WOOD DEVELOPMENT AND PHYSIOLOGY IN A CHANGING CLIMATE

EDITED BY: Guohua Chai, Taku Demura, Xiaohan Yang, Quanzi Li, Wei Li and Meng-Zhu Lu

PUBLISHED IN: Frontiers in Plant Science

frontiers Research Topics

frontiers

ISSN 1664-8714
ISBN 978-2-88976-141-8
DOI 10.3389/978-2-88976-141-8

About Frontiers

Frontiers is more than just an open-access publisher of scholarly articles: it is a pioneering approach to the world of academia, radically improving the way scholarly research is managed. The grand vision of Frontiers is a world where all people have an equal opportunity to seek, share and generate knowledge. Frontiers provides immediate and permanent online open access to all its publications, but this alone is not enough to realize our grand goals.

Frontiers Journal Series

The Frontiers Journal Series is a multi-tier and interdisciplinary set of open-access, online journals, promising a paradigm shift from the current review, selection and dissemination processes in academic publishing. All Frontiers journals are driven by researchers for researchers; therefore, they constitute a service to the scholarly community. At the same time, the Frontiers Journal Series operates on a revolutionary invention, the tiered publishing system, initially addressing specific communities of scholars, and gradually climbing up to broader public understanding, thus serving the interests of the lay society, too.

Dedication to Quality

Each Frontiers article is a landmark of the highest quality, thanks to genuinely collaborative interactions between authors and review editors, who include some of the world's best academicians. Research must be certified by peers before entering a stream of knowledge that may eventually reach the public - and shape society; therefore, Frontiers only applies the most rigorous and unbiased reviews.
Frontiers revolutionizes research publishing by freely delivering the most outstanding research, evaluated with no bias from both the academic and social point of view. By applying the most advanced information technologies, Frontiers is catapulting scholarly publishing into a new generation.

What are Frontiers Research Topics?

Frontiers Research Topics are very popular trademarks of the Frontiers Journals Series: they are collections of at least ten articles, all centered on a particular subject. With their unique mix of varied contributions from Original Research to Review Articles, Frontiers Research Topics unify the most influential researchers, the latest key findings and historical advances in a hot research area! Find out more on how to host your own Frontiers Research Topic or contribute to one as an author by contacting the Frontiers Editorial Office: frontiersin.org/about/contact

WOOD DEVELOPMENT AND PHYSIOLOGY IN A CHANGING CLIMATE

Topic Editors:
Guohua Chai, Qingdao Agricultural University, China
Taku Demura, Nara Institute of Science and Technology (NAIST), Japan
Xiaohan Yang, Oak Ridge National Laboratory (DOE), United States
Quanzi Li, Chinese Academy of Forestry, China
Wei Li, Northeast Forestry University, China
Meng-Zhu Lu, Zhejiang Agriculture & Forestry University, China

Citation: Chai, G., Demura, T., Yang, X., Li, Q., Li, W., Lu, M.-Z., eds. (2022). Wood Development and Physiology in a Changing Climate. Lausanne: Frontiers Media SA. doi: 10.3389/978-2-88976-141-8

Table of Contents

frontiers | Frontiers in Plant Science

EDITORIAL
published: 21 April 2022
doi: 10.3389/fpls.2022.906736

Editorial: Wood Development and Physiology in a Changing Climate

Guohua Chai[1]*, *Mengzhu Lu*[2], *Xiaohan Yang*[3,4], *Taku Demura*[5], *Wei Li*[6] and *Quanzi Li*[7]*

[1] College of Resources and Environment, Qingdao Agricultural University, Qingdao, China, [2] State Key Laboratory of Subtropical Silviculture, School of Forestry and Biotechnology, Zhejiang A&F University, Hangzhou, China, [3] Biosciences Division, Oak Ridge National Laboratory, Oak Ridge, TN, United States, [4] The Center for Bioenergy Innovation, Oak Ridge National Laboratory, Oak Ridge, TN, United States, [5] Division of Biological Science, Graduate School of Science and Technology, Nara Institute of Science and Technology, Nara, Japan, [6] State Key Laboratory of Tree Genetics and Breeding, Northeast Forestry University, Harbin, China, [7] State Key Laboratory of Tree Genetics and Breeding, Chinese Academy of Forestry, Beijing, China

Keywords: tree, wood formation, physiology, biotechnology, metabolism

Editorial on the Research Topic

Wood Development and Physiology in a Changing Climate

Wood of forest trees is a renewable, sustainable and easily workable material and has been widely used in construction, paper making, furniture, and as a feedstock for biofuels. Wood formation is the result of a highly ordered and finely regulated process. Secondary xylem (wood) and phloem are the inner and outer derivative products of the vascular cambium, respectively. Xylem is mainly composed of dead cells with thickened cell walls rich in cellulose, hemicelluloses, and lignin, which are responsible for providing mechanical support and conducting water and minerals for the trees. Phloem transports photoassimilates and signaling molecules, including phytohormones and peptides. Wood structure varies greatly between, and within, tree species. A thorough understanding of developmental processes and metabolic pathways during wood formation would provide a basis for improving wood biomass and modifying properties in forest trees.

Genome sequences of fast-growing tree species, such as *Populus trichocarpa* (Tuskan et al., 2006), *Eucalyptus grandis* (Myburg et al., 2014), *Pinus taeda* (Neale et al., 2014), *Paulownia fortunei* (Cao et al., 2021), *Betula platyphylla* (Chen et al., 2021), and *P. tabuliformis* (Niu et al., 2022), facilitate basic scientific research and motivate the development of biotechnological toolkits for functional genomics. Recently, multi-omics integration has been applied in studying the complexity of wood biology. Through transcriptomic, proteomic, fluxomic and phenomic analyses, Wang et al. (2018) estimated how changes in the expression of wood pathway genes could affect protein abundance, metabolic-flux, metabolite contents, and 25 wood traits, including tree-growth, density, strength, lignin and saccharification. A hierarchical transcriptional regulatory network (TRN), in which the transcription factor (TF) PtrSND1-B1, a master regulator of secondary cell wall (SCW) formation, directs 57 TF-DNA interactions through 17 TFs that transregulate 27 cell wall metabolic genes, was constructed based on quantitative transcriptomics and chromatin binding data (Chen et al., 2019). Despite great progresses in the field of wood biology, a lot of questions remain to be answered on the regulation of wood formation in trees.

This Frontiers Research Topic collected recent advances made through a combination of approaches of genetics and chemistry and improved new insights into the mechanisms of wood biology (anatomy, structure, and function).

This volume is organized in four sections: (1) Growth and Development, (2) Omics Analysis, (3) Gene Discovery, and (4) New Technologies and Resources.

OPEN ACCESS

Edited and reviewed by:
Maurice Bosch,
Aberystwyth University,
United Kingdom

***Correspondence:**
Guohua Chai
chaigh@qau.edu.cn
Quanzi Li
liqz@caf.ac.cn

Specialty section:
This article was submitted to Plant Biotechnology, a section of the journal Frontiers in Plant Science

Received: *29 March 2022*
Accepted: *30 March 2022*
Published: *21 April 2022*

Citation:
Chai G, Lu M, Yang X, Demura T, Li W and Li Q (2022) Editorial: Wood Development and Physiology in a Changing Climate. Front. Plant Sci. 13:906736. doi: 10.3389/fpls.2022.906736

GROWTH AND DEVELOPMENT

Wood formation is initiated from the vascular cambium, and encompasses a series of developmental processes, including cambial division, xylem differentiation, SCW thickening and programmed cell death (PCD). Understanding the mechanisms underlying these processes is essential for optimizing molecular breeding of high-yield trees. Wang D. et al. reviewed the recent discoveries on the regulation of vascular cambium development by multiple internal signals and their crosstalks in trees. This study revealed that there exists a similar but more complex regulatory network orchestrating vascular cambium development in poplar in comparison with Arabidopsis. Jiang et al. summarized the progress in the studies on the transcriptional regulation and signaling of developmental programmed cell death (dPCD) during vegetative and reproductive development. Future perspectives on how to take full advantage of dPCD in plants were discussed, with the goal of improving the efficiency of wood biomass production.

OMICS ANALYSIS

High-throughput sequencing and multi-omics analysis in tree species provide resources for studying the genetic basis of wood formation. Luo et al. compared the regulatory network of wood formation between juvenile wood (JW) and mature wood (MW) forming tissues using RNA sequencing (RNA-Seq) and whole genome bisulfite sequencing (WGBS), and revealed significant differences in transcriptional programs and patterns of DNA methylation between JW and MW. Li et al. employed RNA-Seq and isoform sequencing (Iso-seq) technologies to explore the gene expression profile across wood-forming tissues in the angiosperm *P. alba* × *P. glandulosa* and the gymnosperm *Larix kaempferi* (Lamb.) Carr. Differential mechanisms of wood formation, were identified at the transcriptional and post-transcriptional levels between angiosperm and gymnosperm tree species. Xiao Y. et al. combined transcriptomics, proteomics, and confocal Raman imaging techniques to analyze tension wood (TW), opposite wood (OW), and normal wood (NW) in *Catalpa bungei*, resulting in the identification of several key candidate genes that regulate lignin biosynthesis.

GENE DISCOVERY

Currently, more and more efforts are being made to identify and characterize the genes involved in wood formation for genetic engineering in trees. Six research articles in this Research Topic determined the role of specific genes controlling wood biomass formation and properties. Liu et al. over-expressed the small guanosine triphosphate binding protein gene *PagRabE1b* in poplar and characterized its function in SCW thickening and PCD. Chu et al. showed that the knockdown of poplar microRNA393 (miR393) using the short tandem target mimic (STTM) approach could improve the tree growth and thus improved biomass production. Xiao L. et al. performed an association study as well as epistasis and mendelian randomization (MR) analyses, and revealed the impact of the genetic interaction between PtomiR403b and its target *PtoGT31B-1* on wood formation. During the secondary growth, trees are able to modify the anatomic structure of the wood in response to environmental stresses. Rodriguez-Zaccaro et al. illustrated that the genetic architecture of vessel traits affecting hydraulic physiology and resilience to water stress is under genetic regulation, which is not simply influenced by tree height.

Wood cell walls are composite materials containing cellulose crystals and a tri-component interstitial gel, which is composed of water, hemicelluloses, and lignin. The lignin in dicotyledonous angiosperms is typically polymerized from three monolignol precursors, coniferyl alcohol, sinapyl alcohol, and *p*-coumaroyl alcohol, resulting in guaiacyl (G), syringyl (S), and hydroxyphenyl (H) subunits, respectively (Zhao, 2016). Engineering of lignin quantity and composition is important for reducing biomass recalcitrance. Wang Q. et al. found that the poplar gene *CONIFERALDEHYDE 5-HYDROXYLASE* (*CAld5H2*) was negatively regulated by the BEL1-like homeodomain (BLH) protein PagBLH6a that functions through a combinatorial regulation with multiple TFs for S monolignol biosynthesis. Su et al. revealed that down-regulation of *p-Hydroxycinnamoyl-Coenzyme A: Quinate/Shikimate p-Hydroxycinnamoyltransferase* (*HCT*) expression in poplar changed the contents and micro-distributions of wood cell wall components as well as the morphological characteristics of cells.

NEW TECHNOLOGIES AND RESOURCES

The CRISPR/Cas systems are facile, highly efficient and widely used in diverse cells and organisms (Wada et al., 2022). Woody plants with long-life spans and outcrossing mating systems are difficult subjects for traditional mutagenesis methods. An et al. developed a new mannopine synthase (MAS)-CRISPR/Cas9 system in poplar, which can be used to simultaneously edit multiple genes with higher mutation rates. Mining and establishment of wood-associated databases are helpful for understanding the development and structure of wood. In this issue, two contributions focus on the database of wood formation regulation. Zhuang et al. developed a high-throughput screening system with a library of 517 wood-associated TFs sampled from *P. alba* × *P. glandulosa* cv 84K. Multiple regulatory modules of lignin biosynthesis during wood development were identified by screening this TF library using yeast-one hybrid (Y1H) and yeast-two-hybrid (Y2H) methods. Wang H. et al. established a *P. trichocarpa* stem differentiating xylem (PSDX) database, which integrates 144 RNA-Seq, 33 ChIP-seq, and six single-molecule real-time (SMRT) Iso-seq libraries and presents comprehensive measurements of gene expression and post-transcriptional regulation. Beside these wood-associated databases, Gupta et al. described the economically feasible wood biopreservation platform in *Lannea coromandelica* (Houtt.) Merr. against wood rotting fungi using extracts from weeds viz. *Lantana*

camara L. and *Ageratum conyzoides* L. The use of this plant-based, environmentally sustainable preservative has tremendous potential for wood protection.

Biotechnology has rapidly advanced the practical application of molecular genetics in tree breeding. The articles in this volume provide an excellent update on wood biology research.

AUTHOR CONTRIBUTIONS

All authors participated either in the writing or editing of the editorial. All authors contributed to the article and approved the submitted version.

FUNDING

Financial support for this work was obtained from National Natural Science Foundation of China (31972955 and 32101549), the Central Guidance on Local Science and Technology Development Fund of Shandong Province (YDZX2021112) and the Taishan Scholar Program of Shandong (tsqn202103092).

ACKNOWLEDGMENTS

We thank very much all the authors that have participated in this topic.

REFERENCES

Cao, Y., Sun, G., Zhai, X., Xu, P., Ma, L., Deng, M., et al. (2021). Genomic insights into the fast growth of paulownias and the formation of Paulownia witches' broom. *Mol. Plant* 14, 1668–1682. doi: 10.1016/j.molp.2021.06.021

Chen, H., Wang, J. P., Liu, H., Li, H., Lin, Y. J., Shi, R., et al. (2019). Hierarchical transcription factor and chromatin binding network for wood formation in black cottonwood (*Populus trichocarpa*). *Plant Cell* 31, 602–626. doi: 10.1105/tpc.18.00620

Chen, S., Wang, Y., Yu, L., Zheng, T., Wang, S., Yue, Z., et al. (2021). Genome sequence and evolution of *Betula platyphylla*. *Hortic. Res.* 8, 37. doi: 10.1038/s41438-021-00481-7

Myburg, A., Grattapaglia, D., Tuskan, G., Hellsten, U., Hayes, R. D., Grimwood, J., et al. (2014). The genome of *Eucalyptus grandis*. *Nature* 510, 356–362. doi: 10.1038/nature13308

Neale, D. B., Wegrzyn, J. L., Stevens, K. A., Zimin, A. V., Puiu, D., Crepeau, M. W., et al. (2014). Decoding the massive genome of loblolly pine using haploid DNA and novel assembly strategies. *Genome Biol.* 15, R59. doi: 10.1186/gb-2014-15-3-r59

Niu, S., Li, J., Bo, W., Yang, W., Zuccolo, A., Giacomello, S., et al. (2022). The Chinese pine genome and methylome unveil key features of conifer evolution. *Cell* 185, 204–217.e14. doi: 10.1016/j.cell.2021.12.006

Tuskan, G. A., DiFazio, S., Jansson, S., Bohlmann, J., Grigoriev, I., Hellsten, U., et al. (2006). The genome of black cottonwood, *Populus trichocarpa* (Torr. & Gray). *Science* 313, 1596–1604. doi: 10.1126/science.1128691

Wada, N., Osakabe, K., and Osakabe, Y. (2022). Expanding the plant genome editing toolbox with recently developed CRISPR-Cas systems. *Plant Physiol.* 31, kiac027. doi: 10.1093/plphys/kiac027

Wang, J. P., Matthews, M. L., Williams, C. M., Shi, R., Yang, C., Tunlaya-Anukit, S., et al. (2018). Improving wood properties for wood utilization through multi-omics integration in lignin biosynthesis. *Nat. Commun.* 9, 1579. doi: 10.1038/s41467-018-03863-z

Zhao, Q. (2016). Lignification: flexibility, biosynthesis and regulation. *Trends Plant Sci.* 21, 713–721. doi: 10.1016/j.tplants.2016.04.006

Conflict of Interest: The authors declare that the research was conducted in the absence of any commercial or financial relationships that could be construed as a potential conflict of interest.

Publisher's Note: All claims expressed in this article are solely those of the authors and do not necessarily represent those of their affiliated organizations, or those of the publisher, the editors and the reviewers. Any product that may be evaluated in this article, or claim that may be made by its manufacturer, is not guaranteed or endorsed by the publisher.

frontiers in Plant Science

ORIGINAL RESEARCH
published: 20 May 2021
doi: 10.3389/fpls.2021.655565

PSDX: A Comprehensive Multi-Omics Association Database of *Populus trichocarpa* With a Focus on the Secondary Growth in Response to Stresses

Huiyuan Wang[1], Sheng Liu[2], Xiufang Dai[3], Yongkang Yang[1], Yunjun Luo[2], Yubang Gao[2], Xuqing Liu[1], Wentao Wei[1], Huihui Wang[1], Xi Xu[2], Anireddy S. N. Reddy[4], Pankaj Jaiswal[5], Wei Li[3], Bo Liu[6] and Lianfeng Gu[1]**

[1] Basic Forestry and Proteomics Research Center, College of Forestry, Fujian Agriculture and Forestry University, Fuzhou, China, [2] College of Life Sciences, Fujian Agriculture and Forestry University, Fuzhou, China, [3] State Key Laboratory of Tree Genetics and Breeding, Northeast Forestry University, Harbin, China, [4] Department of Biology and Program in Cell and Molecular Biology, Colorado State University, Fort Collins, CO, United States, [5] Department of Botany and Plant Pathology, Oregon State University, Corvallis, OR, United States, [6] College of Forestry, Fujian Agriculture and Forestry University, Fuzhou, China

OPEN ACCESS

Edited by:
Ralf Alexander Wilhelm, Institute for Biosafety in Plant Biotechnology, Federal Research Centre for Cultivated Plants, Julius Kühn-Institute, Germany

Reviewed by:
Jorge Maurício Mondego, Instituto Agronômico de Campinas (IAC), Brazil
Congting Ye, Xiamen University, China

***Correspondence:**
Bo Liu
liubo@fafu.edu.cn
Lianfeng Gu
lfgu@fafu.edu.cn

Specialty section:
This article was submitted to Plant Biotechnology, a section of the journal Frontiers in Plant Science

Received: *19 January 2021*
Accepted: *26 April 2021*
Published: *20 May 2021*

Citation:
Wang H, Liu S, Dai X, Yang Y, Luo Y, Gao Y, Liu X, Wei W, Wang H, Xu X, Reddy ASN, Jaiswal P, Li W, Liu B and Gu L (2021) PSDX: A Comprehensive Multi-Omics Association Database of Populus trichocarpa With a Focus on the Secondary Growth in Response to Stresses. Front. Plant Sci. 12:655565. doi: 10.3389/fpls.2021.655565

Populus trichocarpa (*P. trichocarpa*) is a model tree for the investigation of wood formation. In recent years, researchers have generated a large number of high-throughput sequencing data in *P. trichocarpa*. However, no comprehensive database that provides multi-omics associations for the investigation of secondary growth in response to diverse stresses has been reported. Therefore, we developed a public repository that presents comprehensive measurements of gene expression and post-transcriptional regulation by integrating 144 RNA-Seq, 33 ChIP-seq, and six single-molecule real-time (SMRT) isoform sequencing (Iso-seq) libraries prepared from tissues subjected to different stresses. All the samples from different studies were analyzed to obtain gene expression, co-expression network, and differentially expressed genes (DEG) using unified parameters, which allowed comparison of results from different studies and treatments. In addition to gene expression, we also identified and deposited pre-processed data about alternative splicing (AS), alternative polyadenylation (APA) and alternative transcription initiation (ATI). The post-transcriptional regulation, differential expression, and co-expression network datasets were integrated into a new *P. trichocarpa* Stem Differentiating Xylem (PSDX) database (http://forestry.fafu.edu.cn/db/SDX), which further highlights gene families of RNA-binding proteins and stress-related genes. The PSDX also provides tools for data query, visualization, a genome browser, and the BLAST option for sequence-based query. Much of the data is also available for bulk download. The availability of PSDX contributes to the research related to the secondary growth in response to stresses in *P. trichocarpa*, which will provide new insights that can be useful for the improvement of stress tolerance in woody plants.

Keywords: plant stress, secondary growth, *Populus trichocarpa*, co-expression, alternative splicing, transcriptome

INTRODUCTION

Plant growth and development are challenged by a variety of abiotic stresses, such as, cold, drought, high salt and heat (Filichkin et al., 2018). Transcription factors (TF) such as NAC, AP2, and MYB are critical master regulators in stress responses (Lindemose et al., 2013). Identification of transcription factor network and their target genes can help us better understand the transcriptional regulation during secondary growth of woody plants. For example, overexpression of *PtrNAC005* and *PtrNAC100* genes in *Populus trichocarpa* (*P. trichocarpa*) showed a strong enhancement in drought tolerance (Li et al., 2019). Using chromatin immunoprecipitation sequencing (ChIP-Seq) protocol for differentiating stem xylem (Li et al., 2014), transcription factor ARBORKNOX1 (ARK1) has been shown to bind near the transcription start sites of thousands of gene loci implicated in diverse functions (Liu et al., 2015b). In addition to transcription factors, the alteration of histone modification and chromatin modifications can regulate the expression level of genes with stressful environmental changes (Kwon et al., 2009; Kim et al., 2012; Perrella et al., 2013). For example, transcription factor PtrAREB1-2 recruits histone acetyltransferase unit of histone acetylase to enrich H3K9ac and RNA polymerase II specifically at drought-responsive genes *PtrNAC006*, *PtrNAC007,* and *PtrNAC120* containing the ABRE *cis*-element, resulting in increased expression of *PtrNAC* genes (Li et al., 2019).

Splicing factors are the key versatile regulators of alternative splicing (AS) and can cause a significant change in splicing profiles in response to different abiotic stresses (Duque, 2011; Reddy et al., 2013). In plants, over 60% of multi-exon genes undergo AS events (Filichkin et al., 2010, 2018; Zhang et al., 2010; Marquez et al., 2012), and the most prevalent AS type is intron retention (IR) in terrestrial plants. AS is involved in the physiological processes of most plants and can respond to environmental stresses (Staiger and Brown, 2013). Interestingly, stress-responsive AS of transcription factors (TFs) has also been reported (Seo et al., 2013). Previous studies have shown that AS is ubiquitous in *P. trichocarpa* (Baek et al., 2008; Srivastava et al., 2009; Bao et al., 2013; Zhao et al., 2014; Tang et al., 2015; Filichkin et al., 2018) and at least 36% of xylem-expressed genes in *P. trichocarpa* are regulated by AS (Bao et al., 2013). For example, *PtrWND1B*, a key gene regulating secondary cell wall in *P. trichocarpa*, encodes two splice isoforms *(PtrWND1B-s* and *PtrWND1B-l*), which cause antagonism in cell wall thickening during fiber development (Zhao et al., 2014). Moreover, dominant-negative regulators are also reported (Li et al., 2012; Lin et al., 2017).

In addition to AS, alternative transcription initiation (ATI) and alternative polyadenylation (APA) can also produce multiple isoforms from one genetic locus (Xing and Li, 2011). ATI and APA refer to one gene has distinct transcription start sites (TSSs) and transcription termination sites (TTSs). For example, *Lon1* preferentially selects proximal TSS under hypoxic-like conditions and causes mitochondrial dysfunction due to protein misfolding in *Arabidopsis* (Daras et al., 2014). Previous studies have shown that 70, 47.9, and 19.7% genes have more than one poly(A) site in *Arabidopsis*, rice, and moso bamboo, respectively (Wu et al., 2011; Fu et al., 2016; Wang et al., 2017), indicating that APA is a widespread post-transcriptional process. APA events are widely involved in abiotic stress response pathways (Ye et al., 2019; Chakrabarti et al., 2020). Post-transcriptional regulations including AS, and APA are regulated by RNA-binding proteins (RBPs). There are more than 800 RNA binding proteins in *Arabidopsis* (Silverman et al., 2013). The RNA recognition motif (RRM) and the K homology (KH) domain are the most prevalent RNA domains in plants. These RBPs regulate the transcriptome *via* AS, APA, and transcript stability (Bailey-Serres et al., 2020). Thus, it is necessary to investigate the dynamics of these RBPs in response to stress.

The development of high-throughput sequencing technology has enabled us to study the transcriptome and post-transcriptional complexities of plants in different tissues and under different environments (Reddy et al., 2020). Single Molecular Real-Time (SMRT) isoform sequencing technology from PacBio which provides evidence in the form of long sequence reads of the cDNAs (Steijger et al., 2013) has important applications in the identification of post-transcriptional regulation such as complex AS (Zhang et al., 2019; Zhao et al., 2019).

Secondary growth in plants refers to the wood formation due to the activities of the secondary meristem, especially vascular cambium (Mellerowicz et al., 2001; Plomion et al., 2001). *P. trichocarpa* is a model of woody plants with a high-quality reference genome (Tuskan et al., 2006), which largely drives the investigation of secondary xylem development including xylem and phloem differentiation and cell proliferation (Jansson and Douglas, 2007; Kaneda et al., 2010). With increasing number of studies using high-throughput transcriptome sequencing to study secondary growth in poplar, huge amounts of data have been generated and publicly released, which provides extremely valuable information for the investigation of the stem-differentiating xylem (SDX) in response to stress. However, a multi-omics database focused on secondary growth in response to stress has never been reported in *P. trichocarpa*. In order to develop such a resource, we collected the majority publicly available peer-reviewed high throughput data on secondary growth in response to stresses in *P. trichocarpa,* which includes multi-omics data on the TF binding, histone modifications, and transcriptomes. Importantly, we processed and analyzed these datasets with unified parameters and integrated them in a unified *P. trichocarpa* Stem Differentiating Xylem (PSDX) database (http://forestry.fafu.edu.cn/db/SDX). The PSDX database is expected to serve as a valuable resource to the scientific community in understanding the interplay between stress responses and secondary growth in *P. trichocarpa*.

MATERIALS AND METHODS

High Throughput Datasets for Construction of PSDX

The *P. trichocarpa* reference genome sequence and annotations (version 3.0) (Tuskan et al., 2006), were obtained from

Phytozome (v.12.1.6) (Goodstein et al., 2012). All the raw RNA-Seq, Iso-Seq, and ChIP-Seq datasets were downloaded from the NCBI SRA database through the Aspera tool. Finally, a total of 144 RNA-Seq (**Supplementary Table 1**) libraries (Lin et al., 2013; Lu et al., 2013; Shi et al., 2017; Filichkin et al., 2018; Li et al., 2019), six Iso-Seq libraries (Filichkin et al., 2018) and 33 ChIP-Seq (**Supplementary Table 1**) libraries (Liu et al., 2014, 2015a,b; Li et al., 2019) were included in this study (**Figure 1**). Besides, the RNA-binding proteins containing RRM and KH domains from *Arabidopsis* were retrieved from a previous study (Lorkovic and Barta, 2002) to search for homologs in *P. trichocarpa*.

ChIP-Seq Data Analysis

For the identification of TF peaks or histone modification sites based on ChIP-Seq data, the sequence reads were aligned to *P. trichocarpa* reference genome using bowtie2 v.2.2.1 (Langmead and Salzberg, 2012) with "-k 2 –no-unal –no-hd –no-sq" parameters. MACS14 was used for peak calling (Zhang et al., 2008). DiffReps (Shen et al., 2013) was used to analyze differential peaks in ChIP-seq signals with "–pval 0.05" parameters (**Figure 2**).

RNA-Seq Data Analysis

In total, 144 RNA-Seq libraries were subjected to transcriptome analysis to calculate gene expression levels and identify AS events. The raw FASTQ files were extracted from the SRA files using fastq-dump v.2.5.7 (Leinonen et al., 2011). Then ht2-filter v1.92.1 of the sequence filter package HTQC (Yang et al., 2013) was used to filter the low-quality bases from single or pair-end reads. The filtered reads were aligned to the *P. trichocarpa* reference genome with hisat2 v.2.0.3-beta (Kim et al., 2015). Only the unique reads were kept. Samtools v.0.1.7 (Li et al., 2009) was used to convert the uniquely SAM files to sorted bam files. Gene expression levels were normalized to FPKM (Fragments Per Kilobase of transcript per Million mapped) for paired-end libraries and RPKM (Reads Per Kilobase of transcript per Million mapped reads) for single-end libraries, respectively. The edgeR package was used for differential gene expression analysis (Robinson et al., 2010). The *P* values less than 0.05 and | Fold Change| greater than 1.5 were considered as statistically significant. In order to identify different AS events, the transcript data was assembled and merged using StringTie v.1.3.3b (Pertea et al., 2015). The obtained BAM file and merged GTF file were used to identify AS events using rMATS v.3.2.2.beta (Shen et al., 2014) with following parameter: -a 8 -c 0.0001 -analysis U –keepTemp to identify differential AS events with false discovery rate (FDR) < 0.05 (**Figure 2**). AS events was visualized by rmats2sashimiplot[1].

Iso-Seq Data Analysis

For the analysis of Iso-Seq data, we obtained high-quality reads of insert (ROI) by ConsensusTools script of SMRT Analysis v.2.3.0 software package from Pacific Biosciences. Then we used pbtranscript.py of SMRT Analysis v.2.3.0 software package to obtain full-length non-chimeric (FLNC) reads. For a small part of the chimeric ROI, they were marked as complete ROI by judging the 5′ primer, 3′ primer, presence of poly(A) and corresponding positional relationship. LSC 1.alpha (Au et al., 2012) was used to correct Iso-Seq. Finally, these corrected Iso-Seq reads were further used as an input file to identify AS events using PRAPI (Gao et al., 2018) with default parameters to identify the post-transcriptional regulation events including ATI, AS, and APA (**Figure 2**).

Identification of RNA-Binding Protein Coding Genes in *Populus trichocarpa*

The RBPs genes in *Arabidopsis* have previously been reported (Lorkovic and Barta, 2002). Firstly, the protein sequence containing the RRM and KH domains was extracted from *Arabidopsis* (TAIR10) gene loci. Then, hmmbuild (Potter et al., 2018) was used to build HMMER matrices with all RBP candidate genes in *Arabidopsis*. Next, homologous RBP candidate genes in *P. trichocarpa* were identified by hmmsearch tool with -E 10^{-5}. All conserved domains of RRM and KH from RBP candidate genes were confirmed by NCBI-CDD.

Identification of Stress Response Genes in *Populus trichocarpa*

In this study, we collected stress tolerance or stress response genes from several public databases and literature sources. To do this, we started by collecting 617 *Arabidopsis* stress tolerance or stress response genes from ASRGDB (Borkotoky et al., 2013) and 106 drought stress response genes in *Arabidopsis* from DroughtDB (Alter et al., 2015). Additionally, we performed a comprehensive review and biocuration of published literature (Villar Salvador, 2013; Hossain et al., 2016; Vats, 2018; Singh et al., 2019). In total, we collected a list of 766 unique *Arabidopsis* stress response genes. To identify putative stress response genes in *P. trichocarpa*, we used blastall (-p blastp, -e 1e-5) with the amino acid sequence of 766 *Arabidopsis* genes as the query. A set of 1,123 *P. trichocarpa* gene with amino acid sequence similarity of more than 50% were identified and retained as candidate stress response genes (**Supplementary Table 2**).

Co-expression Networks Analysis

For the measure of gene co-expression network, we compared the cut-off values of Pearson Correlation Coefficient (PCC) with mutual rank (MR) score (Obayashi and Kinoshita, 2009). The MR values were calculated as described previously (You et al., 2016). According to the methods in previous study (Obayashi and Kinoshita, 2009; You et al., 2016; Tian et al., 2018), we extracted 176 genes with the number of GO terms ranging from 4 to 20 using Receiver Operating Characteristic (ROC) curve and Area under the ROC Curve (AUC) value to evaluate the constructed co-expression network as a specific binary classifier. Based on the co-expression networks with thresholds of PCC > 0.54, PCC > 0.64, PCC > 0.74, PCC > 0.84, MR top3 + MR ≤ 30 or MR top3 + MR ≤ 100, we inferred the true or false determination for GO from pair-wise genes. We used co-expression gene pairs (Potri.008G069600 and Potri.004G162400) from threshold of MR top3 + MR ≤ 30 as example. Potri.008G069600 included four GO terms (GO:0003674, GO:0071704, GO:0003824, and

[1]https://github.com/Xinglab/rmats2sashimiplot/

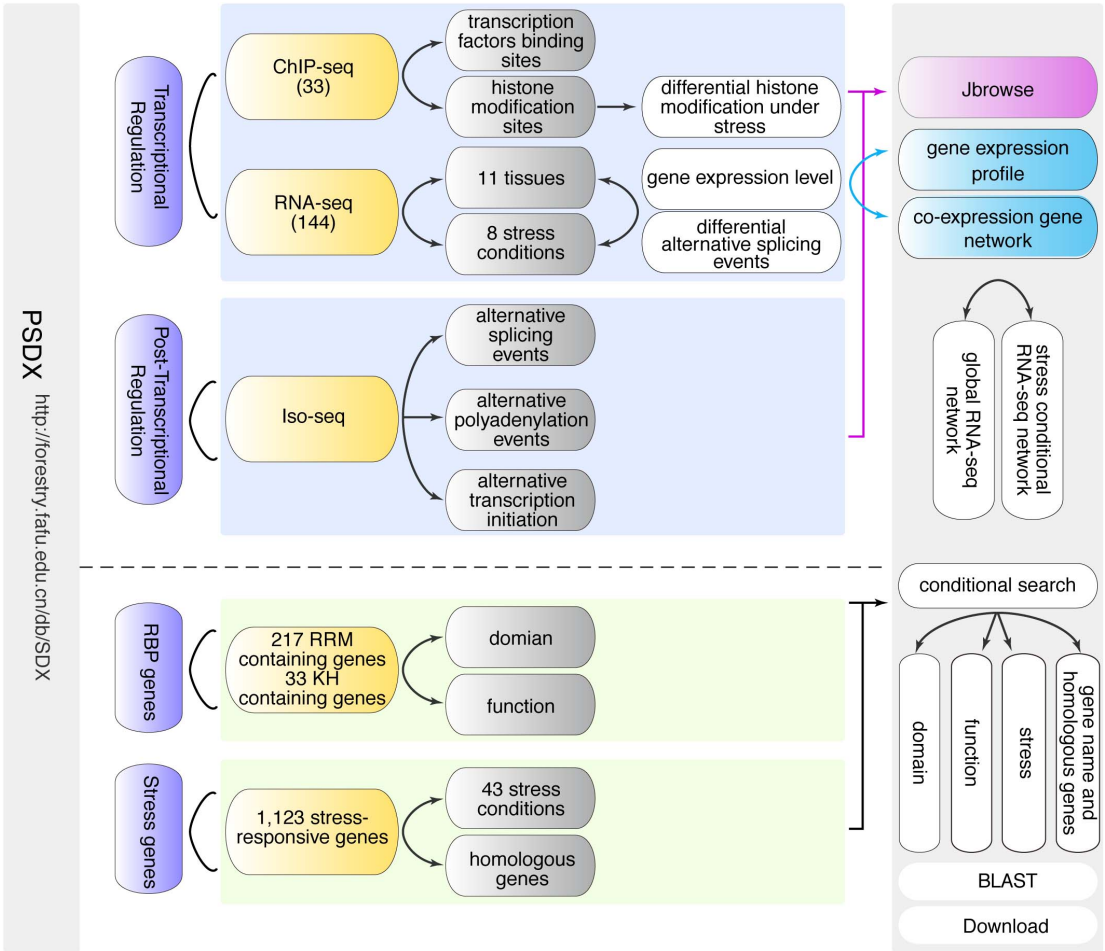

FIGURE 1 | Schematic overview of PSDX database. PSDX consists of two major resources including transcriptional regulation and post-transcriptional regulation under different stress conditions and in different tissues in *P. trichocarpa*. PSDX also includes several other modules: co-expression network, RBP genes, stress-responsive genes, and conditional search.

GO:0006629). Potri.004G162400 included five GO terms (GO:0003674, GO:0003824, GO:0005975, GO:0006006, and GO:0004332). Using Potri.004G162400 as prediction, Potri.008G069600 shown five predicted GO terms including GO:0003674, GO:0003824, GO:0005975, GO:0006006, and GO:0004332. Comparing with the original GO terms of Potri.008G069600 (GO:0003674, GO:0071704, GO:0003824, and GO:0006629), only GO:0003674 and GO:0003824 were true (marked as 1). GO:0005975, GO:0006006, and GO:0004332 were false (marked as 0) (**Supplementary Table 3**). Finally, we selected different thresholds to calculate TPR (true positive rate, TPR) and FPR (false positive rate, FPR). ROC curves and AUC were generated using sklearn plugin. The expression profile and co-expression module was displayed using script from ALCOdb (Aoki et al., 2016).

Database Construction

Populus trichocarpa Stem Differentiating Xylem portal consists of a front-end user interface and a back-end database. The database mainly includes information such as FPKM/RPKM, AS events, APA, ATI, RBP candidate genes, and gene functions, which are presented to the user through the search function module (**Figure 1**). The search function was divided into simple fuzzy (approximate) string searching, single condition or multiple condition joint search, and BLAST search. Both the "Home page" and the "Search page" contained the entry of a simple fuzzy string search enabled by the PHP. The user can input any keyword by fuzzy string searching to query data in MySQL database, and the matching results will be returned to the user. The results data table is displayed using the Bootstrap extension. BLAST search allows the users to perform a sequence-based query. The best matches connect to the gene pages. For the BLAST graphical user interface, we applied a Sequence Server[2] with a modern graphical user interface to set up BLAST+ server (Priyann et al., 2019). Multiple text downloads make it quick and easy to customize the

[2]http://sequenceserver.com

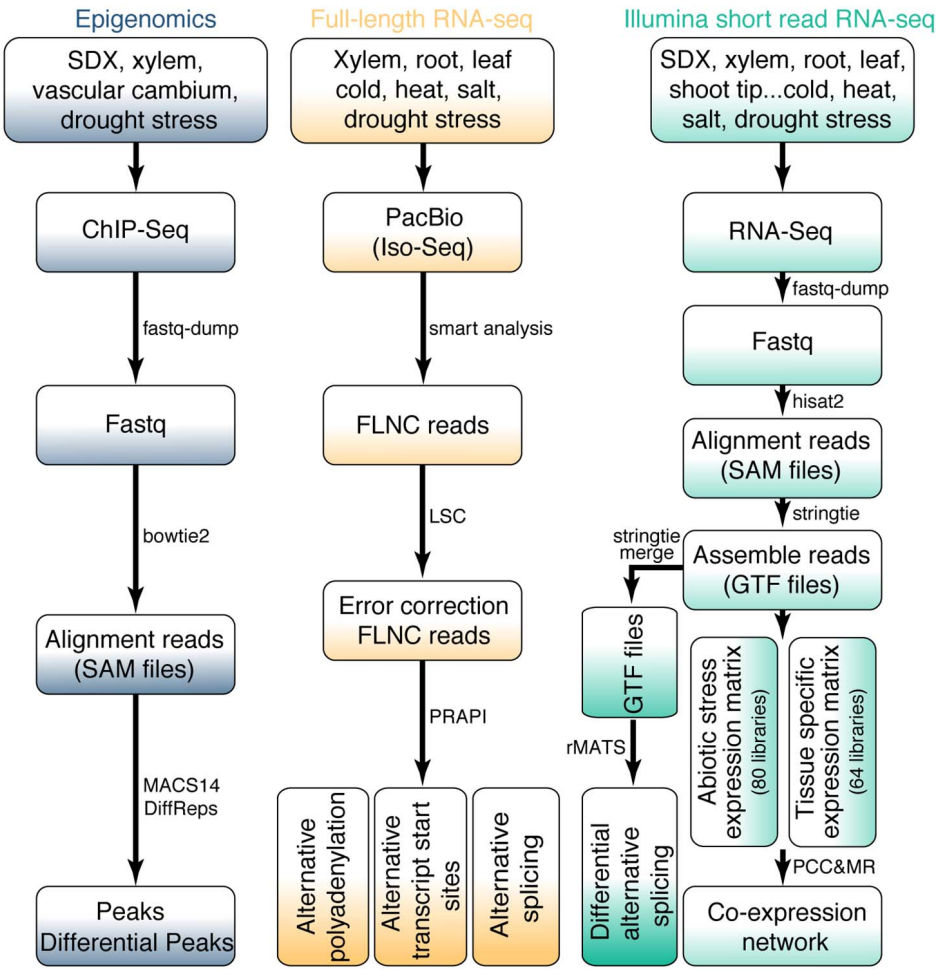

FIGURE 2 | Bioinformatics workflow for omics data. The upper part of the figure shows the data source for RNA-seq and epigenomics. The bioinformatics pipeline for all data processing is shown in the middle and bottom of the figure.

dataset. The JBrowse (Buels et al., 2016) interface is provided to query and visualize the data aligned to the reference genome.

RESULTS AND DISCUSSION

Database Overview and Essential Modules of PSDX

In order to facilitate researchers to access and mine high-throughput sequencing information related to secondary growth upon stress response in *P. trichocarpa,* we constructed an easy-to-use and fully functional web database to query, download, visualize and integrate multi-omics data using a unified portal. The search-query function is the core of the PSDX database, which includes two different built-in search capabilities, including keyword search and BLAST-search (**Figure 1**). When users provide keywords such as gene names, function descriptions, or GO terms in the search box, which will present a drop-down list of search suggestions to auto-complete the keywords (**Figure 1**). After the user submits the keyword, the query function will return a comprehensive data sheet containing pre-computed information based on high throughput sequencing and presents it with a high-resolution figure, and JBrowse genome browser hyperlink.

The gene page includes visualization of the gene structure, gene expression from RNA-Seq, post-transcriptional events from RNA-Seq and Iso-Seq, and other feature information such as functional annotation. The genome browser includes 206 tracks which include the reference genome, gene structure (GFF), and bigwig files for all ChIP-Seq, RNA-Seq and Iso-seq libraries. Users can also upload their local data in standard formats like the BAM, BED, GFF, GTF, VCF, etc., to compare alongside the existing data.

For researchers, interested in profiling sequence-based queries, PSDX's BLAST function module is a preferred tool. Users can paste their own sequence in FASTA format into the text box or drag the FASTA file directly into the text box. Then the system will automatically recognize whether it is a protein sequence or a nucleic acid sequence. After the selection of the appropriate alignment database, the BLAST submit button will be activated, which dramatically reduces the user's burden. After

performing the BLAST comparison, the web browser displays a comparison result report in HTML, XML, or CSV format, which are summarized with the details of each matching alignment and overview graph including the alignment strength and position of each hit. After clicking on the gene name in the BLAST hit results, users can also hyperlink to the detailed page of the PSDX database to view all the information about the gene.

For the export of data, PSDX provides downloads in diverse formats, including CSV, MS-Excel, and TXT. The user can perform a secondary screening of the table in real-time by entering keywords to obtain more accurate results by filter box for the table, which is located at the top right of the data table. Finally, PSDX has created online documentation, which provides a quick start guide on searching, mining, browsing, downloading, and other more comprehensive **Supplementary Material**.

In summary, we integrated transcription factor peaks, gene expression, co-expression network, post-transcriptional regulation information, stress response genes, and RBP candidate genes into one unified database. In the following section, we presented a detailed description of the above six modules.

TF and Differential Histone Modification in Response to Abiotic Stress

To generate a comprehensive chromatin state map of *P. trichocarpa*, we collected the majority of published ChIP-seq libraries, which included peaks of several transcription factors such as ARK1, ARK2, BLR, PCN, and PRE. In total, 15,351 genes with 47,552 TF peaks were identified and integrated in the PSDX database (**Supplementary Table 4**). In addition to TF, H3K9ac modifications are known for their role in drought response in *Arabidopsis* (Kim et al., 2012) and *P. trichocarpa* (Li et al., 2019). Histone acetylation showed alteration in the drought stress-responsive genes under drought stress in *P. trichocarpa* (Li et al., 2019). Thus, we also identified 37,112, 41,613, and 35,703 peaks from different H3K9ac ChIP-seq data (**Supplementary Figure 1** circle 2, 5, and 8). In total, the PSDX database contains 8,359 and 9,360 differential H3K9ac modifications (**Supplementary Table 4**) for 5- and 7-day without watering (drought-like conditions), respectively. The level of H3K9ac also changed in differentially expressed genes under drought stress or drought-responsive genes (**Supplementary Figure 1** circle 3, 4, 6, 7, and 9), which could be visualized at PSDX.

Differential Gene Expression Analysis in Response to Abiotic Stress

In this study, we calculated gene expression in diverse tissues including root, callus, leaf, stem, stem xylem, and shoot tip. Furthermore, we also investigated gene expression patterns under cold, salt, heat, and drought stress conditions. A principal component analysis identified tissues (**Supplementary Figure 2A**) rather than stresses (**Supplementary Figure 2B**), as the main factor driving gene expression, which was consistent with previous research (Appels et al., 2018). In addition, we also conducted Principal Component Analysis and found that the samples can be separated by tissues and treatments (**Supplementary Figure 3**). Next, to identify differentially expressed genes involved in secondary growth, we compared gene expression levels of secondary xylem with that of other tissues. In total, we show that over 21,442 genes are differentially expressed in secondary xylem compared with other tissues. To further investigate which genes are affected in xylem under different stress conditions, we performed differential expression analysis between non-stress and stress conditions in the xylem. In total, we found 19,872 differentially expressed genes in response to different stresses in xylem, which included previously reported Potri.002G081000 (*PtrNAC006*) (Li et al., 2019). Overexpression of Potri.002G081000 (*PtrNAC006*) could significantly improve drought-adaptive capabilities through an increase in the number of xylem vessels (Li et al., 2019). In the search pages of our PDSX, users can use Potri.002G081000 (*PtrNAC006*) as a search condition to get the highly expressed pattern of Potri.002G081000 (*PtrNAC006*) under drought and other stresses in secondary xylem. The user also can get all other specifically expressed genes of secondary xylem in response to different stress.

Stress-Specific Co-expression Networks

We followed previous method (Obayashi and Kinoshita, 2009; You et al., 2016; Tian et al., 2018). In brief, PCC between each pair of genes (A and B) was calculated. The mutual rank (MR) is a refinement of geometric mean of the ranked PCC: $\mathrm{MR(AB)} = \sqrt{Rank(AB) \times Rank(BA)}$. AB represents the order of gene A in gene B's PCC list, whereas BA represents the order of gene B in gene A's PCC list. The highest 5% PCC value of all positive co-expression gene pairs were 0.54 under stress samples (**Supplementary Figure 4**). We selected four PCC thresholds (PCC $>$ 0.54, 0.64, 0.74, and 0.84). Beyond that, we selected two MR thresholds including MRtop3+MR $\leq$ 30 or MRtop3+MR $\leq$ 100. Then, we generate receiver operating characteristic (ROC) curves to compare the performance of different classifiers. The detail steps of how to evaluate the superiority of different classifiers is described in methods. As a result, the AUC of the co-expression network under PCC $>$ 0.74 as cut-off was the best (**Supplementary Figure 5A**). In addition, co-expression networks with thresholds of MR top3+MR $\leq$ 30 and MR $\leq$ 100 were tested and the network with MR top3+MR $\leq$ 30 was the best in all cut-off (**Supplementary Figure 5B**). Thus, we used MR top3+MR $\leq$ 30 as cut-off values for co-expression networks in this study.

Differential Alternative Splicing in Response to Abiotic Stress

We identified 78,526 AS events in 16,545 genes from 144 transcriptome datasets sampled from different stress and tissues. The most common AS types included Exon skipping (ES), Intron Retention (IR), Alternative acceptor sites (AltA), and Alternative donor sites (AltD), respectively (**Figure 3**). The AS events include 28,773 Intron Retention (IR), 13,348 Exon skipping (ES), 24,087 Alternative acceptor sites (AltA), and 12,318 Alternative donor sites (AltD), respectively (**Supplementary Table 5**). Especially, we analyzed the difference in AS events between secondary xylem and other tissues under normal conditions, which revealed

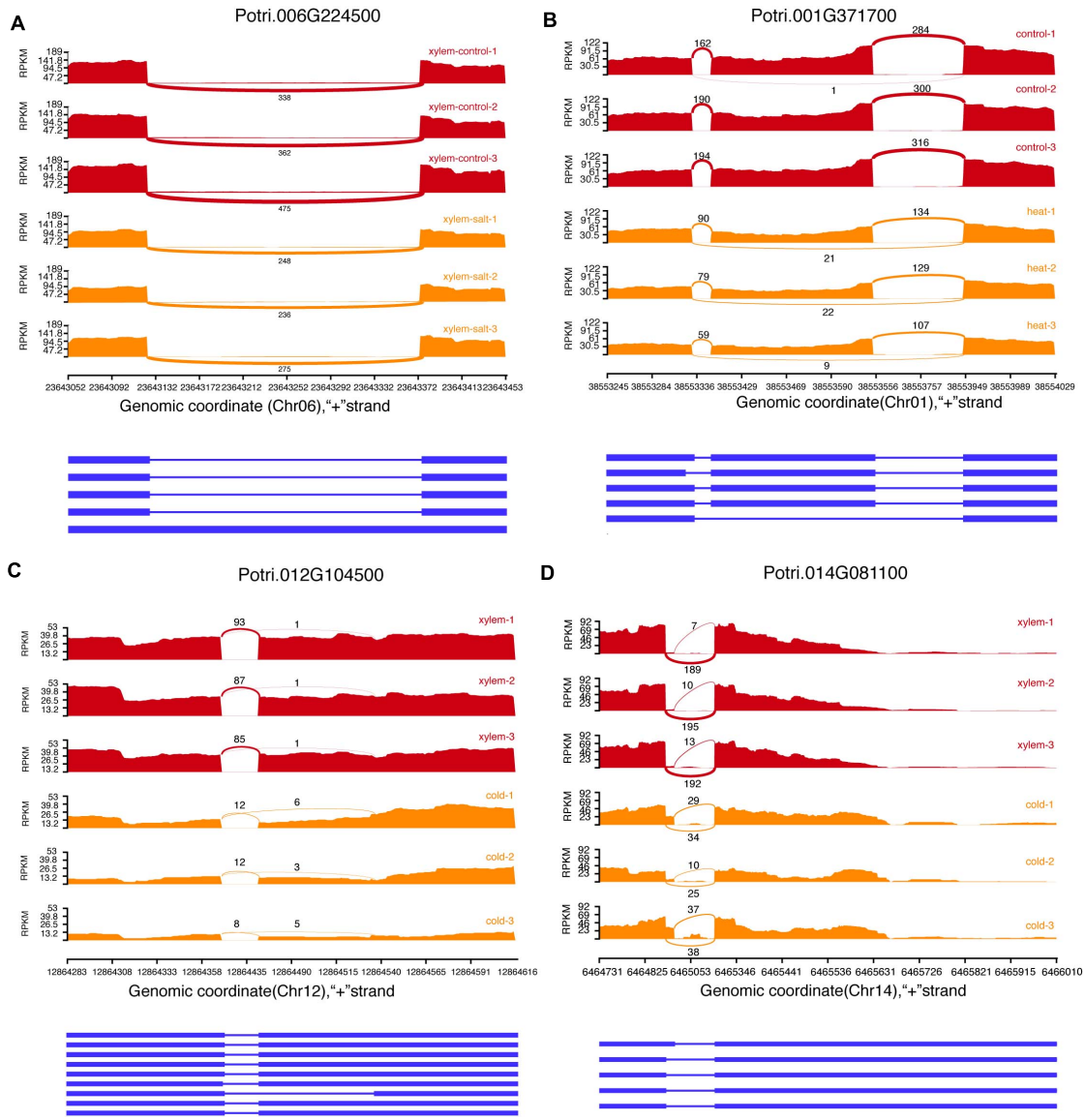

FIGURE 3 | Examples of four alternative splicing events. **(A)** Intron retention (IR). **(B)** Exon skipping (ES). **(C)** Alternative acceptor sites (AltA). **(D)** Alternative donor sites (AltD).

2,178 differential AS events in xylem with secondary growth (**Supplementary Table 6**). To further investigate how AS events affect xylem under different stress conditions, we analyzed differential AS between non-stress control and stress conditions (cold, salt, heat, and drought). In total, 6,559 genes presented 14,003 differential AS events which included 275 stress response genes. For example, Potri.001G448400 (*PtrWND1B*), a key gene regulating secondary cell wall thickening in *P. trichocarpa*, is shown to occur AS in secondary xylem fiber cells (Zhao et al., 2014). In the search pages of PDSX, users can use Potri.001G448400 as a search condition to get the differential AS pattern of this gene under different stresses in secondary xylem. Apart from differential AS in xylem under stress treatment, we also identified 24,103 differentially expressed AS events under other comparisons, which could be searched and visualized at PSDX.

Post-transcriptional Regulation Based on Iso-Seq

Single-molecule real-time (SMRT) Isoform Sequencing (Iso-Seq) presents a great advantage in the identification of post-transcriptional regulation based on full-length splicing isoforms (Gao et al., 2019; Zhang et al., 2019; Zhao et al., 2019). Using Iso-Seq data we identified a total of 58,000 AS events in 9,199 genes which included 22,882 IR, 4,175 ES, 17,031 AltA, and 13,912 AltD, respectively (**Supplementary Table 7**). Among them, 9,490 AS events were identified in

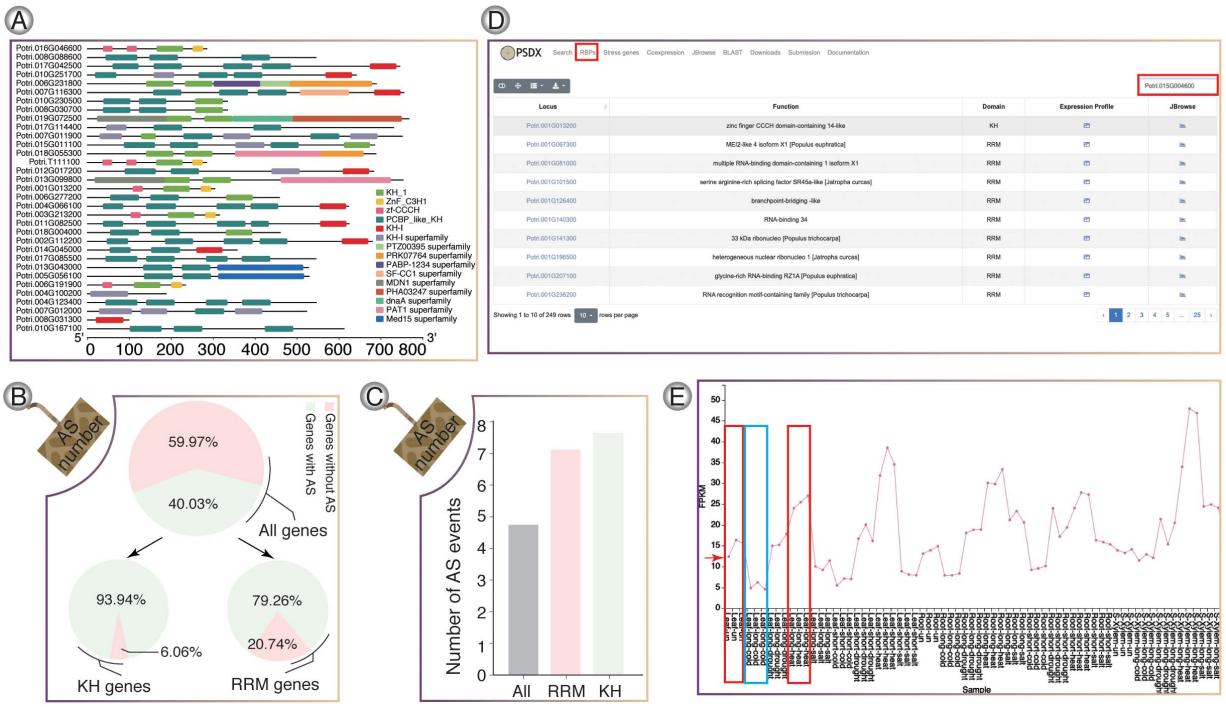

FIGURE 4 | RNA-binding protein genes in *P. trichocarpa*. **(A)** KH-domain structure diagrams. **(B)** Venn diagram shows the percentage of AS in all genes, KH-containing genes, and RRM-containing genes, respectively. **(C)** The average number of AS events for RRM and KH domain genes, respectively. **(D)** The module of RNA binding protein. **(E)** Splicing factor Potri.015G004600 (*PtrSR34A*) was selected as one case, which showed up-regulation upon heat stress (red box) and down-regulation upon cold stress (blue box).

both RNA-seq data and PacBio Iso-seq data (**Supplementary Table 8**). However, RNA-seq libraries presented more AS events which did not detected by PacBio since the 144 RNA-seq libraries contained more tissues and treatment conditions. Subsequently, we merged the gene annotation of RNA-seq and Iso-seq by stringTie and compared merge GTF file with reference annotation using gffcompare (Pertea and Pertea, 2020). The merged GTF file covered all the annotated transcripts. In addition, we obtained 15,720 transcripts within intergenic regions, which did not cover in original annotated transcripts. These new loci can be obtained from download module of PSDX. In addition to AS, we applied PacBio sequencing to identify genome-wide APA and ATI events in *P. trichocarp*a. In total, we identified 165,455 polyadenylation sites from 26,589 genes, of which 21,455 genes had more than one polyadenylation site. Among them, there are 18,637 genes in the same tissue in the control sample. Furthermore, 18,021 genes showed APA events under stress conditions of which 3,590 genes are specifically induced by stress (**Supplementary Figure 6A**). Meanwhile, a comparison of APA genes between different stress and control tissues revealed that APA genes are changed under different stresses (**Supplementary Figures 6B–D**). Further analysis revealed 14,922 genes including 39,606 ATI events (**Supplementary Figure 6E**), which also presented a dynamic change in different tissues and stresses (**Supplementary Figures 6F–H**). All these AS/APA/ATI could be searched and visualized from PSDX.

Compendium of RNA-Binding Genes in Response to Abiotic Stress

RNA-binding proteins genes in *P. trichocarpa* were predicted using hmmbuild (Potter et al., 2018) and hmmsearch. In total, we identified a total of 217 RRM-containing genes (**Supplementary Figure 7**) and 33 KH-containing genes (**Figure 4A**), respectively. In *P. trichocarpa*, 40% of the genes had AS events, while the percentage of AS events for RBP containing the KH and RBP domain is about 94 and 79%, respectively. It was obvious that RBPs showed a higher percentage of AS. The high frequency of AS events in RBPs is consistent with previous studies, which showed that splicing factors are regulated by AS of their own mRNAs (Zhang et al., 2017). RRM and KH domain-containing genes have more splicing isoforms (**Figures 4B,C**). All the stress-induced information for these RBPs could be searched in RBPs pages. Taking Potri.015G004600 (*PtrSR34A*) as an example (**Figure 4D**), *PtrSR34A* showed differential regulation in response to cold and heat stress, respectively (**Figure 4E**). These dynamics change of these RBP in response to stress could play important roles in widespread AS change.

Compendium of Stress Response Genes

In total, 1,123 highly reliable stress response genes were imported into PSDX from module of "Stress genes" (**Figure 5A**). Interestingly, we found that 76% (867) stress response genes have APA events, which suggested that stress response genes are

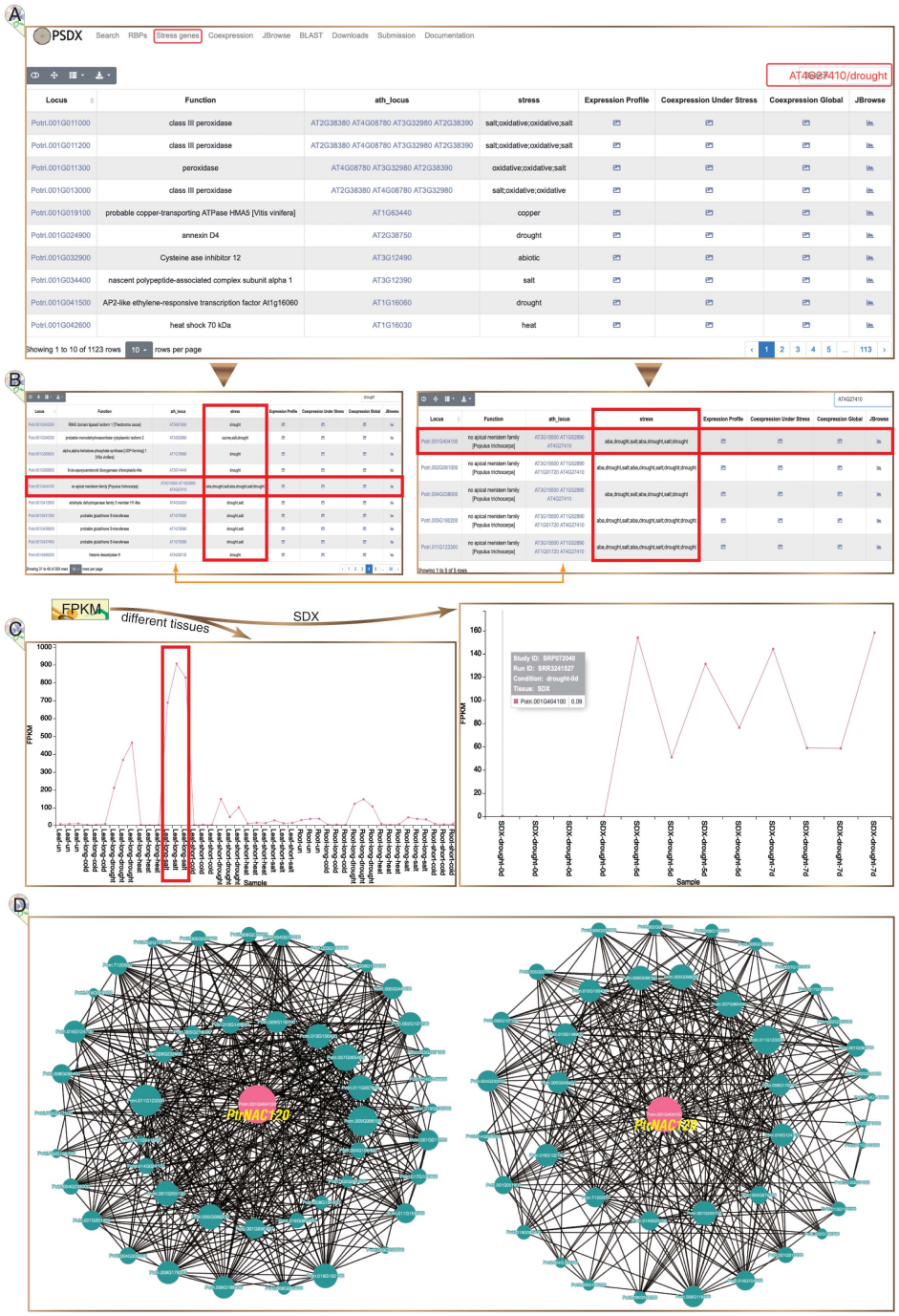

FIGURE 5 | Stress response genes in *P. trichocarpa*. **(A)** The module of stress response genes. **(B)** Following searches, all *P. trichocarpa* genes homologous to AT4G27410 (left panel) and all drought stress-responsive genes (right panel) are returned from a query. **(C)** Potri.001G404100 (*PtrNAC120*) is up-regulated upon drought and salt stress, especially significantly up-regulated under salt stress in leaves (left panel). **(D)** Stress-responsive genes co-expression network is presented under stress treatment libraries (left panel) and all RNA-seq libraries (right panel), respectively.

regulated by APA. This module of "Stress genes" presents all key co-expression profiles under different stresses. The keyword of gene name of *P. trichocarpa* or the homologous gene in *Arabidopsis* can be inputted in the search box. Using drought marker gene Potri.001G404100 (*PtrNAC120*) as an example, the expression profile, co-expression profile, and response in multiple stress can be returned in the result page (**Figure 5B**). *PtrNAC120* showed high up-regulation not only in drought stress but also in salt stress (**Figure 5C**), which indicated that *PtrNAC120* may also play vital roles in salt response. Co-expression profiles

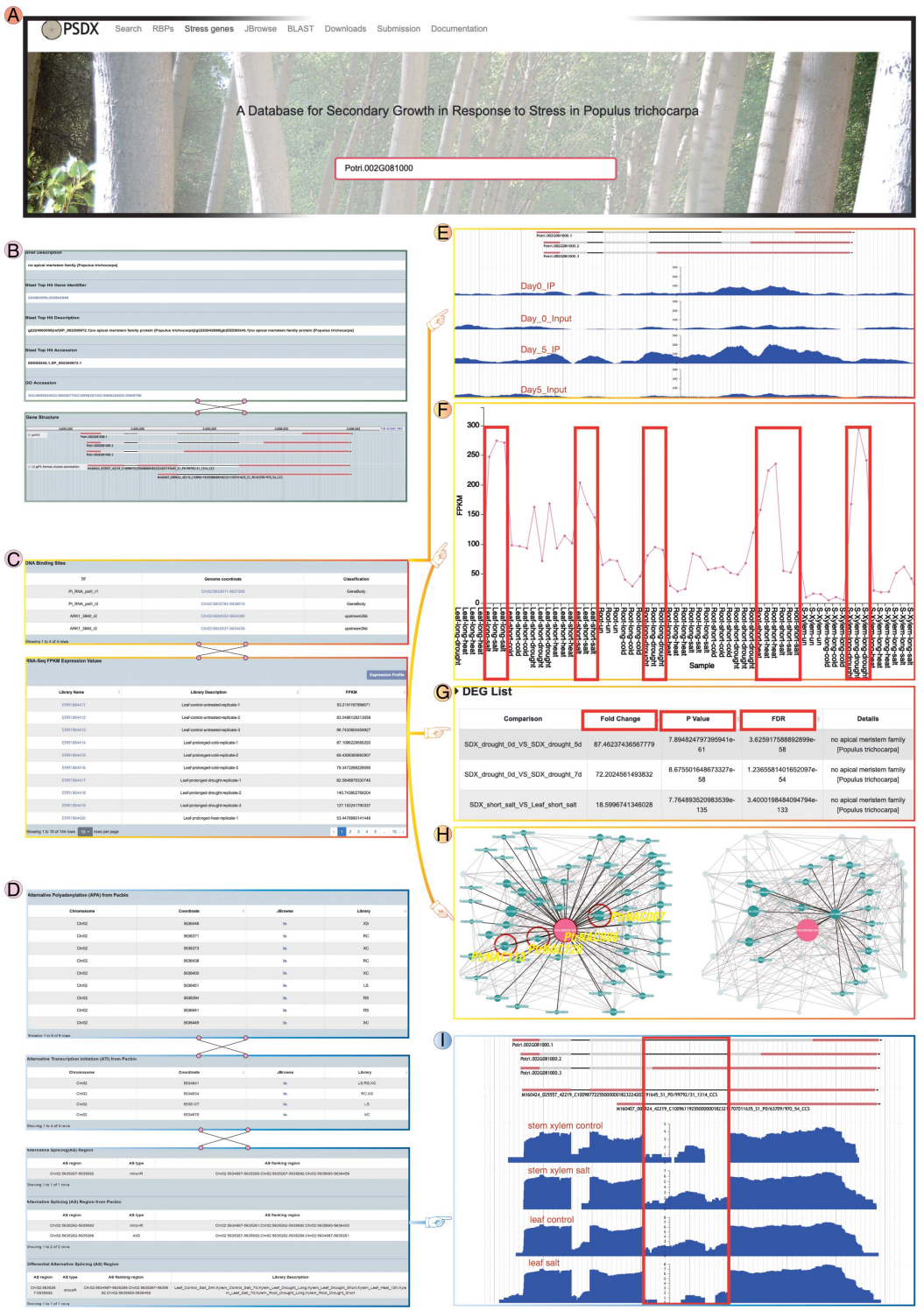

FIGURE 6 | Potri.002G081000 (*PtrNAC006*) was selected as an example to show multi-dimensional omics levels in PSDX. **(A)** PSDX main search interface with Potri.002G081000 (*PtrNAC006*) as an example. **(B)** A brief introduction and gene structure of *PtrNAC006*. **(C)** Transcriptional regulation of *PtrNAC006*. The top panel is the DNA peaks of *PtrNAC006*. All the FPKM values are provided in the bottom panel. **(D)** Post-transcriptional regulation of *PtrNAC006*, which including APA sites, ATI, AS events from short-read RNA-seq and PacBio Iso-seq, and differential AS events. **(E)** Wiggle plot shows increased H3K9ac levels under drought stress. **(F)** *PtrNAC006* is significantly up-regulated under drought and salt stress, respectively. **(G)** Differential expression of *PtrNAC006* in different organs and stresses, users can re-rank the DEG with fold change, *P*-value, and FDR. **(H)** Co-expression network of *PtrNAC006,* which connected with other drought-responsive genes Potri.007G099400 (*PtrNAC007*), Potri.011G123300 (*PtrNAC118*), and Potri.001G404100 (*PtrNac120*). **(I)** The second intron of *PtrNAC006* tends to be included (intron retention) under salt stress in stem xylem. However, the intron tends to be fully spliced under salt stress in the leaf.

shown that, compared to global network, stress-specific co-expression networks had strong evidence for Potri.011G123300 (*PtrNAC118*) co-expressed with *PtrNAC120* (**Figure 5D**), which was reported previously (Li et al., 2019). In addition to the locus name of *P. trichocarpa*, this page is also searchable by *Arabidopsis* homologs locus name.

Case Study of Database Usage

Users can select detailed information according to their own interests. PSDX exhibited differential expression in various tissues under stress and normal conditions. For example, Potri.002G081000 (*PtrNAC006*) showed higher levels in all stress conditions, especially in the drought stress. Taking the query results of drought marker gene *PtrNAC006* as an example (**Figure 6A**). The "main information" page shows some basic information of *PtrNAC006* including the function, gene structure, GO annotation, and sequence (**Figure 6B**). On this page, PSDX also shows transcriptional regulation and post-transcriptional regulation of *PtrNAC006*. For transcriptional regulation of *PtrNAC006*, transcription factor peaks and FPKM in all tissues and stresses can be found on this page (**Figure 6C**). For post-transcriptional regulation, the profile of APA, AS, and ATI can be found in "main information" (**Figure 6D**). The user also can visualize the enrichment of peaks and FPKM values of *PtrNAC006* among different tissues and stresses (**Figures 6E,F**). From the return page, *PtrNAC006* is highly expressed in drought stress, consistent with previous studies (Li et al., 2019; **Figure 6F**). In the "DEG list" module user can filter and sort DEG genes based on fold change, *P* values and FDR (**Figure 6G**). In the "DAS list" module user can also find the DAS events (**Figure 6G**). In the "Co-Expression" page user can obtain other genes that are closely related to the queried gene in expression patterns. *PtrNAC006* is highly co-expressed with Potri.007G099400 (*PtrNAC007*), Potri.011G123300 (*PtrNAC118*) and Potri.001G404100 (*PtrNAC120*) (**Figure 6H**), which was reported previously (Li et al., 2019). For the post-transcriptional regulation, the second intron of *PtrNAC006* is preferentially retained in stem under salt stress. However, the opposite trend was found in leaf and this intron is spliced fully in leaf under salt stress (**Figure 6I**). It will be interesting to investigate the function of these differential splicing isoforms in the future since they show an obvious change in response to stress.

CONCLUSION AND FUTURE DIRECTIONS

Populus is a commercial plantation species due to cellulose and lignin in secondary walls in papermaking (Jansson and Douglas, 2007). However, the mechanisms regulating development in response to different stresses are not yet clear in post-transcriptional level. In this study, we integrated 144 RNA-Seq libraries and 6 Iso-Seq libraries to get information about the normalized gene expression and differential expression analysis between non-stress and stress conditions. Additionally, we also used 33 ChIP-seq libraries from different stresses and tissue to reveal different levels of regulation, which included histone modification sites and TF peaks. Thus, PSDX provided a platform for an integrated analysis of multi-omics data and especially focuses on multi-omics data for wood development in response to stress. With available modern biotechnologies (Lin et al., 2006), PSDX will provide a preliminary resource for characteristics of secondary xylem development using transgenic lines with modified wood-related genes to generate superior wood quality in future.

For the post-transcriptional regulation, 40,284 differential AS events in response to stress were specifically identified. Apart from AS, we identified 21,455 genes with more than one polyadenylation site. Post-transcriptional results were also integrated into the PSDX database, which provides a variety of search methods to query the gene expression and post-transcriptional regulation information of *P. trichocarpa*.

Populus trichocarpa Stem Differentiating Xylem supports the export of search results and download of all original datasets. PSDX also offers a powerful visualization tool and modern BLAST sequence alignment tool, both of which are not only common tools, but also tightly integrated with the data carried by PSDX. For example, a matching gene obtained by BLAST search can be linked to a page of detailed information such as FPKM and AS in different tissues and in response to different stress. With more research on the growth of trees, new high-throughput data from Illumina, PacBio, and Nanopore platforms PSDX data will be processed and released when available.

DATA AVAILABILITY STATEMENT

The original contributions presented in the study are included in the article/**Supplementary Material**, further inquiries can be directed to the corresponding author/s.

AUTHOR CONTRIBUTIONS

LG, WL, and BL conceived and designed the study. HyW, SL, XD, YY, YL, YG, XL, WW, HhW, and XX collected data and conducted analyses. HyW, SL, AR, PJ, and LG contributed to the interpretation of results and drafting the manuscript. All authors read and approved the final manuscript.

FUNDING

This work was supported by the National Key Research and Development Program of China (2016YFD0600106), the Scientific Research Foundation of Graduate School of Fujian Agriculture and Forestry University (324-1122yb061) and Innovation Fund for Science & Technology Project from Fujian Agriculture and Forestry University (CXZX2020093A).

SUPPLEMENTARY MATERIAL

The Supplementary Material for this article can be found online at: https://www.frontiersin.org/articles/10.3389/fpls.2021.655565/full#supplementary-material

Supplementary Figure 1 | Genome-wide distribution of H3K9ac enrichment in *Populus trichocarpa* under drought stress, which is presented in nine circles from 1 (innermost circle) to 9 (outermost circle). The inner-circle 1 represents gene density. Circle 2 shows H3K9ac enrichment distribution after 7 days drought. The color scale ranges from red (high enrichment) to blue (low enrichment). Circle 3 presents differential H3K9ac levels distribution under 7 days drought. The orange dot is increased both H3K9ac level and gene upregulation, the green dot represents a decrease in both H3K9ac level and gene downregulation, the blue dot shows opposite regulation of H3K9ac level and gene regulation, and the yellow dot shows only differential H3K9ac levels. Circle 4 presents differential genes after 7 days of drought (the orange dot shows increased H3K9ac level and gene upregulation, the green dot shows decreased in both H3K9ac level and gene downregulation, the blue dot shows opposite regulation of H3K9ac level and gene regulation, the yellow dot shows only differential gene regulation). Circle 5 presents H3K9ac enrichment distribution after 5 days of drought. Circle 6 shows differential H3K9ac levels distribution after 5 days of drought. Circle 7 presents differentially expressed genes after 5 days of drought. Circle 8 presents H3K9ac enrichment distribution after 0 days drought. Circle 9 presents chromosomes of *P. trichocarpa* and the red line in the track represents drought-responsive genes, which showed that H3K9ac modifications are enriched in drought-responsive genes.

Supplementary Figure 2 | Principal component (PC) analysis plots for different tissues and stress treatments. **(A)** Principal component (PC) analysis plots for different tissues. Different shape means different tissues. "Other" group represent protoplasts with miR397, SND1 or GFP overexpression. "SDX" group represent Stem Differentiating Xylem. **(B)** Principal component (PC) analysis plots for different stress treatments. Different shape means different treatments. "Other" group represent protoplasts with miR397, SND1, or GFP overexpression.

Supplementary Figure 3 | Principal component (PC) analysis plots for different tissues and datasets. Different shape means different datasets. Different color means different tissue. "SDX" group represent Stem Differentiating Xylem.

Supplementary Figure 4 | The distribution of the Pearson Correlation Coefficient of stress-responsive genes under stress.

Supplementary Figure 5 | MR values filtering for stress co-expression network. **(A)** Assessment of PCC co-expression network. **(B)** Assessment of MR co-expression network.

Supplementary Figure 6 | The profile of alternative polyadenylation and alternative transcription initiation. **(A)** All APA genes in control and stress condition. **(B)** APA genes under stress and control in leaf. **(C)** APA genes under stress and control in root. **(D)** APA genes under stress and control in stem xylem. **(E)** All ATI genes in control and stress condition. **(F–H)** ATI genes in leaf, root and stem xylem compare control and stress.

Supplementary Figure 7 | Domain structure diagrams for RRM-domain protein.

Supplementary Table 1 | Sequencing data used in this study.

Supplementary Table 2 | *P. trichocarpa* stress response genes.

Supplementary Table 3 | Values for an example of ROC analysis.

Supplementary Table 4 | ChIP-seq peaks. Sheet 1 are peaks from transcription factors of ARK1, ARK2, BLR, PCN, and PRE. Sheet 2 are 9,360 differential H3K9ac modifications for 7-day without watering. Sheet 3 are 8,359 differential H3K9ac modifications for 5-day without watering.

Supplementary Table 5 | Alternative splicing events from 144 RNA-seq libraries. The first column is the locus name, and the second column is AS events from this gene. Each AS event contains the information of location and type.

Supplementary Table 6 | Differential alternative splicing in stem-differentiating xylem. The first column is the locus name, and the second column is the location information of the AS.

Supplementary Table 7 | Alternative splicing events from Iso-seq. The first column is the locus name, and the second column is all AS events of this gene.

Supplementary Table 8 | Overlapped alternative splicing events between RNA-seq and Iso-seq.

REFERENCES

Alter, S., Bader, K. C., Spannagl, M., Wang, Y., Bauer, E., Schon, C. C., et al. (2015). DroughtDB: an expert-curated compilation of plant drought stress genes and their homologs in nine species. *Database (Oxford)* 2015:bav046. doi: 10.1093/database/bav046

Aoki, Y., Okamura, Y., Ohta, H., Kinoshita, K., and Obayashi, T. (2016). ALCOdb: gene coexpression database for microalgae. *Plant Cell Physiol.* 57:e3. doi: 10.1093/pcp/pcv190

Appels, R., Eversole, K., Feuillet, C., Keller, B., Rogers, J., Stein, N., et al. (2018). Shifting the limits in wheat research and breeding using a fully annotated reference genome. *Science* 361:eaar7191.

Au, K. F., Underwood, J. G., Lee, L., and Wong, W. H. (2012). Improving PacBio long read accuracy by short read alignment. *PLoS One* 7:e46679. doi: 10.1371/journal.pone.0046679

Baek, J.-M., Han, P., Iandolino, A., and Cook, D. R. (2008). Characterization and comparison of intron structure and alternative splicing between *Medicago truncatula*, *Populus trichocarpa*, *Arabidopsis* and rice. *Plant Mol. Biol.* 67, 499–510. doi: 10.1007/s11103-008-9334-4

Bailey-Serres, J., Zhai, J., and Seki, M. (2020). The dynamic kaleidoscope of RNA biology in plants. *Plant Physiol.* 182, 1–9.

Bao, H., Li, E., Mansfield, S. D., Cronk, Q. C. B., El-Kassaby, Y. A., and Douglas, C. J. (2013). The developing xylem transcriptome and genome-wide analysis of alternative splicing in Populus trichocarpa (black cottonwood) populations. *BMC Genomics* 14:359. doi: 10.1186/1471-2164-14-359

Borkotoky, S., Saravanan, V., Jaiswal, A., Das, B., Selvaraj, S., Murali, A., et al. (2013). The *Arabidopsis* stress responsive gene database. *Int. J. Plant Genom.* 2013:949564. doi: 10.1155/2013/949564

Buels, R., Yao, E., Diesh, C. M., Hayes, R. D., Munoz-Torres, M., Helt, G., et al. (2016). JBrowse: a dynamic web platform for genome visualization and analysis. *Genome Biol.* 17, 66. doi: 10.1186/s13059-016-0924-1

Chakrabarti, M., de Lorenzo, L., Abdel−Ghany, S. E., Reddy, A. S., and Hunt, A. G. (2020). Wide−ranging transcriptome remodelling mediated by alternative polyadenylation in response to abiotic stresses in *Sorghum*. *Plant J.* 102, 916–930.

Daras, G., Rigas, S., Tsitsekian, D., Zur, H., Tuller, T., and Hatzopoulos, P. (2014). Alternative transcription initiation and the AUG context configuration control dual-organellar targeting and functional competence of *Arabidopsis* Lon1 protease. *Mol. Plant* 7, 989–1005. doi: 10.1093/mp/ssu030

Duque, P. (2011). A role for SR proteins in plant stress responses. *Plant Signal. Behav.* 6, 49–54.

Filichkin, S. A., Hamilton, M., Dharmawardhana, P. D., Singh, S. K., Sullivan, C., Ben-Hur, A., et al. (2018). Abiotic stresses modulate landscape of poplar transcriptome via alternative splicing, differential intron retention, and isoform ratio switching. *Front. Plant Sci.* 9:5. doi: 10.3389/fpls.2018.00005

Filichkin, S. A., Priest, H. D., Givan, S. A., Shen, R., Bryant, D. W., Fox, S. E., et al. (2010). Genome-wide mapping of alternative splicing in *Arabidopsis thaliana*. *Genome Res.* 20, 45–58. doi: 10.1101/gr.093302.109

Fu, H., Yang, D., Su, W., Ma, L., Shen, Y., Ji, G., et al. (2016). Genome-wide dynamics of alternative polyadenylation in rice. *Genome Res.* 26, 1753–1760. doi: 10.1101/gr.210757.116

Gao, Y., Wang, H., Zhang, H., Wang, Y., Chen, J., and Gu, L. (2018). PRAPI: post-transcriptional regulation analysis pipeline for Iso-Seq. *Bioinformatics* 34, 1580–1582. doi: 10.1093/bioinformatics/btx830

Gao, Y., Xi, F., Liu, X., Wang, H., Reddy, A. S., and Gu, L. (2019). Single-molecule Real-time (SMRT) Isoform Sequencing (Iso-Seq) in plants: the status of the bioinformatics tools to unravel the transcriptome complexity. *Curr. Bioinform.* 14, 566–573.

Goodstein, D. M., Shu, S., Howson, R., Neupane, R., Hayes, R. D., Fazo, J., et al. (2012). Phytozome: a comparative platform for green plant genomics. *Nucleic Acids Res.* 40, D1178–D1186. doi: 10.1093/nar/gkr944

Hossain, M. A., Wani, S. H., Bhattacharjee, S., Burritt, D. J., and Tran, L. S. P. (2016). *Drought Stress Tolerance in Plants*, Vol. 2. Cham: Springer.

Jansson, S., and Douglas, C. J. (2007). Populus: a model system for plant biology. *Annu. Rev. Plant Biol.* 58, 435–458.

Kaneda, M., Rensing, K., and Samuels, L. (2010). Secondary cell wall deposition in developing secondary xylem of poplar. *J. Integr. Plant Biol.* 52, 234–243.

Kim, D., Langmead, B., and Salzberg, S. L. (2015). HISAT: a fast spliced aligner with low memory requirements. *Nat. Methods* 12, 357–U121. doi: 10.1038/nmeth.3317

Kim, J. M., To, T. K., Ishida, J., Matsui, A., Kimura, H., and Seki, M. (2012). Transition of chromatin status during the process of recovery from drought stress in *Arabidopsis thaliana*. *Plant Cell Physiol.* 53, 847–856. doi: 10.1093/pcp/pcs053

Kwon, C. S., Lee, D., Choi, G., and Chung, W. I. (2009). Histone occupancy-dependent and -independent removal of H3K27 trimethylation at cold-responsive genes in *Arabidopsis*. *Plant J.* 60, 112–121. doi: 10.1111/j.1365-313X.2009.03938.x

Langmead, B., and Salzberg, S. L. (2012). Fast gapped-read alignment with Bowtie 2. *Nat. Methods* 9, 357–359. doi: 10.1038/nmeth.1923

Leinonen, R., Sugawara, H., Shumway, M., and International Nucleotide Sequence Database Collaboration (2011). The sequence read archive. *Nucleic Acids Res.* 39, D19–D21. doi: 10.1093/nar/gkq1019

Li, H., Handsaker, B., Wysoker, A., Fennell, T., Ruan, J., Homer, N., et al. (2009). The sequence alignment/map format and SAMtools. *Bioinformatics* 25, 2078–2079. doi: 10.1093/bioinformatics/btp352

Li, Q., Lin, Y. C., Sun, Y. H., Song, J., Chen, H., Zhang, X. H., et al. (2012). Splice variant of the SND1 transcription factor is a dominant negative of SND1 members and their regulation in *Populus trichocarpa*. *Proc. Natl. Acad. Sci. U.S.A.* 109, 14699–14704. doi: 10.1073/pnas.1212977109

Li, S., Lin, Y. J., Wang, P., Zhang, B., Li, M., Chen, S., et al. (2019). The AREB1 transcription factor influences histone acetylation to regulate drought responses and tolerance in *Populus trichocarpa*. *Plant Cell* 31, 663–686. doi: 10.1105/tpc.18.00437

Li, W., Lin, Y. C., Li, Q., Shi, R., Lin, C. Y., Chen, H., et al. (2014). A robust chromatin immunoprecipitation protocol for studying transcription factor-DNA interactions and histone modifications in wood-forming tissue. *Nat. Protoc.* 9, 2180–2193. doi: 10.1038/nprot.2014.146

Lin, S. Z., Zhang, Z. Y., Zhang, Q., and Lin, Y. Z. (2006). Progress in the study of molecular genetic improvements of poplar in China. *J. Integr. Plant Biol.* 48, 1001–1007.

Lin, Y.-C., Li, W., Sun, Y.-H., Kumari, S., Wei, H., Li, Q., et al. (2013). SND1 transcription factor-directed quantitative functional hierarchical genetic regulatory network in wood formation in *Populus trichocarpa*. *Plant Cell* 25, 4324–4341. doi: 10.1105/tpc.113.117697

Lin, Y. J., Chen, H., Li, Q., Li, W., Wang, J. P., Shi, R., et al. (2017). Reciprocal cross-regulation of VND and SND multigene TF families for wood formation in Populus trichocarpa. *Proc. Natl. Acad. Sci. U.S.A.* 114, E9722–E9729. doi: 10.1073/pnas.1714422114

Lindemose, S., O'Shea, C., Jensen, M. K., and Skriver, K. (2013). Structure, function and networks of transcription factors involved in abiotic stress responses. *Int. J. Mol. Sci.* 14, 5842–5878.

Liu, L., Missirian, V., Zinkgraf, M., Groover, A., and Filkov, V. (2014). Evaluation of experimental design and computational parameter choices affecting analyses of ChIP-seq and RNA-seq data in undomesticated poplar trees. *BMC Genomics* 15:S3. doi: 10.1186/1471-2164-15-s5-s3

Liu, L., Ramsay, T., Zinkgraf, M., Sundell, D., Street, N. R., Filkov, V., et al. (2015a). A resource for characterizing genome-wide binding and putative target genes of transcription factors expressed during secondary growth and wood formation in *Populus*. *Plant J.* 82, 887–898. doi: 10.1111/tpj.12850

Liu, L., Zinkgraf, M., Petzold, H. E., Beers, E. P., Filkov, V., and Groover, A. (2015b). The *Populus* ARBORKNOX1 homeodomain transcription factor regulates woody growth through binding to evolutionarily conserved target genes of diverse function. *N. Phytol.* 205, 682–694. doi: 10.1111/nph.13151

Lorkovic, Z. J., and Barta, A. (2002). Genome analysis: RNA recognition motif (RRM) and K homology (KH) domain RNA-binding proteins from the flowering plant *Arabidopsis thaliana*. *Nucleic Acids Re.s* 30, 623–635. doi: 10.1093/nar/30.3.623

Lu, S., Li, Q., Wei, H., Chang, M.-J., Tunlaya-Anukit, S., Kim, H., et al. (2013). Ptr-miR397a is a negative regulator of laccase genes affecting lignin content in *Populus trichocarpa*. *Proc. Natl. Acad. Sci. U.S.A* 110, 10848–10853. doi: 10.1073/pnas.1308936110

Marquez, Y., Brown, J. W. S., Simpson, C., Barta, A., and Kalyna, M. (2012). Transcriptome survey reveals increased complexity of the alternative splicing landscape in *Arabidopsis*. *Genome Research* 22, 1184–1195. doi: 10.1101/gr.134106.111

Mellerowicz, E. J., Baucher, M., Sundberg, B., and Boerjan, W. (2001). Unravelling cell wall formation in the woody dicot stem. *Plant Mol. Biol.* 47, 239–274. doi: 10.1023/a:1010699919325

Obayashi, T., and Kinoshita, K. (2009). Rank of correlation coefficient as a comparable measure for biological significance of gene coexpression. *DNA Res.* 16, 249–260.

Perrella, G., Lopez-Vernaza, M. A., Carr, C., Sani, E., Gossele, V., Verduyn, C., et al. (2013). Histone deacetylase complex1 expression level titrates plant growth and abscisic acid sensitivity in *Arabidopsis*. *Plant Cell* 25, 3491–3505. doi: 10.1105/tpc.113.114835

Pertea, G., and Pertea, M. (2020). GFF Utilities: GffRead and GffCompare. *F1000Res.* 9:304. doi: 10.12688/f1000research.23297.2

Pertea, M., Pertea, G. M., Antonescu, C. M., Chang, T.-C., Mendell, J. T., and Salzberg, S. L. (2015). StringTie enables improved reconstruction of a transcriptome from RNA-seq reads. *Nat. Biotechnol.* 33, 290–295. doi: 10.1038/nbt.3122

Plomion, C., Leprovost, G., and Stokes, A. (2001). Wood formation in trees. *Plant Physiol.* 127, 1513–1523. doi: 10.1104/pp.127.4.1513

Potter, S. C., Luciani, A., Eddy, S. R., Park, Y., Lopez, R., and Finn, R. D. (2018). HMMER web server: 2018 update. *Nucleic Acids Res.* 46, W200–W204. doi: 10.1093/nar/gky448

Priyann, A., Woodcroft, B. J., Rai, V., Moghul, I., Munagala, A., Ter, F., et al. (2019). Sequenceserver: a modern graphical user interface for custom blast databases. *Molecular Biol. Evol.* 36, 2922–2924.

Reddy, A. S., Huang, J., Syed, N. H., Ben-Hur, A., Dong, S., and Gu, L. (2020). Decoding co-/post-transcriptional complexities of plant transcriptomes and epitranscriptome using next-generation sequencing technologies. *Biochem. Soc. Trans.* 48, 2399–2414.

Reddy, A. S., Marquez, Y., Kalyna, M., and Barta, A. (2013). Complexity of the alternative splicing landscape in plants. *Plant Cell* 25, 3657–3683.

Robinson, M. D., McCarthy, D. J., and Smyth, G. K. (2010). edgeR: a bioconductor package for differential expression analysis of digital gene expression data. *Bioinformatics* 26, 139–140.

Seo, P. J., Park, M.-J., and Park, C.-M. (2013). Alternative splicing of transcription factors in plant responses to low temperature stress: mechanisms and functions. *Planta* 237, 1415–1424.

Shen, L., Shao, N. Y., Liu, X. C., Maze, I., Feng, J., and Nestler, E. J. (2013). diffReps: detecting differential chromatin modification sites from ChIP-seq data with biological replicates. *PLoS One* 8:e65598. doi: 10.1371/journal.pone.0065598

Shen, S., Park, J. W., Lu, Z.-x, Lin, L., Henry, M. D., Wu, Y. N., et al. (2014). rMATS: robust and flexible detection of differential alternative splicing from replicate RNA-Seq data. *Proc. Natl. Acad. Sci. U.S.A.* 111, E5593–E5601. doi: 10.1073/pnas.1419161111

Shi, R., Wang, J. P., Lin, Y.-C., Li, Q., Sun, Y.-H., Chen, H., et al. (2017). Tissue and cell-type co-expression networks of transcription factors and wood component genes in Populus trichocarpa. *Planta* 245, 927–938. doi: 10.1007/s00425-016-2640-1

Silverman, I. M., Li, F., and Gregory, B. D. (2013). Genomic era analyses of RNA secondary structure and RNA-binding proteins reveal their significance to post-transcriptional regulation in plants. *Plant Sci.* 205, 55–62. doi: 10.1016/j.plantsci.2013.01.009

Singh, S. P., Upadhyay, S. K., Pandey, A., and Kumar, S. (2019). *Molecular Approaches in Plant Biology and Environmental Challenges*. Mohali, India: Center of Innovative and Applied Bioprocessing (CIAB).

Srivastava, V., Srivastava, M. K., Chibani, K., Nilsson, R., Rouhier, N., Melzer, M., et al. (2009). Alternative splicing studies of the reactive oxygen species gene network in populus reveal two isoforms of high-isoelectric-point superoxide dismutase. *Plant Physiol.* 149, 1848–1859. doi: 10.1104/pp.108.133371

Staiger, D., and Brown, J. W. S. (2013). Alternative splicing at the intersection of biological timing, development, and stress responses. *Plant Cell* 25, 3640–3656. doi: 10.1105/tpc.113.113803

Steijger, T., Abril, J. F., Engstrom, P. G., Kokocinski, F., Hubbard, T. J., Guigo, R., et al. (2013). Assessment of transcript reconstruction methods for RNA-seq. *Nat. Methods* 10, 1177–1184. doi: 10.1038/nmeth.2714

Tang, S., Dong, Y., Liang, D., Zhang, Z., Ye, C.-Y., Shuai, P., et al. (2015). Analysis of the drought stress-responsive transcriptome of black cottonwood (*Populus trichocarpa*) using deep RNA sequencing. *Plant Mol. Biol. Rep.* 33, 424–438. doi: 10.1007/s11105-014-0759-4

Tian, T., You, Q., Yan, H., Xu, W., and Su, Z. (2018). MCENet: a database for maize conditional co-expression network and network characterization collaborated with multi-dimensional omics levels. *J. Genet. Genom.* 45, 351–360. doi: 10.1016/j.jgg.2018.05.007

Tuskan, G. A., DiFazio, S., Jansson, S., Bohlmann, J., Grigoriev, I., Hellsten, U., et al. (2006). The genome of black cottonwood, *Populus trichocarpa* (Torr. & Gray). *Science* 313, 1596–1604.

Vats, S. (2018). *Biotic and Abiotic Stress Tolerance in Plants*. Rajasthan, India: Department of Bioscience & Biotechnology, Banasthali Vidyapith.

Villar Salvador, P. J. E. (2013). in *Plant Responses to Drought Stress. From Morphological to Molecular Features*, ed. R. Aroca (Berlin: Springer-Verlag), 22.

Wang, T., Wang, H., Cai, D., Gao, Y., Zhang, H., Wang, Y., et al. (2017). Comprehensive profiling of rhizome-associated alternative splicing and alternative polyadenylation in moso bamboo (*Phyllostachys edulis*). *Plant J.* 91, 684–699. doi: 10.1111/tpj.13597

Wu, X., Liu, M., Downie, B., Liang, C., Ji, G., Li, Q. Q., et al. (2011). Genome-wide landscape of polyadenylation in *Arabidopsis* provides evidence for extensive alternative polyadenylation. *Proc. Natl. Acad. Sci. U.S.A.* 108, 12533–12538. doi: 10.1073/pnas.1019732108

Xing, D., and Li, Q. Q. (2011). Alternative polyadenylation and gene expression regulation in plants. *Wiley Interdisc. Rev. RNA* 2, 445–458.

Yang, X., Liu, D., Liu, F., Wu, J., Zou, J., Xiao, X., et al. (2013). HTQC: a fast quality control toolkit for Illumina sequencing data. *BMC Bioinform.* 14:33. doi: 10.1186/1471-2105-14-33

Ye, C., Zhou, Q., Wu, X., Ji, G., and Li, Q. Q. (2019). Genome-wide alternative polyadenylation dynamics in response to biotic and abiotic stresses in rice. *Ecotoxicol. Environ. Saf.* 183:109485.

You, Q., Zhang, L., Yi, X., Zhang, K., Yao, D., Zhang, X., et al. (2016). Co-expression network analyses identify functional modules associated with development and stress response in *Gossypium arboreum*. *Sci. Rep.* 6:38436. doi: 10.1038/srep38436

Zhang, G., Guo, G., Hu, X., Zhang, Y., Li, Q., Li, R., et al. (2010). Deep RNA sequencing at single base-pair resolution reveals high complexity of the rice transcriptome. *Genome Res.* 20, 646–654. doi: 10.1101/gr.100677.109

Zhang, G., Sun, M., Wang, J., Lei, M., Li, C., Zhao, D., et al. (2019). PacBio full-length cDNA sequencing integrated with RNA-seq reads drastically improves the discovery of splicing transcripts in rice. *Plant J.* 97, 296–305. doi: 10.1111/tpj.14120

Zhang, H., Lin, C., and Gu, L. (2017). Light regulation of alternative Pre−mRNA splicing in plants. *Photochem. Photobiol.* 93, 159–165.

Zhang, Y., Liu, T., Meyer, C. A., Eeckhoute, J., Johnson, D. S., Bernstein, B. E., et al. (2008). Model-based analysis of ChIP-Seq (MACS). *Genome Biol.* 9:R137. doi: 10.1186/gb-2008-9-9-r137

Zhao, L., Zhang, H., Kohnen, M. V., Prasad, K. V. S. K., Gu, L., and Reddy, A. S. N. (2019). Analysis of transcriptome and epitranscriptome in plants using pacbio iso-seq and nanopore-based direct RNA sequencing. *Front. Genet.* 10:253. doi: 10.3389/fgene.2019.00253

Zhao, Y., Sun, J., Xu, P., Zhang, R., and Li, L. (2014). Intron-mediated alternative splicing of wood-associated nac transcription factor1b regulates cell wall thickening during fiber development in *Populus* Species. *Plant Physiol.* 164, 765–776. doi: 10.1104/pp.113.231134

Conflict of Interest: The authors declare that the research was conducted in the absence of any commercial or financial relationships that could be construed as a potential conflict of interest.

frontiers in Plant Science

ORIGINAL RESEARCH
published: 28 May 2021
doi: 10.3389/fpls.2021.675075

A Comparative Analysis of Transcription Networks Active in Juvenile and Mature Wood in *Populus*

*Laifu Luo[1,2], Yingying Zhu[1], Jinshan Gui[2], Tongmin Yin[3], Wenchun Luo[1], Jianquan Liu[1] and Laigeng Li[2]**

[1] State Key Laboratory of Grassland Agro-Ecosystem, School of Life Sciences, Lanzhou University, Lanzhou, China, [2] National Key Laboratory of Plant Molecular Genetics, CAS Center for Excellence in Molecular Plant Sciences, Institute of Plant Physiology and Ecology, Chinese Academy of Sciences, Shanghai, China, [3] College of Forestry, Nanjing Forestry University, Nanjing, China

Juvenile wood (JW) and mature wood (MW) have distinct physical and chemical characters, resulting from wood formation at different development phases over tree lifespan. However, the regulatory mechanisms that distinguish or modulate the characteristics of JW and MW in relation to each other have not been mapped. In this study, by employing the *Populus* trees with an identical genetic background, we carried out RNA sequencing (RNA-seq) and whole genome bisulfite sequencing (WGBS) in JW and MW forming tissue and analyzed the transcriptional programs in association with the wood formation in different phrases. JW and MW of *Populus* displayed different wood properties, including higher content of cellulose and hemicelluloses, less lignin, and longer and larger fiber cells and vessel elements in MW as compared with JW. Significant differences in transcriptional programs and patterns of DNA methylation were detected between JW and MW. The differences were concentrated in gene networks involved in regulating hormonal signaling pathways responsible for auxin distribution and brassinosteroids biosynthesis as well as genes active in regulating cell expansion and secondary cell wall biosynthesis. An observed correlation between gene expression profiling and DNA methylation indicated that DNA methylation affected expression of the genes related to auxin distribution and brassinosteroids signal transduction, cell expansion in JW, and MW formation. The results suggest that auxin distribution, brassinosteroids biosynthesis, and signaling be the critical molecular modules in formation of JW and MW. DNA methylation plays a role in formatting the molecular modules which contribute to the transcriptional programs of wood formation in different development phases. The study sheds light into better understanding of the molecular networks underlying regulation of wood properties which would be informative for genetic manipulation for improvement of wood formation.

Keywords: juvenile wood, mature wood, wood property, wood formation, RNA-seq, cell wall, cell expansion, DNA methylation

OPEN ACCESS

Edited by:
Guohua Chai,
Qingdao Agricultural University, China

Reviewed by:
Jing Zhang,
University of Helsinki, Finland
Xianhai Zhao,
Brookhaven National Laboratory, United States
Xiaolan Rao,
Hubei University, China

***Correspondence:**
Laigeng Li
lgli@cemps.ac.cn

Specialty section:
This article was submitted to Plant Biotechnology, a section of the journal Frontiers in Plant Science

Received: *02 March 2021*
Accepted: *07 April 2021*
Published: *28 May 2021*

Citation:
Luo L, Zhu Y, Gui J, Yin T, Luo W, Liu J and Li L (2021) A Comparative Analysis of Transcription Networks Active in Juvenile and Mature Wood in Populus. Front. Plant Sci. 12:675075. doi: 10.3389/fpls.2021.675075

INTRODUCTION

Perennial woody plants are characterized by large size and a long lifespan, in which a long non-flowering period of juvenile phase can last years to decades, for example, 3–5 years in *Populus* and 10–15 years in *Pinus* (Braatne et al., 1996; Owens, 2006). Wood produced during juvenile phase is called juvenile wood (JW) which is followed by a mature phase during which trees start flowering and producing mature wood (MW) outside of JW (Basheer-Salimia, 2007). Compared with JW, MW is characterized with longer xylem cells, thicker secondary cell walls, lower density of vessels, higher crystallinity of cellulose in fibers, and smaller microfibril angles (Barrios et al., 2017). Thus, MW is more desirable from a processing and utilization perspective for construction wood, wood pulping, and fiber material production. As a matter of fact, to meet the increasing demand for raw wood material, artificial forest plantation aims to reduce the rotation length and enhance productivity, which makes JW with lower wood quality as a major source for wood industry (Moore and Cown, 2017). This seriously affects the utilization and processing of wood. How to make wood to mature quickly and the proportion of JW to be reduced has become an important aspect of improving wood properties.

Wood formation starts with cell divisions at vascular cambium and subsequent differentiation into secondary xylem through cell expansion, secondary cell wall thickening, and programmed cell death (Fromm, 2013). Plant hormones, such as auxin, brassinosteroids, and gibberellin, participate in regulation of wood formation (Israelsson et al., 2005; Demura and Fukuda, 2007; Choi et al., 2017). The size of wood cells depend on cell expansion process while mechanical and chemical properties of wood are largely determined by secondary cell wall thickening (Cosgrove, 2018). Cell expansion is controlled by extension of the primary cell wall, which is composed of 20–30% cellulose, 30–50% pectins, 20–25% hemicelluloses, and 10% glycoproteins (Mcneil et al., 1984). Following cell expansion, wall thickening is initiated with transcriptional programs for secondary cell wall biosynthesis (Plomion et al., 2001). Secondary cell walls are composed of 40–80% cellulose, 10–40% hemicellulose, 5–25% lignin, and glycoproteins (Kumar et al., 2016). As JW and MW display distinct wood properties, likely the secondary cell formation in JW and MW is differentially regulated.

DNA methylation, a critical epigenetic mechanism among eukaryotes, affects many biological processes. In plant, most of DNA methylation occurs at the fifth carbon of cytosine (including three cytosine contexts, CG, CHG, and CHH, where H represents A, C, or T) to form 5-methylcytosine by DNA methyltransferase (Goll and Bestor, 2005; Law and Jacobsen, 2010; He et al., 2011). Evidence indicates that DNA methylation can regulate gene expression in numerous biological processes including response to abiotic stresses (Wang et al., 2011; Dowen et al., 2012; Ci et al., 2015; Su et al., 2018; Liang et al., 2019), plant development and morphogenesis (Lafon-Placette et al., 2013), and wood formation (Wang et al., 2016). The degree of DNA methylation is also related to plant development phases. The degree of DNA methylation at mature phase was significantly higher than that at juvenile phase in *Pinus radiate* (Fraga et al., 2002a). DNA methylation increases along with the age extension in some species (Fraga et al., 2002b). It is unclear how DNA methylation is involved in regulation of JW and MW formation.

Despite studies which have shown physicochemical difference of wood properties between JW and MW, the molecular regulatory networks underlying formation of the different wood properties is not fully elucidated. In this study, by employing *Populus* trees with an identical genetic background, we analyzed different physical and chemical characters in association with the transcriptomic profiles and DNA methylation during the formation of JW and MW. Correlation analysis revealed the transcriptional networks and DNA methylation that are involved in regulation of wood formation with different wood properties. This study provides an array of mechanistic information for understanding of JW and MW formation, as well as new clues for genetic manipulation for improvement of wood properties.

MATERIALS AND METHODS

Tissue Sampling

Populus trees propagated from the same clone (*Populus deltoides*×*P. euramericana* cv. "*Nanlin895*") were grown in the same plantation located at Siyang, Suqian, Jiangsu, China (33° 47′ N, 118° 22′ E). Wood-forming tissues were sampled from 1-m trunk above the breast height (1.3 m from ground) from 2-year-old (formation of JW) and 8-year-old trees (formation of MW) at fast growing time (May 2017). After bark was removed, wood-forming tissue (developing secondary xylem) was collected directly into liquid nitrogen and stored at −80°C freezer for later analysis (Song et al., 2011). Three trees as biological replicates were sampled (**Supplementary Figure 1**), respectively.

Analysis of Wood Properties

After developing xylem was collected, the tree trunk was used for wood analysis. JW and MW were sampled as illustrated in **Supplementary Figure 1**. Wood tissue was sectioned into 20 μm in thickness and stained with 0.5% phloroglucinol in 12% HCl. Cross sections were observed under a microscope (Olympus, BX53). The number of fibers and vessels and their cross area were counted using Image J. Meanwhile, the wood cells were separated after treatment using acetic acid/hydrogen peroxide (1:1, *v*/*v*) solution at 80°C for 6 h. The separated wood cells were then stained with safranine (1% in water), and the length of fiber cells and vessels was measured under a microscope (Olympus, BX53) using Image J.

Cell Wall Composition Determination

Air-dried wood sample was ground into powder and filtered through 60-mesh sieve. According to our previous established protocol (Yu et al., 2014), alcohol-insoluble residues (AIR) were firstly obtained by extracting the wood powder with 70% ethanol, chloroform/methanol (1:1, *v*/*v*), and acetone. Amylase and pullulanase in 0.1 M sodium acetate buffer (pH 5.0) were used to treat the extracted AIR overnight. For analysis of the sugar in hemicelluloses, AIR was treated with 2 M trifluoroacetic acid (TFA) at 121°C for 90 min. The supernatant was evaporated and incubated in 20 mg/ml fresh sodium borohydride solution

at 40° for 90 min. The product was then neutralized with acetic acid and mixed with 1-methylimidazole and acetic anhydride for acetylation. After extraction with dichloromethane, the product was mixed with ethyl acetate for GC-MS (6890N GC system and 5975 Mass detector, Agilent Technologies, equipped with a SP-2380 capillary column, Supelco, Sigma-Aldrich) analysis. Meanwhile, standard sugars were used to calibrate sugar content determined in samples. The insoluble precipitate from the AIR treated with TFA was collected for crystalline cellulose content determination. The Updegraff reagent (acetic acid:nitric acid:water, 8:1:2, *v*/*v*) was added to the precipitate and incubated at 100°C for 30 min. After washing with H_2O and acetone, the precipitate was incubated with 72% sulfuric acid at room temperature for 1 h. The content of crystalline cellulose was determined by anthrone assay (Foster et al., 2010b). For lignin measurement, AIR was incubated with freshly prepared acetyl bromide (25%, acetyl bromide in acetic acid) at 50°C for 3 h. After cooling, the AIR was mixed with 2 M NaOH, 0.5 M fresh hydroxylamine hydrochloride, and acetic acid. Lignin content was determined using a microplate reader (Varioskan Flash, Thermo) (Foster et al., 2010a).

RNA Isolation and RNA Sequencing

Total RNA was extracted from wood-forming tissues using a mirVana miRNA Isolation Kit (Ambion-1561) following the manufacturer's instruction. After being treated by RNase-free DNase I (Sigma, 4716728001), the quality of total RNA was assessed on NanoDrop spectrophotometer (NanoDrop 2000, Thermo Scientific) and on agarose gel electrophoresis. For RNA sequencing (RNA-seq), cDNA library was generated from 5 μg of total RNA with TruSeq Stranded mRNA LTSample Prep Kit (Illumina, RS-122-2101) and Agencourt AMPure XP (BECKMAN COULTER, A63881). cDNA library was qualified through length distribution of fragments using Agilent 2100 (Bioanalyzer). The 150-bp paired-end sequencing was performed using platform of Illumina HiSeq X10. About five million reads per samples were generated.

DNA Isolation and Bisulfite Sequencing

Genomic DNA was extracted from wood-forming tissues using QIAamp DNA Mini kit (Cat.51306, Qiagen). DNA quantification and integrity were determined by a Nanodrop spectrophotometer (Thermo Fisher Scientific, Inc., Wilmington, DE) and 1% agarose electrophoresis, respectively. Before bisulfite treatment, lambda DNA was added to the purified DNA, which was used as an internal reference to calculate the conversion rate. The mixed DNA was then bisulfite treated using a Zymo Research EZ DNA methylaiton-Glod Kit (Zymo, D05005). Bisulfite sequencing (BS-seq) libraries were constructed by TruSeq® DNA Methylation Kit (Illumina, EGMK91396) following the manufacturer's instruction. After libraries were qualified, sequencing was performed on the Illumina HiSeq X Ten platform and 150 bp paired-end reads were generated.

Analysis of Transcriptome Sequencing Data

Raw reads of sequencing were processed using NGS QC Toolkit to remove low-quality reads (Patel and Jain, 2012). The cleaned reads were mapped to *Populus trichocarpa*'s genome (http://phytozome.jgi.doe.gov/) using hisat2 with default parameters (Kim et al., 2015). Gene expression level was measured as fragments per kilobase per million reads (FPKM) using cufflinks (Trapnell et al., 2010; Roberts et al., 2011). Read counts for each gene in each sample were obtained using htseq-count and standardized by rlog (Anders et al., 2015). Principle component analysis (PCA) was performed by plotPCA of DEseq2 R package with default parameters. Differential expression genes (DEGs) were identified using the DESeq R package by estimation of Size Factors and nbinomTest. Analysis of DEGs with gene ontology (GO) enrichment and the Kyoto Encyclopedia of Genes and Genomes (KEGG) (Kanehisa et al., 2008) pathway enrichment was performed using R based on the hypergeometric distribution.

Analysis of Genome Bisulfite Sequencing

The raw reads of BS-seq were cleaned using Fastp (Chen et al., 2018) by removing adapters, ploy-N, and low-quality reads. The remaining high-quality clean reads were mapped to the *Populus trichocarpa*'s genome (http://phytozome.jgi.doe.gov/) using Bismark software with default parameters (Krueger and Andrews, 2011). Methylcytosine (mC) sites were identified using MethylKit (Akalin et al., 2012). With default parameters, MethylKit was applied for PCA analysis. Differentially methylated regions (DMRs) were identified using MethylKit software with a *Q* value (*p*-value corrected by FDR method) threshold of 0.05 and an absolute delta cutoff of 10% between the two groups. Analysis of DMGs with GO enrichment and KEGG pathway enrichment was performed according to the same method used for DEGs analysis.

Quantitative Real-Time PCR

The first-strand cDNA was synthesized from 2 μg of total RNA using a cDNA Synthesis SuperMix (TransGen Biotech, AT311-03). Using cDNA as template, quantitative real-time PCR (qRT-PCR) was performed using *Perfectstart*™ Green qPCR SuperMix (TransGen, AQ601) and a Quantstudio™ 3 Real-Time PCR Detection System (Thermo). The primers used for selected genes are listed in **Supplementary Table 13**, and *TUB9* was used as an internal control to normalize gene expression.

RESULTS

Properties of JW and MW in *Populus*

To examine the properties of the JW and MW produced in *Populus*, plantation-grown trees that were propagated from a single clone were sampled. Three trees at 2 and 8 years old were collected with trunk at breast height, respectively (**Supplementary Figure 1**). In wood anatomical section, difference in the ratio of fiber cell/vessel, the length and size of fibers and vessels was observed between JW and MW (**Figures 1A–D**). MW contained higher ratio of fiber cell/vessel,

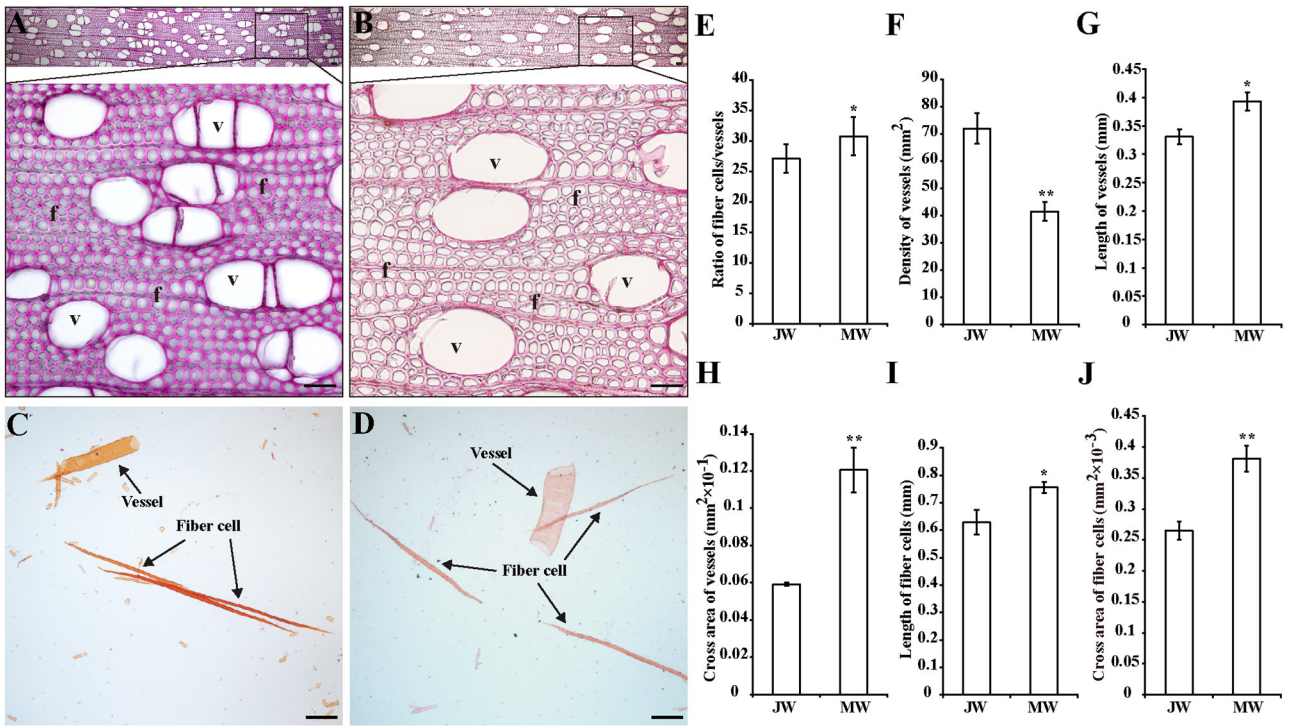

FIGURE 1 | Properties of the wood produced in juvenile phase (JP) and mature phase (MP). **(A,B)** Wood sections stained with phloroglucinol in different magnifications from juvenile wood (JW) **(A)** and mature wood (MW) **(B)**. Bars = 50 μm. **(C,D)** Fibers and vessels from JW **(C)** and MW **(D)**. Bars = 200 μm. **(E)** Ratio of numbers of fiber cells/vessels. **(F)** Density of vessels. **(G,H)** Length and cross area of vessels. The values were means ± SE of 500 and 800 independent vessels from JW and MW, respectively. **(I,J)** Length and cross area of fiber cells. The values were means ± SE of 1,000 independent fibers from JW and MW, respectively. Significance was determined by Student's *t*-test (*$p < 0.05$ and **$p < 0.01$). f, fiber cell; v, vessel.

lower density of vessel cell in wood section, and longer and larger fiber cell and vessel than those in JW (**Figures 1E–J**). Chemical analysis indicated that MW contained higher content of crystalline cellulose and lower content of lignin compared with JW (**Table 1**). Sugar composition in hemicelluloses also showed difference between JW and MW. MW contained higher xylose, mannose, glucose, and arabinose but lower galactose compared with JW (**Table 1**). These results indicated that JW and MW in *Populus* displayed different cellular structures and chemical compositions.

TABLE 1 | Chemical composition in JW and MW of *Populus*.

Chemical composition (μg/mg AIR)	JW	MW
Cellulose	400.3 ± 24.4	432.4 ± 27.0*
Lignin	223.1 ± 9.7	206.7 ± 18.9*
Hemicellulose		
Xylose	145.9 ± 14.8	192.4 ± 18.1**
Mannose	27.2 ± 4.7	36.8 ± 4.2**
Galactose	2.7 ± 0.5	1.8 ± 0.33*
Glucose	62.4 ± 6.5	69.8 ± 6.0*
Arabinose	2.5 ± 0.2	3.6 ± 0.3**

*Sugar content in hemicelluloses is calculated on the basis of standard sugar calibration. Significance was determined by Student's t-test (*p < 0.05 and **p < 0.01).*

Transcriptional Profiles in Formation of JW and MW

To dissect the gene expression involved in *Populus* wood formation, transcripts were profiled in the wood-forming tissues undergoing formation of JW and MW *via* high-throughput RNA-seq. Assessment of the RNA-seq data and biological repeats validated the high quality of the sequence data generated from the wood-forming tissues (**Supplementary Table 1**, The raw data in Sequence Read Archive (SRA), ID: PRJNA705066). A total of 300.5 million raw reads were obtained from six samples, and about 284.8 million high-quality reads (more than 94% of raw reads) were obtained after filtering and removal of low-quality reads. More than 86% of the high-quality reads per sample were mapped to the reference genome, corresponding to expression of ∼20,000 genes out of 41,335 predicted genes in each sample. Meanwhile, PCA indicated that the transcript profiles showed a clear separation between JW and MW (**Supplementary Figure 2A**), suggesting the different transcription activities in formation of JW and MW.

A group of 3,992 genes were identified (FPKM ≥3, fold change >2, and *p* value FDR <0.05) for their differential expression in JW and MW (**Supplementary Figure 2B**; **Supplementary Table 2**). The DEGs included 2,110 higher

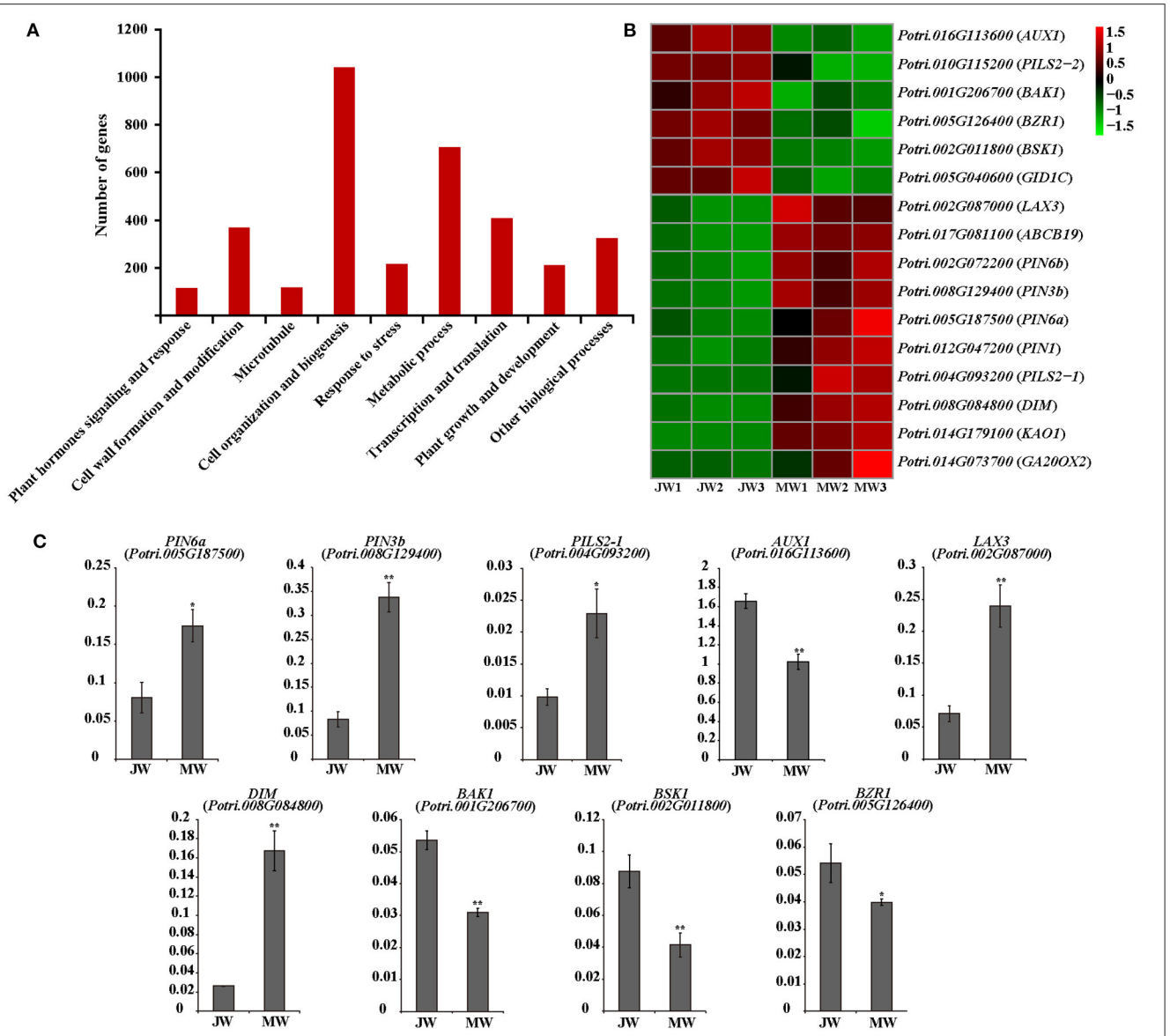

FIGURE 2 | (A) The functional of the differentially expressed genes (DEGs). **(B)** The heat map of genes related to plant hormones. **(C)** The results of quantitative real-time PCR of selected genes related to plant hormones in JW and MW. Significance was determined by Student's *t*-test (*$p < 0.05$ and **$p < 0.01$).

expression in JW and 1,882 higher expression in MW. As indicated by GO and KEGG enrichment analysis, the DEGs were primarily associated with plant hormones signaling and response, cell wall formation and modification, microtubule, cell organization and biogenesis, transcription, and other biological processes (**Figure 2A**; **Supplementary Tables 3, 4**).

Expression of Hormone-Related Genes in Wood Formation at Different Phases

Among the detected DEGs were included ample hormone-related genes. Particularly, genes of auxin transportation, brassinosteroids (BR) biosynthesis, and signaling were identified for their remarkable difference of expression in JW and MW (**Figure 2B**). The homologs of *AUX1*, *LAX3*, *PILS2*, and *ABCB19* which are related to auxin transport (Enders and Strader, 2015) had high expression level in JW and MW (FPKM >100). Intriguingly, the homolog (*Potri.016G113600*) of *AUX1* which facilitates auxin influx was expressed in JW higher than in MW, while the homolog (*Potri.017G081100*) of *ABCB19* which facilitates the efflux of auxin was expressed in MW higher than in JW. Furthermore, four homologs of *PIN1*, *PIN3*, and *PIN6*, encoded the auxin transporters that mediate that auxin efflux (Liu et al., 2014; Enders and Strader, 2015), were identified in DEGs, and their expression in MW was much higher than in JW (**Figure 2B**). In addition, the PIN-LIKES (PILS), which are thought to be located on the endoplasmic reticulum (ER), may transport auxin from the cytoplasm into the ER (Enders and Strader, 2015). One

PILS2 homolog (*Potri.004G093200*) was expressed in MW 13 times higher than in JW (**Figure 2B**). The differential expression of the auxin-related genes was verified by qRT-PCR determination (**Figure 2C**). These data indicate that the genes involved in IAA transport were differentially expressed in MW and JW.

Genes involved in BR biosynthesis and signaling were readily noticed among DEGs. The homolog (*Potri.008G084800*) of *DIM*/*DWF1* which is a key gene for BR biosynthesis in *Arabidopsis* (Klahre et al., 1998; Youn et al., 2018) was expressed in MW 5.6 times higher than in JW (**Figure 2B**). Additionally, several genes involved in BR signaling were differentially expressed between JW and MW (**Figure 2B**). The homolog of *BRI1-associated receptor kinase* (*BAK1*) (*Potri.001G206700*), *brassinosteroid signaling positive regulator* (*BZR1*) (*Potri.005G126400*), and *BR signaling kinase 1* (*BSK1*) (*Potri.002G011800*) were downregulated in MW compared with JW. qRT-PCR determination confirmed the differential expression (**Figure 2C**). On the other hand, although the genes involved in other hormones signaling such as gibberellins (GAs) were detected to be differentially expressed between JW and MW (**Figure 2B**), their expression profiles were unable to be verified. Together, the results suggest that auxin and BR may be involved in the regulation of JW and MW formation.

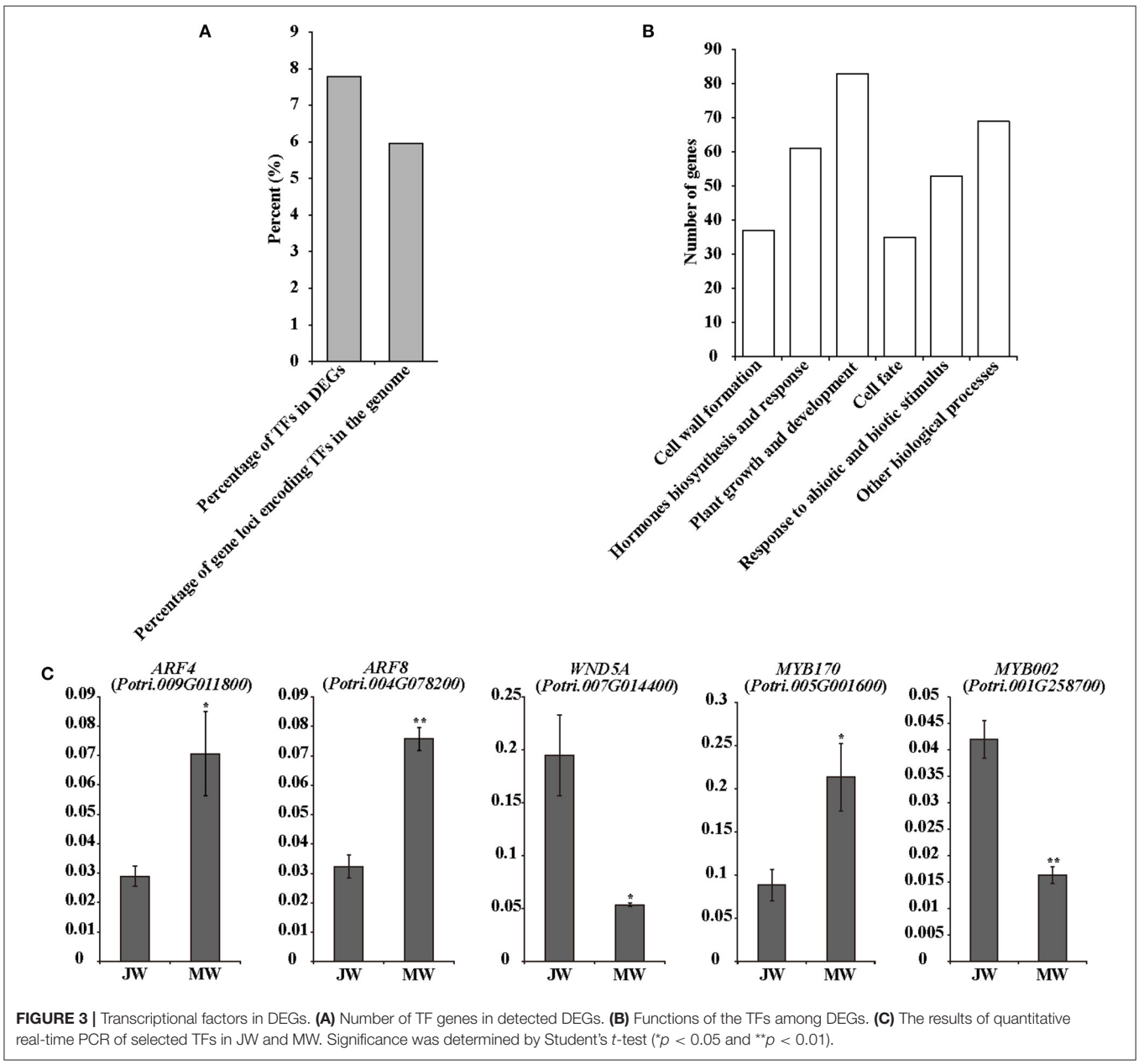

FIGURE 3 | Transcriptional factors in DEGs. **(A)** Number of TF genes in detected DEGs. **(B)** Functions of the TFs among DEGs. **(C)** The results of quantitative real-time PCR of selected TFs in JW and MW. Significance was determined by Student's *t*-test (*$p < 0.05$ and **$p < 0.01$).

Expression of Transcriptional Factor Genes in the Formation of JW and MW

The identified 3,992 DEGs included 305 transcription factor (TF) genes, 7.6% of all DEGs, which is higher than 6% of TF genes in *Populus* genome (PlantTFDB, http://planttfdb.cbi.pku.edu.cn) (Jin et al., 2014) (**Figure 3A**; **Supplementary Table 5**), implying that expression of transcription factor genes is altered in higher proportion. Among the TF genes, 105 TF genes were upregulated in MW, and the rest were downregulated in MW. GO annotation analysis indicated that the TFs in the DEGs were primarily associated with hormone biosynthesis and responses, plant growth and development, cell fate, cell wall formation, and response to abiotic and biotic stimuli (**Figure 3B**).

Several TF genes that are involved in auxin signaling were differentially expressed in JW and MW (**Supplementary Table 5**). The DEGs contained nine *auxin response factor* (*ARF*) genes with four upregulated and five downregulated in JW. In addition, three homologs of *SHI-RELATED SEQUENCEs* (*SRSs*) that play a role in activation of auxin biosynthesis (Eklund et al., 2010) were upregulated in MW. One homolog of *AINTEGUMENTA-LIKE 6* (*AIL6*) that is involved in regulation of auxin biosynthesis (Pinon et al., 2013) displayed higher expression in MW. The differential expression determined by RNA-seq and qRT-PCR analyses was well-correlated (**Figure 3C**; **Supplementary Figure 3**).

The DEGs included a number of TFs related to regulation of cell wall formation, such as the homologs of *SND1*, *NST1 VND1*, and *VND4* (**Supplementary Table 5**), which were key TFs for regulation of secondary cell wall biosynthesis (Zhong et al., 2010; Hussey et al., 2013; Kumar et al., 2016). *PtrMYB26*, *PtrMYB90*, and *PtrMYB152* which were reported to directly regulate lignin biosynthesis in *Populus* (Zhong et al., 2011; Wang et al., 2014; Li et al., 2015) were expressed higher in JW than in MW. This is in agreement with the higher lignin content in JW. Furthermore, expression of *PtrMYB170* and *PtrMYB121*, which may play a role in resource acquisition and allocation for xylem development (Romano et al., 2012), were upregulated in MW. One homolog (*Potri.006G241700*) of *MYB3R1*, which

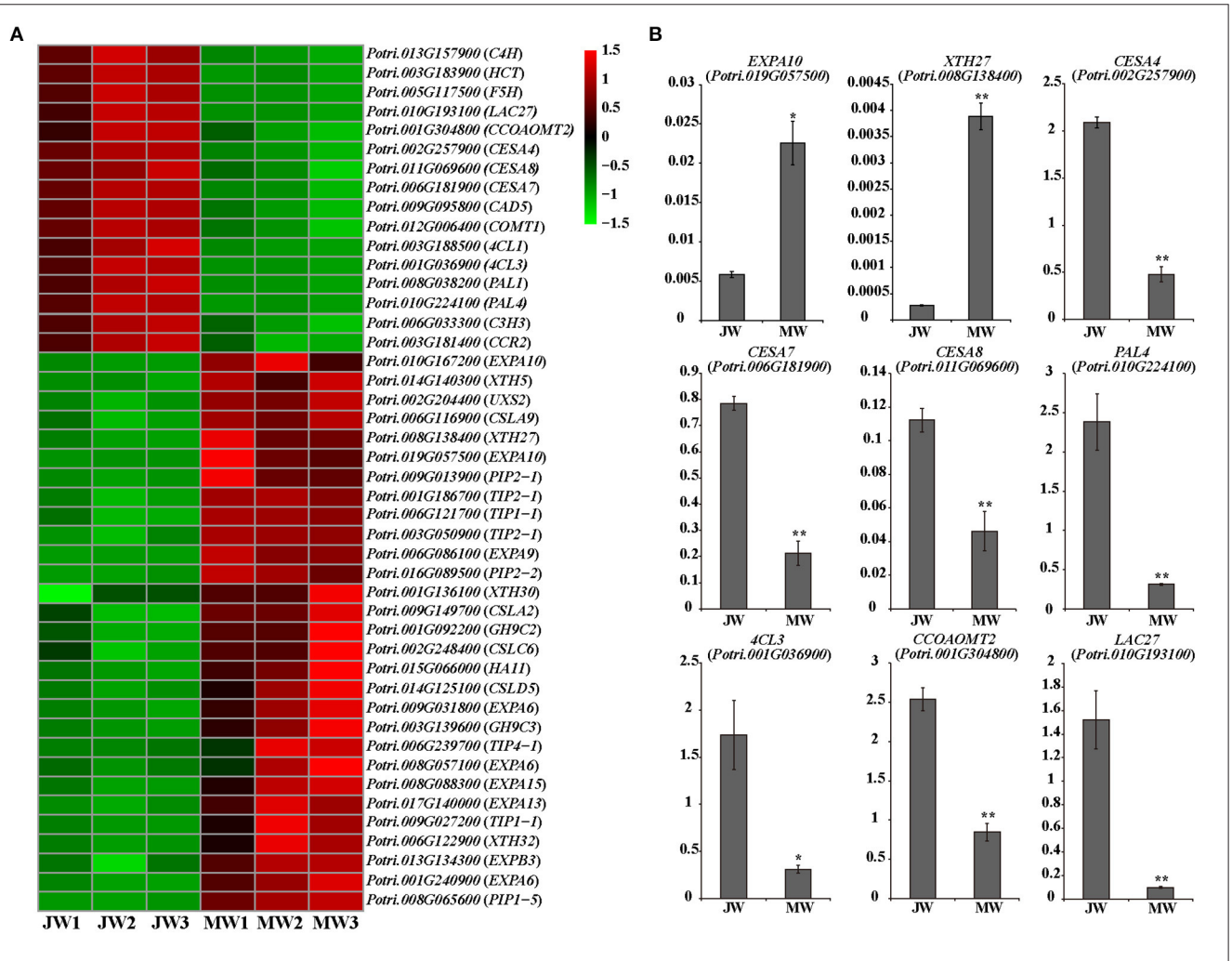

FIGURE 4 | Differentially expressed genes involved in cell wall formation in JW and MW. **(A)** The heat map of genes related to cell wall formation. **(B)** The results of quantitative real-time PCR of selected genes related to cell wall formation in JW and MW. Significance was determined by Student's *t*-test (*$p < 0.05$ and **$p < 0.01$).

played a role in activating expression of the genes in cell cycle (Haga et al., 2011), showed higher expression in MW. *PtrERF118* (*Potri.018G028000*), which was identified as a TF-regulating xylem cell expansion in *Populus* (Vahala et al., 2013; Seyfferth et al., 2018), was upregulated in MW. These results suggest that the transcriptional networks in relation to auxin biosynthesis and signaling, secondary cell wall formation, and xylem cell differentiation were differentially regulated in the formation of JW and MW.

Expression of the Cell Wall Formation Genes in JW and MW

The DEGs included a large number of genes responsible for cell wall biosynthesis (**Figure 4**; **Supplementary Table 6**). It is worth noting that among the DEGs, a large number of genes related to turgor maintenance and cell expansion were identified, of which the majority were upregulated in MW (**Figure 4A**; **Supplementary Table 6**). Cell turgor pressure is closely related to cell expansion, it can induce irreversible cell expansion (Genard et al., 2001). Five *TIPs* and three *PIPs* which are related to maintenance of turgor pressure were upregulated in MW. On the other hand, nine *EXPAs* and four *XTHs* which were related to cell wall loosening (Mcqueenmason et al., 1992; Van Sandt et al., 2007; Nishikubo et al., 2011) were identified upregulated in MW (**Figure 4A**). In addition, the homologs of *FUC1*, *PAEs*, *PMEs*, and *PMRs*, which play a role in modifying cell wall for cell wall loosening (Gou et al., 2012; Kato et al., 2018), were also upregulated in MW. Meanwhile, the homolog of *HA11* (a PM H+-ATPase) were upregulated in MW. The PM H+-ATPase can reduce the pH in the apoplast space to activate expansins and other cell wall loosening proteins as well as promote the absorption of water to provide turgor pressure for cell expansion (Spartz et al., 2014). These changes of the gene expression were confirmed by qRT-PCR (**Figure 4B**). These results support the observation that MW is formed with larger and longer fibers and vessel elements.

Expression of the genes for monolignol biosynthesis was consistently lower in MW, including five *PAL* homologs, *C4H1* and *C4H2*, *4CL1* and *4CL5*, *HCT1*, *C3H3*, *CSE2*, *CCoAOMT1* and *CCoAOMT2*, *CCR2*, *F5H1* and *F5H2*, *COMT1*, and *CAD* (**Figure 4A**). This may reflect less lignin biosynthesis in MW. After biosynthesis, monolignols are polymerized by laccases or peroxidases. Among detected, 11 *laccase* (*LAC*) genes including homologs of *LAC2*, *LAC10*, *LAC11*, and *LAC17* were downregulated in MW. Interestingly, among the 10 detected *peroxidase* genes, two *peroxidase*s were expressed higher in JW and the other eight were expressed higher in MW. It is worthy of further investigating whether the different members of *LAC* or *PRX* act in different phases of wood formation. Cellulose is synthesized by cellulose synthase complex (CSC) of synthases (CesAs) (Song et al., 2010; McFarlane et al., 2014). It is interesting to notice that the homologs of *CesA4*, *CesA7*, and *CesA8*, which form CSCs for cell wall thickening (Song et al., 2010; Watanabe et al., 2015; Xi et al., 2017), were downregulated in MW (**Figures 4A,B**). As cellulose synthesis is affected by CesA modifications at protein level (Polko and Kieber, 2019), it is unclear whether modification of CesAs are involved in regulating cellulose synthesis in JW and MW.

A number of genes for biosynthesis of hemicelluloses were differentially expressed in JW and MW (**Figure 4A**). UDP-glucuronic acid decarboxylase (UXS) catalyzes UDP-glucuronic acid (UDP-GlcA) to biosynthesis of UDP-Xyl (Kuang et al., 2016), which is a donor for biosynthesis of xylan, a major secondary cell wall hemicellulose. *Cellulose synthase-like D* (*CSLD*) involved xylan synthesis (Bernal et al., 2007). *Cellulose synthase-like A* (*CSLA*) encodes mannan synthase (Liepman et al., 2005; Suzuki et al., 2006; Verhertbruggen et al., 2011). Homologs of *UXS, CSLC*, *CSLD*, and *CLSA* showed higher expression in MW. The results support a higher content of xylan and mannan deposited in MW than in JW (**Table 1**).

DNA Methylation in Formation of JW and MW

The differential gene expression in different growth phases prompted us to examine the whole genome bisulfite sequencing (WGBS). The bisulfite sequencing showed that 87.6–91.9% of the reads was qualified for methylation assay against the *Populus* genome (http://phytozome.jgi.doe.gov/) (**Supplementary Table 7**, The raw data in Sequence Read Archive (SRA), ID: PRJNA705570). Overall, the methylation level was different within cytosine methylation contexts (CG, CHG, and CHH). The context of CG had higher methylation level, while CHG and CHH had lower (**Supplementary Table 8**). The DNA methylation context patterns displayed a similarity with those previously observed in *Populus* (Vining et al., 2012; Su et al., 2018). PCA showed that JW and MW had distinct DNA methylation (**Figure 5A**). Comparison of the DNA methylation in JW and MW revealed 12,176 differentially methylated regions (DMRs) (with methylation difference $\geq$10, *Q*-value $<$0.05). Majority of DMRs were in the contexts of CG sites (10,303) and CHG sites (1,663) (**Supplementary Figure 4A**; **Supplementary Table 9**), Among them, 10,237 DMRs were located in gene body and/or flanking regions ($\pm$2 kb), named differentially methylated genes (DMGs). In MW, 5,414 DMGs showed higher methylation while JW contained 4,849 DMGs with higher methylation (**Figure 5B**; **Supplementary Table 10**), suggesting that different DNA methylations occurred in the formation of JW and MW. Analysis of the correlation between DMGs and DEGs indicated that DMRs in gene promoter region were more likely to affect gene expression (**Supplementary Figure 4B**). About 20% DEGs (802) displayed different methylation (**Supplementary Table 11**). These DEGs were closely related to plant hormone signaling and response, cell wall formation and modification, metabolic process, transcription and translation, etc. (**Supplementary Figure 4C**; **Supplementary Table 12**). For example, the homologs of *ARFs*, *BAK1*, *BSK1*, and *BZR1*, which are involved in auxin and BR signaling, were differential methylated in their different gene regions in JW and MW (**Figure 5C**; **Supplementary Table 11**). Furthermore, several genes related to cell wall formation such as *XTH30*, *PAEs*, *WND1B*, *CESA4*, *CESA7*, and *CESA8* (**Figure 5C**; **Supplementary Table 11**) showed differential methylation in JW

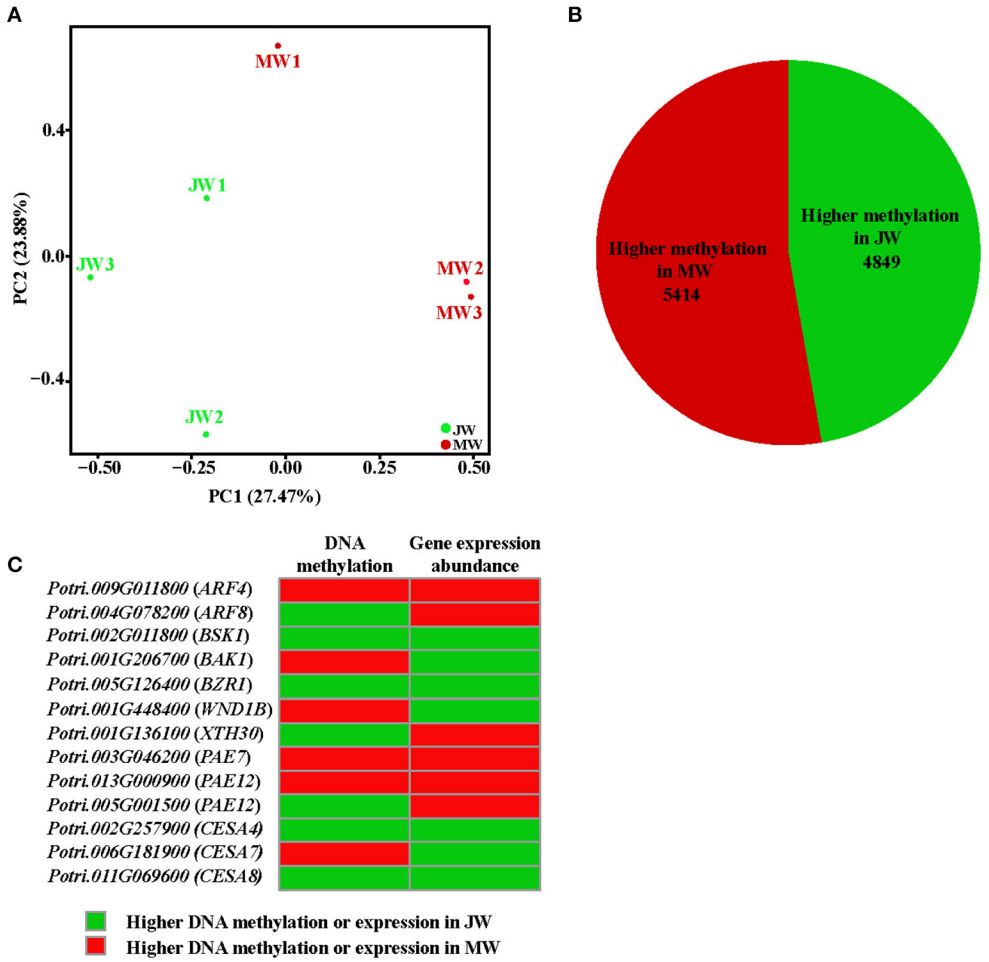

FIGURE 5 | The methylation profile of JW and MW. **(A)** Principal component analysis (PCA) of DNA methylation in each sample. **(B)** The number of higher methylation genes in DMGs. **(C)** Methylation and expression of genes related to wood formation.

and MW. In addition, several DMRs in intergenic region were neighbored to the homologs of *PILS2*, *AUX1*, *PIN7*, *WND2A*, *MYBs*, and *PAL1*, which are involved in auxin distribution and cell wall biosynthesis (**Supplementary Table 11**). In summary, the results revealed that DNA methylation displayed a clear difference in the formation of JW and MW, which may play a role in regulating gene expression in different growth phases, particularly for the genes involved in hormone signal transduction, cell division, and cell wall biosynthesis in wood formation.

DISCUSSION

At a given point of tree development, wood can be differentiated into juvenile wood and mature wood which have distinct properties (Basheer-Salimia, 2007; Barrios et al., 2017). In the present study, we profiled the transcriptome and DNA methylation patterns in JW and MW derived from an identical genetic background in order to uncover the paths involved in wood formation at different developmental phases. Different transcription profiles and DNA methylation were identified in the formation of JW and MW. Differences in gene expression were primarily associated with plant hormones including auxin and BR signaling and response, cell wall formation and modification, cell organization and biogenesis, and transcription regulation processes. Different patterns of DNA methylation were also detected in genes involved in auxin transport, BR signaling, and cell expansion which suggest a role for the epigenetic regulation of JW and MW formation.

Different expressions of auxin transport genes were observed in JW and MW. Relative to JW, we observed that the genes related to auxin influx (homolog of *AUX1*) (Enders and Strader, 2015) were downregulated in MW, while the genes related to auxin efflux (homologs of *PINs*, *PILSs*, *ABCB19*) (Liu et al., 2014; Enders and Strader, 2015) were upregulated in MW. Meanwhile, the different members of the *AUX1/LAX3* family were that expressed in JW and MW imply a possibility that formation of JW and MW involves distinct auxin molecule formats, as *AUX1/LAX* members correspond with different auxin formats (Enders and

Strader, 2015). Further characterization of PIN, ABCB, AUX1, and LAX3 proteins in association with auxin in the JW-/MW-forming tissues would be able to provide mechanistic evidence for verification of the findings. However, current results indicate that auxin transport plays a role in regulating the formation of JW and MW.

Furthermore, we also found that homolog of *DIM* which is a key gene for BR biosynthesis (Klahre et al., 1998) was upregulated in MW, while homologs of *BAK1*, *BSK1*, and *BZR1* which are marker genes for BR signaling (Li et al., 2002; Nam and Li, 2002; Wang et al., 2002; Tang et al., 2008) showed downregulated expression in MW, suggesting that BR signaling plays a role in regulating MW formation. Studies have shown that BR promotes wood formation (Du et al., 2020). It is worthy of studying whether BR manipulates wood properties in wood formation because the properties of JW and MW are different.

DNA methylation acts as an epigenetic mechanism to regulate gene expression in plants (Fraga et al., 2002a; Vining et al., 2012; Matzke and Mosher, 2014; Liang et al., 2019). In this study, we found that the methylation level of the auxin transport genes *PILS2*, *AUX1*, and *PIN7* was different between JW and MW. In addition, the different degrees of DNA methylation were also detected in the BR signaling genes *BAK1*, *BSK1*, and *BZR1*. It is likely that the different expressions of these genes in JW and MW may be related to their DNA methylation changes over the developmental process. Further investigation of the DNA methylation effect on the transcription activities of the auxin and BR genes would help in the revelation of the molecular pathways underlying the alternation of the hormone signaling during different development phases in perennial trees. In summary, the present results suggest that auxin distribution and transportation, BR biosynthesis, and signaling are involved in regulating the wood formation at juvenile and mature phase. DNA methylation plays an important role in regulating the expression of the auxin and BR genes at different development phases.

In consistent with the hormone signaling changes, the downstream biological processes in response to auxin and BR also showed alternation in JW and MW. For instance, TFs such as *ARFs*, *SRSs*, *AP2*, and *MYB3R1* and genes related to cell loosing and cell expansion such as *HA11*, *XTHs*, *FUC1*, *PAEs*, *PMEs*, *PMRs*, *PIPs*, and *TIPs*, of which the expression is responding to auxin signaling (Guilfoyle and Hagen, 2007; Spartz et al., 2014), showed differential expression in formation of JW and MW. These transcription regulations are in agreement with the MW properties that have significantly longer and larger fiber cells and vessels.

Cell wall composition (including lignin, cellulose, and hemicellulose) which is closely related to wood properties is rather different in JW and MW (**Table 1**). Expressions of the genes related to lignin biosynthesis were downregulated, and the genes for hemicelluloses biosynthesis were upregulated in MW, consistent with the result of less lignin content and higher hemicellulose content in MW. Interestingly, expression of the cellulose biosynthesis genes (such as *CesA4*, *CesA7*, and *CesA8*) was downregulated in MW compared with JW. However, the cellulose content was higher in MW. As this discrepancy requires further verification, regulation of the CesA activity at protein level may be considered. It is known that protein phosphorylation plays a crucial role in regulating CesA catalytic activity and motility (Chen et al., 2010; Speicher et al., 2018; Polko and Kieber, 2019). More evidence is needed for the elucidation of the different cellulose accumulations in JW and MW.

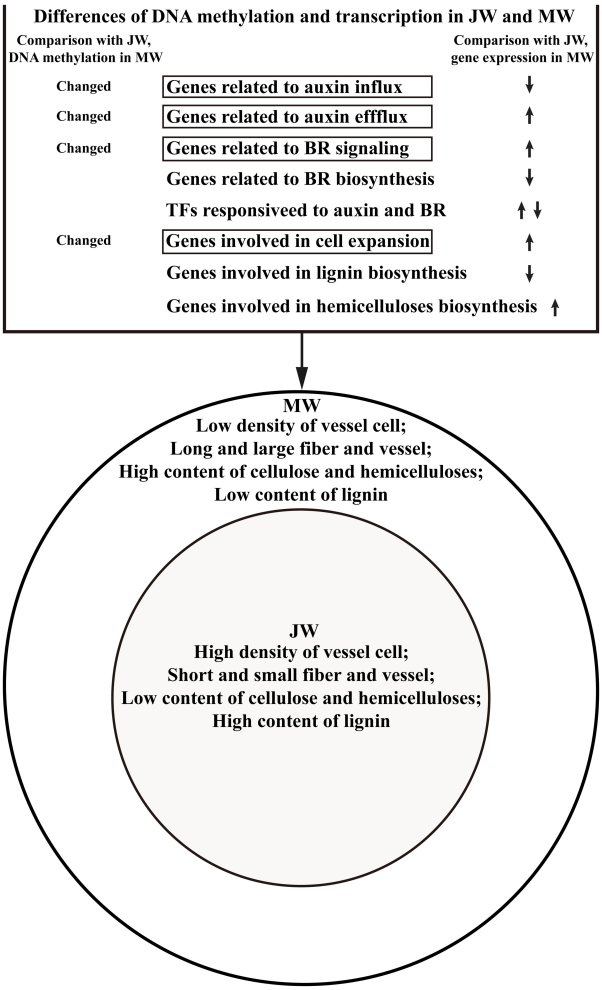

FIGURE 6 | Outline of the DAN methylation and transcription regulation in formation of JW and MW.

CONCLUSIONS

In this study, we analyzed transcription profiles and genome-wide DNA methylation in association with the wood properties of JW and MW by employing *Populus* trees with an identical genetic background. Results suggest that auxin distribution and BR signaling may act as major mechanisms to modulate the wood formation in different development phases. In response to the hormone signaling alteration, the transcription activities are modulated, leading to the formation of different wood properties in JW and MW. Furthermore, results also indicate that the transcription modulation of the hormone-related genes may be

regulated through DNA methylation. The study outlines a picture of the main transcription networks related to wood formation in JW and MW and a possible role of DNA methylation in tuning the transcriptional network (**Figure 6**). These findings shed light toward a better mechanistic understanding of wood formation in different development phases and new evidence to inform the engineering of wood properties.

DATA AVAILABILITY STATEMENT

The data presented in the study are deposited in Sequence Read Archive (SRA) repository, the RNA-seq accession number: PRJNA705066 and DNA methylation accession number: PRJNA705570). Supporting results of this article are included in **Supplementary Material**.

AUTHOR CONTRIBUTIONS

LLu performed experiments, analyzed data, and wrote the manuscript. YZ and JL analyzed data and wrote the manuscript. JG conducted RNA-seq analysis and wrote the manuscript. TY prepared the tree samples and analyzed data. LLi conceived the project, analyzed data, and wrote the manuscript. All authors have read and approved the final manuscript.

FUNDING

This work was supported by the National Key Research and Development Program of China (2016YFD0600104), the National Nature Science Foundation of China (31630014), the Youth Innovation Promotion Association CAS (Grant No. 2017318), and the Chinese Academy of Sciences (XDB27020104).

ACKNOWLEDGMENTS

We thank Wenli Hu for assistance with the GC-MS analysis (SIPPE) and Shumin Cao and Zhi Xie for assistance with the tissue sampling.

SUPPLEMENTARY MATERIAL

The Supplementary Material for this article can be found online at: https://www.frontiersin.org/articles/10.3389/fpls.2021.675075/full#supplementary-material

REFERENCES

Akalin, A., Kormaksson, M., Li, S., Garrett-Bakelman, F. E., Figueroa, M. E., Melnick, A., et al. (2012). methylKit: a comprehensive R package for the analysis of genome-wide DNA methylation profiles. *Genome Biol.* 13:R87. doi: 10.1186/gb-2012-13-10-r87

Anders, S., Pyl, P. T., and Huber, W. (2015). HTSeq-a python framework to work with high-throughput sequencing data. *Bioinformatics* 31, 166–169. doi: 10.1093/bioinformatics/btu638

Barrios, A., Trincado, G., and Watt, M. S. (2017). Wood properties of juvenile and mature wood of *Pinus radiata* D. Don trees growing on contrasting sites in Chile. *Forest Sci.* 63, 184–191. doi: 10.5849/forsci.2016-060

Basheer-Salimia, R. (2007). Juvenility, maturity, and rejuvenation in woody plants. *Hebron Univ. Res. J.* 3, 17–43.

Bernal, A. J., Jensen, J. K., Harholt, J., Sorensen, S., Moller, I., Blaukopf, C., et al. (2007). Disruption of ATCSLD5 results in reduced growth, reduced xylan and homogalacturonan synthase activity and altered xylan occurrence in Arabidopsis. *Plant J.* 52, 791–802. doi: 10.1111/j.1365-313X.2007.03281.x

Braatne, J. H., Rood, S. B., and Heilman, P. E. (1996). *Life History, Ecology, and Conservation of Riparian Cottonwoods in North America*. Ottawa: NRC research press.

Chen, S., Ehrhardt, D. W., and Somerville, C. R. (2010). Mutations of cellulose synthase (CESA1) phosphorylation sites modulate anisotropic cell expansion and bidirectional mobility of cellulose synthase. *Proc. Natl. Acad. Sci. U.S.A.* 107, 17188–17193. doi: 10.1073/pnas.1012348107

Chen, S., Zhou, Y., Chen, Y., and Gu, J. (2018). fastp: an ultra-fast all-in-one FASTQ preprocessor. *Bioinformatics* 34, i884–i890. doi: 10.1093/bioinformatics/bty560

Choi, H., Dang, T. V. T., and Hwang, I. (2017). Emergence of plant vascular system: roles of hormonal and non-hormonal regulatory networks. *Curr. Opin. Plant Biol.* 35, 91–97. doi: 10.1016/j.pbi.2016.11.013

Ci, D., Song, Y. P., Tian, M., and Zhang, D. Q. (2015). Methylation of miRNA genes in the response to temperature stress in Populus simonii. *Front. Plant Sci.* 6:921. doi: 10.3389/fpls.2015.00921

Cosgrove, D. J. (2018). Diffuse growth of plant cell walls. *Plant Physiol.* 176, 16–27. doi: 10.1104/pp.17.01541

Demura, T., and Fukuda, H. (2007). Transcriptional regulation in wood formation. *Trends Plant Sci.* 12, 64–70. doi: 10.1016/j.tplants.2006.12.006

Dowen, R. H., Pelizzola, M., Schmitz, R. J., Lister, R., Dowen, J. M., Nery, J. R., et al. (2012). Widespread dynamic DNA methylation in response to biotic stress. *Proc. Natl. Acad. Sci. U.S.A.* 109, E2183–2191. doi: 10.1073/pnas.1209329109

Du, J., Gerttula, S., Li, Z. H., Zhao, S. T., Li-Liu, Y., Liu, Y., et al. (2020). Brassinosteroid regulation of wood formation in poplar. *New Phytol.* 225, 1516–1530. doi: 10.1111/nph.15936

Eklund, D. M., Staldal, V., Valsecchi, I., Cierlik, I., Eriksson, C., Hiratsu, K., et al. (2010). The *Arabidopsis thaliana* STYLISH1 protein acts as a transcriptional activator regulating auxin biosynthesis. *Plant Cell.* 22, 349–363. doi: 10.1105/tpc.108.064816

Enders, T. A., and Strader, L. C. (2015). Auxin activity: past, present, and future. *Am. J. Bot.* 102, 180–196. doi: 10.3732/ajb.1400285

Foster, C. E., Martin, T. M., and Pauly, M. (2010a). Comprehensive compositional analysis of plant cell walls (*Lignocellulosic biomass*) part I: lignin. *J. Vis. Exp.* 1745. doi: 10.3791/1745

Foster, C. E., Martin, T. M., and Pauly, M. (2010b). Comprehensive compositional analysis of plant cell walls (*Lignocellulosic biomass*) part II: carbohydrates. *J. Vis. Exp.* 1837. doi: 10.3791/1837

Fraga, M. F., Canal, M. J., and Rodriguez, R. (2002a). Phase-change related epigenetic and physiological changes in *Pinus radiata* D. Don. *Planta* 215, 672–678. doi: 10.1007/s00425-002-0795-4

Fraga, M. F., Rodriguez, R., and Canal, M. J. (2002b). Genomic DNA methylation-demethylation during aging and reinvigoration of *Pinus radiata*. *Tree Physiol.* 22, 813–816. doi: 10.1093/treephys/22.11.813

Fromm, J. (2013). "Xylem development in trees: from cambial divisions to mature wood cells," in *Cellular Aspects of Wood Formation. Plant Cell Monographs, Vol. 20*, ed J. Fromm (Berlin Heidelberg: Springer), 3–39. doi: 10.1007/978-3-642-36491-4_1

Genard, M., Fishman, S., Vercambre, G., Huguet, J. G., Bussi, C., Besset, J., et al. (2001). A biophysical analysis of stem and root diameter variations in woody plants. *Plant Physiol.* 126, 188–202. doi: 10.1104/pp.126.1.188

Goll, M. G., and Bestor, T. H. (2005). Eukaryotic cytosine methyltransferases. *Annu. Rev. Biochem.* 74, 481–514. doi: 10.1146/annurev.biochem.74.010904.153721

Gou, J. Y., Miller, L. M., Hou, G. C., Yu, X. H., Chen, X. Y., and Liu, C. J. (2012). Acetylesterase-mediated deacetylation of pectin impairs cell elongation, pollen germination, and plant reproduction. *Plant Cell.* 24, 50–65. doi: 10.1105/tpc.111.092411

Guilfoyle, T. J., and Hagen, G. (2007). Auxin response factors. *Curr. Opin. Plant Biol.* 10, 453–460. doi: 10.1016/j.pbi.2007.08.014

Haga, N., Kobayashi, K., Suzuki, T., Maeo, K., Kubo, M., Ohtani, M., et al. (2011). Mutations in MYB3R1 and MYB3R4 cause pleiotropic developmental defects and preferential down-regulation of multiple G2/M-specific genes in *Arabidopsis*. *Plant Physiol.* 157, 706–717. doi: 10.1104/pp.111.180836

He, X. J., Chen, T. P., and Zhu, J. K. (2011). Regulation and function of DNA methylation in plants and animals. *Cell Res.* 21, 442–465. doi: 10.1038/cr.2011.23

Hussey, S. G., Mizrachi, E., Creux, N. M., and Myburg, A. A. (2013). Navigating the transcriptional roadmap regulating plant secondary cell wall deposition. *Front. Plant Sci.* 4:325. doi: 10.3389/fpls.2013.00325

Israelsson, M., Sundberg, B., and Moritz, T. (2005). Tissue-specific localization of gibberellins and expression of gibberellin-biosynthetic and signaling genes in wood-forming tissues in aspen. *Plant J.* 44, 494–504. doi: 10.1111/j.1365-313X.2005.02547.x

Jin, J., Zhang, H., Kong, L., Gao, G., and Luo, J. (2014). PlantTFDB 3.0: a portal for the functional and evolutionary study of plant transcription factors. *Nucleic Acids Res.* 42, D1182–1187. doi: 10.1093/nar/gkt1016

Kanehisa, M., Araki, M., Goto, S., Hattori, M., Hirakawa, M., Itoh, M., et al. (2008). KEGG for linking genomes to life and the environment. *Nucleic Acids Res.* 36, D480–D484. doi: 10.1093/nar/gkm882

Kato, S., Hayashi, M., Kitagawa, M., Kajiura, H., Maeda, M., Kimura, Y., et al. (2018). Degradation pathway of plant complex-type N-glycans: identification and characterization of a key alpha1,3-fucosidase from glycoside hydrolase family 29. *Biochem. J.* 475, 305–317. doi: 10.1042/BCJ20170106

Kim, D., Landmead, B., and Salzberg, S. L. (2015). HISAT: a fast spliced aligner with low memory requirements. *Nat. Methods* 12, 357–U121. doi: 10.1038/nmeth.3317

Klahre, U., Noguchi, T., Fujioka, S., Takatsuto, S., Yokota, T., Nomura, T., et al. (1998). The *Arabidopsis* DIMINUTO/DWARF1 gene encodes a protein involved in steroid synthesis. *Plant Cell.* 10, 1677–1690. doi: 10.1105/tpc.10.10.1677

Krueger, F., and Andrews, S. R. (2011). Bismark: a flexible aligner and methylation caller for Bisulfite-Seq applications. *Bioinformatics* 27, 1571–1572. doi: 10.1093/bioinformatics/btr167

Kuang, B. Q., Zhao, X. H., Zhou, C., Zeng, W., Ren, J. L., Ebert, B., et al. (2016). Role of UDP-glucuronic acid decarboxylase in xylan biosynthesis in Arabidopsis. *Mol. Plant.* 9, 1119–1131. doi: 10.1016/j.molp.2016.04.013

Kumar, M., Campbell, L., and Turner, S. (2016). Secondary cell walls: biosynthesis and manipulation. *J. Exp. Bot.* 67, 515–531. doi: 10.1093/jxb/erv533

Lafon-Placette, C., Faivre-Rampant, P., Delaunay, A., Street, N., Brignolas, F., and Maury, S. (2013). Methylome of DNase I sensitive chromatin in Populus trichocarpa shoot apical meristematic cells: a simplified approach revealing characteristics of gene-body DNA methylation in open chromatin state. *New Phytol.* 197, 416–430. doi: 10.1111/nph.12026

Law, J. A., and Jacobsen, S. E. (2010). Establishing, maintaining and modifying DNA methylation patterns in plants and animals. *Nat. Rev. Genet.* 11, 204–220. doi: 10.1038/nrg2719

Li, C. F., Wang, X. Q., Ran, L. Y., Tian, Q. Y., Fan, D., and Luo, K. M. (2015). PtoMYB92 is a transcriptional activator of the lignin biosynthetic pathway during secondary cell wall formation in *Populus tomentosa*. *Plant Cell Physiol.* 56, 2436–2446. doi: 10.1093/pcp/pcv157

Li, J., Wen, J. Q., Lease, K. A., Doke, J. T., Tax, F. E., and Walker, J. C. (2002). BAK1, an Arabidopsis LRR receptor-like protein kinase, interacts with BRI1 and modulates brassinosteroid signaling. *Cell* 110, 213–222. doi: 10.1016/S0092-8674(02)00812-7

Liang, X. L., Hou, X., Li, J. Y., Han, Y. Q., Zhang, Y. X., Feng, N. J., et al. (2019). High-resolution DNA methylome reveals that demethylation enhances adaptability to continuous cropping comprehensive stress in soybean. *BMC Plant Biol.* 19:79. doi: 10.1186/s12870-019-1670-9

Liepman, A. H., Wilkerson, C. G., and Keegstra, K. (2005). Expression of cellulose synthase-like (Csl) genes in insect cells reveals that CslA family members encode mannan synthases. *Proc. Natl. Acad. Sci. U.S.A.* 102, 2221–2226. doi: 10.1073/pnas.0409179102

Liu, B. B., Zhang, J., Wang, L., Li, J. B., Zheng, H. Q., Chen, J., et al. (2014). A survey of Populus PIN-FORMED family genes reveals their diversified expression patterns. *J. Exp. Bot.* 65, 2437–2448. doi: 10.1093/jxb/eru129

Matzke, M. A., and Mosher, R. A. (2014). RNA-directed DNA methylation: an epigenetic pathway of increasing complexity. *Nat. Rev. Genet.* 15, 394–408. doi: 10.1038/nrg3683

McFarlane, H. E., Doring, A., and Persson, S. (2014). The cell biology of cellulose synthesis. *Annu. Rev. Plant Biol.* 65, 69–94. doi: 10.1146/annurev-arplant-050213-040240

Mcneil, M., Darvill, A. G., Fry, S. C., and Albersheim, P. (1984). Structure and function of the primary-cell walls of plants. *Annu. Rev. Biochem.* 53, 625–663. doi: 10.1146/annurev.bi.53.070184.003205

Mcqueenmason, S., Durachko, D. M., and Cosgrove, D. J. (1992). 2 Endogenous proteins that induce cell-wall extension in plants. *Plant Cell* 4, 1425–1433. doi: 10.1105/tpc.4.11.1425

Moore, J. R., and Cown, D. J. (2017). Corewood (Juvenile wood) and its impact on wood utilisation. *Curr. Rep.* 3, 107–118. doi: 10.1007/s40725-017-0055-2

Nam, K. H., and Li, J. M. (2002). BRI1/BAK1, a receptor kinase pair mediating brassinosteroid signaling. *Cell* 110, 203–212. doi: 10.1016/S0092-8674(02)00814-0

Nishikubo, N., Takahashi, J., Roos, A. A., Derba-Maceluch, M., Piens, K., Brumer, H., et al. (2011). Xyloglucan endo-transglycosylase-mediated xyloglucan rearrangements in developing wood of hybrid aspen. *Plant Physiol.* 155, 399–413. doi: 10.1104/pp.110.166934

Owens, J. N. (2006). *The Reproductive Biology of Lodgepole Pine*, Columbia: Forest Genetics Council of BC (FGC).

Patel, R. K., and Jain, M. (2012). NGS QC toolkit: a toolkit for quality control of next generation sequencing data. *PLoS ONE* 7:e30619. doi: 10.1371/journal.pone.0030619

Pinon, V., Prasad, K., Grigg, S. P., Sanchez-Perez, G. F., and Scheres, B. (2013). Local auxin biosynthesis regulation by PLETHORA transcription factors controls phyllotaxis in *Arabidopsis*. *Proc. Natl. Acad. Sci. U.S.A.* 110, 1107–1112. doi: 10.1073/pnas.1213497110

Plomion, C., Leprovost, G., and Stokes, A. (2001). Wood formation in trees. *Plant Physiol.* 127, 1513–1523. doi: 10.1104/pp.010816

Polko, J. K., and Kieber, J. J. (2019). The regulation of cellulose biosynthesis in plants. *Plant Cell.* 31, 282–296. doi: 10.1105/tpc.18.00760

Roberts, A., Trapnell, C., Donaghey, J., Rinn, J. L., and Pachter, L. (2011). Improving RNA-Seq expression estimates by correcting for fragment bias. *Genome Biol.* 12:R22. doi: 10.1186/gb-2011-12-3-r22

Romano, J. M., Dubos, C., Prouse, M. B., Wilkins, O., Hong, H., Poole, M., et al. (2012). AtMYB61, an R2R3-MYB transcription factor, functions as a pleiotropic regulator via a small gene network. *New Phytol.* 195, 774–786. doi: 10.1111/j.1469-8137.2012.04201.x

Seyfferth, C., Wessels, B., Jokipii-Lukkari, S., Sundberg, B., Delhomme, N., Felten, J., et al. (2018). Ethylene-related gene expression networks in wood formation. *Front. Plant Sci.* 9:272. doi: 10.3389/fpls.2018.00272

Song, D., Shen, J., and Li, L. (2010). Characterization of cellulose synthase complexes in Populus xylem differentiation. *New Phytol.* 187, 777–790. doi: 10.1111/j.1469-8137.2010.03315.x

Song, D. L., Xi, W., Shen, J. H., Bi, T., and Li, L. G. (2011). Characterization of the plasma membrane proteins and receptor-like kinases associated with secondary vascular differentiation in poplar. *Plant Mol. Biol.* 76, 97–115. doi: 10.1007/s11103-011-9771-3

Spartz, A. K., Ren, H., Park, M. Y., Grandt, K. N., Lee, S. H., Murphy, A. S., et al. (2014). SAUR inhibition of PP2C-D phosphatases activates plasma membrane H+-ATPases to promote cell expansion in *Arabidopsis*. *Plant Cell.* 26, 2129–2142. doi: 10.1105/tpc.114.126037

Speicher, T. L., Li, P. Z. Q., and Wallace, I. S. (2018). Phosphoregulation of the plant cellulose synthase complex and cellulose synthase-like proteins. *Plants-Basel* 7:52. doi: 10.3390/plants7030052

Su, Y. T., Bai, X. T., Yang, W. L., Wang, W. W., Chen, Z. Y., Ma, J. C., et al. (2018). Single-base-resolution methylomes of *Populus euphratica* reveal the association between DNA methylation and salt stress. *Tree Genet. Genom.* 14:86. doi: 10.1007/s11295-018-1298-1

Suzuki, S., Li, L. G., Sun, Y. H., and Chiang, V. L. (2006). The cellulose synthase gene superfamily and biochemical functions of xylem-specific cellulose synthase-like genes in *Populus trichocarpa*. *Plant Physiol.* 142, 1233–1245. doi: 10.1104/pp.106.086678

Tang, W. Q., Kim, T. W., Oses-Prieto, J. A., Sun, Y., Deng, Z. P., Zhu, S. W., et al. (2008). BSKs mediate signal transduction from the receptor kinase BRI1 in *Arabidopsis*. *Science* 321, 557–560. doi: 10.1126/science.1156973

Trapnell, C., Williams, B. A., Pertea, G., Mortazavi, A., Kwan, G., van Baren, M. J., et al. (2010). Transcript assembly and quantification by RNA-Seq reveals unannotated transcripts and isoform switching during cell differentiation. *Nat. Biotechnol.* 28, 511–U174. doi: 10.1038/nbt.1621

Vahala, J., Felten, J., Love, J., Gorzsas, A., Gerber, L., Lamminmaki, A., et al. (2013). A genome-wide screen for ethylene-induced ethylene response factors (ERFs) in hybrid aspen stem identifies ERF genes that modify stem growth and wood properties. *New Phytol.* 200, 511–522. doi: 10.1111/nph.12386

Van Sandt, V. S., Suslov, D., Verbelen, J. P., and Vissenberg, K. (2007). Xyloglucan endotransglucosylase activity loosens a plant cell wall. *Ann Bot*. 100, 1467–1473. doi: 10.1093/aob/mcm248

Verhertbruggen, Y., Yin, L., Oikawa, A., and Scheller, H. V. (2011). Mannan synthase activity in the CSLD family. *Plant Signal Behav*. 6, 1620–1623. doi: 10.4161/psb.6.10.17989

Vining, K. J., Pomraning, K. R., Wilhelm, L. J., Priest, H. D., Pellegrini, M., Mockler, T. C., et al. (2012). Dynamic DNA cytosine methylation in the *Populus trichocarpa* genome: tissue-level variation and relationship to gene expression. *BMC Genomics* 13:27. doi: 10.1186/1471-2164-13-27

Wang, Q. S., Ci, D., Li, T., Li, P. W., Song, Y. P., Chen, J. H., et al. (2016). The Role of DNA Methylation in xylogenesis in different tissues of poplar. *Front. Plant Sci.* 7:1003. doi: 10.3389/fpls.2016.01003

Wang, S. C., Li, E. Y., Porth, I., Chen, J. G., Mansfield, S. D., and Douglas, C. J. (2014). Regulation of secondary cell wall biosynthesis by poplar R2R3 MYB transcription factor PtrMYB152 in *Arabidopsis*. *Sci Rep-UK*. 4:5054. doi: 10.1038/srep05054

Wang, W. S., Pan, Y. J., Zhao, X. Q., Dwivedi, D., Zhu, L. H., Ali, J., et al. (2011). Drought-induced site-specific DNA methylation and its association with drought tolerance in rice (*Oryza sativa* L.). *J. Exp. Bot.* 62, 1951–1960. doi: 10.1093/jxb/erq391

Wang, Z. Y., Nakano, T., Gendron, J., He, J. X., Chen, M., Vafeados, D., et al. (2002). Nuclear-localized BZR1 mediates brassinosteroid-induced growth and feedback suppression of brassinosteroid biosynthesis. *Dev. Cell*. 2, 505–513. doi: 10.1016/S1534-5807(02)00153-3

Watanabe, Y., Meents, M. J., McDonnell, L. M., Barkwill, S., Sampathkumar, A., Cartwright, H. N., et al. (2015). Visualization of cellulose synthases in *Arabidopsis* secondary cell walls. *Science* 350, 198–203. doi: 10.1126/science.aac7446

Xi, W., Song, D. L., Sun, J. Y., Shen, J. H., and Li, L. G. (2017). Formation of wood secondary cell wall may involve two type cellulose synthase complexes in *Populus*. *Plant Mol. Biol.* 93, 419–429. doi: 10.1007/s11103-016-0570-8

Youn, J. H., Kim, T. W., Joo, S. H., Son, S. H., Roh, J., Kim, S., et al. (2018). Function and molecular regulation of DWARF1 as a C-24 reductase in brassinosteroid biosynthesis in *Arabidopsis*. *J. Exp. Bot*. 69, 1873–1886. doi: 10.1093/jxb/ery038

Yu, L. L., Chen, H. P., Sun, J. Y., and Li, L. G. (2014). PtrKOR1 is required for secondary cell wall cellulose biosynthesis in *Populus*. *Tree Physiol.* 34, 1289–1300. doi: 10.1093/treephys/tpu020

Zhong, R. Q., Lee, C. H., and Ye, Z. H. (2010). Evolutionary conservation of the transcriptional network regulating secondary cell wall biosynthesis. *Trends Plant Sci.* 15, 625–632. doi: 10.1016/j.tplants.2010.08.007

Zhong, R. Q., McCarthy, R. L., Lee, C., and Ye, Z. H. (2011). Dissection of the transcriptional program regulating secondary wall biosynthesis during wood formation in poplar. *Plant Physiol.* 157, 1452–1468. doi: 10.1104/pp.111.181354

Conflict of Interest: The authors declare that the research was conducted in the absence of any commercial or financial relationships that could be construed as a potential conflict of interest.

frontiers in Plant Science

ORIGINAL RESEARCH
published: 04 June 2021
doi: 10.3389/fpls.2021.686024

A Small Guanosine Triphosphate Binding Protein *PagRabE1b* Promotes Xylem Development in Poplar

Ying-Li Liu[1], *Li-Juan Wang*[1,2], *Yu Li*[1,3], *Ying-Hua Guo*[1], *Yuan Cao*[1] *and Shu-Tang Zhao*[1,2*]

[1] State Key Laboratory of Tree Genetics and Breeding, Research Institute of Forestry, Chinese Academy of Forestry, Beijing, China, [2] Co-innovation Center for Sustainable Forestry in Southern China, Nanjing Forestry University, Nanjing, China, [3] Key Laboratory of Plant Molecular Physiology, Institute of Botany, Chinese Academy of Sciences, Beijing, China

Rab GTPases are the subfamily of the small guanosine triphosphate (GTP)-binding proteins which participated in the regulation of various biological processes. Recent studies have found that plant Rabs play some specific functions. However, the functions of *Rabs* in xylem development in trees remain unclear. In this study, functional identification of *PagRabE1b* in *Populus* was performed. Quantitative reverse transcription PCR (qRT-PCR) results showed that *PagRabE1b* was highly accumulated in stems, especially in phloem and xylem tissues. Overexpression of *PagRabE1b* in poplar enhanced programmed cell death (PCD) and increased the growth rate and the secondary cell wall (SCW) thickness. Quantitative analysis of monosaccharide content showed that various monosaccharides were significantly increased in secondary xylem tissues of the overexpressed lines. Flow cytometry analysis revealed that the number of apoptotic cells in *PagRabE1b-OE* lines is more than a wild type (WT), which indicated that *PagRabE1b* may play an important role in PCD. Further studies showed that overexpression of *PagRabE1b* increased the expression level of genes involved in SCW biosynthesis, PCD, and autophagy. Collectively, the results suggest that *PagRabE1b* plays a positive role in promoting the xylem development of poplar.

Keywords: poplar, small gtp binding protein, *PagRabE1b*, cell wall, wood formation

OPEN ACCESS

Edited by:
Guohua Chai,
Qingdao Agricultural University, China

Reviewed by:
Yuxiang Cheng,
Northeast Forestry University, China
Bo Zheng,
Huazhong Agricultural University, China

***Correspondence:**
Shu-Tang Zhao
zhaost318@163.com

Specialty section:
This article was submitted to Plant Biotechnology, a section of the journal Frontiers in Plant Science

Received: *26 March 2021*
Accepted: *14 May 2021*
Published: *04 June 2021*

Citation:
Liu Y-L, Wang L-J, Li Y, Guo Y-H, Cao Y and Zhao S-T (2021) A Small Guanosine Triphosphate Binding Protein PagRabE1b Promotes Xylem Development in Poplar. Front. Plant Sci. 12:686024. doi: 10.3389/fpls.2021.686024

INTRODUCTION

Trees are the most abundant natural sources important for sustainable energy and the sinks of atmospheric carbon dioxide (Zhang et al., 2015; Zhong and Ye, 2015). Wood biomass is mainly composed of the secondary cell wall (SCW) and is widely used in many applications, such as house construction, biofuels, pulping, and paper-making. Because of the substantial economic value of wood, elucidating the molecular regulatory mechanism of wood formation will be useful for the manipulation of wood quality and quantity through molecular breeding.

The development of SCW is a complicated procedure requiring synchronization of several regulatory and metabolic pathways. Previous studies have revealed that the SCW biosynthesis is mainly regulated by transcriptional regulatory networks of NAC and MYB transcription factor (TF) families (Zhong and Ye, 2015). During SCW formation, several NAC TFs are considered as

master switches and in the top layer of the SCW regulatory network (Xie et al., 2018). A series of additional TFs, such as *MYB46* and *MBY83*, belong to the second layer of a transcriptional network of the SCW formation. In addition, several other MYB TFs in the third layer have been identified as direct targets of *MYB46/83* (Zhang et al., 2018a); most of these MYB members positively regulate SCW biosynthesis. SCWs mainly consist of cellulose, hemicelluloses, and lignin. Cellulose taking about 40–50% of wood components is glucose polymers. Hemicelluloses constitute a major part of lignocellulosic biomass, mainly including xyloglucans, xylans, mannans, glucomannans, and β-(1→ 3, 1→ 4)-glucans (Scheller and Ulvskov, 2010). Lignin is a complex three-dimensional polyphenolic polymer of *p*-hydroxyphenyl (H), guaiacyl (G), and syringyl (S) lignins (Boerjan et al., 2003). Monolignol biosynthesis is carried out through the common phenylpropanoid pathway, and several central genes involved in lignin synthesis during secondary wall formation in *Populus* had been well-identified (Wang et al., 2018). Finally, the lignified vessel and fiber cells undergo programmed cell death (PCD) for complete lysis of cell content in the maturation of xylem cells (Courtois-Moreau et al., 2009).

Small GTPases also play important roles in the regulation of cell wall development by monitoring cytoskeletal arrangement and membrane trafficking (Oda and Fukuda, 2014). In the eukaryotic, the Ras subfamily of small GTPases comprises five families: Ras, Rab, Ran, Arf, and Rho (Hall, 1998). Rho and Rab of plants play critical roles in the development of primary and SCWs (Oda and Fukuda, 2014). ROPGEF4 and ROPGAP3 mediate Rho GTPase ROP11 to originate the fundamental patterning of SCWs in xylem cells, and then ROP11 interacts withMIDD1 to provoke local depolymerization of cortical microtubules (Oda and Fukuda, 2012). In *Arabidopsis*, a boundary of the ROP domain (BDR1) and Wallin (WAL) complex regulates cell wall development. BDR1 could recruit WAL to the plasma membrane and then regulate an ROP-act in a pathway to shape pit boundaries (Sugiyama et al., 2019). Rab GTPase has also been shown to play important roles in SCW deposition. Overexpression of a constitutively active mutant of *RabG3b* (RabG3bCA) stimulated both autophagy and tracheary element formation in *Arabidopsis* (Kwon et al., 2010) and increased xylem growth due to the stimulation of autophagy during xylem development in *Populus* (Kwon et al., 2011).

The Rab family in plants is categorized into eight subfamilies (RabA-RabH) (Vernoud et al., 2003). We found out that there was a total of 67 *PtRab* genes in *Populus trichocarpa* and were grouped into eight subfamilies (Zhang et al., 2018b). Most of the *PtRab* genes were preferentially expressed in phloem and xylem. During the development of the poplar stem, the majority of *PtRabs* were preferentially expressed in the transition region from primary growth to secondary growth. These results suggested that the *PtRab* genes might participate in the biological processes related to xylem development. In this study, we explored the function of *PagRabE1b* in xylem development using transgenics overexpressing constitutively active mutant and native *PagRabE1b*, which revealed that *PagRabE1b* influenced both SCW biosynthesis and final PCD during wood formation.

MATERIALS AND METHODS

Plant Materials and Growth Conditions

Hybrid poplar (*Populus alba* × *Populus glandulosa*, *Pag*) clone 84 K was used for gene transformation. Plants were cultivated for 4 weeks under *in vitro* conditions and then transplanted to the soil and grown for 12 weeks in a greenhouse (16-h light: 8-h dark, 25°C: 20°C, with relative humidity in the range 50–60%).

Vector Construction and Plant Transformation

PagRabE1b and *PagRabE1b* (Q74L) (point mutation of Q74 to L in motif 2, a constitutively active form of *PagRabE1b*) genes were cloned into the pMDC32 plant expression vector and transformed into poplars previously (Zhang et al., 2018b). Two overexpression lines of *PagRabE1b* and *PagRabE1b* (Q74L) with high expression levels were selected and named as OE-1 and OE-9 for *PagRabE1b* and QL-8 and QL-13 for *PtRabE1b* (Q74L), respectively.

Histological Analyses

The basal stems of wild type (WT), OE-1, OE-9, QL-8, and QL-13 plants were sectioned for histology using a vibratome (VT1000S; Leica, Wetzlar, Germany) to a thickness of 50 μm. Then, the sections were stained with 0.05% toluidine blue (TBO) for 60 s at room temperature, rinsed three times in water, and photographed with an Olympus BX51 microscope (Du et al., 2020).

Wall Thickness Measurement

Secondary cell wall thickness was observed by using confocal laser scanning microscopy (CLSM) and transmission electron microscopy (TEM). The 15th internodes of 2-month-old WT and *PagRabE1b* transgenic plants were sectioned using a vibratome at a thickness of 50 μm. CLSM pictures were captured with an LSM880 microscopy (Zeiss) using 488-nm laser excitation (5% power). TEM observation was implemented as described by Zhao et al. (2020). The 20th internodes from 3-month-old WT and transgenic plants were cut into 2-mm pieces, which were fixed using 2.5% paraformaldehyde and 0.5% glutaraldehyde in PBS (0.1 M, pH 7.4) with vacuum infiltration. The pieces were then washed three times with 0.1 M PBS and further fixed in 1% osmic acid for 2 h at room temperature. Ultrathin sections were made and photographed using an HT-7700 microscope (Hitachi) and a Gatan *ORIUS*^{TM} *SC*1000CCD Camera (Gatan Inc., USA). The cell wall thickness of at least 100 cells from three individual plants of each line was measured using ImageJ software and analyzed statistically using Student's *t*-test.

Analysis of SCW Composition

The 10th to 20th internodes of 3-month-old WT and *PagRabE1b* transgenic plants were collected and freeze-dried at −60°C on a vacuum freeze. The dried stems were powdered by ball milling and used to measure alcohol-insoluble residues according to Zhao et al. (2020). The monosaccharide content was analyzed through GC-MS (Agilent, Santa Clara,

CA, USA). Three biological replicates were analyzed for each line.

Programmed Cell Death Analysis of Stem-Differentiating Xylem Protoplasts

The *Populus* protoplasts from SDX isolation were carried out as previously described by Lin et al. (2013)and Wang et al. (2020) with minor modifications. Briefly, the debarked stem segments of 3-month-old WT and *PagRabE1b* transgenic poplars were incubated in a cell wall digestion enzyme solution [1.5% (wt/vol) Cellulase R-10 and 0.4% (wt/vol) pectolyase Y-23 in 20-mM MES,0.6-M mannitol and 20-mM KCl solution, 10-mM $CaCl_2$, and 0.1% (wt/vol) BSA, pH 5.7] for 40 min in the dark at room temperature. Protoplasts were filtered through a 70-μm cell strainer and spun down at 150 × g for 5 min. Protoplasts were resuspended in W5 solution (2-mM MES, pH 5.7, 125-mM $CaCl_2$, 154-mM NaCl, 0.1-M glucose, and 5-mM KCl). The isolated protoplasts were resuspended in a 195-μl prediluted binding buffer, and 5-μl Annexin V-FITC solution (Solarbio, Beijing, China) was added, mixed, and incubated for 30 min at room temperature, and then added 1 μl of the 20-μg ml^{-1} propidium iodide (PI) storage solution. After the addition of another 300-μl binding buffer, the suspended protoplasts were analyzed using a BD Aria SORP cell sorter (BD Biosciences, USA) with 488-nm excitation for FITC and 530 nm for PI. Three independent sets of experiments were performed.

Gene Expression Analysis

The apex, stems, and roots were harvested from 8-week-old poplars and were sampled for quantitative reverse transcription PCR (qRT-PCR). For sampling, the xylem and phloem–cambium tissues from stems of 8-week-old poplar were debarked and scraped with a sterile double-edged razor blade from the outer of the debarked stem or the inner surface of the peeled bark. To examine the expression levels of marker genes involved in xylem development by qRT-PCR, 2-month-old WT and *PagRabE1b* transgenic plants were debarked, and developing xylems were scraped. Total RNA was extracted from all the samples using the RNeasy Plant Mini Kit (Qiagen, Hilden, Germany) and genomic DNA was eliminated with the on-column treatment of RNase-free DNase I (Qiagen, Hilden, Germany). First-strand complementary DNA (cDNA) was synthesized with about 1-μg RNA using the SuperScript III reverse transcription kit (Invitrogen) according to the instruction of the manufacturer. Primers with annealing temperatures of 58–60°C and amplification lengths of 100–250 bp were designed using Primer3 software (http://primer3.ut.ee/). All primers were listed in **Supplementary Table 1**. qRT-PCR was carried out using KAPA SYBR FAST qPCR master mixture on Roche LightCycler 480 (Roche Applied Science, Penzberg, Upper Bavaria, Germany) according to the instructions of the manufacturer. All experiments were performed in three biological replicates and three technical replicates. The *PagActin* gene (Potri.001G309500) was used as the internal control (Wang et al., 2016; Zhao et al., 2020).

RESULTS

Expression Pattern of *PagRabE1b*

To investigate the expression pattern of *PagRabE1b*, qRT-PCR was used to analyze the gene expression in tissues collected from the apex, stems, and roots. The results revealed that *PagRabE1b* expression could be detected in all the tissues and was high in xylem and phloem–cambium (**Figure 1A**). A similar expression pattern was also observed by analysis of the AspWood database (http://aspwood.popgenie.org) (Sundell et al., 2017), which showed that *PagRabE1b* is highly expressed in expanding xylem (**Figure 1B**). These results suggested a potential role of *PagRabE1b* in xylem development in poplar.

Overexpression of *PagRabE1b* Promotes Xylem Development in Transgenic Poplar

Mutation of particular residues of small GTPases can generate constitutively active forms, which can be used to explore Rab functions. Overexpression of constitutively active RabG3b stimulated autophagy and increased xylem development in *Arabidopsis* and *Populus* (Kwon et al., 2010, 2011). To elucidate the function of *PagRabE1b* in xylem development, transgenic poplars with *PagRabE1b* and *PagRabE1b* (Q74L) overexpression were generated under the control of the CaMV 35S promoter. Two independently transgenic lines (OE-1, OE-9) with higher expression of *PagRabE1b* and two lines with overexpressing a constitutively active form of *PagRabE1b* (Q74L) (QL-8, QL-13) (Zhang et al., 2018b) were selected for further analysis (**Figures 2A,B**). All WT and transgenic lines were grown in the greenhouse under the same environmental conditions. Compared with the WT, 2-month-old transgenic plants of *PagRabE1b* and *PagRabE1b* (Q74L) exhibited rapid growth and development (**Figure 2A**). Quantitative measurement of the growth rate and basal stem diameter showed that *PagRabE1b* transgenic plants had a 20.3–28.9% increase in the growth rate and an 11.8–26.5% increase in stem width compared with wild-type plants (**Figures 2C,D**). To examine whether the xylem development was altered in *PagRabE1b* transgenic poplars, cross-sections of basal stems from 3-month-old WT and *PagRabE1b* transgenic lines were analyzed. Compared with the WT, xylem width was significantly increased in all *PagRabE1b* overexpression lines (**Figure 3A**). Quantitative analysis showed that the xylem radial width was increased by 27–50% in *PagRabE1b* transgenic plants compared with WT plants (**Figure 3B**). All these results suggested that *PagRabE1b* may play critical roles in regulating poplar secondary growth and xylem development.

PagRabE1b Overexpression Affects SCW Deposition

Several studies have suggested that RabGTPase has positive roles in the controlling of SCW development. Therefore, we first examined the SCW structure by lignin autofluorescence using CLSM. The results showed that lignification and SCW deposition were increased in *PagRabE1b* transgenic plants than in WT (**Supplementary Figure 1**). Then, transverse-sections of the 20th internode of 3-month-old transgenic plants were used to

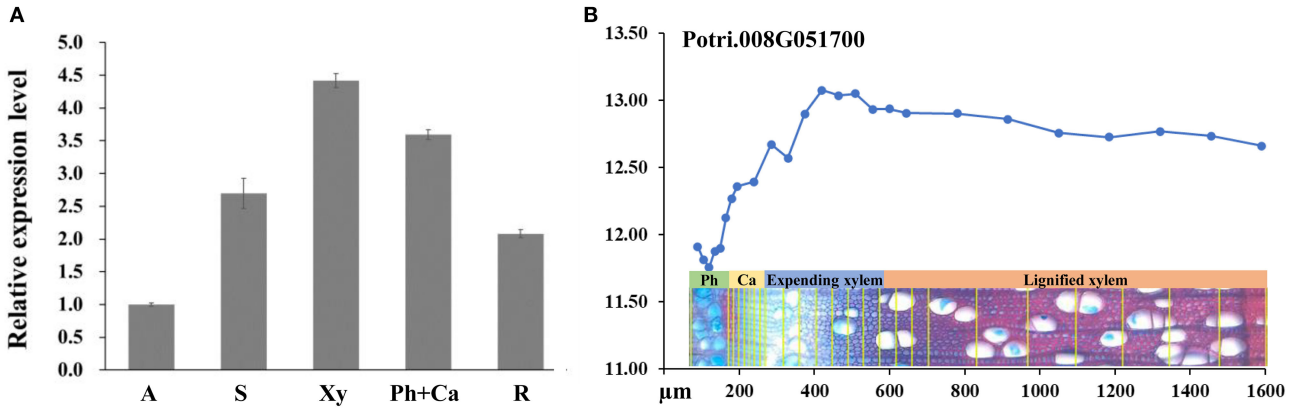

FIGURE 1 | Expression patterns of *PagRabE1b* in poplar. **(A)** Quantitative reverse transcription PCR (qRT-PCR) was carried out to analyze the gene expression levels of *PagRabE1b* indifferent tissues of poplar. The *actin* gene was used as an internal control. **(B)** Expression profiles of *PagRabE1b* among developing phloem, cambium, and developing xylem. Data were derived from the AspWood database (http://aspwood.popgenie.org) (Sundell et al., 2017). A, apex; S, stem; Xy, xylem; Ph, phloem; Ca, cambium; R, root.

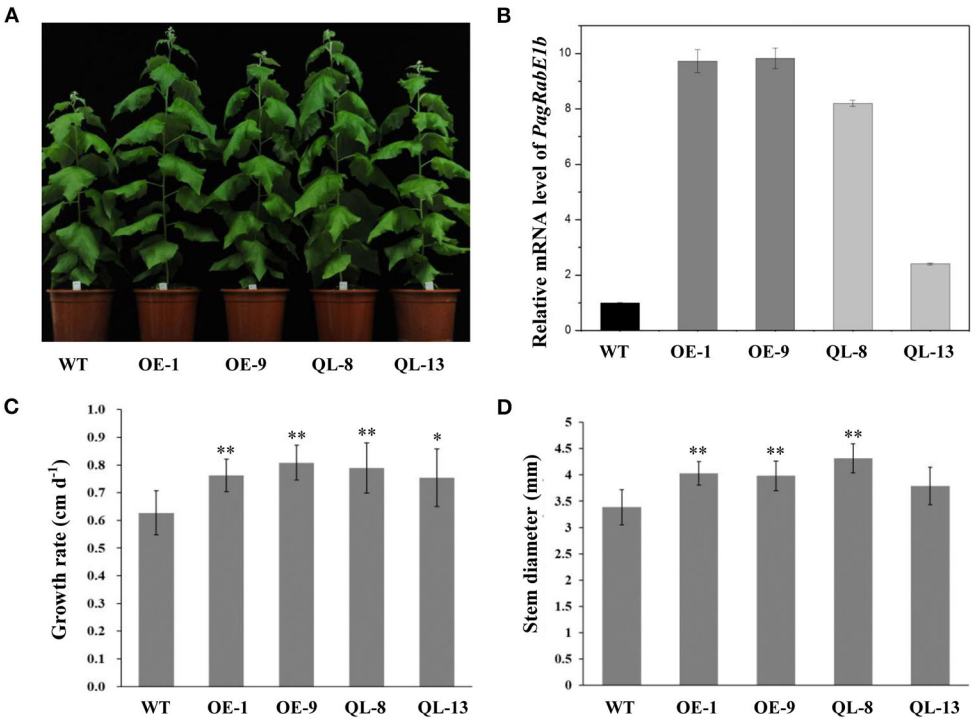

FIGURE 2 | Growth phenotypes of *PagRabE1b* transgenic poplars compared with wild type (WT). **(A)** A photograph of WT and *PagRabE1b* overexpression lines. Bar = 10 cm; **(B)** qRT-PCR analyses of the transcript levels of *PagRabE1b* in WT, OE-1, OE-9, QL-8, and QL-13 lines. **(C,D)** The growth rate and basal diameter of 3-month-old WT, OE-1, OE-9, QL-8, and QL-13 lines. The growth rate and diameter: means ± SD of six clonally propagated plants. Student's *t*-test; $^{*}P < 0.05$; $^{**}P < 0.01$.

examine the SCW structure using TEM. The results showed that the cell walls of xylem fiber cells were thicker in all *PagRabE1b* overexpression plants than in WT plants (**Figure 3C**). Statistical analysis showed that the SCW thickness of xylem fibers was increased by 10.2, 23.5, 17.65, and 13.1 in-OE-1, OE-9, QL-8, and QL-13 plants, respectively (**Figure 3D**).

The differences in SCW thickness may indicate changes in cell wall composition, and therefore, we determined the chemical components of the SCWs using the stem of wild-type and transgenic plants. Overexpression of *PagRabE1b* appeared to have a remarkable effect on monosaccharide contents. The contents of glucose and galactose were significantly increased in all transgenic plants compared with WT. Among these, the content of glucose was increased by 36.1–170% in *PagRabE1b* and *PagRabE1b* (Q74L) overexpression lines than in WT. In addition, the contents of fructose, arabinose,

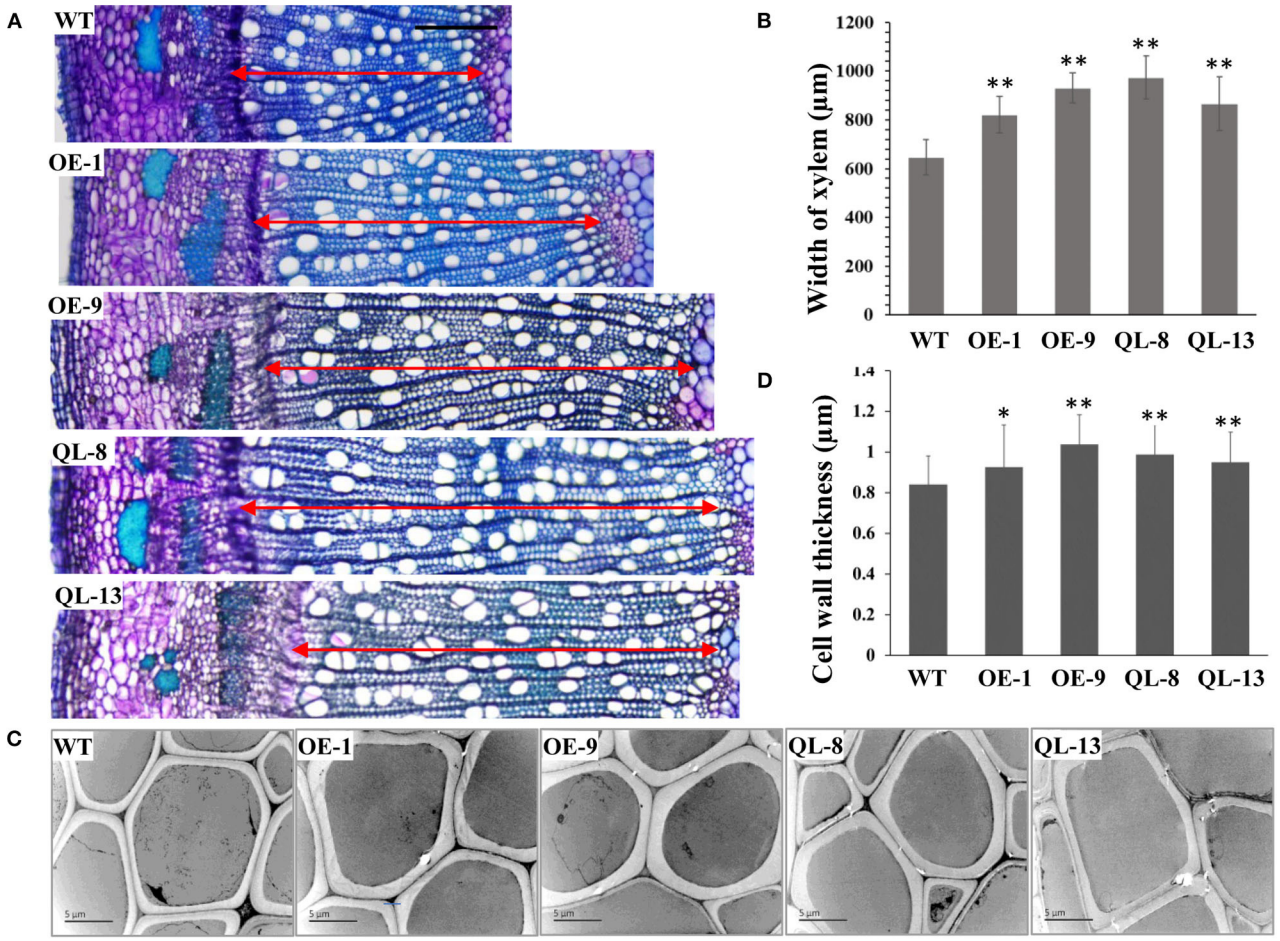

FIGURE 3 | Xylem development was increased by *PagRabE1b* overexpression. **(A)** Transverse sections of the basal stems of 3-month-old WT, OE-1, OE-9, QL-8, and QL-13 plants. Bar = 200 μm; **(B)** Transmission electron microscopy (TEM) examination of the cell wall thickness of xylem fiber cells in 3-month-old WT, OE-1, OE-9, QL-8, and QL-13. Bar = 5 μm. **(C)** Statistical analysis of xylem width in the stems of WT, OE-1, OE-9, QL-8, and L-13 lines. **(D)** Statistical analysis of the cell wall thickness of WT, OE-1, OE-9, QL-8, and QL-13 lines. Student's *t*-test; $^{*}P < 0.05$; $^{**}P < 0.01$.

mannose, xylose, and galactose were significantly increased in the *PagRabE1b*or *PagRabE1b* (Q74L) transgenic lines compared with WT (**Figure 4**). These results suggest that *PagRabE1b* positively regulates secondary wall biosynthesis in *Populus*.

PagRabE1b Promotes the PCD Process in Xylem Formation

Programmed cell death is a pivotal step in xylem formation and is required for the complete maturation of both TEs and fiber cells during xylem development. To investigate the differences of PCD between *PagRabE1b* transgenic and WT plants, protoplasts were isolated from the SDX and analyzed by flow cytometry. Loss of plasma membrane irregularity is one of the earliest characteristics in PCD with exposing phospholipid phosphatidylserine (PS) to the exterior cellular environment. FITC-conjugated Annexin V has a high affinity with PS and acts as a sensitive probe for flow cytometric analysis of the early stage of PCD (O'brien et al., 1998). PI is commonly used to detect dead cells in a population since it is not permeant to live cells. Flow cytometry assay showed that the proportion of apoptotic cells was significantly different in WT and *PagRabE1b* transgenic plants. WT plants contained the lowest percentage (34.3%) of FITC positive cells, while PagRabE1bOE-9 and PagRabE1bQL-8 plants had the higher percentage (56.0 and 45.9%, respectively), of FITC positive cells (**Figure 5**). Similar to the FITC staining, PagRabE1bOE-9, and PagRabE1bQL-8 plants displayed a significant increase in PI-positive cells (41.5 and 34.8%, respectively), compared with WT plants (20.5%) (**Figure 5**). This result indicates that *PagRabE1b* has a positive role in PCD during xylem development.

Expression Analysis of Xylem Development-Related Genes

Since manipulation of *PagRabE1b* expression resulted in changes in SCW thickness and PCD of xylem cells, we examined the expression of key genes involved in wood formation by qRT-PCR. As expected, xylem differentiation- and secondary wall

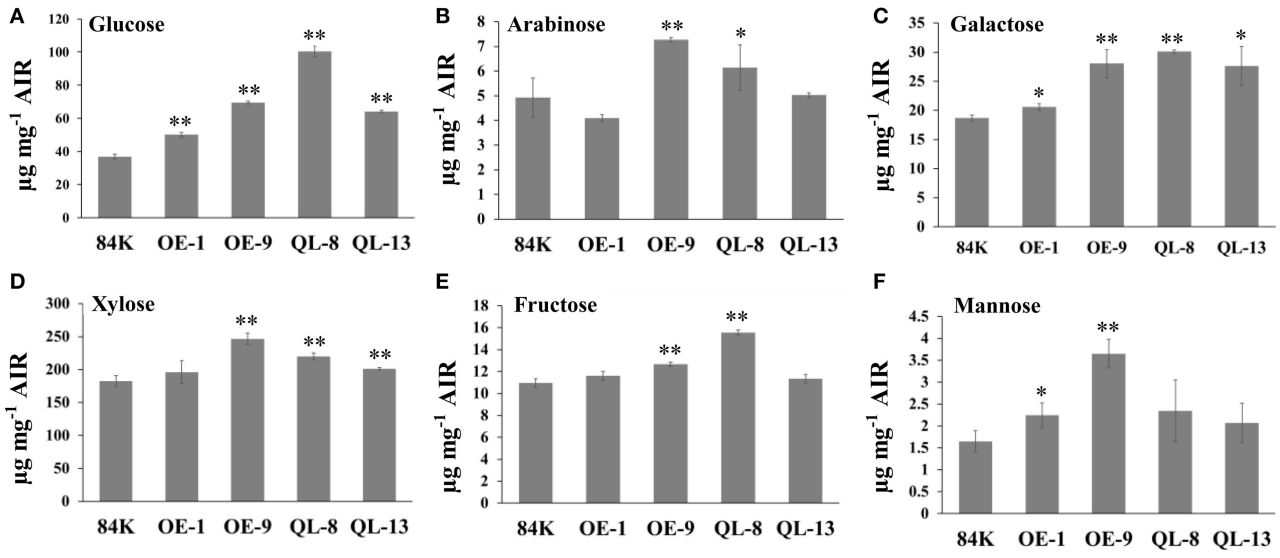

FIGURE 4 | *PagRabE1b* promotes accumulation of monosaccharide content in secondary xylem tissues of transgenic plants. **(A)** Glucose; **(B)** arabinose; **(C)** galactose; **(D)** xylose; **(E)** fructose; **(F)** mannose. Student's *t*-test; $^{*}P < 0.05$; $^{**}P < 0.01$.

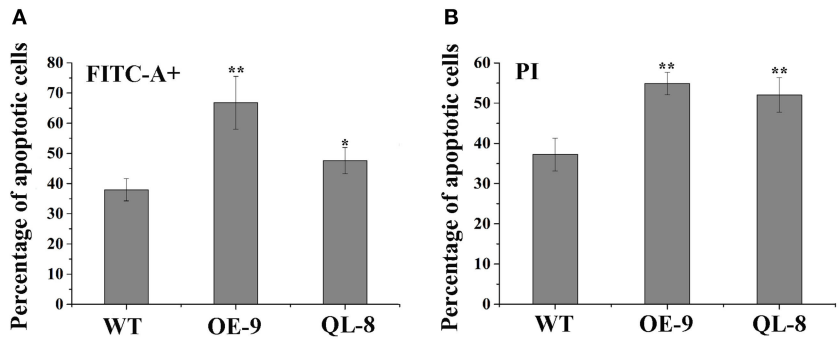

FIGURE 5 | Flow cytometry analyses of the protoplasts from poplar stem-differentiating xylem (SDX) stained with **(A)** annexin V-FITC and **(B)** propidium iodide (PI). Results are means ± SD of three biological replicates. Student's *t*-test; $^{*}P < 0.05$; $^{**}P < 0.01$.

regulation-related NAC and MYB genes, such as *SND1-A1* (ortholog of *AtSND1*), *VND6-C1* (*AtVND6*), *MYB21* (*AtMYB46* and *AtMYB83*), *MYB031* (*AtMYB69*), *MYB090* (*AtMYB52* and *AtMYB54*), *MYB127* (*AtMYB67*), and *MYB128* (*AtMYB103*), were upregulated (**Figure 6**, **Supplementary Figure 2**). SCW synthesis-related genes containing homologs of *Arabidopsis CESA4*, *CESA7*, CESA8, *LAC4*, and *LAC17* were also upregulated. Additionally, we also examined the expression levels of PCD-related genes (*Peroxidase*, *VPE*, *MC9ATG8d1*, *ATG8f2*, and *ATG8i*) (Kwon et al., 2011) (**Figure 6**, **Supplementary Figure 2**). All these genes were upregulated in OE-1, OE-9, QL-8, and QL-13 plants. These results suggest that *PagRabE1b* overexpression can activate the expression of wood formation-related genes in transgenic plants.

DISCUSSION

Wood formation is a complicated biological process, including the division and differentiation of the vascular cambium, cell elongation, SCW deposition, and PCD. Although the transcriptional regulatory network was outlined on the SCW synthesis of xylem cells (Zhang et al., 2018a), the precise regulatory mechanisms of xylem cell differentiation during xylem formation remain elusive. Previous research suggests that small GTPases may activate autophagy during wood formation (Kwon et al., 2011), other than regulate SCW development in the xylem of higher plants (Oda and Fukuda, 2014). Therefore, in this study, we further investigated the function of *PagRabE1b* in xylem development in poplar.

Eight of the 11 ROP genes in *Arabidopsis* were expressed in xylem tissues (Winter et al., 2007). In poplar, more than half of the *PtRab* genes were highly expressed in phloem and xylem (Zhang et al., 2018b). In this study, the qRT-PCR analysis showed that *PagRabE1b* was highly expressed in xylem and phloem–cambium (**Figure 1**). Similarly, the *Eucalyptus* ROP GTPase gene was found preferentially expressed in the cambium area and developing xylem (Foucart et al., 2009). Since cambium includes newly differentiating xylem cells (close to developing xylem) with

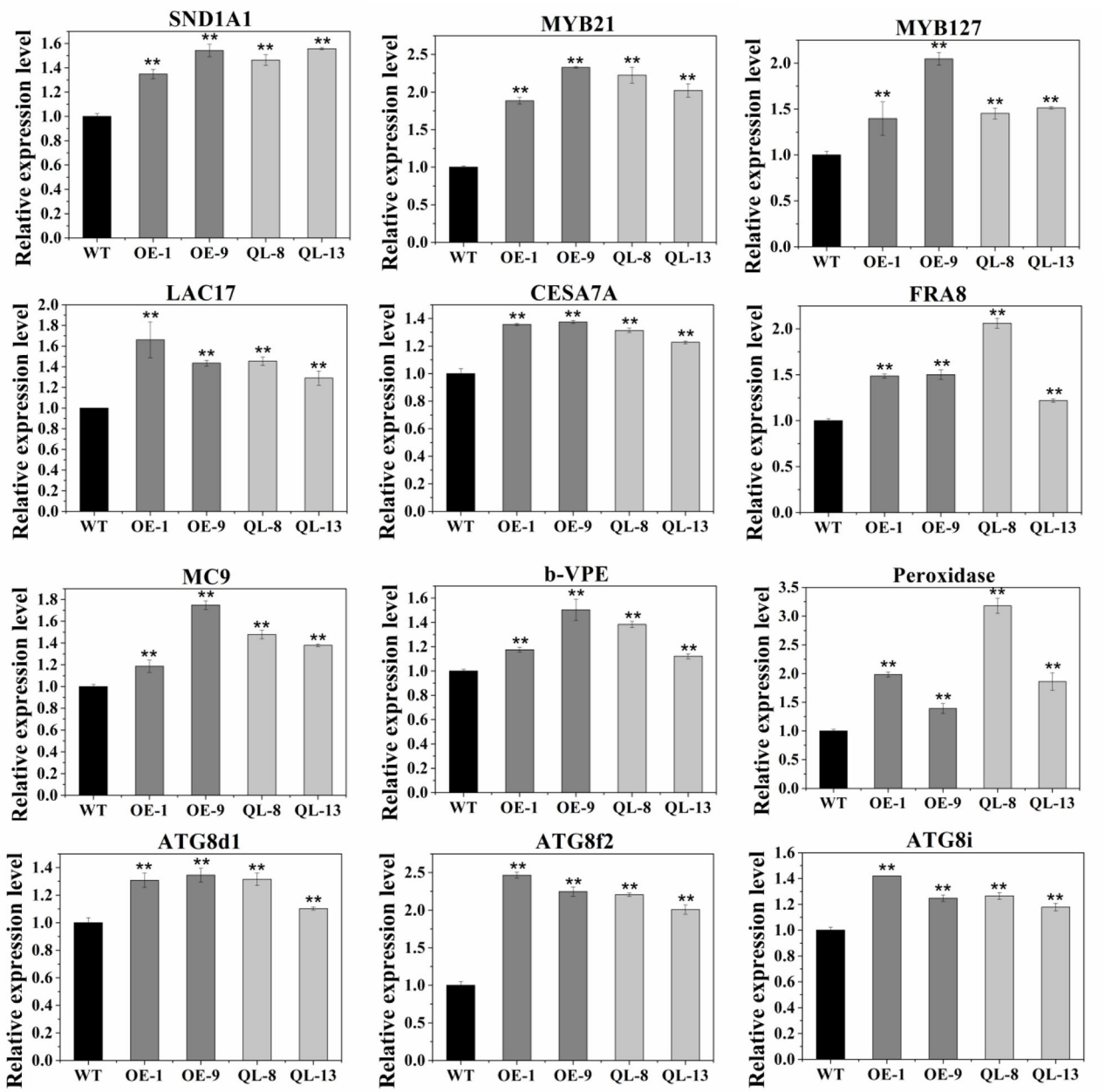

FIGURE 6 | Expression analysis of xylem development-related genes in WT, OE-1, OE-9, QL-8, and QL-13 lines. The poplar actin gene was used as an internal control. Results are means ± SD of three biological replicates. Student's *t*-test; $^{**}P < 0.01$.

higher expression than other cell types as shown in **Figure 1**, we propose that the involvement of *PagRabE1b* gene in the process of xylem development.

To investigate the role of *RabE1b* in woody plants, transgenic poplars overexpressing *PagRabE1b* were generated. The overexpression of *PagRabE1b* leads to an increase in both plant length and stem thickness in poplar (**Figure 2**). These phenotypic alterations are similar to that with *Arabidopsis RabG3b* overexpression (Kwon et al., 2011). In contrast, the reduced plant size and drastically altered leaf morphology were observed in the *Arabidopsis RabE1d* downregulated transgenic plants (Speth et al., 2009). In addition, virus-induced gene silencing of *NbRabE1* caused various phenotypes, such as growth retardation, premature senescence, and aberrant leaf development (Ahn et al., 2013). These results prove that Rab GTPase plays a pivotal role in plant growth and development.

Phenotypic examination revealed that overexpression of *PagRabE1b* enhanced SCW thickness of fiber cells in poplar stems (**Figure 3**). Chemical components measurement showed an increase in cell wall constituents in the stems of transgenic

plants (**Figure 4**). To better explain these phenotypes, we used qRT-PCR analyses and found that the expression of marker genes involved in xylem differentiation, cell wall synthesis, and PCD was upregulated in *PagRabE1b* OE plants (**Figure 6**). The NAC TFs, including SND1 and VND6, were considered as master switches (Zhang et al., 2018b) their orthologs PtrVND6 and PtrSND1 function together for reciprocal cross-regulation of xylem development in poplar (Lin et al., 2017). MYB46 and MYB83 were made up of the second layer of the regulatory network of SCW biosynthesis (Zhang et al., 2018a). Upregulation of which genes increased the biosynthesis of lignin, cellulose, and xylan, and led to the ectopic deposition of SCW (McCarthy et al., 2009; Chai et al., 2014). *LAC17*, *CESA4A*, *CESA7A*, and *FRA8* were the enzymes that catalyzed the synthesis of lignin and cellulose. These data indicated that *PagRabE1b* plays a role in xylem differentiation at a higher level, rather than its function in mediating secretory vesicle transportation from the Golgi to the PM to provide substrates for SCW synthesis.

Programmed cell death occurs in the final stage during xylem cell development, which is essential to form empty, water-conducting tracheids or vessels through autolytic processes (Fukuda, 2000). In poplar, autophagosome- and autolysosome-like structures were observed in developing xylem cells in WT, and more accumulation was detected in RabG3bCA overexpression plants (Kwon et al., 2011). In this study, three autophagy-related genes, *ATG8d1*, *ATG8f2*, and *ATG8i* (Courtois-Moreau et al., 2009), and three PCD-related genes, *peroxidase*, *VPE*, and *MC9*, were highly expressed in growing stems of *PagRabE1b* OE plants (**Figure 6**). Flow cytometry analysis showed that the number of apoptotic cells in overexpression transgenic materials was more than that of WT. All these results suggest that *PagRabE1b* positively affects the whole xylem differentiation process, including the final cell lysisin poplar.

In conclusion, the study provided evidence that *PagRabE1b* acts as a positive factor for xylem differentiation and secondary wall formation. This finding provides new information on understanding the regulatory network of wood formation in woody plants.

DATA AVAILABILITY STATEMENT

The original contributions presented in the study are included in the article/**Supplementary Material**, further inquiries can be directed to the corresponding author/s.

AUTHOR CONTRIBUTIONS

S-TZ conceived and designed the experiments. Y-LL, L-JW, YL, Y-HG, and YC performed the experiments. Y-LL and S-TZ wrote the manuscript. All authors contributed to the article and approved the submitted version.

FUNDING

This work was supported by the National Nonprofit Institute Research Grant of CAF (CAFYBB2012039) and the National Key Program on Transgenic Research (2018ZX08020002).

ACKNOWLEDGMENTS

We thank Dr. Meng-Zhu Lu (Zhejiang Agriculture and Forestry University) and Dr. Jin Zhang (Zhejiang Agriculture and Forestry University) for the critical reading and revision of the manuscript. We thank the flow cytometry Core at National Center for Protein Sciences at Peking University for technical help.

SUPPLEMENTARY MATERIAL

The Supplementary Material for this article can be found online at: https://www.frontiersin.org/articles/10.3389/fpls.2021.686024/full#supplementary-material

Supplementary Figure 1 | The microscopic images by confocal laser scanning microscopy (CLSM) of Rab transgenic poplars and wild type (WT). **(A,B)** WT; **(C)** OE-1; **(D)** OE-9; **(E)** QL-8; **(F)** QL-13.

Supplementary Figure 2 | Quantitative reverse transcription PCR (qRT-PCR) analysis of xylem development-related genes in WT and transgenic lines. The poplar act in the gene was used as an internal control. Results are means ± SD of three biological replicates. Student's *t*-test; $^{*}P < 0.05$; $^{**}P < 0.01$.

Supplementary Table 1 | List of primers used in this study.

REFERENCES

Ahn, C. S., Han, J. A., and Pai, H. S. (2013). Characterization of in vivo functions of *Nicotiana benthamianaRabE1*. *Planta* 237, 161–172. doi: 10.1007/s00425-012-1760-5

Boerjan, W., Ralph, J., and Baucher, M. (2003). Lignin biosynthesis. *Annu. Rev. Plant Biol.* 54, 519–546. doi: 10.1146/annurev.arplant.54.031902.134938

Chai, G., Qi, G., Cao, Y., Wang, Z., Yu, L., Tang, X., et al. (2014). Poplar *PdC3H17* and *PdC3H18* are direct targets of *PdMYB3* and *PdMYB21*, and positively regulate secondary wall formation in *Arabidopsis* and poplar. *New Phytol.* 203, 520–534. doi: 10.1111/nph.12825

Courtois-Moreau, C. L., Pesquet, E., Sjodin, A., Muniz, L., Bollhoner, B., Kaneda, M., et al. (2009). A unique program for cell death in xylem fibers of *Populus* stem. *Plant J.* 58, 260–274. doi: 10.1111/j.1365-313X.2008.03777.x

Du, J., Gerttula, S., Li, Z., Zhao, S. T., Liu, Y. L., Liu, Y., et al. (2020). Brassinosteroid regulation of wood formation in poplar. *New Phytol.* 225, 1516–1530. doi: 10.1111/nph.15936

Foucart, C., Jauneau, A., Gion, J. M., Amelot, N., Martinez, Y., Panegos, P., et al. (2009). Overexpression of *EgROP1*, a *Eucalyptus* vascular-expressed Rac-like small GTPase, affects secondary xylem formation in *Arabidopsis thaliana*. *New Phytol.* 183, 1014–1029. doi: 10.1111/j.1469-8137.2009.02910.x

Fukuda, H. (2000). Programmed cell death of tracheary elements as a paradigm in plants. *Plant Mol. Biol.* 44, 245–253. doi: 10.1007/978-94-010-0934-8_1

Hall, A. (1998). Rho GTPases and the actin cytoskeleton. *Science* 279, 509–514. doi: 10.1126/science.279.5350.509

Kwon, S. I., Cho, H. J., Jung, J. H., Yoshimoto, K., Shirasu, K., and Park, O. K. (2010). The Rab GTPase RabG3b functions in autophagy and contributes to tracheary element differentiation in *Arabidopsis*. *Plant J.* 64, 151–164. doi: 10.1111/j.1365-313X.2010.04315.x

Kwon, S. I., Cho, H. J., Lee, J. S., Jin, H., Shin, S. J., Kwon, M., et al. (2011). Overexpression of constitutively active *Arabidopsis* RabG3b promotes xylem development in transgenic poplars. *Plant Cell Environ.* 34, 2212–2224. doi: 10.1111/j.1365-3040.2011.02416.x

Lin, Y. C., Li, W., Sun, Y. H., Kumari, S., Wei, H., Li, Q., et al. (2013). SND1 transcription factor-directed quantitative functional hierarchical genetic regulatory network in wood formation in *Populus trichocarpa*. *Plant Cell* 25, 4324–4341. doi: 10.1105/tpc.113.117697

Lin, Y. J., Chen, H., Li, Q., Li, W., Wang, J. P., Shi, R., et al. (2017). Reciprocal cross-regulation of VND and SND multigene TF families for wood formation in *Populus trichocarpa*. *Proc. Natl. Acad. Sci. U.S.A.* 114, E9722–E9729. doi: 10.1073/pnas.1714422114

McCarthy, R. L., Zhong, R., and Ye, Z. H. (2009). MYB83 is a direct target of SND1 and acts redundantly with MYB46 in the regulation of secondary cell wall biosynthesis in *Arabidopsis*. *Plant Cell Physiol.* 50, 1950–1964. doi: 10.1093/pcp/pcp139

O'brien, I. E. W., Baguley, B. C., Murray, B. G., Morris, B. A. M., and Ferguson, I. B. (1998). Early stages of the apoptotic pathway in plant cells are reversible. *Plant J.* 13, 803–814. doi: 10.1046/j.1365-313X.1998.00087.x

Oda, Y., and Fukuda, H. (2012). Initiation of cell wall pattern by a Rho- and microtubule-driven symmetry breaking. *Science* 337, 1333–1336. doi: 10.1126/science.1222597

Oda, Y., and Fukuda, H. (2014). Emerging roles of small GTPases in secondary cell wall development. *Front. Plant Sci.* 5:428. doi: 10.3389/fpls.2014.00428

Scheller, H. V., and Ulvskov, P. (2010). Hemicelluloses. *Annu. Rev. Plant Biol.* 61, 263–289. doi: 10.1146/annurev-arplant-042809-112315

Speth, E. B., Imboden, L., Hauck, P., and He, S. Y. (2009). Subcellular localization and functional analysis of the *Arabidopsis* GTPase RabE. *Plant Physiol.* 149, 1824–1837. doi: 10.1104/pp.108.132092

Sugiyama, Y., Nagashima, Y., Wakazaki, M., Sato, M., Toyooka, K., Fukuda, H., et al. (2019). A Rho-actin signaling pathway shapes cell wall boundaries in *Arabidopsis* xylem vessels. *Nat. Commun.* 10:468. doi: 10.1038/s41467-019-08396-7

Sundell, D., Street, N. R., Kumar, M., Mellerowicz, E. J., Kucukoglu, M., Johnsson, C., et al. (2017). AspWood: high-spatial-resolution transcriptome profiles reveal uncharacterized modularity of wood formation in *Populus tremula*. *Plant Cell* 29, 1585–1604. doi: 10.1105/tpc.17.00153

Vernoud, V., Horton, A. C., Yang, Z., and Nielsen, E. (2003). Analysis of the small GTPase gene superfamily of *Arabidopsis*. *Plant Physiol.* 131, 1191–1208. doi: 10.1104/pp.013052

Wang, J. P., Matthews, M. L., Williams, C. M., Shi, R., Yang, C., Tunlaya-Anukit, S., et al. (2018). Improving wood properties for wood utilization through multi-omics integration in lignin biosynthesis. *Nat. Commun.* 9:1579. doi: 10.1038/s41467-018-03863-z

Wang, Y., Chen, Y., Ding, L., Zhang, J., Wei, J., and Wang, H. (2016). Validation of reference genes for gene expression by quantitative real-time RT-PCR in stem segments spanning srimary to secondary srowth in *Populus tomentosa*. *PLoS ONE*11:e0157370. doi: 10.1371/journal.pone.0157370

Wang, Z., Mao, Y., Guo, Y., Gao, J., Liu, X., Li, S., et al. (2020). MYB transcription factor161 mediates feedback regulation of secondary wall-associated NAC-Domain1 family genes for wood formation. *Plant Physiol.* 184, 1389–1406. doi: 10.1104/pp.20.01033

Winter, D., Vinegar, B., Nahal, H., Ammar, R., Wilson, G. V., and Provart, N. J. (2007). An "Electronic Fluorescent Pictograph" browser for exploring and analyzing large-scale biological data sets. *PLoS ONE* 2:e718. doi: 10.1371/journal.pone.0000718

Xie, M., Zhang, J., Tschaplinski, T. J., Tuskan, G. A., Chen, J. G., and Muchero, W. (2018). Regulation of lignin biosynthesis and its role in growth-defense tradeoffs. *Front. Plant. Sci.* 9:1427. doi: 10.3389/fpls.2018.01427

Zhang, J., Li, Y., Liu, B., Wang, L., Zhang, L., Hu, J., et al. (2018b). Characterization of the *PopulusRab* family genes and the function of *PtRabE1b* in salt tolerance. *BMC Plant Biol.* 18:124. doi: 10.1186/s12870-018-1342-1

Zhang, J., Serra, J. A. A., and Helariutta, Y. (2015). Wood development: growth through knowledge. *Nat. Plants* 1:15060. doi: 10.1038/nplants.2015.60

Zhang, J., Xie, M., Tuskan, G. A., Muchero, W., and Chen, J. G. (2018a). Recent advances in the transcriptional regulation of secondary cell wall biosynthesis in the woody plants. *Front. Plant Sci.* 9:1535. doi: 10.3389/fpls.2018.01535

Zhao, Y., Song, X., Zhou, H., Wei, K., Jiang, C., Wang, J., et al. (2020). *KNAT2/6b*, a class I KNOX gene, impedes xylem differentiation by regulating NAC domain transcription factors in poplar. *New Phytol.* 225, 1531–1544. doi: 10.1111/nph.16036

Zhong, R. Q., and Ye, Z. H. (2015). Secondary cell walls: biosynthesis, patterned deposition and transcriptional regulation. *Plant Cell Physiol.* 56, 195–214. doi: 10.1093/pcp/pcu140

Conflict of Interest: The authors declare that the research was conducted in the absence of any commercial or financial relationships that could be construed as a potential conflict of interest.

frontiers in Plant Science

ORIGINAL RESEARCH
published: 25 June 2021
doi: 10.3389/fpls.2021.695223

BEL1-like Homeodomain Protein BLH6a Is a Negative Regulator of *CAld5H2* in Sinapyl Alcohol Monolignol Biosynthesis in Poplar

Qiao Wang[1,2†], *Xinren Dai*[1†], *Hongying Pang*[1†], *Yanxia Cheng*[1], *Xiong Huang*[1,2], *Hui Li*[1], *Xiaojing Yan*[1], *Fachuang Lu*[3], *Hairong Wei*[4], *Ronald R. Sederoff*[5] *and Quanzi Li*[1,2*]

[1] State Key Laboratory of Tree Genetics and Breeding, Chinese Academy of Forestry, Beijing, China, [2] Research Institute of Forestry, Chinese Academy of Forestry, Beijing, China, [3] Department of Energy Great Lakes Bioenergy Research Center, Wisconsin Energy Institute, Madison, WI, United States, [4] College of Forest Resources and Environmental Science, Michigan Technological University, Houghton, MI, United States, [5] Forest Biotechnology Group, Department of Forestry and Environmental Resources, North Carolina State University, Raleigh, NC, United States

OPEN ACCESS

Edited by:
Hong Luo,
Clemson University, United States

Reviewed by:
Gilles Pilate,
Institut National de la Recherche Agronomique (INRA), France
Akiyoshi Kawaoka,
Akita Jujo Chemicals Co., Ltd., Japan

***Correspondence:**
Quanzi Li
liqz@caf.ac.cn

[†]These authors have contributed equally to this work

Specialty section:
This article was submitted to Plant Biotechnology, a section of the journal Frontiers in Plant Science

Received: *14 April 2021*
Accepted: *02 June 2021*
Published: *25 June 2021*

Citation:
Wang Q, Dai X, Pang H, Cheng Y, Huang X, Li H, Yan X, Lu F, Wei H, Sederoff RR and Li Q (2021) BEL1-like Homeodomain Protein BLH6a Is a Negative Regulator of CAld5H2 in Sinapyl Alcohol Monolignol Biosynthesis in Poplar. Front. Plant Sci. 12:695223. doi: 10.3389/fpls.2021.695223

Lignin is one of the major components of xylem cell walls in tree stems. The lignin in the wood of most flowering plants (dicotyledonous angiosperms) is typically polymerized from three monolignol precursors, coniferyl alcohol, sinapyl alcohol, and *p*-coumaroyl alcohol, resulting in guaiacyl (G), syringyl (S), and hydroxyphenyl (H) subunits, respectively. In this study, we focus on the transcriptional regulation of a coniferaldehyde 5-hydroxylase (*CAld5H2*) gene, which encodes a key enzyme for sinapyl alcohol biosynthesis. We carried out a yeast one-hybrid (Y1H) screen to identify candidate upstream transcription factors (TFs) regulating *CAld5H2.* We obtained 12 upstream TFs as potential regulators of *CAld5H2.* One of these TF genes, BLH6a, encodes a BEL1-like homeodomain (BLH) protein and negatively regulated the *CAld5H2* promoter activity. The direct regulation of *CAld5H2* promoter by BLH6a was supported by chromatin immunoprecipitation–quantitative polymerase chain reaction (ChIP–qPCR) and dominant repression of BLH6a in transgenic plants. Luciferase complementation imaging analyses showed extensive protein–protein interactions among these 12 TFs. We propose that BLH6a is a negative regulator of *CAld5H2,* which acts through combinatorial regulation of multiple TFs for sinapyl alcohol (S monolignol) biosynthesis in poplar.

Keywords: lignin, *CAld5H2*, BEL1-like homeodomain protein, transcription factor, yeast one hybrid

INTRODUCTION

Lignin is a polyphenolic polymer deposited in the secondary cell walls (SCWs) of vascular plants (Sarkanen and Ludwig, 1971). Many different phenylpropanoid subunits may be incorporated into lignin, but the wood of trees within the angiosperms typically contains three predominant lignin subunits, hydroxyphenyl (H), guaiacyl (G), and syringyl (S), derived from *p*-coumaryl, coniferyl, and sinapyl alcohols, also called monolignols. Lignin composition depends on the relative abundance of monolignols, which are polymerized by radical coupling reactions (Ralph et al., 2004). In angiosperm wood, typically in dicots, lignin is composed primarily of G and S subunits, with minor amounts of H subunits. The proportion of G and S subunits in lignin is different between cell types. Vessel elements are specialized for water transport, and fiber cells provide

mechanical support. In the wood of poplar, guaiacyl lignin is predominant in vessel cell walls, whereas S subunits are mainly located in fiber cell walls (Zhou et al., 2011). In gymnosperms, the mature xylem contains one major type of cell (tracheids), which carries out both support and transport. Tracheid lignin has mainly G subunits with only minor amounts of H subunits in their cell walls (Sarkanen and Ludwig, 1971).

In angiosperms, 11 enzyme families comprise a branched grid-like pathway that converts phenylalanine to three major monolignols (Boerjan et al., 2003; Vanholme et al., 2013) (**Figure 1**). These enzyme families are designated PAL (phenylalanine ammonia-lyase, EC 4.3.1.5), C4H (cinnamate 4-hydroxylase, EC 1.14.13.11), C3H (*p*-coumaroyl-CoA 3-hydroxylase, EC 1.14.14.1), 4CL (*p*-coumarate CoA ligase, EC 6.2.1.12), HCT (hydroxycinnamoyltransferase, EC 2.3.1.133), CSE (caffeoyl shikimate esterase, EC 3.1.1-), CCoAOMT (caffeoyl-CoA *O*-methyltransferase, EC 2.1.1.104), CCR (cinnamoyl-CoA reductase, EC 1.2.1.44), F5H/CAld5H [ferulate/coniferaldehyde 5-hydroxylase (CAld5H2), EC 1.14.13], COMT (caffeic acid 3-*O*-methyltransferase, EC 2.1.1.6), and CAD (cinnamyl alcohol dehydrogenase, EC 1.1.1.95). In this pathway, coniferaldehyde is converted to coniferyl alcohol by CAD for G monolignol production. Alternatively, coniferaldehyde can be converted to sinapyl alcohol in three steps by three consecutive enzymes, CAld5H/F5H, COMT, and CAD. CAld5H/F5H is a key enzyme in directing S lignin production (Osakabe et al., 1999). Overexpression of *F5H* driven by a *C4H* promoter caused an increase (29.5%) in sinapyl alcohol level in hybrid poplar (Stewart et al., 2009).

Many transcription factors (TFs) in the transcriptional network regulating the SCW synthesis have been characterized (Ko et al., 2014). In the top layer of the gene regulatory network (GRN), NAC [no apical meristem (NAM), arabidopsis transcription activator factor (ATAF1/2), and cup-shaped cotyledon (CUC)] and v-myb avian myeloblastosis viral oncogene homolog (MYB) members, such as secondary wall-associated NAC domain protein1/vascular-related NAC-domain6 (SND1/VND6) (Minoru et al., 2005; Zhong et al., 2006) and MYB46/83 (Zhong et al., 2007; McCarthy et al., 2009; Zhong and Ye, 2012), are master regulators activating SCW synthesis. Most TFs in the GRN are activators and a few are repressors, indicating fine-tuning of the transcriptional control in SCW biosynthesis (Ko et al., 2014). Some TFs in the network directly regulate genes encoding pathway enzymes for cellulose, hemicellulose, and lignin biosynthesis (Ohashiito et al., 2010; Kim et al., 2013). The TFs that directly regulate lignin biosynthesis could act to differentially activate or repress lignin pathway genes. For example, MYB46 directly regulates nine of the 10 *Arabidopsis* lignin pathway genes characterized (Ko et al., 2014), whereas MYB58 directly activates all 10 of the *Arabidopsis* lignin pathway genes (Zhou et al., 2009). In Medicago, SND1 directly activates *F5H*, but the SND1 in *Arabidopsis* does not (Zhong et al., 2008; Zhao et al., 2010), indicating that the GRN for SCW synthesis may not be the same in different plant species.

Wood provides large quantities of material for the production of pulp, paper, timber, and lignocellulosic biofuels. For pulp, paper, and chemical feedstock production, lignin is a major barrier to such applications and must be removed. The content, composition, and structure of lignin affect the process efficiency of woody biomass (Studer et al., 2011; Li et al., 2014). Lignin composition, calculated as the S/G ratio, is an important factor affecting the pulp yield than the lignin content (Río et al., 2005; Studer et al., 2011). High pulp yield is correlated with a high S/G ratio (Río et al., 2005). Hardwood is generally delignified more readily than softwood due to the abundance of S subunits in the hardwood lignin (Sarkanen and Ludwig, 1971; Chang and Sarkanen, 1973). Wood with a higher proportion of S subunits is preferred for paper/pulping and biofuel production (Wagner et al., 2015).

The favorable properties of lignin with a higher S subunit content have motivated efforts to increase the S lignin content in wood through genetic modification. Overexpression of *CAld5H* had a 64% increase in the S/G ratio in poplar (Li et al., 2003). Lignin polymers that contain S units have been generated in conifer cells by overexpression of *F5H* in *Pinus radiata* tracheary element cultures. Co-transformation of *F5H* and *COMT* resulted in a two to three times higher S/G ratio than *F5H* alone (Wagner et al., 2015).

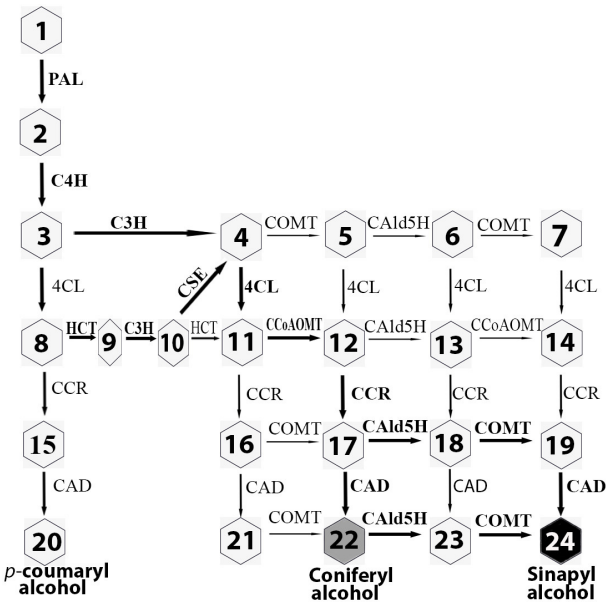

FIGURE 1 | Monolignol biosynthetic pathway in poplar. Bold arrows indicate the main metabolic flux. Eleven enzyme families are PAL, phenylalanine ammonia-lyase; C4H, cinnamate 4-hydroxylase; C3H, *p*-coumaroyl-CoA 3-hydroxylase; 4CL, *p*-coumarate CoA ligase; HCT, hydroxycinnamoyltransferase; CSE, caffeoyl shikimate esterase; CCoAOMT, caffeoyl-CoA *O*-methyltransferase; CCR, cinnamoyl-CoA reductase; CAld5H, coniferaldehyde 5-hydroxylase; COMT, caffeic acid 3-*O*-methyltransferase; CAD, cinnamyl alcohol dehydrogenase. The metabolites are shown in numbers. 1: phenylalanine; 2: cinnamic acid; 3: 4-hydroxycinnamic acid; 4: caffeic acid; 5: ferulic acid; 6: 5-hydroxyferulic acid; 7: sinapic acid; 8: *p*-coumaroyl-CoA; 9: *p*-coumaroyl shikimic acid; 10: caffeoyl shikimic acid; 11: caffeoyl-CoA; 12: feruloyl-CoA; 13: 5-dydroxyferuloyl-CoA; 14: sinapoyl-CoA; 15: *p*-coumaraldehyde; 16: caffeyl aldehyde; 17: coniferaldehyde; 18: 5-hydroxyconiferaldehyde; 19: sinapaldehyde; 20: *p*-coumaryl alcohol (H monolignol); 21: caffeyl alcohol; 22: coniferyl alcohol (G monolignol); 23:5-hydroxyconiferyl alcohol; 24: sinapyl alcohol (S monolignol).

To learn more about the GRN that determines SCW biosynthesis, we identified and characterized TFs regulating sinapyl alcohol (monolignol) biosynthesis. We conducted a yeast one hybridization (Y1H) screening of a library of TFs from *Populus trichocarpa,* using the *CAld5H2* promoter as bait, and identified 12 candidates as potential targets. Among the 12 TFs, two BEL1-like homeodomain (BLH) 6 proteins, BLH6a and BLH6b, bound *CAld5H2* promoter specifically.

We characterized the functions of BLH6a. Transient overexpression and dominant repression of *BLH6a* regulation inhibited *CAld5H2* expression, and extensive protein–protein interactions were detected among the 12 TFs. Our results suggest that a complex GRN with combinatorial and redundant elements may control the *CAld5H* gene expression for S lignin biosynthesis.

MATERIALS AND METHODS

Plant Materials

Populus alba × *Populus glandulosa* and *Nicotiana benthamiana* plants were grown in a room with long-day conditions (16-h light/8-h dark) at 25 ± 1°C. The *P. alba* × *P. glandulosa* sterile plants used for transformation were propagated by microcuttings in bottles and cultured on 0.5 × the Murashige and Skoog (MS) medium.

Yeast One-Hybrid

Total RNAs were extracted from differentiating xylem of 6-month-old *P. trichocarpa* trees using an RNeasy Plant Mini Kit (QIAGEN Inc., Valencia, CA, USA) and reverse-transcribed to complementary DNAs (cDNAs) by using the PrimeScript™ RT Reagent Kit (TaKaRa, Dalian, China). The cDNAs were used as templates to amplify the coding region of 213 TFs (**Supplementary Data Sheet 1**) with the Phanta Max Super-Fidelity DNA Polymerase (Vazyme Biotech Co., Ltd., Nanjing, Jiangsu, China). About 202 PCR fragments were digested with corresponding restriction enzymes and cloned into the pGADT7 vectors by T4 DNA ligases. About 11 PCR fragments were cloned into the pGADT7 vector through the recombination method by using the ClonExpressII One Step Cloning Kit (Vazyme Biotech Co., Ltd., Nanjing, Jiangsu, China). The full lengths of coding regions cloned in pGADT7 were sequence confirmed. The coding regions of 14 TFs were synthesized and cloned into pGADT7. Total 227 TF-prey plasmids were constructed.

Genomic DNA was extracted from young leaves using a DNeasy Plant Mini Kit (QIAGEN Inc., Valencia, CA, USA). Gene promoter regions were amplified from genomic DNA and cloned into the pABAi vector by T4 DNA ligases. The resultant DNA-bait plasmid was linearized by *Bstb*I and integrated into the Y1HGold Strain (Clontech Laboratories, Inc., Mountain View, CA, USA). Four transformants were tested on the SD/-ura medium with the addition of Aureobasidin A (AbA) ranging from 100 to 500 μg/ml, and the DNA-bait strain with optimal AbA concentration was selected for Y1H.

The 227 TF-prey plasmids were individually transformed into the DNA-bait strain, and the transformants were selected on the SD/-ura-leu medium. The positive strains were diluted with 0.9% NaCl and screened on the SD/-ura-leu+AbA medium for identifying the TF–DNA interaction.

Effector-Reporter-Based Transactivation/Repression Assays

The 2-kb *CAld5H2* promoter was amplified from *P. alba* × *P. glandulosa* genomic DNA and cloned into *pBG3-LZ004-LUC* (luciferase) (Chen et al., 2017) by using the ClonExpressII One Step Cloning Kit (Vazyme Biotech Co., Ltd., Nanjing, Jiangsu, China), generating the reporter construct *pBG3-pCAld5H2:LUC*. The full-length coding regions of *BLH6a*, *BLH6b*, and *BLH2* were amplified from *P. alba* × *P. glandulosa* xylem cDNA and cloned into the pENTR/D TOPO Vector (Invitrogen Co., Carlsbad, CA, USA). After being verified by sequencing, the genes were Gateway cloned into the pGWB17 Vector by LR Clonase II (Invitrogen), generating the effector constructs *pBWB17-35S:BLH6a*, *pBWB17-35S:BLH6b*, and *pBWB17-35S:BLH2*. The resultant reporter constructs and effector constructs were transformed into *Agrobacterium* GV3101. *Agrobacterium* containing an effector construct and a reporter construct were co-injected into the tobacco leaves. After 48 h, the LUC luminescence was detected under a Promega GloMax®-20/20 Luminometer (Promega Corp., Madison, WI, USA). The primers used for the promoter and gene amplification are listed in **Supplementary Table 1**.

Transcriptional Activation/Inhibition Assays in Yeast

The full-length coding region of *BLH6a* was amplified from *P. alba* × *P. glandulosa* xylem cDNA with the Phanta Max Super-Fidelity DNA Polymerase (Vazyme Biotech Co., Ltd., Nanjing, Jiangsu, China) and cloned into pGBKT7 and pGBKT7-VP16 vector using the ClonExpressII One Step Cloning Kit (Vazyme Biotech Co., Ltd., Nanjing, Jiangsu, China), generating BD-BLH6 and BD-VP16:BLH6a. The constructs were transformed into the yeast strain, yeast two hybridization, Y2H Gold (Clontech Laboratories, Inc., Mountain View, CA, USA). Transformants were grown on the SD/-Trp medium for the selection of positive clones and then transferred to the SD/-Trp-His-Ade medium for the transcriptional activation/inhibition assays with X-α-gal used as an indicator.

Chromatin Immunoprecipitation–Quantitative PCR Assay

The fragment of 3× FLAG was amplified from the *pCM1307-N-Flag-HA vector* (Zhou et al., 2012), cloned into the pENTR/D TOPO Vector (Invitrogen), and LR ligated into *pUC19-35S-RfA-35S-sGFP* (Li et al., 2012) to generate *pUC19-35S-FLAG-35S-sGFP*. BLH6a coding sequences were amplified from *P. alba* × *P. glandulosa* xylem cDNA and cloned into *pUC19-35S-FLAG-35S-sGFP*, generating *pUC19-35S-Flag:BLH6a-35S-sGFP*. Primers are listed in **Supplementary Table 1**. Plasmid DNA for the protoplast transfection was prepared using the EndoFree Plasmid Kit (QIAGEN Inc., Valencia, CA, USA). Leaf protoplasts were prepared from mesophyII of leaves in tissue culture bottles

following the published protocol (Lee et al., 2017), and xylem protoplasts were prepared as described previously (Lin et al., 2014). Plasmids were transferred into protoplasts, and each chromatin immunoprecipitation (ChIP) assay was performed using 5×10^6 protoplasts with anti-FLAG antibodies as described before (Yan et al., 2019). One-fiftieth of the supernatants before adding antibodies were used as input in the qPCR. qPCR was conducted using the Green Premix Ex Tag II (TaKaRa, Dalian, China) and detected by the Roche LightCycler 480 II (Roche Co., Basel, Switzerland), with 18S as the reference.

RNA *in-situ* Hybridization

The eighth and nineth internodes of 3-month-old *P. alba* × *P. glandulosa* stems were fixed in formalin/acetic acid/alcohol (FAA) and embedded in paraplast. The 8 μm microsections were prepared for the *in situ* hybridization. PCR fragments of ∼250 bp, amplified with gene-specific primers (**Supplementary Table 1**), were used as templates to synthesize antisense and sense probes with T7 RNA polymerases using the Digoxigenin (DIG) RNA Labeling Kit (Roche). The hybridization and immunological detection were performed as previously described (Liu et al., 2018). The hybridization solution contains 10× *in situ* salts, deionized formamide, 50% dextran sulfate, 50× Denhardt's solution, and 100 ng/ml tRNA. Signals were detected using anti-DIG antibodies conjugated with alkaline phosphatase, and photographs were taken under an OLYMPUS BX51 Microscope (Olympus Corp., Tokyo, Japan).

Yeast Two Hybridization

The full-length coding regions of *BLH6b* and *BLH2* were amplified from *P. alba* × *P. glandulosa* xylem cDNA with the Phanta Max Super-Fidelity DNA Polymerase (Vazyme Biotech Co., Ltd., Nanjing, Jiangsu, China) and cloned into the pGADT7 vector by using the ClonExpressII One Step Cloning Kit (Vazyme Biotech Co., Ltd., Nanjing, Jiangsu, China), generating AD fusion vectors. The full-length coding region of *BLH6a* was cloned into the pGBKT7 vector, generating the BD-BLH6a vector. The BD-BLH6a and AD fusion vectors were co-transformed into the yeast strain *Saccharomyces cerevisiae* Y2HGold as described in the Yeast Protocols Handbook (Clontech Laboratories, Inc., Mountain View, CA, USA). Transformants were grown on the SD/-Leu-Trp medium and then screened on the SD/-Ade-His-Leu-Trp medium.

Luciferase Complementation Imaging Assays

The coding region of 12 TFs was amplified from *P. alba* × *P. glandulosa* xylem cDNA, and, by using the ClonExpressII One Step Cloning Kit (Vazyme Biotech Co., Ltd., Nanjing, Jiangsu, China), they were cloned into *pCAMBIA1300-cLUC* and *pCAMBIA1300-nLUC*, which were pre-linearized by *Kpn*I/*Sal*I (Song et al., 2011), generating *TF-nLUC* and *TF-cLUC*. Primers used for the vector construction are shown in **Supplementary Table 1**. After confirmation by sequencing, the vectors were transformed into *Agrobacteriu*m GV3101. Equal concentrations and volumes of *Agrobacterium* cultures were mixed and co-infiltrated into the *N. benthamiana* leaves. After incubation for 36 h, the LUC fluorescence was detected under a Berthold NightSHADE LB985 *in vivo* Plant Imaging System (Berthold Technologies GmbH, Bad Wildbad, Germany).

Vector Construction and Transgenic Production

Two oligos EAR-motif repression domain (SRDX)-F and SRDX-R (**Supplementary Table 1**) were synthesized. After denature and annealing, the double-strand DNA fragment was ligated into *pBI121* at *BamH*I/*Sac*I, generating *pBI121-35S-SRDX*. This vector contains a short sequence between 35S promoter and stops codon, encoding a 12 amino acid (LDLDLELRLGFA) plant-specific SRDX (Mitsuda et al., 2011).

The full-length coding region of *BLH6a* was amplified by 121BLH6a-F/R from *P. alba* × *P. glandulosa* xylem cDNA and inserted into *pBI121-35S-SRDX* using the ClonExpressII One Step Cloning Kit (Vazyme Biotech Co., Ltd., Nanjing, Jiangsu, China), generating *pBI121-35S-BLH6a:SRDX*. The resultantly plasmid was transformed into *Agrobacterium* GV3101, and transformation in *P. alba* × *P. glandulosa* was conducted by the leaf disk method. The leaves were cut at vein area, immersed in *Agrobacterium* culture for 15 min. After incubated on the co-cultivation medium (1 × MS, pH 5.7–5.9, 5 mg/L 6BA, 0.05 mg/L NAA) in dark for 4 days, the explants were transferred to the selection medium (1× MS, pH 5.7–5.9, 0.5 mg/L 6BA, 0.05 mg/L NAA, 200 mg/L timentin, 50 mg/L kanamycin) under light with the medium substitution every 2 weeks. The generated shoots were cut and transferred to the rooting medium (0.5× MS, pH 5.7–5.9, 0.2 mg/L NAA, 0.05 mg/L IBA, 200 mg/L timentin, 50 mg/L kanamycin) for the root induction.

Quantitative Reverse Transcription-PCR

Total RNAs were extracted from differentiating xylem of 6-month-old trees using the RNeasy Plant Mini Kit (QIAGEN Inc., Valencia, CA, USA). The total RNAs were reverse transcribed to cDNA using a PrimeScript™ RT Reagent Kit with gDNA Eraser (TaKaRa, Dalian, China). The PCR was conducted using the Green Premix Ex Tag II (TaKaRa, Dalian, China) and detected by the Roche LightCycler 480 II. Actin was used as the reference.

Stem Sectioning and Light Microscopy

The stem fragments, close to the bottom node, were collected from the seventh to 14th internodes, immobilized with glue (LOCTITE 495), and sectioned by an oscillating Leica VT 1000 S Microtome (Leica Microsystems, Wetzlar, Germany). The section thickness was 40 μm. The sections were stained in 0.05% (w/v) toluidine blue (TBO) dye for 1 min and observed under an OLYMPUS BX51 Microscope (Olympus Corp., Tokyo, Japan).

Lignin Content and Composition

The stems below the 20th internode were collected from 9-month-old trees, and bark was removed. Dried wood was ground, lyophilized, and extracted with chloroform/methanol (2:1, v/v). The lignin content was determined by the Klason method as described before (Lu et al., 2013). Lignin compositions were determined by the thioacidolysis method (Lapierre et al., 1995).

RESULTS

Identification of 12 TF Candidates That Bound the *P. trichocarpa cAld5H2* Promoter

In *P. trichocarpa*, two closely related genes *CAld5H1* (Potri.005G117500) and *CAld5H2* (Potri.007G016400) are key genes in S monolignol biosynthesis with redundant functions (Wang et al., 2012). These enzymes comprise a key branch point in monolignol biosynthesis because they regulate the relative abundance of substrate that becomes coniferyl alcohol as opposed to 5-hydroxyconiferyl alcohol. These enzymes act on coniferyl alcohol directly or they may act on the aldehyde intermediates converting coniferylaldehyde to 5-hydroxyconiferaldehyde. The synthesis of 5-hydroxy intermediates determines the amount of sinapylaldehyde and sinapyl alcohol that is formed and therefore the relative abundance of sinapyl and coniferyl alcohol. The ratio of these alcohols is a major determinant of the ratio of S and G subunits polymerized into lignin (Osakabe et al., 1999; Wang et al., 2014, 2018).

We conducted a Y1H screening to identify TFs that could directly regulate *CAld5H* genes. Using our previous RNA-seq data (Shi et al., 2017) from xylem, phloem, leaves, and shoot tips from *P. trichocarpa*, we obtained 227 TFs differentially expressed in xylem compared to three other tissues [fold change >1, and false discovery rate (FDR) <0.05] (**Supplementary Data Sheet 1**). We generated a TF-prey library by cloning 227 TFs into the yeast expression vector pGADT7. We isolated the 2 kb promoter of *CAld5H2* from *P. trichocarpa* genomic DNA and used it as bait to screen the TF-prey library. The 227 TF-prey plasmids were individually transformed into the bait-strain and selected on the SD/-leu-ura medium containing AbA, we obtained 57 TF containing clones that could grow on the selective medium.

To eliminate the false positives from the 57 TF candidates, we performed co-expression analysis of 57 TFs with *CAld5H* genes using the AspWood web resource (http://aspwood.popgenie.org). AspWood provides a high-spatial-resolution gene expression profile of 25–28 stem cryosections in *P. tremula*, from phloem to cambium and then to wood-forming tissues, enabling the co-expression network analysis (Sundell et al., 2017). Of the 57 TF genes that passed the screen, 12 were co-expressed with both *CAld5H2 and CAld5H1* transcripts (**Supplementary Figure 1**, **Supplementary Table 2**). Their expression levels were low in the cambium (sections 5–9). Starting from section 9 in the wood-forming tissue, their expression levels gradually increased and were maintained at a higher level (**Supplementary Figure 2**), indicating their roles in xylem cell differentiation and SCW biosynthesis during wood formation. We chose these 12 TFs for further characterization.

To identify how many TFs among these 12 could interact with the *CAld5H2* promoter among the monolignol pathway gene promoters, we conducted Y1H assays to compare these 12 TFs with other monolignol pathway gene promoters isolated from *P. trichocarpa*, including *CAD1*, *C3H3*, *COMT2*, *CCR2*, *PAL4*, *HCT1*, *4CL3*, *4CL5*, and *C4H2*. Among these 12 TFs, only the homologs of BLH6a (Potri.004G159300) and BLH6b (Potri.009G120800) bound *CAld5H2* promoter specifically. BLH2 (Potri.005G129500) bound both *CAld5H2* and *CAld5H1* promoters, but not other promoters (**Figures 2A,B**). This three TFs belong to the BLH family, indicating that the BLH protein family may be more specific in binding to *CAld5H* promoters. The other nine TFs recognized promoters of other genes in the monolignol pathway (**Figures 2A,B**), suggesting that they regulate other steps in monolignol biosynthesis.

All 12 Selected TFs Bound the Fragments 6 and 7 of the *CAld5H2* Promoter

To identify the specific binding regions of these 12 TFs in the *CAld5H2* promoter in *P. trichocarpa*, we divided the 2 kb promoter into seven fragments (**Figure 2C**). The Y1H assays were conducted to examine the interactions of 12 TFs with the seven fragments. The self-activation in the bait strains containing fragments 1, 2, and 4 was very strong, and therefore these fragments were removed in the study. The Y1H assays showed that all 12 TFs could bind fragment 6 of *CAld5H2* promoter, and eight TFs could bind fragment 7. Fragment 3 of the promoter was recognized by BLH6a, VAL2a, and VAL2b. None of the TFs bound to fragment 5 (**Figure 2D**).

Fragments 6 and 7 are major binding sites for all 12 TFs. We used PlantPAN 3.0 (http://plantpan.itps.ncku.edu.tw/index.html) to characterize the specificity of cis-acting regulatory DNA elements and to identify possible binding to TF families. Besides the CAAT box and TATA box, multiple cis-acting regulatory elements were found, including WBOXATNPR1, MYBCOREATCYCB1, DOFCOREZM, and SURECOREATSULTR11 (**Supplementary Data Sheet 2**). The possible TF families that could bind to these motifs include AT-HOOK, Dof, ATA, ALE, WOX, MYB, bZIP, bHLH, NAC, HD-ZIP, and ZF-H (**Supplementary Data Sheet 2**). Fragments 6 and 7 contain motifs for recognition by the families of 12 TFs, such as the "TGAC" element in motif WBOXATNPR1 for BLH proteins, and the "CANNTG" element in YCCONSENSUSAT motif for bHLH and bZIP TFs (Murre et al., 1989; Ledent and Vervoort, 2001; Kondhare et al., 2019). This analysis supports the binding of 12 TFs to the *CAld5H2* promoter.

P. alba × *P. glandulosa* BLH6a Negatively Regulated *CAld5H2* Promoter Activity

Among the three potential *CAld5H2*-specific upstream regulators, BLH2, also named WBLH2 (Chen et al., 2019), has been implicated as an upstream regulator and was shown to bind the *CAld5H1* promoter by ChIP–PCR in *P. trichocarpa* (Chen et al., 2019). Although *BLH6a* (also named WBLH3 (Chen et al., 2019) has been implicated as a target of PtrMYB021, the regulatory function of these two BLH6 members on the monolignol pathway genes was not studied before.

To investigate whether the two BLH6 homologs regulate *CAld5H2 in vivo*, we conducted effector-reporter-based transactivation/repression assays. The reporter constructs, carrying a *LUC* luciferase gene under the control of the *P. alba* × *P. glandulosa CAld5H2* promoter and was co-expressed transiently in *N. benthamiana* leaves with effector construct harboring either *BLH6a* or *BLH6b* from the *P. alba* × *P. glandulosa* hybrid. BLH6a repressed reporter activity, but BLH6b did not (**Figure 3A**). BLH2 also inhibited *CAld5H2*

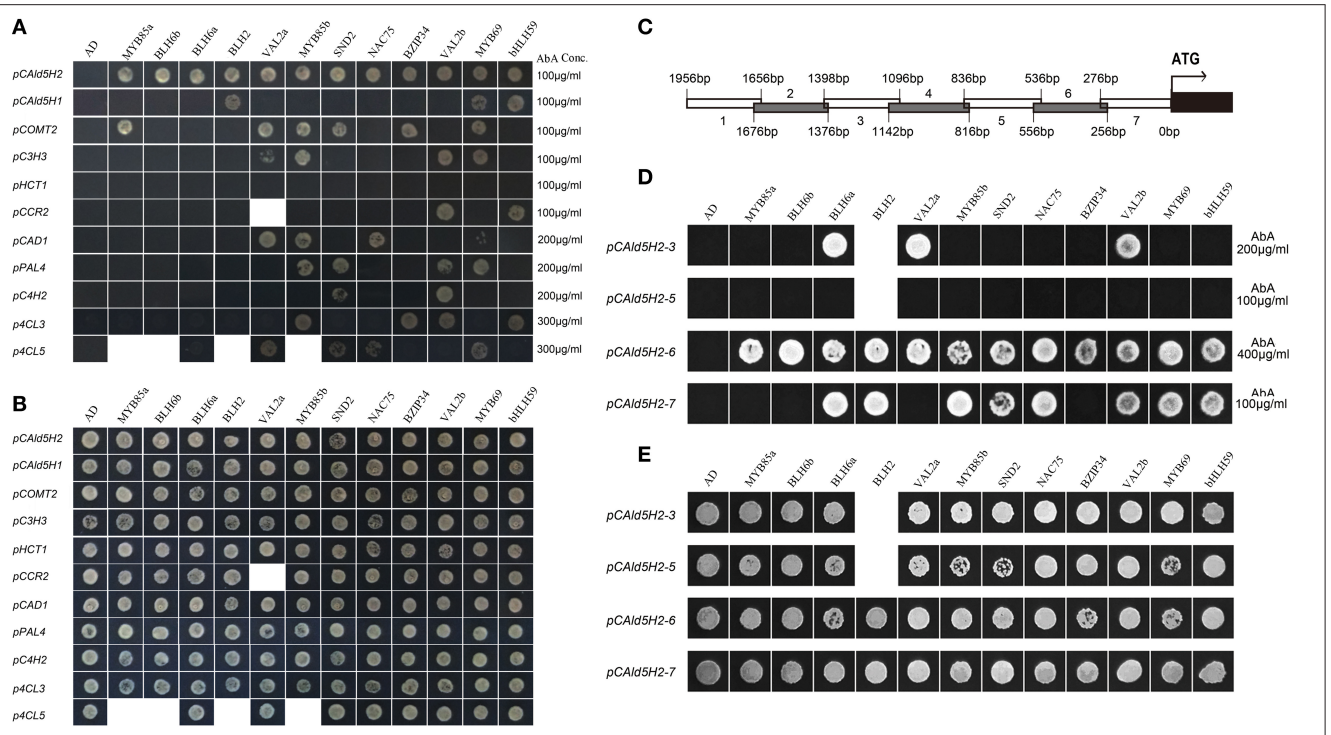

FIGURE 2 | Yeast one hybridization. **(A,B)** Yeast one-hybrid (Y1H) of 12 transcription factors (TFs) with 11 monolignol pathway genes in *Populus trichocarpa*. TF-prey plasmids were transformed into bait strains and grown on SD/-ura-leu. We did not obtain transformants for *VAL2a* transformed into *CCR2* promoter strain, and for *MYB85a*, *BLH6b*, *BLH2*, and *MYB85b* transformed into *4CL5* promoter strain **(B)**. The transformants were selected on SD/-ura-leu+AbA **(A)**. The concentrations of Aureobasidin A (AbA) are shown on right. **(C–E)** Y1H of 12 TFs with seven fragments of *CAld5H2* promoter in *P. trichocarpa*. **(C)** The 2 kb *P. trichocarpa CAld5H2* promoter was divided into seven fragments. Each fragment is about 300 bp long and two adjacent fragments have a 20–46 bp overlap. **(D)** Y1H assays of 12 TFs with fragments (3, 5, 6, and 7) of *CAld5H2* promoters. The self-activation of fragments 1, 2, and 4 are too higher (1,000 μg/ml) to be removed. The transformants were grown on SD/-ura-leu+AbA for selection. The AbA concentrations were shown on the right. **(E)** The transformants were grown on SD/-ura-leu.

promoter activity (**Figure 3A**). We further used the yeast system to detect the activation/repression activity of BLH6a. Yeast with *BLH6a* overexpression could not grow on the medium lacking histidine (**Figure 3B**), showing that BLH6a could not activate *HIS3* expression. Compared to the VP16 alone, BLH16a:VP16 fusion disturbed the activation of an α-galactosidase gene (**Figure 3B**), indicating that BLH6a is a transcriptional repressor, not an activator.

We further used ChIP assays in both xylem and leaf protoplasts to examine the interaction of BLH6a and *CAld5H2* promoters. In comparison with a negative control of overexpression of FLAG alone, the *CAld5H2* promoter region was significantly enriched in the immunoprecipitation in both xylem and leaf protoplasts overexpressing FLAG:BLH6a fusion (**Figure 3C**), confirming the direct binding of BLH6a to *CAld5H2* promoter.

BLH6a Was Co-expressed With *CAld5H* Genes in *P. alba* × *P. glandulosa* Differentiating Xylem

The proposed interaction of BHL6a with the *CAld5H2* promoter requires that both genes are expressed in the same cells. We used RNA *in situ* hybridization (RISH) to examine the co-expression of *BLH6a* with *CAld5H* genes in cells of differentiating xylem. *BLH6a* and *BLH6b* are a paralogous gene pair, with 90% nucleotide identity; thus, it is difficult to distinguish transcripts of the two genes using an RNA probe. Similarly, RNA probes for *CAld5H* RISH could not distinguish *CAld5H1* and *CAld5H2*. The RISH detected *CAld5H1/2* transcripts in cross-sections of differentiating xylem, including vessels and fiber cells (**Figure 4**), consistent with the function of *CAld5H* in monolignol biosynthesis during the SCW biosynthesis. *BLH6a/b* transcripts were also detected in both vessels and fiber cells, in the early stages of the xylem differentiation (**Figure 4**). We also selected two TFs (bZIP34 and bHLH59), which did not specifically bind the *CAldH2* promoter, for RISH. These two genes showed the same expression pattern as *CAld5H1/2* (**Figure 4**). The RISH showed that *bZIP34* and *bHLH59* were co-expressed with *CAld5H1/2* in all cell types of differentiating xylem, and *BLH6a/b* were co-expressed with *CAld5H1/2* in the early stage of the xylem cell differentiation.

Protein–Protein Interactions Among 12 TF Candidates

All the identified 12 TFs could bind the 556 bp promoter region (fragments 6–7) of *CAld5H2*. It would be interesting

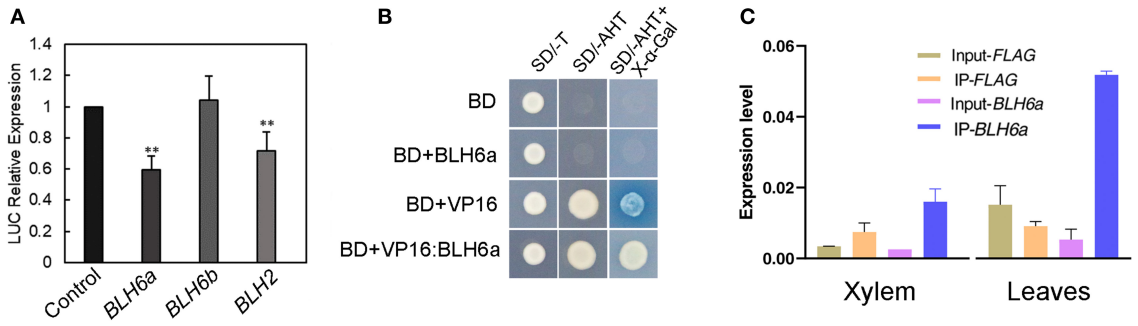

FIGURE 3 | BLH6a is a transcriptional repressor of *CAld5H2* in *P. alba* × *P. glandulosa*. **(A)** Effector-reporter-based gene activation/repression assay. *LUC* gene was driven by the *P. alba* × *P. glandulosa CAld5H2* promoter in the reporter construct. Each TF gene from *P. alba* × *P. glandulosa* was driven by the 35S promoter in the effector construct. Effect construct and reporter construct were co-infiltrated in the tobacco leaves by *Agrobacterium* for the LUC activity determination. The reporter construct alone was the control. **(B)** Transactivation/repressor activity detections in yeast strain Y2HGold. SD/-T, single dropout medium lacking tryptophan; SD/-AHT, triple dropout medium lacking adenine, histidine, and tryptophan; BD, GAL4-binding domain. **(C)** Chromatin immunoprecipitation (ChIP) assays in xylem (left) and leaf (right) protoplasts. ChIP was conducted in protoplasts overexpressing *FLAG* and *FLAG:BLH6a*, respectively, and followed by qPCR. Input-FLAG and Input-BLH6a were IP using one-fiftieth of the supernatants before adding antibodies in the *FLAG* and *FLAG:BLH6a* overexpression protoplasts, respectively. IP-FLAG and IP-BLH6a were IP with FLAG antibodies in *FLAG* and *FLAG:BLH6a* overexpression protoplasts, respectively. Error bars represent SD ($n = 3$). $^{**}p < 0.01$, determined by Student's t test.

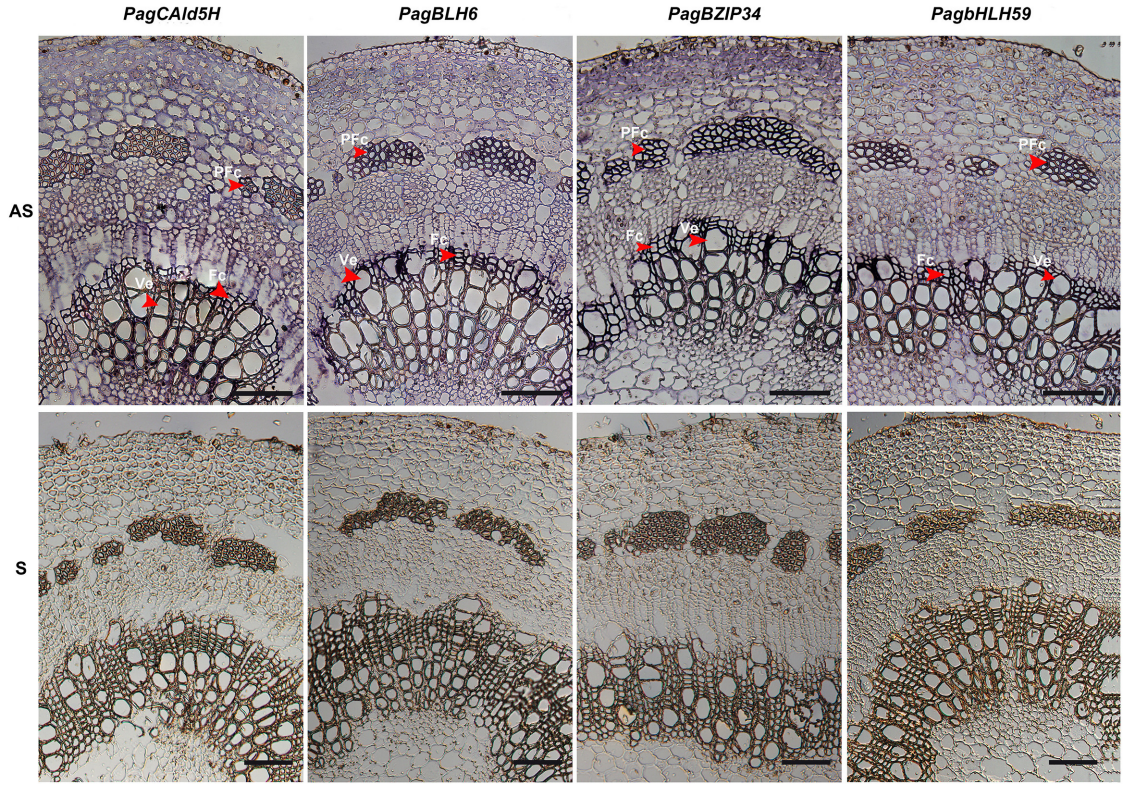

FIGURE 4 | RNA *in situ* localization of *CAld5H*, *BLH6*, *BZIP34*, and *bHLH59* in the 8–9 internode stems of *P. alba* × *P. glandulosa stems*. Bars = 200 μm. Arrows show the signals of the vessels (Ve), fiber cells (Fc), and phloem fiber cell (PFc) in the differentiating xylem where signals of RNA *in situ* hybridization were intensified. AS and S represent the sections hybridized with antisense and sense probes, respectively.

to know how they cooperatively regulate *CAld5H2*. We first examined the interactions of BLH6a with other two *CAld5H2*-specific TFs BLH6b and BLH2 by Y2H, and the assays showed that BLH6a could form a dimer with BLH6b and BLH2 (**Figure 5A**). We further conducted firefly LCI assays for the three BLH members in the *N. benthamiana*

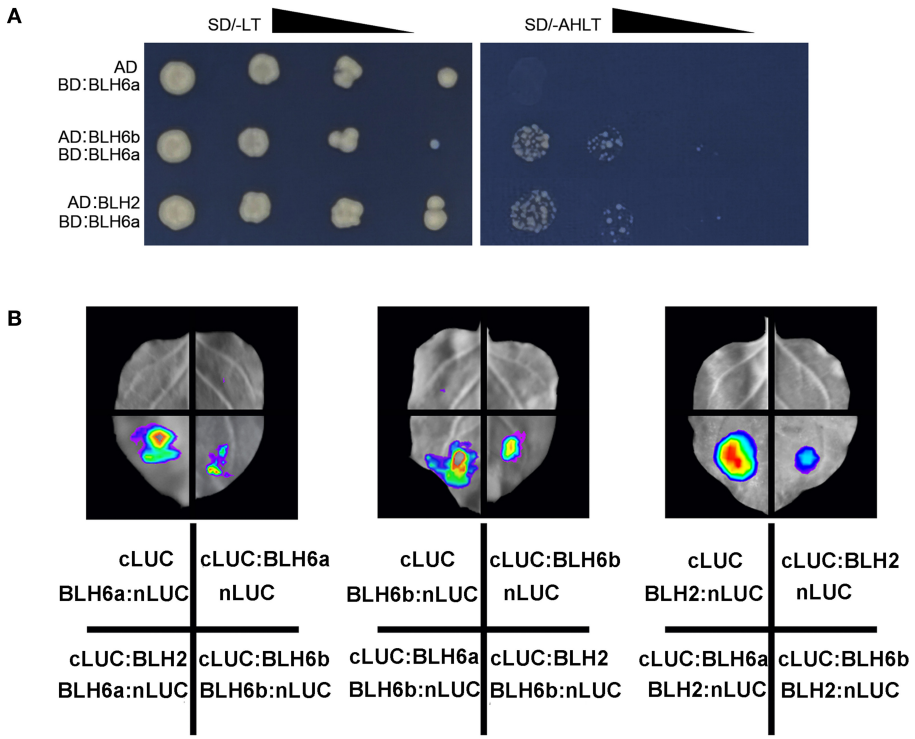

FIGURE 5 | Protein–protein interactions of BLH6a, BLH6b, and BLH2. **(A)** Yeast two hybridizations. BLH6a was fused with Gal4-binding domain (BD). BLH6b and BLH2 were fused with activation domain (AD). The resulting AD constructs (AD:BLH6b, AD:BLH2) and BD construct (BD:BLH6a) were co-transfected into a yeast cell, grown on the SD/-Leu-Trp medium (SD/-LT), and selected on the SD/-Ade-His-Leu-Trp medium (SD/-AHLT). **(B)** Luciferase complementation imaging (LCI) assays for the detection of the interactions between two proteins of BLH6a, BLH6b, and BLH, with one of them being fused to the N-terminal portion of LUC (nLUC), and the other being fused to the C-terminal portion of LUC (cLUC).

leaves (**Figure 5B**). A strong LUC signal was detected when *BLH6a-nLUC* and *cLUC-BLH2* were co-infiltrated, and reciprocal co-infiltration of *BLH2-nLUC* and *cLUC-BLH6a* also had strong luminescence. Similarly, when each pair of *BLH6a-nLUC/cLUC-BLH6b*, *BLH6b-nLUC/-cLUC-BLH6a*, *BLH6b-nLUC/cLUC-BLH2*, and *BLH2-nLUC/cLUC-BLH6b* was co-infiltrated into tobacco leaves, the LUC luminescence was observed. However, no LUC luminescence was observed in negative controls (*cLUC/BLH6a-nLUC*, *cLUC-BLH6a/nLUC*, *cLUC/BLH6b-nLUC*, *cLUC-BLH6b/nLUC*, *cLUC/BLH2-nLUC*, and *cLUC-BLH2/nLUC*). The LCI assays for the interaction among BLH6a, BLH6b, and bHLH2 were repeated four times. All had positive luminescence, showing that these three proteins could interact with each other.

We further used the LCI assays to examine the remaining possible interactions between any two TFs among 12 TFs. For each two TFs, we examined their interactions reciprocally (i.e., TF1:nLUC/TF2:cLUC and TF2:nLUC/TF1:cLUC), and each assay was conducted twice. Theoretically, 66 interactions could exist among 12 TFs for the heterodimer formation. Our LCI assay identified 58 interactions (**Supplementary Figure 3**, **Supplementary Table 3**). Among 58 interactions, 52 were detected for both combinations (TF1:nLUC/TF2:cLUC and TF2:nLUC/TF1:cLUC), and six interactions were detected for one combination (either TF1:nLUC/TF2:cLUC or TF2:nLUC/TF1:cLUC). Except for MYB85b, all other 11 TFs could form homodimers (**Supplementary Figure 3**).

Dominant Repression by *BLH6a* in *P. alba* × *P. glandulosa* Inhibited *CAld5H* Gene Expression and Affected SCW Biosynthesis in Differentiating Xylem

Arabidopsis BLH6 was identified as a transcriptional repressor of REVOLUTA during the SCW formation (Liu et al., 2014). Our results showed that BLH6a is a transcriptional repressor of *CAld5H2* in poplar. We identified 12 upstream TFs of CAld5H2, indicating a possibility of redundancy of these TFs. To avoid the redundancy, we exploited the Chimeric REpressor gene Silencing Technology (CRES-T) (Mitsuda et al., 2011) to investigate the regulation of BLH6a on CAld5H2 *in vivo*. We obtained 36 transgenic *P. alba* × *P. glandulosa* lines for overexpression of *BLH6a:SRDX*, which encoded a chimeric repressor generated by the fusion of the BLH6a protein with a plant-specific SRDX. All transgenic lines grew as normal as wild type (WT). After the quantitative reverse transcription (qRT)-PCR analysis of transgene (*BLH6a:SRDX*) in the xylem of 36 transgenic lines (**Supplementary Figure 4**), we selected two lines (#2 and #29)

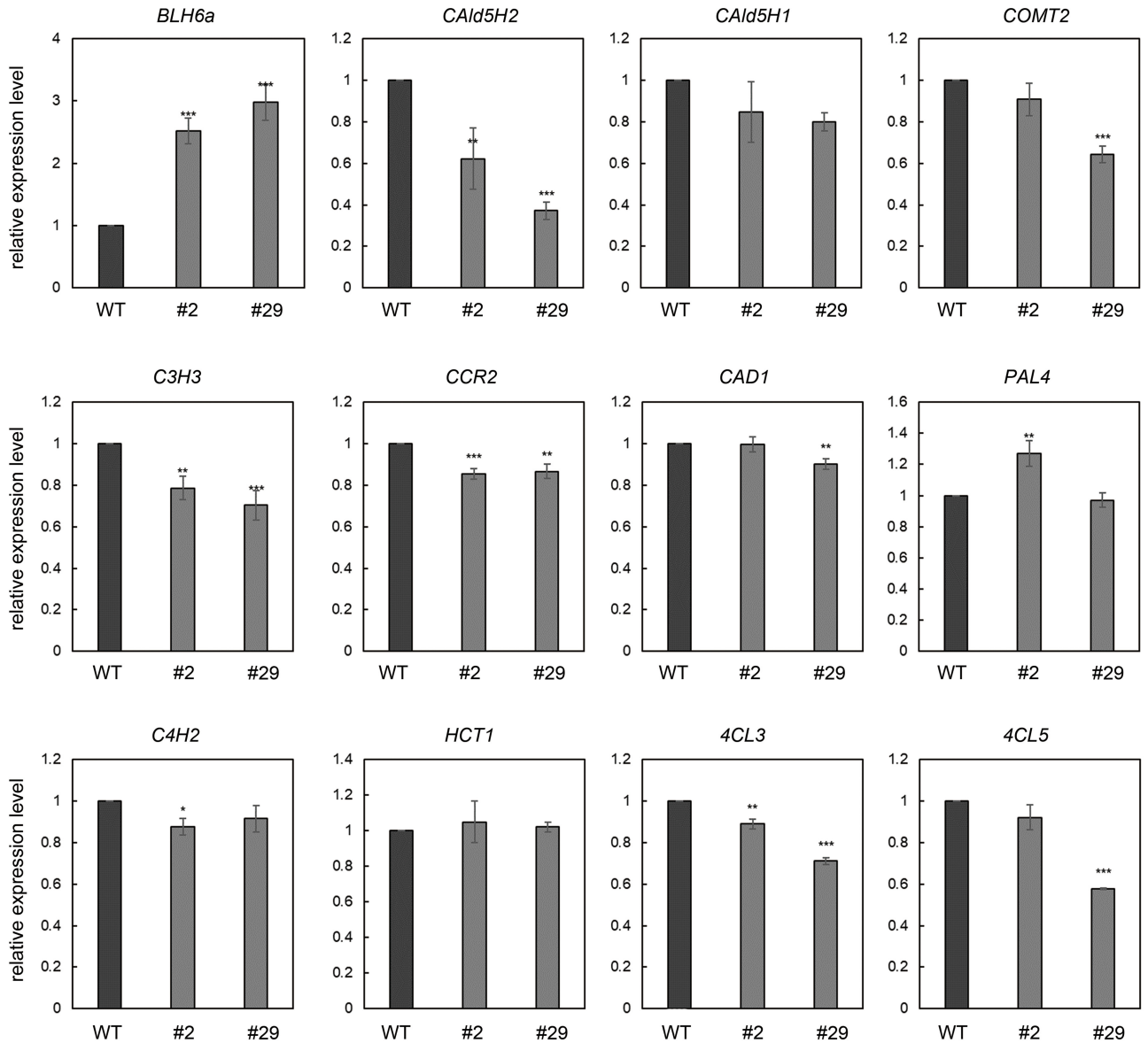

FIGURE 6 | qRT-PCR analysis of monolignol pathway genes in the differentiating xylem of *BLH6a:SRDX* overexpression transgenic *P. alba* × *P. glandulosa*. The transcript abundance in wild type (WT) and transgenic lines 2 and 29 was determined for transgene *BLH6a:SRDX* and monolignol pathway genes *CAld5H2*, *CAld5H1*, *COMT2*, *CAD1*, *C3H3*, *CCR2*, *C4H2*, *4CL3*, *4CL5*, *PAL4*, and *HCT1*. Asterisks highlight significant differences by the Student's *t*-test: $*p < 0.5$, $**p < 0.01$; $***p < 0.001$.

to measure the expression levels of *CAld5H2* and *CAld5H1*, and nine other genes encoding the enzymes of monolignol pathway, including *PAL4*, *CAD1*, *COMT2*, *C3H3*, *C4H2*, *CCR2*, *4CL3*, *4CL5*, and *HCT1*. Compared to WT, *CAld5H2* transcript levels were significantly reduced in both lines 2 and 29. The reduction in transcript abundance of *CAld5H2* in line 29 (62.9%) is greater than line 2 (37.7%), in accordance with the higher transgene expression level in line 29 (**Figure 6**). The transcript abundance of *CAld5H1* in lines 2 and 29 was not changed significantly. Transcript reduction was also observed for *COMT2*, *CAD1*, *C3H3*, *CCR2*, *4CL3*, and *4CL5*, but the extent of reduction is much less than that of *CAld5H2* (**Figure 7**). The qRT-PCR results indicate that BLH6a may interact more specifically with the *CAld5H2* promoter, consistent with the results of Y1H assays (**Figure 2**).

To study the effects of dominant repression of BLH6a regulation on the wood formation, we used lines 2 and 29 to examine the cell wall structure at the seventh and the 14th stem internodes using light microscopy. Line 29 had a higher level of *BLH6a:SRDX* overexpression than line 2. Accordingly, it was observed that the cell wall thickness of vessels and fiber cells in both the seventh and the 14th

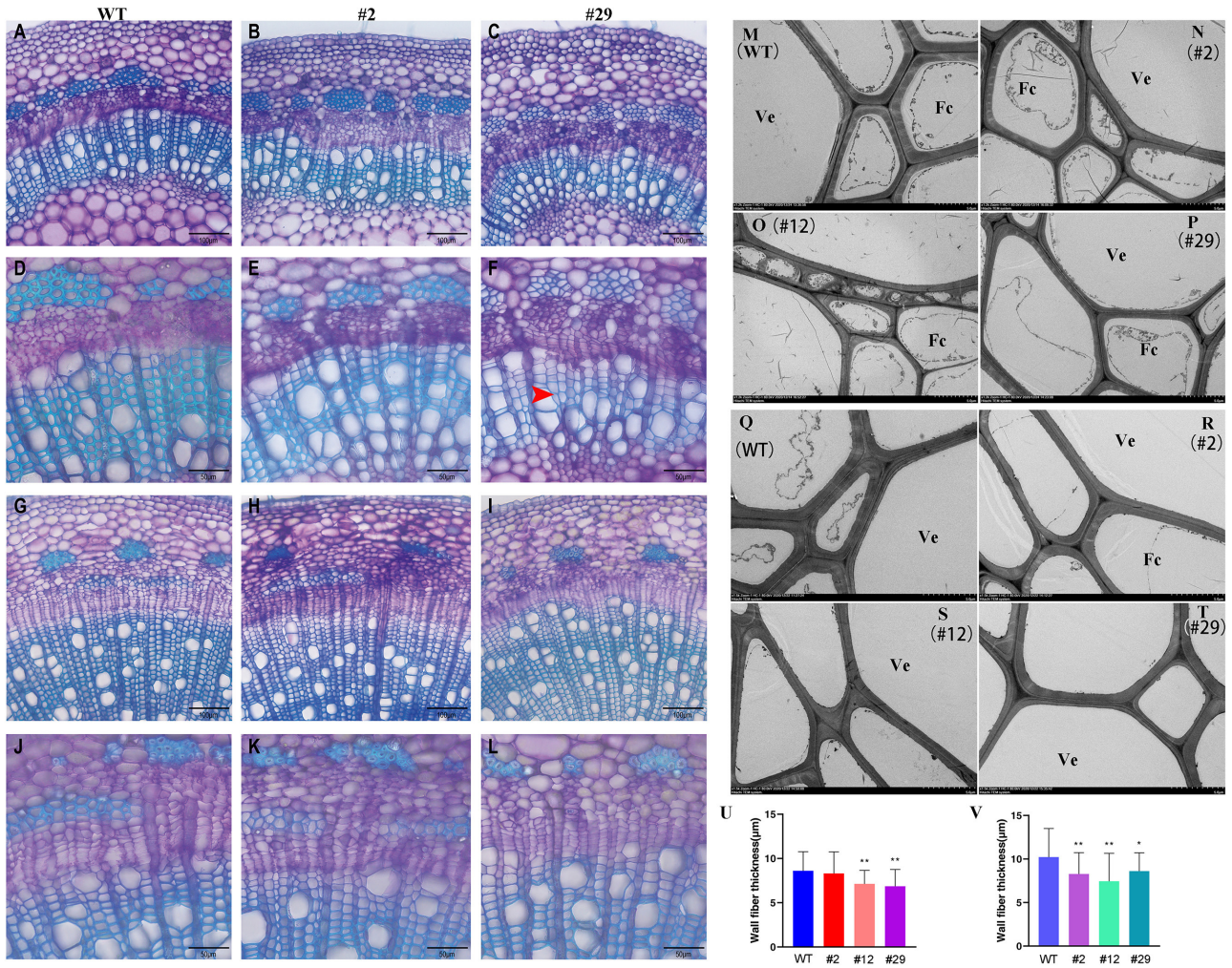

FIGURE 7 | Comparison of xylem structure between *P. alba* × *P. glandulosa BLH6a* dominant repression transgenics and WT. **(A–L)** Light microscopy. **(A–C)** Cross sections of the seventh internode from WT **(A)**, transgenic lines 2 **(B)**, and 29 **(C)** at 200 magnification. **(D–F)** Cross sections of the seventh internode from WT **(D)**, transgenic lines 2 **(E)**, and 29 **(F)** at 400 magnification. **(G–I)** Cross sections of the 14th internode from WT **(G)**, transgenic lines 2 **(H)**, and 29 **(I)** at 200 magnification. **(J–L)** Cross sections of the 14th internode from WT **(J)**, transgenic lines 2 **(K)**, and 29 **(L)** at ×400 magnification. Bars = 100 μm in **(A–C**, **G–I)** and 50 μm in **(D–F**, **J–L)**. The red arrow shows the thinner cell wall. **(M–T)** Transmission electron microscopy. **(M–P)** Cross-sections of the eighth internode from WT **(M)**, transgenic lines 2 **(N)**, 12 **(O)**, and 29 **(P)**. **(Q–T)** Cross-sections of the 14th internode from WT **(Q)**, transgenic lines 2 **(R)**, 12 **(S)**, and 29 **(T)**. Bars = 5 μm. Ve, Vessel; Fc, Fiber cell. **(U,V)** Statistics of fiber cell wall thickness in the eighth internode **(U)** and the 14th internode **(V)** of WT, transgenic lines 2, 12, and 29. $*p < 0.05$, $**p < 0.01$, determined by the Student's *t*-test.

internodes of line 29 was decreased (**Figures 7A–L**). We further used transmission electron miscopy to compare the xylem cell wall thickness between transgenic lines (#2, #12, and #29) and WT. Transgenic line 12 had a similar expression level of *BLH6a:SRDX* as line 29 (**Supplementary Figure 4**). The measurement of 50 fiber cells showed that the cell wall thickness was significant decreased in both the eighth and the 14th internodes of lines 12 and 29 (**Figures 7M–V**), indicating that the overexpression of *BLH6a:SRDX* affected the SCW formation in the differentiating xylem.

To investigate effects on lignin biosynthesis by the *BLH6a:SRDX* overexpression, we determined lignin content and composition in transgenic lines 2 and 29 (**Table 1**). We only observed a slight and significant decrease of cellulose content in line 29. Compared to WT, the contents of lignin and the three monomers were not changed significantly, showing that lignin biosynthesis is not affected significantly in the transgenic wood.

DISCUSSION

Wood is the major resource for timber, paper, and pulping. Because wood is composed of SCW in vascular plants, extensive studies have been carried out to understand the composition, function, and biosynthesis of the SCW, particularly in the model plant *Arabidopsis thaliana* and several species of poplar. In these model systems, many TFs, including NACs and MYBs,

TABLE 1 | Lignin content and compositions in the *BLH6a:SRDX* overexpression transgenics.

Line	Cellulose content	Hemicellulose content	Acid-insoluable lignin (%CWR)	Acid-soluable lignin (%CWR)	H (μmol/g CWR)	G (μmol/g CWR)	S (μmol/g CWR)
WT	48.53 ± 0.37	16.67 ± 0.34	19.88 ± 0.26	6.34 ± 0.17	2.86 ± 0.11	226.86 ± 0.22	488.83 ± 10.69
#2	47.10 ± 0.29	17.18 ± 0.45	19.24 ± 0.10	6.76 ± 0.01	2.60 ± 0.19	221.44 ± 4.71	547.59 ± 12.91
#29	46.21 ± 0.11*	16.73 ± 0.26	20.37 ± 0.69	6.45 ± 0.12	2.75 ± 0.01	241.82 ± 7.17	532.77 ± 9.68

Values are means ± SE. SEs represent two biological replicates. WT, wild type; #2, BLH6a:SRDX overexpression transgenic poplar line 2; #29, transgenic line 29. The asterisk represents the significant increase of cellulose content in #29 by the Student's t-test ($p < 0.05$).*

were identified as key regulators during the SCW formation (Zhong et al., 2008; Ye and Zhong, 2015). Hierarchical gene regulatory networks (hGRNs) controlling SCW thickening are under construction using many different bioinformatic and biochemical strategies and techniques. One recent combination of methods used top-down Gaussian Graphical Modeling (GGM) to infer correlated molecular interactions and the direction of the correlated effects (Lin et al., 2013; Chen et al., 2019). Network construction uses relative abundance based on the global transcript sequencing (RNA-seq), chromatin binding to construct a four-layered hGRN directed by PtrSND1-B1, a master regulatory NAC protein affecting wood formation (Lin et al., 2013; Chen et al., 2019). Alternatively, bottom-up GGM was used to build a two-layered hGRN for laccases, which polymerize lignin monomers (Lu et al., 2013). Using enhanced Y1H to identify protein–DNA interactions, networks controlling the vascular cambium development and SCW formation have been constructed (Taylor-Teeples et al., 2015; Xu et al., 2016; Yeh et al., 2019; Smit et al., 2020). Through transcriptional network construction, additional interactions and feedback, and feed-forward regulations, have been described (Ko et al., 2014; Smit et al., 2020). In this study, we constructed a TF-prey library containing 227 xylem-specific TFs and conducted Y1H assays to identify TFs regulating *CAld5H2* in hybrid poplar. We identified 12 TF candidates and focused on the characterization of three BLH family proteins. BLH proteins belong to the plant-specific three-amino acid loop extension (TALE) superclass of the homeodomain protein family. In *Arabidopsis*, BLH6a has been indicated to regulate SCW formation through interacting with KNOTTED ARABIDOPSIS THALIANA7 (KNAT7) (Liu et al., 2014), and BLH2 has been indicated to regulate demethylesterification of homogalacturonan in seed mucilage (Xu et al., 2020). In the *Arabidopsis blh6* mutant, expressions of some of CELLULOSE SYNTHASE (CESA) and lignin pathway genes, such as *CesA7*, *CesA8*, and *F5H*, were increased (Liu et al., 2014). Our results confirmed the regulation of BLH6a on *CAld5H2* in poplar by transient overexpression, stable dominate repression, and ChIP–qPCR. Our analyses on the activation/repression ability of poplar BLH6a are consistent with the conclusion that *Arabidopsis* BLH6 is a transcriptional repressor (Liu et al., 2014). Because BLH6a is a transcriptional repressor, overexpression of *BLH6a:SRDX* would enhance its repression ability, which will cause a similar phenotype of overexpression transgenics. Consistently, decreased cell wall thickness is observed in *Arabidopsis* overexpressing a *BLH6* gene (Liu et al., 2014).

Different methods for the hGRN construction and TF identification have their advantages and limitations. Each method may generate false positives. For network prediction by GGM algorithms, more samples with more variation of the gene expression levels improve the precision of the network. The constructed networks and TFs included in the network by different strategies are not the same. For example, NAC123 directly targets *CCoAOMT1* in *P. trichocarpa* by ChIP–qPCR in xylem protoplasts (Chen et al., 2019). Our Y1H showed that NAC123 (also named SND2 in this study) could bind the promoters of *CAld5H2*, *COMT2*, *PAL4*, *C4H2,* and *4CL5*. In the *P. trichocarpa* network (Chen et al., 2019), the TF WBLH2 interacts with *CAld5H1* and *HCT1* promoters, whereas in this study its homolog BLH2 from *P. alba* × *P. glandulosa* bound *CAld5H2* and *CAld5H1* promoters and did not bind the promoters of other monolignol pathway genes. Further experiments, such as ChIP assays in xylem cells (not xylem protoplasts) and electrophoretic mobility shift assays (EMSA) are needed to verify these interactions. The protein–DNA interactions ought to be proven before carrying out experiments to show that they are expressed in the same cells. Based on transcriptome data from a series of xylem cryosections (Sundell et al., 2017), our 12 TF genes are co-expressed with *CAld5H2* (**Supplementary Figure 1**). The RISH has provided evidence of co-expression of *BLH6a/b*, *BZIP34*, and *bHLH59* with *CAld5H1/2*. Further experiments, laser capture microdissection, or single-cell RNA sequencing (scRNA-seq) may provide additional information on gene co-expression.

Note that the networks constructed in different species may not be the same. In *Arabidopsis*, MYB46/83, which is located in the second layer directly regulated by SND1, can directly regulate the bottom layer SCW biosynthetic genes, including three CesA encoding genes (*CesA4*, *7,* and *8*), seven monolignol pathway genes (*PAL1*, *2*, *4*, *4CL3*, *CCR*, *CCoAOMT1*, and *CAD*) and four xylan biosynthetic pathway enzyme encoding genes (*FRA8*, *IRX8*, *IRX9*, and *IRX14*) (Zhong and Ye, 2012; Kim et al., 2013; Ko et al., 2014). However, in *P. trichocarpa*, using ChIP assays in xylem protoplasts overexpressing *PtrMYB021* (homolog of MYB46) only identifies four bottom layer genes (*PtrIRX9*, *PtrIRX14-L*, *PtrFRA-1*, and *PtrPAL2*) as the direct targets of PtrMYB021 (Chen et al., 2019). Further ChIP assays on the five TFs (targets of PtrMYB021) in the third layer, including PtrMYB090, PtrMYB161, PtrMYB174, PtrNAC123, PrWBLH1,

and PtrWBLH2, identified three *CesA* gene promoters and 10 monolignol pathway gene promoters (Chen et al., 2019).

The poplar genome has had a historical whole-genome duplication event, generating about 8,000 pairs of duplicated genes (Tuskan et al., 2006). During evolution, both promoter and gene body between the gene pair could have diverged. In *Arabidopsis*, MYB85 overexpression induces *4CL* expression and causes ectopic lignin deposition (Zhong et al., 2008). In our study, the identified 12 TFs contain two poplar MYB85 paralogs (MYB85a and MYB85b). Y1H assays showed that MYB85a only interacted with *CAld5H2* and *COMT2* promoters, whereas MYB85b interacted with *CAdl5H2*, *COMT2*, *C3H3*, *CAD1*, *PAL4*, and *4CL3* promoters, showing the different abilities of these two MYB85 members in activating monolignol biosynthesis. In *P. trichocarpa,* the two homologs 4CL3 and 4CL5 have different regulatory metabolic activity, indicating that the difference in promotor binding of *4CL3* and *4CL5* may be related to their different metabolic roles (Chen et al., 2013). All 12 TFs could bind the *CAld5H2* promoter, but only three TFs could bind the *CAld5H1* promoter, indicating promoter divergence.

Many studies have shown that one gene may be regulated by multiple TFs, and multiple TFs binding to the same promoter could regulate target genes by forming protein complexes (Chen et al., 2019). Pairwise interactions among three TFs, PtrMYB090, PtrMYB161, and PtrWBLH1 have been detected in *P. trichocarpa*, and these three TFs may form a ternary complex regulating *CAld5H*. Our LCI assays for pairwise interactions among 12 TFs identified extensive interactions between TFs, indicating many TFs may form many dimers. In the *BLH6a:SRDX* overexpression transgenics, the *CAld5H2* gene was downregulated up to 62%, but the *CAld5H1* gene was not downregulated significantly. S lignin content was not changed in the *BLH6a:SRDX* overexpression transgenic wood, which could be due to the redundancy between *CAld5H1* and *CAld5H2*. Thus, it is necessary to perform Y1H to identify the TFs that specifically bind to the *CAld5H1* promoter. Although the CRES-T technology could avoid redundancy, using the SRDX system for a transcriptional repressor may not make much difference in some cases, which may be another possible reason for the unchanged S lignin content. When the TF of interest is a transcriptional repressor, transgenic plants expressing a chimeric repressor exhibit an enhanced phenotype (Mitsuda et al., 2011). Further using the CRISPR-CAS9 system to knock out the candidate TF genes regulating *CAld5H1/2* in poplar is needed to understand their roles in lignin biosynthesis. Although lignin content and composition did not show alteration in *BLH6a:SRDX* overexpression transgenic wood compared to WT, we observed that the xylem cell wall thickness was decreased significantly. This phenotype may be caused by the interactions of BLH6a with other TFs. The conserved BELL and SKY domains in BLH proteins comprise a conserved bipartite MID domain, which can interact with the KNAT MEINOX domain to form heterodimers (Bellaoui et al., 2001), and the decrease is likely associated with the repression of *REVOLUTA* by BLH6 and KNT7 interactions. OVATE FAMILY PROTEIN1 (OFP1) and OFP4 are components of the BLH6-KNAT7 multi-protein complex and may modulate the activity of the BLH6-KNAT7 complex (Liu and Douglas, 2015). Further investigations are needed to study the heterodimer formation among the identified TFs for efficient regulation of *CAld5H* promoter activity.

Multiple TFs may have the combinatorial coordination to activate or suppress target gene expression. Transcriptional activation and repression strength and sequence specificity of TFs depend on their expression levels. The RISH showed *BLH6a* transcript abundance in the vessels and fiber cells at the early stages of xylem differentiation. Two other genes *BZIP34* and *bHLH59*, which were expressed throughout the xylem, have the same expression profile with *CAld5H1/2*. These 12 genes may function at different locations, either activating or suppressing *CAld5H* genes. Different cells may have different proportions of different protein–protein interactions, thus affecting *CAld5H* gene expression through different protein complex composition and abundance. Further investigation is needed to determine whether these TFs are activators or repressors and to study their potential for redundant and combinatorial regulation.

CONCLUSION

We identified 12 upstream candidates of *CAld5H2.* The regulation of one TF, BLH6a, on *CAld5H2* was substantiated by transient effector–reporter assays, dominant repression, and ChIP–qPCR. Further understanding the TFs regulating *CAld5H2* and their mechanisms of action will lead to novel strategies for engineering S subunit levels in lignin. Such information will be important for the development of S subunits in gymnosperm wood, which are currently absent in gymnosperms.

DATA AVAILABILITY STATEMENT

The original contributions presented in the study are included in the article/**Supplementary Material**, further inquiries can be directed to the corresponding author/s.

AUTHOR CONTRIBUTIONS

QL designed and supervised the project. QW, XD, HP, YC, XH, HL, and XY performed the experiments. FL, HW, RS, and QL analyzed the data. QW, HW, RS, and QL wrote the manuscript. All authors contributed to the article and approved the submitted version.

FUNDING

This work was supported by grants from Fundamental Research Funds of the Chinese Academy of Forestry (CAFYBB2017ZY001 and CAFYBB2016ZX001-1), Natural Science Foundation of China (31670667), and the National Key Research and Development Program of China (2016YFD0600103).

ACKNOWLEDGMENTS

We thank Dr. Chengcai Chu for the *pBG3-LZ004* vector, Dr. Yan Guo for the pCM1307-N-FLAG-HA vector, Dr. Keming Luo for pGBKT7-VP16 vector, Jiaqiang Sun for *pGWB17*, *p1300-35S-nLUC*, and *p1300-35S-cLUC* vectors, and Dr. Wei Li for *Populus trichocarpa* developing xylem.

SUPPLEMENTARY MATERIAL

The Supplementary Material for this article can be found online at: https://www.frontiersin.org/articles/10.3389/fpls.2021.695223/full#supplementary-material

Supplementary Figure 1 | Co-expression analysis of 12 TF genes with *CAld5H1* and *CAld5H2*.

Supplementary Figure 2 | Expression patterns of 12 TFs and two *CAld5H* genes in stem cryosections of *P. tremula*.

Supplementary Figure 3 | Protein–protein interactions among 12 TFs by LCI assays.

Supplementary Figure 4 | qRT-PCR of transgene *BLH6a:SRDX* in the leaves of 36 transgenic lines.

Supplementary Table 1 | Primers used in this study.

Supplementary Table 2 | 12 TF candidates regulating *CAld5H2*.

Supplementary Table 3 | Summary of interactions among 12 TFs.

Supplementary Data Sheet 1 | 227 xylem-specific TFs in *Populus trichocarpa*.

Supplementary Data Sheet 2 | Sequence motif analysis of the fragments 6 and 7 in *CAld5H2* promoter.

REFERENCES

Bellaoui, M., Pidkowich, M. S., Samach, A., Kushalappa, K., Kohalmi, S. E., Modrusan, Z., et al. (2001). The Arabidopsis BELL1 and KNOX TALE homeodomain proteins interact through a domain conserved between plants and animals. *Plant Cell* 13, 2455–2470. doi: 10.1105/tpc.010161

Boerjan, W., Ralph, J., and Baucher, M. (2003). Lignin biosynthesis. *Annu. Rev. Plant. Biol.* 54, 519–546. doi: 10.1146/annurev.arplant.54.031902.134938

Chang, H.-m., and Sarkanen, K. (1973). Species variation in lignin. *TAPPI* 56, 132–134.

Chen, H., Song, J., Williams, C. M., Shuford, C. M., Liu, J., Wang, J. P., et al. (2013). Monolignol pathway 4-coumaric acid:CoA ligases in Populus trichocarpa: novel specificity, metabolic regulation, and simulation of CoA ligation fluxes. *Plant Physiol.* 161, 1501–1516. doi: 10.1104/pp.112.210971

Chen, H., Wang, J. P., Liu, H., Li, H., Lin, Y.-C. J., Shi, R., et al. (2019). Hierarchical transcription factor and chromatin binding network for wood formation in black cottonwood (*Populus trichocarpa*). *Plant Cell* 31, 602–626. doi: 10.1105/tpc.18.00620

Chen, J., Nolan, T., Ye, H., Zhang, M., Tong, H., Xin, P., et al. (2017). *Arabidopsis* WRKY46, WRKY54 and WRKY70 transcription factors are involved in brassinosteroid-regulated plant growth and drought response. *Plant Cell* 29, 1425–1439. doi: 10.1105/tpc.17.00364

Kim, W. C., Ko, J. H., Kim, J. Y., Kim, J. M., Bae, H. J., and Han, K. H. (2013). MYB46 directly regulates the gene expression of secondary wall-associated cellulose synthases in *Arabidopsis*. *Plant J.* 73, 26–36. doi: 10.1111/j.1365-313x.2012.05124.x

Ko, J. H., Jeon, H. W., Kim, W. C., Kim, J. Y., and Han, K. H. (2014). The MYB46/MYB83-mediated transcriptional regulatory programme is a gatekeeper of secondary wall biosynthesis. *Ann. Bot.* 114:1099. doi: 10.1093/aob/mcu126

Kondhare, K. R., Vetal, P. V., Kalsi, H. S., and Banerjee, A. K. (2019). BEL1-like protein (StBEL5) regulates CYCLING DOF FACTOR1 (StCDF1) through tandem TGAC core motifs in potato. *J. Plant Physiol.* 241:153014. doi: 10.1016/j.jplph.2019.153014

Lapierre, C., Pollet, B., and Rolando, C. (1995). New insights into the molecular architecture of hardwood lignins by chemical degradative methods. *Res. Chem. Intermediat.* 21, 397–412. doi: 10.1007/BF03052266

Ledent, V., and Vervoort, M. (2001). The basic helix-loop-helix protein family: comparative genomics and phylogenetic analysis. *Genome Res.* 11, 754–770. doi: 10.1101/gr.177001

Lee, J. H., Jin, S., Sun, Y. K., Kim, W., and Ji, H. A. (2017). A fast, efficient chromatin immunoprecipitation method for studying protein-DNA binding in Arabidopsis mesophyll protoplasts. *Plant Methods* 13:42. doi: 10.1186/s13007-017-0192-4

Li, L., Zhou, Y., Cheng, X., Sun, J., Marita, J. M., Ralph, J., et al. (2003). Combinatorial modification of multiple lignin traits in trees through multigene cotransformation. *Proc. Natl. Acad. Sci. U. S. A.* 100, 4939–4944. doi: 10.1073/pnas.0831166100

Li, Q., Lin, Y.-C., Sun, Y.-H., Song, J., Chen, H., Zhang, X.-H., et al. (2012). Splice variant of the SND1 transcription factor is a dominant negative of SND1 members and their regulation in *Populus trichocarpa*. *Proc. Natl. Acad. Sci. U. S. A.* 109, 14699–14704. doi: 10.1073/pnas.1212977109

Li, Q., Song, J., Peng, S., Wang, J. P., Qu, G. Z., Sederoff, R. R., et al. (2014). Plant biotechnology for lignocellulosic biofuel production. *Plant Biotechnol. J.* 12, 1174–1192. doi: 10.1111/pbi.12273

Lin, Y.-C., Li, W., Chen, H., Li, Q., Sun, Y.-H., Shi, R., et al. (2014). A simple improved-throughput xylem protoplast system for studying wood formation. *Nat. Protocols* 9, 2194–2205. doi: 10.1038/nprot.2014.147

Lin, Y.-C., Li, W., Sun, Y.-H., Kumari, S., Wei, H., Li, Q., et al. (2013). SND1 transcription factor–directed quantitative functional hierarchical genetic regulatory network in wood formation in *Populus trichocarpa*. *Plant Cell* 25, 4324–4341. doi: 10.1105/tpc.113.117697

Liu, C., Xue, Z., Tang, D., Shen, Y., Shi, W., Shi, W., et al. (2018). Ornithine δ-aminotransferase is critical for floret development and seed setting through mediating nitrogen reutilization in rice. *Plant J.* 96, 842–854. doi: 10.1111/tpj.14072

Liu, Y., and Douglas, C. J. (2015). A role for OVATE FAMILY PROTEIN1 (OFP1) and OFP4 in a BLH6-KNAT7 multi-protein complex regulating secondary cell wall formation in *Arabidopsis thaliana*. *Plant Signal. Behav.* 10:e1033126. doi: 10.1080/15592324.2015.1033126

Liu, Y., You, S., Taylor-Teeples, M., Li, W. L., Schuetz, M., Brady, S. M., et al. (2014). BEL1-LIKE HOMEODOMAIN6 and KNOTTED ARABIDOPSIS THALIANA7 interact and regulate secondary cell wall formation *via* repression of *REVOLUTA*. *Plant Cell* 26, 4843–4861. doi: 10.1105/tpc.114.128322

Lu, S., Li, Q., Wei, H., Chang, M.-J., Tunlaya-Anukit, S., Kim, H., et al. (2013). Ptr-miR397a is a negative regulator of laccase genes affecting lignin content in *Populus trichocarpa*. *Proc. Natl. Acad. Sci. U. S. A.* 110, 10848–10853. doi: 10.1073/pnas.1308936110

McCarthy, R. L., Zhong, R., and Ye, Z. H. (2009). MYB83 is a direct target of SND1 and acts redundantly with MYB46 in the regulation of secondary cell wall biosynthesis in *Arabidopsis*. *Plant Cell Physiol.* 50, 1950–1964. doi: 10.1093/pcp/pcp139

Minoru, K., Makiko, U., Nobuyuki, N., Gorou, H., Masatoshi, Y., Jun, I., et al. (2005). Transcription switches for protoxylem and metaxylem vessel formation. *Genes Dev.* 19:1855. doi: 10.1101/gad.1331305

Mitsuda, N., Matsui, K., Ikeda, M., Nakata, M., Oshima, Y., Nagatoshi, Y., et al. (2011). CRES-T, an effective gene silencing system utilizing chimeric repressors. *Methods Mol. Biol.* 754, 87–105. doi: 10.1007/978-1-61779-154-3_5

Murre, C., Mccaw, P. S., Vaessin, H., Caudy, M., and Lassar, A. B. (1989). Interactions between heterologous helix-loop-helix proteins generate complexes that bind specifically to a common DNA sequence. *Cell* 58, 537–544. doi: 10.1016/0092-8674(89)90434-0

Ohashiito, K., Oda, Y., and Fukuda, H. (2010). *Arabidopsis* VASCULAR-RELATED NAC-DOMAIN6 directly regulates the genes that govern programmed cell death and secondary wall formation during xylem differentiation. *Plant Cell* 22, 3461–3473. doi: 10.1105/tpc.110.075036

Osakabe, K., Tsao, C. C., Li, L., Popko, J. L., Umezawa, T., Carraway, D. T., et al. (1999). Coniferyl aldehyde 5-hydroxylation and methylation direct syringyl lignin biosynthesis in angiosperms. *Proc. Natl. Acad. Sci. U. S. A.* 96, 8955–8960. doi: 10.1073/pnas.96.16.8955

Ralph, J., Lundquist, K., Brunow, G., Lu, F., Kim, H., Schatz, P. F., et al. (2004). Lignins: natural polymers from oxidative coupling of 4-hydroxyphenyl- propanoids. *Phytochem. Rev.* 3, 29–60. doi: 10.1023/B:PHYT.0000047809.65444.a4

Río, J. C. D., Gutiérrez, A., Hernando, M., Landín, P., Romero, J., and Martínez, Á. T. (2005). Determining the influence of eucalypt lignin composition in paper pulp yield using Py-GC/MS. *J. Anal. Appl. Pyrol.* 74, 110–115. doi: 10.1016/j.jaap.2004.10.010

Sarkanen, K. V., and Ludwig, C. H. (1971). *Lignins: Occurrence, Formation, Structure and Reactions*. New York, NY: Wiley-Interscience.

Shi, R., Wang, J. P., Lin, Y.-C., Li, Q., Sun, Y.-H., Chen, H., et al. (2017). Tissue and cell-type co-expression networks of transcription factors and wood component genes in *Populus trichocarpa*. *Planta* 245, 927–938. doi: 10.1007/s00425-016-2640-1

Smit, M. E., McGregor, S. R., Sun, H., Gough, C., Bågman, A.-M., Soyars, C. L., et al. (2020). A PXY-mediated transcriptional network integrates signaling mechanisms to control vascular development in *Arabidopsis*. *Plant Cell* 32, 319–335. doi: 10.1105/tpc.19.00562

Song, S., Qi, T., Huang, H., Ren, Q., Wu, D., Chang, C., et al. (2011). The jasmonate-ZIM domain proteins interact with the R2R3-MYB transcription factors MYB21 and MYB24 to affect jasmonate-regulated stamen development in *Arabidopsis*. *Plant Cell* 23, 1000–1013. doi: 10.1105/tpc.111.083089

Stewart, J. J., Akiyama, T., Chapple, C., Ralph, J., and Mansfield, S. D. (2009). The effects on lignin structure of overexpression of ferulate 5-hydroxylase in hybrid poplar1. *Plant Physiol.* 150, 621–635. doi: 10.1104/pp.109.137059

Studer, M. H., Demartini, J. D., Davis, M. F., Sykes, R. W., Brian, D., Martin, K., et al. (2011). Lignin content in natural Populus variants affects sugar release. *Proc. Natl. Acad. Sci. U. S. A.* 108, 6300–6305. doi: 10.1073/pnas.1009252108

Sundell, D., Street, N. R., Kumar, M., Mellerowicz, E. J., Kucukoglu, M., Johnsson, C., et al. (2017). AspWood: High-spatial-resolution transcriptome profiles reveal uncharacterized modularity of wood formation in *Populus tremula*. *Plant Cell* 29, 1585–1604. doi: 10.1105/tpc.17.00153

Taylor-Teeples, M., Lin, L., de Lucas, M., Turco, G., Toal, T. W., Gaudinier, A., et al. (2015). An *Arabidopsis* gene regulatory network for secondary cell wall synthesis. *Nature* 517, 571–575. doi: 10.1038/nature14099

Tuskan, G. A., DiFazio, S., Jansson, S., Bohlmann, J., Grigoriev, I., Hellsten, U., et al. (2006). The genome of black cottonwood, *Populus trichocarpa* (Torr. & Gray). *Science* 313, 1596–1604. doi: 10.1126/science.1128691

Vanholme, R., Cesarino, I., Rataj, K., Xiao, Y., Sundin, L., Goeminne, G., et al. (2013). Caffeoyl shikimate esterase (CSE) is an enzyme in the lignin biosynthetic pathway in *Arabidopsis*. *Science* 341, 1103–1106. doi: 10.1126/science.1241602

Wagner, A., Tobimatsu, Y., Phillips, L., Flint, H., Geddes, B., Lu, F., et al. (2015). Syringyl lignin production in conifers: Proof of concept in a Pine tracheary element system. *Proc. Natl. Acad. Sci. U. S. A.* 112:6218. doi: 10.1073/pnas.1411926112

Wang, J. P., Matthews, M. L., Williams, C. M., Rui, S., Yang, C., Tunlaya-Anukit, S., et al. (2018). Improving wood properties for wood utilization through multi-omics integration in lignin biosynthesis. *Nat. Comm.* 9:1579. doi: 10.1038/s41467-018-03863-z

Wang, J. P., Naik, P. P., Chen, H.-C., Shi, R., Lin, C.-Y., Liu, J., et al. (2014). Complete proteomic-based enzyme reaction and inhibition kinetics reveal how monolignol biosynthetic enzyme families affect metabolic flux and lignin in *Populus trichocarpa*. *Plant Cell* 26, 894–914. doi: 10.1105/tpc.113.120881

Wang, J. P., Shuford, C. M., Li, Q., Song, J., Lin, Y. C., Sun, Y. H., et al. (2012). Functional redundancy of the two 5-hydroxylases in monolignol biosynthesis of *Populus trichocarpa*: LC-MS/MS based protein quantification and metabolic flux analysis. *Planta* 236, 795–808. doi: 10.1007/s00425-012-1663-5

Xu, H., Cao, D., Feng, J., Wu, H., Lin, J., and Wang, Y. (2016). Transcriptional regulation of vascular cambium activity during the transition from juvenile to mature stages in *Cunninghamia lanceolata*. *J. Plant Physiol.* 200, 7–17. doi: 10.1016/j.jplph.2016.06.003

Xu, Y., Wang, Y., Wang, X., Pei, S., Kong, Y., Hu, R., et al. (2020). Transcription factors BLH2 and BLH4 regulate demethylesterification of homogalacturonan in seed mucilage. *Plant Physiol.* 183, 96–111. doi: 10.1104/pp.20.00011

Yan, X., Ma, L., Pang, H., Wang, P., Liu, L., Cheng, Y., et al. (2019). METHIONINE SYNTHASE1 is involved in chromatin silencing by maintaining DNA and histone methylation. *Plant Physiol.* 181, 249–261. doi: 10.1104/pp.19.00528

Ye, Z.-H., and Zhong, R. (2015). Molecular control of wood formation in trees. *J. Exp. Bot.* 66, 4119–4131. doi: 10.1093/jxb/erv081

Yeh, C.-S., Wang, Z., Miao, F., Ma, H., Kao, C.-T., Hsu, T.-S., et al. (2019). A novel synthetic-genetic-array–based yeast one-hybrid system for high discovery rate and short processing time. *Genome Res.* 29, 1343–1351. doi: 10.1101/gr.245951.118

Zhao, Q., Wang, H., Yin, Y., Xu, Y., Chen, F., and Dixon, R. A. (2010). Syringyl lignin biosynthesis is directly regulated by a secondary cell wall master switch. *Proc. Natl. Acad. Sci. U. S. A.* 107, 14496–14501. doi: 10.1073/pnas.1009170107

Zhong, R., Demura, T., and Ye, Z. H. (2006). SND1, a NAC domain transcription factor, is a key regulator of secondary wall synthesis in fibers of *Arabidopsis*. *Plant Cell* 18, 3158–3170. doi: 10.1105/tpc.106.047399

Zhong, R., Lee, C., Zhou, J., Mccarthy, R. L., and Ye, Z. H. (2008). A battery of transcription factors involved in the regulation of secondary cell wall biosynthesis in *Arabidopsis*. *Plant Cell* 20, 2763–2782. doi: 10.1105/tpc.108.061325

Zhong, R., Richardson, E. A., and Ye, Z. H. (2007). The MYB46 transcription factor is a direct target of SND1 and regulates secondary wall biosynthesis in *Arabidopsis*. *Plant Cell* 19, 2776–2792. doi: 10.1105/tpc.107.053678

Zhong, R., and Ye, Z. H. (2012). MYB46 and MYB83 bind to the SMRE sites and directly activate a suite of transcription factors and secondary wall biosynthetic genes. *Plant Cell Physiol.* 53, 368–380. doi: 10.1093/pcp/pcr185

Zhou, C., Li, Q., Chiang, V. L., Lucia, L. A., and Griffis, D. P. (2011). Chemical and spatial differentiation of syringyl and guaiacyl lignins in poplar wood *via* time-of-flight secondary ion mass spectrometry. *Anal. Chem.* 83, 7020–7026. doi: 10.1021/ac200903y

Zhou, H., Zhao, J., Yang, Y., Chen, C., Liu, Y., Jin, X., et al. (2012). UBIQUITIN-SPECIFIC PROTEASE16 modulates salt tolerance in *Arabidopsis* by regulating Na^+/H^+ antiport activity and serine hydroxymethyltransferase stability. *Plant Cell* 24, 5106–5122. doi: 10.1105/tpc.112.106393

Zhou, J., Lee, C., Zhong, R., and Ye, Z. H. (2009). MYB58 and MYB63 are transcriptional activators of the lignin biosynthetic pathway during secondary cell wall formation in *Arabidopsis*. *Plant Cell* 21, 248–266. doi: 10.1105/tpc.108.063321

Conflict of Interest: The authors declare that the research was conducted in the absence of any commercial or financial relationships that could be construed as a potential conflict of interest.

frontiers in Plant Science

CORRECTION
published: 09 September 2021
doi: 10.3389/fpls.2021.761291

Corrigendum: BEL1-like Homeodomain Protein BLH6a Is a Negative Regulator of *CAld5H2* in Sinapyl Alcohol Monolignol Biosynthesis in Poplar

Qiao Wang[1,2†], Xinren Dai[1†], Hongying Pang[1†], Yanxia Cheng[1], Xiong Huang[1,2], Hui Li[1], Xiaojing Yan[1], Fachuang Lu[3], Hairong Wei[4], Ronald R. Sederoff[5] and Quanzi Li[1,2]*

[1] State Key Laboratory of Tree Genetics and Breeding, Chinese Academy of Forestry, Beijing, China, [2] Research Institute of Forestry, Chinese Academy of Forestry, Beijing, China, [3] Department of Energy Great Lakes Bioenergy Research Center, Wisconsin Energy Institute, Madison, WI, United States, [4] College of Forest Resources and Environmental Science, Michigan Technological University, Houghton, MI, United States, [5] Forest Biotechnology Group, Department of Forestry and Environmental Resources, North Carolina State University, Raleigh, NC, United States

Keywords: lignin, *CAld5H2*, BEL1-like homeodomain protein, transcription factor, yeast one hybrid

OPEN ACCESS

Approved by:
Frontiers Editorial Office, Frontiers Media SA, Switzerland

***Correspondence:**
Quanzi Li
liqz@caf.ac.cn

[†] These authors have contributed equally to this work

Specialty section:
This article was submitted to Plant Biotechnology, a section of the journal Frontiers in Plant Science

Received: *19 August 2021*
Accepted: *20 August 2021*
Published: *09 September 2021*

Citation:
Wang Q, Dai X, Pang H, Cheng Y, Huang X, Li H, Yan X, Lu F, Wei H, Sederoff RR and Li Q (2021) Corrigendum: BEL1-like Homeodomain Protein BLH6a Is a Negative Regulator of CAld5H2 in Sinapyl Alcohol Monolignol Biosynthesis in Poplar. Front. Plant Sci. 12:761291. doi: 10.3389/fpls.2021.761291

A Corrigendum on

BEL1-like Homeodomain Protein BLH6a is a Negative Regulator of *CAld5H2* in Sinapyl Alcohol Monolignol Biosynthesis in Poplar

by Wang, Q., Dai, X., Pang, H., Cheng, Y., Huang, X., Li, H., Yan, X., Lu, F., Wei, H., Sederoff, R. R., and Li, Q. (2021). Front. Plant Sci. 12:695223. doi: 10.3389/fpls.2021.695223

When originally published, the article title contained a typographical error. The correct gene name should be "*CAld5H2*" instead of "*CAl5H2*" as originally published. The correct title is "BEL1-like Homeodomain Protein BLH6a is a Negative Regulator of *CAld5H2* in Sinapyl Alcohol Monolignol Biosynthesis in Poplar."

The authors state that this does not change the scientific conclusions of the article in any way. The original article has been updated.

frontiers in Plant Science

ORIGINAL RESEARCH
published: 02 July 2021
doi: 10.3389/fpls.2021.698602

Investigation Into Different Wood Formation Mechanisms Between Angiosperm and Gymnosperm Tree Species at the Transcriptional and Post-transcriptional Level

Hui Li[1,2†], *Guanghui Chen*[3†], *Hongying Pang*[1], *Qiao Wang*[1,4] *and Xinren Dai*[1*]

[1] State Key Laboratory of Tree Genetics and Breeding, Chinese Academy of Forestry, Beijing, China, [2] Guangzhou Institute of Forestry and Landscape Architecture, Guangzhou, China, [3] Shandong Peanut Research Institute, Shandong Academy of Agricultural Sciences, Qingdao, China, [4] Research Institute of Forestry, Chinese Academy of Forestry, Beijing, China

Enormous distinctions of the stem structure and cell types between gymnosperms and angiosperms tree species are expected to cause quite different wood physical and mechanical attributes, however, the molecular mechanisms underlying the differing wood morphology are still unclear. In this study, we compared the transcriptomes obtained by RNA-Seq between *Populus alba* × *P. glandulosa* clone 84K, and *Larix kaempferi* (Lamb.) Carr trees. Available genome resource served as reference for *P. alba* × *P. glandulosa* and the Iso-Seq results of a three-tissues mixture (xylem, phloem, and leaf) were used as the reference for *L. kaempferi* to compare the xylem-specifically expressed genes and their alternative splicing model. Through screening, we obtained 13,907 xylem-specifically expressed genes (5,954 up-regulated, 7,953 down-regulated) in the xylem of *P. alba* × *P. glandulosa*, and 2,596 xylem-specifically expressed genes (1,648 up-regulated, 948 down-regulated) in the xylem of *L. kaempferi*. From the GO and KEGG analyses, some genes associated with two wood formation-related pathways, namely those for phenylpropanoid biosynthesis, and starch and sucrose metabolism, were successfully screened. Then the distributions and gene expression models between *P. alba* × *P. glandulosa* and *L. kaempferi* in those pathways were compared, which suggested differential wood formation processes between the angiosperm and gymnosperm trees. Furthermore, a Weight Gene Co-expression Network Analysis (WGCNA) for total xylem-specifically expressed genes in two species was conducted, from which wood formation-related modules were selected to build a co-expression network for the two tree species. The genes within this co-expression network showed different co-expression relationships between the angiosperm and gymnosperm woody species. Comparing the alternative splicing events for wood formation-related genes suggests a different post-transcriptional regulation process exists between the angiosperm and gymnosperm trees. Our research thus provides the foundation for the in-depth investigation of different wood formation mechanisms of angiosperm and gymnosperm species.

Keywords: angiosperm, gymnosperm, transcriptome, co-expression network, alternative splicing, wood formation

OPEN ACCESS

Edited by:
Wei Li,
Northeast Forestry University, China

Reviewed by:
Qingzhang Du,
Beijing Forestry University, China
Akiyoshi Kawaoka,
Akita Jujo Chemicals Co, Ltd., Japan

***Correspondence:**
Xinren Dai
xinrend@caf.ac.cn

† These authors contributed equally to this work

Specialty section:
This article was submitted to Plant Biotechnology, a section of the journal Frontiers in Plant Science

Received: *21 April 2021*
Accepted: *01 June 2021*
Published: *02 July 2021*

Citation:
Li H, Chen G, Pang H, Wang Q and Dai X (2021) Investigation Into Different Wood Formation Mechanisms Between Angiosperm and Gymnosperm Tree Species at the Transcriptional and Post-transcriptional Level. Front. Plant Sci. 12:698602. doi: 10.3389/fpls.2021.698602

INTRODUCTION

Seed-bearing plants are the primary plant species on our planet and are composed of two main phyla, gymnosperms and angiosperms, which appeared ca. 300 million years ago (Pavy et al., 2012). Gymnosperms include seed-bearing plants that are woody, herbaceous, or climbing (vines), consisting of four extant sub-phyla: Cycadophyta (cycads), Ginkgophyta (*Ginkgo biloba* L.), Coniferophyta (conifers), and Gnetophyta (gnetophytes). Among them, the conifers are the most numerous gymnosperms found on earth, comprising 50 genera and 550 species, and they are widely distributed throughout the Northern Hemisphere (Carvalho et al., 2013). For the angiosperms, taxonomists have identified about 352,000 species, making it the most diversiform group on earth (www.theplantlist.org). All of these angiosperm species originated from one single ancestor ca. 167–199 million years ago (Bell et al., 2010), and diverged into eight extant clades, namely the Amborellales, Nymphaeales, Austrobaileyales, Monocots, Magnoliids, Ceratophyllales, Chloranthales and Eudicots. Among them, the Eudicots is the primary clade, containing about 262,000 species (Zeng et al., 2014).

Wood represents a renewable natural resource for feedstocks used in several bio-economy products, such as pulp, paper, and biomaterials, and potentially biofuels as well. It is also a major carbon sink in natural ecosystems. The stem of woody plants is mainly composed of secondary xylem (Li et al., 2010). The most striking divergent characteristics between gymnosperm and angiosperm wood are in their anatomical structure and chemical composition (Jokipii-Lukkari et al., 2018). In gymnosperm trees, tracheids provide both water transport and mechanical support; in angiosperms, vessel elements are responsible for carrying water, with fibers providing mechanical support for the stem. To some extent, however, the tracheids in gymnosperms are similar to the vessel in angiosperms (Courtois-Moreau et al., 2009; Dieset, 2011). Vessel elements appear only in angiosperm species and are shaped by the need for rapid and efficient water transport capacity (Sperry et al., 2006). Wood formation in tree species requires the complex coordination of two highly ordered processes, cell differentiation and secondary cell wall (SCW) thickening, which are initiated from the vascular cambium and result in thick-walled xylem cells (Zhao et al., 2014). Secondary walls of xylem cells are composed of high-content cellulose and lignin (Li et al., 2010). Importantly, the amount and chemical structure of lignin in SCWs differs between gymnosperms and angiosperms, and these differences are closely related to plant evolution (Vanholme et al., 2010; Nawawi et al., 2016). The lignin in gymnosperms is exclusively polymerized from guaiacyl (G) units, while both G units and syringyl (S) units are the major components of lignin in angiosperms (Sarkanen, 1971; Higuchi et al., 1977; Boerjan et al., 2003; Weng et al., 2008).

In the last few decades, significant progress has been made in uncovering the molecular players involved in SCW biosynthesis in tree species, including hormonal signals, receptor kinases, and the transcriptional network which controls SCW formation. Both NAC and MYB master switches and their downstream transcription factors (TFs) have been shown to play critical roles during SCW formation (Yamamoto et al., 1997; Aspeborg et al., 2005; Li et al., 2012; Zhong and Ye, 2014; Ye and Zhong, 2015; Zhang et al., 2018; Du et al., 2019; Wang et al., 2019). Genes encoding the enzymes for the biosynthesis of SCW cellulose, hemicelluloses, and lignin have been identified and most of them are now functionally characterized in *Populus* and *Eucalyptus* (Suzuki et al., 2006; Shi et al., 2009; Lu et al., 2013; Yuan et al., 2014; Ye and Zhong, 2015; Kim et al., 2019; Wang et al., 2019). Many recent studies aiming to identify those key genes involved in wood development in many plant species were carried out to investigate xylem evolution at the transcriptome level (Cronk and Forest, 2017; He and Groover, 2017; Sundell et al., 2017; Tuskan et al., 2018; Roodt et al., 2019). The expanding genomic resources of tree species are invaluable for exploring secondary xylem formation and its evolution. Yet woody gymnosperm species typically have large genome sizes and high heterozygosity, so their transcriptome analyses remain limited by the poor quality of assembled genomes.

Alternative splicing (AS) is an important model of post-transcriptional regulation that can increase transcriptional and proteomic diversity in eukaryotic organisms (Chen and Manley, 2009). AS that combines different transcript splice junctions results in transcripts with shuffled exons, alternative 5′ or 3′ splicing sites, retained introns, and different transcript termini. In plants, 33−60% of the mRNAs are alternatively spliced (Shen et al., 2014), of which more than 60% are in the form of retained introns (Zhang et al., 2010; Syed et al., 2012). Transcriptome analysis has revealed that approximately 36% of wood-expressed genes undergo AS in the xylem of *P. trichocarpa* (Bao et al., 2013), and that 28.3% and 20.7% of the highly expressed transcripts in developing xylem tissue undergo AS events in *Populus* and *Eucalyptus*, respectively (Xu et al., 2014). Interestingly, most of the key TFs in the first layer of SCW regulatory network also undergo AS. In *Populus*, *PtrSND1-A2*^{IR}, a splice variant of stem-differentiating xylem (SDX)- SND1, acts as a dominant negative regulator of the SND1 transcriptional network (Li et al., 2012). *PtrSND1-A2*^{IR} is derived from *PtrSND1-A2* (also named *PtrWND1B/PtrVNS11*), having lost its DNA binding and activation domain but retaining its dimerization capability; it represses the transcription of *PtrSND1* members and their target gene *PtrMYB021* by translocating into the nucleus exclusively as a heterodimeric partner with full-size PtrSND1s (Li et al., 2012). This is the first time to report about the TF family's auto-repression by its own splice variant found in plants (Zhang et al., 2018; Camargo et al., 2019). Other research has shown that overexpression of *PtrSND1-A2* enhances fiber cell wall thickening, while overexpression of *PtrSND1-A2*^{IR} (*PtrWND1B-l*) inhibits the fiber cell wall-thickening process (Zhao et al., 2014). *VND6*, another key TF in the first layer of the SCW regulatory network, was also confirmed to undergo alternative splicing during wood formation in poplar (Lin et al., 2017). Its splice variant, *PtrVND6-C1*^{IR} derived from *PtrVND6-C1* (*PtVNS01/PtrWND5A*), suppresses the protein functioning of all *PtrVND6* and *PtrSND1* family members, whereas *PtrVND6-C1*^{IR} is unable to suppress *PtrSND1-A2*; further, *PtrSND1-A2*^{IR} has no effect on *PtrVND6-C1*^{IR}. Both *PtrVND6-C1*^{IR} and *PtrSND1-A2*^{IR} function together in the reciprocal cross-regulation of VND and SND members to maintain homeostasis during xylem differentiation

and plant development. Recently, for a gymnosperm species, *LaSCL6*, a member of the GRAS transcription factor family, was determined to have two variants which are differentially expressed during the growth and development in *L. kaempferi* (Zang et al., 2019). Our knowledge of AS of other genes, especially the key TFs in SCW regulatory network, is still vastly limited.

Although some molecular players are distinguished by their conserved functions during wood formation in gymnosperms and angiosperms, wood formation between gymnosperms and angiosperms is clearly different (i.e., xylem cell type and wood composition, among others). This suggests their gene regulatory networks are also not the same and that certain genes may have distinct functions in the two tree species above. Here, we employed next-generation sequencing and Iso-Seq technology to explore the gene expression model across wood-forming tissues in the angiosperm *P. alba* × *P. glandulosa* and the gymnosperm *L. kaempferi*. By screening xylem specific-expressed genes, associating these genes with wood-formation related pathways, building a co-expression network and analyzing the AS of common genes among the two tree species, differential mechanisms of wood formation between angiosperm and gymnosperm tree species were investigated and preliminarily discussed. Our research provides theoretical support for searching for the differing wood formation mechanisms between angiosperm and gymnosperm species.

MATERIALS AND METHODS

Plant Materials Collection and RNA Extraction

Samples were collected from 10-year-old *P. alba* × *P. glandulosa* trees in the Beiwu garden (39°59′N, 116°15′E; Beijing, China) and 10-year-old *L. kaempferi* tress in the Dagujia seed orchard (42°22′N, 124°51′E; Liaoning Province, China) as describe in He et al. (2020). Briefly, the bark and phloem were peeled off at breast height, the immature xylem and phloem were collected from each species by scratching with single-end razors. These, along with leaf samples, were immediately frozen in liquid nitrogen. Each sample was collected from three trees per species as three biological replicates. Total RNAs were extracted by using the improved CTAB method (Lorenz et al., 2010). The RNA was precipitated by ethanol, and then dissolved in RNase-free water. After digesting it with DNaseI, we used the Agilent 2100 Bioanalyzer and NanoDrop to measure the RNA concentration, RIN value, 28s/18s value, and size of the fragment, to confirm the integrity and purity of RNA in the samples.

Construction of a PacBio Library With Different Library Sizes and Sequencing

To correct the Hi-Seq results and analyze AS events in the two tree species, we also constructed PacBio libraries. By taking 1 μg RNA subsamples, first-strand cDNA was synthesized using the Clontech SMARTer PCR cDNA synthesis Kit (cat. no. 634926, http://www.clontech.com/), with an anchored olig (dT) 30 as the primer. Then the double-strand cDNA was amplified by carrying out a long PCR (LD-PCT) using the Advantage 2 PCT kit (Clonetech, cat. No.639206). The 1–2 kb, 2–3 kb, and 3–6 kb cDNA fragments were generated by the BluePinppin size-selection system (Sage Science, http://www.sagescience.com/). For those transcripts whose size was more than 3 kb, we generated the BluePippin selection again. The PacBio libraries were then constructed with a Pacific Biosciences SMARTbell template Prep Kit 1.0 (part 100-259-100, http://www.pacb.com/), following the manufacture's protocol. These libraries were later sequenced on a PacBio RSII real-time (RT) platform, using the SMRT Cell 8 Pac v3 (part100-171-800) with a total of 8 SMRT cells: that is, the 1–2 k and 2–3 k libraries were each sequenced with 3 SMRT cells, while the 3–6 k libraries were sequenced with 2 SMRT cells.

RNA-Seq Library Construction and Sequencing

We used magnetic beads with Oli (dT) to enrich the mRNA and broke it into pieces by applying a fragmentation buffer. Employing these mRNAs as the template, random hexamers were used to synthesize the first-strand cDNA. Next, together with buffer, the dNTPs, RNaseH, and DNA polymerase I synthesized the second-strand cDNA. Each cDNA library was purified and to it a joint end with A was added. Following their PCR amplification, the ensuing PCR products were sequenced by the Illumina HiSeq 2500 platform to generate 100-bp paired sequence reads.

Analysis of PacBio Single-Molecule Reads

We used the SMRT Analysis Server (v2.3) to handle the Raw SMRT sequencing reads in order to obtain the Full-Length non-chimeric Read (FLNC). The first step in doing this was to properly deal with the inserted anti-molecular sequence and assess the length of cDNAs loaded into SMRT cell using these parameters "minFullPasses" = 0, "minPredictedAccruacy" = 80, "numThreads" = 12. Reads-of-Insert can be obtained from a single molecular inserted sequence. After removing the cDNA primer and polyA, we classified the Reads-of-Insert into full-length or non-full-length, chimeric or non-chimeric, fragments with these two parameter settings: "min_seq_len" = 300, "cpus" = 12. The full-length and non-chimeric transcripts were corrected, using the Interactive Clustering and Erro Correction (ICE) algorithm, to obtain the corresponding sequences. Then the cover rating for these corresponding sequences was predicted, after which the non-full length and non-chimeric sequences were corrected by the Quiver algorithm.

Completing these steps left us with high- and low-quality full-length transcripts. The LSC software was then used to correct the FLNC by referencing short reads of HiSeq (Au et al., 2012). For each corrected FLNC, we used the CD-HIT-EST to reduce the redundant highly similar transcripts (Li and Godzik, 2006); these transcripts were merged by Cogent software to obtain the unigenes. For their annotation, unigenes were BLAST-searched to NR (ftp://ftp.ncbi.nlm.nih.gov/blast/db), NT (ftp://ftp.ncbi.nlm.nih.gov/blast/db), COG (http://www.ncbi.nlm.nih.gov/COG), KEGG (http://www.genome.jp/kegg) and Swiss-Prot (http://ftp.ebi.ac.uk/pub/databases/swissprot) databases. According to those annotations of the NR database, Blast2GO (https://www.blast2go.com)

(Conesa et al., 2005) was used to obtain the annotations from the GO database. According to the latter, the CDs of best-matched unigenes were selected for further analysis. For those unigenes that could not be annotated by any database, ESTscan software was relied upon to build a model and predict the CDs for them (Iseli et al., 1999).

Read Mapping and Differentially Expressed Genes (DEGs) Analyses

Raw data were filtered using the NGS QC Toolkit to obtain clean reads. These were mapped onto the genome or PacBio Isoform transcripts via Hierarchical Indexing for Spliced Alignment of Transcripts (HISAT) (Kim et al., 2015). The mapped output was processed by Cufflinks to obtain the Fragments per Kilobase Million (FPKM) for all genes in each sample, for which correlations among different replicate samples were determined by calculating Pearson correlation. Using the DEseq2 software (Love et al., 2014), we obtained the DEGs among the types of plant tissue. The DEGs in the two species were filtered according to these criteria: the DEGs that had a $\log_2$ (X vs. P or L) $\geq$ 1 (Q-value $\leq$ 0.05) were designated as up-regulated genes in xylem compared to phloem and leaf parts; those DEGs that met $\log_2$ (X vs. P or L) ≤ -1 (*Q*-value $\leq$ 0.05) were considered down-regulated genes compared with the other two tissue types. The intersection of X vs. P and X vs. L correspond to the xylem-specifically expressed genes.

GO and KEGG Analysis for Xylem-Specifically Expressed Genes

For all DEGs, their Gene Ontology (GO) enrichment analysis was conducted using GOseq and topGO (Young et al., 2010). To do this, we first mapped all the detected genes in the two tree species to the GO database (http://geneontology.org/), to obtain their GO annotations. According to these results, we enriched the xylem-specifically expressed genes by comparing them to the reference gene background by applying the hypergeometric test. The gene numbers for each term were then calculated, among which the significantly enriched GO terms were determined. We also mapped all detected genes to the Kyoto Encyclopedia of Genes and Genomes (KEGG) database (https://www.kegg.jp/), to obtain their corresponding KEGG annotations. According to the KEGG annotations, we enriched the xylem-specifically expressed genes in the main biochemical and signal transduction pathways and identified those significantly enriched metabolic pathways or signal transduction pathways. The "phyper" package for the R computing platform was used to calculate the *p* values, as described in Li et al. (2020).

Association of mRNAs in Wood Formation-Related Pathways

Based on the KEGG results, we located the enriched xylem-specifically expressed genes in two pathways, the phenylpropanoid biosynthesis pathway, and the starch and sucrose pathway, to derive and display a putative gene expression model. These pathways were visualized in Chewdraw software (version Professional 15.0). The heatmaps were drawn with TBtools 0.6669 (Chen et al., 2020).

Weighted Gene Co-expression Network Analysis (WGCNA) for Xylem-Specifically Expressed Genes

We used "WGNCA" package in R software to carry out a co-expression network analysis for xylem-specifically expressed genes in the two tree species. Then, for each module per species, we also conducted GO and KEGG analyses. After combining these GO and KEGG results, we selected the modules in which wood formation-related genes were evidently enriched.

Network Building for Wood-Formation Related Genes

To discern the possible relationships among wood formation-related genes, we chose the top 50,000 gene relation pairs in the selected edge file of WGCNA and imported these pairs into Cytoscape software (Kohl et al., 2011). According to the GO and KEGG analyses and BLASTn results in the selected module of each species, we built co-expression networks of wood formation-related genes in Cytoscape software to depict the co-expression relationships of the two tree species.

Identification of Alternative Splicing (AS)

To classify the AS events, Cogent software was used to reconstruct the PacBio transcripts and this yielded the UniTransModels. After blasting the non-redundant transcripts to UniTransModels, using GMAP software, the output results from GMAP were inputted into SUPPA software to detect the AS events (Li et al., 2017).

Verification of RNA-Seq Result and AS Events

To validate the RNA-Seq and AS events experimentally, PCRs were run for eight pairs of homologous genes that underwent different AS types in the two tree species. For each sample, 1 mg of total RNA was reverse-transcribed into first-strand cDNA, by using the PrimeScript RT reagent Kit gDNA Eraser (Takara, Dalian, China). The primers were designed based on the consensus gene sequences of the two tree species, and these primer sequences are listed in **Supplementary Tables 1A,B**. For validation of RNA-Seq results, we chose several genes from both *P. alba* × *P. glandulosa* and *L. kaempferi* to perform the qRT-PCR, by following the instructions for SYBR® Premix Ex Taq™ II (Takara), for the xylem, phloem, and leaf tissues, respectively. Linear fitting between RNA-Seq and qRT-PCR data was done in Origin 2016 software. To validate the AS events, the PCR was run in a 25-ml reaction system, using the High-Fidelity PCR Master Mix (NEB), whose procedure went as follows: initial denaturation at 98°C for 1 min, 98°C for 10 s, 60°C for 30 s, and 72°C for 1–3 min (35 cycles) and a final extension at 72°C for 5 min. All the PCR products were visualized by 1.5% agarose gel electrophoresis analysis.

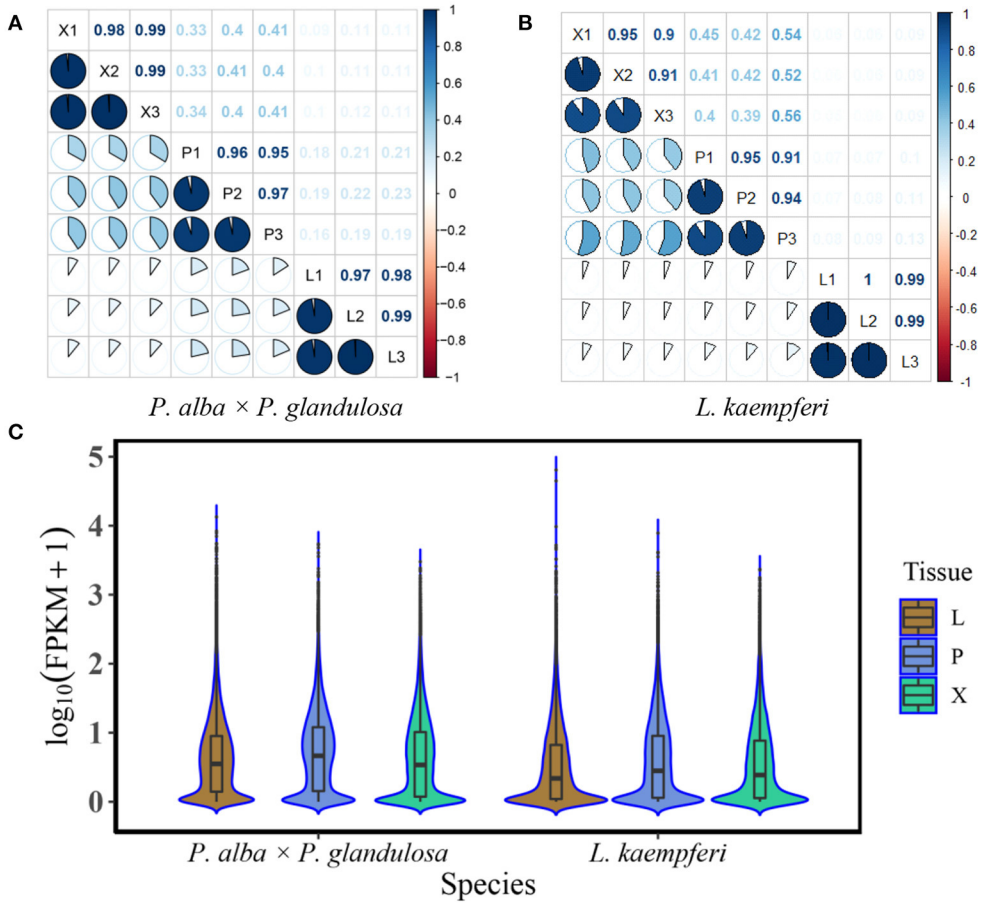

FIGURE 1 | Correlation analysis and the gene expression distributions of different tissues in the two tree species. **(A)** Correlations among different tissues and replicates of the angiosperm *Populus alba* × *P. glandulosa* clone 84K (*P. alba* × *P. glandulosa*). **(B)** Correlations among different tissues and replicates of the gymnosperm *Larix kaempferi* (Lamb.) Carr (*L. kaempferi*). **(C)** Gene expression distribution of different tissues (Xylem: X; Phloem: P; Leaf: L) in two tree species. Box plots appear in the center of the violin graphs. The top edge, middle edge, and bottom edge represent third quartile, median, and first quartile, respectively. The expression levels of the genes were standardized by the $\log_{10}$ (FPKM) algorithm. FPKM represents Fragments per Kilobase Million.

RESULTS

Global Analysis of RNA-Seq for the Two Tree Species

We conducted the RNA-Seq of xylem, phloem, and leaf tissues of two tree species, with three biological replicates per tissue. Before the formal data analysis, we tested for correlations (using Pearson's r) among the different replicates and tissue types (**Figure 1**). The tests confirmed that the three replicates of the same tissue in each of the species were strongly correlated, having r values > 0.8 (**Figures 1A,B**), thus showing that their transcriptome data was suitable for further analysis. We also derived key statistics for gene expression levels in different tissue of the two tree species. In*P. alba* × *P. glandulosa*, two high proportions of expressed genes focus at 0.1 and 1.0, respectively. By contrast, there was only one high proportion of expressed genes focus at 0.1 in *L. kaempferi*. The median gene expression levels in the three tissues of *P. alba* × *P. glandulosa* were about 0.8–0.9, and higher than those of *L. kaempferi* (**Figure 1C**). These phenomena reflected different gene expression distributions between angiosperm and gymnosperm tree species.

We next profiled the RNA transcriptome for three tissues (xylem, phloem and leaves) of the two tree species. In *P. alba* × *P. glandulosa*, we obtained 50,995,164, 56,113,145, and 50,995,164 clean reads in the xylem, phloem, and leaves, respectively; in *L. kaempferi*, the corresponding counts were 66,463,409, 77,166,823, and 63,449,442 clean reads. The reads from *P. alba* × *P. glandulosa* were mapped to the reference genome (https://bigd.big.ac.cn/), while those reads from *L. kaempferi* were mapped to the SMRT library which had corrected by RNA-Seq data. The mapping rates for xylem, phloem, and leaf tissue were 95.39 95.41 and 95.60 for *P. alba* × *P. glandulosa*, and 46.79 41.41 and 54.95 for *L. kaempferi*, respectively. Eventually, we obtained 44,561 genes in xylem, 47,465 in phloem, and 48,091 in leaves of *P. alba* × *P. glandulosa*, and likewise, 21,535 genes in xylem, 22,986 in phloem and 23,233 in leaves of *L. kaempferi* (**Table 1**).

TABLE 1 | Summary information of the RNA-Seq results for the two tree species.

Species	Tissue	Total reads	Mapped reads	Mapping rate%	Number of gene
Populus alba × *P. glandulosa*	xylem	50,995,164	48,644,287	95.39	44,561
	phloem	56,113,145	53,537,552	95.41	47,465
	leaf	50,995,164	48,751,377	95.60	48,091
Larix kaempferi	xylem	66,463,409	24,451,888	46.79	21,535
	phloem	77,166,823	31,954,781	41.41	22,986
	leaf	63,449,442	34,865,468	54.95	23,233

Screening of Xylem-Specifically Expressed Genes in the Two Tree Species

To understand the expression discrepancy of RNAs in three different tissues of the two tree species, we conducted a DEG analysis for *P. alba* × *P. glandulosa,* we obtained 9,025 up-regulated DEGs and 12,024 down-regulated DEGs in the X vs. P group, and 12,086 up-regulated DEGs and 19,241 down-regulated DEGs in the X vs. L group (**Figure 2A**; **Supplementary Tables 2A,B**). For *L. kaempferi*, we obtained 2,746 up-regulated DEGs and 2,080 down-regulated DEGs in the X vs. P group, and 3,150 up-regulated DEGs and 3,063 down-regulated DEGs in the X vs. L group (**Figure 2B**; **Supplementary Tables 2C,D**). By taking the overlapping intersection of X vs. P and X vs. L, finally, we finally obtained 5,954 up-regulated DEGs and 7,953 down-regulated DEGs in the xylem of *P. alba* × *P. glandulosa* (**Figure 2A**), and 1,648 up-regulated and 948 down-regulated DEGs in the xylem of *L. kaempferi* (**Figure 2B**).

Validation of RNA-Seq Results by qRT-PCR

To detect and check the robustness of our RNA-Seq results, we selected four genes in *P. alba* × *P. glandulosa*: Pop_G14G045130 (*PagBXL2*), Pop_G16G060785 (*PagIRX9*), Pop_G06G002976 (*PagPME2*), and Pop_A14G029833 (*PagARA12*), and similarly four genes in *L. kaempferi*: Lkgene4125 (*LkIRX9H*), Lkgene760 (*LkMSR2*), Lkgene166 (*LkC4H*), and Lkgene11869 (*LkSUS4*). These were used to perform qRT-PCR in xylem, phloem, and leaf tissues (**Figure 3**). In *P. alba* × *P. glandulosa*, except for Pop_G06G002976, the other three genes were significantly up-regulated or down-regulated in xylem when compared to the other tissues. In *L. kaempferi*, all four selected genes were significantly up-regulated or down-regulated in xylem (**Figure 3**). Hence, the qRT-PCR results agreed with the RNA-Seq analysis. The linear relationship between the RNA-Seq and qRT-PCR results was fitted in the Origin software; this showed their data were significantly correlated (p value = 1.47E-14). The slope of the fitted line was 20.15, indicating a positive relationship between RNA-Seq and qRT-PCR results, and the goodness-of-fit was $R^2 = 0.553$ (**Figure 3**). Taken together, these results indicated our RNA-Seq results were reliable and useful for further analysis.

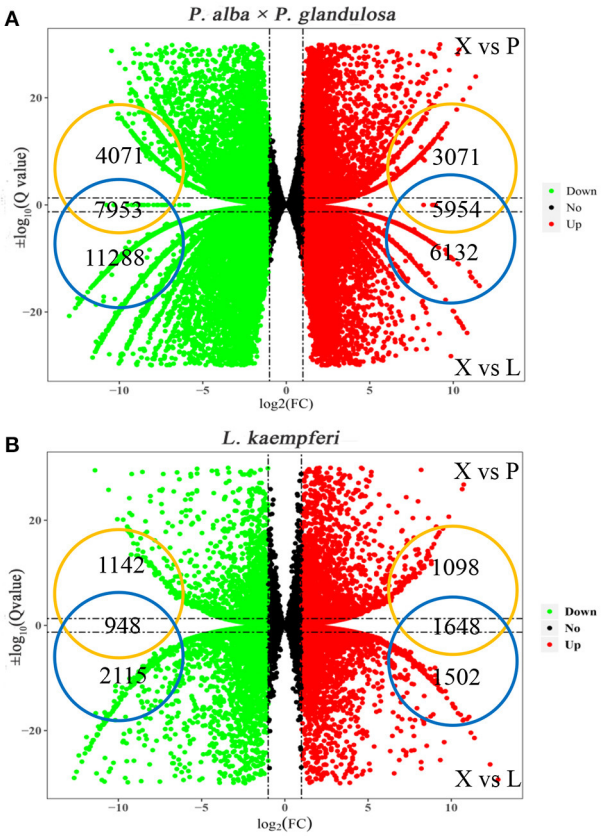

FIGURE 2 | Distributions of up- and down-regulated DEGs in the two tree species. **(A)** Up and down-regulated DEGs in *P. alba* × *P. glandulosa*. **(B)** Up and down-regulated DEGs in *L. kaempferi*. In both panels, X vs. P represents the differential expression analysis between the xylem and phloem; likewise, X vs. L represents the differential expressed analysis between the xylem and leaf. The vertical dotted lines correspond to the $\log_2$ (fold- change) = ±1, while the horizontal dotted lines are positioned at $\log_{10}$ (Q-value) = ±1.3 (Q-value = 0.05). The genes at the intersection of two groups are the up- and down-regulated genes in xylem tissue.

GO Analysis and Functional Classification for Xylem-Specifically Expressed Genes

By filtering the DEGs, we obtained 13,907 xylem-specifically expressed genes (5,954 up-regulated, 7,953 down-regulated) in *P. alba* × *P. glandulosa*, and 2,596 xylem-specifically expressed genes (1,648 up-regulated, 948 down-regulated) in *L. kaempferi*. To assess and compare the functional differences of these genes between the two species, we implemented GO and KEGG analyses. Three main ontologies—biological process (BP), cellular component (CC), and molecular function (MF)—were considered here. To fully display the GO terms, we reordered them according to the Q-values of the GO results and selected only the top 10 GO terms in each ontology category for the visualization.

In *P. alba* × *P. glandulosa*, 13,907 xylem-specifically expressed genes were clustered in 50 GO terms. Under BP, genes were significantly enriched in single organism

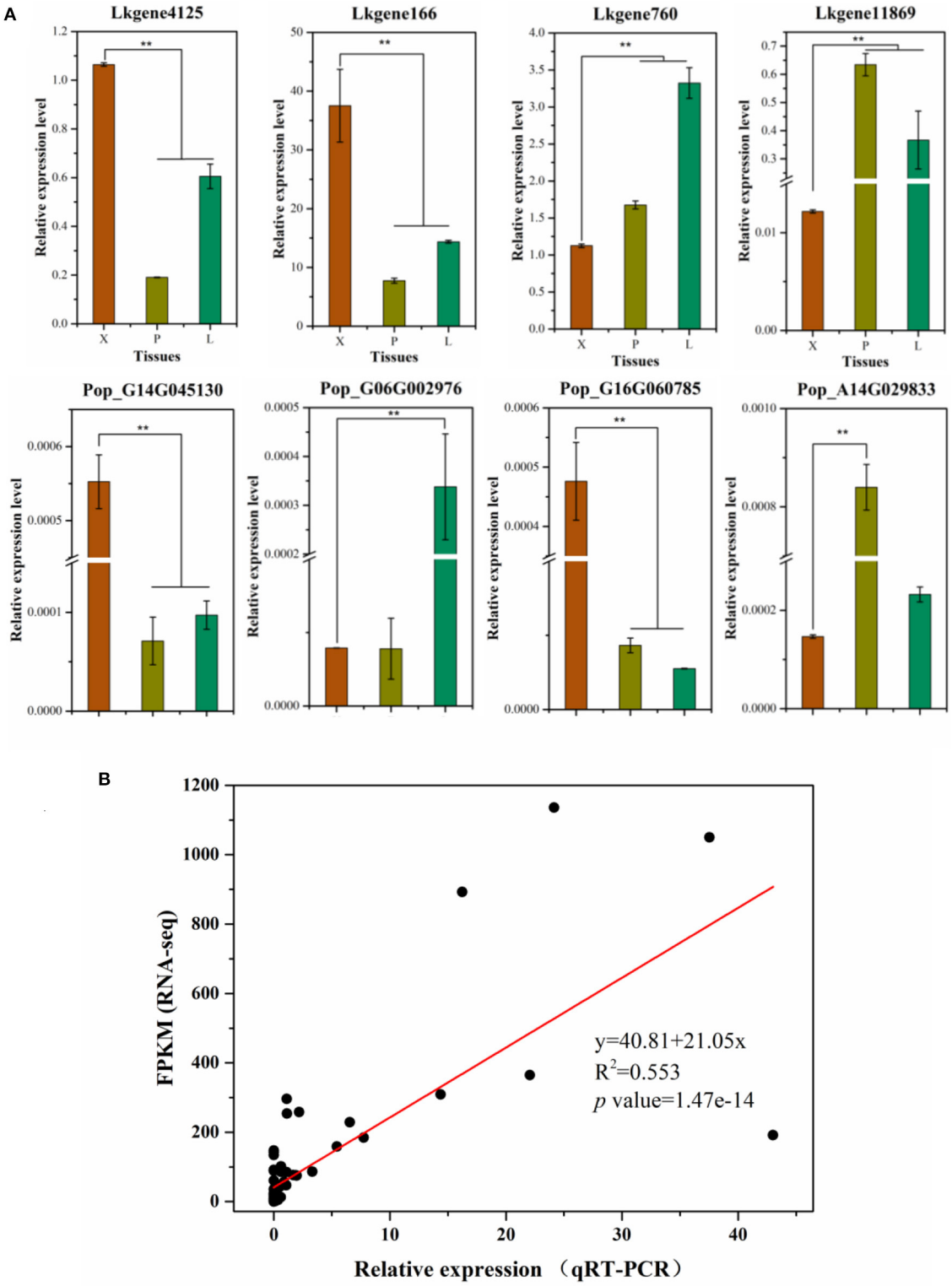

FIGURE 3 | Validation of RNA-Seq results by qRT-PCR. **(A)** The qRT-PCR results for selected genes in the two tree species. **(B)** Linear regression for the RNA-Seq and qRT-PCR results. In this graph, gene expression levels in RNA-Seq are standardized by FPKM, the expression levels in qRT-PCR were standardized by the $2^{-\Delta ct}$ algorithm. In **(A)**, the relative expression levels in the three tissue types are shown as the mean ± sd; the ** indicates a significant difference at $P < 0.01$ according to a one-way ANOVA.

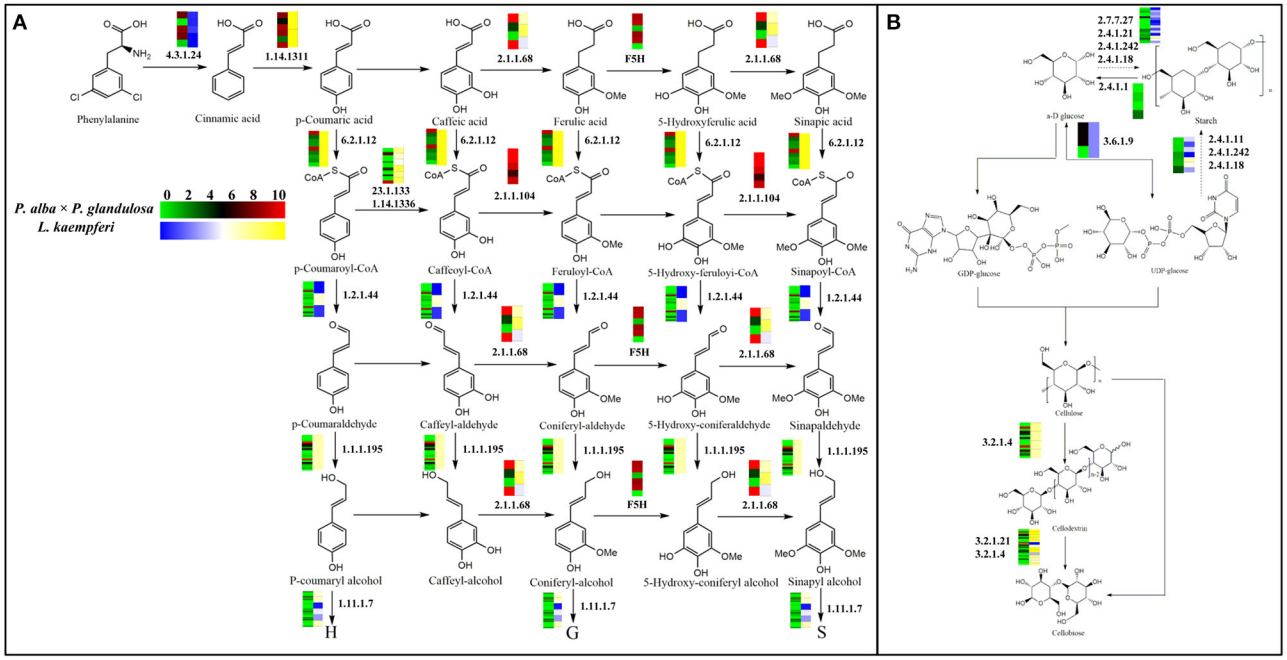

FIGURE 4 | Gene expression model for the lignin and cellulose biosynthesis pathway. **(A)** Branch of phenylpropanoid biosynthesis pathway that is related to lignin biosynthesis. **(B)** Branch of starch and sucrose metabolism pathway that is related to cellulose biosynthesis. The heatmaps in each pathway are visualized according to gene expression levels. In the color bar, red indicates a high expression level and green a low expression level in *P. alba* × *P. glandulosa*; yellow corresponds to high expression level and blue a low expression level in *L. kaempferi*. The dotted arrows in the pathways denote an indirect linkage. The solid arrows refer to a direct relationship during compound synthesis. Numbers in the graph are EC identifier of corresponding enzyme.

process (GO: 0044699, *Q*-value = 1.4E-07), localization (GO: 0051179, *Q*-value = 5.45E-05), and growth (GO: 0040007, *Q*-value = 0.017); under MF, genes were significantly enriched in transporter activity (GO: 0005215, *Q*-value = 2.20E-14) and electron carrier activity (GO: 0009055, *Q*-value = 1.1E-4); finally, under CC, genes were significantly enriched in membrane (GO: 0016020, *Q*-value = 3.16E-58), membrane part (GO: 0044425, *Q*-value = 3.16E-58), supramolecular fiber (GO: 0099512, *Q*-value = 1E-5), extracellular region (GO: 0005576, *Q*-value = 1.1E-3), cell junction (GO: 0030054, *Q*-value = 2.37E-2), and symplast (GO: 0055044, *Q*-value = 2.37E-2) (**Supplementary Table 3A**). In *L. kaempferi*, 2,596 xylem-specifically expressed genes were enriched in 43 GO terms. Under BP, genes were significantly enriched only in single organism process (GO: 0044699, *Q*-value = 6.84E-09); under MF, genes were significantly enriched in catalytic activity (GO: 0005576, *Q*-value = 1.903E-33), nucleic acid binding transcription factor activity (GO: 0099512, *Q*-value = 6.0E-08), and structural molecule activity (GO: 0044425, *Q*-value = 9.05E-3); under CC, genes were significantly enriched in membrane part (GO: 0003824, *Q*-value = 3.486E-11), membrane (GO: 0001071, *Q*-value = 2.39E-2), and nucleoid (GO: 0005198, *Q*-value = 2.7E-2) (**Supplementary Table 3C**). In **Supplementary Figures 1A,C,** more detailed GO terms are shown for the two species. According to the GO results, genes in *P. alba* × *P. glandulosa* tend to increase plant growth and enable the directed movement of substances within cells; in contrast, genes in *L. kaempferi* involved in the structural integrity of a complex or its assembly within or outside a cell, catalyzed reactions process. In sum, our GO analysis results indicated different functions between the angiosperm and gymnosperm trees.

For the KEGG analysis, we reordered the results according to the Rich factor and chose the top 30 pathways for visualization purposes. In *P. alba* × *P. glandulosa*, 13,907 xylem-specifically expressed genes were enriched in 132 pathways. The top three significantly enriched pathways were photosynthesis (ko00195), metabolic pathways (ko01100), and photosynthesis-antenna proteins (ko00196) (**Supplementary Figure 1B**; **Supplementary Table 3B**) with corresponding enriched gene numbers of 99, 1,605, and 34 respectively. In *L. kaempferi*, 2,596 xylem-specifically expressed genes were clustered in 112 pathways; its top three significantly enriched pathways were starch and sucrose metabolism (ko00500), flavonoid biosynthesis (ko00941), and metabolic pathways (ko01100). The enriched gene numbers respectively were 196, 59, and 655 (**Supplementary Figure 1D**; **Supplementary Table 3D**). Hence, these KEGG results also uncovered different gene functions during the metabolism process between the two tree species.

Association of Xylem-Specifically Expressed Genes With Lignin and Cellulose-Formation Related Pathways

Here, we selected two main pathways related to wood formation: phenylpropanoid biosynthesis, and starch and sucrose

metabolism (**Figure 4**), and went on to associate each with those xylem-specifically expressed genes according to the KEGG results. Evidently, in both pathways, most of those genes were active in the same step during lignin and cellulose synthesis processes in the two species. Yet differences did exist between these tree species. For instance, in the phenylpropanoid biosynthesis pathway, during the transformation from ferulic acid to 5-hydroxyl ferulic acid, coniferyl-aldehyde to 5-hydroxy-coniferaldehyde, and coniferyl-alcohol to 5-hydroy-coniferyl alcohol, we found that six highly expressed genes (homologous to *FAH1*) participated in these steps in *P. alba* × *P. glandulosa*. These genes encode enzymes that catalyze the hydroxylation of coniferyl alcohol and coniferaldehyde during syringyl lignin formation (Wu et al., 2018). In stark contrast, such genes were apparently absent in *L. kaempferi* (**Figure 4A**; **Supplementary Tables 4A,B**).

During the biosynthesis process of cinnamic acid from phenylalanine, most genes in *P. alba* × *P. glandulosa* were highly expressed, whereas most genes in *L. kaempferi* were expressed at low levels. In the synthesis process converting cafferyl-CoA to feruloyl-CoA, and 5-hydroxy-feruloyl CoA to sinapoyl-CoA, we identified five active genes (homologous to *CCoAOMT1* and *CCOAMT*) in *P. alba* × *P. glandulosa* (**Figure 4A**; **Supplementary Tables 4A,B**), known to related to lignin content and composition (Xie et al., 2019). In the starch and sucrose metabolism pathway, four genes (homologous to*PHS1* and *DPE2*) were expressed in *P. alba* × *P. glandulosa*, these participating in the transformation from starch to α-D glucose (**Figure 4B**; **Supplementary Tables 4A,B**). These divergent results may explain why the compound synthesis mechanism differs between gymnosperm and angiosperm species during their wood formation.

Although both tree species also harbor homologous genes involved in the same steps, their respective expression patterning was not totally identical, with certain discrepancies among them. For example, during the formation of an alcohol-derived compound from an aldehyde-derived compound, we distinguished 21 genes—homologous to *CAD4*, *6*, *7*, *9*, *K9L2.15*,0.18,0.19,0.20, *MEE23*, *T17H7.1*, and *FOX2*—expressed in these steps in *P. alba* × *P. glandulosa*. Among them, CAD (cinnamyl alcohol dehydrogenase) family members are involved in lignin biosynthesis and catalyze the final step specific for the production of lignin monomers (Kim et al., 2004). A member of the BBE-like family, *T17H7.1*, mediates the oxidation of cinnamyl alcohol and of *p*-hydroxylated derivatives of cinnamyl alcohol during the monolignin metabolism process (Daniel et al., 2015). Yet only Lkgene2978 (homologous to *F19I3.4*) was expressed in *L. kaempferi* (**Figure 4A**, **Supplementary Tables 4A,B**). This disparity between species suggests that *P. alba* × *P. glandulosa* relies on a more complicated mechanism than the gymnosperm species during these steps of wood formation. Nevertheless, despite belong to different phyla, *P. alba* × *P. glandulosa* and *L. kaempferi* have expression models with notable similarities. For example, some genes found (homologous to *T16L4.190*) participated in the reciprocal transformation between α-D glucose and UDP-glucose in both *P. alba* × *P. glandulosa* and *L. kaempferi* (**Figure 4B**; **Supplementary Table 4B**). This emphasizes that different species within the same phyla could be similar in some aspects.

WGCNA Analysis and Co-expression Network Building for Wood-Formation Related Genes in the Two Tree Species

To better understand the relationships among those xylem-specifically expressed genes, we performed a WGCNA analysis (Lukens and Downs, 2012) (**Supplementary Figure 2**). For *P. alba* × *P. glandulosa*, its 13,907 xylem-specifically expressed genes could be divided into 20 dynamic modules. After merging them, eventually we obtained four modules: a dark magenta module, an orange module, a saddle brown module, and a white module (**Supplementary Figure 2A**). For *L. kaempferi*, its 2,596 xylem-specifically expressed genes were divided into 22 dynamic modules. After merging those, three modules were obtained: a dark green module, a green module, and a midnight blue module (**Supplementary Figure 2B**).

After doing the WGCNA analysis for each selected module per species, the top 50,000 gene pairs ordered by the edge weight coefficient were chosen to build a gene co-expression network (**Figure 5**; **Supplementary Table 5**). A follow-up GO analysis was then performed for each module, from which only the top five GO numbers in BP are shown graphically (**Figure 5**). For *P. alba* × *P. glandulosa*, the GO analysis showed that more of its wood formation-related genes were clustered in the orange module. Among these top five GO terms, GO: 0009808 had a relationship with lignin biosynthesis (**Figure 5**; **Supplementary Table 5C**). In *L. kaempferi*, the genes were significantly enriched in starch metabolic process (GO: 0005982) and starch biosynthetic process (GO: 0019252) in the dark green module (**Figure 5**; **Supplementary Table 5I**), as were the phenylpropanoid catabolic process (GO: 0046271), lignin catabolic process (GO: 0046274), lignin metabolic process (GO: 0009808), and phenylpropanoid metabolic process (GO: 0009698) in the midnight blue module (**Figure 5**; **Supplementary Table 5M**).

Combining the GO and KEGG results and the BLASTn to *Arabidopsis*, we then screened the wood formation-related genes among all xylem-specifically expressed genes and built the former's co-expression network in the two tree species (**Figure 6**). In the resulting co-expression network, 36 co-expressed genes were specific to *P. alba* × *P. glandulosa* (**Supplementary Table 6A**), 34 co-expressed genes were specific to *L. kaempferi* (**Supplementary Table 6B**), and 27 genes were shared by the two species (**Supplementary Table 6C**). Of the 36 specifically expressed genes in *P. alba* × *P. glandulosa*, four NAC members (*VND1*, *VND5*, *SND2*, *SND3*), two MYB members (*MYB26*, *MYB52*), two laccase members (*LAC2*, *LAC4*), and two cysteine protease members (*XCP1*, *XCP2*) were obtained. Among these, *SND2* is known to play a crucial role in the biosynthesis of cellulose, mannan, and xylan, in addition to cell wall modification and lignin polymerization, but not so in monolignol biosynthesis. The *SND2* promotes the up-regulation of several TF genes, such as *MYB103* and *SND1*, and it occupies a subordinate position in the transcriptional regulatory network

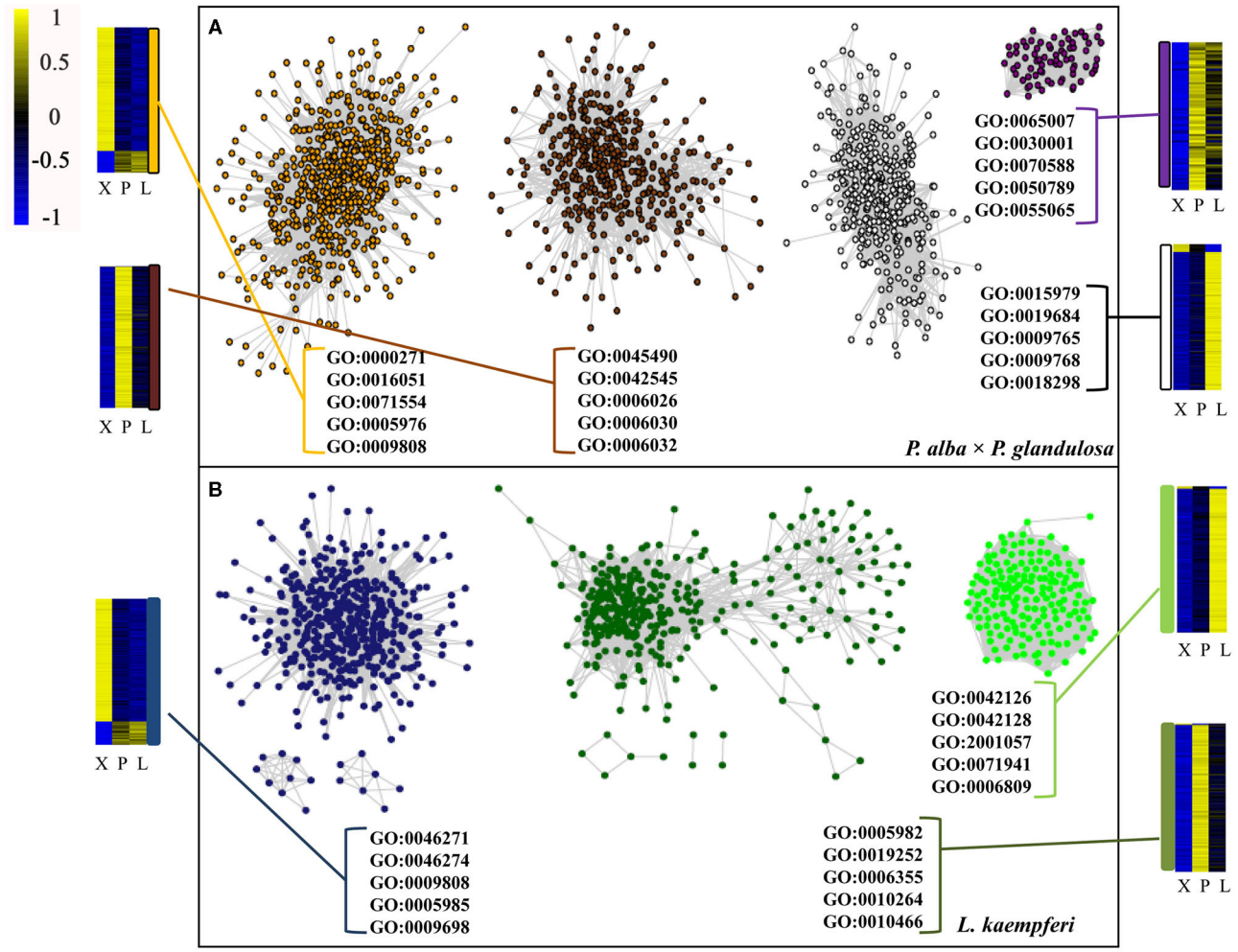

FIGURE 5 | Co-expression network and GO analysis for each module in the two tree species. **(A)** Co-expression network in *P. alba* × *P. glandulosa*. **(B)** Co-expression network in *L. kaempferi*. In these networks, only the top 50 000 gene co-expression pairs are displayed. Only the top five GO terms under the biological process category appear in each module. The heatmaps are for gene expression levels in the different modules.

(Hussey et al., 2011). *SND3* is directly activated by *SND1/NST1* and *VND6/VND7*, yet there is still no evidence to prove *SND3* is a direct target of *VND6* or *VND7* (Hussey et al., 2011). Both *VND1* and *VND5* are specifically expressed in vessels, where they activate the expression of secondary wall biosynthetic genes for cellulose, xylan, and lignin and concomitantly induce the ectopic deposition of secondary walls (Zhou et al., 2014).

We also obtained two notable cysteine protease gene family members, *XCP1* and *XCP2*, in the co-expression network of *P. alba* × *P. glandulosa*. This gene family is involved in other PCD (programmed cell death) events that contribute to plant organ senescence, plant defense responses, and nutrient mobilization. Both *XCP1* and *XCP2* are frequently used as markers for xylogenesis, and prominently positioned in models of TEs' (tracheary elements) PCD to carry out their autolysis. They are dispersed in the cytoplasmic compartment and imported into the vacuole (Funk et al., 2002; Avci et al., 2008; Zhang et al., 2014). In our results, however, the absence of *XCP1* and *XCP2* in *L. kaempferi* (**Supplementary Table 6B**) may have led to a TE PCD process unlike that which characterizes *P. alba* × *P. glandulosa*.

In 34 specifically expressed genes in *L. kaempferi* (**Supplementary Table 6B**), one NAC member (*ANAC075*), three laccase members (*LAC5*, *LAC12*, *LAC13*), and one *MYB* member (*MYB61*) were obtained. Among them, we know that *ANAC075* promotes the expression of the secondary wall-associated TF called *MYB46* (Endo et al., 2015) and functions upstream of *NAC030*, *VND7*, *NAC101*, *VND6*, *LBD30*, and *ASL19* (Sakamoto and Mitsuda, 2015). We then verified the co-expression relation for all the genes forming the network via AspWood web resources (http://aspwood.popgenie.org). We used BLASTn to find the homologous genes in both tree species (**Supplementary Tables 6D,E**). As **Figure 6** shows, for *P. alba* × *P. glandulosa*, 59 out of 63 genes in its network were

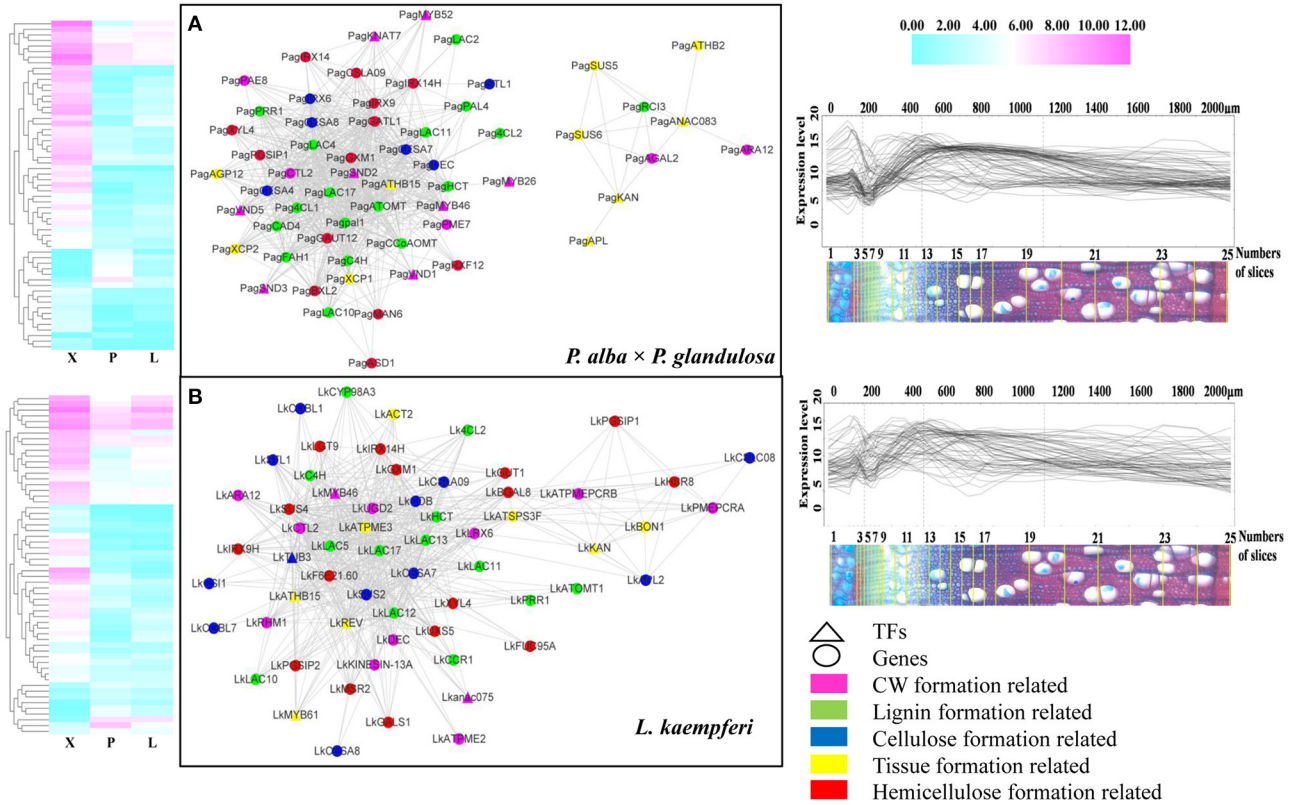

FIGURE 6 | Co-expression network of wood formation-related genes in the two tree species. **(A)** Network for wood formation-related genes in *P. alba* × *P. glandulosa*. **(B)** Network for wood formation-related genes in *L. kaempferi*. The heatmaps (left) and gene expression abundance curves (right) depict the corresponding genes in each co-expression network. The scales above the expression curves indicate the slice position; the scales under expression curves indicate the number of slices. Gene expression abundance curves were derived and drawn using an online tool (http://aspwood.popgenie.org).

co-expressed in xylem (**Figure 6A**; **Supplementary Table 6D**). Similarly, in *L. kaempferi*, 57 out of 64 genes in its network were co-expressed in xylem (**Figure 6B**, **Supplementary Table 6E**). For either tree species, the genes in the co-expression network corresponded to actual co-expression relationships present across xylem tissue ($\geq 300\,\mu m$). This suggests our co-expression networks were robust and valid for inference.

Comparison of Alternative Splicing Mode for Part of Wood-formation Related Genes in the Two Tree Species

Seven AS forms were detected, namely the alternative 3′ splice site (A3SS), alternative 5′ splice site (A5SS), alternative first exon, alternative last exon, mutually exclusive exon, retained intron (RI), and skipped exon (**Figure 7A**). We derived an AS model of genes expressed in xylem of *P. alba* × *P. glandulosa* and *L. Kaempferi* (**Figure 7B**). This showed similar proportions for different tree species, in that A3SS, A5SS, and RI are the main splicing models. Further investigation of the common wood formation-related genes for both species showed that *CSLA9*, *UGD2*, and *DEC* featured AS. The verification of AS in both tree species was pursued and these results confirmed that *CSLA9* in *L. kaempferi* accorded with the putative AS results presented in **Figure 8**. Although our bioinformatic analysis indicated the gene *CSLA9* also can undergo AS in *P. alba* × *P. glandulosa*, our RT-PCR result failed to detect it. We also confirmed AS variants of *UGD2* in *L. kaempferi*, and those of *DEC* in *P. alba* × *P. glandulosa* (**Figure 8**). Collectively, these results demonstrated there is differential post-transcriptional regulation in *P. alba* × *P. glandulosa* and *L. kaempferi*, which could point to the possible causes for the differing wood structure in these two kinds of trees.

DISCUSSION

In comparison to gymnosperm species, angiosperms underwent massive adaptive radiation to supplant the gymnosperms as the world's dominant vascular plant group (Sanderson and Donoghue, 1994; Pavy et al., 2012). During evolutionary process, angiosperm wood form their own structure characters which is mostly composed of vessels, rays, fibers, and parenchyma cells and sharply contrast to the relatively simple gymnosperms' wood which mainly consists of tracheid and rays (Zhang et al., 2017). Besides these wood structural differences, gymnosperms and angiosperms also differ in their HD-Zip III genes and hemicelluloses ingredients (Côté et al., 2010); in the binding of

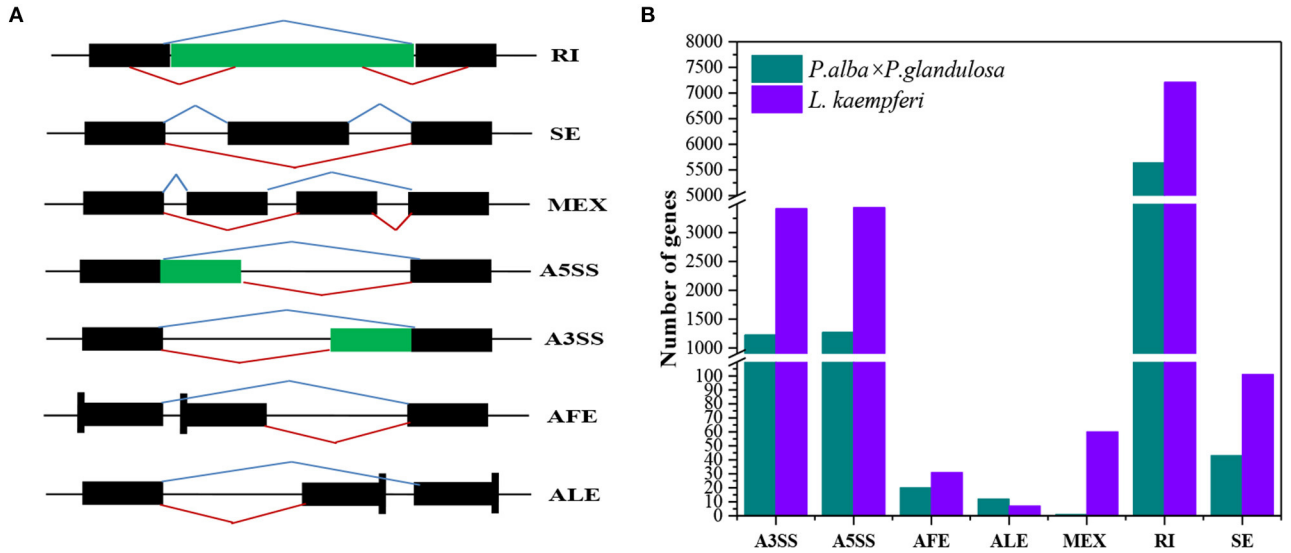

FIGURE 7 | Comparison of different alternative splicing events between the two tree species. **(A)** Splicing patterns of seven kinds of alternative splicing. **(B)** Distributions of seven kinds of alternative splicing in each of the two tree species. A3SS, alternative 3′ splice site; A5SS, alternative 5′ splice site; AFE, alternative first exon; ALE, alternative last exon; MEX, mutually exclusive exon; RI, retained intron; SE, skipped exon. Black blocks are exons, while the green blocks and black lines represent introns. Blue broken lines above the block(s) represent normal transcripts; red broken lines are the alternative splicing events.

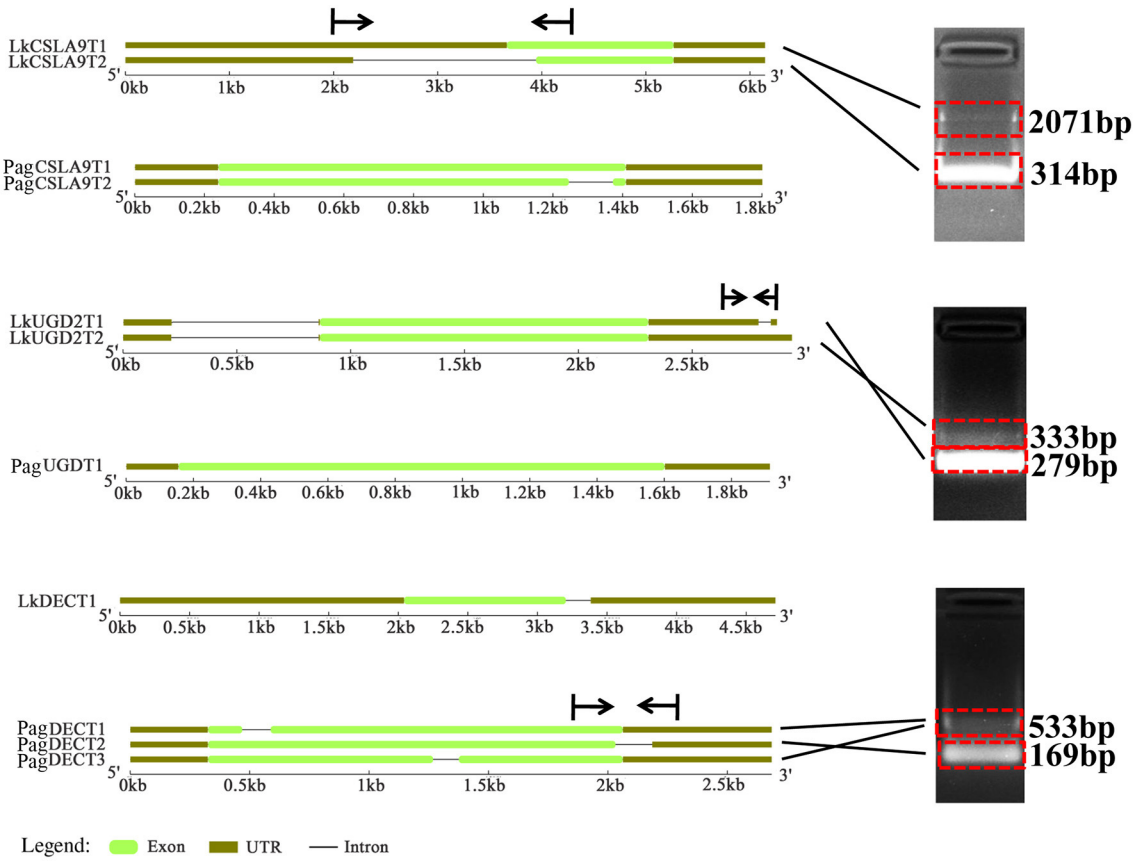

FIGURE 8 | Comparison of the gene structure for three common genes and their variants in the two tree species. Vertical lines and arrows indicate the position of designed primers and amplification direction of fragments, respectively.

multiple xylan chains to adjacent planes of the cellulose fibril (Marta et al., 2016); metabolically, in the formation of syringyl lignin (Nakamura et al., 1974), and; in their cell wall-associated peroxidases involved in xylem lignification (Mcdougall, 2001).

Gene co-expression represents interactive relationships among genes to a certain extent (Mitsuda and Ohme-Takagi, 2009). For TFs, their co-expression is indicative of coding function-related or protein–protein interactions (Mitsuda and Ohme-Takagi, 2009), and more generally, co-expressed genes may have up- or down-stream relationships in the transcriptional cascade (Hirai et al., 2007). In the constructed co-expression network, we detected similar and different co-expressed genes between the two tree species (**Supplementary Tables 6A–C**). Although both species do share some common genes, these genes still had some differences in their structure. For example, in their investigation of the structure of HD-Zip III family between angiosperms and gymnosperms, Côté et al. (2010) found that gymnosperm sequences derived from lineages that diverged earlier than angiosperm sequences, and that some sequences were lost in angiosperms indicates the full-length cDNA is longer in gymnosperms than angiosperms. Consistent with the above research (Côté et al., 2010), our gene structure analysis showed that *UGD2*, *CSLA9*, and *DEC* in *L. kaempferi* are longer than in *P. alba* × *P. glandulosa,* especially in the UTR region, suggesting lost sequences in *P. alba* × *P. glandulosa*.

Both FAH1 and CYP98A3 are members of P450 (Cytochrome P450). We found that *FAH1*, also named *F5H*, was expressed specifically in the xylem of *P. alba* × *P. glandulosa* (**Figure 4A**, **Supplementary Table 6A**). In contrast, *CYP98A3* was expressed only in the xylem of *L. kaempferi* (**Supplementary Table 6B**) where it could catalyze the hydroxylation of shikimic acid and quinic acid to form monolignin. Its substrate mainly includes *p*-coumarate, *p*-coumaraldehyde, and *p*-coumaroyl methyl ester, which differs from *FAH1*. Other studies also found that *CYP98A3* could participate in the biosynthesis process of the coumarins scopoletin and scopolin (Schoch et al., 2001; Abdulrazzak et al., 2006). Previous research indicated that *FAH1* is associated with S-lignin monomer formation, in that the expression of *FAH1* could increase the ratio of S/G (Boerjan et al., 2003). In our study, *FAH1* was only present in *P. alba* × *P. glandulosa*, indicating a high syringyl lignin content and high proportion of S/G in this species. This result is consistent with work by Boerjan et al. (2003), which revealed that most dicotyledonous angiosperms (hardwood) are rich in G and S lignin monomers yet poor in the H lignin monomer. In gymnosperms (softwood), the G lignin monomer is the main lignin monomer and S and H lignin monomers' content is low (Boerjan et al., 2003). This implies a pronounced difference in the lignin monomer formation process between angiosperm and gymnosperm plants. We found *SND2* was specific to *P. alba* × *P. glandulosa* whereas *ANAC075* was specific to *L. kaempferi*. Both *SND2* and *ANAC075* can influence glucose and xylose and lignin contents, but *ANAC075* has a greater transcriptional activation ability than does *SND2*, suggesting a different wood formation mechanism between angiosperm and gymnosperm species (Sakamoto and Mitsuda, 2015).

Although MYB family members were found in the studied two tree species, *MYB26* and *MYB52* were specifically expressed in the xylem of *P. alba* × *P. glandulosa* (**Supplementary Table 6A**). *MYB26* localizes to the nucleus and regulates endothelial development and the secondary wall- thickening process (Yang et al., 2007). *MYB52* is involved in both the ABA response and cell wall biosynthesis, and its overexpression in *Arabidopsis* improves this plant's drought tolerance and salt-sensitivity (Park et al., 2011). Even so, *MYB52*, *SND2*, and *SND3* together with *KAN7* can also influence the secondary cell wall-thickening process in fiber cells under the control of *SND1* (Zhong et al., 2008). *MYB61* mainly participates in xylem formation, by inducing qualitative changes to the xylem cell structure and lateral root development (Romano et al., 2012). The characteristic expression model in *P. alba* × *P. glandulosa* illustrated a distinctive wood formation process when compared with that of gymnosperm species. Laccase genes were reportedly active in the late stage of lignin formation and could promote lignification of the secondary xylem cell walls (Brown et al., 2005) and their different subcellular localization implies different functions among the laccase members. For instance, some research indicates that laccase can play additional roles in plants that go beyond the lignification process (Cai et al., 2006). In our results, we found co-expression of laccase members *LAC2* and *LAC4* in *P. alba* × *P. glandulosa*, and likewise that of *LAC5*, *LAC12*, and *LAC13* in *L. kaempferi*, which suggests laccase genes may be the key factors influencing wood structure. Fine-scale distinctions among these laccase genes' functioning deserve further investigation.

Alternative splicing (AS) is a criticalpost-regulation process for the expression of genes. In this way, different transcripts could encode different proteins to perform various functions and this contributes to the variety of transcripts and proteins available for use (Chen and Manley, 2009; Reddy and Yamile, 2013). Researchers have since discovered that approximately 30 to 60% of mRNAs have variants (Zhang et al., 2010; Shen et al., 2014). According to our results, AS events characterized about 14.5% of the genes (8,207 of 56,711) in *P. alba* × *P. glandulosa*, but this was threefold greater, at 46.7% (14,259 of 30,726 genes), in *L. kaempferi*. Compared with other research (Zhang et al., 2010; Shen et al., 2014), our results uncovered a lower proportion of AS events in *P. alba* × *P. glandulosa*, perhaps due to the quality of its references. A previous study also showed that the retained intron is the main AS form, constituting approximately 60% of all AS events in plants (Syed et al., 2012). Similarly, in our study, the chief form of AS encountered was the retained intron, occurring in about 68.7% of genes (5,639 out of 8,207) in *P. alba* × *P. glandulosa* and 50.6% of those (7,209 out of 14,259) in *L. kaempferi*.

CONCLUSION

In this study, we compared the xylem-specifically expressed genes between *P. alba* × *P. glandulosa* and *L. kaempferi* trees on the transcriptional level and post-transcriptional level. Our results showed that differences exist in the enriched GO

terms and KEGG pathways, gene expression models of the lignin and cellulose biosynthesis-related pathway, co-expression relationships, and alternative splicing forms, which together indicates different wood formation processes between *P. alba* × *P. glandulosa* and *L. kaempferi*. Our research provides a timely foundation for the further discovery and elucidation of differing wood formation mechanisms between angiosperm and gymnosperm species.

DATA AVAILABILITY STATEMENT

The original contributions presented in the study are publicly available. This data can be found at: NCBI repository, accession number: PRJNA723483.

AUTHOR CONTRIBUTIONS

HL and XD conceived and designed the study. QW and XD collected the plant materials. XD, QW, and HL extracted the RNA. HP, XD, and HL conducted the validation of RNA-Seq and alternative splicing events. HL and GC performed the bioinformatics analyses and carried out the data visualization. HL and XD wrote the manuscript. All of the authors revised and approved the manuscript.

FUNDING

This research was supported by the Fundamental Research Funds for the Central Non-profit Research Institution of CAF (CAFYBB2018ZY001-8 and CAFYBB2017ZY001) and the Youth Program of National Natural Science Foundation of China (31800267).

SUPPLEMENTARY MATERIAL

The Supplementary Material for this article can be found online at: https://www.frontiersin.org/articles/10.3389/fpls.2021.698602/full#supplementary-material

REFERENCES

Abdulrazzak, N., Pollet, B., Ehlting, J., Larsen, K., Asnaghi, C., Ronseau, S., et al. (2006). A coumaroyl-ester-3-hydroxylase insertion mutant reveals the existence of nonredundant meta-hydroxylation pathways and essential roles for phenolic precursors in cell expansion and plant growth. *Plant Physiol.* 140, 30–48. doi: 10.1104/pp.105.069690

Aspeborg, H., Schrader, J., Coutinho, P. M., Stam, M., Kallas, Å., Djerbi, S., et al. (2005). Carbohydrate-active enzymes involved in the secondary cell wall biogenesis in hybrid aspen. *Plant Physiol.* 137, 983–997. doi: 10.1104/pp.104.055087

Au, K. F., Underwood, J. G., Lee, L., and Wong, W. H. (2012). Improving PacBio long read accuracy by short read alignment. *PLoS ONE*. 7:e46679. doi: 10.1371/journal.pone.0046679

Avci, U., Petzold, H. E., Ismail, I. O., Beers, E. P., and Haigler, C. H. (2008). Cysteine proteases XCP1 and XCP2 aid micro-autolysis within the intact central vacuole during xylogenesis in *Arabidopsis* roots. *Plant J.* 56, 303–315. doi: 10.1111/j.1365-313X.2008.03592.x

Bao, H., Li, E., Mansfield, S. D., Cronk, Q. C., El-Kassaby, Y. A., and Douglas, C. J. (2013). The developing xylem transcriptome and genome-wide analysis of alternative splicing in *Populus trichocarpa* (black cottonwood) populations. *BMC Genomics* 14:359. doi: 10.1186/1471-2164-14-359

Bell, C. D., Soltis, D. E., and Soltis, P. S. (2010). The age and diversification of the angiosperms re-revisited. *Am. J. Bot.* 97, 1296–1303. doi: 10.3732/ajb.0900346

Boerjan, W., Ralph, J., and Baucher, M. (2003). Lignin biosynthesis. *Annu. Rev. Plant Biol.* 54, 519–546. doi: 10.1146/annurev.arplant.54.031902.134938

Brown, D. M., Zeef, L. A., Ellis, J., Goodacre, R., and Turner, S. R. (2005). Identification of novel genes in *Arabidopsis* involved in secondary cell wall formation using expression profiling and reverse genetics. *Plant Cell* 17, 2281–2295. doi: 10.1105/tpc.105.031542

Cai, X., Davis, E. J., Ballif, J., Liang, M., Bushman, E., Haroldsen, V., et al. (2006). Mutant identification and characterization of the laccase gene family in *Arabidopsis*. *J. Exp. Bot.* 57, 2563–2569. doi: 10.1093/jxb/erl022

Camargo, E. L., Ployet, R., Cassan-Wang, H., Mounet, F., and Grima-Pettenati, J. (2019). Digging in wood: new insights in the regulation of wood formation in tree species. *Adv. Bot. Res.* 89, 201–233. doi: 10.1016/bs.abr.2018.11.007

Carvalho, A., Paiva, J., Louzada, J., and Lima-Brito, J. (2013). The transcriptomics of secondary growth and wood formation in conifers. *Mol. Biol. Int.* 2013, 1–12. doi: 10.1155/2013/974324

Chen, C., Chen, H., Zhang, Y., Thomas, H. R., Frank, M. H., He, Y., et al. (2020). TBtools: an integrative toolkit developed for interactive analyses of big biological data. *MOL PLANT*, 13, 1194–1202. doi: 10.1016/j.molp.2020.06.009

Chen, M., and Manley, J. L. (2009). Mechanisms of alternative splicing regulation: insights from molecular and genomics approaches. *Nat. Rev. Mol. Cell Biol.* 10, 741–754. doi: 10.1038/nrm2777

Conesa, A., Götz, S., García-Gómez, J. M., Terol, J., Talón, M., and Robles, M. (2005). Blast2GO: a universal tool for annotation, visualization and analysis in functional genomics research. *Bioinformatics* 21, 3674–3676. doi: 10.1093/bioinformatics/bti610

Côté, C. L., Boileau, F., Roy, V., Ouellet, M., Levasseur, C., Morency, M.-J., et al. (2010). Gene family structure, expression and functional analysis of HD-Zip III genes in angiosperm and gymnosperm forest trees. *BMC Plant Biol.* 10, 1–17. doi: 10.1186/1471-2229-10-273

Courtois-Moreau, C. L., Pesquet, E., Sjödin, A., Muñiz, L., Bollhöner, B., Kaneda, M., et al. (2009). A unique program for cell death in xylem fibers of *Populus* stem. *Plant J.* 58, 260–274. doi: 10.1111/j.1365-313X.2008.03777.x

Cronk, Q. C. B., and Forest, F. (2017). "The evolution of angiosperm trees: from palaeobotany to genomics," in *Comparative and Evolutionary Genomics of Angiosperm Trees. Plant Genetics and Genomics: Crops and Models*, eds A. Groover and Q. Cronk (Cham: Springer), 1–17. doi: 10.1007/7397_2016_31

Daniel, B., Pavkov-Keller, T., Steiner, B., Dordic, A., Gutmann, A., Nidetzky, B., et al. (2015). Oxidation of monolignols by members of the berberine bridge enzyme family suggests a role in plant cell wall metabolism. *J. Bio. Chem.* 290, 18770–18781. doi: 10.1074/jbc.M115.659631

Dieset, A. (2011). *Genetic variation of xylem formation in Norway spruce (Picea abies (L.) Karst.) clones with contrasting growth rhytm* (Master thesis). Norwegian University of Life Sciences, Ås, Norway.

Du, J., Gerttula, S., Li, Z., Zhao, S. T., Liu, Y. L., Liu, Y., et al. (2019). Brassinosteroid regulation of wood formation in poplar. *New Phytol.* 225, 1516–1530. doi: 10.1111/nph.15936

Endo, H., Yamaguchi, M., Tamura, T., Nakano, Y., Nishikubo, N., Yoneda, A., et al. (2015). Multiple classes of transcription factors regulate the expression of *vascular-related NAC-DOMAIN7*, a master switch of xylem vessel differentiation. *Plant Cell Physiol.* 56, 242–254. doi: 10.1093/pcp/pcu134

Funk, V., Kositsup, B., Zhao, C., and Beers, E. P. (2002). The *Arabidopsis* xylem peptidase XCP1 is a tracheary element vacuolar protein that may be a papain ortholog. *Plant Physiol.* 128, 84–94. doi: 10.1104/pp.010514

He, S., Xie, Y., Sun, X., and Zhang, S. (2020). Comparative transcriptome analyses reveal candidate genes regulating wood quality in Japanese larch (*Larix kaempferi*). *J. For. Res.* 31, 65–73. doi: 10.1007/s11676-019-00997-8

He, X., and Groover, A. T. (2017). "The genomics of wood formation in angiosperm trees," in *Comparative and Evolutionary Genomics of Angiosperm Trees. Plant Genetics and Genomics: Crops and Models*, eds E. Groover A. and E. Cronk Q. (Cham: Springer), 205–225. doi: 10.1007/7397_2016_17

Higuchi, T., Shimada, M., Nakatsubo, F., and Tanahashi, M. (1977). Differences in biosyntheses of guaiacyl and syringyl lignins in woods. *Wood Sci. Technol.* 11, 153–167.

Hirai, M. Y., Sugiyama, K., Sawada, Y., Tohge, T., Obayashi, T., Suzuki, A., et al. (2007). Omics-based identification of *Arabidopsis* Myb transcription factors regulating aliphatic glucosinolate biosynthesis. *Proc. Natl. Sci. U S A.* 104, 6478–6483. doi: 10.1073/pnas.0611629104

Hussey, S. G., Mizrachi, E., Spokevicius, A. V., Bossinger, G., Berger, D. K., and Myburg, A. A. (2011). *SND2*, a NAC transcription factor gene, regulates genes involved in secondary cell wall development in *Arabidopsis* fibres and increases fibre cell area in *Eucalyptus*. *BMC Plant Biol.* 11, 1–17. doi: 10.1186/1471-2229-11-173

Iseli, C., Jongeneel, C. V., and Bucher, P. (1999). "ESTScan: a program for detecting, evaluating, and reconstructing potential coding regions in EST sequences," in *Proceedings of the International Conference on Intelligent Systems for Molecular Biology* (Heidelberg), 138–148.

Jokipii-Lukkari, S., Delhomme, N., Schiffthaler, B., Mannapperuma, C., Prestele, J., Nilsson, O., et al. (2018). Transcriptional roadmap to seasonal variation in wood formation of Norway Spruce. *Plant Physiol.* 176, 2851–2870. doi: 10.1104/pp.17.01590

Kim, D., Langmead, B., and Salzberg, S. L. (2015). HISAT: a fast spliced aligner with low memory requirements. *Nat. Methods* 12 357–360. doi: 10.1038/nmeth.3317

Kim, M.-H., Cho, J.-S., Jeon, H.-W., Sangsawang, K., Shim, D., Choi, Y.-I., et al. (2019). Wood transcriptome profiling identifies critical pathway genes of secondary wall biosynthesis and novel regulators for vascular cambium development in *Populus*. *Genes*. 10:690. doi: 10.3390/genes10090690

Kim, S.-J., Kim, M.-R., Bedgar, D. L., Moinuddin, S. G., Cardenas, C. L., Davin, L. B., et al. (2004). Functional reclassification of the putative cinnamyl alcohol dehydrogenase multigene family in *Arabidopsis*. *Proc. Natl. Sci. U S A.* 101, 1455–1460. doi: 10.1073/pnas.0307987100

Kohl, M., Wiese, S., and Warscheid, B. (2011). Cytoscape: software for visualization and analysis of biological networks. *Methods Mol. Biol.* 696, 291–303. doi: 10.1007/978-1-60761-987-1_18

Li, H., Huang, X., Li, W., Lu, Y., and Li, Q. (2020). MicroRNA comparison between poplar and larch provides insight into the different mechanism of wood formation. *Plant Cell Rep.* 39, 1199–1217. doi: 10.1007/s00299-020-02559-3

Li, J., Harata-Lee, Y., Denton, M. D., Feng, Q., Rathjen, J. R., Qu, Z., et al. (2017). Long read reference genome-free reconstruction of a full-length transcriptome from *Astragalus membranaceus* reveals transcript variants involved in bioactive compound biosynthesis. *Cell Discov.* 3, 1–13. doi: 10.1038/celldisc.2017.31

Li, Q., Lin, Y.-C., Sun, Y.-H., Song, J., Chen, H., Zhang, X.-H., et al. (2012). Splice variant of the SND1 transcription factor is a dominant negative of SND1 members and their regulation in *Populus trichocarpa*. *Proc. Natl. Sci. U S A.* 109, 14699–14704. doi: 10.1073/pnas.1212977109

Li, W., and Godzik, A. (2006). Cd-hit: a fast program for clustering and comparing large sets of protein or nucleotide sequences. *Bioinformatics* 22, 1658–1659. doi: 10.1093/bioinformatics/btl158

Li, X., Wu, H. X., and Southerton, S. G. (2010). Comparative genomics reveals conservative evolution of the xylem transcriptome in vascular plants. *BMC Evol. Biol.* 10, 1–14. doi: 10.1186/1471-2148-10-190

Lin, Y.-C. J., Chen, H., Li, Q., Li, W., Wang, J. P., Shi, R., et al. (2017). Reciprocal cross-regulation of VND and SND multigene TF families for wood formation in *Populus trichocarpa*. *Proc. Natl. Sci. U S A.* 114, E9722–E9729. doi: 10.1073/pnas.1714422114

Lorenz, W. W., Yu, Y.-S., and Dean, J. F. (2010). An improved method of RNA isolation from loblolly pine (*P. taeda* L.) and other conifer species. *J. Vis. Exp.* 36:e1751. doi: 10.3791/1751

Love, M., Anders, S., and Huber, W. (2014). Differential analysis of count data–the DESeq2 package. *Genome Biol.* 15:550. doi: 10.1186/s13059-014-0550-8

Lu, S., Li, Q., Wei, H., Chang, M.-J., Tunlaya-Anukit, S., Kim, H., et al. (2013). Ptr-miR397a is a negative regulator of laccase genes affecting lignin content in *Populus trichocarpa*. *Proc. Natl. Sci. U S A.* 110, 10848–10853. doi: 10.1073/pnas.1308936110

Lukens, L., and Downs, G. (2012). "Bioinformatics techniques for understanding and analyzing tree gene expression data," in Genomics of Tree Crops, eds E. Schnell R.J. and E. Priyadarshan P.M. (New York, NY: Springer), 17–38. doi: 10.1007/978-1-4614-0920-5_2

Marta, Busse-Wicher, Li, A., Silveira, Rodrigo, L., Caroline, S., et al. (2016). Evolution of xylan substitution patterns in gymnosperms and angiosperms: implications for xylan interaction with cellulose. *Plant physiol.* 171, 2418–2431. doi: 10.1104/pp.16.00539

Mcdougall, G. J. (2001). Cell-wall-associated peroxidases from the lignifying xylem of angiosperms and gymnosperms: monolignol oxidation. *Holzforschung* 55, 246–249. doi: 10.1515/HF.2001.040

Mitsuda, N., and Ohme-Takagi, M. (2009). Functional analysis of transcription factors in *Arabidopsis*. *Plant Cell Physiol.* 50, 1232–1248. doi: 10.1093/pcp/pcp075

Nakamura, Y., Fushiki, H., and Higuchi, T. (1974). Metabolic differences between gymnosperms and angiosperms in the formation of syringyl lignin. *Phytochemistry* 13, 1777–1784. doi: 10.1016/0031-9422(74)85088-0

Nawawi, D. S., Syafii, W., Akiyama, T., and Matsumoto, Y. (2016). Characteristics of guaiacyl-syringyl lignin in reaction wood in the gymnosperm *Gnetum gnemon* L. *Holzforschung* 70, 593–602. doi: 10.1515/hf-2015-0107

Park, M. Y., Kang, J. Y., and Kim, S. Y. (2011). Overexpression of AtMYB52 confers ABA hypersensitivity and drought tolerance. *Mol Cells.* 31, 447–454. doi: 10.1007/s10059-011-0300-7

Pavy, N., Pelgas, B., Laroche, J., Rigault, P., Isabel, N., and Bousquet, J. (2012). A spruce gene map infers ancient plant genome reshuffling and subsequent slow evolution in the gymnosperm lineage leading to extant conifers. *BMC Biol.* 10, 1–19. doi: 10.1186/1741-7007-10-84

Reddy, Anireddy S. N., Yamile, Marquez, et al. (2013). Complexity of the alternative splicing landscape in plants. *Plant Cell* 25, 3657–3683. doi: 10.1105/tpc.113.117523

Romano, J. M., Dubos, C., Prouse, M. B., Wilkins, O., and Campbell, M. M. (2012). AtMYB61, an R2R3-MYB transcription factor, functions as a pleiotropic regulator via a small gene network. *New Phytol.* 195, 774–786. doi: 10.1111/j.1469-8137.2012.04201.x

Roodt, D., Li, Z., Van de Peer, Y., and Mizrachi, E. (2019). Loss of wood formation genes in monocot genomes. *Genome Biol Evol.* 11, 1986–1996. doi: 10.1093/gbe/evz115

Sakamoto, S., and Mitsuda, N. (2015). Reconstitution of a secondary cell wall in a secondary cell wall-deficient *Arabidopsis* mutant. *Plant Cell Physiol.* 56, 299–310. doi: 10.1093/pcp/pcu208

Sanderson, M. J., and Donoghue, M. J. (1994). Shifts in diversification rate with the origin of angiosperms. *Science.* 264, 1590–1593. doi: 10.1126/science.264.5165.1590

Sarkanen, K. (1971). "Classification and distribution," in *Lignins Occurrence, Formation, Structure and Reactions*, eds E. Sarkanen, K.V. and Ludwig, C.H. (New York: Wiley-Interscience). 43–94.

Schoch, G., Goepfert, S., Morant, M., Hehn, A., Meyer, D., Ullmann, P., et al. (2001). CYP98A3 from *Arabidopsis thaliana* is a 3′-hydroxylase of phenolic esters, a missing link in the phenylpropanoid pathway. *J. Biol. Chem.* 276, 36566–36574. doi: 10.1074/jbc.M104047200

Shen, Y., Zhou, Z., Wang, Z., Li, W., Fang, C., Wu, M., et al. (2014). Global dissection of alternative splicing in paleopolyploid soybean. *Plant Cell.* 26, 996–1008. doi: 10.1105/tpc.114.122739

Shi, R., Sun, Y.-H., Li, Q., Heber, S., Sederoff, R., and Chiang, V. L. (2009). Towards a systems approach for lignin biosynthesis in *Populus trichocarpa*: transcript abundance and specificity of the monolignol biosynthetic genes. *Plant Cell Physiol.* 51, 144–163. doi: 10.1093/pcp/pcp175

Sperry, J. S., Hacke, U. G., and Pittermann, J. (2006). Size and function in conifer tracheids and angiosperm vessels. *Am. J. Bot.* 93, 1490–1500. doi: 10.3732/ajb.93.10.1490

Sundell, D., Street, N. R., Kumar, M., Mellerowicz, E. J., Kucukoglu, M., Johnsson, C., et al. (2017). AspWood: high-spatial-resolution transcriptome profiles reveal uncharacterized modularity of wood formation in *Populus tremula*. *Plant Cell.* 29, 1585–1604. doi: 10.1105/tpc.17.00153

Suzuki, S., Li, L., Sun, Y.-H., and Chiang, V. L. (2006). The cellulose synthase gene superfamily and biochemical functions of xylem-specific

cellulose synthase-like genes in *Populus trichocarpa*. *Plant physiol*. 142, 1233–1245.doi: 10.1104/pp.106.086678

Syed, N. H., Kalyna, M., Barta, B., et al. (2012). Alternative splicing in plants - coming of age. *Trends Plant Sci*. 17, 616–623. doi: 10.1016/j.tplants.2012.06.001

Tuskan, G. A., Groover, A. T., Schmutz, J., DiFazio, S. P., Myburg, A., Grattapaglia, D., et al. (2018). Hardwood tree genomics: unlocking woody plant biology. *Front. Plant Sci*. 9, 1799–1799. doi: 10.3389/fpls.2018.01799

Vanholme, R., Demedts, B., Morreel, K., Ralph, J., and Boerjan, W. (2010). Lignin biosynthesis and structure. *Plant Physiol*. 153, 895–905. doi: 10.1104/pp.110.155119

Wang, J. P., Matthews, M. L., Naik, P. P., Williams, C. M., Ducoste, J. J., Sederoff, R. R., et al. (2019). Flux modeling for monolignol biosynthesis. *Curr. Opin. Biotechnol*. 56, 187–192. doi: 10.1016/j.copbio.2018.12.003

Weng, J.-K., Li, X., Stout, J., and Chapple, C. (2008). Independent origins of syringyl lignin in vascular plants. *Proc. Natl. Sci. U S A*. 105, 7887–7892. doi: 10.1073/pnas.0801696105

Wu, Z., Wang, N., Hisano, H., Cao, Y., and Fu, C. (2018). Simultaneous regulation of *F5H* in COMT-RNAi transgenic switchgrass alters effects of *COMT* suppression on syringyl lignin biosynthesis. *Plant Biotechnol. J*. 17, 836–845. doi: 10.1111/pbi.13019

Xie, H., Engle, N. L., Venketachalam, S., Yoo, C. G., Barros, J., Lecoultre, M., et al. (2019). Combining loss of function of Folylpolyglutamate synthetase1 and *caffeoyl-coa 3-o-methyltransferase1* for lignin reduction and improved saccharification efficiency in *Arabidopsis thaliana*. *Biotechnol. Biofuels*. 12, 1–20. doi: 10.1186/s13068-019-1446-3

Xu, P., Kong, Y., Song, D., Huang, C., Li, X., and Li, L. (2014). Conservation and functional influence of alternative splicing in wood formation of *Populus* and *Eucalyptus*. *BMC Genom*. 15, 1–12. doi: 10.1186/1471-2164-15-780

Yamamoto, R., Demura, T., and Fukuda, H. (1997). Brassinosteroids induce entry into the final stage of tracheary element differentiation in cultured *Zinnia* cells. *Plant Cell Physiol*. 38, 980–983. doi: 10.1093/oxfordjournals.pcp.a029262

Yang, C., Xu, Z., Song, J., Conner, K., Barrena, G. V., and Wilson, Z. A. (2007). *Arabidopsis MYB26/MALE STERILE35* regulates secondary thickening in the endothecium and is essential for anther dehiscence. *Plant Cell*. 19, 534–548. doi: 10.1105/tpc.106.046391

Ye, Z.-H., and Zhong, R. (2015). Molecular control of wood formation in trees. *J. Exp. Bot*. 66, 4119–4131. doi: 10.1093/jxb/erv081

Young, M. D., Wakefield, M. J., Smyth, G. K., and Oshlack, A. (2010). Gene ontology analysis for RNA-seq: accounting for selection bias. *Genome Biol*. 11, 1–12. doi: 10.1186/gb-2010-11-2-r14

Yuan, Y., Teng, Q., Zhong, R., and Ye, Z.-H. (2014). Identification and biochemical characterization of four wood-associated glucuronoxylan methyltransferases in *Populus*. *PLoS ONE*. 9:e87370. doi: 10.1371/journal.pone.0087370

Zang, Q.-L., Li, W.-F., and Qi, L.-W. (2019). Regulation of *LaSCL6* expression by genomic structure, alternative splicing, and microRNA in *Larix kaempferi*. *Tree Genet. Genomes* 15, 1–7. doi: 10.1007/s11295-019-1362-5

Zeng, L., Zhang, Q., Sun, R., Kong, H., Zhang, N., and Ma, H. (2014). Resolution of deep angiosperm phylogeny using conserved nuclear genes and estimates of early divergence times. *Nat. Commun*. 5, 1–12. doi: 10.1038/ncomms5956

Zhang, B., Tremousaygue, D., Denance, N., van Esse, H. P., Horger, A. C., Dabos, P., et al. (2014). PIRIN2 stabilizes cysteine protease XCP2 and increases susceptibility to the vascular pathogen *Ralstonia solanacearum* in *Arabidopsis*. *Plant J*. 79, 1009–1019. doi: 10.1111/tpj.12602

Zhang, G., Guo, G., Hu, X., Zhang, Y., Li, Q., Li, R., et al. (2010). Deep RNA sequencing at single base-pair resolution reveals high complexity of the rice transcriptome. *Genome Res.* 20, 646–654. doi: 10.1101/gr.100677.109

Zhang, J., Xie, M., Tuskan, G. A., Muchero, W., and Chen, J.-G. (2018). Recent advances in the transcriptional regulation of secondary cell wall biosynthesis in the woody plants. *Front. Plant Sci*. 9:1535. doi: 10.3389/fpls.2018.01535

Zhang, M., Ji, C., Zhu, J., et al. (2017). Comparison of wood physical and mechanical traits between major gymnosperm and angiosperm tree species in China. *Wood Sci. Technol*. 51, 1405–1419. doi: 10.1007/s00226-017-0954-1

Zhao, Y., Sun, J., Xu, P., Zhang, R., and Li, L. (2014). Intron-mediated alternative splicing of *PtrWND1B* regulates cell wall thickening during fiber development in *Populus*. *Plant Physiol*. 164, 765–776. doi: 10.1104/pp.113.231134

Zhong, R., Lee, C., Zhou, J., McCarthy, R. L., and Ye, Z.-H. (2008). A battery of transcription factors involved in the regulation of secondary cell wall biosynthesis in *Arabidopsis*. *Plant Cell*. 20, 2763–2782. doi: 10.1105/tpc.108.061325

Zhong, R., and Ye, Z.-H. (2014). Complexity of the transcriptional network controlling secondary wall biosynthesis. *Plant Sci*. 229, 193–207. doi: 10.1016/j.plantsci.2014.09.009

Zhou, J., Zhong, R., and Ye, Z. H. (2014). *Arabidopsis* NAC domain proteins, VND1 to VND5, are transcriptional regulators of secondary wall biosynthesis in vessels. *PLoS ONE*. 9:e105726. doi: 10.1371/journal.pone.0105726

Conflict of Interest: The authors declare that the research was conducted in the absence of any commercial or financial relationships that could be construed as a potential conflict of interest.

frontiers in Plant Science

METHODS
published: 12 July 2021
doi: 10.3389/fpls.2021.703546

An Improved CRISPR/Cas9 System for Genome Editing in *Populus* by Using Mannopine Synthase (MAS) Promoter

Yi An[1†], *Ya Geng*[1†], *Junguang Yao*[1], *Chun Wang*[2] *and Juan Du*[3*]

[1] State Key Laboratory of Subtropical Silviculture, School of Forestry and Biotechnology, Zhejiang A&F University, Hangzhou, China, [2] State Key Laboratory of Rice Biology, China National Rice Research Institute, Chinese Academy of Agricultural Sciences, Hangzhou, China, [3] College of Life Sciences, Zhejiang University, Hangzhou, China

Gene editing technology in woody plants has great potential for understanding gene function, and altering traits affecting economically and ecologically important traits. Gene editing applications in woody species require a high genome editing efficiency due to the difficulty during transformation and complexities resulting from gene redundancy. In this study, we used poplar 84K (*Populus alba* × *P. glandulosa*), which is a model hybrid for studying wood formation and growth. We developed a new CRISPR/Cas9 system to edit multiple genes simultaneously. Using this system, we successfully knocked out multiple targets of the PHYTOENE DESATURASE 8 in poplar. We found the mutation rate of our CRISPR/Cas9 system is higher (67.5%) than existing reports in woody trees. We further improved the mutation rate up to 75% at editing sites through the usage of the mannopine synthase (MAS) promoter to drive Cas9. The MAS-CRISPR/Cas9 is an improved genome-editing tool for woody plants with a higher efficiency and a higher mutation rate than currently available technologies.

Keywords: poplar 84K, CRISPR/Cas9, 35S promoter, MAS promoter, *PagPDS* gene, high efficiency

OPEN ACCESS

Edited by:
Quanzi Li,
Chinese Academy of Forestry, China

Reviewed by:
Yuxiang Cheng,
Northeast Forestry University, China
Keming Luo,
Southwest University, China

***Correspondence:**
Juan Du
djuan@zju.edu.cn

These authors have contributed equally to this work

Specialty section:
This article was submitted to Plant Biotechnology, a section of the journal Frontiers in Plant Science

Received: *30 April 2021*
Accepted: *16 June 2021*
Published: *12 July 2021*

Citation:
An Y, Geng Y, Yao J, Wang C and Du J (2021) An Improved CRISPR/Cas9 System for Genome Editing in Populus by Using Mannopine Synthase (MAS) Promoter. Front. Plant Sci. 12:703546. doi: 10.3389/fpls.2021.703546

INTRODUCTION

Poplars (*Populus*) have tremendous economic and ecological value because of their timber, bioenergy applications, rapid pulp production rotation, as well as their key ecological roles in temperate forests across the northern hemisphere (Jansson and Douglas, 2007; Polle et al., 2013). With a modest genome size, high levels of genetic diversity, and a rapid growth rate (Wullschleger et al., 2002), poplars became a model system for woody plants. Hybrid poplars have been genetically modified for studying wood formation, including perennial secondary vascular cambium activity and secondary cell wall deposition (Qiu et al., 2019). Despite existence of some promising approaches for creating knockout mutants in *Populus* (Fan et al., 2015; Zhou et al., 2015; An et al., 2020a,b; Wang et al., 2020), large-scale gene mutational resources are still lacking for poplars, motivating us to build a robust and high-efficient gene editing system for *Populus*.

Currently, CRISPR/Cas9 technology is the most effective gene editing technology. In plants, the CRISPR/Cas9 system has not only been used in the study of gene function, but also plays an important role in the improvement of plant traits. Woody plants with long-life spans and outcrossing mating systems are difficult subjects for traditional mutagenesis methods (Bewg et al., 2018). Currently, there are about ten woody plants species that have been successful edited using CRISPR/Cas9 technology: apple (Nishitani et al., 2016), citrus (Jia et al., 2017), grape (Nakajima et al., 2017), cassava (Odipio et al., 2017), cacao (Fister et al., 2018), coffee (Breitler et al., 2018),

kiwifruit (Wang et al., 2018), parasponia andersonii (Van Zeijl et al., 2018), pomegranate (Chang et al., 2019), and poplar (Fan et al., 2015; Zhou et al., 2015; Wang et al., 2020). Three kinds of *Populus* have been edited via CRISPR/Cas9, including *Populus tomentosa Carr* (Fan et al., 2015), 717 (*Populus tremula* × *P. alba*) (Zhou et al., 2015), and Shanxin yang (*Populus davidiana* × *P. bolleana*) (Wang et al., 2020). Extensively cultivated in China and Korea, the hybrid clone 84K (*Populus alba* × *P. glandulosa*) is a model hybrid for the study wood formation and stress response and also has relatively high rates of transformation compared with other woody plants (Li et al., 2017; Qiu et al., 2019). The recent availability of poplar 84K genome sequence facilitates functional genomic studies and the ability to design CRISPR/CAS9 approaches to target specific genes or even multiple genes (Huang et al., 2020). Therefore, it is of high priority to develop a high-efficiency gene editing system in the 84K poplar genotype.

To develop a simple and efficient gene-editing system for poplar 84K, and for editing multiple genes, we used the existing conventional isocaudomer technique using constructs based on pC1300-Cas9 (binary vector) and SK-gRNA (intermediate vector driven by AtU6-26). The system has the potential to edit an unlimited number of target genes simultaneously (Wang et al., 2015). The promoter is the key to driving the expression of transformed genes. Previous studies conducted on tobacco and maize indicated that the *mannopine synthase*

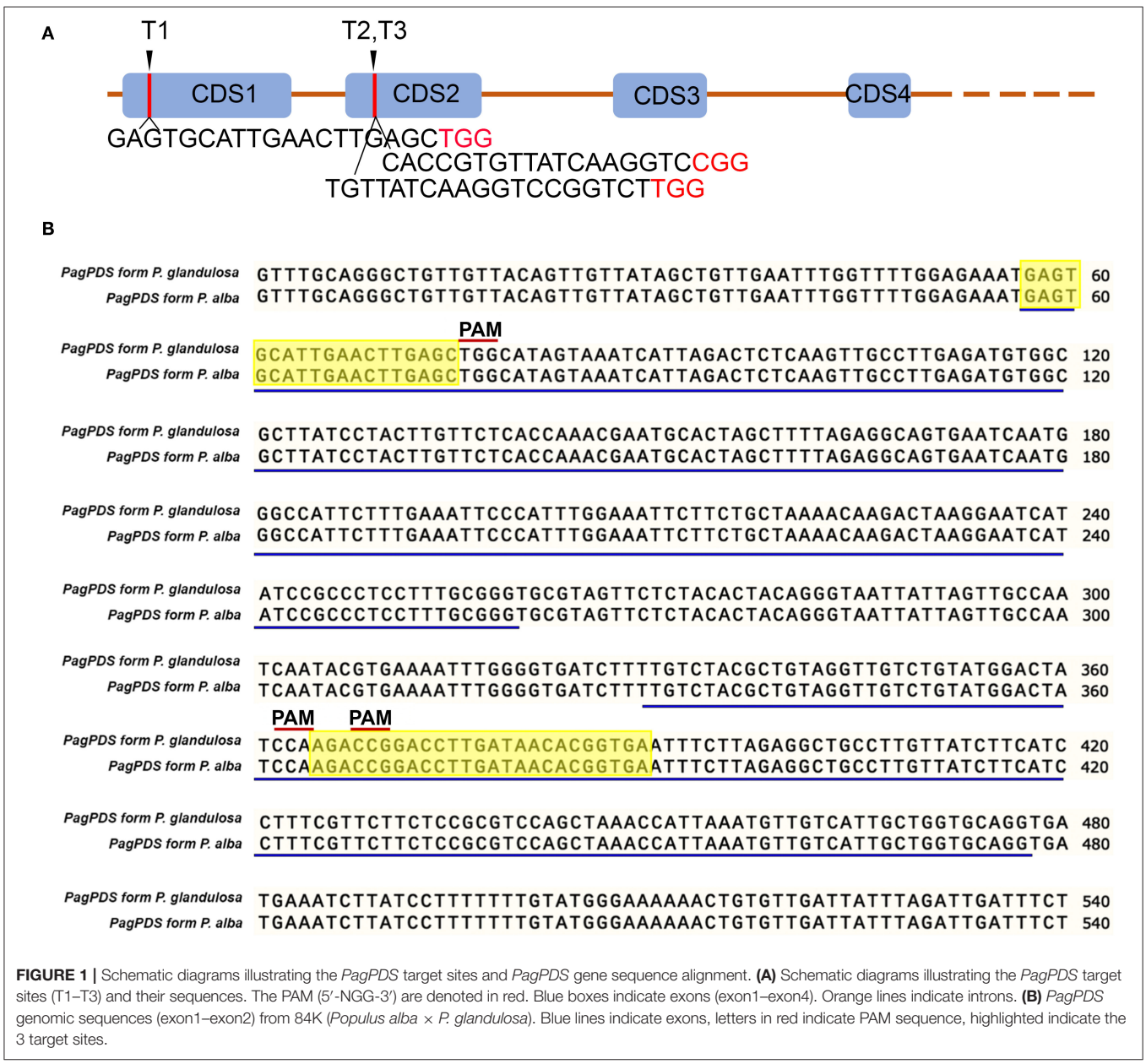

FIGURE 1 | Schematic diagrams illustrating the *PagPDS* target sites and *PagPDS* gene sequence alignment. **(A)** Schematic diagrams illustrating the *PagPDS* target sites (T1–T3) and their sequences. The PAM (5′-NGG-3′) are denoted in red. Blue boxes indicate exons (exon1–exon4). Orange lines indicate introns. **(B)** *PagPDS* genomic sequences (exon1–exon2) from 84K (*Populus alba* × *P. glandulosa*). Blue lines indicate exons, letters in red indicate PAM sequence, highlighted indicate the 3 target sites.

(*MAS*) promoter could increase the direct expression of β-glucuronidase activity to 2–20 fold compared with the commonly used enhanced CaMV 35S promoter (Ni et al., 1995; Lee et al., 2007). We hypothesized that MAS promoter could similarly drive Cas9 to enhance editing events in 84K. Therefore, we constructed a new gene editing system which used 35S/MAS promoter to drive Cas9 and studied the editing efficiency in poplar 84K. The new system successfully editing multiple targets of phytoene desaturase gene 8 (*PDS*) with high mutation rates.

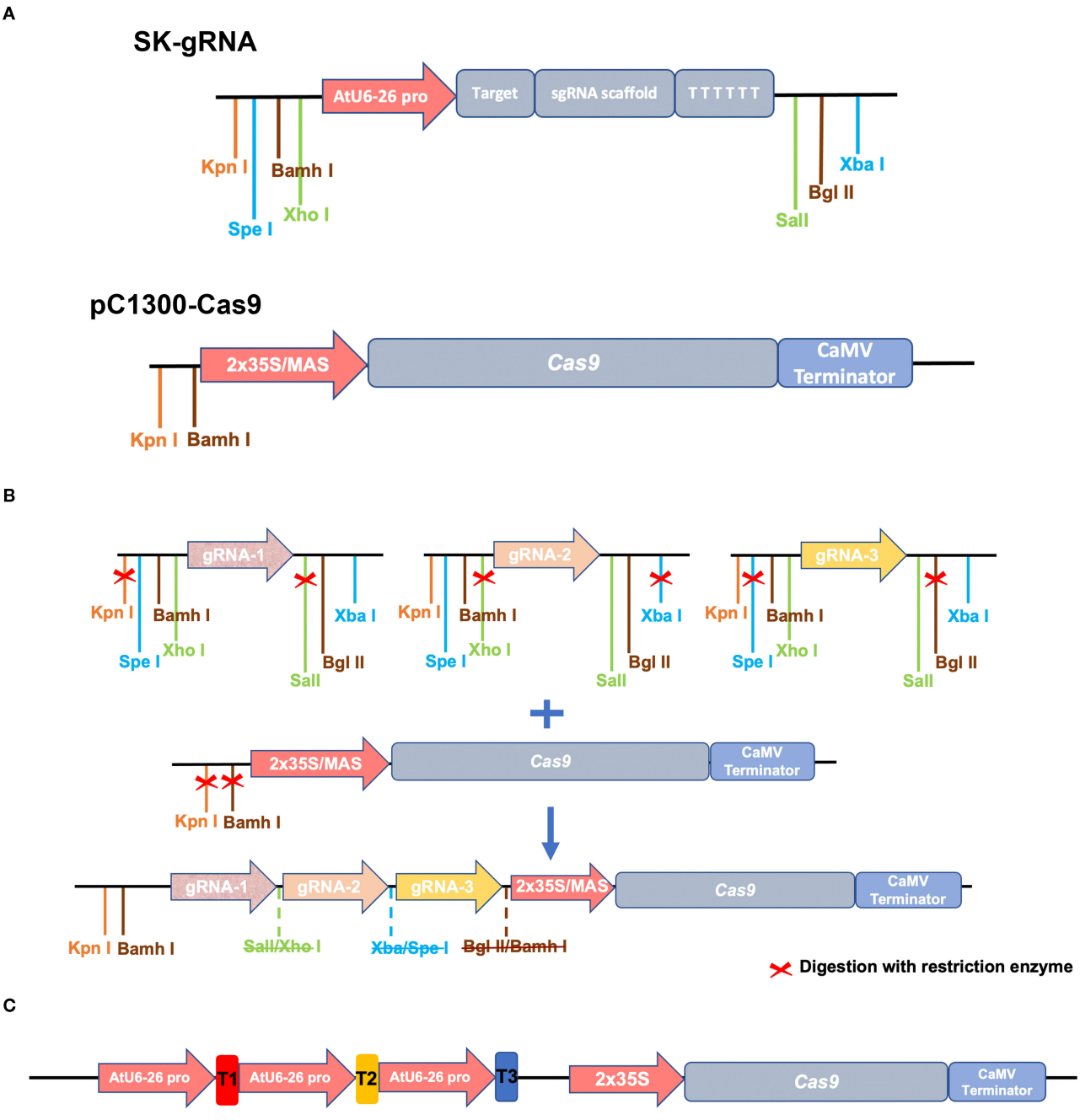

FIGURE 2 | Schematic diagram illustrating the structure of vectors and construction strategy. **(A)** The intermediate vector SK-gRNA contains the U6 promotor, an sgRNA scaffold, and the terminator. The restriction sites used for cloning are indicated. Binary vector pC1300-Cas9 contains the 2 × 35S or MAS promotor, a codon-optimized Cas9 coding sequence, and the CaMV terminator. **(B)** Vector construction strategy. *Kpn* I and *BamH* I sites are indicated in front of the 2 × 35S or MAS promotor. Three gRNA scaffolds with *PagPDS* targets are, respectively, digested (contains *Kpn* I, *BamH* I, *Xho* I, *Sal* I, *Xba* I, and *Spel* I) and cloned into pC1300-Cas9 between the *Kpn* I and *BamH* I sites in a one-step ligation. **(C)** Structure of destination vectors used in the CRISPR/Cas9 system.

MATERIALS AND METHODS

Cloning of *PagPDS* Fragments and Selection of Target Site

Wide-type (WT) poplar 84K genomic DNA was extracted by the cetyltrimethylammonium bromide (CTAB) method (Fan et al., 2015). The phytoene desaturase gene (*PDS*) was cloned from extracted genomic DNA. Briefly, primers were designed against *PagPDS* from genome sequence of poplar 84K. The primers are PagPDS_F: GTTTGCAGGGCTGTTGTTACAGTT and PagPDS_R: CATTTAATGGTGCAGGGAGAACTTCAG. The amplification reaction was conducted at 95°C for 5 min, 35 cycles at 95°C for 30 s, 58°C for 30 s, 72°C for 35 s, and 72°C for 10 min. The amplicon product was electrophoresed on an ethidium bromide-stained agarose gel (1%). DNA was extracted from gel using the TIANgel Midi Purification Kit (Tiangen, Beijing, China) and cloned into the pMD18-T Simple vector and then confirmed by Sanger sequencing. The single-guide RNA (sgRNA) sequence for *PDS* was designed (**Figure 1A**) based on the allelic variation of *PagPDS* in **Figure 1B**. Three sgRNAs were designed to target three conserved sites optimizing GC content and PAM sequence.

Vector Construction

The system is comprised of two vectors, the first of which is pC1300-Cas9, which was based on the pCAMBIA1300 backbone, which has been frequently used for *Agrobacterium-mediated* transformation in *Populus*. The vector contains the codon-optimized *Streptococcus pyogenes* Cas9 gene driven by the 2xCaMV35S promoter. pC1300-Cas9 contains *Kpn* I and *BamH* I restriction enzyme sites, which are designed for allowing integration of gRNA cassettes. Then, we developed novel vectors based on pC1300-Cas9 backbone, introducing the Superpromoter to drive Cas9 expression, with the aim to increase the expression level of Cas9 in the *Populus* cells. The Superpromoter is a synthetic promoter consists of a trimer of the octopine synthase transcriptional activating element affixed to the mannopine synthase2# transcriptional activating element plus minimal promoter (Lee et al., 2007). The MAS promoter sequence is shown in **Supplementary Sequence 1**.

Three sgRNAs guiding sequences were inserted into the SK-gRNA vector (Wang et al., 2015) between the two *Aar* I sites using annealed oligonucleotides (we named the resulting three vectors SK-gRNA1, SK-gRNA2, and SK-gRNA3). The pC1300-Cas9 vector contains the codon-optimized *Streptococcus pyogenes* Cas9 gene and the *Kpn* I and *BamH* I isocaudomer enzyme sites, which are designed to allow integration of gRNA cassettes. The SK-gRNA vector also contains isocaudomer restriction enzyme sites, namely *Spel/ Xba* I, *Xho* I/*Sal* I, and *BamH* I/BgI II sites (**Figure 2A**). The steps of vector construction are shown in **Figure 2B**. The three vectors (SK-gRNA1, SK-gRNA2, and SK-gRNA3) were digested separately with restriction enzymes, and then inserted into the pC1300-2 × 35S-Cas9

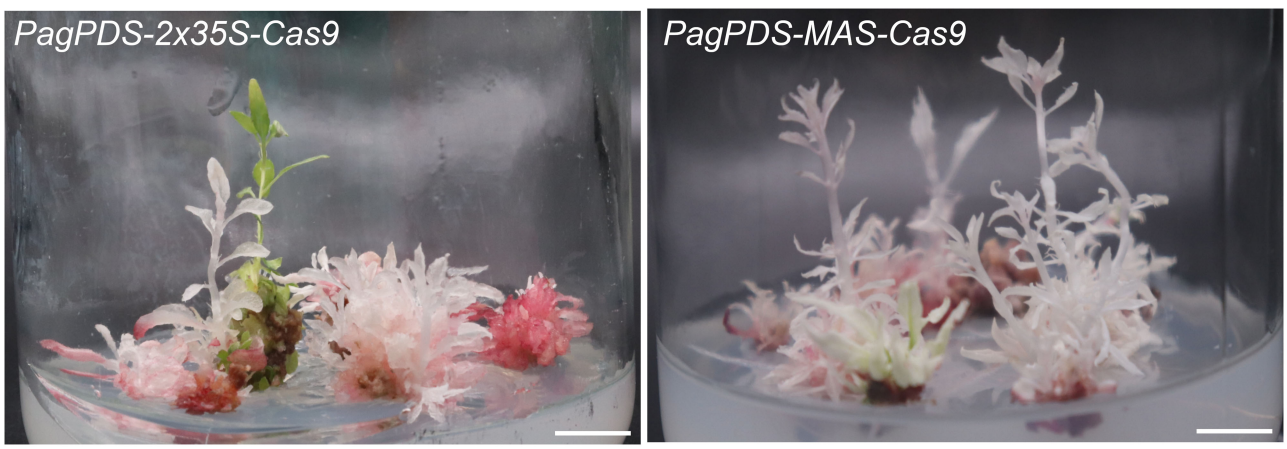

FIGURE 3 | Phenotypes of the *PagPDS-2 × 35S/MAS*-Cas9-mediated transgenic plants. Scale bar = 1 cm.

TABLE 1 | Determination of mutation rate in transgenic T_0 poplar plants generated with the *PagPDS-2 × 35S/MAS*-Cas9 system.

Target gene	Number of plants examined	Number of plants with mutations	Mutation rate (%)	Albinism phenotype		Pale green phenotype	
				Number	%	Number	%
PagPDS-2 × 35S-Cas9	40	27	67.5	21	77.8	6	22.2
PagPDS-MAS-Cas9	40	30	75	23	76.7	7	23.3
CK	40	0	0	ND	ND	ND	ND

CK, Empty vector; ND, not determined.

and pC1300-MAS-Cas9 binary vector between the *Kpn* I and *Bam*H I sites by one-step ligation (Wang et al., 2015). The constructed vectors were named *PagPDS*-2 × 35S-Cas9, and *PagPDS*-MAS-Cas9, respectively. The final vector diagram is shown in **Supplementary Figure 1** and the Cas9 sequence in **Supplementary Sequence 2**. The construct was sequenced and the expected sequences confirmed.

Transformation and Regeneration

The vector containing CRISPR/Cas9 with gRNA expression

A

PagPDS-2x35S-Cas9

phenotype	target1	target2	
	GGAGAAATGAGTGCATTGAACTTG-AGCTGGCATAG	ACTATCCAAGACCGGACCTTGATAACACGGTGAATTTC	
		target3	
		ACTATCCAAGACCGGACCTTGATAACACGGTGAATTTC	
albinism	GGAGAAATGAGTGCATTGAACTTGTAGCTGGCATAG	ACTATCCA-----GGACCTTGATAACACGGTGAATTTC	+1/-5 x1
	GGAGAAATGAGTGCATTGAACTTGTAGCTGGCATAG	ACTATCCA-----GGACCTTGATAACACGGTGAATTTC	+1/-5
albinism	GGAGAAATGAGTGCATTGAACTTGAAGCTGGCATAG	ACTATCCAA-----GACCTTGATAACACGGTGAATTTC	+1/-5 x1
	GGAGAAATGAGTGCATTGAACTTGAAGCTGGCATAG	ACTATCCAA-----GACCTTGATAACACGGTGAATTTC	+1/-5
albinism	GGAGAAATGAGTGCATTGAACTTGTAGCTGGCATAG	ACTATCCAAGA--GGACCTTGATAAAGACGGTGAATTTC	+3/-4 x1
	GGAGAAATGAGTGCATTGAACTTGTAGCTGGCATAG	ACTATCCA-----GGACCTTGATAACACGGTGAATTTC	+1/-5
albinism	GGAGAAATGAGTGCATTGAACTTGTAGCTGGCATAG	ACTATCCA-----GGACCTTGATAACACGGTGAATTTC	+1/-5 x2
	GGAGAAATGAGTGCATTGAACTTGTAGCTGACATAA	ACTATCCAAGA--GGACCTTGATAACACGGTGAATTTC	+3/-4
albinism	GGAGAAATGAGTGCATTGAACTTGTAGCTGGCATAG	ACTATCCA-----GGACCTTGATAACACGGTGAATTTC	+1/-5 x15
	GGAGAAATGAGTGCATTGAACTTGTAGCTGGCATAG	ACTATCCAAGA--GGACCTTGATAACACGGTGAATTTC	+1/-2
albinism	GGAGAAATGAGTGCATTGAA----------	----------CTTGATAACACGGTGAATTTC	-305 x1
	GGAGAAATGAGTGCATTGAA----------	----------CTTGATAACACGGTGAATTTC	-305
pale	GGAGAAATGAGTGCATTGAACTTGTAGCTGGCATAG	ACTATCCA-----GGACCTTGATAACACGGTGAATTTC	+1/-5 x3
	GGAGAAATGAGTGCATTGAACTTG-AGCTGGCATAG	ACTATCCAAGA--GGACCTTGATAACACGGTGAATTTC	-2
pale	GGAGAAATGAGTGCATTGAACTTG-AGCTGGCATAG	ACTATCCAAGA--GGACCTTGATAACACGGTGAATTTC	-2 x1
	GGAGAAATGAGTGCATTGAACTTG-AGCTGGCATAG	ACTATCCAAGA--GGACCTTGATAACACGGTGAATTTC	-2
pale	GGAGAAATGAGTGCATTGAACTTGTAGCTGGCATAG	ACTATCCAAGA--GGACCTTGATAACACGGTGAATTTC	+1/-2 x2
	GGAGAAATGAGTGCATTGAACTTG-AGCTGGCATAG	ACTATCCAAGACCGGACCTTGATAACACGGTGAATTTC	-
green	GGAGAAATGAGTGCATTGAACTTG-AGCTGGCATAG	ACTATCCAAGACCGGACCTTGATAACACGGTGAATTTC	- x13
	GGAGAAATGAGTGCATTGAACTTG-AGCTGGCATAG	ACTATCCAAGACCGGACCTTGATAACACGGTGAATTTC	-

B

PagPDS-MAS-Cas9

phenotype	target1	target2	
	GGAGAAATGAGTGCATTGAACTTGAGCTGGCATAG	ACTATCCAAGACCGGACCTTGATAACACGGTGAATTTC	
		target3	
		ACTATCCAAGACCGGACCTTGATAACACGGTGAATTTC	
albinism	GGAGAAATGAGTGCATTGAA----------	----------CTTGATAACACGGTGAATTTC	-305 x15
	GGAGAAATGAGTGCATTGAA----------	----------CTTGATAACACGGTGAATTTC	-305
albinism	GGAGAAATGAGTGCATTGAACTTG----------	----------CCGGATAACACGGTGAATTTC	303/+ x2
	GGAGAAATGAGTGCATTGAACTTG----------	----------CCGGATAACACGGTGAATTTC	303/+2
albinism	GGAGAAATGAGTGCATTGAACTTG----------	----------CTTGATAACACGGTGAATTTC	-301 x1
	GGAGAAATGAGTGCATTGAACTTG----------	----------CTTGATAACACGGTGAATTTC	-301
albinism	GGAGAAATGAGTGCATTGAACTTGTAGCTGGCATAG	ACTATCCAAGACCG----------GGATTTC	-16+2 x1
	GGAGAAATGAGTGCATTGAACTTGTAGCTGGCATAG	ACTATCCAAGACCG----------GGATTTC	-16+2
albinism	GGAGAAATGAGTGCATTGAACTTGTAGCTTGG-ATAG	ACTATGCCAGCTCGGACCTTGATAACACGGTGAATTTC	-5+4 x1
	GGAGAAATGAGTGCATTGAACTTGT-CTTGGATAG	ACTATGCCAGCTCGGACCTTGATAACACGGTGAATTTC	-2+1
albinism	GGAGAAATGAGTGCATCGAACTT-AGCTGGCATAG	ACTATCCAAGA-CGGACCTTGATAACACGGTGAATTTC	-3+1 x1
	GGAGAAATGAGTGCATTGAACTTGGGTCCGGTCTTGGATAG	ACTATGC-----CAGCTCTTGATAACACGGTGAATTTC	-18+13
albinism	GGAGAAATGAGTGCATTGAACTT-AGCTGGCATAG	ACTATCCAAGA-CGGACCTTGATAACACGGTGAATTTC	-2 x1
	GGAGAAATGAGTGCATTGAACTT-AGCTGGCATAG	ACTATCCAAGA-CGGACCTTGATAACACGGTGAATTTC	-2
albinism	GGAGAAATGAGTGCATTGAACTTG----------	----------CTTGATAACACGGTGAATTTC	-301 x1
	GGAGAAATGAGTGCATTGAACTTGTAGCTGGCATAG	ACTATCCA-ACCGGACTCTTGATAACACGGTGAATTTC	-2/+1
pale	GGAGAAATGAGTGCATTGAACTTGTAGCTGGCATAG	ACTATCCA-----GGACCTTGATAACACGGTGAATTTC	-6/+1 x4
	GGAGAAATGAGTGCATTGAACTTGAGCTGGCATAG	ACTATCCAAGACCGGACCTTGATAACACGGTGAATTTC	-
pale	GGAGAAATGAGTGCATTGAACTTG----------	----------CTTGATAACACGGTGAATTTC	-301 x3
	GGAGAAATGAGTGCATTGAACTTGAGCTGGCATAG	ACTATCCAAGACCGGACCTTGATAACACGGTGAATTTC	-
green	GGAGAAATGAGTGCATTGAACTTGAGCTGGCATAG	ACTATCCAAGACCGGACCTTGATAACACGGTGAATTTC	- x10
	GGAGAAATGAGTGCATTGAACTTGAGCTGGCATAG	ACTATCCAAGACCGGACCTTGATAACACGGTGAATTTC	-

FIGURE 4 | CRISPR/Cas9-mediated gene editing in transgenic poplar plants. **(A)** Editing situation in *PagPDS-2 × 35S-Cas9* plants. **(B)** Editing situation in *PagPDS-MAS-Cas9* plants.

TABLE 2 | Summary of the mutation types at each target site.

	PagPDS-2 × 35S-Cas9		*PagPDS-MAS-Cas9*	
	T1	**T2/T3**	**T1**	**T2/T3**
Biallelic mutation	1	21	3	2
Homozygous	20	4	19	20
Heterozygous	5	2	7	7
Unmodified	14	13	11	11
Mutation rate	65%	67.5%	72.5%	72.5%

cassettes was then transformed into the *Agrobacterium* tumefaciens strain GV3101 (Han et al., 2000; Li et al., 2017; An et al., 2020b). Briefly, *Agrobacterium* cells harboring the vectors were harvested by centrifugation and then resuspended to OD_{600} = 0.3–0.4. Poplar 84K leaf disks were soaked for 20 min on a shaker with the resuspended cells at room temperature. The inoculated leaf disks were co-cultivated at 22°C in the dark for 2 to 3 days. The leaf discs were then washed with sterile double-distilled water and cultured on a callus-induction medium for 10 to 30 days in the dark. The transgenic lines were selected by culturing on medium supplemented with hygromycin (2.0 mg/L). The gene-edited plants were vegetatively propagated in half-strength Murashige and Skoog medium (pH 5.7) containing 0.8% (w/v) agar at room temperature under the light intensity of 50 μmol m^{-2} s^{-1} and a 16/8 h (light/dark) photoperiod.

Detection of Mutations

For analysis of the mutations of edited *PagPDS* in transgenic T_0 plants, genomic DNA was extracted from stable transgenic or wild-type plants using CTAB as described above. The genomic DNAs were used as templates to amplify the endogenous *PagPDS* fragment by Polymerase Chain Reaction (PCR). The primers used for PCR were PagPDS_Mut_F: AACTGGGTATGCGAAGACTTCC and PagPDS_Mut_R: GATTTCATCACCTGCACCAGCAAT. The primers amplified the region spanning the three target sites of the Cas9 system (target 1: 5′-GAGTGCATTGAACTTGAGCTGG-3′; target 2: 5′-CCAAGACCGGACCTTGATAACA-3′; target 3: 5′-CCGGACCTTGATAACACGGTGA-3′). The PCR products were amplified and cloned into the pMD18-T Simple vector as mentioned above for Sanger sequencing to evaluate the editing outcomes of CRISPR/Cas9 transfection. Finally, individual sequences were aligned to the wild-type sequence using SnapGene to determine the mutations effects on predicted modified peptide sequences.

RESULTS

CRISPR/Cas9 Targeted Mutagenesis in *PagPDS*

To establish a new CRISPR/Cas9 genome editing system in poplars, we cloned the phytoene desaturase gene 8 from the hybrid poplar 84K and selected three target sites with 5′-NGG-3′ PAMs of two exons. We named the three target sites T1, T2, and T3 (**Figure 1A**). The multiple CRISPR RNA (crRNA) cassettes were driven by the *Arabidopsis* RNA polymerase III promoter AtU6-26 while Cas9 was driven by the 2 × 35S promoter or MAS promoter in pCambia1300 binary vectors (**Figure 2A**). The target sequence was confirmed by amplification and sequencing. The three gRNAs were inserted into the *pC1300-2 × 35S-Cas9* and *pC1300-MAS-Cas9* binary vectors between the *Kpn* I and *BamH* I sites by a one-step ligation (**Figure 2B**). Two constructs (**Figure 2C**) were introduced into the poplar 84K via *Agrobacterium*-mediated transformation. The transgenic plants were selected by culture on ½ MS medium supplemented with hygromycin and grown with a light and dark cycles of 16/8 h.

Phenotypes of *PagPDS-2 × 35S-Cas9* Transgenic Plants

Forty positive candidate transgenic lines were obtained for *PagPDS-2 × 35S-Cas9* and confirmed by DNA PCR amplification. Both biallelic homozygous and heterozygous mutants of *PDS* are known to exhibit albino phenotypes (Fan et al., 2015). Here, albino seedlings were observed, confirming that mutations were generated at the *PDS* gene (**Figure 3**). To evaluate the simultaneous editing of multiple target sites, the genomic DNA of 40 transgenic plants was extracted independently, and the targeted sequences of *PDS* were amplified by PCR. The sequencing results showed 67.5% (27 out of 40) mutation rate. Out of 40 albino seedlings, 77.8% (21 out of 27) were albinos and 22.2% (6 out of 27) showed pale green phenotype (**Table 1**). At the T1 site, all seedlings carried mutations, and 53.75% of the mutations were a mononucleotide insertion. At T2/T3 loci, deletions were noted ranging from 2 to 5 nt near the PAM. Gene editing data are presented in **Figure 4A**. At the T1 locus, five plants had a mutation in one allele while 21 plants had mutations in both alleles, including 20 homozygous mutations and 1 biallelic mutations. At T2/T3 loci, the mutation rate was 67.5% (27 out of 40), including 21 biallelic mutations and four homozygous mutations (**Table 2**).

Phenotypes of *PagPDS-MAS-Cas9* Transgenic Plants

To explore the activity of the MAS promoter in poplars, we used the same method to construct a vector with MAS driving expression of Cas9. This construct was introduced into poplar 84K resulting in 40 transgenic lines, of which30 were albino. In the MAS-Cas9 system, the mutation rate was 75% (30 out of

40), which was higher than that of the 2 × 35S-Cas9 system. 76.7% (23 of 30) of mutant plants were albinos and 23.3% (7 out of 30) showed a pale green phenotype (**Table 1**). Sequencing of the albino plants was used to define the resulting mutations. Large deletions were found between T1 and T2/T3 (**Figure 4B**). At mutation site T1, 29 plants (72.5%) had at least one allele edited while 22 plants had the edited mutations in both alleles, including 19 homozygous mutations and 3 biallelic mutations. At the T2/T3 loci, the mutation rate was 72.5%, including 20 homozygous mutations and 2 biallelic mutations (**Table 2**).

DISCUSSION

In this study, we established a simplified method for creating mutations with high frequency directly in the model poplar 84K genotype. We used two vectors to construct an engineered binary vector based on the classical isocaudomer technique to simplify the procedures. With appropriate restriction enzyme sites, as many as three gRNAs or more can be assembled together in one step in a single ligation reaction, which enables creating mutations in multiple target sites within a single plant. This system both simplifies the procedures for gene editing, and also increases the frequency of mutations.

Our ability to successfully target multiple sites of the *PagPDS* genes in *Populus* make demonstrates the ability to edit multiple genes at the same time, including duplicated homologous genes. Gene duplication is common in poplar and other trees, so the simple system could be applied to edit all homologs in trees. In order to better compare the editing efficiency with the binary pYLCRIPSR/Cas9, three target sites were selected using the criteria of Fan et al. (2015). The mutation rate in our system is improved to higher rate, 67.5% in CaMV 35S promoter-based system and 75% in pC1300-MAS-Cas9 system than the reported mutation rate (51.7%) in *Populus tomentosa Carr* (Fan et al., 2015). Indeed in our pC1300-MAS-Cas9 system, there is high editing efficiency, which is of practical importance as it reduces the work and effort of producing and evaluating enough transgenic lines to recover desired mutations. Based on previous studies, the MAS promoter increases the expression of gene fusions in tobacco and maize (Ni et al., 1995; Lee et al., 2007). It is thus likely that the MAS promoter promoted the expression of Cas9 in our experiments in poplar, enriching the variety and efficiency of edits.

Our a high-efficiency genome-editing tool of pC1300-MAS-Cas9 will facilitate gene functional research in woody tree species. In future studies we will directly test whether the PC1300-MAS-Cas9 has high editing efficiency in other woody plants and trees.

DATA AVAILABILITY STATEMENT

The original contributions presented in the study are included in the article/**Supplementary Material**, further inquiries can be directed to the corresponding author/s.

AUTHOR CONTRIBUTIONS

YA, JD, and CW designed the research and wrote the paper. YA, CW, JY, and YG performed the research. YA and JY analyzed data. All authors reviewed the manuscript.

FUNDING

This research was supported by National Key Program on Transgenic Research (2018ZX08020002) to Zhejiang University (JD). It was supported by the by the National Natural Science Foundation of China (31901327) to YA.

ACKNOWLEDGMENTS

We thank Dr. Andrew Groover for help with editing the manuscripts.

SUPPLEMENTARY MATERIAL

The Supplementary Material for this article can be found online at: https://www.frontiersin.org/articles/10.3389/fpls.2021.703546/full#supplementary-material

REFERENCES

An, Y., Geng, Y., Yao, J., Fu, C., Lu, M., Wang, C., et al. (2020a). Efficient genome editing in populus using CRISPR/Cas12a. *Front. Plant Sci.* 11:593938. doi: 10.3389/fpls.2020.593938

An, Y., Zhou, Y., Han, X., Shen, C., Wang, S., Liu, C., et al. (2020b). The GATA transcription factor GNC plays an important role in photosynthesis and growth in poplar. *J. Exp. Bot*. 71, 1969–1984. doi: 10.1093/jxb/erz564

Bewg, W. P., Ci, D., and Tsai, C. J. (2018). Genome editing in trees: from multiple repair pathways to long-term stability. *Front. Plant Sci*. 9:1732. doi: 10.3389/fpls.2018.01732

Breitler, J.-C., Dechamp, E., Campa, C., Zebral Rodrigues, L. A., Guyot, R., Marraccini, P., et al. (2018). CRISPR/Cas9-mediated efficient targeted mutagenesis has the potential to accelerate the domestication of *Coffea canephora*. *Plant Cell Tissue Organ. Cult*. 134, 383–394. doi: 10.1007/s11240-018-1429-2

Chang, L., Wu, S., and Tian, L. (2019). Effective genome editing and identification of a regiospecific gallic acid 4-O-glycosyltransferase in pomegranate (*Punica granatum* L.). *Hortic. Res*. 6:123. doi: 10.1038/s41438-019-0206-7

Fan, D., Liu, T., Li, C., Jiao, B., Li, S., Hou, Y., et al. (2015). Efficient CRISPR/Cas9-mediated targeted. Mutagenesis in *Populus* in the first generation. *Sci. Rep*. 5:12217. doi: 10.1038/srep12217

Fister, A. S., Landherr, L., Maximova, S. N., and Guiltinan, M. J. (2018). Transient expression of CRISPR/Cas9 machinery targeting TcNPR3 enhances defense response in *Theobroma cacao*. *Front. Plant Sci*. 9:268. doi: 10.3389/fpls.2018.00268

Han, K. H., Meilan, R., Ma, C., and Strauss, S. H. (2000). An *Agrobacterium tumefaciens* transformation protocol effective on a variety of cottonwood hybrids (genus *Populus*). *Plant Cell Rep*. 19, 315–320. doi: 10.1007/s002990050019

Huang, X., Chen, S., Peng, X., Bae, E.-K., Dai, X., Liu, G., et al. (2020). An improved draft genome sequence of hybrid *Populus alba* × *Populus glandulosa*. *J. For. Res.* 32, 1663–1672. doi: 10.1007/s11676-020-01235-2

Jansson, S., and Douglas, C. J. (2007). Populus: a model system for plant biology. *Annu. Rev. Plant Biol.* 58, 435–458. doi: 10.1146/annurev.arplant.58.032806.103956

Jia, H., Xu, J., Orbovic, V., Zhang, Y., and Wang, N. (2017). Editing citrus genome via SaCas9/sgRNA system. *Front. Plant Sci.* 8:2135. doi: 10.3389/fpls.2017.02135

Lee, L. Y., Kononov, M. E., Bassuner, B., Frame, B. R., Wang, K., and Gelvin, S. B. (2007). Novel plant transformation vectors containing the superpromoter. *Plant Physiol.* 145, 1294–1300. doi: 10.1104/pp.107.106633

Li, S., Zhen, C., Xu, W., Wang, C., and Cheng, Y. (2017). Simple, rapid and efficient transformation of genotype Nisqually-1: a basic tool for the first sequenced model tree. *Sci. Rep.* 7:2638. doi: 10.1038/s41598-017-02651-x

Nakajima, I., Ban, Y., Azuma, A., Onoue, N., Moriguchi, T., Yamamoto, T., et al. (2017). CRISPR/Cas9-mediated targeted mutagenesis in grape. *PLoS ONE* 12:e0177966. doi: 10.1371/journal.pone.0177966

Ni, M., Cui, D., Einstein, J., Narasimhulu, S., Vergara, C. E., and Gelvin, S. B. (1995). Strength and tissue specificity of chimeric promoters derived from the octopine and mannopine synthase genes. *Plant J.* 7, 661–676. doi: 10.1046/j.1365-313X.1995.7040661.x

Nishitani, C., Hirai, N., Komori, S., Wada, M., Okada, K., Osakabe, K., et al. (2016). Efficient genome editing in apple using a CRISPR/Cas9 system. *Sci. Rep.* 6:31481. doi: 10.1038/srep31481

Odipio, J., Alicai, T., Ingelbrecht, I., Nusinow, D. A., Bart, R., and Taylor, N. J. (2017). Efficient CRISPR/Cas9 genome editing of phytoene desaturase in cassava. *Front. Plant Sci.* 8:1780. doi: 10.3389/fpls.2017.01780

Polle, A., Janz, D., Teichmann, T., and Lipka, V. (2013). Poplar genetic engineering: promoting desirable wood characteristics and pest resistance. *Appl. Microbiol. Biotechnol.* 97, 5669–5679. doi: 10.1007/s00253-013-4940-8

Qiu, D., Bai, S., Ma, J., Zhang, L., Shao, F., Zhang, K., et al. (2019). The genome of *Populus alba* × *Populus tremula* var. glandulosa clone 84K. *DNA Res.* 26, 423–431. doi: 10.1093/dnares/dsz020

Van Zeijl, A., Wardhani, T. A. K., Seifi Kalhor, M., Rutten, L., Bu, F., Hartog, M., et al. (2018). CRISPR/Cas9-Mediated mutagenesis of four putative symbiosis genes of the tropical tree parasponia andersonii reveals novel phenotypes. *Front. Plant Sci.* 9:284. doi: 10.3389/fpls.2018.00284

Wang, C., Shen, L., Fu, Y., Yan, C., and Wang, K. (2015). A simple CRISPR/Cas9 system for multiplex genome editing in rice. *J. Genet. Genomics* 42, 703–706. doi: 10.1016/j.jgg.2015.09.011

Wang, J., Wu, H., Chen, Y., and Yin, T. (2020). Efficient CRISPR/Cas9-mediated gene editing in an interspecific hybrid poplar with a highly heterozygous genome. *Front. Plant Sci.* 11:996. doi: 10.3389/fpls.2020.00996

Wang, X., Tu, M., Wang, D., Liu, J., Li, Y., Li, Z., et al. (2018). CRISPR/Cas9-mediated efficient targeted mutagenesis in grape in the first generation. *Plant Biotechnol. J.* 16, 844–855. doi: 10.1111/pbi.12832

Wullschleger, S. D., Jansson, S., and Taylor, G. (2002). Genomics and forest biology: *Populus* emerges as the perennial favorite. *Plant Cell* 14, 2651–2655. doi: 10.1105/tpc.141120

Zhou, X., Jacobs, T. B., Xue, L. J., Harding, S. A., and Tsai, C. J. (2015). Exploiting SNPs for biallelic CRISPR mutations in the outcrossing woody perennial *Populus* reveals 4-coumarate:CoA ligase specificity and redundancy. *New Phytol.* 208, 298–301. doi: 10.1111/nph.13470

Conflict of Interest: The authors declare that the research was conducted in the absence of any commercial or financial relationships that could be construed as a potential conflict of interest.

frontiers in Plant Science

ORIGINAL RESEARCH
published: 14 July 2021
doi: 10.3389/fpls.2021.714907

Knockdown of miR393 Promotes the Growth and Biomass Production in Poplar

Liwei Chu[1], *Xuejiao He*[1], *Wenbo Shu*[3], *Lijuan Wang*[1,2] *and Fang Tang*[1,2*]

[1] State Key Laboratory of Tree Genetics and Breeding, Key Laboratory of Tree Breeding and Cultivation of the National Forestry and Grassland Administration, Research Institute of Forestry, Chinese Academy of Forestry, Beijing, China, [2] Co-innovation Center for Sustainable Forestry in Southern China, Nanjing Forestry University, Nanjing, China, [3] Key Laboratory of Horticultural Plant Biology of Ministry of Education, College of Horticulture and Forestry Sciences, Huazhong Agricultural University, Wuhan, China

Short tandem target mimic (STTM), which is composed of two short sequences mimicking small RNA target sites, separated by a linker of optimal size, can block the functions of all members in a miRNA family. microRNA393 (miR393), which is one of the conserved miRNA families in plants, can regulate plant root growth, leaf development, plant architecture, and stress resistance. In order to verify the role of miR393 in the secondary growth of trees, we created its STTM transgenic poplar lines (STTM393). The expression of miR393 in STTM393 lines was reduced by over 10 times compared with the control plants. STTM393 lines showed promoted growth with about 20% higher, 15% thicker, and 2–4 more internodes than the control plants after 3 months of growth. The cross-section of the stems showed that STTM393 lines had wider phloem, xylem, and more cambium cell layers than control plants, and the lignin content in STTM393 lines was also higher as revealed by staining and chemical determination. Based on the transcriptome analysis, the genes related to the auxin signaling pathway, cell cyclin, cell expansion, and lignin synthesis had higher expression in STTM393 lines than that in control plants. The higher expression levels of *FBL* family members suggested that the auxin signaling pathway was strengthened in STTM393 lines to promote plant growth. Therefore, the knockdown of miR393 using the STTM approach provides a way to improve poplar growth and biomass production.

Keywords: miR393, STTM, plant growth, auxin signaling pathway, RNA-seq, poplar

OPEN ACCESS

Edited by:
Guohua Chai,
Qingdao Agricultural University, China

Reviewed by:
Jianhua Wei,
Beijing Academy of Agricultural and Forestry Sciences, China
Lin Zhang,
Central South University Forestry and Technology, China

****Correspondence:***
Fang Tang
tangfangcaf@126.com

Specialty section:
This article was submitted to Plant Biotechnology, a section of the journal Frontiers in Plant Science

Received: *26 May 2021*
Accepted: *21 June 2021*
Published: *14 July 2021*

Citation:
Chu L, He X, Shu W, Wang L and Tang F (2021) Knockdown of miR393 Promotes the Growth and Biomass Production in Poplar. Front. Plant Sci. 12:714907. doi: 10.3389/fpls.2021.714907

INTRODUCTION

Poplar is one of the important carbon-neutral biomass for the production of timber products, paper pulping, chemicals, and biofuels (Gui et al., 2020). At present, there is a large demand for wood, and cultivating fast-growing trees like poplar is a promising way to solve this problem. To further improve poplar growth and biomass production, substantial efforts have been made to identify the functions of genes and small RNAs that regulate poplar growth (Lucas et al., 2013; Sundell et al., 2017; Busov, 2018). MicroRNAs (miRNAs) can negatively regulate the transcription and post-transcription of their specific target genes by binding their near-perfect complementary sites through its 20–24 nucleotides, which can lead to the target mRNA degradation and/or translational repression (Meyers et al., 2008; Voinnet, 2009).

In previous studies, in order to understand miRNA functions, the major approaches were used by generating the transgenic lines in which the genes that encode miRNAs or the target gene of miRNAs were overexpressed (Zhu et al., 2009; Zhang et al., 2010; Curaba et al., 2013). However, these approaches were insufficient to fully understand miRNA functions. First, one miRNA often targeted multiple genes for regulation, and modifying one target gene could not possibly reveal the functions of other target genes (Bartel, 2009). Second, overexpressing the miRNAs could only result in a decrease in the expression level of miRNA target genes and an inability to obtain the information of gain of functions of the target genes. On the contrary, miRNAs tend to be gene families, and thus previous approaches could generally overexpress only one member at a time (Sieber et al., 2007; Curaba et al., 2013).

Short tandem target mimic (STTM) can explore the functions of miRNAs by simultaneously blocking all the members in an miRNA family so as to achieve a gain-function of target genes through a single genetic transformation event (Yan et al., 2012). STTM is an artificial, short (∼100 nt), non-coding RNA that is composed of two miRNA-binding sites and a spacer/linker. The two binding sites are complementary to the target small RNAs except for the central 3-nucleotide bulge, which sticks out between the 10th and 11th nucleotides of the targeted small RNA, so that the binding sites can trap miRNAs without being cleaved by them (Tang et al., 2012). STTM can be expressed through either stable plant transformation or virus-based transient expression systems (Sha et al., 2014; Teotia et al., 2017) and has been used to knockdown the target miRNA expression in *Arabidopsis* (Yan et al., 2012), soybean (Wong et al., 2014), tomato (Cao et al., 2016), cotton (Gu et al., 2014), and maize (Liu et al., 2019).

As one of the conserved miRNA families in plants, miR393 had been studied in several species like *Arabidopsis* (Navarro et al., 2006), rice (Bian et al., 2012), barley (Yuan et al., 2019), and poplar (Lu et al., 2008), and it was found that miR393 affected the plant root system (Vidal et al., 2010), leaf development (Si-Ammour et al., 2011), seedling growth and drought stress tolerance (Yuan et al., 2019), and salinity and alkaline stress (Gao et al., 2011). In *Arabidopsis*, miR393, which is encoded by MIR393a and MIR393b, can regulate its target genes including four F-box family auxin receptor genes (*Transport Inhibitor Response Protein 1*, *TIR1*) by splicing (Zhang et al., 2006; Si-Ammour et al., 2011; Wójcik and Gaj, 2016). *TIR1* family members affect different phenotypes including rooting, seedling growth, and seed coat development by regulating the auxin pathway (Parry et al., 2009; Hu et al., 2012). In poplar, the *FBL* family, which are homologous genes of the *TIR* family in *Arabidopsis*, have eight members, and *FBL1-FBL4* have been confirmed to be cleaved by miR393 (Shu et al., 2015; Tang et al., 2020). There are four members in the miR393 family of poplar, in which the mature miR393 encoded by different precursors share the same sequences (PmiREN, V2) (Guo et al., 2019). In a previous study, we analyzed the expression of miR393 in different tissues of poplar at multiple developmental stages and found that its expression was low in young tissues but high in mature tissues, especially in old stem (Tang et al., 2020). This suggests that miR393 may play a role in the vascular tissue development, which deserves further investigation.

In this study, we created miR393 STTM transgenic poplar (*Populus alba* × *Populus glandulosa*) in which the expression of miR393 was significantly reduced. The transgenic lines showed increased plant height, ground diameter, number of internodes, width of xylem, and total biomass production compared with the non-transgenic control plants. Accordingly, a large number of genes related to plant growth and wood formation were upregulated in STTM393 transgenic lines in order to inhibit the expression of miR393. The results support that blocking the function of miR393 by the STTM approach can promote plant growth and increase biomass production.

MATERIALS AND METHODS

STTM393 Vector Construction and Transformation

The construction of the STTM393 vector was based on the previous method (Tang et al., 2012; Peng et al., 2018). Two primers with the sequences to form hairpin were synthesized according to the sequence of mature miR393, which is conserved across all the sequenced poplar species so far. The primer sequences were as follows: STTM393-Forward Primer: 5′-gcc**ATTTAAAT**atggtctaaagaagaaggatGATCAATGCGAtcgTCCCTTTGGAgaattcggtacgctgaaatcaccag-3′ and STTM393-Reverse Primer: 5′-gcc**ATTTAAAT**tagaccataacaacaacaacTCCAAAGGGAcgaTCGCATTGATCaagcttgggctgtcctctccaaatg-3′. The *SwaI* site "**ATTTAAAT,**" the *EcoRI* site "gaattc," the *HindII* site "aagctt," the artificial linker (20 nts) with the lowercase nucleotides, the "tcg" bulge in the middle of miR393 sequences, and the complementary sequences to d35S and T-35S of the pOT2 vector with lowercase nucleotides at the 3′-end were embedded in these two synthesized primers. Then, the pOT2 vector was used as a template for PCR amplification, and the linker PCR product was subjected to *SwaI* digestion and a subsequent self-ligation, which resulted in pOT2-STTM393. Finally, the pOT2 with STTM393 structure was sub-cloned into a binary vector pFGC5941, which was used to transform into 84K poplar (*P. alba* × *P. glandulosa*) by *Agrobacterium*-mediated leaf disk method. The positively transformed lines identified by resistance screening and expression analysis were used for further phenotypic observation.

Plant Phenotypic Determination and Chemical Composition Measurement

The plantlets of STTM393 transgenic lines and 84K controls were grown in the culture medium for 1 month and then transferred to the soil pots. Seedlings were grown in a culture room under long-day conditions (16 h light/8 h dark) at 25/22°C (day/night) and in a greenhouse under natural light with daytime and nighttime temperatures of 24–30°C in the Chinese Academy of Forestry (Beijing, China). The plant height, ground diameter, and internode number were measured every month. The plant height is the length from the top of the plant to the base of the stem; the ground diameter is the diameter of the last internode at the

base of the stem, and the number of internodes is the internode from the first expanded leaf to the last internode at the stem base. Stem tissues were sectioned by Leica VT1000S vibrating-blade microtome (Leica, Germany) with a thickness of 70 μm. The sections were stained by using toluidine blue (TBO) and phloroglucinol-HCl and were observed under Olympus BX51 microscope (Olympus, Tokyo, Japan). The stems of 6-month-old plants from 16th to 40th were used for cellulose, hemicellulose, and lignin content determination, according to the published protocol (Wang et al., 2020). Six STTM393 lines and 84K control plants were analyzed in this study, and each line included 6–10 vegetatively propagated individuals for the experiment. Data from each experiment were subjected to either an ANOVA or a *t*-test. All statistical analyses were performed using the SPSS Version 17.0 (SPSS, NY, United States). The phenotyping of STTM393 transgenic lines and 84K control plants was performed on three batches of plants.

Total RNA Extraction and cDNA Synthesis

Total RNA was extracted using the LC Sciences Total RNA Purification Kit (#TRK-1001, LC Sciences, TX, United States) according to the previous modified methods (Tang et al., 2019). The integrity of total RNA was further assessed by 1.5% agarose gel electrophoresis, and the RNA concentration and purity were determined by NanoDrop™ 8000 Spectrophotometer (Thermo Fisher Scientific, MA, United States). Only RNA samples with an A260/A280 ratio between 1.9 and 2.1 and an A260/A230 ratio >1.80 were used for cDNA synthesis. We used a universal reverse transcription (RT) PCR method, in which the total RNA will be added by a poly(A) tail before RT (Tang et al., 2016). First, 2 μg of the total RNA was polyadenylated with ATP by poly(A) polymerase (PAP) at 37°C for 1 h in a 20-μl reaction mixture using the Poly(A) Tailing Kit (#AM1350, Invitrogen, MA, United States). Then, 10 μl (1 μg) of the E-PAP-treated total RNA was reverse transcribed with a poly(T) adapter universal RT-primer (5′-AAC GAG ACG ACG ACA GAC TTT TTT TTT TTT TTTV-3′) using PrimeScript™ RT reagent Kit (#RR037, TaKaRa, Shiga, Japan) following the instruction of the manufacturer. The cDNA was diluted 20-fold with nuclease-free water for quantitative real-time reverse transcription PCR (qRT-PCR).

Quantitative Real-Time PCR Analysis

Quantitative real-time PCR was performed on the LightCycler® 480 System (Roche Molecular Systems, Basel, Switzerland). The reaction mixture contained 10 μl of KAPA SYBR FAST qPCR Master Mix (# K4601, KAPA Biosystems, MA, United States), 2 μl of 20-fold diluted cDNA, 0.4 μM each of a forward and a reverse primer (**Supplementary Table 1**), and ddH_2O in a final volume of 20 μl. Amplifications were performed with the following program: 95°C for 3 s; 40 cycles of 95°C for 10 s, 60°C for 30 s, and 72°C for 3 s. No-template reactions were used as negative controls, and *protein phosphatase 2A-2* (*PP2A-2*) and *polyubiquitin* (*UBQ*) were used as reference genes (Tang et al., 2019). Each sample was assessed in four technical replicates, and the experiment was repeated three times.

High-Throughput Transcriptome Sequencing

The top five internodes of 3-month-old STTM393 lines (STTM393-2, STTM393-8, and STTM393-16) and 84K control plants were collected, among which 3–5 individuals in a line were randomly selected as a biological replicate, and each line had three biological replicates. The cDNA library construction and high-throughput sequencing of the above samples were performed by Biomarker Technologies (BMK, Beijing, China). The sequencing library used the NEBNext Ultra™ RNA Library Prep Kit for Illumina (NEB, MA, United States). The library was sequenced with Illumina Novaseq 6000, and the reading length was 2 × 150 bp (PE150). Clean data were obtained by removing the sequences containing adapter, poly-N, and low quality from raw data. Using Hisat2 software, the obtained clean data were compared with the genome of 717 poplar (*Populus tremula* × *P. alba*) (http://128.192.158.63/index.php/databases/spta-717-genome). The number of allowed mismatched nucleotides was set to "0" or "1." After that, String-Tie (version 2.1.4) was used for transcriptional assembly and new transcriptional prediction, and the alternative splicing types and corresponding expression levels of each sample were obtained by ASprofile software. The quantification of gene expression level was estimated by the number of fragments per kilobase of transcript per million fragments (FPKM). EBSeq (Version 1.5.4) software was used to analyze the differential expression between STTM393 lines and 84K control samples. Genes with an adjusted FDR < 0.05 found by DESeq2 were assigned as differentially expressed. Gene ontology (GO) enrichment analysis of differentially expressed genes (DEGs) was carried out by GOseq R software, and the DEGs in the KEGG pathway were enriched by KOBAS software. The original transcriptome data were submitted to the NCBI public database Sequence Read Archive (SRA, PRJNA724789).

RESULTS

STTM393 Promotes Poplar Growth

We obtained 30 STTM393 transgenic lines by *Agrobacterium*-mediated leaf disk method, and qRT-PCR showed that the expression of miR393 in 13 randomly selected lines was reduced over 10 times (**Supplementary Figure 1**). Six STTM393 transgenic lines with different expression levels were randomly selected for phenotype observation. The height, ground diameter, and internode number of these STTM393 transgenic plants at different developmental stages were significantly higher than those of 84K control plants (**Supplementary Figure 2**). Three STTM393 lines (i.e., STTM393-2, STTM393-8, and STTM393-16) with obvious phenotypic changes were used for further analysis.

The transgenic plants of STTM393-2, STTM393-8, and STTM393-16 grew faster than the control plants from tissue culture to soil cultivation. The plant height and root length of their 1-month-old tissue culture plantlets were longer than the control plantlets (**Supplementary Figure 3A**). Similarly, the STTM393 transgenic plants transferred to soil for 1 month (2-month-old plants) had significantly higher plant

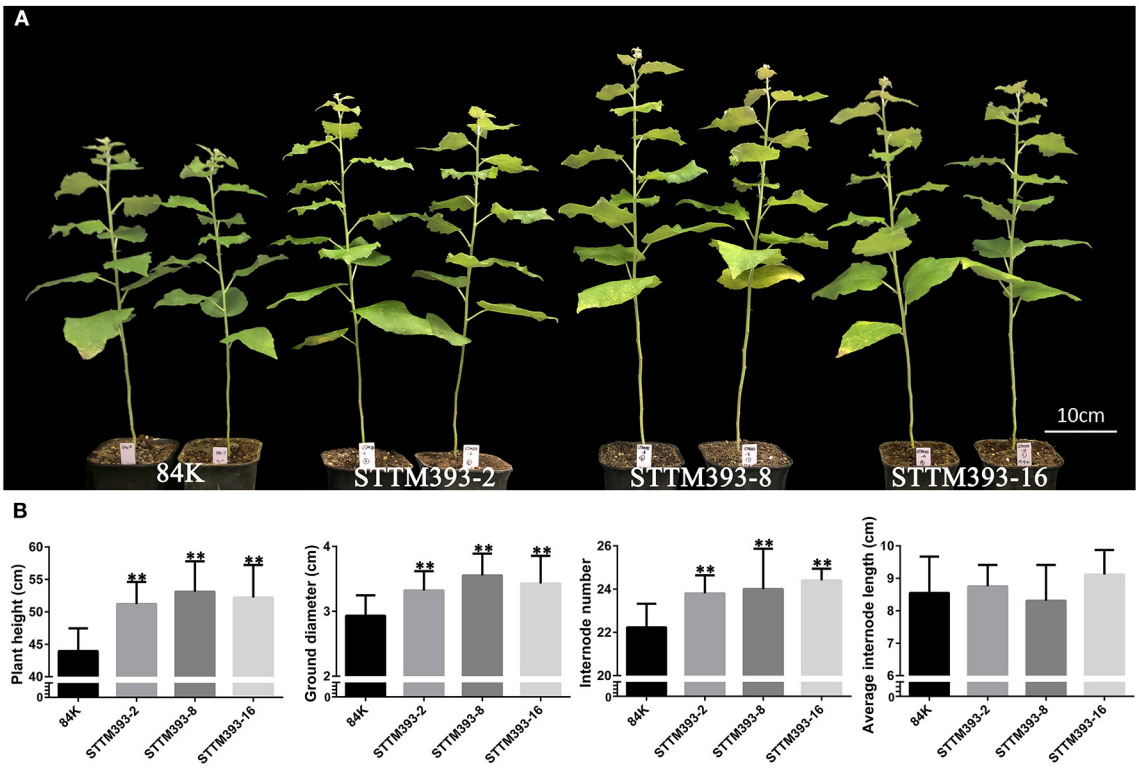

FIGURE 1 | The phenotypes of STTM393 transgenic plants. **(A)** 3-month-old STTM393 and 84K control plants. **(B)** The height, ground diameter, internode number, and average internode length of 3-month-old STTM393-2, STTM393-8, STTM393-16, and 84K control plants. The bars represent means ± SD ($n = 10$), $^{**}P \leq 0.01$.

height, ground diameter, and internode number than those of the control plants (**Supplementary Figures 3B–E**). The height, ground diameter, and internode number of each 3-month-old STTM393 lines were 15–35, 15–25, and 7–13% higher than those of the control, respectively. However, the average internode length of STTM393 plants was not significantly different from that of the control plants (**Figure 1**). The three transgenic lines were grown three times, and similar results were obtained (**Supplementary Figure 4**). Therefore, the knockdown of miR393 family may promote plant growth in poplar.

STTM393 Enhances Wood Formation

To investigate the function of miR393 in wood formation, we prepared the stem cross-sections to observe the vascular tissue of STTM393 lines. The results showed that the 15th internode of 3-month-old STTM393 transgenic plants was significantly larger in diameter than that of the control plants, while the cell layers of cambium and the width of phloem, xylem, and pith were also larger than of the control plants (**Figure 2**). This indicates that STTM393 transgenic plants can enhance the xylem development probably due to the high activity of cambium cells.

Phloroglucinol staining showed that lignin deposition was increased in both the fiber and vessel cell walls of STTM393 transgenic lines, as revealed by the dark pink color (**Figures 3A,B**). Therefore, the content of lignin, cellulose, and hemicellulose in the stems of STTM393 transgenic lines and the controls was chemically determined. The STTM393 lines had significantly higher lignin content but lower cellulose content than the 84K controls (**Figure 3C**). However, there was no significant difference in the relative hemicelluloses content between STTM393 transgenic and control plants (**Figure 3C**). This suggests that the inhibition of miR393 expression may increase the lignin content in the secondary cell wall.

STTM393 Increases the Expression of *PagFBLs*

We detected the expression levels of miR393 in the stems of 3-month-old STTM393 lines and 84K controls. The expression values of miR393 were reduced by 78, 88, and 91% in STTM393-2, STTM393-8, and STTM393-16 lines, respectively, compared with the control plants (**Figure 4A**). It indicates that the STTM of miR393 indeed causes the inhibition of the expression of miR393. *FBL* family members are the target genes of miR393 in poplar (Tang et al., 2020); thus, we detected *PagFBLs* expression in STTM393 lines and control plants by qRT-PCR and found that the expression levels of eight *PagFBL* genes were increased in STTM393 transgenic lines (**Figure 4B**). These results suggest that STTM393 can increase the expression of *PagFBLs* by inhibiting the function of miR393.

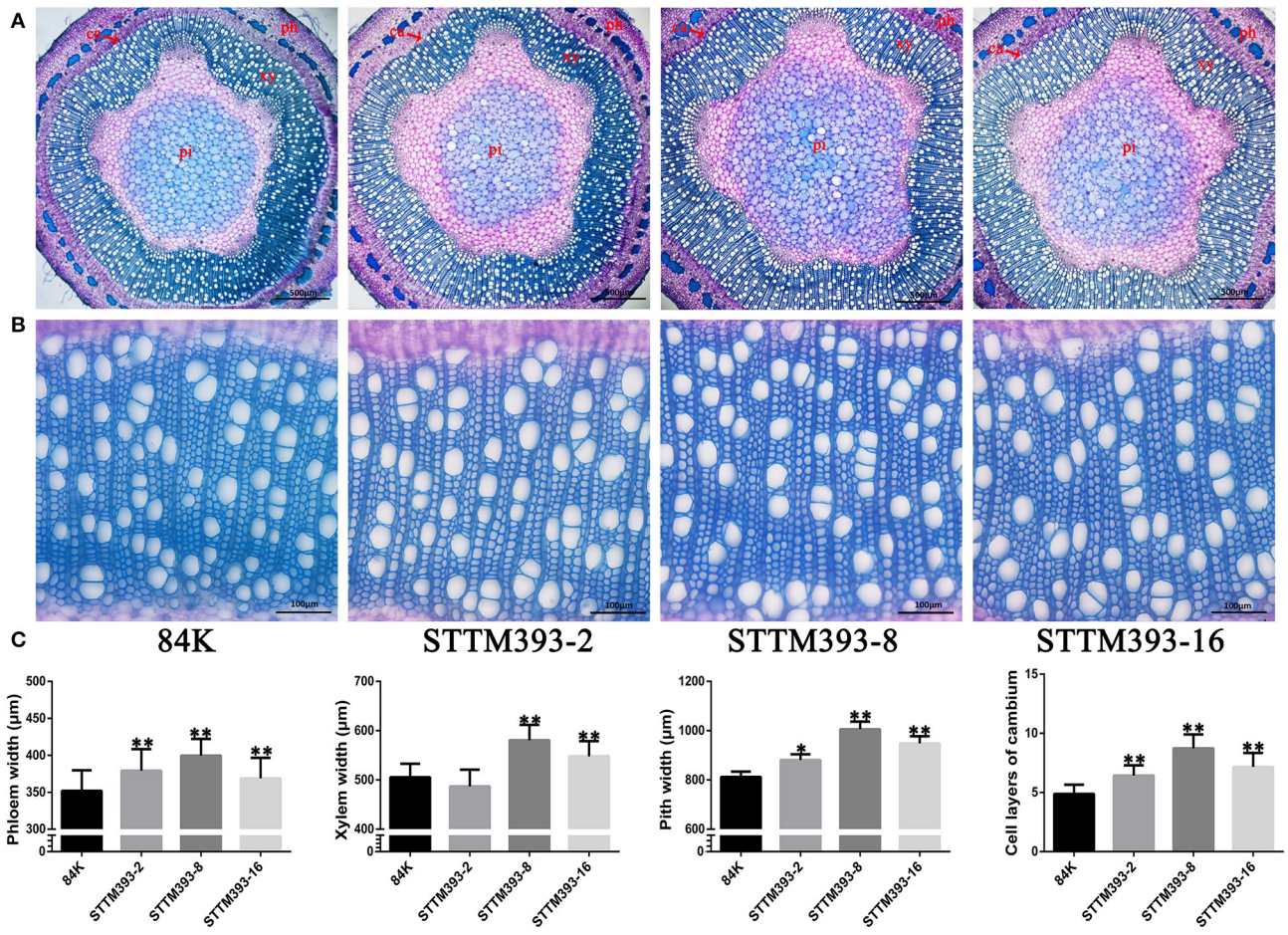

FIGURE 2 | The vascular tissues in STTM393 transgenic plants. **(A)** The cross-sections of the 15th internode of 3-month-old STTM393 and 84K control plants stained by toluidine blue (TBO), Bar = 500 μm. ph, phloem; xy, xylem; pi, pith; ca, cambium. **(B)** The magnified xylem region of **(A)**, Bar = 100 μm. **(C)** The statistical data for phloem, xylem, pith, and cambium layers of 3-month-old STTM393 lines and 84K control plants. The bars represent means ± SD ($n > 40$). $^{**}P \leq 0.01$, $^{*}0.01 < P \leq 0.05$.

Inhibition of miR393 Affects Genes Related to Plant Growth and Wood Formation

To understand which genes would be affected due to the inhibited miR393 expression, the expression of genes in three STTM393 lines (STTM393-2, STTM393-8, and STTM393-16) and control plants was detected by RNA sequencing. The results showed that there were 863 differentially expressed genes in the three STTM393 lines compared with the control, 431 of which were upregulated, and 432 were downregulated (**Supplementary Table 2**). The biological function of the upregulated genes was mainly enriched in the xyloglucan metabolic process (GO:0010411), cell wall biogenesis (GO:0042546), cell wall organization (GO:0071555), and response to auxin (GO:0009733), while that of the downregulated genes was mainly enriched in response to stimulus (GO:0050896), response to stress (GO:0006950), cellular response to sulfur starvation (GO:0010438), and response to an inorganic substance (GO:0010035).

Notably, the expression of genes related to auxin signal transduction had been upregulated, such as auxin-responsive protein (*SAUR1* and *SAUR78*), indole-3-acetic acid-amido synthetase (*GH3.6*), and indole-3-acetic acid-induced protein (*ARG7*). In addition, one auxin transporter protein, *AUX1*, and two homologous genes of the auxin-binding protein, *ABP19a*, had higher expression in STTM393 lines than in the control (**Table 1**). In STTM393 lines, several cell wall loosening factors including expansin (*EXP*), xyloglucan endotransglucosylase/hydrolase (*XTH*), glucan endo-1, 3-beta-glucosidase (*GLC*), and galacturonosyltransferase-like (*GATL*) were upregulated. Furthermore, the expression of cyclin genes regulating cell cycle transition was also upregulated, for example, cyclin D 1;1 (*CYCD1;1*), cyclin D 3;1 (*CYCD3;1*), and cyclin P 4;1 (*CYCP4;1*), all highly expressed in STTM393 transgenic lines. The higher expression of cell cycle-related genes may explain why the growth rate of STTM393 lines is faster than the controls.

In accordance with the relatively high content of lignin but low content of cellulose in STTM393 transgenic plants, the genes

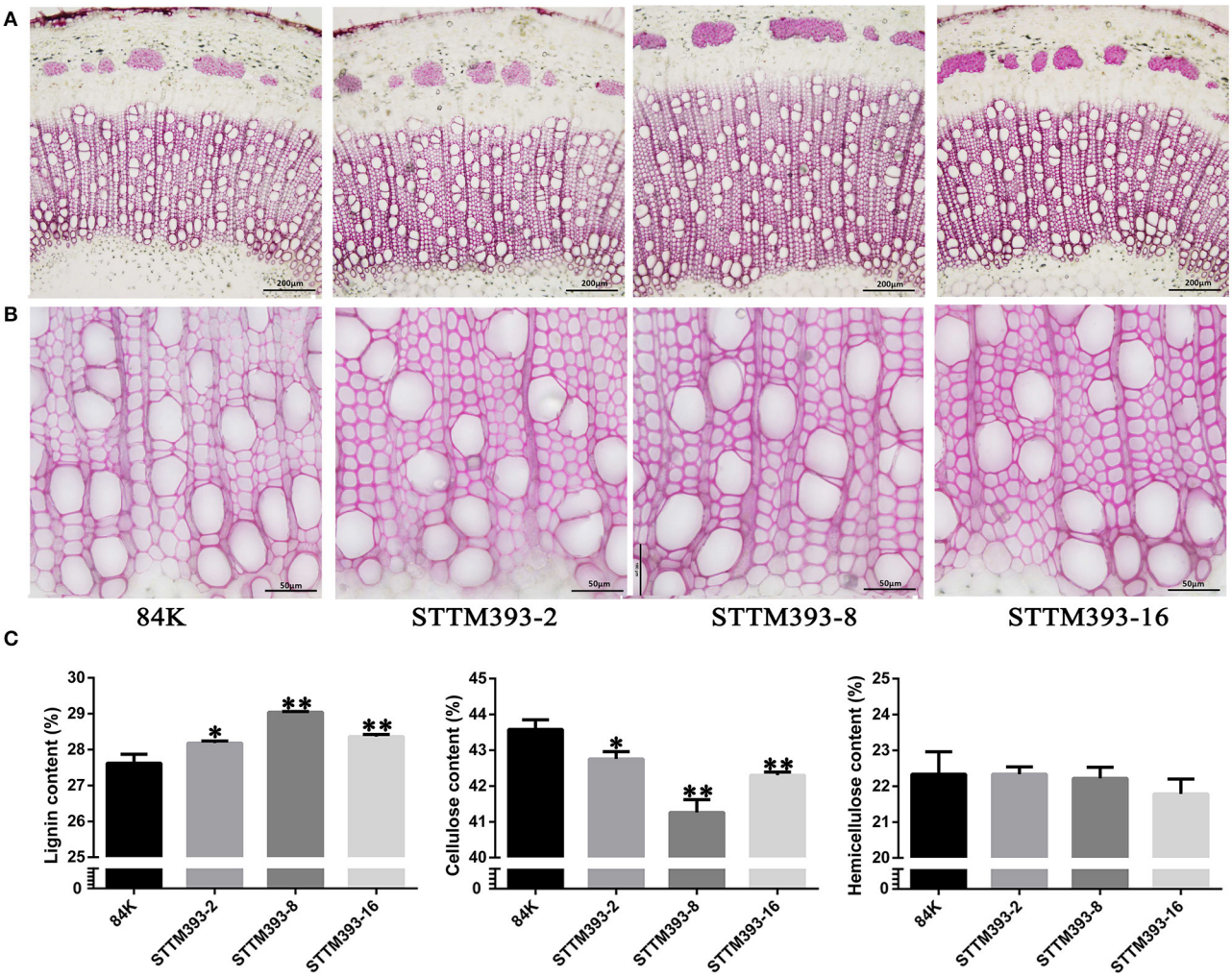

FIGURE 3 | The chemical composition analysis in STTM393 transgenic plants. **(A)** The cross-sections of the 15th internode of 6-month-old STTM393 and 84K control plants stained by phloroglucinol-HCl, Bar = 200 μm. **(B)** The magnified xylem region of **(A)**, Bar = 50 μm. **(C)** The lignin, cellulose, and hemicellulose content of stem from 16th to 40th internodes of 6-month-old STTM393 lines and 84K control plants. The bars represent means ± SD ($n > 6$). $^{**}P \leq 0.01$, $^{*}0.01 < P \leq 0.05$.

involved in the lignin synthesis pathway, such as cinnamoyl-CoA reductase (*CCR1* and *CCRL6*), caffeic acid 3-*O*-methyltransferase (*OMT1*), peroxidase (*PER9* and *PER73*), and benzylalcohol *O*-acetyltransferase (*BEAT*), were upregulated, while cellulose synthase-like genes (*CSLG3* and *CSLE1*) were downregulated (**Table 1**). The homologous genes of *CESA1* and *CESA6*, which are involved in the cellulose synthesis in the primary cell wall, exhibited higher expression in STTM393 lines. Therefore, the inhibition of the miR393 expression can increase the expression of genes related to lignification, thus promoting wood formation.

The expression levels of some genes mentioned above were verified by qRT-PCR. *PP2A-2* and *UBQ* were selected as reference genes for qRT-PCR. The expression trends of the genes calculated with *PP2A-2* (**Figure 5**) were consistent with those calculated with *UBQ* (**Supplementary Figure 5**). The relative expression levels of these genes obtained *via* qRT-PCR were consistent with that from the RNA sequencing data.

DISCUSSION

As an important regulator in the auxin signaling pathway, miR393 is involved in root development and stress resistance in herbaceous plants. For instance, the overexpression of miR393 can cause phenotypic changes in the length of main roots and the number of lateral roots in *Arabidopsis* and rice (Chen et al., 2011; Bian et al., 2012). We previously found that miR393 was highly expressed in developing secondary vascular tissues in poplar (Tang et al., 2016), but, so far, the role of miR393 in vascular tissue development has not been fully investigated. In this study, we blocked the miR393 expression in transgenic poplars using STTM technology and found its role in strengthening auxin signaling, which led to the promotion of secondary growth and production of high biomass in transgenic poplars.

To access the role of miR393 in secondary growth, we generated miR393 inhibition lines using the STTM approach.

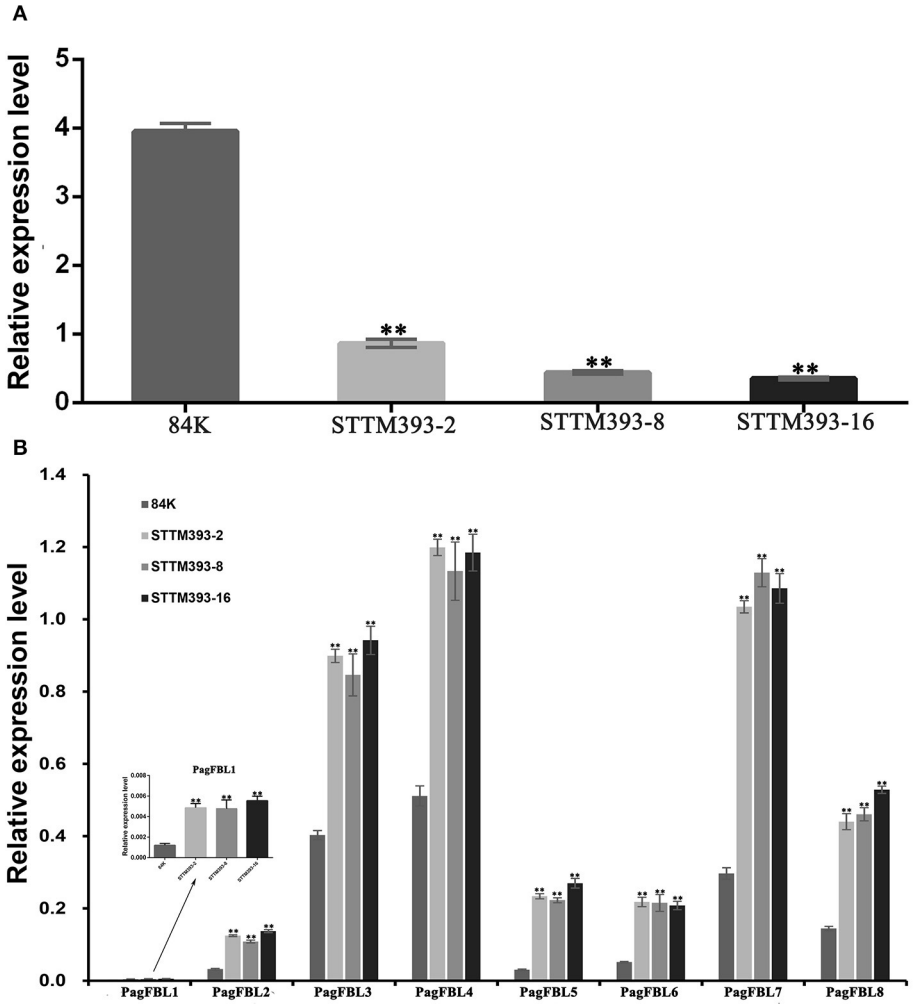

FIGURE 4 | The expression of miR393 and *PagFBLs* in STTM393 lines by quantitative real-time reverse transcription (qRT)-PCR. The relative expression of miR393 **(A)** and eight members from *PagFBL* family **(B)** was detected by qRT-PCR in the 3-month-old STTM393 lines and 84K control plants. $^{**}P \leq 0.01$.

The plant height, ground diameter, and the number of internodes of STTM393 transgenic lines were all increased significantly, and this was opposite to the phenotype of the miR393 overexpression that inhibit apical meristem development observed in *Arabidopsis* (Wang et al., 2017). Interestingly, the cambium zone, pith, xylem, and phloem regions of the STTM393 lines were wider than the non-transgenic control plants, indicating that STTM393 could promote cell division, resulting in the increase of cell numbers in the pith, xylem, cambium, and phloem, which eventually led to the increase of stem diameter.

Previous studies had shown that miR393 in *Arabidopsis* and poplar played the role of splicing the target gene, *TIR1*, and its homologous, *FBLs* (Vidal et al., 2010; Chen et al., 2011; Tang et al., 2020). In this study, we found that the expression levels of all *FBL* family members were increased in the STTM393 lines, indicating that the function of miR393 on *FBLs* was successfully inhibited. A previous study suggested that *FBL1-FBL4* in *FBL* family members could be cleaved by miR393 (Tang et al., 2020). However, in this study, we found that the expression levels of all *FBL* members were increased using the STTM approach. These results suggest that miR393 may be tolerant to the mismatch with the target sequences. Overexpression of *PagFBL1* could promote the growth and root development in poplar (Shu et al., 2018); thus, the promoted secondary growth in STTM393 transgenic plants might be due to the increased expression of *FBL* family members.

Auxin is a very important hormone in controlling plant growth and development, and the FBL family members as putative auxin receptors mediate the auxin signaling pathway. To further investigate the role of auxin signaling in the development of secondary vascular tissues, we used RNA sequencing to check the genes changed in expression due to the inhibition of miR393. The downstream genes of the auxin signaling pathway, such as *SAUR78* and *GH3.6*, were upregulated, of which *GH3.6* was known to be regulated by *PagFBL1* and might modulate adventitious rooting (Shu et al., 2018), while the overexpression

TABLE 1 | The differently expressed genes related to plant growth and wood formation.

#ID	84K	S393-2	S393-8	S393-16	Change	Gene name	Annotation
Auxin signal transduction							
Potri.008G066400.1	3.81	6.46	6.84	7.00	Up	AUX1	Auxin transporter-like protein 1
Potri.001G169000.1	90.36	339.12	255.85	213.42	Up	ABP19a	Auxin-binding protein
Potri.013G141900.1	507.95	1108.03	840.21	863.32	Up	ABP19a	Auxin-binding protein
Potri.004G165500.1	2.59	5.26	6.99	4.90	Up	SAUR1	Auxin-responsive protein
Potri.004G165600.1	0.74	2.11	4.28	4.30	Up	SAUR1	Auxin-responsive protein
Potri.003G071000.1	1.32	5.92	7.58	3.07	Up	SAUR78	Auxin-responsive protein
Potri.001G410400.1	4.10	7.14	8.73	8.19	Up	GH3.6	Indole-3-acetic acid-amido synthetase
Potri.011G129700.1	3.64	6.38	7.91	10.50	Up	GH3.6	Indole-3-acetic acid-amido synthetase
Potri.004G165800.1	0.60	2.26	2.69	4.33	Up	ARG7	Indole-3-acetic acid-induced protein
Cell expansion							
Potri.013G060800.1	21.93	41.26	46.23	44.81	Up	EXPA10	Expansin-A10
Potri.009G141400.1	2.63	11.30	10.54	9.52	Up	EXPL2	Expansin-like A2
Potri.002G236200.1	16.16	37.93	54.84	32.96	Up	XTH2	Xyloglucan endotransglucosylase/hydrolase 2
Potri.004G021000.1	18.89	60.70	65.11	43.95	Up	XTH8	Xyloglucan endotransglucosylase/hydrolase 8
Potri.019G125000.1	35.85	163.80	178.76	105.74	Up	XTH9	Xyloglucan endotransglucosylase/hydrolase 9
Potri.006G071200.1	7.73	40.09	23.95	21.20	Up	XTH23	Xyloglucan endotransglucosylase/hydrolase 23
Potri.018G095100.2	0.05	1.31	2.34	1.57	Up	XTH23	Xyloglucan endotransglucosylase/hydrolase 23
Potri.004G132700.1	1.22	2.01	2.15	2.70	Up	GLC11	Glucan endo-1,3-beta-glucosidase 11
Potri.008G055900.1	5.63	9.82	12.37	11.35	Up	GLC1	Glucan endo-1,3-beta-glucosidase 1
Potri.008G192600.1	0.79	2.20	3.02	2.26	Up	GATL9	Probable galacturonosyltransferase-like 9
Potri.010G038300.1	5.32	17.42	16.08	11.07	Up	GATL9	Probable galacturonosyltransferase-like 9
Potri.009G006500.1	21.21	43.10	45.58	28.49	Up	IRX7	Glucuronoxylan glucuronosyltransferase
Cell cyclin							
Potri.007G005700.1	0.72	1.71	2.75	1.63	Up	CYCD1;1	Cyclin-D1-1
Potri.009G086700.1	18.22	30.55	33.24	24.59	Up	CYCD1;1	Cyclin-D1-1
Potri.002G123000.1	8.96	12.58	16.04	13.59	Up	CYCD3;1	Cyclin-D3-1
Potri.012G115600.1	2.71	5.59	6.22	4.26	Up	CYCP4;1	Cyclin-P4-1
Potri.014G050400.1	21.52	56.45	69.92	44.15	Up	CYCP4;1	Cyclin-P4-1
Lignin							
Potri.002G004500.1	9.86	17.34	14.05	12.90	Up	CCR1	Cinnamoyl-CoA reductase 1
Potri.013G079500.2	2.64	9.01	9.23	6.20	Up	CCRL6	Cinnamoyl-CoA reductase-like
Potri.014G106500.2	1.70	3.07	2.72	3.48	Up	OMT1	Caffeic acid 3-O-methyltransferase
Potri.007G053400.1	9.25	18.01	17.71	12.44	Up	PER73	Peroxidase 73
Potri.002G031200.1	0.25	0.60	0.80	0.87	Up	PER9	Peroxidase 9
Potri.005G028200.1	12.56	34.36	38.49	25.00	Up	BEAT	Acetyl-CoA-benzylalcohol acetyltransferase
Potri.019G001400.1	2.99	6.26	7.54	5.16	Up	BEAT	Acetyl-CoA-benzylalcohol acetyltransferase
Potri.005G028500.1	9.96	27.35	29.87	20.98	Up	BEAT	Acetyl-CoA-benzylalcohol acetyltransferase
Cellulose							
Potri.005G087500.1	29.09	52.39	53.63	46.34	Up	CESA6	Cellulose synthase 6
Potri.018G029400.1	51.33	81.41	84.90	69.36	Up	CESA1	Cellulose synthase 1
Potri.003G142300.1	18.82	9.94	10.25	10.79	Down	CSLG3	Cellulose synthase like G3
Potri.006G004300.1	50.81	32.43	29.52	30.59	Down	CSLE1	Cellulose synthase like E1
Potri.006G004300.10	4.00	2.66	1.52	2.28	Down	CSLE1	Cellulose synthase like E1

of *SAUR78* promoted plant growth in *Arabidopsis* (Li et al., 2015). Several cyclin genes, including *CYCD* and *CYCP*, were also upregulated in the STTM393 lines. Cyclin D can regulate cell transformation from the G1 phase to the S phase to start the cell cycle by promoting DNA synthesis and cell proliferation (Lu et al., 2011). Overexpression of *CYCD2* in tobacco could increase the rate of plant growth and biological yield by accelerating the rate of cell division (Cockcroft et al., 2000). Similarly, *CYCD3* was a positive regulator of cambial cell proliferation and secondary growth (Collins et al., 2015). Therefore, the strengthened auxin

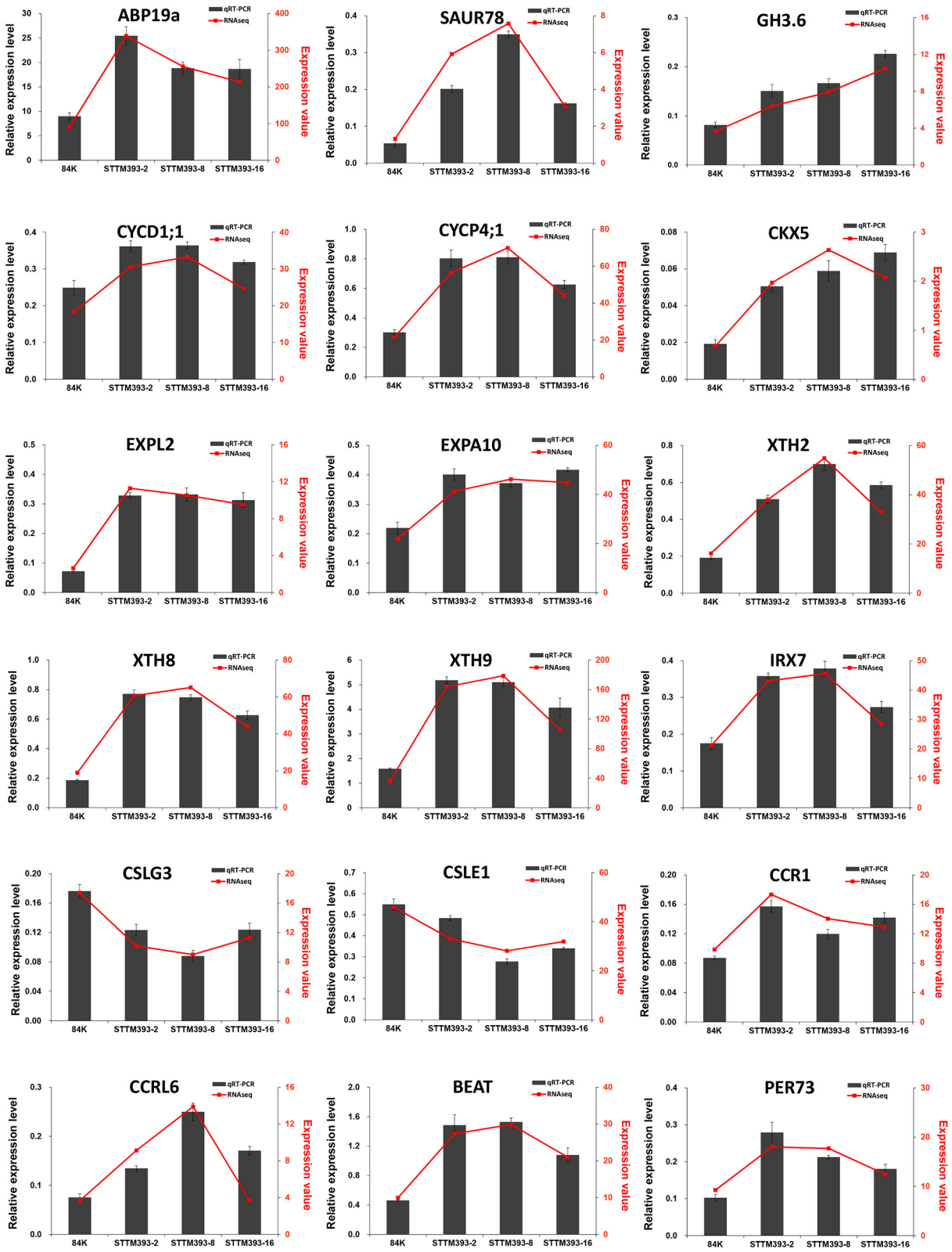

FIGURE 5 | Validation of key genes related to plant growth and wood formation by qRT-PCR using *PP2A-2* as reference gene. The column represents the results of qRT-PCR, with the coordinate axis on the left (dark-grey). The line represents the results of transcriptome, with the coordinate axis on the right (red).

signaling also leads to the activation of cell cycles to accelerate cell division and thus promote the secondary growth of poplar.

Plant cell wall loosening is a necessary physiological process during cell expansion and elongation throughout the entire growth and development of plants. It is due to the hydrolysis of polysaccharides in the cell wall caused by the action of cell wall loosening factors (Zhao and Li, 2011). The expression levels of several cell wall loosening factors, such as *EXPA10*, *XTH2*, *XTH8*, *XTH9,* and *XTH23* genes, were upregulated in the transgenic lines. Previous studies have shown that *EXPA* is involved in the regulation of xylem formation (Gray-Mitsumune et al., 2004), while *XTH* family members are involved in the cell wall synthesis in poplar (Mellerowicz and Sundberg, 2008), but *XTH9* mutation leads to shorter internode length (Hyodo et al., 2003). The upregulation of these genes provides support to the observed fast xylem development in transgenic lines. In addition, the lignin synthesis pathway genes, *CCR1*, *CCRL6*, *PER73,* and *BEAT*, were upregulated in the STTM393 lines, in comparison with the control plants. The increased expression of key enzymes in the lignin synthesis pathway can promote lignin synthesis (Xie et al., 2018). On the contrary, the expression levels of two cellulose synthase-related genes, *CSLG3* and *CSLE1*, in STTM393 lines were decreased. This was in accordance with the observation that STTM393 lines exhibited higher lignin content but lower cellulose content in stems.

In summary, the STTM approach can block the function of miR393, thus increasing the expression of its target genes *FBLs*. The strengthened auxin signaling promotes secondary growth of and biomass production in transgenic poplars, by changing a series of downstream genes orchestrating cambium activity, xylem development, and cell wall synthesis. This study provides additional support, that is, manipulating auxin signaling regulators could enhance trees for fast growth and biomass production.

DATA AVAILABILITY STATEMENT

The datasets presented in this study can be found in online repositories. The names of the repository/repositories and accession number(s) can be found below: SRA, PRJNA724789.

AUTHOR CONTRIBUTIONS

FT designed the study. FT constructed the STTM393 vector and LC transformed it into poplar. FT, XH, and LC investigated the growth data of STTM393 transgenic and control plants. FT and XH completed the section and microscopic observation of different stem nodes of STTM393 plants. FT and LC analyzed the data and drafted the manuscript. WS and LW helped in the interpretation of results. All of the authors carefully checked and approved this manuscript.

FUNDING

This work was supported by the National Natural Science Foundation of China (31700592), the Fundamental Research Funds for the Central Non-profit Research Institution of CAF (CAFYBB2017QA003), and the National Key Research and Development Program of China (2016YFD0600100).

ACKNOWLEDGMENTS

We thank Zhongyong Chen and Jun'e Mu of the Chinese Academy of Forestry for their valuable technical contribution for the transformation and tissue culture of poplar.

SUPPLEMENTARY MATERIAL

The Supplementary Material for this article can be found online at: https://www.frontiersin.org/articles/10.3389/fpls.2021.714907/full#supplementary-material

REFERENCES

Bartel, D. P. (2009). MicroRNAs: target recognition and regulatory functions. *Cell* 136, 215–233. doi: 10.1016/j.cell.2009.01.002

Bian, H., Xie, Y., Guo, F., Han, N., Ma, S., Zeng, Z., et al. (2012). Distinctive expression patterns and roles of the miRNA393/TIR1 homolog module in regulating flag leaf inclination and primary and crown root growth in rice (Oryza sativa). *New Phytol.* 196, 149–161. doi: 10.1111/j.1469-8137.2012.04248.x

Busov, V. (2018). Manipulation of growth and architectural characteristics in trees for increased woody biomass production. *Front. Plant Sci.* 9:1505. doi: 10.3389/fpls.2018.01505

Cao, D., Wang, J., Ju, Z., Liu, Q., Li, S., Tian, H., et al. (2016). Regulations on growth and development in tomato cotyledon, flower and fruit via destruction of miR396 with short tandem target mimic. *Plant Science*. 247, 1–12. doi: 10.1016/j.plantsci.2016.02.012

Chen, Z.-H., Bao, M.-L., Sun, Y.-Z., Yang, Y.-J., Xu, X.-H., Wang, J.-H., et al. (2011). Regulation of auxin response by miR393-targeted transport inhibitor response protein 1 is involved in normal development in Arabidopsis. *Plant Mol. Biol.* 77, 619–629. doi: 10.1007/s11103-011-9838-1

Cockcroft, C., den Boer, B., Healy, S., and Murray, J. (2000). Cyclin D control of growth rate in plants. *Nature* 405, 575–579. doi: 10.1038/35014621

Collins, C., Gowda, M., and Jahn, C. (2015). CYCD3 D-type cyclins regulate cambial cell proliferation and secondary growth in Arabidopsis. *J. Exp. Bot*. 66, 4595–4606. doi: 10.1093/jxb/erv218

Curaba, J., Talbot, M., Li, Z., and Helliwell, C. (2013). Over-expression of microRNA171 affects phase transitions and floral meristem determinancy in barley. *BMC Plant Biol.* 13:6. doi: 10.1186/1471-2229-13-6

Gao, P., Bai, X., Yang, L., Lv, D., Pan, X., Li, Y., et al. (2011). Osa-MIR393: a salinity- and alkaline stress-related microRNA gene. *Mol. Biol. Rep.* 38, 237–242. doi: 10.1007/s11033-010-0100-8

Gray-Mitsumune, M., Mellerowicz, E., Abe, H., Schrader, J., Winzéll, A., Sterky, F., et al. (2004). Expansins abundant in secondary xylem belong to subgroup A of the -expansin gene family. *Plant Physiol.* 135, 1552–1564. doi: 10.1104/pp.104.039321

Gu, Z., Huang, C., Li, F., and Zhou, X. (2014). A versatile system for functional analysis of genes and microRNAs in cotton. *Plant Biotechnol. J.* 12, 638–649. doi: 10.1111/pbi.12169

Gui, J., Lam, P. Y., Tobimatsu, Y., Sun, J., Huang, C., Cao, S., et al. (2020). Fiber-specific regulation of lignin biosynthesis improves biomass quality in Populus. *New Phytol*. 226, 1074–1087. doi: 10.1111/nph.16411

Guo, Z., Kuang, Z., Wang, Y., Zhao, Y., Tao, Y., Cheng, C., et al. (2019). PmiREN: a comprehensive encyclopedia of plant miRNAs. *Nucleic Acids Res.* 48, D1114–D1121. doi: 10.1093/nar/gkz894

Hu, Z., Keceli, M., Kalliola, M., Li, J., Survila, M., Heino, P., et al. (2012). F-box protein AFB4 plays a crucial role in plant growth, development and innate immunity. *Cell Res.* 22, 777–781. doi: 10.1038/cr.2012.12

Hyodo, H., Yamakawa, S., Takeda, Y., Tsuduki, M., Yokota, A., Nishitani, K., et al. (2003). Active gene expression of a xyloglucan endotransglucosylase/hydrolase gene, XTH9, in inflorescence apices is related to cell elongation in Arabidopsis thaliana. *Plant Mol. Biol.* 52, 473–482. doi: 10.1023/A:1023904217641

Li, Z., Chen, H., Li, Q., Tao, J., Bian, X.-H., Ma, B., et al. (2015). Three SAUR proteins SAUR76, SAUR77 and SAUR78 promote plant growth in Arabidopsis. *Sci. Rep*. 5:12477. doi: 10.1038/srep12477

Liu, X., Liu, S., Wang, R., Chen, X., Fan, Z., Wu, B., et al. (2019). Analyses of miRNA functions in maize using a newly developed ZMBJ-CMV-2bN81-STTM vector. *Front. Plant Sci.* 10:1277. doi: 10.3389/fpls.2019.01277

Lu, M., Yao, C., Lai, D., and Xu, H. (2011). Cyclin D1 and cell cycle regulation. *Biotechnol. Bull.* 10, 55–59. doi: 10.13560/j.cnki.biotech.bull.1985.2011.10.025

Lu, S., Sun, Y.-H., and Chiang, V. L. (2008). Stress-responsive microRNAs in Populus. *Plant J.* 55, 131–151. doi: 10.1111/j.1365-313X.2008.03497.x

Lucas, W. J., Groover, A., Lichtenberger, R., Furuta, K., Shri-Ram, Y., Helariutta, Y., et al. (2013). The plant vascular system: evolution, development and functions. *J. Integr. Plant Biol.* 55, 294–388. doi: 10.1111/jipb.12041

Mellerowicz, E., and Sundberg, B. (2008). Wood cell walls: biosynthesis, developmental dynamics and their implications for wood properties. *Curr. Opin. Plant Biol.* 11, 293–300. doi: 10.1016/j.pbi.2008.03.003

Meyers, B. C., Axtell, M. J., Bartel, B., Bartel, D. P., Baulcombe, D., Bowman, J. L., et al. (2008). Criteria for annotation of plant MicroRNAs. *Plant Cell* 20, 3186–3190. doi: 10.1105/tpc.108.064311

Navarro, L., Dunoyer, P., Jay, F., Arnold, B., Dharmasiri, N., Estelle, M., et al. (2006). A plant miRNA contributes to antibacterial resistance by repressing auxin signaling. *Science* 312, 436–439. doi: 10.1126/science.1126088

Parry, G., Calderon-Villalobos, L. I., Prigge, M., Peret, B., Dharmasiri, S., Itoh, H., et al. (2009). Complex regulation of the TIR1/AFB family of auxin receptors. *Proc. Natl. Acad. Sci. U. S. A.* 106, 22540–22545. doi: 10.1073/pnas.0911967106

Peng, T., Qiao, M., Liu, H., Teotia, S., Zhang, Z., Zhao, Y., et al. (2018). A resource for inactivation of microRNAs using short tandem target mimic technology in model and crop plants. *Mol. Plant* 11, 1400–1417. doi: 10.1016/j.molp.2018.09.003

Sha, A., Zhao, J., Yin, K., Tang, Y., Wang, Y., Wei, X., et al. (2014). Virus-based microRNA silencing in plants. *Plant Physiol.* 164, 36–47. doi: 10.1104/pp.113.231100

Shu, W., Liu, Y., Guo, Y., Zhou, H., Zhang, J., Zhao, S., et al. (2015). A Populus TIR1 gene family survey reveals differential expression patterns and responses to 1-naphthaleneacetic acid and stress treatments. *Front. Plant Sci.* 6:714. doi: 10.3389/fpls.2015.00719

Shu, W., Zhou, H., Jiang, C., Zhao, S., Wang, L., Li, Q., et al. (2018). The auxin receptor TIR1 homolog (PagFBL1) regulates adventitious rooting through interactions with Aux/IAA28 in Populus. *Plant Biotechnol. J.* 17, 338–349. doi: 10.1111/pbi.12980

Si-Ammour, A., Windels, D., Arn-Bouldoires, E., Kutter, C., Ailhas, J., Meins, F., et al. (2011). miR393 and secondary siRNAs regulate expression of the TIR1/AFB2 auxin receptor clade and auxin-related development of Arabidopsis leaves. *Plant Physiol.* 157, 683–691. doi: 10.1104/pp.111.180083

Sieber, P., Wellmer, F., Gheyselinck, J., Riechmann, J., and Meyerowitz, E. (2007). Redundancy and specialization among plant microRNAs: role of the MIR164 family in developmental robustness. *Development* 134, 1051–1060. doi: 10.1242/dev.02817

Sundell, D., Street, N. R., Kumar, M., Mellerowicz, E. J., Kucukoglu, M., Johnsson, C., et al. (2017). AspWood: high-spatial-resolution transcriptome profiles reveal uncharacterized modularity of wood formation in Populus tremula. *Plant Cell* 29, 1585–1604. doi: 10.1105/tpc.17.00153

Tang, F., Chu, L., He, X., Shu, W., and Lu, M. (2020). Identification of regulation of poplar miR393 on FBL family genes. *J. Central South Univ. Forest. Technol.* 40, 146–153. doi: 10.14067/j.cnki.1673-923x.2020.05.017

Tang, F., Chu, L., Shu, W., He, X., Wang, L., and Lu, M. (2019). Selection and validation of reference genes for quantitative expression analysis of miRNAs and mRNAs in Poplar. *Plant Methods* 15:35. doi: 10.1186/s13007-019-0420-1

Tang, F., Wei, H., Zhao, S., Wang, L., Zheng, H., and Lu, M. (2016). Identification of microRNAs Involved in Regeneration of the Secondary Vascular System in *Populus tomentosa* Carr. *Front. Plant Sci.* 7:724. doi: 10.3389/fpls.2016.00724

Tang, G., Yan, J., Gu, Y., Qiao, M., Fan, R., Mao, Y., et al. (2012). Construction of short tandem target mimic (STTM) to block the functions of plant and animal microRNAs. *Methods* 58, 118–125. doi: 10.1016/j.ymeth.2012.10.006

Teotia, S., Zhang, D., and Tang, G. (2017). Knockdown of rice microRNA166 by short tandem target mimic (STTM). *Methods Mol. Biol.* 1654, 337–349. doi: 10.1007/978-1-4939-7231-9_25

Vidal, E., Araus, V., Lu, C., Parry, G., Green, P., Coruzzi, G., et al. (2010). Nitrate-responsive miR393/AFB3 regulatory module controls root system architecture in *Arabidopsis thaliana*. *Proc. Natl. Acad. Sci. U. S. A.* 107, 4477–4482. doi: 10.1073/pnas.0909571107

Voinnet, O. (2009). Origin, biogenesis, and activity of plant MicroRNAs. *Cell* 136, 669–687. doi: 10.1016/j.cell.2009.01.046

Wang, F., Shi, D., Han, J., Zhang, G., Jiang, X., Yang, M., et al. (2020). Comparative study on pretreatment processes for different utilization purposes of switchgrass. *ACS Omega* 5, 21999–22007. doi: 10.1021/acsomega.0c01047

Wang, L., Liu, Z., Qiao, M., and Xiang, F. (2017). miR393 inhibits in vitro shoot regeneration in Arabidopsis thaliana via repressing TIR1. *Plant Sci.* 266, 1–8. doi: 10.1016/j.plantsci.2017.10.009

Wójcik, A., and Gaj, M. (2016). miR393 contributes to the embryogenic transition induced *in vitro* in Arabidopsis via the modification of the tissue sensitivity to auxin treatment. *Planta* 244, 231–243. doi: 10.1007/s00425-016-2505-7

Wong, J., Gao, l., Yang, Y., Zhai, J., Arikit, S., Yu, Y., et al. (2014). Roles of small RNAs in soybean defense against *Phytophthora sojae* infection. *Plant J.* 79, 928–940. doi: 10.1111/tpj.12590

Xie, M., Zhang, J., Tschaplinski, T., Tuskan, G., Chen, J.-G., and Muchero, W. (2018). Regulation of lignin biosynthesis and its role in growth-defense tradeoffs. *Front. Plant Sci.* 9:1427. doi: 10.3389/fpls.2018.01427

Yan, J., Gu, Y., Jia, X., Kang, W., Pan, S., Tang, X., et al. (2012). Effective small RNA destruction by the expression of a short tandem target mimic in Arabidopsis. *Plant Cell* 24, 415–427. doi: 10.1105/tpc.111.094144

Yuan, W., Suo, J., Shi, B., Zhou, C., Bai, B., Bian, H., et al. (2019). The barley miR393 has multiple roles in regulation of seedling growth, stomatal density, and drought stress tolerance. *Plant Physiol. Biochem.* 142, 303–311. doi: 10.1016/j.plaphy.2019.07.021

Zhang, B., Pan, X., Cannon, C., Cobb, G., and Anderson, T. (2006). Conservation and divergence of plant microRNA genes. *Plant J.* 46, 243–259. doi: 10.1111/j.1365-313X.2006.02697.x

Zhang, X., Zou, Z., Gong, P., Zhang, J., Ziaf, K., Li, H., et al. (2010). Over-expression of microRNA169 confers enhanced drought tolerance to tomato. *Biotechnol. Lett.* 33, 403–409. doi: 10.1007/s10529-010-0436-0

Zhao, Y., and Li, L. (2011). Plant cell wall loosening factors. *Plant Physiol. J.* 47, 925–935. doi: 10.13592/j.cnki.ppj.2011.10.008

Zhu, Q.-H., Upadhyaya, N., Gubler, F., and Helliwell, C. (2009). Over-expression of miR172 causes loss of spikelet determinacy and floral organ abnormalities in rice (Oryza sativa). *BMC Plant Biol.* 9:149. doi: 10.1186/1471-2229-9-149

Conflict of Interest: The authors declare that the research was conducted in the absence of any commercial or financial relationships that could be construed as a potential conflict of interest.

frontiers in Plant Science

ORIGINAL RESEARCH
published: 16 July 2021
doi: 10.3389/fpls.2021.696747

Economically Feasible Wood Biopreservation Platform in *Lannea coromandelica* (Houtt.) Merr. Against Wood Rotting Fungus Through Bio-Prospecting Weed Extracts

Heena Gupta[1]*, *Kulwant Rai Sharma*[1] and *J. N. Sharma*[2]

[1] Department of Forest Products, College of Forestry, Dr. Y. S. Parmar University of Horticulture and Forestry Nauni, Solan, India, [2] Department of Plant Pathology, College of Horticulture, Dr. Y. S. Parmar University of Horticulture and Forestry Nauni, Solan, India

As an alternative to synthetic preservatives, the use of plant-based, environmentally sustainable preservatives for wood protection has tremendous potential. The current research analyzed the dimensional stability and longevity of *Lannea coromandelica* wood using weed extracts viz. *Lantana camara* L. and *Ageratum conyzoides* L., respectively. Petroleum ether (PE) and methanolic weed extracts were used to treat wood blocks (5 cm × 2.5 cm × 2.5 cm) at varying concentrations ranging from 0.25 to 2.00%. The PE extract of *A. conyzoides* resulted in maximum swelling (tangential plane, 6.30%) at 2.00%, volumetric swelling coefficient (13.17%) at 1.50%, and volumetric shrinkage coefficient (7.71%) at 1.00% concentration, while maximum shrinkage (tangential plane, 4.10%) in methanol (M) extract was observed. In *L. camara* methanolic extract (1.00%), maximum anti-shrink efficiency (37.01%) was recorded. *In vitro* mycelial growth of the wood-rotting fungus was completely inhibited by PE extract from both weeds. However, the methanolic extract of *A. conyzoides* resulted in maximal inhibition (75.93%) at a concentration of 2.00%. Also, PE extract (2.00%) of *A. conyzoides* reduced the fungal colonization to 50%, as compared with control. The lowest weight loss (decay test, 12 weeks) was observed at a 2.00% concentration of *L. camara* PE extract. The present research highlighted that both *A. conyzoides* and *L. camara* could be used as an environmentally sustainable wood preservative substitute that will encourage the utilization of *L. coromandelica* in wood-based industries.

Keywords: ***Lannea coromandelica*, antifungal, dimensional stability, durability, preservative, wood**

OPEN ACCESS

Edited by:
Guohua Chai,
Qingdao Agricultural University, China

Reviewed by:
Emil Engelund Thybring,
University of Copenhagen, Denmark
Sreenivasan Sasidharan,
Universiti Sains Malaysia (USM), Malaysia

***Correspondence:**
Heena Gupta
gheena88@gmail.com

Specialty section:
This article was submitted to Plant Biotechnology, a section of the journal Frontiers in Plant Science

Received: *17 April 2021*
Accepted: *17 June 2021*
Published: *16 July 2021*

Citation:
Gupta H, Sharma KR and Sharma JN (2021) Economically Feasible Wood Biopreservation Platform in Lannea coromandelica (Houtt.) Merr. Against Wood Rotting Fungus Through Bio-Prospecting Weed Extracts. Front. Plant Sci. 12:696747. doi: 10.3389/fpls.2021.696747

INTRODUCTION

Wood is one of the most important and versatile natural resources of humanity, assisting various nations in achieving sustainable development and improving technology and welfare (Daly-Hassen et al., 2014; Verhaegen et al., 2014). The strong mechanical properties of wood and its ease of processing and satisfying aesthetic appearance have not only led to its widespread use in tools, furniture, buildings, and decorations (Qiu et al., 2018) but also in the emerging fields of transparent materials (Zhu et al., 2016, Yu et al., 2017), water clean-up and extraction (Liu et al., 2017; Zhu et al., 2017; Wang et al., 2019), energy storage (Yang et al., 2018),

stimuli-responsive materials (Li et al., 2018), and electronic devices (Chen et al., 2018). Since wood, underexposed environmental conditions, is vulnerable to deterioration caused by various organisms and abiotic influences, it must have high natural durability for these applications. The constitutive biopolymers (cellulose, lignin, and hemicelluloses) of wood are subjected to intense and progressive oxidative degradation processes (photo-oxidation, chemical oxidation, thermal decomposition, and photolysis reactions) as a result of environmental factors (sunlight radiation, primarily UV component; moisture produced by dewing, raining, and snowing; chemical pollutants; fire; heat/cold variations; wind abrasion-particulates; atmospheric oxygen), which affects the natural durability of the wood (dimensional stability, surface integrity) and causes significant structural and color changes (discoloration), as well as a progressive reduction in its resistance to biological agents (biodegradation or decay development) and mechanical properties (Teaca et al., 2019).

Several wood species (*Tectona grandis*, *Cedrus deodara*, etc.) have very good natural resilience against destructive wood agents, but global demand has outstripped supply or availability in the marketplace. Furthermore, timber production from government forest areas in India accounts for 3.35% of total demand, or 153 million m^3 in 2020 (projected), while potential timber production accounts for 45% of total demand for raw wood by various wood-based industries (Brocco et al., 2017; Vanam, 2019). The decline in raw material supply, especially for traditional/primary timber species, is continually impeding the production activities of wood-based industries, resulting in limited output and growth globally (Purnomo et al., 2011; Zhou et al., 2015; Antwi-Boasiako and Boadu, 2016). Importing raw materials could solve the problem, but it would raise the cost of operations and goods, slowing the development of local industries. To ensure a consistent supply of raw materials, one of the best strategies would be introducing lesser used timber species (LUS) into the market, as LUS is abundant in many sustainably managed tropical forests, lowering costs (Antwi-Boasiako and Boadu, 2016).

As a result, *Lannea coromandelica*, a fast-growing deciduous tropical tree in the Anacardiaceae family widely distributed in waste places and forests throughout India, Bangladesh, and some other tropical countries, was chosen for this reason (Reddy et al., 2011; Weerapreeyakul et al., 2016). However, despite having a density of 0.77 gm/cm^3 (at 12% MC), this species is rated as non-durable or non-resistant to natural decay agents as resistance to natural decay depends on higher extractive content rather than the higher density.

Furthermore, the difficulty in seasoning has limited the use of the species in furniture production, house building, and other structural purposes (Rahman et al., 2013). However, synthetic wood preservatives can enhance its durability for a variety of end-uses. While chemical preservation of wood is one of the most effective methods for inducing dimensional stability, UV resistance, and biological resistance in wood (Rowell, 2005), it is costly and becoming increasingly restricted due to both pronounced toxicity and harmful environmental effects (Kartal et al., 2015; Teaca et al., 2019). Furthermore, the treated wood needs maintenance throughout its existence, posing a risk in the disposal and reuse of this material (Wang et al., 2016). Concerns about the environmental effects of conventional wood preservatives have fueled the need for the production of alternative wood protection agents and methods based on natural materials that are both cost-effective and environmentally friendly (Edlich et al., 2005; Singh and Singh, 2012; Mohammed et al., 2016; Tchinda et al., 2018). The high availability and rapid proliferation of invasive plants (e.g., *Ageratum conyzoides*, *Eupatorium* sp., *Lantana camara*, *Mikania micrantha*, and *Parthenium hysteophorus*) will not only improve the overall economic feasibility of the process but may also solve the problems associated with extreme ecological impacts that result in the loss of biodiversity and ecosystem services by altering native biodiversity, community structure, composition, and functions (Negi et al., 2019; Broda, 2020).

Taking that into consideration, two noxious weed species, *L. camara* L. (Verbenaceae) and *A. conyzoides* L. (Asteraceae), with antifungal properties, were chosen for the study with the goal of bio-prospecting weed extracts for providing an economical and environmentally friendly biopreservation platform in *L. coromandelica* (Houtt.) Merr. against *Laetiporus sulphureus* (Bull.: Fr.) Murr., a common wood-rotting fungus.

MATERIALS AND METHODS

Experimental Location

The experiment was conducted in the Department of Forest Products, Dr. Y. S. Parmar University of Horticulture and Forestry, Nauni, Solan (H.P.) (30.8613° N, 77.1708° E) located at 1,275 m a.s.l.

Wood Material

The wood blocks [5.0 cm (longitudinal) × 2.5 cm (radial) × 2.5 cm (tangential)] from air-dried sapwood of *L. coromandelica* were prepared at the sawmill workshop of the Department of Forest Products, Nauni, Solan (Himachal Pradesh, India). The blocks were oven-dried at 105 ± 2°C until constant weight is attained before the subsequent treatments. No observable signs of defects, infection by mold, or wood-destroying fungi and termite were detected on wood samples. The density of the oven-dried specimens was in the range of (0.56 to 0.77) (Gupta et al., 2016). To ensure maximum uptake of the treatment solutions, none of the surfaces of the wood samples was sealed. Three replicates, each with six wood blocks, were cut for the tests, along with control samples.

Plant Material and Extracts Preparation

Two obnoxious weeds, viz., *A. conyzoides* L. and *L. camara* L. were collected from University premises. The botanical identity was confirmed by comparing with the herbarium specimens and a voucher specimen with accession number 7307 and 12674, respectively, deposited at the Herbarium of Department of Forest Products. PE and M were used as extraction solvents for comparison in this study. PE was selected because of its low polarity and ability to remove oils, fats, sterols, and terpenes (Pramod et al., 2017). On the other hand, M is known for its low

toxicity, high polarity, and efficiency in extracting various polar phytocompounds (phenolics, flavonoids, and so on) (Swamy et al., 2015). The grounded leaves of *L. camara* and aerial parts of *A. conyzoides* (100.0 g each) were extracted sequentially first with refluxing PE (Sigma-Aldrich, St. Louis, MO) in a Soxhlet extractor for 10 cycles. The residual PE was allowed to evaporate from the material and was subsequently extracted with refluxing M (Merck, India). The solvents were separated from the respective solution by rotary evaporation and preserved separately at 4°C until further use. The extracts were named E1 (*L. camara* PE extract), E2 (*L. camara* M extract), E3 (*A. conyzoides* PE extract), E4 (*A. conyzoides* M extract). The soxhlet extractions were replicated thrice.

Treatment Method

The surface-applied treatment steeping was conducted. The PE and M extracts of *Lantana* (L) and *Ageratum* (A) were prepared at different concentrations of 0.25, 0.50, 1.00, 1.50, and 2.00% (w/v) by diluting the respective amount of extract in 5% M (v/v). The oven-dried wood blocks (M_1) (six in each replicate) were immersed in a solution of each concentration of extracts for 72 h at room temperature. After the treatment, the excess extract was wiped off the surface of the wood blocks, and the wet weight (M_2) and dimensions of all the treated wood blocks were evaluated. The retentions for each treatment were calculated according to Equation (1):

$$R = \frac{G \times C}{V} \times 10\ Kgm^{-3} \quad (1)$$

where G (M_2-M_1) is the grams of treatment solution absorbed by the wood block; C is the Grams of preservative solutions in 100 g of the treatment solution; V is the volume of wood block in cubic centimeters.

All the wood blocks were oven-dried at (103- ± 2°C; 24 h). The treated and untreated samples were conditioned at 20 ± 2°C and 65 ± 5% relative humidity (RH). The dimensions and weight (M_3) were recorded and evaluated for weight percent gain (WPG) (Equation 2):

$$WPG\ (\%) = \frac{M_3 - M_1}{M_1} \times 100 \quad (2)$$

where M_3 is the oven-dried weight of the sample after treatment; M_1 is the oven-dried weight of the sample before treatment.

Dimensional Stability

The dimensional stabilities of the treated and untreated wood samples were determined by measuring swelling (S_w) and shrinkage (S_h) [tangential (T), radial (R) direction], T/R shrinkage ratio, volumetric swelling (VS), volumetric swelling (S), and anti-shrink efficiency (ASE). The oven-dried treated and untreated wood blocks (conditioned before) were soaked for 1 week in distilled water at room temperature until completely saturated. Then, the wood blocks were removed, and the dimensions in wet condition were recorded. The treated and untreated samples were conditioned at 20 ± 2°C and 65 ± 5% RH followed by oven-dried at 103 ± 2°C to a constant weight, and the dimensions were recorded again to the nearest millimeter with a digital Vernier caliper. Percentage swelling and shrinkage in tangential and radial directions were measured using (Equation 3) and (Equation 4):

$$S_w\ (\%) = \frac{(D_s - D_o)}{D_o} \times 100 \quad (3)$$

$$S_h\ (\%) = \frac{(D_s - D_{oo})}{D_s} \times 100 \quad (4)$$

where D_s is dimension at saturation; D_o is dimension at oven-dried condition before saturation; D_{oo} is dimension at oven-dried condition after saturation.

The T/R shrinkage ratio, according to Priadi et al. (2020) (Equation 5),

$$T/R = \frac{Tangential\ shrinkage\ (\%)}{Radial\ shrinkage\ (\%)} \times 100 \quad (5)$$

The volumetric swelling coefficient (S) (Equation 6), volumetric shrinkage coefficient (VS) (Equation 7), and anti-shrink efficiency (ASE) (Equation 8) were calculated according to Rowell and Ellis (1978):

$$S = \frac{V_2 - V_1}{V_1} \times 100 \quad (6)$$

where V_2 = volume of wood sample after at wet condition (cm^3); V_1 = volume of oven-dried samples before wetting (cm^3).

$$VS = \frac{V_2 - V_1}{V_2} \times 100 \quad (7)$$

where V_2 = volume of wood sample after at wet condition (cm^3); V_1 = volume of oven-dried samples after wetting (cm^3).

$$ASE = \frac{S_1 - S_2}{S_1} \times 100 \quad (8)$$

where S_1 is the volumetric shrinkage coefficient of untreated wood samples and S_2 is the volumetric shrinkage coefficient of treated wood samples.

Fungal Strain

Laetiporus sulphureus (MTCC 1067), used in the study, was procured from the Microbial Type Culture Collection and Gene Bank (MTCC), CSIR-Institute of Microbial Technology, Chandigarh, India. Fresh colonies of the fungi were grown in 4% malt powder and 2% agar culture media in a growing chamber at 20 ± 2°C and 65 ± 5% relative humidity. Once the mycelia covered the whole Petri dish, the colonies were refrigerated (8°C), and 2 days before their further use, the colonies were returned to the growing chamber at 20 ± 2°C and 65 ± 5% relative humidity.

Antifungal Assay

The method of Falck (1907) and Xie et al. (2017) with slight modifications was employed for antifungal evaluation of PE and M extracts of *L. camara* and *A. conyzoides*, which were tested

at 0.25, 0.50, 1.00, 1.50, and 2.00% concentrations against *L. sulphureus* in 9 cm Petri dishes. Double strength potato dextrose agar (PDA) medium was prepared by doubling the amount of constituents except distilled water, and the medium was sterilized at 1.05 kg/cm^2 pressure for 20 min. Simultaneously, double concentrations of different plant extracts were also prepared in sterilized distilled water to get desired concentration of plant extracts after mixing the fungicide solutions in the double strength media. Plant extract solutions were added separately to equal quantities of double-strength PDA medium aseptically before pouring in Petri plates. These plates were then inoculated with the 7-day-old culture of the fungus. A control treatment was also maintained in which only plain sterilized water was added to the double strength medium. Each treatment was replicated thrice, and the inoculated plates were incubated at 27 ± 1°C in a BOD incubator for 5–7 days. The colony diameter of test fungi was recorded till the mycelia reached the edges of the control plates. The antifungal index was calculated according to Equation (9):

$$Antifungal\ index = \left(1 - Da/Db\right) \times 100 \quad (9)$$

where Da = the diameter of the growth zone in the experimental plate (mm), Db = the diameter of the growth zone in the control plate (mm).

Decay Test

The block decay test was performed following a modified version of the Sarker et al. (2006). The glass jars (500 mL) containing growth media (100 mL), 2% malt powder, and 2% agar were inoculated with one plug (Ø 5.5 mm) of the actively growing *L. sulphureous* under sterile conditions. The jars were sealed with parafilm and incubated at 25 ± 1°C and 65 ± 5% RH till the colonies reached the edge of the glass jars. The treated as well as untreated wood blocks were exposed to fungus by placing them on mycelia grown in the jars and incubated again at 25 ± 1°C and 65 ± 5% RH for 21 days for visual observation of the fungal growth by the naked eye using the following scale:

Disease Rating Scale	Surface coverage
0	0%
1	1–25%
2	26–50%
3	51–75%
4	>76%

Percent fungus colonization index and growth inhibition were calculated according to McKinney (1923) (Equation 10) and Vincent (1947) (Equation 11), respectively.

$$Percent\ fungus\ colonization\ Index = \frac{Sum\ of\ all\ disease\ ratings}{Total\ number\ of\ ratings \times Maximum\ grade} \times 100 \quad (10)$$

$$Fungus\ growth\ inhibition\ (\%) = \frac{C - T}{C} \times 100 \quad (11)$$

where C = fungus colonization in control (%) and T = fungus colonization in treated wood (%).

These samples were continued to be incubated at 25 ± 1°C and 65 ± 5% RH for 12 weeks. After exposure, the samples were then taken out of the jars, and hyphae from the surface of the wood were gently removed with a brush. Wood samples were oven-dried at 103 ± 3°C for 24 h and weighed to calculate the mass loss according to Equation (12):

$$ML\ (\%) = \frac{M_0 - M_1}{M_0} \times 100 \quad (12)$$

where ML is the mass loss (%), M_0 is the oven-dry weight of the sample before fungi test (g), and M_1 is the oven-dried weight after fungi test (g).

Statistical Analysis

The data recorded from the laboratory experiments were subjected to the statistical ANOVA using SPSS Version 25.0 (IBM SPSS Statistics for Windows, IBM Corporation, Armonk, NY) following Completely randomized block design (factorial). Means were expressed as mean ± SE and grouped using Tukey's honestly significant difference test at a significance level of 0.05.

RESULTS

Extractive Retention and WPG

The data pertaining to the retention of *L. camara* and *A. conyzoides* extracts at different concentrations in *L. coromandelica* wood blocks are presented in **Table 1**. With increasing concentration, the extract retentions were found to increase significantly ($p < 0.01$). The wood blocks treated with the highest concentration (2.00%) of plant extracts retained 7.45 kg/m^3 (E1), 7.37 kg/m^3 (E2), 6.75 kg/m^3 (E4), and 6.08 kg/m^3 (E3). Whereas, lowest retentions (0.76 kg/m^3, E4; 0.95 kg/m^3, E1; 1.08 kg/m^3, E2; 1.12 kg/m^3, E3) was observed at 0.25% concentration of plant extracts. Whereas, lowest retentions (0.76 kg/m^3, E4; 0.95 kg/m^3, E1; 1.08 kg/m^3, E2; 1.12 kg/m^3, E3) was observed at 0.25% concentration of plant extracts. The data on wood retention were in line with that of WPG. In general, with increasing extract concentration an increase in WPG was observed ($p < 0.01$) (**Table 1**). Similarly, as reported for retention data, negative WPG were observed at low concentrations of 0.25 and 0.50%, while highest at 2.00% concentration.

Dimensional Stability

The relative dimensional changes [swelling (Sw) and shrinkage (Sh)] in untreated and treated wood blocks of *L. coromandelica* are presented in **Table 2**. The results revealed significant differences for swelling and shrinkage in radial and tangential directions and volumetric coefficient ($p < 0.01$). The greater dimensional changes of untreated wood in the tangential direction (Sw: 4.24%; Sh: 3.62%) than in the radial direction (Sw: 3.98%; Sh: 3.30%) were observed (due to the small dimensional changes of the examined samples, being in the range 0.2–0.4%, measurements on swelling and shrinkage in the longitudinal direction were not given). The treatments with E1 and E2 significantly reduced the moisture-dependent

TABLE 1 | Retention (kg/m^3), weight percent gain (WPG, %), and mass loss (ML, %) of untreated and plant extracts treated *Lannea coromandelica* wood blocks.

Treatment	Concentration (%)	Retention (Kg/m^3)	WPG (%)	Mass Loss (ML) (%)
Untreated/ Control	/	/	/	31.60 ± 0.28^{k}
E1	0.25	1.12 ± 0.01^{a}	-2.46 ± 0.22^{ab}	28.24 ± 0.09^{hi}
	0.50	2.17 ± 0.10^{b}	-0.88 ± 0.02^{c}	27.06 ± 0.23^{fgh}
	1.00	4.31 ± 0.02^{c}	0.68 ± 0.21^{de}	25.71 ± 0.05^{ef}
	1.50	7.36 ± 0.06^{d}	1.17 ± 0.11^{e}	19.40 ± 0.05^{b}
	2.00	7.45 ± 0.12^{d}	1.39 ± 0.09^{e}	16.43 ± 0.15^{a}
E2	0.25	1.08 ± 0.01^{a}	-2.13 ± 0.11^{ab}	29.11 ± 0.31^{ij}
	0.50	2.20 ± 0.10^{b}	-0.97 ± 0.25^{c}	28.99 ± 0.35^{ij}
	1.00	3.54 ± 0.01^{c}	1.08 ± 0.13^{e}	26.50 ± 0.45^{fg}
	1.50	5.19 ± 0.07^{d}	1.15 ± 0.09^{e}	24.78 ± 0.43^{de}
	2.00	7.37 ± 0.09^{e}	1.18 ± 0.06^{e}	21.78 ± 0.35^{c}
E3	0.25	0.95 ± 0.01^{a}	-1.89 ± 0.11^{b}	27.73 ± 0.42^{ghi}
	0.50	1.94 ± 0.11^{b}	-0.79 ± 0.19^{c}	26.77 ± 0.34^{fgh}
	1.00	3.84 ± 0.04^{c}	0.16 ± 0.10^{d}	24.96 ± 0.14^{e}
	1.50	6.07 ± 0.12^{d}	0.68 ± 0.05^{de}	19.61 ± 0.21^{b}
	2.00	6.09 ± 0.15^{d}	0.74 ± 0.04^{de}	17.11 ± 0.25^{a}
E4	0.25	0.76 ± 0.02^{a}	-2.77 ± 0.14^{a}	29.90 ± 0.38^{j}
	0.50	1.51 ± 0.03^{b}	-0.59 ± 0.04^{c}	27.89 ± 0.35^{ghi}
	1.00	3.56 ± 0.06^{c}	0.80 ± 0.16^{de}	24.80 ± 0.32^{de}
	1.50	4.74 ± 0.15^{d}	0.81 ± 0.07^{e}	22.96 ± 0.06^{d}
	2.00	6.75 ± 0.22^{e}	0.96 ± 0.03^{de}	21.68 ± 0.06^{c}

Data represent the mean of three replicates ± Standard error (SE). Different superscripts letters in a column specify a statistically significant difference between the means ($P \leq 0.05$, Turkey's HSD Test).

dimensional changes in all directions over control. The lowest radial (2.75%; 1.50%), tangential (2.70%; 1.00%), and volumetric swelling (6.44%; 0.25%) values were obtained for E2. The highest radial (6.00%; 1.50%), tangential (6.30%; 2.00%), and volumetric swelling (13.17%; 1.50%) values were measured for E3. The swelling of wood blocks in radial and tangential directions increased with an increase in extract concentration while the wood shrinkage followed a reducing trend. The minimum shrinkage values for radial (2.01%), tangential (2.09%) direction, and volumetric swelling (4.57%) values were obtained for E1 at 2.00% concentration. The maximum radial (3.73%; 0.25%), and volumetric shrinkage (7.71%; 1.00%) values were recorded for E3, whereas the highest tangential shrinkage (4.10%; 1.50%) for E4. The percentage of shrinkage reduced (ASE) as a result of extracts treatment ($p < 0.05$) is presented in **Figure 1**. In comparison with the control, there was more variability between different plant extracts and among blocks treated with the same plant extract. The ASE for E1 and E2 treatments were registered with positive values, and the maximum ASE (37.57%) was registered for E1 at 1.00% concentration and lowest (7.77%) for E2 at 0.25%. The ASE values obtained for E3 and E4 treatments were generally lower than those obtained for previous treatments, with negative values ranging from −7 to −1% obtained at low concentrations. The other positive results for E3 and E4 ranged between a minimum of 9.88% (1.00%; E4) and a maximum of 24.06% (2.00%; E4).

In vitro Antifungal Assay

The antifungal activity of the selected plant of *L. camara* (E1, E2) and *A. conyzoides* (E3, E4) extracts against the wood-rotting fungus *L. sulphureus* were shown in **Figure 2** (antifungal assay) and **Figure 3** (antifungal index). The results revealed that E1 (**Figure 2**) as well as E3 (**Figure 2**) showed the best activity against *L. sulphureus* and induced 100% antifungal index at all the test concentrations. In contrast, the other extracts, i.e., E2 (**Figure 2**) and E4 (**Figure 2**), showed relatively lower activity. E4 exhibited the highest antifungal index of 75.93% at 2.00% concentration, but E2 (**Figures 2**, **3**) expressed reduced antifungal activities at the same concentration with the antifungal index lower than 41.85%. Despite greater variation between concentrations, the extracts (E2; **Figure 2**, E4; **Figure 2**) demonstrated dose-dependent antifungal activity that increased with increasing concentrations from 0.25 to 2.00%. The least antifungal activities of extracts E2 (**Figure 2**) and E4 (**Figure 2**) were observed at the lowest concentration (0.25%) with an antifungal index lower than 20% (10.04 and 18.89%, respectively).

Visual Observations

Visual observation of mycelium growth on the wood surface was used to assess the antifungal activities of *L. camara,* and *A. conyzoides* extracts treated wood blocks. The results of fungal inhibition determined after 21 days of incubation are shown in

TABLE 2 | Dimensional stability (swelling and shrinkage) of untreated and plant extracts treated wood blocks of *Lannea coromandelica*.

Treatment	Concentration (%)	Swelling			Shrinkage		
		Swelling (R, %)	Swelling (T, %)	Volumetric swelling (%)	Shrinkage (R, %)	Shrinkage (T, %)	Volumetric Shrinkage (%)
Untreated/ Control	/	3.98 ± 0.11^{abcd}	4.24 ± 0.04^{bcde}	9.09 ± 0.15^{cde}	3.30 ± 0.08^{bcde}	3.62 ± 0.03^{bcde}	7.20 ± 0.08^{ghi}
E1	0.25	2.88 ± 0.07^{abc}	3.03 ± 0.36^{abc}	6.64 ± 0.73^{ab}	3.24 ± 0.22^{abcde}	2.89 ± 0.28^{abcde}	6.22 ± 0.16^{def}
	0.50	3.03 ± 0.36^{abcd}	3.18 ± 0.14^{abc}	6.66 ± 0.24^{ab}	2.47 ± 0.06^{abcd}	2.81 ± 0.11^{abcde}	5.62 ± 0.20^{bcde}
	1.00	3.34 ± 0.17^{ab}	3.37 ± 0.17^{abc}	7.27 ± 0.11^{abc}	2.47 ± 0.09^{abcd}	2.72 ± 0.08^{abcde}	4.49 ± 0.04^{a}
	1.50	3.57 ± 0.10^{abcd}	3.71 ± 0.20^{abcde}	7.92 ± 0.31^{abcd}	2.28 ± 0.16^{abc}	2.37 ± 0.28^{abc}	5.31 ± 0.12^{abcd}
	2.00	4.09 ± 0.33^{abcd}	3.98 ± 0.32^{abcde}	8.74 ± 0.09^{bcde}	2.01 ± 0.16^{a}	2.09 ± 0.34^{a}	4.57 ± 0.06^{a}
E2	0.25	3.63 ± 0.13^{abcd}	2.88 ± 0.12^{ab}	6.72 ± 0.03^{a}	3.05 ± 0.07^{abcde}	3.24 ± 0.15^{abcde}	6.63 ± 0.25^{fgh}
	0.50	3.21 ± 0.38^{abcd}	3.40 ± 0.10^{abcd}	6.88 ± 0.34^{ab}	3.03 ± 0.28^{abcde}	2.86 ± 0.09^{abcde}	5.98 ± 0.08^{cdef}
	1.00	3.05 ± 0.11^{abc}	2.70 ± 0.24^{a}	7.20 ± 0.15^{abc}	2.53 ± 0.11^{abcde}	2.65 ± 0.21^{abcde}	5.75 ± 0.06^{bcdef}
	1.50	2.75 ± 0.07^{a}	3.45 ± 0.12^{abcd}	7.31 ± 0.28^{abc}	2.55 ± 0.12^{abcde}	2.64 ± 0.03^{abcde}	5.06 ± 0.13^{abc}
	2.00	3.90 ± 0.14^{abcd}	4.43 ± 0.15^{cde}	9.09 ± 0.03^{cde}	2.17 ± 0.11^{ab}	2.20 ± 0.21^{ab}	4.95 ± 0.21^{ab}
E3	0.25	4.36 ± 0.27^{cd}	4.80 ± 0.44^{de}	10.02 ± 0.72^{def}	3.73 ± 0.22^{e}	3.87 ± 0.04^{de}	7.50 ± 0.21^{hi}
	0.50	4.49 ± 0.18^{d}	4.91 ± 0.26^{e}	10.23 ± 0.57^{ef}	3.61 ± 0.13^{de}	3.08 ± 0.47^{abcde}	7.47 ± 0.28^{hi}
	1.00	4.51 ± 0.31^{d}	5.10 ± 0.31^{ef}	11.65 ± 0.30^{fg}	2.74 ± 0.34^{abcde}	2.94 ± 0.21^{abcde}	7.71 ± 0.08^{i}
	1.50	6.00 ± 0.22^{e}	6.25 ± 0.36^{f}	13.17 ± 0.59^{g}	2.61 ± 0.43^{abcde}	2.57 ± 0.47^{abcd}	6.03 ± 0.04^{def}
	2.00	5.98 ± 0.26^{e}	6.30 ± 0.26^{f}	13.13 ± 0.27^{g}	2.50 ± 0.09^{abcde}	2.43 ± 0.03^{abcde}	5.93 ± 0.18^{cdef}
E4	0.25	4.10 ± 0.06^{abcd}	4.21 ± 0.17^{bcde}	9.26 ± 0.13^{cde}	3.47 ± 0.09^{cde}	3.75 ± 0.25^{cde}	7.51 ± 0.12^{hi}
	0.50	4.18 ± 0.11^{bcd}	4.36 ± 0.04^{cde}	9.27 ± 0.08^{cde}	3.23 ± 0.30^{abcde}	3.72 ± 0.08^{cde}	7.26 ± 0.15^{ghi}
	1.00	4.35 ± 0.25^{cd}	4.40 ± 0.02^{cde}	9.38 ± 0.05^{cde}	3.26 ± 0.14^{bcde}	3.77 ± 0.13^{cde}	6.49 ± 0.03^{efg}
	1.50	4.32 ± 0.28^{cd}	4.41 ± 0.02^{cde}	9.50 ± 0.29^{de}	2.28 ± 0.07^{abc}	4.10 ± 0.15^{e}	5.55 ± 0.15^{bcd}
	2.00	4.39 ± 0.06^{cd}	5.01 ± 0.21^{e}	10.17 ± 0.47^{ef}	2.08 ± 0.19^{ab}	4.06 ± 0.30^{e}	5.47 ± 0.08^{bcde}

Data represent the mean of three replicates ± SE. Different superscripts letters in a column specify a statistically significant difference between the means ($P \leq 0.05$, Tukey's HSD test).

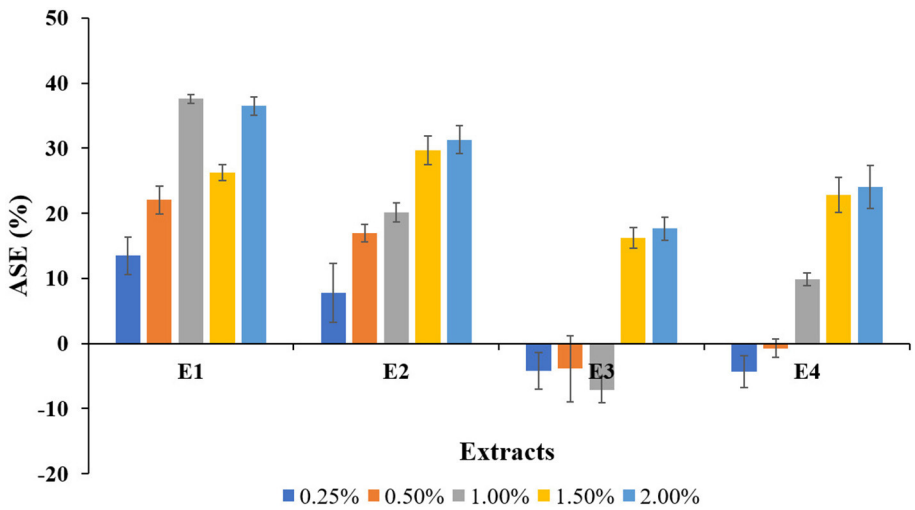

FIGURE 1 | Anti-shrink efficiency (ASE) values for the plant extracts treated wood blocks of *Lannea coromandelica*.

Figure 4. L. sulphureous grew quickly on untreated wood blocks, and the surface of the wood blocks was completely overgrown (rating scale 5), indicating complete fungal colonization (100%). However, the types and concentrations of extracts had a significant effect on the mycelial linear growth of test fungi. They showed remarkable inhibition effects over the control. Furthermore, an increase in fungal inhibition was observed with increasing extract concentrations. The PE extracts of both plants (E1 and E3) inhibited the growth of the test fungi significantly, with the highest fungal inhibition (50.00%) recorded for E3 at 2.00% concentration and the lowest (16.77%) recorded for E1 and E3 at 0.25% concentration. While the effect of methanolic extracts

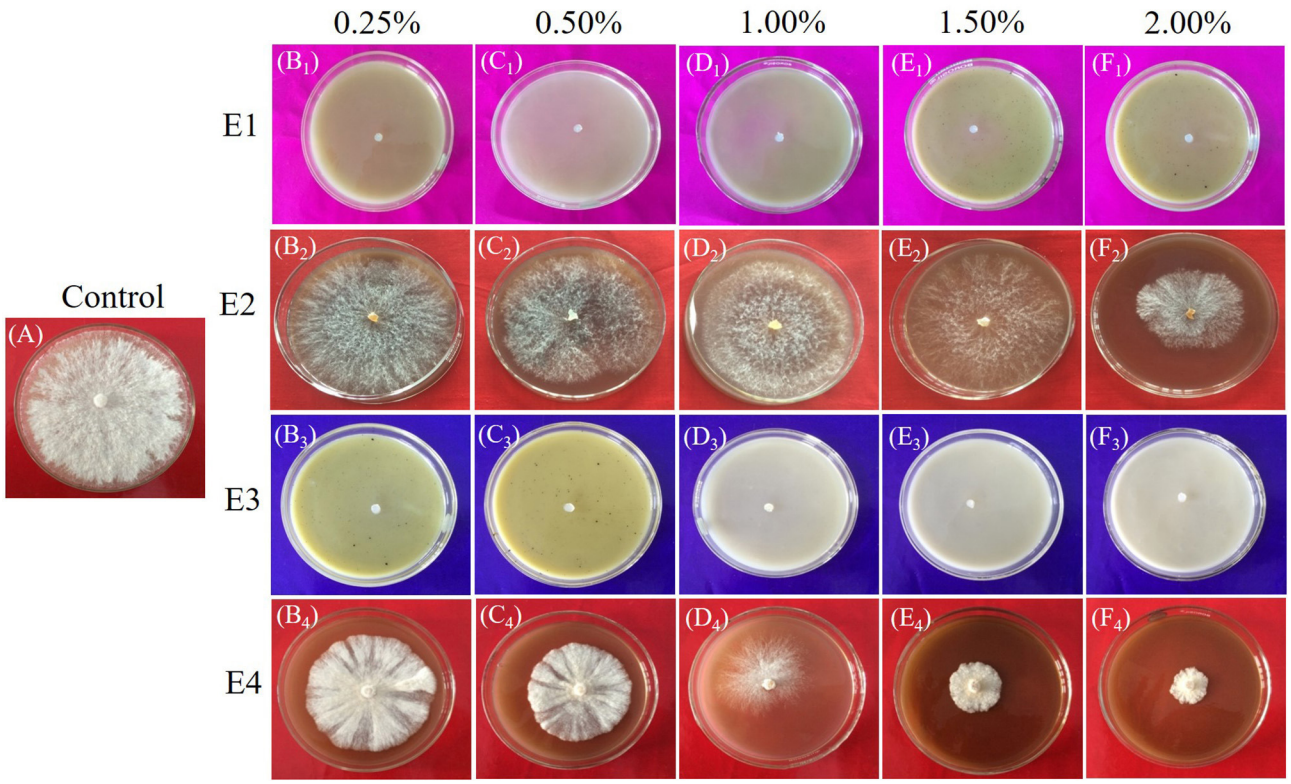

FIGURE 2 | (A–F) Antifungal activity of *Laetiporus sulphureus* against **(A)** Control (PDA+ test fungi) and at 0.25, 0.50, 1.00, 1.50, and 2.00% concentrations of extracts (PDA+ extracts+ test fungi) E1 **(B_1-F_1)**; E2 **(B_2-F_2)**; E3 **(B_3-F_3)**; and E4 **(B_4-F_4)**.

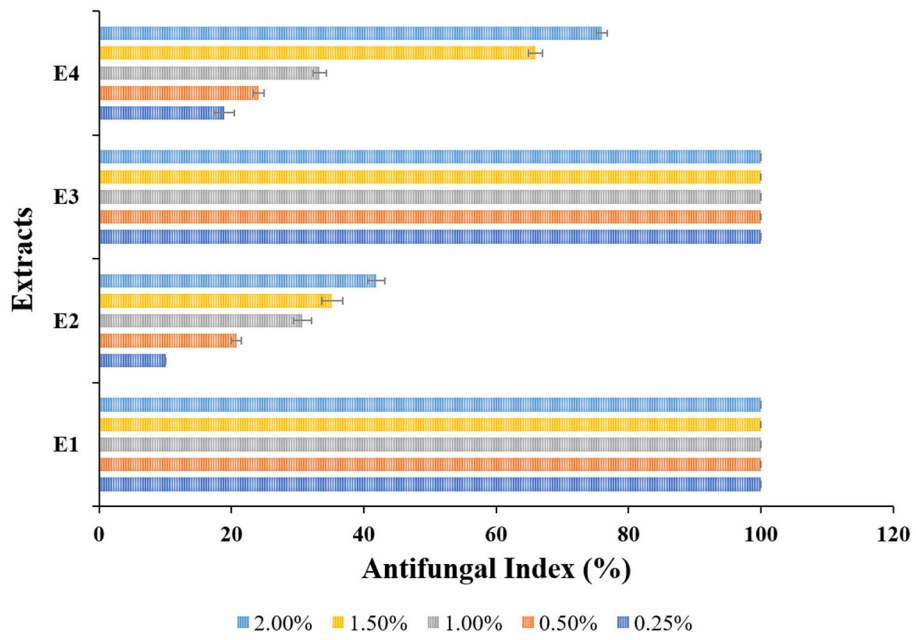

FIGURE 3 | Antifungal index (%) of different extracts from *Lantana camara* (E1, E2) and *Ageratum conyzoides* (E3, E4) against *Laetiporus sulphureus* at 0.25, 0.50, 1.00, 1.50, and 2.00% concentrations.

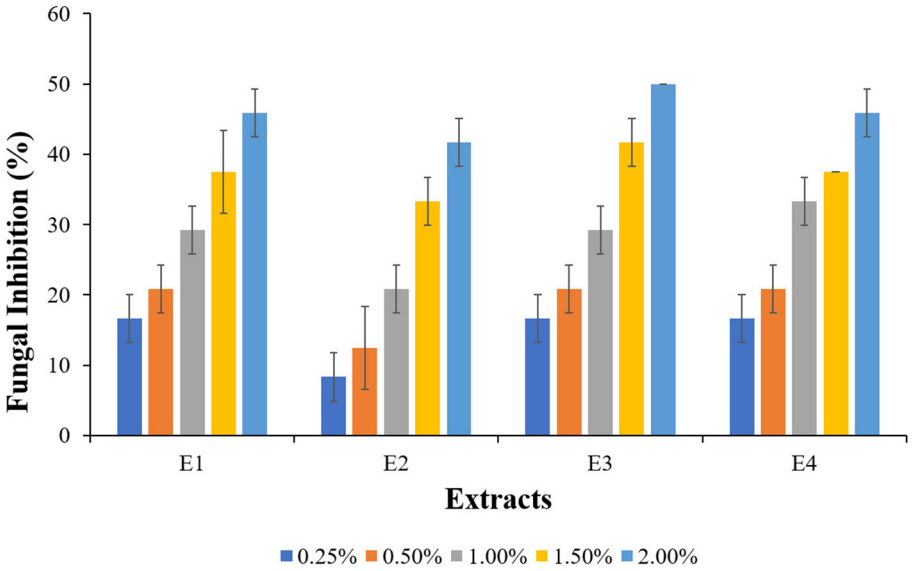

FIGURE 4 | Fungal inhibition in plant extracts treated wood blocks of *Lannea coromandelica*.

(E2 and E4) was lower in comparison, test fungi inhibition was found to be 46% (E2; 8.33% and E4; 45.00%).

Resistance Against Decay Fungi

The mean percentage mass loss (ML) of extract-treated *L. coromandelica* wood blocks tested after exposure to *L. sulphureous* for 12 weeks ($p < 0.01$) are shown in **Table 1**. The highest ML (31.60%) was recorded in untreated wood blocks. Both the plants improved the wood resistance as the treated wood blocks showed an ML of <30%. The blocks treated with PE extracts (E1 and E3) displayed more decay resistance with ML as ranged between (16–28%) compared with 21–30% for M extracts (E2 and E4). The fungal resistance improved with increasing concentration from 0.25 to 2.00%. The minimum ML (16.77%) was recorded in E1 at 2.00% concentration, representing >45% reduction in ML over control followed by E3 (17.11%). Although the M extracts (E2 and E4) were comparatively less effective, but offered decay resistance higher than the control with the lowest ML (21.68%) at 2.00% concentration.

DISCUSSION

Extractive Retention and WPG

The retention of the preservative is a significant factor demonstrating the quality of impregnation (Dong et al., 2020). Retention is primarily determined by treatment conditions (such as duration and preservative type) and concentration. The variation in retention was observed with extract type, with E1 having the best retention. E1 appears to have sufficient viscosity to allow for good penetration into the wood. With increasing concentrations of plant extracts, the retention of wood blocks has increased. Several authors have discussed the linear relationship between increasing preservative retention and increasing preservative concentration (Syazwan et al., 2017; Ouyang et al., 2018; Shukla et al., 2019). The heterogeneous texture, density, and porosity of wood species significantly impact retention values, whereas the particle size of the extracts is responsible for the penetration efficiency of the retention rate. The extract retention data agreed with WPG regarding the amount of extractive that entered the wood blocks (lumen and/or cell wall). The variations in WPG can be attributed to moisture content, variation in wood density, and absorption and intensity of interaction of extracts with different wood elements present in the microstructure of *L. coromandelica* wood. On the other hand, negative retention can be related to extractives leached from wood during treatment with extract solutions. While investigating the potential use of the Maillard reaction to modify wood, Peeters et al. (2018) reported similar incompetent treatments with $MgCl_2$, in that the weight percentage gains were negative (as much as 5 to 6% WPG in the case of glucosamine with magnesium chloride), indicating removal of cell wall components as a result of the reaction.

Dimensional Stability

Wood swelling is related to increased moisture content, while shrinkage is related to decreased moisture content. Because wood is anisotropic, swelling and shrinkage occur at different rates and magnitudes in different directions, most notably in the tangential direction, followed by the radial direction, and are negligible in the longitudinal direction (Cai et al., 2019). This is because microfibrils in the tangential plane are parallel to the axis of the cell wall, whereas the radial plane has a restraining effect due to the presence of wood rays (radial microfibril orientation) (Elaieb et al., 2019). When compared with untreated wood blocks, the extracts of *L. camara* (E1 and E2) demonstrated reduced dimensional changes (swelling and shrinkage; different planes, volumetric), revealing the ability of these extracts to

improve the dimensional stability of *L. coromandelica* wood blocks. The findings are consistent with those of Var and Kardas (2019), that discovered that salt natural geothermal water (SNGW) treatments reduced the swelling values of pine woods. However, the performance of A. conyzoides (E3 and E4) extracts was lower in providing dimensional stability over control. Temiz et al. (2013) reported higher swelling (tangential plane) of *Arundo donax* bio-oil treated samples than control. The increasing tangential and radial swelling with increased extract concentrations are in line with the finding of Shuib (2011), Okon (2014), Bossu et al. (2016), and Ney et al. (2019).

The extracts of *L. camara* (E1 and E2) reduced the shrinkage values in tangential as well as radial direction with an increase in extract concentration representing reduction improvement of

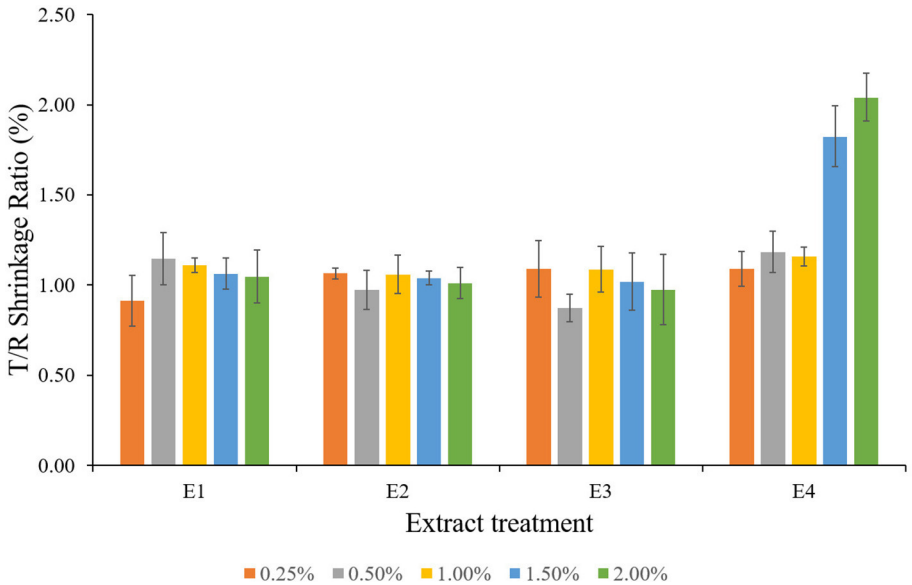

FIGURE 5 | Tangential-radial shrinkage ratio (T/R) of plant extract treated wood blocks of *Lannea coromandelica*.

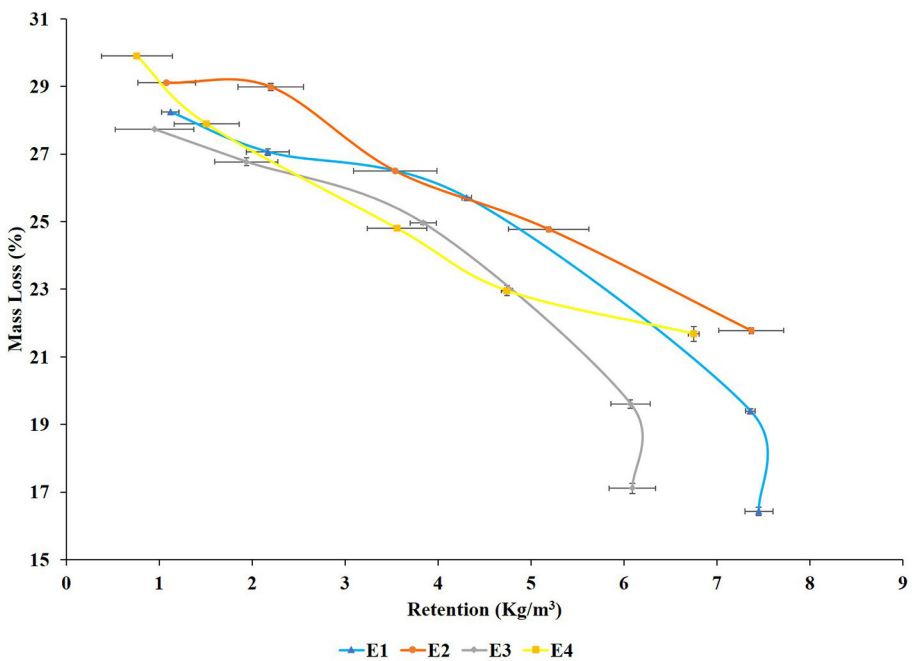

FIGURE 6 | Mass loss concerning extractive retention of *Lannea coromandelica* wood blocks.

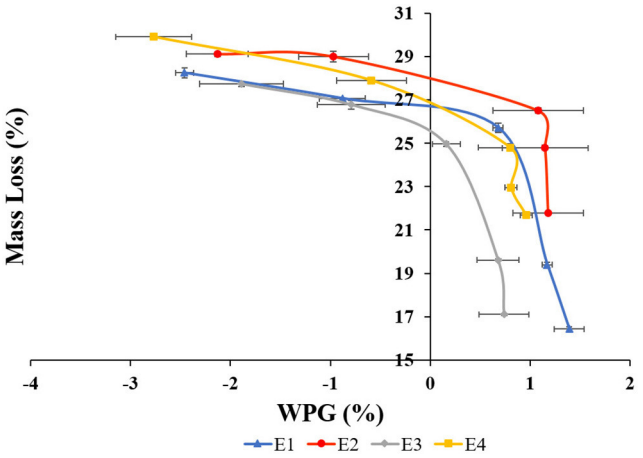

FIGURE 7 | Mass loss concerning weight percent gain (WPG) of *Lannea coromandelica* wood blocks.

20–42%; E1, 10–39%; E2 in the tangential direction, and 2–39%; E1, 7–34%; E2 in the radial direction. The shrinkage reduction in the tangential direction was observed to be greater than the reductions in radial directions, which could be due to the vertical orientation of microfibrils in the S2 layer of the cell wall, which is consistent with the findings of Barnett and Bonham (2004) and Okon et al. (2018). The tangential microfibril angle is greater than the radial and longitudinal microfibril angles, resulting in greater tangential shrinkage reduction compared with radial and longitudinal shrinkage (Okon et al., 2018). After treatment, the volumetric swelling of the wood indicated the amount of extract present in the cell wall because the increase in wood volume occurs only after the reagent penetrates the cell wall via pores. Untreated samples had a high volumetric swelling coefficient compared with E1 and E2 extract-treated wood, indicating low cell wall-filling/bulking. Similarly, the plant extract-treated blocks showed a significant increase in volumetric swelling coefficients but decreased volumetric shrinkage coefficients as extract concentration increased. The findings are consistent with those of Salim et al. (2010), Bazyar (2012), and Wu et al. (2012). The tangential-radial shrinkage ratio (T/R ratio) of *L. coromandelica* wood was affected by the extract treatment. The lower T/R ratio of wood treated with E1 and E2 (**Figure 5**) suggested that *Lantana* extracts (E1 and E2) had a better ability to provide dimensional stability. T/R ratios close to one indicated better dimensional stability of wood, whereas Bowyer et al. (2007) stated that T/R ratios greater than two indicated worse dimensional stability of wood. Priadi et al. (2020) reported similar results while evaluating the dimensional stability, color change, and durability of modified red jabon (*Antochephalus macrophyllus*) wood by double impregnation with boron and methyl methacrylate (MMA) and heat treatment.

ASE compares the volumetric shrinkages of extract-treated blocks to those of untreated blocks to determine the contribution of the extracts to shrinkage suppression. The results clearly showed that treated wood blocks had higher ASE values than untreated ones (ASE = 0), implying that, due to bulking effect, the extracts were effective in reducing shrinkage of wood specimens, thus providing good dimensional stability, as previously explained (Li et al., 2000; Gabrielli and Kamke, 2010). The low and negative values for *A. conyzoides* extracts can be attributed to the fact that the extracts only penetrated a thin layer inside the wood blocks and thus did not counteract shrinkage. The larger dimensional changes will influence the smaller dimensional changes of the untreated samples in the E3, and E4 treated blocks compared with E1 and E2. As a result, rather than concluding a problem with the treated blocks, it can be assumed that the behavior of untreated wood blocks resulted in these lower ASE values. The current findings are consistent with Pepin et al. (2018) and Antonelli et al. (2020).

Antifungal Activity

As environmental awareness has grown, the focus has shifted to the development of environmentally friendly plant-based wood protectants as an alternative to synthetic wood preservatives. The *in vitro* fungicidal activity of PE (E1 and E3) and M (E2 and E4) extracts against *L. sulphureus* was evaluated to assess the potentials of *L. camara* and *A. conyzoides* for use as wood bioprotectants. All the extracts exhibited remarkable antifungal activity over control, and the PE extracts (E1 and E3) were found to completely inhibit the studied fungi even at the lowest studied concentration. However, M extracts (E2 and E4) were observed to have a comparatively high susceptibility to fungus. The findings are consistent with Linthoingambi and Singh (2013) that observed that the PE leaf extract of *Tithonia diversifolia* had the highest antifungal activity, followed by M and chloroform extracts. Several researchers have reported complete inhibition of *L. sulphureus* (Cheng et al., 2005, 2006; Wang et al., 2005; Xie et al., 2015, 2017). However, the high susceptibility of M extract contradicted the findings of Tripathi et al. (2009), Fayaz et al. (2017). The strong antifungal activities of *L. camara* and *A. conyzoides* plant extracts against a wide variety of fungi have been attributed to the presence of Propanoic acid, 2-hydroxy-, ethyl ester in Cabrido and Demayo (2018); and Precocene II (6,7-dimethoxy-2,2-dimethyl-2-chromene) (Moreira et al., 2007; Adebayo et al., 2010; Yadav et al., 2019) phytochemicals, respectively.

The visual observation of mycelium growth on the wood surface after 21 d of incubation enabled the degree of antifungal activity of the extracts treated wood blocks to be assessed. The findings on fungal inhibition at high extract concentrations of extracts were consistent with the findings of Salem et al. (2016) on fungal inhibition of *P. rigida* heartwood extract at 2% concentration and Mansour and Salem (2015) on fungal inhibition of *Cupressus sempervirens* methanolic extract treated *Acacia saligna* wood *Trichoderma harzianum* at 5%, 10%, and 20% concentrations. In addition to the results obtained, it is also important to highlight that the surface coverage of *L. sulphureous* on the treated wood blocks was less than the controls. When testing wood preservatives, the absence of fungal colonization of the wood was also considered important (Bahmani et al., 2016). Although the extracts demonstrated good antifungal activity after 21 d of incubation, this is only an *in vitro* indicative study, and the experimental conditions did not account for all ecological and

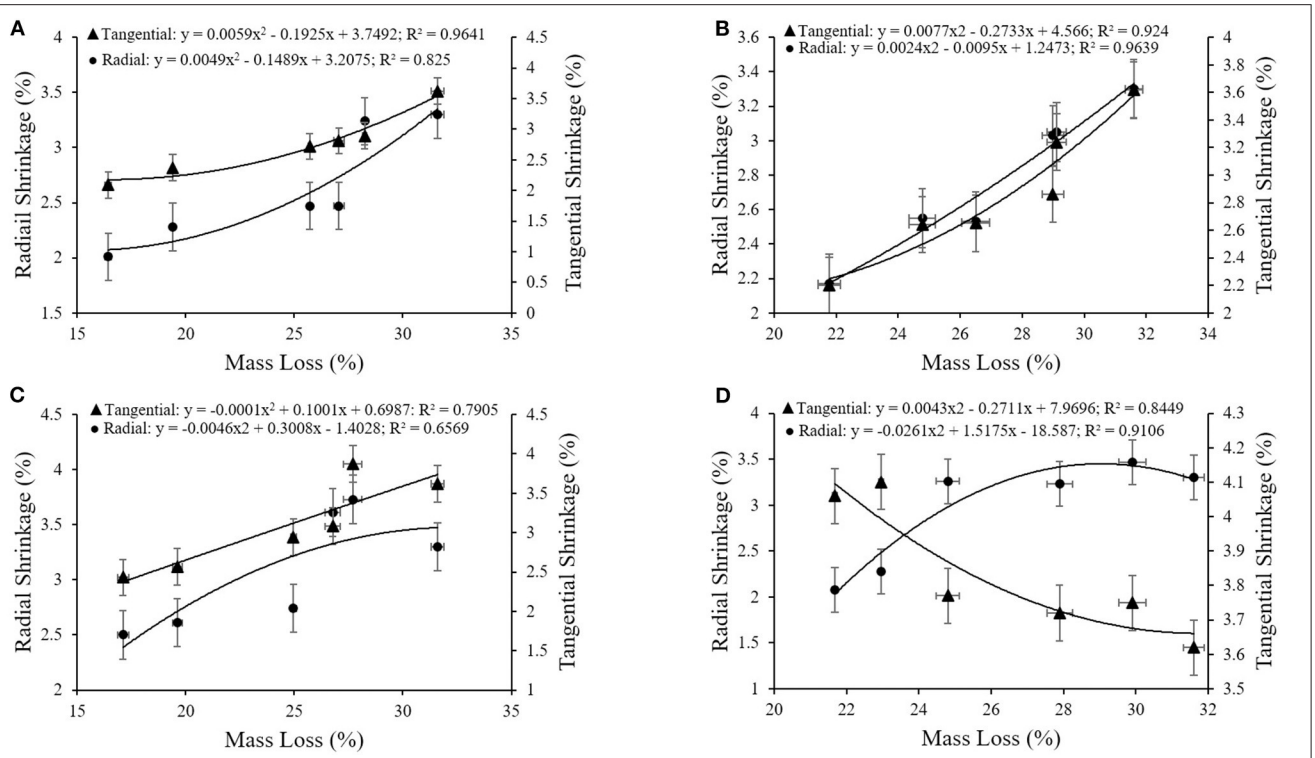

FIGURE 8 | (A–D) Relationship between the mass loss and tangential and radial shrinkages for **(A)** E1; **(B)** E2; **(C)** E3; **(D)** E4.

endemic factors. Under field conditions, large-scale studies are economically necessary to test the selected plant extracts.

Decay Test

As a result of biodeterioration of lignocellulosic materials, wood-decaying fungi cause significant losses in wood and other wood-based products (Kositchaiyong et al., 2014; Taghiyari et al., 2014; Xu et al., 2015; Kwaśniewska-Sip et al., 2018). As a result, assessing the resistance of lignocellulosic material to decay fungi and improving the durability of wood and wood-based products is needed to assess the suitability of a timber species for a specific purpose (Sundararaj et al., 2015; Barton-Pudlik et al., 2017). Twelve weeks of exposure to basidiomycetes fungi culminated in the highest ML of untreated *L. coromandelica* control wood blocks, revealing the non-durability of sapwood (Durability class III; field testing, Sundararaj et al., 2015), if not treated with preservatives. The treatment of wood blocks with the selected plant extracts revealed better performance against the test fungi, although the extracts did not provide complete protection. Since the mass loss is relatively less for treated blocks, it can be inferred that the extract might have formed a protective layer over the surface of wood blocks, at least throughout fungal decay (12 weeks). These results were similar to those previously reported by Nayeri et al. (2017), Kwaśniewska-Sip et al. (2018), Ouyang et al. (2018), Izadyar et al. (2020), Ahadnezhad et al. (2021). The differences in ML varied depending on the plant extracts and the concentration used. Despite the fact that all of the wood blocks had complete fungal coverage after 12 weeks of exposure, the resistance provided by PE extracts (E1 and E3) was significantly higher. The results demonstrated a close relationship between ML in the decay test and extracted concentration, with increasing plant extract concentrations reducing decay. The growth of the test fungi on the treated samples was also slowed at low concentrations. Extracts from the selected plant species contained the phytochemicals that slowed fungal attack and reduced weight loss in a susceptible wood species, *L. coromandelica*. The findings of this study are consistent with those stated by Kadir and Hale (2019). The increased resistance of *L. coromandelica* treated wood blocks to test fungi demonstrates the ability of plant extracts to increase durability.

A correlation between retention of extracts (**Figure 6**), WPG (**Figure 7**), and ML was also observed as the decay resistance improved with increasing retention and WPG. The results are in line with those reported by Nayeri et al. (2017), Kwaśniewska-Sip et al. (2018), Ouyang et al. (2018), Zelinka et al. (2020). The close relationships between dimensional stability and ML (described by second-degree polynomials) are also confirmed by coefficients of determination. A high correlation was observed between the mass loss and tangential shrinkage for E1 ($R^2 = 0.96$; **Figure 8A**) and E2 ($R^2 = 0.92$; **Figure 8B**); between mass loss and radial shrinkage for E2 ($R^2 = 0.96$; **Figure 8B**) and E4 ($R^2 = 0.94$; **Figure 8D**). Whereas, a weaker correlation between mass loss and radial ($R^2 = 0.66$) and tangential ($R^2 = 0.79$) shrinkages were recorded for E3 (**Figure 8C**). A similar high correlation in oak wood buried in waterlogged peat was reported by Babiński et al. (2019).

CONCLUSIONS

Overall, the research findings revealed that treatments with plant extracts increased dimensional stability and decay resistance significantly and also demonstrated their practicable utilization as a preservative. Thus, the extracts have the potential to be developed as a natural fungicide and as a suitable substitute for synthetic preservatives. However, although these plant extracts proved to be effective in laboratory conditions and can be used as an alternative to conventional wood preservatives, more testing is needed to determine their effectiveness in field conditions while considering all ecological and endemic factors. Furthermore, because our study used PE and M extraction, more research is needed to determine the ecotoxicity and efficacy of extractives and their mechanism of inhibition. Furthermore, the technical and economic feasibility of extracting these weed species should be confirmed.

DATA AVAILABILITY STATEMENT

The original contributions generated for the study are included in the article/supplementary material, further inquiries can be directed to the corresponding author/s.

AUTHOR CONTRIBUTIONS

HG and KS conceived the concept. HG, KS, and JS framed the experimental design and wrote and edited the manuscript. HG took the data and conducted statistical analysis. All authors contributed to the article and approved the submitted version.

FUNDING

This study was funded by the Department of Science and Technology (DST), Government of India, under the INSPIRE-Fellowship Programme.

ACKNOWLEDGMENTS

The authors are thankful to the HOD (Forest Products), KS, Dr. YSP UHF, Nauni, Solan for providing necessary facilities. The authors are also thankful to the WST lab and pathology lab staff members for their kind cooperation.

REFERENCES

Adebayo, A. H., Zeng, G. Z., Zhang, Y. M., Ji, C. J., Akindahunsi, A. A., and Tan, N. H. (2010). Toxicological evaluation of precocene II isolated from *Ageratum conyzoides* L. (Asteraceae) in Sprague Dawley rats. *Afr. J. Biotechnol.* 9, 2938–2944.

Ahadnezhad, M., Izadyar, S., and Efhamisisi, D. (2021). Investigation of fungal decay of Poplar wood treated with pistachio resin. *Bioresources* 16, 779–788. doi: 10.15376/biores.16.1.779-788

Antonelli, F., Galotta, G., Sidoti, G., Zikeli, F., Nisi, R., Davidde Petriaggi, B., et al. (2020). Cellulose and lignin nano-scale consolidants for waterlogged archaeological wood. *Front. Chem.* 8:32. doi: 10.3389/fchem.2020.00032

Antwi-Boasiako, C., and Boadu, K. B. (2016). The level of utilization of secondary timber species among furniture producers. *South-East Eur. For.* 7, 39–47. doi: 10.15177/seefor.16-08

Babiński, L., Fabisiak, E., Zborowska, M., Michalska, D., and Pradzyński, W. (2019). Changes in oak wood buried in waterlogged peat: shrinkage as a complementary indicator of the wood degradation rate. *Eur. J. Wood Wood Prod.* 77, 691–703. doi: 10.1007/s00107-019-01420-z

Bahmani, M., Schmidt, O., Fathi, L., and Frühwald, A. (2016). Environment-friendly short-term protection of palm wood against mould and rot fungi. *Wood Mater. Sci. Eng.* 11, 239–247. doi: 10.1080/17480272.2014.981581

Barnett, J. R., and Bonham, V. A. (2004). Cellulose microfibril angle in the cell wall of wood fibres. *Biol. Rev. Camb. Philos. Soc.* 79, 461–472. doi: 10.1017/S1464793103006377

Barton-Pudlik, J., Czaja, K., Grzymek, M., and Lipok, J. (2017). Evaluation of wood-polyethylene composites biodegradability caused by filamentous fungi. *Int. Biodeterior. Biodegradation* 118, 10–18. doi: 10.1016/j.ibiod.2017.01.014

Bazyar, B. (2012). Decay resistance and physical properties of oil heat treated aspen wood. *Bioresources* 7, 696–705.

Bossu, J., Beauchêne, J., Estevez, Y., Duplais, C., and Clair, B. (2016). New insights on wood dimensional stability influenced by secondary metabolites: the case of a fast-growing tropical species *Bagassa guianensis* Aubl. *PLoS ONE* 11:e0150777. doi: 10.1371/journal.pone.0150777

Bowyer, J. L., Shmulsky, R., and Haygreen, J. G. (2007). *Forest Products and Wood Science*. 5th Edn. Ames, IA: Blackwell Publishing Professional.

Brocco, V. F., Paes, J. B., da Costa, L. G., Brazolin, S., and Arantes, M. D. C. (2017). Potential of teak heartwood extracts as a natural wood preservative. *J. Clean. Prod.* 142, 2093–2099. doi: 10.1016/j.jclepro.2016.11.074

Broda, M. (2020). Natural compounds for wood protection against pungi-a review. *Molecules* 25:3538. doi: 10.3390/molecules25153538

Cabrido, C., and Demayo, C. G. (2018). Antimicrobial and cellular metabolic effects of the ethanolic extract of the dallas red variety of *Lantana camara*. *Pharmacophore* 9, 10–18.

Cai, C., Heräjärvi, H., and Haapala, A. (2019). Effects of environmental conditions on physical and mechanical properties of thermally modified wood. *Can. J. For. Res.* 49, 1434–1440. doi: 10.1139/cjfr-2019-0180

Chen, C., Song, J., Zhu, S., Li, Y., Kuang, Y., Wan, J., et al. (2018). Scalable and sustainable approach toward highly compressible, anisotropic, lamellar carbon sponge. *Chem* 4, 544–554. doi: 10.1016/j.chempr.2017.12.028

Cheng, S. S., Lin, H. Y., and Chang, S. T. (2005). Chemical composition and antifungal activity of essential oils from different tissues of Japanese cedar (*Cryptomeria japonica*). *J. Agric. Food Chem.* 53, 614–619. doi: 10.1021/jf0484529

Cheng, S. S., Liu, J. Y., Hsui, Y. R., and Chang, S. T. (2006). Chemical polymorphism and antifungal activity of essential oils from leaves of different provenances of indigenous cinnamon (*Cinnamomum osmophloeum*). *Bioresour. Technol.* 97, 306–312. doi: 10.1016/j.biortech.2005.02.030

Daly-Hassen, H., Kasraoui, M., and Karra, C. (2014). Industrial timber production in Tunisia: despite reforestation, dependence on imports is increasing. *Bois Forêts Des Tropiques* 322, 29–37. doi: 10.19182/bft2014.322.a31232

Dong, H., Bahmani, M., Rahimi, S., and Humar, M. (2020). Influence of copper and biopolymer/Saqez resin on the properties of poplar wood. *Forests* 11:667. doi: 10.3390/f11060667

Edlich, R., Winters, K. L., and Long, I. I. I., W. B. (2005). Treated wood preservatives linked to aquatic damage, human illness, and death—a societal problem. *J. Long Term Eff. Med. Implants* 15, 209–224. doi: 10.1615/JLongTermEffMedImplants.v15.i2.80

Elaieb, M. T., Shel, F., Jalleli, M., Langbour, P., and Candelier, K. (2019). Propiedades físicas de la madera de cuatro especies de latifoliadas de porosidad anular: influencia de los radios sobre las contracciones tangencial y radial. *Madera y Bosques* 25, 1–18. doi: 10.21829/myb.2019.2521695

Falck, R. (1907). Wachtumgesetze, wachstum Laktorehnund temperature wertder holzersterenden. *Mycetur* 32, 38–39.

Fayaz, M., Bhat, M. H., Fayaz, M., Kumar, A., and Jain, A. K. (2017). Antifungal activity of *Lantana camara* L. leaf extracts in different solvents against some pathogenic fungal strains. *Pharmacologia* 8, 105–112. doi: 10.5567/pharmacologia.2017.105.112

Gabrielli, C. P., and Kamke, F. A. (2010). Phenol-formaldehyde impregnation of densified wood for improved dimensional stability. *Wood Sci. Technol.* 44, 95–104. doi: 10.1007/s00226-009-0253-6

Gupta, H., Sharma, K. R., and Dutt, B. (2016). Effect of plant extracts treatment on specific gravity of *Lannea coromandelica* (Houtt.) Merr. wood. *Ecol. Environ. Conserv.* 22, 1857–1860.

Izadyar, S., Babaei, Y., and Efhamisisi, D. (2020). Effect of natural resin from wild Pistachio trees on physical properties and durability of beech wood: alone and in combination with boric acid. *Drvna Industr. Znanstveni Casopis Za Pitanja Drvne Tehnologije* 71, 379–388. doi: 10.5552/drvind.2020.1949

Kadir, R., and Hale, M. (2019). Biocidal potential of the extractives of four Malaysian timbers against subterranean termites and wood decay fungi. *Eur. J. Wood Wood Prod.* 77, 147–155. doi: 10.1007/s00107-018-1361-5

Kartal, S. N., Terzi, E., Yilmaz, H., and Goodell, B. (2015). Bioremediation and decay of wood treated with ACQ, micronized ACQ, nano-CuO and CCA wood preservatives. *Int. Biodeterior. Biodegrad.* 99, 95–101. doi: 10.1016/j.ibiod.2015.01.004

Kositchaiyong, A., Rosarpitak, V., Hamada, H., and Sombatsompop, N. (2014). Anti-fungal performance and mechanical–morphological properties of PVC and wood/PVC composites under UV-weathering aging and soil-burial exposure. *Int. Biodeterior. Biodegrad.* 91, 128–137. doi: 10.1016/j.ibiod.2014.01.022

Kwaśniewska-Sip, P., Cofta, G., and Nowak, P. B. (2018). Resistance of fungal growth on Scots pine treated with caffeine. *Int. Biodeterior. Biodegrad.* 132, 178–184. doi: 10.1016/j.ibiod.2018.03.007

Li, J. Z., Furuno, T., and Katoh, S. (2000). Dimensional stability and flame resistance of silicate-acetylated and -propionylated wood composites. *J. Wood Chem. Technol.* 20, 441–453. doi: 10.1080/02773810009351893

Li, Y., Hui, B., Lv, M., Li, J., and Li, G. (2018). Inorganic–organic hybrid wood in response to visible light. *J. Mater. Sci.* 53, 3889–3898. doi: 10.1007/s10853-017-1775-1

Linthoingambi, W., and Singh, M. S. (2013). Antimicrobial activities of different solvent extracts of *Tithonia diversifolia* (Hemsely) A. Gray. *Asian J. Plant Sci. Res.* 3, 50–54.

Liu, K.-K., Jiang, Q., Tadepalli, S., Raliya, R., Biswas, P., Naik, R. R., et al. (2017). Wood–graphene oxide composite for highly efficient solar steam generation and desalination. *ACS Appl. Mater. Interfaces* 9, 7675–7681. doi: 10.1021/acsami.7b01307

Mansour, M. M. A., and Salem, M. Z. M. (2015). Evaluation of wood treated with some natural extracts and Paraloid B-72 against the fungus *Trichoderma harzianum*: wood elemental composition, *in-vitro* and application evidence. *Int. Biodeterior. Biodegrad.* 100, 62–69. doi: 10.1016/j.ibiod.2015.02.009

McKinney, H. H. (1923). Influence of soil temperature and moisture on infection of wheat seedlings by *Helminthosporium sativum*. *J. Agric. Res.* 26, 195–217.

Mohammed, S. A., Madhan, B., Demissie, B. A., Velappan, B., and Selvi, A. T. (2016). Rumex abyssinicus (mekmeko) Ethiopian plant material for preservation of goat skins: approach for cleaner leather manufacture. *J. Clean. Prod.* 133, 1043–1052. doi: 10.1016/j.jclepro.2016.06.043

Moreira, M. D., Picanço, M. C., Barbosa, L. C., de, A., Guedes, R. N. C., Campos, M. R. de, Silva, G. A., et al. (2007). Plant compounds insecticide activity against Coleoptera pests of stored products. *Pesq. Agropec. Bras.* 42, 909–915. doi: 10.1590/S0100-204X2007000700001

Nayeri, H. R., Tarmian, A., Abdulkhani, A., and Ebrahimi, G. (2017). Decay resistance of wood impregnated with monoethanolamine and sodium bisulfite pulping black liquors. *Maderas Cienc. Tecnol.* 19, 507–516. doi: 10.4067/S0718-221X2017005001001

Negi, G. C. S., Sharma, S., Vishvakarma, S. C. R., Samant, S. S., Maikhuri, R. K., Prasad, R. C., et al. (2019). Ecology and use of *Lantana camara* in India. *Bot. Rev.* 85, 109–130. doi: 10.1007/s12229-019-09209-8

Ney, F. P., Malco, D. C. L., Senoro, D. B., and Catajay-Mani, M. (2019). The bio-mechanical properties of coco wood applied with Neem extracts: a potential preservative for sustainable building in Marinduque, Philippines. *Sustain. Environ. Res.* 29, 1–13. doi: 10.1186/s42834-019-0041-4

Okon, K. E. (2014). Variations in specific gravity and shrinkage in wood of a 25-year-old *Gmelina arborea* in Oluwa forest reserve, South West Nigeria. *Arch. Appl. Sci. Res.* 6, 271–276.

Okon, K. E., Lin, F., Lin, X., Chen, C., Chen, Y., and Huang, B. (2018). Modification of Chinese fir (Cunninghamia lanceolata L.) wood by silicone oil heat treatment with micro-wave pretreatment. *Eur. J. Wood Wood Prod.* 76, 221–228. doi: 10.1007/s00107-017-1165-z

Ouyang, H., Liu, Z., Wang, L., Peng, W., Deng, H., and Ashraf, M. A. (2018). Fungicidal activity and bamboo preservation of *Pinus elliottii* needles extracts. *Wood Res.* 63, 533–546.

Peeters, K., Larnøy, E., Kutnar, A., and Hill, C. A. S. (2018). An examination of the potential for the use of the Maillard reaction to modify wood. *Int. Wood Prod. J.* 9, 108–114. doi: 10.1080/20426445.2018.1471840

Pepin, S., Blanchet, P., and Landry, V. (2018). "Development and characterisation of a penetrating barrier treatment for wood protection," in *Proceedings of the Canadian Wood Preservation Association 39th Annual Meeting* (Vancouver, BC), 66–77.

Pramod, P. S., Trimbakrao, K. S., and Vanita, A. (2017). Evaluation of unsaponified petroleum ether extract of *Lantana camara* L. leaves for antioxidant activity and oxidative stability. *Indian J. Pharm. Educ. Res.* 51, 692–699. doi: 10.5530/ijper.51.4.102

Priadi, T., Orfian, G., Cahyono, T. D., and Iswanto, A. H. (2020). Dimensional stability, color change, and durability of boron-mma treated red jabon (*Antochephalus macrophyllus*) wood. *J. Korean Wood Sci. Technol.* 48, 315–325. doi: 10.5658/WOOD.2020.48.3.315

Purnomo, H., Abdullah, L., and Irawati, R. H. (2011). "Systems dynamics approach to balancing wood supply and demand for sustaining furniture industry," in *Paper Presented in 19th International Congress on Modelling and Simulation, 12-16 December 2011* (Perth, WA), 338–344.

Qiu, H., Yang, S., Han, Y., Shen, X., Fan, D., Li, G., et al. (2018). Improvement of the performance of plantation wood by grafting water-soluble vinyl monomers onto cell walls. *ACS Sustain. Chem. Eng.* 6, 14450–14459. doi: 10.1021/acssuschemeng.8b03112

Rahman, K. S., Shaikh, A., Rahman, M., Alam, D., and Alam, M. (2013). The potential for using stem and branch of bhadi (*Lannea coromandelica*) as a lignocellulosic raw material for particleboard. *Int. Res. J. Biol. Sci.* 2, 8–12.

Reddy, A. K., Joy, J. M., and Kumara, C. K. A. (2011). *Lannea coromandelica*: the researcher's tree. *J. Pharm. Res.* 4, 577–579.

Rowell, R. M. (2005). "Chemical modification of wood," in *Handbook of Wood Chemistry and Wood Composite*, ed R. M. Rowell (Madison, WI: Taylor and Francis; CRC Press), 381–420.

Rowell, R. M., and Ellis, W. D. (1978). Determination of dimensional stabilization of wood using the water-soak method. *Wood Fiber Sci.* 10, 104–111.

Salem, M. Z. M., Zidan, Y. E., El Hadidi, N. M. N., Mansour, M. M. A., and Elgat, W. A. A. A. (2016). Evaluation of usage three natural extracts applied to three commercial wood species against five common molds. *Int. Biodeterior. Biodegra.* 110, 206–226. doi: 10.1016/j.ibiod.2016.03.028

Salim, R., Ashaari, Z., Samsi, H. W., Wahab, R., and Alamjuri, R. H. (2010). Effect of oil heat treatment on physical properties of semantan bamboo (*Gigantochloa scortechinii* Gamble). *Mod. Appl. Sci.* 4:107. doi: 10.5539/mas.v4n2p107

Sarker, P. K., Rahman, M. A., Bulbul, M. R., Das, T., and Ilias, G. N. M. (2006). *Standard Test Methods for Wood Preservatives by Laboratory Agar-Block Test.* The International Research Group on Wood Preservation, Doc. No. IRG/WP06, 20350, 18–22.

Shuib, N. S. (2011). *Physical and mechanical properties of extracted wood of Tectona grandis and antifungal test of the extractive with Phanerochaete chrysosporium* [Doctoral dissertation], Universiti Sains Malaysia, Gelugor, Malaysia.

Shukla, S. R., Zhang, J., and Kamdem, D. P. (2019). Pressure treatment of rubberwood (*Heavea brasiliensis*) with waterborne micronized copper azole: effects on retention, copper leaching, decay resistance and mechanical properties. *Constr. Build. Mater.* 216, 576–587. doi: 10.1016/j.conbuildmat.2019.05.013

Singh, T., and Singh, A. P. (2012). A review on natural products as wood protectant. *Wood Sci. Technol.* 46, 851–870. doi: 10.1007/s00226-011-0448-5

Sundararaj, R., Shanbhag, R. R., Nagaveni, H. C., and Vijayalakshmi, G. (2015). Natural durability of timbers under Indian environmental

conditions–An overview. *Int. Biodeterior. Biodegrad.* 103, 196–214. doi: 10.1016/j.ibiod.2015.04.026

Swamy, M. K., Sinniah, U. R., and Akhtar, M. (2015). *In vitro* pharmacological activities and GC-MS analysis of different solvent extracts of *Lantana camara* leaves collected from tropical region of Malaysia. *Evid Based Compl. Alt.* 2015, 1–9. doi: 10.1155/2015/506413

Syazwan, M., Azmi, B., Wai, L. C., Yhaya, M. F., Bin, I.smail, N., Tajarudin, H. A., et al. (2017). Preservation of rubber wood against biological decay by salts derived from leachate. *Wood Res.* 62, 863–872.

Taghiyari, H. R., Bari, E., Schmidt, O., Ghanbary, M. A. T., Karimi, A., and Tahir, P. M. D. (2014). Effects of nanowollastonite on biological resistance of particleboard made from wood chips and chicken feather against Antrodia vaillantii. *Int. Biodeterior. Biodegrad.* 90, 93–98. doi: 10.1016/j.ibiod.2014.02.012

Tchinda, J.-B. S., Ndikontar, M. K., Belinga, A. D. F., Mounguengui, S., Njankouo, J. M., Durmaçay, S., et al. (2018). Inhibition of fungi with wood extractives and natural durability of five Cameroonian wood species. *Ind. Crops Prod.* 123, 183–191. doi: 10.1016/j.indcrop.2018.06.078

Teaca, C. A., Roşu, D., Mustată, F., Rusu, T., Roşu, L., Roşca, I., et al. (2019). Natural bio-based products for wood coating and protection against degradation: a review. *Bioresources* 14, 4873–4901. doi: 10.15376/biores.14.2.Teaca

Temiz, A., Akbas, S., Panov, D., Terziev, N., Alma, M. H., Parlak, S., et al. (2013). Chemical composition and efficiency of bio-oil obtained from giant cane (*Arundo donax* L.) as a wood preservative. *Bioresources* 8, 2084–2098. doi: 10.15376/biores.8.2.2084-2098

Tripathi, S., Rawat, K., Dhyani, S., and Pant, H. (2009). Potential of *Lantana camara* Linn. weed against wood destroying fungi. *Indian For.* 135:403.

Vanam, B. (2019). Timber trade in India-challenges and policies. *EPRA Int. J. Multidiscip. Res.* 12, 119–122. doi: 10.36713/epra2013

Var, A. A., and Kardas, I. (2019). Changes in physical, mechanical, shrinking and swelling properties of pine wood species treated with salt natural geothermal waters as environmentally safe resources. *Appl. Ecol. Environ. Res.* 17, 14053–14068. doi: 10.15666/aeer/1706_1405314068

Verhaegen, D., Randrianjafy, H., Andriatsitohaina, H. R., Rakotonirina, M.-C. T., Andriamampianina, N., Montagne, P., et al. (2014). *Eucalyptus robusta* for sustainable fuelwood production in Madagascar: review of knowledge and future prospects. *Bois Forets Tropiques* 320, 15–30. doi: 10.19182/bft2014.320.a20541

Vincent, J. M. (1947). Distortion of fungal hyphae in the presence of certain inhibitors. *Nature* 159:850. doi: 10.1038/159850b0

Wang, K., Liu, X., Tan, Y., Zhang, W., Zhang, S., and Li, J. (2019). Two-dimensional membrane and three-dimensional bulk aerogel materials via top-down wood nanotechnology for multibehavioral and reusable oil/water separation. *Chem. Eng. J.* 371, 769–780. doi: 10.1016/j.cej.2019.04.108

Wang, L., Chen, S. S., Tsang, D. C. W., Poon, C.-S., and Shih, K. (2016). Recycling contaminated wood into eco-friendly particleboard using green cement and carbon dioxide curing. *J. Clean. Prod.* 137, 861–870. doi: 10.1016/j.jclepro.2016.07.180

Wang, S. Y., Chen, P. F., and Chang, S. T. (2005). Antifungal activities of essential oils and their constituents from indigenous cinnamon (*Cinnamomum osmophloeum*) leaves against wood decay fungi. *Bioresour. Technol.* 96, 813–818. doi: 10.1016/j.biortech.2004.07.010

Weerapreeyakul, N., Junhom, C., Barusrux, S., and Thitimetharoch, T. (2016). Induction of apoptosis in human hepatocellular carcinoma cells by extracts of *Lannea coromandelica* (Houtt.) Merr. *and Diospyros castanea* (Craib) Fletcher. *Chin. Med.* 11, 1–10. doi: 10.1186/s13020-016-0091-z

Wu, G., Lang, Q., Chen, H., Pu, J. (2012). Physical and chemical performance of eucalyptus wood with impregnated chemicals. *Bioresources.* 7, 0816–0826

Xie, Y., Wang, Z., Huang, Q., and Zhang, D. (2017). Antifungal activity of several essential oils and major components against wood-rot fungi. *Ind. Crops Prod.* 108, 278–285. doi: 10.1016/j.indcrop.2017.06.041

Xie, Y., Yang, Z., Cao, D., Rong, F., Ding, H., and Zhang, D. (2015). Antitermitic and antifungal activities of eugenol and its congeners from the flower buds of *Syzgium aromaticum* (clove). *Ind Crops Prod.* 77, 780–786. doi: 10.1016/j.indcrop.2015.09.044

Xu, K., Feng, J., Zhong, T., Zheng, Z., and Chen, T. (2015). Effects of volatile chemical components of wood species on mould growth susceptibility and termite attack resistance of wood plastic composites. *Int. Biodeterior. Biodegrad.* 100, 106–115. doi: 10.1016/j.ibiod.2015.02.002

Yadav, N., Ganie, S. A., Singh, B., Chhillar, A. K., and Yadav, S. S. (2019). Phytochemical constituents and ethnopharmacological properties of *Ageratum conyzoides* L. *Phytother Res.* 33, 2163–2178. doi: 10.1002/ptr.6405

Yang, H., Wang, Y., Yu, Q., Cao, G., Yang, R., Ke, J., et al. (2018). Composite phase change materials with good reversible thermochromic ability in delignified wood substrate for thermal energy storage. *Appl. Energy.* 212, 455–464. doi: 10.1016/j.apenergy.2017.12.006

Yu, Z., Yao, Y., Yao, J., Zhang, L., Chen, Z., Gao, Y., et al. (2017). Transparent wood containing Cs × WO 3 nanoparticles for heat-shielding window applications. *J. Mater. Chem. A* 5, 6019–6024. doi: 10.1039/C7TA00261K

Zelinka, S. L., Kirker, G. T., Bishell, A. B., and Glass, S. V. (2020). Effects of wood moisture content and the level of acetylation on brown rot decay. *Forests* 11:299. doi: 10.3390/f11030299

Zhou, J., Fu, W., Qing, Y., Han, W., Zhao, Z., and Zhang, B. (2015). Fabrication and performance of a glue-pressed engineered honeycomb bamboo (GPEHB) structure with finger-jointed ends as a potential substitute for wood lumber. *Bioresources* 10, 3302–3313. doi: 10.15376/biores.10.2.3302-3313

Zhu, M., Li, T., Davis, C. S., Yao, Y., Dai, J., Wang, Y., et al. (2016). Transparent and haze wood composites for highly efficient broadband light management in solar cells. *Nano Energy* 26, 332–339. doi: 10.1016/j.nanoen.2016.05.020

Zhu, M., Li, Y., Chen, G., Jiang, F., Yang, Z., Luo, X., et al. (2017). Tree-inspired design for high-efficiency water extraction. *Adv. Mater.* 29:1704107. doi: 10.1002/adma.201704107

Conflict of Interest: The authors declare that the research was conducted in the absence of any commercial or financial relationships that could be construed as a potential conflict of interest.

frontiers in Plant Science

MINI REVIEW
published: 29 July 2021
doi: 10.3389/fpls.2021.702928

Transcriptional Regulation and Signaling of Developmental Programmed Cell Death in Plants

*Cheng Jiang[1], Jiawei Wang[1], Hua-Ni Leng[2], Xiaqin Wang[1], Yijing Liu[1], Haiwen Lu[1], Meng-Zhu Lu[1] and Jin Zhang[1]**

[1] State Key Laboratory of Subtropical Silviculture, College of Forestry and Biotechnology, Zhejiang A&F University, Hangzhou, China, [2] Department of Horticultural Science, North Carolina State University, Raleigh, NC, United States

Developmental programmed cell death (dPCD) has multiple functions in plant growth and development, and is of great value for industrial production. Among them, wood formed by xylem dPCD is one of the most widely used natural materials. Therefore, it is crucial to explore the molecular mechanism of plant dPCD. The dPCD process is tightly regulated by genetic networks and is involved in the transduction of signaling molecules. Several key regulators have been identified in diverse organisms and individual PCD events. However, complex molecular networks controlling plant dPCD remain highly elusive, and the original triggers of this process are still unknown. This review summarizes the recent progress on the transcriptional regulation and signaling of dPCD during vegetative and reproductive development. It is hoped that this review will provide an overall view of the molecular regulation of dPCD in different developmental processes in plants and identify specific mechanisms for regulating these dPCD events. In addition, the application of plants in industrial production can be improved by manipulating dPCD in specific processes, such as xylogenesis.

Keywords: programmed cell death, signaling, transcriptional regulation, plant development, cell differentiation

OPEN ACCESS

Edited by:
Elizabeth P. B. Fontes, Universidade Federal de Viçosa, Brazil

Reviewed by:
Ting Zhao, Zhejiang University, China
Yunjun Zhao, Brookhaven National Laboratory (DOE), United States

****Correspondence:***
Jin Zhang
zhangj@zafu.edu.cn
orcid.org/0000-0002-8397-5078

Specialty section:
This article was submitted to Plant Biotechnology, a section of the journal Frontiers in Plant Science

Received: *30 April 2021*
Accepted: *02 July 2021*
Published: *29 July 2021*

Citation:
Jiang C, Wang J, Leng H-N, Wang X, Liu Y, Lu H, Lu M-Z and Zhang J (2021) Transcriptional Regulation and Signaling of Developmental Programmed Cell Death in Plants. Front. Plant Sci. 12:702928. doi: 10.3389/fpls.2021.702928

INTRODUCTION

Programmed cell death (PCD) is considered a behavior of self-salvage that is genetically controlled to eliminate no longer needed and damaged cells selectively or to differentiate specific cell types for efficient utilization of nutrition, reproduction, and other aspects (Daneva et al., 2016). In plants, PCD can be classified into developmentally induced PCD (dPCD, triggered as the ultimate step of cell-type specific differentiation programs) and environmentally induced PCD (ePCD, triggered by diverse abiotic stresses) according to the way it is triggered (Petrov et al., 2015; Huysmans et al., 2017). In an early work, PCD and autolysis were considered to be interchangeable or distinct in various studies. However, in some cases of developmental cell death, PCD and autolysis can easily be distinguished as two different biological processes with unique biochemical mechanisms and functional purposes (Escamez and Tuominen, 2014). dPCD occurs during vegetative and reproductive development and is the final differentiation process in specific cell types, such as xylem, root cap cells, trichomes, and anther tapetum (Olvera-Carrillo et al., 2015).

Over the last two decades, numerous studies unscrambling dPCD have focused on (1) the extracellular and intracellular signals that initiate dPCD or are altered during dPCD (Gechev and Hille, 2005), (2) the transcriptional regulation of specific gene expression to control dPCD (Cubría-Radío and Nowack, 2019), and (3) hydrolytic enzymes such as proteases and nucleases, which

are key executors of dPCD (Buono et al., 2019). The aim of this review is to shed light on the most common instances of dPCD in plant development, focusing on the molecular regulation of the dPCD process, to discuss future research directions contributing to a clear understanding of the mechanisms of dPCD and to take full advantage of dPCD in plants to improve the efficiency of production.

TRANSCRIPTIONAL REGULATION OF dPCD

Transcriptional Regulation of Reproductive dPCD

Reproductive growth is a critical process for plant population survival and genetic diversity. Recently, Wang et al. (2021) summarized the regulatory framework of flower-specific dPCD such as tapetal degeneration, pollen tube rupture, transmitting tract formation, and self-incompatibility. Here, we focus on the transcriptional regulation of dPCD in male and female germ cell formation, and fertilization and seed development.

Male Germ Cell Formation

Dehiscence of the anther and release of pollen rely on the PCD of the tapetum, and the precise timing of its degeneration is crucial for pollen maturation (Gómez et al., 2015). The transcriptional regulation mechanism that controls dPCD during tapetum differentiation has been reported. A group of basic helix–loop–helix (bHLH) transcription factors (TFs) can positively regulate tapetal PCD. bHLH142 acts downstream of the bHLH TF UNDEVELOPED TAPETUM1 (OsUDT1) and regulates the bHLH TF *ETERNAL TAPETUM1* (*OsEAT1*) to induce tapetal PCD. Furthermore, two genes (*AP25* and *AP37*) that encode aspartic proteases for tapetal PCD are under the regulation of OsEAT1 (Ko et al., 2014). In rice, TAPETUM DEGENERATION RETARDATION (OsTDR) activates a cysteine protease-encoding gene (*OsCP1*) to induce tapetal PCD, and its activation is repressed by an aldehyde dehydrogenase (OsALDH) (Xie et al., 2020). TDR INTERACTING PROTEIN2 (OsTIP2) can interact with and directly regulate the expression of *OsTDR* and *OsEAT1* (Fu et al., 2014). PERSISTENT TAPETAL CELL encoding genes (*OsPTC1* and *OsPTC2*) were proved to regulate the expression of *OsEAT1*, *OsAP1*, and *OsAP25* (Uzair et al., 2020). *Arabidopsis AtMYB80* might suppress tapetal PCD by influencing the expression of the papain-like cysteine protease gene *AtCEP1*, but the precise regulation mechanism is still unclear (Zhang et al., 2014). In addition, AtMYB80 might activate the PCD-inhibiting aspartic protease *UNDEAD*, and a mutation in *AtMYB80* caused precocious tapetum degeneration in *Arabidopsis* (Phan et al., 2011). These results show that a regulatory network is crucial for the precise timing of tapetal PCD and male fertility (**Figure 1**).

Female Germ Cell Formation

Female gametophytes develop inside the ovules, which originate from a meiotic product. One functional megaspore survives, and three megaspores degenerate. During these processes, the expression of *Arabinogalactan protein 18* (*AtAGP18*) is needed in the abaxial pole of the ovule to ensure the survival of functional megaspores (Demesa-Arévalo and Vielle-Calzada, 2013). The nucellus is an ephemeral tissue whose degeneration is controlled by female gametophytes (Chen et al., 2014). The TF OsMADS29 can regulate the expression of the cysteine protease gene (*CEP*), thereby promoting nucellar degeneration in rice (Yin and Xue, 2012). Another PCD-related *CEP* gene, a *vacuolar processing enzyme* (*HvVPE*), was shown to be upregulated during nucellar cell death in barley (Radchuk et al., 2011).

Fertilization and Seed Development

During fertilization, several cells are tightly controlled for elimination. Pollen tubes growth toward the ovule is guided by the transmitting tract, the death of which is considered to be important. Cell death of the transmitting tract to make way for growing pollen tubes is regulated by two bHLH TFs (*AtSTY* and *AtHEC*) and two auxin response factor (ARF) genes (*AtARF6* and *AtARF8*) (Kaminaka et al., 2006). Once pollen tubes arrive at ovules, synergids undergo cell death, and three synergid-expressed genes, *FERONIA* (*AtFER*), *LORELEI* (*AtLRE*), and *NORTIA* (*AtNTA*), are required (Kessler and Grossniklaus, 2011). AtMYB97, AtMYB101, and AtMYB120 positively regulate receptive synergid degeneration after the proper discharge of sperm cells (Liang et al., 2013). ZHOUPI (AtZOU/AtRGE1) and INDUCER OF CBP EXPRESSION 1 (AtICE1) promote the breakdown of the embryo-surrounding region, and loss-of-function mutants of these genes lead to misshaped embryos (Denay et al., 2014).

Transcriptional Regulation of Vegetative dPCD

Xylogenesis

Secondary xylem is the most abundant biomass produced by plants and concurrently functions in structural and mechanical support and transport tissues distributing water and solutes. Xylogenesis consists of xylem generation, differentiation, and PCD processes (Escamez and Tuominen, 2014). In this process, a typical dPCD event is the formation of the tracheal element (TE), which loses its contents and forms a functional region composed of hollow, dead tubes. VASCULAR NAC DOMAIN (VNDs) and NAC SECONDARY WALL THICKENING PROMOTING FACTOR (NSTs) are known to function as key regulators of TE secondary cell wall (SCW) formation and cell death (Zhang et al., 2018a). These NAC TFs are regarded as first layer regulators in the progression of the SCW regulatory network, subsequently regulating the second layer master switches *MYB46* and *MYB83* (Zhong et al., 2007). VNDs also regulate the expression of TE differentiation inhibitors, such as *SUPPRESSOR OF ACAULIS 51* (*SAC51*) and *XYLEM NAC DOMAIN 1* (*XND1*) (Zhong et al., 2010). Moreover, hydrolytic enzymes downstream of VNDs, such as xylem cysteine proteinase (AtXCP1 and AtXCP2) and metacaspase9 (AtMC9), are the executors of autolysis during dPCD.

Root Cap

The root cap ensheathes the root and has important functions for root growth, gravity sensing, root system architecture, and

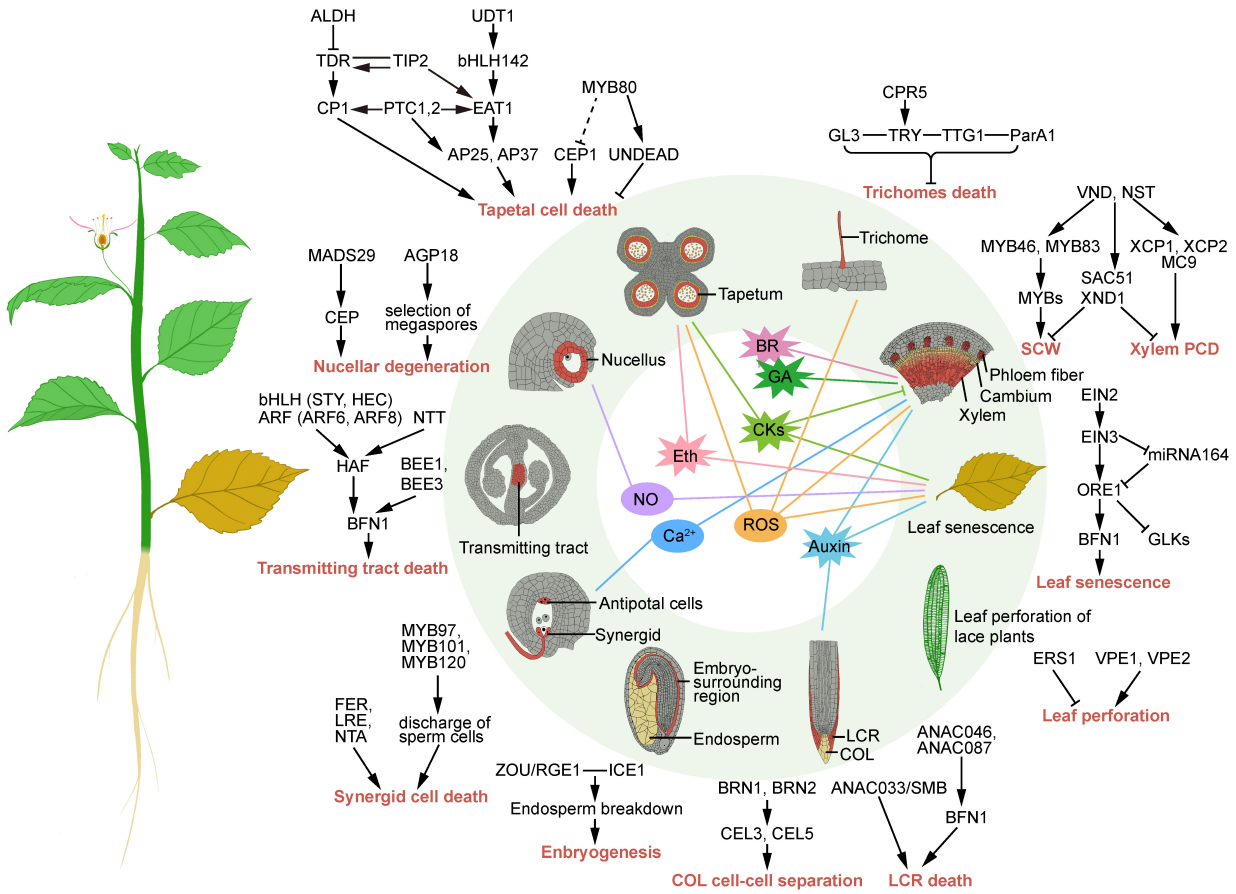

FIGURE 1 | Schematic representation of the transcriptional regulation and signaling of developmental programmed cell death in plants. Arrows and a "T" at the ends of lines represent transcriptional activation and repression, respectively. Lines without arrows or a "T" represent protein-protein interactions; dotted line represents unclear regulation.

protection of the stem cells in the root tip (Kumpf and Nowack, 2015). The root cap has to maintain its size and position at the root tip by sloughing old cells and producing new cells; the disposal of old cells is a PCD process. In *Arabidopsis*, the root cap can be distinguished into two tissue types, the central columella root cap (COL) and the peripheral lateral root cap (LRC). Two NACs, BEARSKIN1 (AtBRN1) and AtBRN2, regulate root cap-expressed *CELLULASE3* (*AtCEL3*) and *AtCEL5,* and control cell-cell separation in mature COL layers (Bennett et al., 2010). The TF ANAC033/SOMBRERO was shown to transcriptionally control LRC differentiation and preparation for cell death (Fendrych et al., 2014). In addition, two other NACs (AtANAC087 and AtANAC046) are sufficient to activate the expression of cell death-associated genes and induce dPCD *via* the nuclease BIFUNCTIONAL NUCLEASE1 (AtBFN1) (Huysmans et al., 2018).

Leaf Morphogenesis

The production of various leaf shapes during leaf morphogenesis is also regulated by dPCD. Leaf perforation exists in lace plants, and few aroids are caused by PCD (Gunawardena, 2008). The transcription level of the ethylene receptor gene *AmERS1a* was significantly reduced in leaves undergoing PCD, indicating that ethylene plays an important role in dPCD during lace plant perforation (Rantong et al., 2015). Two *VPE* genes (*AmVPE1* and *AmVPE2*) were identified with high expression levels in the preperforation developmental stage and late window stage of lace plants, respectively (Rantong and Gunawardena, 2018). However, the detailed transcriptional regulation mechanism is still unclear.

Leaf Senescence

The last stage of leaf senescence is a PCD process influenced by numerous internal and external environmental signals, which are controlled by a very complex gene regulatory network (Woo et al., 2019). Ethylene controls the leaf senescence PCD by the trifurcate pathway. ETHYLENE-INSENSITIVE2 (AtEIN2) perceiving ethylene activates the expression of *AtEIN3*, which represses *miR164* (Li et al., 2013). *MiR164* subsequently suppresses the expression of *ORESARA1/ANAC092 (AtORE1)*, which directly contributes to controlling AtBFN1 (Matallana-Ramirez et al., 2013), and inhibits the activity of the chloroplast-supporting TFs GOLDEN-LIKE1 (AtGLK1) and AtGLK2 (Rauf et al., 2013).

Trichome Differentiation

Trichomes are epidermal outgrowths that play various protective roles and provide valuable resources for plant development. Trichome cells were proved to die finally with chromatin condensation, nuclear fragmentation, and endoplasmic reticulum dilation (Papini et al., 2010). Trichome death is also regulated by *CONSTITUTIVE PATHOGEN RESPONSE5* (*AtCPR5*) through linking endoreduplication and cell division (Kirik et al., 2001), and the effects of the *cpr5* mutant were epistatic to those of trichome developmental regulators TRIPTYCHON (AtTRY) and GLABRA3 (AtGL3) (Brininstool et al., 2008). In *Nicotiana*, silencing *TRANSPARENT TESTA GLABRA1* (*NtTTG1*) in trichomes resulted in the elimination of hypersensitive cell death induced by ParA1 (Wang et al., 2009).

SIGNALS CONTROLLING DEVELOPMENTAL PCD

Plant Hormones

Auxin was reported to be involved in xylem formation, root cap morphogenesis, and leaf senescence. Dying cells were shown to facilitate the production of indole-3-acetic acid (IAA), as their proteins were hydrolyzed and some of the tryptophan was released to adjacent cells (Sheldrake, 2021). The auxin dynamics among dying cells and adjacent cells play a crucial role in plant growth and development through PCD. The levels of auxin immediately increase around differentiating xylem cells in leaf veins, petals, and roots when they are dying (Brunoud et al., 2012). When polar auxin transport is inhibited, xylem differentiation is further induced locally, along with high levels of auxin (Ravichandran et al., 2020). In this process, differentiating xylem cells were considered "stem-cell organizers" leading to the formation of a new organizer adjacent to cambial stem cells and differentiation into mature xylem themselves. In the lateral root cap, PCD and auxin form a cyclic action that regulates the periodicity of lateral organ induction, coordinating primary root growth with root branching (Xuan et al., 2016). Furthermore, in senescent leaves, tryptophan and auxin levels increase dramatically, which accelerates leaf senescence (Araújo et al., 2011). These studies indicate that auxin acts as an important signal involved in cell differentiation, especially in developmentally controlled cell death. Furthermore, it mainly appears to initiate these processes (Vanneste and Friml, 2009).

Cytokinin plays a central role in cell division and differentiation through an antagonistic interaction with auxin. Cytokinin can also affect the dPCD of xylem, leaves during senescence, and tapetum. In *Arabidopsis*, the cell fate to protoxylem exhibits high auxin and low cytokinin signaling, while the cell fate to procambium exhibits high cytokinin but low auxin signaling in roots (Bishopp et al., 2011). In a loss-of-function mutant of the cytokinin receptor *AtAHK3*, leaf senescence was delayed with reduced sensitivity to cytokinin (Kim et al., 2006). Through expression analysis of phytohormone biosynthesis and signaling genes, cytokinin is needed during earlier stages of rice tapetum and not needed at the uninuclear microspore stage (Hirano et al., 2008). Therefore, regulating cytokinin at low levels ensures well-organized PCD in plants. It has also been demonstrated that high levels of cytokinin call induce PCD in root cortex cells of *Vicia faba* ssp. minor seedlings (Kunikowska et al., 2013) and in cultured *Arabidopsis* cells (Vescovi et al., 2012).

Ethylene is widely known as the plant hormone responsible for a number of developmental processes. Tapetal cell death and leaf senescence require ethylene. The reduction of ethylene production and signal transduction leads to delayed leaf senescence (Graaff et al., 2006). Some plants form aerenchyma in response to a hypoxic environment; however, blocking the ethylene receptor that makes the cells insensitive to ethylene can avoid PCD to allow aerenchyma to form (Liu et al., 2019). Ethylene signaling is needed for the induction of PCD in epidermal cells of deepwater rice (Steffens and Sauter, 2005). The expression and activation of signaling genes involved in ethylene specifically occurred in tapetal cells concurrently, which regulated tapetal cell death (Hirano et al., 2008). In addition, ethylene is also an active signal in floral organ formation and development (Wang et al., 2010).

Moreover, several other phytohormones are also involved in dPCD-related processes, e.g., gibberellin is essential in vascular differentiation (Eriksson et al., 2000), brassinosteroids initiate TE differentiation (Milhinhos and Miguel, 2013), salicylic acid is associated with hypersensitive reaction and has dual functions in cell death control (Radojičić et al., 2018), and jasmonic acid is necessary for leaf senescence (He et al., 2002). In summary, phytohormones play many roles in plant dPCD. However, the molecular and biochemical mechanisms of plant hormones as signals for the dPCD of different tissues and organs remain to be elucidated (**Figure 1**).

Reactive Oxygen Species

Continuously generated reactive oxygen species (ROS), such as singlet oxygen ($^1O_2$), superoxide ($O_2^{\cdot -}$), hydrogen peroxide (H_2O_2), and hydroxyl radical (HO), act as signaling molecules that coordinate various plant processes, namely, tapetal cell death, trichome death, xylogenesis, and leaf senescence (Gechev et al., 2006). ROS are regarded not only as signals but also as byproducts of aerobic pathways generated in different cellular compartments and cause PCD at higher concentrations (Gechev and Hille, 2005). MAPKs involved in relaying the H_2O_2 signal mediate PCD triggered by chloroplast-generated H_2O_2 (Liu et al., 2007). The chloroplast protein EXECUTER1, acting together with EXECUTER2, could transfer oxidative signals from the plastid to the nucleus, leading to cell death (Lee et al., 2007). The H_2O_2 signal transmitted to ROS-specific TFs could lead to H_2O_2-dependent cell death (Gadjev et al., 2006). In the rice *mads3* mutant, anthers exhibit oxidative stress-related phenotypes, since tapetal PCD occurs prematurely (Hu et al., 2011). ROS production by NADPH oxidases also acts on tapetal PCD progression (Xie et al., 2014). Elimination of H_2O_2 through non-enzymatic and enzymatic pathways maintains the level of ROS, while catalase, peroxidase, ascorbate peroxidase, and glutathione reductase are considered to be the main H_2O_2 scavengers, which can effectively reduce the amount of H_2O_2 (Kapoor et al., 2015). In summary, the role of ROS in the dPCD process strictly depends

on its concentration, and its interaction with other signaling molecules also determines cell fate (Niu and Liao, 2016).

Nitric Oxide

Nitric oxide (NO) is a small gaseous and highly reactive molecule that can take part in a wide range of physiological processes, such as nucellar degeneration and leaf senescence. Due to NO being highly reactive, a series of NO derivatives could be formed, resulting in a redox-mediated modification in plants. The effects of NO as an activator or repressor seem to be due to the concentration and timing patterns of NO (Mur et al., 2012). High levels of NO are associated with the progression of natural senescence, cell death, and DNA fragmentation (Carimi et al., 2005). Studies have indicated that NO and H_2O_2 can be induced to synthesize each other and that the signaling crosstalk between H_2O_2 and NO synergistically regulates leaf cell death and delays senescence (Iakimova and Woltering, 2015). During nucellar cell degeneration, considerable production of NO and H_2O_2 caused an induction of caspase-like proteases, leading to nucellar dPCD (Lombardi et al., 2010). In addition, rapid and transient increases in ROS and NO were also detected by self-incompatibility in the pollen tube growth of *Papaver* (Wilkins et al., 2011).

Calcium

Ca^{2+} is a core signaling molecule in plants that is involved in many physiological processes, such as PCD of synergids and xylogenesis (Uslu and Grossmann, 2016). The change in intracellular Ca^{2+} concentration plays an important role in signaling transmission during a series of cellular processes (Kong et al., 2015). The Ca^{2+} increase in the cytosol was verified to be an early signal that occurred upstream of the vacuolar breakdown in self-incompatibility (Wilkins et al., 2015). Calcium-mediated signaling between two synergids determined their fate (death or survival) in the control of sperm delivery (Ngo et al., 2014). In xylogenic *Zinnia* cultures, Ca^{2+} influx into the cell was required for cell death and implicated as a trigger after SCW deposition (Groover and Jones, 1999). Ca^{2+} influx has been demonstrated to be mediated by H_2O_2 signaling in the plasma membrane of root cells, resulting in root elongation (Han et al., 2014). Because of various types of Ca^{2+} receptors and channels, Ca^{2+} signaling can be delivered widely. For example, Ca^{2+}-dependent DNases (CaN) participate in the PCD of secretory cavity cells through nuclear DNA degradation in *Citrus* (Bai et al., 2020). In *Eucommia ulmoides*, *EuCaN1*, and *EuCaN2* were identified to be involved in secondary xylem development (Chen et al., 2012).

CONCLUSION AND FUTURE PERSPECTIVES

Current studies have shown that the fate of cells undergoing PCD is controlled by complex signaling and transcriptional regulatory networks. Transcriptional regulation has been revealed to play a key role in specific dPCD events. However, the link between signaling pathways and dPCD-related gene expression regulation is rarely clearly established. Especially in woody plants, the signal transduction and transcriptional regulatory mechanism of dPCD during wood formation are still unclear. Recently, Zhang et al. (2018b) used a combination of expression quantitative trait loci (eQTL) analysis and genome-wide association study (GWAS) to successfully identify crucial genes that control metabolite synthesis and further upstream transcription factors. This approach provides a new strategy for exploring new regulatory mechanisms in biological processes. Therefore, combining cell biology, biochemistry, and molecular biology methods to detect how signaling pathways control dPCD through gene regulatory networks will become an overall trend in future research. Specifically, xylogenesis contributes to the largest bioenergy source, in which the components and contents of SCW are the main influencing factors in the improvement of industrial production. In short, the analysis of the molecular regulation mechanism of plant dPCD can lay the foundation for regulating specific developmental processes of plants through genetic engineering methods and further applying their products to industrial production.

AUTHOR CONTRIBUTIONS

JZ conceived the study. CJ and JZ collected and synthesized the data and draft the manuscript. JW, H-NL, XW, YL, HL, and M-ZL revised the manuscript. All authors contributed to the article and approved the submitted version.

FUNDING

This study was supported by the National Natural Science Foundation of China (32001285) to CJ, the National Key R&D Program "International Cooperation in Science and Technology Innovation between Governments" (2019YFE0119100) to M-ZL, and the Zhejiang A&F University Research and Development Fund Talent Startup Project (2021LFR013) to JZ.

REFERENCES

Araújo, W. L., Ishizaki, K., Nunes-Nesi, A., Tohge, T., Larson, T. R., Krahnert, I., et al. (2011). Analysis of a range of catabolic mutants provides evidence that phytanoyl-coenzyme a does not act as a substrate of the electron-transfer flavoprotein/electron-transfer flavoprotein:ubiquinone oxidoreductase complex in *Arabidopsis* during dark-induced senes. *Plant Physiol.* 157, 55–69. doi: 10.1104/pp.111.182188

Bai, M., Liang, M., Huai, B., Gao, H., Tong, P., Shen, R., et al. (2020). Ca^{2+}-dependent nuclease is involved in DNA degradation during the formation of the secretory cavity by programmed cell death in fruit of *Citrus grandis* 'Tomentosa'. *J. Exp. Bot.* 71, 4812–4827. doi: 10.1093/jxb/eraa199

Bennett, T., Toorn, A. V. D., Sanchez-Perez, G. F., Campilho, A., Willemsen, V., Snel, B., et al. (2010). SOMBRERO, BEARSKIN1, and BEARSKIN2 regulate root cap maturation in *Arabidopsis*. *Plant Cell* 22, 640–54. doi: 10.1105/tpc.109.072272

Bishopp, A., Help, H., El-Showk, S., Weijers, D., Scheres, B., Friml, J., et al. (2011). A mutually inhibitory interaction between auxin and cytokinin specifies vascular pattern in roots. *Curr. Biol.* 21, 917–926. doi: 10.1016/j.cub.2011.04.017

Brininstool, G., Kasili, R., Simmons, L. A., Kirik, V., Hülskamp, M., and Larkin, J. C. (2008). Constitutive expressor of Pathogenesis-Related Genes5 affects cell wall biogenesis and trichome development. *BMC Plant Biol.* 8:58. doi: 10.1186/1471-2229-8-58

Brunoud, G., Wells, D. M., Oliva, M., Larrieu, A., Mirabet, V., Burrow, A. H., et al. (2012). A novel sensor to map auxin response and distribution at high spatio-temporal resolution. *Nature* 482, 103–106. doi: 10.1038/nature10791

Buono, R. A., Hudecek, R., and Nowack, M. K. (2019). Plant proteases during developmental programmed cell death. *J. Exp. Bot.* 70, 2097–2112. doi: 10.1093/jxb/erz072

Carimi, F., Zottini, M., Costa, A., Cattelan, I., Michele, R. D., Terzi, M., et al. (2005). NO signalling in cytokinin-induced programmed cell death. *Plant Cell Environ.* 28, 1171–1178. doi: 10.1111/j.1365-3040.2005.01355.x

Chen, G. H., Sun, J. Y., Liu, M., Jie, L., and Yang, W. C. (2014). SPOROCYTELESS is a novel embryophyte-specific transcription repressor that interacts with TPL and TCP proteins in *Arabidopsis*. *J. Genet. Genomics* 41, 617–625. doi: 10.1016/j.jgg.2014.08.009

Chen, H. M., Yu, P., Zeng, J., Qi, D., Yin, S. Y., Liu, C., et al. (2012). The Ca^{2+}-dependent DNases are involved in secondary xylem development in *Eucommia ulmoides*. *J. Integr. Plant Biol.* 54, 456–470. doi: 10.1111/j.1744-7909.2012.01134.x

Cubría-Radío, M., and Nowack, M. K. (2019). Transcriptional networks orchestrating programmed cell death during plant development. *Curr. Top. Dev. Biol.* 131, 161–184. doi: 10.1016/bs.ctdb.2018.10.006

Daneva, A., Gao, Z., Durme, M. V., and Nowack, M. K. (2016). Functions and regulation of programmed cell death in plant development. *Annu. Rev. Cell Dev. Bi.* 32, 441–468.

Demesa-Arévalo, E., and Vielle-Calzada, J. P. (2013). The classical arabinogalactan protein AGP18 mediates megaspore selection in *Arabidopsis*. *Plant Cell* 25, 1274–1287. doi: 10.1105/tpc.112.106237

Denay, G., Cre, Ff, A., Moussu, S., Wagnon, P., Thévenin, J., et al. (2014). Endosperm breakdown in *Arabidopsis* requires heterodimers of the basic helix-loop-helix proteins ZHOUPI and INDUCER OF CBP EXPRESSION 1. *Development* 141, 1222–1227. doi: 10.1242/dev.103531

Eriksson, M. E., Israelsson, M., Olsson, O., Moritz, T. (2000). Increased gibberellin biosynthesis in transgenic trees promotes growth, biomass production and xylem fiber length. *Nat. Biotechnol.* 18, 784–788. doi: 10.1038/77355

Escamez, S., and Tuominen, H. (2014). Programmes of cell death and autolysis in tracheary elements: when a suicidal cell arranges its own corpse removal. *J. Exp. Bot.* 65, 1313–1321. doi: 10.1093/jxb/eru057

Fendrych, M., Hautegem, T. V., Durme, M. V., Olvera-Carrillo, Y., Huysmans, M., Karimi, M., et al. (2014). Programmed cell death controlled by ANAC033/SOMBRERO determines root cap organ size in *Arabidopsis*. *Curr. Biol.* 24, 931–940. doi: 10.1016/j.cub.2014.03.025

Fu, Z., Yu, J., Cheng, X., Zong, X., Xu, J., Chen, M., et al. (2014). The Rice basic Helix-Loop-Helix transcription factor TDR INTERACTING PROTEIN2 ss a central switch in early anther development. *Plant Cell* 26, 1512–1524. doi: 10.1105/tpc.114.123745

Gadjev, I., Vanderauwera, S., Gechev, T. S., Laloi, C., Minkov, I. N., Shulaev, V., et al. (2006). Transcriptomic footprints disclose specificity of reactive oxygen species signaling in *Arabidopsis*. *Plant Physiol.* 141, 436–445. doi: 10.1104/pp.106.078717

Gechev, T. S., Breusegem, F. V., Stone, J. M., Denev, I., and Laloi, C. (2006). Reactive oxygen species as signals that modulate plant stress responses and programmed cell death. *BioEssays* 28, 1091–1101. doi: 10.1002/bies.20493

Gechev, T. S., and Hille, J. (2005). Hydrogen peroxide as a signal controlling plant programmed cell death. *J. Cell Biol.* 168, 17–20. doi: 10.1083/jcb.200409170

Gómez, J. F., Talle, B., and Wilson, Z. A. (2015). Anther and pollen development: a conserved developmental pathway. *J. Integr. Plant Biol.* 57, 876–891. doi: 10.1111/jipb.12425

Graaff, E. V. D., Schwacke, R., Schneider, A., Desimone, M., Flügge, U., and Kunze, R. (2006). Transcription analysis of *Arabidopsis* membrane transporters and hormone pathways during developmental and induced leaf senescence. *Plant Physiol.* 141, 776–792. doi: 10.1104/pp.106.079293

Groover, A., and Jones, A. M. (1999). Tracheary element differentiation uses a novel mechanism coordinating programmed cell death and secondary cell wall synthesis. *Plant Physiol.* 119, 375–384. doi: 10.1104/pp.119.2.375

Gunawardena, A. H. L. A. N. (2008). Programmed cell death and tissue remodelling in plants. *J. Exp. Bot.* 59, 445–451. doi: 10.1093/jxb/erm189

Han, S., Fang, L., Ren, X., Wang, W., and Jiang, J. (2014). MPK6 controls H_2O_2-induced root elongation by mediating Ca^{2+} influx across the plasma membrane of root cells in *Arabidopsis* seedlings. *New Phytol.* 205, 695–706. doi: 10.1111/nph.12990

He, Y., Fukushige, H., and Gan, H. S. (2002). Evidence supporting a role of jasmonic acid in *Arabidopsis* leaf senescence. *Plant Physiol.* 128, 876–884. doi: 10.1104/pp.010843

Hirano, K., Aya, K., Hobo, T., Sakakibara, H., Kojima, M., Shim, R. A., et al. (2008). Comprehensive transcriptome analysis of phytohormone biosynthesis and signaling genes in microspore/pollen and tapetum of rice. *Plant Cell Physiol.* 49, 1429–1450. doi: 10.1093/pcp/pcn123

Hu, L., Liang, W., Yin, C., Cui, X., Zong, J., Wang, X., et al. (2011). Rice MADS3 regulates ROS homeostasis during late anther development. *Plant Cell* 23, 515–533. doi: 10.1105/tpc.110.074369

Huysmans, M., Buono, R. A., Skorzinski, N., Radio, M. C., Winter, F. D., Parizot, B., et al. (2018). NAC transcription factors ANAC087 and ANAC046 control distinct aspects of programmed cell death in the *Arabidopsis* columella and lateral root cap. *Plant Cell* 30, 2197–2213. doi: 10.1105/tpc.18.00293

Huysmans, M., Saul, L. A., Coll, N. S., and Nowack, M. K. (2017). Dying two deaths-programmed cell death regulation in development and disease. *Curr. Opin. Plant Biol.* 35, 37–44. doi: 10.1016/j.pbi.2016.11.005

Iakimova, E. T., and Woltering, E. J. (2015). Nitric oxide prevents wound-induced browning and delays senescence through inhibition of hydrogen peroxide accumulation in fresh-cut lettuce. *Innov. Food Sci. Emerg.* 30, 157–169. doi: 10.1016/j.ifset.2015.06.001

Kaminaka, H., Näke, C., Epple, P., Dittgen, J., Schütze, K., Chaban, C., et al. (2006). bZIP10-LSD1 antagonism modulates basal defense and cell death in *Arabidopsis* following infection. *EMBO J.* 25, 4400–4411. doi: 10.1038/sj.emboj.7601312

Kapoor, D., Sharma, R., Handa, N., Kaur, H., Rattan, A., Yadav, P., et al. (2015). Redox homeostasis in plants under abiotic stress: role of electron carriers, energy metabolism mediators and proteinaceous thiols. *Front. Env. Sci.* 3:13. doi: 10.3389/fenvs.2015.00013

Kessler, S. A., and Grossniklaus, U. (2011). She's the boss: signaling in pollen tube reception. *Curr. Opin. Plant Biol.* 14, 622–627. doi: 10.1016/j.pbi.2011.07.012

Kim, H. J., Ryu, H., Hong, S. H., Woo, H. R., Lim, P. O., Lee, I. C., et al. (2006). Cytokinin-mediated control of leaf longevity by AHK3 through phosphorylation of ARR2 in *Arabidopsis*. *Proc. Natl. Acad. Sci. U. S. A.* 103, 814–819. doi: 10.1073/pnas.0505150103

Kirik, V., Bouyer, D., Schbinger, U., Bechtold, N., Herzog, M., Bonneville, J.-M., et al. (2001). CPR5 is involved in cell proliferation and cell death control and encodes a novel transmembrane protein. *Curr. Biol.* 11, 1891–1895. doi: 10.1016/s0960-9822(01)00590-5

Ko, S. S., Li, M. J., Ku, S. B., Ho, Y. C., Lin, Y. J., Chuang, M. H., et al. (2014). The bHLH142 transcription factor coordinates with TDR1 to modulate the expression of EAT1 and regulate pollen development in rice. *Plant Cell* 26, 2486–2504. doi: 10.1105/tpc.114.126292

Kong, D., Ju, C., Parihar, A., Kim, S., Cho, D., and Kwak, J. M. (2015). *Arabidopsis* glutamate receptor homolog3.5 modulates cytosolic Ca^{2+} level to counteract effect of abscisic acid in seed germination. *Plant Physiol.* 167, 1630–1642. doi: 10.1104/pp.114.251298

Kumpf, R. P., and Nowack, M. K. (2015). The root cap: a short story of life and death. *J. Exp. Bot.* 19, 5651–62. doi: 10.1093/jxb/erv295

Kunikowska, A., Byczkowska, A., and Kazmierczak, A. (2013). Kinetin induces cell death in root cortex cells of *Vicia faba* ssp. minor seedlings. *Protoplasma* 250, 851–861. doi: 10.1007/s00709-012-0466-7

Lee, K. P., Kim, C., Landgraf, F., and Apel, K. (2007). EXECUTER1- and EXECUTER2-dependent transfer of stress-related signals from the plastid to the nucleus of *Arabidopsis thaliana*. *Proc. Natl. Acad. Sci. U. S. A.* 104, 10270–10275. doi: 10.1073/pnas.0702061104

Li, Z., Peng, J., Wen, X., and Guo, H. (2013). Ethylene-insensitive 3 is a senescence-associated gene that accelerates age-dependent leaf senescence by directly repressing *miR164* transcription in *Arabidopsis*. *Plant Cell* 25, 3311–3328. doi: 10.1105/tpc.113.113340

Liang, Y., Tan, Z. M., Zhu, L., Niu, Q. K., Zhou, J. J., Li, M., et al. (2013). MYB97, MYB101 and MYB120 function as male factors that control pollen tube-synergid interaction in *Arabidopsis thaliana* fertilization. *PLoS Genet.* 9:e1003933. doi: 10.1371/journal.pgen.1003933

Liu, H., Hao, N., Jia, Y., Liu, X., Ni, X., Wang, M., et al. (2019). The ethylene receptor regulates *Typha angustifolia* leaf aerenchyma morphogenesis and cell fate. *Planta* 250, 381–390. doi: 10.1007/s00425-019-03177-4

Liu, Y., Ren, D., Pike, S., Pallardy, S., Gassmann, W., and Zhang, S. (2007). Chloroplast-generated reactive oxygen species are involved in hypersensitive response-like cell death mediated by a mitogen-activated protein kinase cascade. *Plant J.* 51, 941–954. doi: 10.1111/j.1365-313x.2007.03191.x

Lombardi, L., Ceccarelli, N., Picciarelli, P., Lorenzi, R. (2010). Nitric oxide and hydrogen peroxide involvement during programmed cell death of Sechium edule nucellus. *Physiol. Plant.* 140, 89–102. doi: 10.1111/j.1399-3054.2010.01381.x

Matallana-Ramirez, L. P., Rauf, M., Farage-Barhom, S., Dortay, H., Xue, G. P., Dröge-Laser, W., et al. (2013). NAC transcription factor ORE1 and senescence-induced *BIFUNCTIONAL NUCLEASE1* (*BFN1*) constitute a regulatory cascade in *Arabidopsis*. *Mol. Plant* 6, 1438–1452. doi: 10.1093/mp/sst012

Milhinhos, A., and Miguel, C. M. (2013). Hormone interactions in xylem development: a matter of signals. *Plant Cell Rep.* 32, 867–883. doi: 10.1007/s00299-013-1420-7

Mur, L. A. J., Mandon, J., Persijn, S., Cristescu, S. M., Moshkov, I. E., Novikova, G. V., et al. (2012). Nitric oxide in plants: an assessment of the current state of knowledge. *AoB Plants* 5:pls052. doi: 10.1093/aobpla/pls052

Ngo, Q. A., Vogler, H., Lituiev, D. S., Nestorova, A., and Grossniklaus, U. (2014). A calcium dialog mediated by the *FERONIA* signal transduction pathway controls plant sperm delivery. *Dev. Cell* 29, 491–500. doi: 10.1016/j.devcel.2014.04.008

Niu, L., and Liao, W. (2016). Hydrogen peroxide signaling in plant development and abiotic responses: crosstalk with nitric oxide and calcium. *Front. Plant Sci.* 7:230. doi: 10.3389/fpls.2016.00230

Olvera-Carrillo, Y., Bel, M. V., Hautegem, T. V., Fendrych, M., Huysmans, M., Simaskova, M., et al. (2015). A conserved core of programmed cell death indicator genes discriminates developmentally and environmentally induced programmed cell death in plants. *Plant Physiol.* 169, 2683–2699.

Papini, A., Tani, G., Falco, P. D., and Brighigna, L. (2010). The ultrastructure of the development of *Tillandsia* (*Bromeliaceae*) trichome. *Flora* 205, 94–100. doi: 10.1016/j.flora.2009.02.001

Petrov, V., Hille, J., Mueller-Roeber, B., and Gechev, T. S. (2015). ROS-mediated abiotic stress-induced programmed cell death in plants. *Front. Plant Sci.* 6:69. doi: 10.3389/fpls.2015.00069

Phan, H. A., Iacuone, S., Li, S. F., and Parish, R. W. (2011). The MYB80 transcription factor is required for pollen development and the regulation of tapetal programmed cell death in *Arabidopsis thaliana*. *Plant Cell* 23, 2209–2224. doi: 10.1105/tpc.110.082651

Radchuk, V., Weier, D., Radchuk, R., Weschke, W., and Weber, H. (2011). Development of maternal seed tissue in barley is mediated by regulated cell expansion and cell disintegration and coordinated with endosperm growth. *J. Exp. Bot.* 62, 1217–1227. doi: 10.1093/jxb/erq348

Radojičić, A., Li, X., and Zhang, Y. (2018). Salicylic acid: a double-edged sword for programed cell death in plants. *Front. Plant Sci.* 9:1133. doi: 10.3389/fpls.2018.01133

Rantong, G., Evans, R., and Gunawardena, A. H. L. A. N. (2015). Lace plant ethylene receptors, AmERS1a and AmERS1c, regulate ethylene-induced programmed cell death during leaf morphogenesis. *Plant Mol. Biol.* 89, 215–227. doi: 10.1007/s11103-015-0356-4

Rantong, G., and Gunawardena, A. H. L. A. N. (2018). Vacuolar processing enzymes, AmVPE1 and AmVPE2, as potential executors of ethylene regulated programmed cell death in the lace plant (*Aponogeton madagascariensis*). *Botany* 96, 235–247. doi: 10.1139/cjb-2017-0184

Rauf, M., Arif, M., Dortay, H., Matallana-Ramírez, L. P., Waters, M. T., Nam, H. G., et al. (2013). ORE1 balances leaf senescence against maintenance by antagonizing G2-like-mediated transcription. *EMBO Rep.* 14, 382–388. doi: 10.1038/embor.2013.24

Ravichandran, S. J., Linh, N. M., and Scarpella, E. (2020). The canalization hypothesis-challenges and alternatives. *New Phytol.* 227, 1051–1059. doi: 10.1111/nph.16605

Sheldrake, A. R. (2021). The production of auxin by dying cells. *J. Exp. Bot.* 72, 2288–2300. doi: 10.1093/jxb/erab009

Steffens, B., and Sauter, M. (2005). Epidermal cell death in rice is regulated by ethylene, gibberellin, and abscisic acid. *Plant Physiol.* 139, 713–721. doi: 10.1104/pp.105.064469

Uslu, V. V., and Grossmann, G. (2016). The biosensor toolbox for plant developmental biology. *Curr. Opin. Plant Biol.* 29, 138–147. doi: 10.1016/j.pbi.2015.12.001

Uzair, M., Xu, D., Schreiber, L., Shi, J., Liang, W., Jung, K., et al. (2020). PERSISTENT TAPETAL CELL 2 is required for normal tapetal programmed cell death and pollen wall patterning. *Plant Physiol.* 182, 962–976. doi: 10.1104/pp.19.00688

Vanneste, S., and Friml, J. (2009). Auxin: a trigger for change in plant development. *Cell* 136, 1005–1016. doi: 10.1016/j.cell.2009.03.001

Vescovi, M., Riefler, M., Gessuti, M., Novak, O., Schmulling, T., and Schiavo, L. F. (2012). Programmed cell death induced by high levels of cytokinin in *Arabidopsis* cultured cells is mediated by the cytokinin receptor CRE1/AHK4. *J. Exp. Bot.* 63, 2825–2832. doi: 10.1093/jxb/ers008

Wang, D. H., Li, F., Duan, Q. H., Han, T., Xu, Z. H., and Bai, S. N. (2010). Ethylene perception is involved in female cucumber flower development. *Plant J.* 61, 862–872. doi: 10.1111/j.1365-313x.2009.04114.x

Wang, Y., Liu, R., Chen, L., Liang, Y., Wu, X., Li, B., et al. (2009). Nicotiana tabacum TTG1 contributes to ParA1-induced signalling and cell death in leaf trichomes. *J. Cell Sci.* 122, 2673–2685. doi: 10.1242/jcs.049023

Wang, Y., Ye, H., Bai, J., and Ren, F. (2021). The regulatory framework of developmentally programmed cell death in floral organs: a review. *Plant Physiol. Biochem.* 158, 103–112. doi: 10.1016/j.plaphy.2020.11.052

Wilkins, K. A., Bancroft, J., Bosch, M., Ings, J., Smirnoff, N., and Franklintong, V. E. (2011). ROS and NO mediate actin reorganization and programmed cell death in the self-incompatibility response of *Papaver*. *Plant Physiol.* 156, 404–416. doi: 10.1104/pp.110.167510

Wilkins, K. A., Bosch, M., Haque, T., Teng, N., Poulter, N. S., and Franklin-Tong, V. E. (2015). Self-incompatibility-induced programmed cell death in *Papaver* pollen involves dramatic acidification of the incompatible pollen tube cytosol. *Plant Physiol.* 167, 766–779. doi: 10.1104/pp.114.252742

Woo, H. R., Kim, H. J., Lim, P. O., and Nam, H. G. (2019). Leaf senescence: systems and dynamics aspects. *Annu. Rev. Plant Biol.* 70, 15.11–15.30.

Xie, H. T., Wan, Z. Y., Li, S., and Zhang, Y. (2014). Spatiotemporal production of reactive oxygen species by NADPH oxidase is critical for tapetal programmed cell death and pollen development in *Arabidopsis*. *Plant Cell* 26, 2007–2023. doi: 10.1105/tpc.114.125427

Xie, X., Zhang, Z., Zhao, Z., Xie, Y., Li, H., Ma, X., et al. (2020). The mitochondrial aldehyde dehydrogenase OsALDH2b negatively regulates tapetum degeneration in rice. *J. Exp. Bot.* 71, 2551–2560. doi: 10.1093/jxb/eraa045

Xuan, W., Band, L. R., Kumpf, R. P., Damme, D. V., Parizot, B., Rop, G. D., et al. (2016). Cyclic programmed cell death stimulates hormone signaling and root development in *Arabidopsis*. *Science* 351, 384–387. doi: 10.1126/science.aad2776

Yin, L. L., and Xue, H. W. (2012). The *MADS29* transcription factor regulates the degradation of the nucellus and the nucellar projection during rice seed development. *Plant Cell* 24, 1049–1065. doi: 10.1105/tpc.111.094854

Zhang, D., Di, L., Lv, X., Wang, Y., Xun, Z., Liu, Z., et al. (2014). The cysteine protease CEP1, a key executor involved in tapetal programmed cell death, regulates pollen development in *Arabidopsis*. *Plant Cell* 26, 2939–2961. doi: 10.1105/tpc.114.127282

Zhang, J., Xie, M., Tuskan, G. A., Muchero, W., and Chen, J. G. (2018a). Recent advances in the transcriptional regulation of secondary cell wall biosynthesis in the woody plants. *Front. Plant Sci.* 9:1535. doi: 10.3389/fpls.2018.01535

Zhang, J., Yang, Y., Zheng, K., Xie, M., Feng, K., Jawdy, S. S., et al. (2018b). Genome-wide association studies and expression-based quantitative trait loci analyses

reveal roles of HCT2 in caffeoylquinic acid biosynthesis and its regulation by defense-responsive transcription factors in Populus. *New Phytol.* 220, 502–516. doi: 10.1111/nph.15297

Zhong, R., Lee, C., and Ye, Z. H. (2010). Global analysis of direct targets of secondary wall NAC master switches in *Arabidopsis*. *Mol. Plant* 3, 1087–1103. doi: 10.1093/mp/ssq062

Zhong, R., Richardson, E. A., and Ye, Z. H. (2007). The MYB46 transcription factor is a direct target of SND1 and regulates secondary wall biosynthesis in *Arabidopsis*. *Plant Cell* 19, 2776–2792. doi: 10.1105/tpc.107.053678

Conflict of Interest: The authors declare that the research was conducted in the absence of any commercial or financial relationships that could be construed as a potential conflict of interest.

Publisher's Note: All claims expressed in this article are solely those of the authors and do not necessarily represent those of their affiliated organizations, or those of the publisher, the editors and the reviewers. Any product that may be evaluated in this article, or claim that may be made by its manufacturer, is not guaranteed or endorsed by the publisher.

frontiers in Plant Science

MINI REVIEW
published: 18 August 2021
doi: 10.3389/fpls.2021.700928

Vascular Cambium: The Source of Wood Formation

Dian Wang[1], Yan Chen[2], Wei Li[3], Quanzi Li[4], Mengzhu Lu[5], Gongke Zhou[6] and Guohua Chai[6]**

[1]College of Agronomy, Qingdao Agricultural University, Qingdao, China, [2]College of Landscape Architecture and Forestry, Qingdao Agricultural University, Qingdao, China, [3]State Key Laboratory of Tree Genetics and Breeding, Northeast Forestry University, Harbin, China, [4]State Key Laboratory of Tree Genetics and Breeding, Chinese Academy of Forestry, Beijing, China, [5]State Key Laboratory of Subtropical Silviculture, School of Forestry and Biotechnology, Zhejiang A&F University, Hangzhou, China, [6]College of Resources and Environment, Qingdao Agricultural University, Qingdao, China

Wood is the most abundant biomass produced by land plants and is mainly used for timber, pulping, and paper making. Wood (secondary xylem) is derived from vascular cambium, and its formation encompasses a series of developmental processes. Extensive studies in *Arabidopsis* and trees demonstrate that the initiation of vascular stem cells and the proliferation and differentiation of the cambial derivative cells require a coordination of multiple signals, including hormones and peptides. In this mini review, we described the recent discoveries on the regulation of the three developmental processes by several signals, such as auxin, cytokinins, brassinosteroids, gibberellins, ethylene, TDIF peptide, and their cross talk in *Arabidopsis* and *Populus*. There exists a similar but more complex regulatory network orchestrating vascular cambium development in *Populus* than that in *Arabidopsis*. We end up with a look at the future research prospects of vascular cambium in perennial woody plants, including interfascicular cambium development and vascular stem cell regulation.

Keywords: wood, vascular cambium, hormones and peptides, cross talk regulation, *Arabidopsis* and *Populus*

OPEN ACCESS

Edited by:
Raju Datla, Global Institute for Food Security (GIFS), Canada

Reviewed by:
Melis Kucukoglu, University of Helsinki, Finland
Célia M. Miguel, University of Lisbon, Portugal

***Correspondence:**
Guohua Chai
chaigh@qau.edu.cn
Gongke Zhou
zhougk@qau.edu.cn

Specialty section:
This article was submitted to Plant Development and EvoDevo, a section of the journal Frontiers in Plant Science

Received: *27 April 2021*
Accepted: *27 July 2021*
Published: *18 August 2021*

Citation:
Wang D, Chen Y, Li W, Li Q, Lu M, Zhou G and Chai G (2021) Vascular Cambium: The Source of Wood Formation. Front. Plant Sci. 12:700928. doi: 10.3389/fpls.2021.700928

INTRODUCTION

Vascular plants, particularly tree species, undergo two distinct phases of growth and development. During primary growth, shoot apical meristems (SAMs) and root apical meristems (RAMs) are responsible for the aboveground and underground organ growth, respectively. At the peripheral region of SAM, procambium cells produce primary vascular bundles (**Figure 1**; also see Nieminen et al., 2015). After the primary vascular system is established, fascicular cambium located at the center of primary vascular bundles undergoes extension into the interfascicular region, forming a ring of vascular cambium (**Figure 1**; Nieminen et al., 2015). Vascular cambium is a cylindrical secondary meristem whose activity gives rise to the secondary growth. Like SAM and RAM, vascular cambium contains bifacial cambium stem cells in *Arabidopsis* (Shi et al., 2019; Smetana et al., 2019). However, stem cell activities of the three types of meristems are preferentially regulated by different members of the WUSCHEL-RELATED HOMEOBOX (WOX) and CLAVATA3/EMBRYO SURROUNDING REGION-RELATED (CLE) gene families: SAM is associated with WUSCHEL (WUS) and CLAVATA3 (CLV3; Mayer et al., 1998; Schoof et al., 2000), RAM with WOX5 and

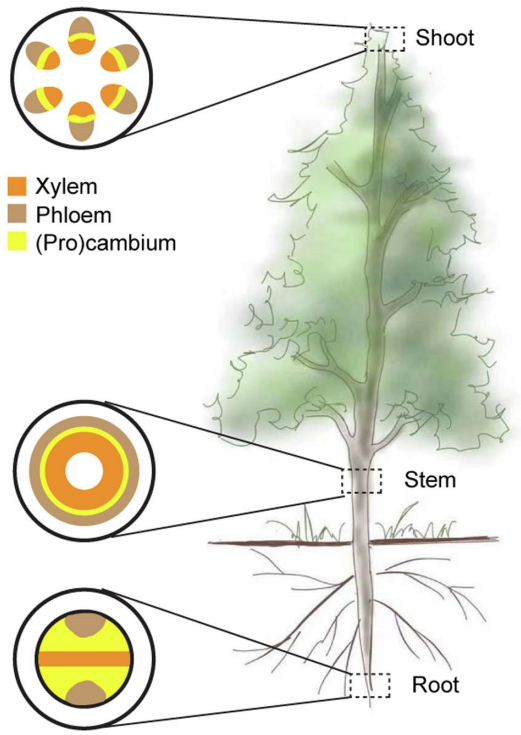

FIGURE 1 | A schematic view of vascular tissue organization in shoot, stem, and root of vascular plants. Xylem and phloem tissues are initiated from procambium in vascular plants. Shoot apical meristems and root apical meristems are two primary meristems, and vascular cambium is a cylindrical secondary meristem in stems. The xylem is represented in orange, the phloem in brown, and the cambium in yellow.

CLE40 (Sarkar et al., 2007; Berckmans et al., 2020), and vascular cambium with WOX4 and CLE41/44 (Hirakawa et al., 2010; Ji et al., 2010).

Secondary xylem (wood) and phloem are the inner and outer derivative products of the vascular cambium. Xylem is mainly comprised with dead cells with thickened cell walls rich in cellulose, hemicelluloses, and lignin and responsible for providing mechanical support and conducting water and minerals for the plant. Phloem transports photoassimilates and signaling molecules, including phytohormones and peptides, from the source organs to the sink organs. Fusiform initials and ray initials are morphologically distinct meristematic cells in vascular cambium of woody stems (Mauseth, 2016). The fusiform initials (>90% of the vascular cambium) are oriented longitudinally relative to the stem and undergo periclinal divisions that produce phloem and xylem mother cells (Mizrachi and Myburg, 2016; Fischer et al., 2019). The ray initials are isodiametric and produce the radially orientated ray cells that serve radial transport and storage.

The activity of the vascular cambium is regulated by endogenous developmental programs and environmental cues. In recent years, considerable progress in the molecular mechanism of the development of vascular cambium has been achieved in the model plants *Arabidopsis* and *Populus*. It has been shown that the establishment and maintenance of vascular cambium involve the coordination of multiple regulators, including hormones, peptides, and transcription factors (**Figure 2**; also see the reviews by Miyashima et al., 2013; Mizrachi and Myburg, 2016; Chiang and Greb, 2019). However, our knowledge about the development and regulation of vascular cambium, compared to SAM and RAM, is limited. This mini review focuses on recent progresses in the regulatory networks responsible for the vascular cambium identity and activity in poplar.

ESTABLISHMENT OF THE VASCULAR CAMBIUM

Because vascular procambial cells are imbedded under layers of other tissues in stems, our current understanding of procambium initiation and regulation is derived from studies in *Arabidopsis* embryos, RAMs, and leaf venation systems. Functional characterization of a serial of *Arabidopsis* mutants shows that vascular cambium initiation requires the cross talk regulation of multiple hormones (**Figure 2A**). Auxin plays a central role in regulating the initiation and maintenance of procambial stem cells (Ibañes et al., 2009; Weijers and Wagner, 2016). In pre-procambial strands, MONOPTEROS (MP)/AUXIN RESPONSE FACTOR 5 (ARF5) is activated in response to auxin and positively regulates the number of vascular initial cells through induction of the expression of the auxin efflux carrier gene *PIN-FORMED1* (*PIN1*; Wenzel et al., 2007). Periodic auxin maxima controlled by polar transport but not overall auxin levels is required to determine the radial pattern of vascular bundles in postembryonic growth (Ibañes et al., 2009). MP/ARF5 positively regulates TARGET OF MONOPTEROS 5 (TMO5), which forms a dimer complex with LONESOME HIGHWAY (LHW) to control the procambium cell divisions in roots (De Rybel et al., 2014; Ohashi-Ito et al., 2014). MP/ARF5 activates ATHB8-targeted PIN1 in response to auxin, forming a self-reinforcing mechanism of auxin flow during the formation of vein procambium (Donner et al., 2009). ATHB8, a HD-ZIP III transcription factor, is shown to restrict preprocambial cell specification to a narrow zone and stabilize preprocambial cell fate (Baima et al., 2001; Donner et al., 2009). *REVOLUTA* is another member of the *Arabidopsis* HD-ZIP III gene family, and its *Populus* ortholog, *PopREVOLUTA*, influences vascular cambium initiation in *Populus* stems (Robischon et al., 2011).

Cytokinin (CK) is another major hormone that regulates procambium identity and activity in *Arabidopsis* (**Figure 2A**). Mutation of three CK receptor genes *CYTOKININ RESPONSE 1* (*CRE1*), *ARABIDOPSIS HISTIDINE KINASE 2* (*AHK2*), and *AHK3* results in a severely reduced numbers of periclinal divisions in the procambium cells of the primary roots (Inoue et al., 2001). Accordingly, transgenic *Arabidopsis* plants overexpressing *CYTOKININ OXIDASES/DEHYDROGENASES 2* (*CKX2*), a CK degrading enzyme gene, under the control of *CRE1* promoter show the *cre1ahk2ahk3* phenotype (Mähönen et al., 2006). Moreover, the establishment of

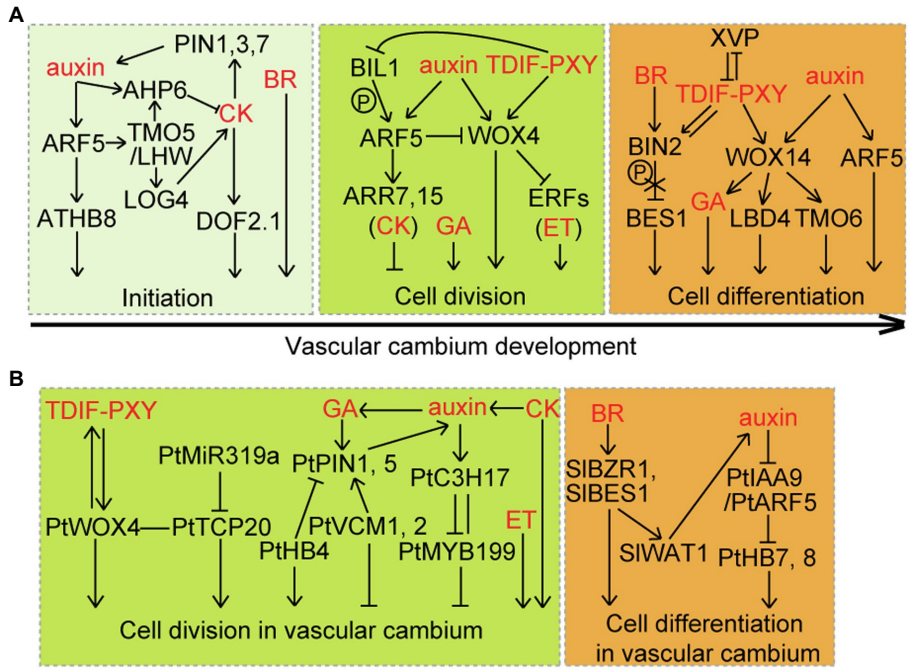

FIGURE 2 | Coordination of multilayered signaling pathways on vascular cambium. **(A)** In *Arabidopsis*, vascular cambium initiation and the proliferation and differentiation of cambia derivative cells require a coordination of multiple signals, including auxin, cytokinin (CK), brassinosteroid (BR), gibberellin (GA), ethylene (ET), and TDIF-PXY. TDIF peptides are synthesized in the phloem and move to the cambium at which they bind to the PXY receptor. **(B)** Cross talk regulation of cell division and differentiation by multiple signals in the vascular cambium of *Populus* (Pt) and tomato (Sl) stems. There is a similar but more complex regulatory network orchestrating vascular cambium development in *Populus* than that in *Arabidopsis*.

procambium cell identity requires a mutually inhibitory interaction between CK and auxin signaling (**Figure 2A**). Reduced CK signaling changes the subcellular polarity of PIN1, PIN3, and PIN7, while auxin is able to activate the expression of *ARABIDOPSIS HISTIDINE PHOSPHOTRANSFER 6* (*AHP6*), an inhibitor of CK signaling (Mähönen et al., 2006; Bishopp et al., 2011). Auxin-induced TMO5/LHW dimer directly activates *LONELY GUY 4* (*LOG4*) that encodes for a rate-limiting enzyme in CK biosynthesis (De Rybel et al., 2014). CK-dependent procambium cell divisions are controlled by the DOF transcription factor DOF2.1 downstream of TMO5/LHW (Smet et al., 2019).

Brassinosteroids (BRs) serve as a key promoting signal for procambial division during primary growth (**Figure 2A**). In the stem of *Arabidopsis*, the number of vascular bundles (VB) is obviously increased in gain-of-function BR-signaling mutants, such as *brassinosteroid insensitive 2* (*bin2*) and *brassinazole-resistant 1-1D* (*bzr1-1D*), while loss-of-function BR-signaling mutant *brassinosteroid insensitive 1-116* (*bri1-116*) and BR synthesis mutant *constitutive photomorphogenesis and dwarfism* (*cpd*) have fewer VBs than wild-type plants (Ibañes et al., 2009).

REGULATION OF VASCULAR CAMBIUM ACTIVITY

Trees display prominent secondary growth in the stem and root, with similar vascular cell types to *Arabidopsis* (Mizrachi and Myburg, 2016). Studies in *Arabidopsis* stems and roots indicate an important regulatory function for hormones (auxin, CK, and ethylene) and TRACHEARY ELEMENT DIFFERENTIATION INHIBITORY FACTOR (TDIF) peptide in the proliferation of vascular cambium (Ortega-Martinez et al., 2007; Matsumoto-Kitano et al., 2008; Suer et al., 2011; Fischer et al., 2019; Smetana et al., 2019). WOX4 is considered to be a central regulator of vascular cambium division (**Figure 2A**), because it activates a cambium-specific transcriptional network and integrates auxin, ethylene, and TDIF-PXY (PHLOEM INTERCALATED WITH XYLEM) signaling for cambium division (Hirakawa et al., 2010; Ji et al., 2010; Suer et al., 2011; Etchells et al., 2012; Brackmann et al., 2018; Zhang et al., 2019). WOX4 is required for auxin-dependent stimulation of cambium activity (Suer et al., 2011). Auxin-induced MP/ARF5 directly attenuates the activity of the stem cell-promoting *WOX4* gene, and cell-autonomously restricts the number of stem cells in stems (Brackmann et al., 2018). The TDIF peptides encoded by *CLE41* and *CLE44* are synthesized in the phloem and travel to the cambium where they bind and activate PXY, stimulating *WOX4* transcription and promoting cambium proliferation in stems (Hirakawa et al., 2010). Ethylene and TDIF signaling converge at WOX4 to regulate cambium activity (Etchells et al., 2012; Yang et al., 2020b). BIN2-LIKE 1 (BIL1), a glycogen synthase kinase 3, functions as a mediator that links auxin-CK signaling with TDIF-PXY signaling for the maintenance of cambial activity (Han et al., 2018).

Phosphorylation of MP/ARF5 by BIL1 enhances its negative effect on the activity of vascular cambial, which upregulates ARABIDOPSIS RESPONSE REGULATOR 7 (ARR7) and ARR15, two negative regulators of CK signaling. BIL1 activity is inhibited by PXY, attenuating the effect of MP/ARF5 on *ARR7* and *ARR15* expressions and increasing vascular cambial activities.

Regulation of vascular cambium activity by auxin, CK, ethylene, and TDIF-PXY signaling is relatively conserved between trees and *Arabidopsis* (**Figure 2**). Auxin shows the highest level at the cambium zone, and its level declines near the mature xylem cells during wood formation in trees (Nilsson et al., 2008; Immanen et al., 2016). Overexpression of the stabilized form of INDOLE ACETIC ACID 3 (IAA3) that perturbs auxin signaling in hybrid aspen represses periclinal division of cambial cells but enlarges cell file harboring anticlinal cell division (Nilsson et al., 2008). Auxin-responsive *Pa*C3H17-*Pa*MYB199 module promotes cambium division by a dual regulatory mechanism in *Populus* stems (Tang et al., 2020). Auxin promotes direct repression of *PaMYB199* expression by *Pa*C3H17 and also enhances the *Pa*C3H17-*Pa*MYB199 interaction, attenuating *Pa*MYB199 inhibition of cambial cell division. Consistent with this, dominant repressors of *Pa*C3H17 or overexpression of *PaMYB199* result in a reduction in the number of cambial cell layers, while transgenic poplars overexpressing *PaC3H17* or repressing *PaMYB199* have the opposite phenotype. In addition, the regulation of vascular cambium activity is associated with feedback mediation of auxin homeostasis in trees. Downregulation of the *Populus* HD-ZIP III gene *PtrHB4* enhances *PtrPIN1* expression and causes drastic defects in interfascicular cambium, indicating that *Ptr*HB4 induces interfascicular cambium formation during the development of the secondary vascular system (Zhu et al., 2018). VASCULAR CAMBIUM-RELATED MADS 1 (VCM1) and VCM2 inhibit vascular cambium proliferation activity and secondary growth through direct upregulation of *PtrPIN5* expression in *Populus* stems (Zheng et al., 2021). These findings indicate more fine regulation of cambial activity by auxin signaling in trees than in *Arabidopsis*.

CK is another important regulator of cambial activity during wood formation (**Figure 2B**). Inhibition of cambial CK signaling by overexpression of *Arabidopsis AtCKX2* under the promoter of a birch *CRE1* gene leads to a reduced number of cambial cells in poplar stems, while increased vascular division is observed in transgenic poplars expressing the *Arabidopsis* CK biosynthetic gene *ISOPENTENYL TRANSFERASE 7* (*IPT7*) under the control of the cambium-specific *PttLMX5* promoter (Nieminen et al., 2008; Immanen et al., 2016). Elevated CK levels cause an increase of auxin level at the cambium zone, highlighting the interconnected nature of auxin and CK gradients (Immanen et al., 2016). A recent study uncovers the mechanism of CK signaling associated with its spatial enrichment to regulate vascular development in *Populus* (Fu et al., 2021). The local CK signaling in the developing secondary phloem regulates the activity of vascular cambium in a non-cell-autonomous manner.

In addition to auxin and CK, gibberellin (GA), ethylene, and TDIF-PXY signaling promote cambial cell division and radial growth in trees (**Figure 2B**). Transgenic poplar lines overexpressing *GA 20-OXIDASE*, encoding a GA biosynthesis enzyme, promote over-production of GA and cambium proliferation (Eriksson et al., 2000). Ethylene-overproducing and ethylene-insensitive poplars show increased and reduced cambium division, respectively (Love et al., 2009). Overexpression of *Ptt*CLE41, a TDIF-like peptide, together with its receptor *Ptt*PXYa affects the rate of cambial cell division and woody tissue organization in both hybrid aspen and poplar (Etchells et al., 2015; Kucukoglu et al., 2017). *Ptt*WOX4 stimulates the cambium proliferation downstream of TDIF-PXY signaling, as is similar to the manner of the *Arabidopsis* TDIF-PXY-WOX module. One difference is that in *Populus, PttWOX4a/b* expression is not responsive to auxin treatments, but upstream genes, such as *PttPXYa* and *PttCLE41a/d*, are responsive (Kucukoglu et al., 2017). The cross talk of hormones in regulation of cambium activity was also found in trees. For instance, GA coordinates with auxin for inducing cambium division through upregulating 83% of auxin-responsive genes, including *PttPIN1*, while auxin treatment upregulates GA biosynthesis genes and downregulates GA degradation genes in wood-forming tissues (Björklund et al., 2007).

REGULATION OF CAMBIUM DERIVATIVE CELLS DIFFERENTIATION

The regulatory roles of auxin, BR, and GA in cell differentiation in the vascular cambium are studied in *Arabidopsis* or/and trees (**Figure 2**). Since 20 years ago, the IAA12/BODENLOS (BDL)-ARF5/MP module in auxin signaling has been identified to control provascular specification and patterning during embryo-genesis in *Arabidopsis* (Hardtke and Berleth, 1998). Recently, the *Pto*IAA9-*Pto*ARF5 module from *Populus* has been validated to mediate auxin-triggered cell differentiation of early developing xylem (Xu et al., 2019). With auxin treatment, *Pto*IAA9 protein is degraded, inducing *Pto*ARF5-activated gene expression, and the activated *PtoIAA9* switches-off auxin signaling in a self-controlled manner during wood formation. BRs play a regulatory role in differentiation of vascular tissues, in addition to inducing cambium initiation during primary growth. Mutation of both BRI-LIKE 1 (BRL1) and BRL3, two *Arabidopsis* vascular-specific BR receptors, causes expanded phloem development at the expense of xylem in stems (Cano-Delgado et al., 2004). *bri1-ethylmethylsulfone-suppressor 1-D* (*bes1-D*), a gain-of-function BR-signaling mutants, exhibits an increase of xylem differentiation (Kondo et al., 2014). Similarly, inhibition of BR synthesis results in decreased secondary vascular differentiation and cell wall biosynthesis, while elevated BR levels cause increases in secondary growth in *Populus* (Du et al., 2020). A recent study indicates that BR signaling is tightly connected with local intracellular auxin homeostasis during cell differentiation in the vascular cambium of tomato stems (Lee et al., 2021). BZR1/BES1-activated WALLS ARE THIN1 (WAT1), an auxin efflux carrier, facilitates cell differentiation in the vascular cambium by enhancing local auxin signaling. In addition, GA is shown to induce vascular cell differentiation and lignification downstream of *WOX14* gene in the stem of *Arabidopsis* (Mauriat and Moritz, 2009; Denis et al., 2017).

TDIF-PXY signaling is a mediator that induces cell differentiation in the vascular cambium in *Arabidopsis* (**Figure 2A**). Transgenic plants overexpressing *CLE41* or *CLE44* display abnormal vascular patterning with a xylem intermixed with phloem phenotype during both primary and secondary growths (Fisher and Turner, 2007; Etchells and Turner, 2010). TDIF signaling regulation of xylem differentiation is fine-tuned by the NAC transcription factor XYLEM DIFFERENTIATION AND ALTERED VASCULAR PATTERNING (XVP; Yang et al., 2020a). XVP negatively regulates the TDIF-PXY module, and it also forms a complex with TDIF co-receptors PXY-BAK1 (BRI1-associated receptor kinase 1). *XVP* expression is suppressed by TDIF by a feedback mechanism. Overexpression of *PttCLE41* or *PttPXY* (the orthologs to *Arabidopsis CLE41* and *PXY*, respectively) in hybrid aspen or poplar causes defects in the patterning of the vascular tissues and shows inhibited plant growth (Etchells et al., 2015; Kucukoglu et al., 2017), suggesting a similar regulation of xylem differentiation by the TDIF-PXY module in trees. The cross talk between TDIF-PXY signaling module and BR or auxin occurs in controlling vascular cell differentiation in *Arabidopsis* (**Figure 2A**). PXY physically interacts with BIN2 at the plasma membrane, and the treatments by TDIF peptide enhance the activity of BIN2 in a PXY-dependent manner (Kondo et al., 2014). Transcriptional regulatory network mediated by PXY comprises 690 transcription factor-promoter interactions, of which a feed-forward loop containing WOX14, TMO6 and their downstream gene LATERAL ORGAN BOUNDARIES DOMAIN4 (LBD4) determines the arrangement of vascular tissue (Smit et al., 2020).

The HD-ZIP III and NAC transcription factors are important regulators of vasculature organization. In *Arabidopsis* vascular tissues, mutation of one or several members of HD-ZIP III family results in an amphicribal vascular bundle pattern (phloem surrounding xylem), whereas gain-of-function mutants display amphivasal bundles (McConnell et al., 2001; Emery et al., 2003; Ramachandran et al., 2017). *PtrHB5* and *PtrHB7* are the orthologs of *Arabidopsis POPCORONA* and *AtHB8* in *Populus*, respectively. Both genes correspondingly induce cambium activity and xylem differentiation in stems during secondary growth (Du et al., 2011; Zhu et al., 2013). Interestingly, *PtrHB7* was identified as a direct target of the *Ptr*IAA9-*Ptr*ARF5 module during xylem cell differentiation (Xu et al., 2019). This places *Ptr*HB7 in the regulatory network of auxin-induced xylem differentiation in woody stems. The *Arabidopsis* NAC genes *VASCULAR-RELATED NAC DOMAINs* (*VNDs*) act as master regulators of xylem differentiation capable of switching on the developmental program (Kubo et al., 2005; Zhou et al., 2014), while other members of this family, *NAC SECONDARY WALL THICKENING PROMOTING FACTOR 1, 3* (*NST1, 3*), can promote fiber differentiation in stems (Zhong et al., 2006; Mitsuda et al., 2007). Four *Populus* orthologs of NST1/3 redundantly control SCW formation in xylem fibers, phloem fibers, and xylem ray parenchyma cells (Takata et al., 2019), indicating a conserved role of these NACs in wood formation. Some NAC genes impede xylem differentiation and secondary wall deposition involving *Pag*KNAT2/6b and *Pto*TCP20 in *Populus* (Hou et al., 2020; Zhao et al., 2020). *Pag*KNAT2/6b directly activates *PagXND1a* expression but represses *PagNST3s* and *PagVND6* expression in wood-forming tissues (Zhao et al., 2020). *Pto*TCP20 interacts with *Pto*WOX4a to control vascular cambium proliferation and also activates *PtoWND6* expression to promote secondary xylem differentiation (Hou et al., 2020).

FUTURE OUTLOOK

Wood formation of tree species involves a complex regulatory network underlying cambial initiation, tissue patterning, and cell differentiation. Understanding the vascular cambium development is a basis for genetic modification of wood biomass and properties in trees. Extensive studies in the model tree *Populus* indicate the cross talk regulation of vascular cambium development by multiple signals, including auxin, CK, BR, and TDIF-PXY, similar to regulatory programs of *Arabidopsis* vascular development (**Figure 2**). However, based on genome sequences, it is predicted that 1.4~1.6 *Populus* homologs correspond to each *Arabidopsis* gene (Tuskan et al., 2006). These *Populus* duplicated genes may undergo divergent fates, such as nonfunctionalization (loss of original functions), neofunctionalization (acquisition of novel functions), or subfunctionalization (partition of original functions). This may explain the emerging more complex mechanisms underlying vascular cambium maintenance and differentiation in trees than in *Arabidopsis*.

In recent years, the studies on the vascular cambium formation and regulation in trees have been greatly facilitated by new technologies, such as the genome-editing, integrated-omics, and more advanced microscopy. Therefore, the following key questions are anticipated to be addressed in the near future.

1. How do the interfascicular cambial cells function in woody stems?

With the onset of the secondary growth, fascicular cambia are interconnected with interfascicular cambia located between the vascular bundles, forming a complete vascular cambium in woody stems (**Figure 1**). The interfascicular cambia are known to originate from the parenchymatic cells in the interfascicular region. Currently, our understanding regarding how the parenchymatic cells differentiate and develop into new procambium strands in the interfascicular region is limited, compared with extensive studies on fascicular cambia. To our knowledge, the HD-ZIP III gene *PtrHB4* is the only gene that is shown to induce interfascicular cambium division in *Populus* stems (Zhu et al., 2018). Analysis of time-spatial features of parenchymatic cells action and mining the related genes in trees are essential in the future. The application of single-cell RNA sequencing, computational modeling, or biosensor may be helpful for addressing this question.

2. How is the vascular cambium activity maintained in trees?

Vascular cambium of trees is able to ensure both increased stem girth and annual renewal of vascular tissues over its lifespan. Even in 667-year-old *Ginkgo biloba* trees, the vascular cambium still maintains activity (Wang et al., 2020). A key question for wood biology is how vascular cambium activity maintained? In *Populus*, multiple signals mediate the coordinated regulation of vascular cambium activity, as is more complex than that in *Arabidopsis* (**Figure 2**). It is therefore critical to investigate what signals and how these signals drive the activity of cambial stem cells under certain circumstances? Identification of reliable cell-specific makers thus to analyze gene expression

in each layer of cambial cells is essential for understanding the gene regulation of vascular stem cells in trees.

AUTHOR CONTRIBUTIONS

DW and GC drafted the manuscript. GZ, YC, WL, QL, and ML edited the manuscript. All authors approved the final version.

FUNDING

Financial support for this work was obtained from the National Key Scientific Research Project of China (2016YFD0600104), the National Natural Science Foundation of China (31972955, 31770315, 31972860, and 31900227), the Taishan Scholar Program of Shandong (tsqn202103092), and First Class Grassland Science Discipline Program of Shandong Province.

REFERENCES

Baima, S., Possenti, M., Matteucci, A., Wisman, E., Altamura, M. M., Ruberti, I., et al. (2001). The Arabidopsis ATHB-8 HD-zip protein acts as a differentiation-promoting transcription factor of the vascular meristems. *Plant Physiol.* 126, 643–655. doi: 10.1104/pp.126.2.643

Berckmans, B., Kirschner, G., Gerlitz, N., Stadler, R., and Simon, R. (2020). CLE40 signaling regulates root stem cell fate. *Plant Physiol.* 182, 1776–1792. doi: 10.1104/pp.19.00914

Bishopp, A., Help, H., El-Showk, S., Weijers, D., Scheres, B., Friml, J., et al. (2011). A mutually inhibitory interaction between auxin and cytokinin specifies vascular pattern in roots. *Curr. Biol.* 21, 917–926. doi: 10.1016/j.cub.2011.04.017

Björklund, S., Antti, H., Uddestrand, I., Moritz, T., and Sundberg, B. (2007). Cross-talk between gibberellin and auxin in development of *Populus* wood: gibberellin stimulates polar auxin transport and has a common transcriptome with auxin. *Plant J.* 52, 499–511. doi: 10.1111/j.1365-313X.2007.03250.x

Brackmann, K., Qi, J., Gebert, M., Jouannet, V., Schlamp, T., Grunwald, K., et al. (2018). Spatial specificity of auxin responses coordinates wood formation. *Nat. Commun.* 9:875. doi: 10.1038/s41467-018-03256-2

Cano-Delgado, A., Yin, Y., Yu, C., Vafeados, D., Mora-Garcia, S., Cheng, J. C., et al. (2004). BRL1 and BRL3 are novel brassinosteroid receptors that function in vascular differentiation in Arabidopsis. *Development* 131, 5341–5351. doi: 10.1242/dev.01403

Chiang, M. H., and Greb, T. (2019). How to organize bidirectional tissue production? *Curr. Opin. Plant Biol.* 51, 15–21. doi: 10.1016/j.pbi.2019.03.003

De Rybel, B., Adibi, M., Breda, A. S., Wendrich, J. R., Smit, M. E., Novák, O., et al. (2014). Plant development. Integration of growth and patterning during vascular tissue formation in Arabidopsis. *Science* 345:1255215. doi: 10.1126/science.1255215

Denis, E., Kbiri, N., Mary, V., Claisse, G., Silva, N. C., Kreis, M., et al. (2017). WOX14 promotes bioactive gibbrellin synthesis and vascular cell differentiation in Arabidopsis. *Plant J.* 90, 560–572. doi: 10.1111/tpj.13513

Donner, T. J., Sherr, I., and Scarpella, E. (2009). Regulation of preprocambial cell state acquisition by auxin signaling in Arabidopsis leaves. *Development* 136, 3235–3246. doi: 10.1242/dev.037028

Du, J., Gerttula, S., Li, Z., Zhao, S., Liu, Y., Liu, Y., et al. (2020). Brassinosteroid regulation of wood formation in poplar. *New Phytol.* 225, 1516–1530. doi: 10.1111/nph.15936

Du, J., Miura, E., Robischon, M., Martinez, C., and Groover, A. (2011). The *Populus* Class III HD ZIP transcription factor POPCORONA affects cell differentiation during secondary growth of woody stems. *PLoS One* 6:e17458. doi: 10.1371/journal.pone.0017458

Emery, J. F., Floyd, S. K., Alvarez, J., Eshed, Y., Hawker, N. P., Izhaki, A., et al. (2003). Radial patterning of Arabidopsis shoots by class III HD-ZIP and KANADI genes. *Curr. Biol.* 13, 1768–1774. doi: 10.1016/j.cub.2003.09.035

Eriksson, M. E., Israelsson, M., Olsson, O., and Moritz, T. (2000). Increased gibberellin biosynthesis in transgenic trees promotes growth, biomass production and xylem fiber length. *Nat. Biotechnol.* 18, 784–788. doi: 10.1038/77355

Etchells, J. P., Mishra, L. S., Kumar, M., Campbell, L., and Turner, S. R. (2015). Wood formation in trees is increased by manipulating PXY-regulated cell division. *Curr. Biol.* 25, 1050–1055. doi: 10.1016/j.cub.2015.02.023

Etchells, J. P., Provost, C. M., and Turner, S. R. (2012). Plant vascular cell division is maintained by an interaction between PXY and ethylene signalling. *PLoS Genet.* 8:e1002997. doi: 10.1371/journal.pgen.1002997

Etchells, J. P., and Turner, S. R. (2010). The PXY-CLE41 receptor ligand pair defines a multifunctional pathway that controls the rate and orientation of vascular cell division. *Development* 137, 767–774. doi: 10.1242/dev.044941

Fischer, U., Kucukoglu, M., Helariutta, Y., and Bhalerao, R. P. (2019). The dynamics of cambial stem cell activity. *Annu. Rev. Plant Biol.* 70, 293–319. doi: 10.1146/annurev-arplant-050718-100402

Fisher, K., and Turner, S. (2007). PXY, a receptor-like kinase essential for maintaining polarity during plant vascular-tissue development. *Curr. Biol.* 17, 1061–1066. doi: 10.1016/j.cub.2007.05.049

Fu, X., Su, H., Liu, S., Du, X., Xu, C., and Luo, K. (2021). Cytokinin signaling localized in phloem noncell-autonomously regulates cambial activity during secondary growth of *Populus* stems. *New Phytol.* 230, 1476–1488. doi: 10.1111/nph.17255

Han, S., Cho, H., Noh, J., Qi, J., Jung, H. J., Nam, H., et al. (2018). BIL1-mediated MP phosphorylation integrates PXY and cytokinin signalling in secondary growth. *Nat. Plants* 4, 605–614. doi: 10.1038/s41477-018-0180-3

Hardtke, C. S., and Berleth, T. (1998). The Arabidopsis gene MONOPTEROS encodes a transcription factor mediating embryo axis formation and vascular development. *EMBO J.* 17, 1405–1411. doi: 10.1093/emboj/17.5.1405

Hirakawa, Y., Kondo, Y., and Fukuda, H. (2010). TDIF peptide signaling regulates vascular stem cell proliferation via the WOX4 homeobox gene in Arabidopsis. *Plant Cell* 22, 2618–2629. doi: 10.1105/tpc.110.076083

Hou, J., Xu, H., Fan, D., Ran, L., Li, J., Wu, S., et al. (2020). MiR319a-targeted PtoTCP20 regulates secondary growth via interactions with PtoWOX4 and PtoWND6 in *Populus tomentosa*. *New Phytol.* 228, 1354–1368. doi: 10.1111/nph.16782

Ibañes, M., Fàbregas, N., Chory, J., and Caño-Delgado, A. I. (2009). Brassinosteroid signaling and auxin transport are required to establish the periodic pattern of Arabidopsis shoot vascular bundles. *Proc. Natl. Acad. Sci. U. S. A.* 106, 13630–13635. doi: 10.1073/pnas.0906416106

Immanen, J., Nieminen, K., Smolander, O. P., Kojima, M., Alonso Serra, J., Koskinen, P., et al. (2016). Cytokinin and auxin display distinct but interconnected distribution and signaling profiles to stimulate cambial activity. *Curr. Biol.* 26, 1990–1997. doi: 10.1016/j.cub.2016.05.053

Inoue, T., Higuchi, M., Hashimoto, Y., Seki, M., Kobayashi, M., Kato, T., et al. (2001). Identification of CRE1 as a cytokinin receptor from Arabidopsis. *Nature* 409, 1060–1063. doi: 10.1038/35059117

Ji, J., Strable, J., Shimizu, R., Koenig, D., Sinha, N., and Scanlon, M. J. (2010). WOX4 promotes procambial development. *Plant Physiol.* 152, 1346–1356. doi: 10.1104/pp.109.149641

Kondo, Y., Ito, T., Nakagami, H., Hirakawa, Y., Saito, M., Tamaki, T., et al. (2014). Plant GSK3 proteins regulate xylem cell differentiation downstream of TDIF-TDR signalling. *Nat. Commun.* 5:3504. doi: 10.1038/ncomms4504

Kubo, M., Udagawa, M., Nishikubo, N., Horiguchi, G., Yamaguchi, M., Ito, J., et al. (2005). Transcription switches for protoxylem and metaxylem vessel formation. *Genes Dev.* 19, 1855–1860. doi: 10.1101/gad.1331305

Kucukoglu, M., Nilsson, J., Zheng, B., Chaabouni, S., and Nilsson, O. (2017). WUSCHEL-RELATED HOMEOBOX4 (WOX4)-like genes regulate cambial cell division activity and secondary growth in Populus trees. *New Phytol.* 215, 642–657. doi: 10.1111/nph.14631

Lee, J., Kim, H., Park, S. G., Hwang, H., Yoo, S. I., Bae, W., et al. (2021). Brassinosteroid-BZR1/2-WAT1 module determines the high level of auxin signalling in vascular cambium during wood formation. *New Phytol.* 230, 1503–1516. doi: 10.1111/nph.17265

Love, J., Björklund, S., Vahala, J., Hertzberg, M., Kangasjärvi, J., and Sundberg, B. (2009). Ethylene is an endogenous stimulator of cell division in the cambial meristem of *Populus*. *Proc. Natl. Acad. Sci. U. S. A.* 106, 5984–5989. doi: 10.1073/pnas.0811660106

Mähönen, A. P., Higuchi, M., Törmäkangas, K., Miyawaki, K., Pischke, M. S., Sussman, M. R., et al. (2006). Cytokinins regulate a bidirectional phosphorelay network in Arabidopsis. *Curr. Biol.* 16, 1116–1122. doi: 10.1016/j.cub.2006.04.030

Matsumoto-Kitano, M., Kusumoto, T., Tarkowski, P., Kinoshita-Tsujimura, K., Vaclavikova, K., Miyawaki, K., et al. (2008). Cytokinin kinins are central regulators of cambial activity. *Proc. Natl. Acad. Sci. U. S. A.* 105, 20027–20031. doi: 10.1073/pnas.0805619105

Mauriat, M., and Moritz, T. (2009). Analyses of GA20ox- and GID1-over-expressing aspen suggest that gibberellins play two distinct roles in wood formation. *Plant J.* 58, 989–1003. doi: 10.1111/j.1365-313X.2009.03836.x

Mauseth, J. D. (2016). *Botany: An Introduction to Plant Biology*. Burlington: Jones & Bartlett Learning.

Mayer, K. F. X., Schoof, H., Haecker, A., Lenhard, M., Jurgens, G., and Laux, T. (1998). Role of WUSCHEL in regulating stem cell fate in the Arabidopsis shoot meristem. *Cell* 95, 805–815. doi: 10.1016/S0092-8674(00)81703-1

McConnell, J. R., Emery, J., Eshed, Y., Bao, N., Bowman, J., and Barton, M. K. (2001). Role of PHABULOSA and PHAVOLUTA in determining radial patterning in shoots. *Nature* 411, 709–713. doi: 10.1038/35079635

Mitsuda, N., Iwase, A., Yamamoto, H., Yoshida, M., Seki, M., Shinozaki, K., et al. (2007). NAC transcription factors, NST1 and NST3, are key regulators of the formation of secondary walls in woody tissues of Arabidopsis. *Plant Cell* 19, 270–280. doi: 10.1105/tpc.106.047043

Miyashima, S., Sebastian, J., Lee, J. Y., and Helariutta, Y. (2013). Stem cell function during plant vascular development. *EMBO J.* 32, 178–193. doi: 10.1038/emboj.2012.301

Mizrachi, E., and Myburg, A. A. (2016). Systems genetics of wood formation. *Curr. Opin. Plant Biol.* 30, 94–100. doi: 10.1016/j.pbi.2016.02.007

Nieminen, K., Blomster, T., Helariutta, Y., and Mähönen, A. P. (2015). Vascular cambium development. *Arabidopsis Book* 13:e0177. doi: 10.1199/tab.0177

Nieminen, K., Immanen, J., Laxell, M., Kauppinen, L., Tarkowski, P., Dolezal, K., et al. (2008). Cytokinin signaling regulates cambial development in poplar. *Proc. Natl. Acad. Sci. U. S. A.* 105, 20032–20037. doi: 10.1073/pnas.0805617106

Nilsson, J., Karlberg, A., Antti, H., Lopez-Vernaza, M., Mellerowicz, E., Perrot-Rechenmann, C., et al. (2008). Dissecting the molecular basis of the regulation of wood formation by auxin in hybrid aspen. *Plant Cell* 20, 843–855. doi: 10.1105/tpc.107.055798

Ohashi-Ito, K., Saegusa, M., Iwamoto, K., Oda, Y., Katayama, H., Kojima, M., et al. (2014). A bHLH complex activates vascular cell division via cytokinin action in root apical meristem. *Curr. Biol.* 24, 2053–2058. doi: 10.1016/j.cub.2014.07.050

Ortega-Martinez, O., Pernas, M., Carol, R. J., and Dolan, L. (2007). Ethylene modulates stem cell division in the *Arabidopsis thaliana* root. *Science* 317, 507–510. doi: 10.1126/science.1143409

Ramachandran, P., Carlsbecker, A., and Etchells, J. P. (2017). Class III HD-ZIPs govern vascular cell fate: an HD view on patterning and differentiation. *J. Exp. Bot.* 68, 55–69. doi: 10.1093/jxb/erw370

Robischon, M., Du, J., Miura, E., and Groover, A. (2011). The *Populus* class III HD ZIP, popREVOLUTA, influences cambium initiation and patterning of woody stems. *Plant Physiol.* 155, 1214–1225. doi: 10.1104/pp.110.167007

Sarkar, A. K., Luijten, M., Miyashima, S., Lenhard, M., Hashimoto, T., Nakajima, K., et al. (2007). Conserved factors regulate signalling in *Arabidopsis thaliana* shoot and root stem cell organizers. *Nature* 446, 811–814. doi: 10.1038/nature05703

Schoof, H., Lenhard, M., Haecker, A., Mayer, K. F., Jurgens, G., and Laux, T. (2000). The stem cell population of Arabidopsis shoot meristems in maintained by a regulatory loop between the CLAVATA and WUSCHEL genes. *Cell* 10, 635–644. doi: 10.1016/s0092-8674(00)80700-x

Shi, D., Lebovka, I., López-Salmerón, V., Sanchez, P., and Greb, T. (2019). Bifacial cambium stem cells generate xylem and phloem during radial plant growth. *Development* 146:dev171355. doi: 10.1242/dev.171355

Smet, W., Sevilem, I., de Luis Balaguer, M. A., Wybouw, B., Mor, E., Miyashima, S., et al. (2019). DOF2.1 controls cytokinin-dependent vascular cell proliferation downstream of TMO5/LHW. *Curr. Biol.* 29, 520.e6–529.e6. doi: 10.1016/j.cub.2018.12.041

Smetana, O., Mäkilä, R., Lyu, M., Amiryousefi, A., Rodríguez, F. S., Wu, M. F., et al. (2019). High levels of auxin signalling define the stem-cell organizer of the vascular cambium. *Nature* 565, 485–489. doi: 10.1038/s41586-018-0837-0

Smit, M. E., McGregor, S. R., Sun, H., Gough, C., Bågman, A., Soyars, C. L., et al. (2020). A PXY-mediated transcriptional network integrates signaling mechanisms to control vascular development in Arabidopsis. *Plant Cell* 32, 319–335. doi: 10.1105/tpc.19.00562

Suer, S., Agusti, J., Sanchez, P., Schwarz, M., and Greb, T. (2011). WOX4 imparts auxin responsiveness to cambium cells in Arabidopsis. *Plant Cell* 23, 3247–3259. doi: 10.1105/tpc.111.087874

Takata, N., Awano, T., Nakata, M. T., Sano, Y., Sakamoto, S., Mitsuda, N., et al. (2019). Populus NST/SND orthologs are key regulators of secondary cell wall formation in wood fibers, phloem fibers and xylem ray parenchyma cells. *Tree Physiol.* 39, 514–525. doi: 10.1093/treephys/tpz004

Tang, X., Wang, D., Liu, Y., Lu, M., Zhuang, Y., Xie, Z., et al. (2020). Dual regulation of xylem formation by an auxin-mediated PaC3H17-PaMYB199 module in *Populus*. *New Phytol.* 225, 1545–1561. doi: 10.1111/nph.16244

Tuskan, G. A., Difazio, S., Jansson, S., Bohlmann, J., Grigoriev, I., Hellsten, U., et al. (2006). The genome of black cottonwood, *Populus trichocarpa* (Torr. & Gray). *Science* 313, 1596–1604. doi: 10.1126/science.1128691

Wang, L., Cui, J., Jin, B., Zhao, J., Xu, H., Lu, Z., et al. (2020). Multifeature analyses of vascular cambial cells reveal longevity mechanisms in old *Ginkgo biloba* trees. *Proc. Natl. Acad. Sci. U. S. A.* 117, 2201–2210. doi: 10.1073/pnas.1916548117

Weijers, D., and Wagner, D. (2016). Transcriptional responses to the auxin hormone. *Annu. Rev. Plant Biol.* 67, 539–574. doi: 10.1146/annurev-arplant-043015-112122

Wenzel, C. L., Schuetz, M., Yu, Q., and Mattsson, J. (2007). Dynamics of MONOPTEROS and PIN-FORMED1 expression during leaf vein pattern formation in *Arabidopsis thaliana*. *Plant J.* 49, 387–398. doi: 10.1111/j.1365-313X.2006.02977.x

Xu, C., Shen, Y., He, F., Fu, X., Yu, H., Lu, W., et al. (2019). Auxin-mediated Aux/IAA-ARF-HB signaling cascade regulates secondary xylem development in Populus. *New Phytol.* 222, 752–767. doi: 10.1111/nph.15658

Yang, J. H., Lee, K. H., Du, Q., Yang, S., Yuan, B., Qi, L., et al. (2020a). A membrane-associated NAC domain transcription factor XVP interacts with TDIF co-receptor and regulates vascular meristem activity. *New Phytol.* 226, 59–74. doi: 10.1111/nph.16289

Yang, S., Wang, S., Li, S., Du, Q., Qi, L., Wang, W., et al. (2020b). Activation of ACS7 in Arabidopsis affects vascular development and demonstrates a link between ethylene synthesis and cambial activity. *J. Exp. Bot.* 71, 7160–7170. doi: 10.1093/jxb/eraa423

Zhang, J., Eswaran, G., Alonso-Serra, J., Kucukoglu, M., Xiang, J., Yang, W., et al. (2019). Transcriptional regulatory framework for vascular cambium development in Arabidopsis roots. *Nat. Plants* 5, 1033–1042. doi: 10.1038/s41477-019-0522-9

Zhao, Y., Song, X., Zhou, H., Wei, K., Jiang, C., Wang, J., et al. (2020). KNAT2/6b, a class I KNOX gene, impedes xylem differentiation by regulating NAC domain transcription factors in poplar. *New Phytol.* 225, 1531–1544. doi: 10.1111/nph.16036

Zheng, S., He, J., Lin, Z., Zhu, Y., Sun, J., and Li, L. (2021). Two MADS-box genes regulate vascular cambium activity and secondary growth by modulating auxin homeostasis in *Populus*. *Plant Commun.* 2:100134. doi: 10.1016/j.xplc.2020.100134

Zhong, R., Demura, T., and Ye, Z. (2006). SND1, a NAC domain transcription factor, is a key regulator of secondary wall synthesis in fibers of Arabidopsis. *Plant Cell* 18, 3158–3170. doi: 10.1105/tpc.106.047399

Zhou, J., Zhong, R., and Ye, Z. H. (2014). Arabidopsis NAC domain proteins, VND1 to VND5, are transcriptional regulators of secondary wall biosynthesis in vessels. *PLoS One* 9:e105726. doi: 10.1371/journal.pone.0105726

Zhu, Y., Song, D., Sun, J., Wang, X., and Li, L. (2013). PtrHB7, a class III HD-Zip gene, plays a critical role in regulation of vascular cambium differentiation in Populus. *Mol. Plant* 6, 1331–1343. doi: 10.1093/mp/sss164

Zhu, Y., Song, D., Xu, P., Sun, J., and Li, L. (2018). A HD-ZIP III gene, PtrHB4, is required for interfascicular cambium development in Populus. *Plant Biotechnol. J.* 16, 808–817. doi: 10.1111/pbi.12830

Conflict of Interest: The authors declare that the research was conducted in the absence of any commercial or financial relationships that could be construed as a potential conflict of interest.

Publisher's Note: All claims expressed in this article are solely those of the authors and do not necessarily represent those of their affiliated organizations, or those of the publisher, the editors and the reviewers. Any product that may be evaluated in this article, or claim that may be made by its manufacturer, is not guaranteed or endorsed by the publisher.

frontiers in Plant Science

ORIGINAL RESEARCH
published: 23 August 2021
doi: 10.3389/fpls.2021.705596

Genetic Regulation of Vessel Morphology in *Populus*

F. Daniela Rodriguez-Zaccaro[1,2], *Isabelle M. Henry*[2] *and Andrew Groover*[1,2]*

[1]US Forest Service, Pacific Southwest Research Station, Davis, CA, United States, [2]Department of Plant Biology, University of California, Davis, Davis, CA, United States

During secondary growth, forest trees can modify the anatomy of the wood produced by the vascular cambium in response to environmental conditions. Notably, the trees of the model angiosperm genus, *Populus*, reduce the risk of cavitation and hydraulic failure under water stress by producing water-conducting vessel elements with narrow lumens, which are more numerous and more interconnected with each other. Here, we determined the genetic architecture of vessel traits affecting hydraulic physiology and resilience to water stress. Vessel traits were measured for clonally replicated genotypes of a unique *Populus deltoides* x *nigra* population carrying genomically defined insertions and deletions that create gene dosage variation. We found significant phenotypic variation for all traits measured (mean vessel diameter, height-corrected mean vessel diameter, vessel frequency, height-corrected vessel frequency, vessel grouping index, and mean vessel circularity), and that all traits were under genetic control and showed moderate heritability values, ranging from 0.32 to 0.53. Whole-genome scans of correlations between gene dosage and phenotypic traits identified quantitative trait loci for tree height, mean vessel diameter, height-corrected mean vessel diameter, height-corrected vessel frequency, and vessel grouping index. Our results demonstrate that vessel traits affecting hydraulic physiology are under genetic control, and both pleiotropic and trait-specific quantitative trait loci are found for these traits.

Keywords: forest tree, drought, wood formation cambium activity, genomics, forest tree growth

OPEN ACCESS

Edited by:
Wei Li,
Northeast Forestry University, China

Reviewed by:
Hari Chhetri,
Oak Ridge National Laboratory (DOE), United States
Dennis William Stevenson,
New York Botanical Garden, United States

***Correspondence:**
Andrew Groover
agroover@fs.fed.us

Specialty section:
This article was submitted to Plant Development and EvoDevo, a section of the journal Frontiers in Plant Science

Received: *05 May 2021*
Accepted: *05 July 2021*
Published: *23 August 2021*

Citation:
Rodriguez-Zaccaro FD, Henry IM and Groover A (2021) Genetic Regulation of Vessel Morphology in Populus. Front. Plant Sci. 12:705596. doi: 10.3389/fpls.2021.705596

INTRODUCTION

Wood (secondary xylem) is the water conducting tissue of tree stems, and the anatomical features of wood can have profound effects on water transport and vulnerability to hydraulic failure during water stress (Rodriguez-Zaccaro and Groover, 2019). Vessel elements are the primary water conducting cells in most angiosperms including trees of the model genus *Populus*. Vessel differentiation starts with the commitment of terminal cell fate and cessation of cell division, followed by cell expansion, construction of a rigid secondary cell wall, and programmed cell death to produce water conducting cell corpse (Groover and Jones, 1999; Turner et al., 2007). In *Populus*, stems undergoing secondary growth, the vessel elements differentiate from the xylem mother cells derived from the fusiform initials of the vascular cambium and join end-on-end to create longer water conducting tubes termed as vessels (Larson, 1994; Sperry et al., 2006). Pits between adjacent vessel elements and between vessel elements and other cells, such as ray parenchyma, provide additional routes for water to pass both between and

out of vessel elements. Importantly, secondary growth can be altered to produce wood anatomy and vessel morphologies that mitigate water stress during drought or maximize water conduction for fast growth under permissive conditions (Tyree, 1989; Tyree and Sperry, 1989; Tyree and Zimmermann, 2002). To what degree these changes reflect the passive or indirect responses of development to environmental conditions, as opposed to genetically regulated responses, remains unclear.

Together, the anatomical properties of vessels have a profound effect on water conduction physiology (Rodriguez-Zaccaro and Groover, 2019). Vessel lumen diameter directly affects the rate of water transport through secondary xylem with wider vessels contributing to greater water transport efficiency. This can be partially explained through the Hagen-Poiseuille law, modeling the volumetric flow rate of a liquid moving through a tube as being proportional to the fourth power of the radius of the tube (Venturas et al., 2017). Consequently, a small increase in vessel width can produce a large increase in water flow and allow for greater photosynthesis and growth rates (Brodribb and Feild, 2000). Larger vessel diameters, however, have been associated with greater vulnerability to cavitation due to drought and other abiotic stressors (Gleason et al., 2016; Hacke et al., 2016). Cavitation results in the formation of air-pockets within the xylem network, which can lead to lethal hydraulic failure (Tyree, 1989). Vessel frequency (VF), which is the number of vessels within a given area of xylem, and vessel grouping index (VGI), a measure of vessel clustering and interconnectivity, can also affect hydraulic function. A greater VF can increase water transport efficiency and buffer the xylem network from hydraulic failure by allowing for a larger fraction of smaller diameter vessels that remain functional under water stress compared to lower VF xylem (Baas et al., 1983; Villar-Salvador et al., 1997). Similarly, a greater VGI can lead to increased hydraulic efficiency and mitigate the effects of cavitation by providing xylem sap alternate routes to bypass embolized vessels (Carlquist, 1984; Lens et al., 2011). Greater VGI, however, has also been related to increased vulnerability to cavitation due to a likely increase in the probability of embolism spread in a more interconnected xylem network (Loepfe et al., 2007). A trait that has not been well studied in the context of hydraulic function is vessel shape or cross-sectional circularity. According to microchannel fluid mechanics, a more circular conduit can transport fluids more efficiently than conduits with more irregular shapes (White, 2011). Vessel circularity has also been related to safety from water stress with more circular vessels able to withstand large negative pressures within the xylem network without imploding and disrupting water transport (Cochard et al., 2004). Non-lumen fraction (NF) is the proportion of xylem area that is not made up of vessel lumen area. This trait has been previously positively related to wood mechanical strength and density (Searson et al., 2004; Zanne et al., 2010), an important trait that helps to determine commercial wood quality.

Several stem and wood anatomical traits have been shown to be correlated to each other (von Arx et al., 2013; Hajek et al., 2014) although cause and effect for these correlations are not known. For example, mean vessel diameter (MVD) and VF are often negatively correlated (Chauhan et al., 1999; Sellin et al., 2008). Some studies have suggested that this correlation is the result of a trade-off between hydraulic conductivity and mechanical support in stems (Wagner et al., 1998; Barbour and Whitehead, 2003); a positive correlation leading to larger and more numerous vessels could result in mechanically weaker stems that are selected against. MVD and VF are also known to predictably scale with tree height (TH); larger trees tend to have wider and less numerous vessels compared to smaller trees at the same sampling height (Olson et al., 2014). Some hydraulic optimality models suggest that vessel width and quantity are influenced by height. The Hagen-Poiseuille law predicts that longer conduits are more resistant to flow than shorter conduits of equal diameter. Wider vessels, then, are thought to compensate for the decrease in water transport efficiency that would otherwise result from the longer conductive pathways necessarily present in taller trees (Olson and Rosell, 2013). However, the correlation between tree height and vessel traits is not perfect, and it is unclear to what degree the observed variation in vessel traits could be the result of genetic regulation independent from tree size.

The regulation of cell expansion and final diameter in vessel elements likely involves the regulation of cell turgor and cell wall expansion. The experimental manipulation of potassium, a primary osmoticum of plant cells likely involved in cell turgor regulation, can be used to alter the diameter of differentiating vessel elements (Cutter and Morphey, 1978). However, there is less evidence that the manipulation of secondary cell wall formation can have similar effects. For example, well-characterized *irregular xylem* (*irx*) mutants with physically compromised vessels with crumpled cell walls are not significantly defective in terms of cell diameter (Turner and Somerville, 1997). Whether turgor regulation, cell wall regulation, or other unknown factors, such as the timing of transition from cell division to cell expansion, are the most critical factors that influencing the final cell diameter and morphology remains uncertain. One reason for this knowledge gap is that experimental systems to investigate the genetic and genomic properties of vessel element morphology within relevant species, including forest trees, have been historically lacking.

We previously developed *Populus* germplasm with the goal of performing functional genomic experiments directly in a forest tree species with extensive secondary growth and wood formation. To create this resource, pollen from a *Populus nigra* male tree was irradiated to create chromosomal breaks prior to crossing with two *Populus deltoides* females to produce a large F1 hybrid population (Henry et al., 2015). The insertions and deletions in each F1 individual create structural variation and associated gene dosage variation in the affected regions. Insertions and deletions were genomically mapped for each F1 individual, allowing genome-wide surveys linking gene dosage variation with phenotypes to identify dosage quantitative trait locus (dQTL; Bastiaanse et al., 2019, 2021). The genetic architecture of multiple biomass and phenology-related traits were previously dissected using this resource, including the identification of dQTL for multiple traits, and demonstrated that gene dosage is a major source of phenotypic variation in

this population (Bastiaanse et al., 2019, 2021). These results are relevant to natural genetic variation in *Populus*, where, similar to other plant species that have been surveyed, structural and gene dosage variation is prevalent (Pinosio et al., 2016; Zhang et al., 2019).

Here, we used the same poplar irradiation hybrid germplasm to estimate the genetic architecture of prominent vessel element and stem traits including MVD, VF, VGI, mean vessel circularity (MVC), tree height (TH), non-lumen fraction (NF), and bark thickness (BT). We report correlations among all traits measured including tree height and vessel traits. All traits showed modest heritabilities, indicating that there is a significant genetic component underlying the observed phenotypic variation for vessel traits. Additionally, dQTL are reported for MVD, tree height-corrected mean vessel diameter (cMVD), tree height-corrected vessel frequency (cVF), and VGI. We provide evidence of dQTL commonly shared by correlated traits, as well as trait-specific dQTL, suggesting that independent regulatory factors exist for both correlated and uncorrelated traits. Together, our results show that vessel traits are under genetic regulation and are not simply a passive consequence of tree height, and that system genetic approaches could now be used to further dissect these traits and identify candidate genes using this same genomics resource.

MATERIALS AND METHODS

Plant Materials

A subset of 201 poplar hybrid genotypes was included from a larger dosage mutant pedigree developed and described by Henry et al. (2015). Briefly, the pedigree was produced by crossing two female *P. deltoides* with gamma-irradiated pollen of a male *P. nigra*. The F1 hybrids were then completely sequenced using Illumina short reads. Relative sequencing read coverage values were used to detect the insertions and deletions (indel mutations) across F1 hybrids that together cover the entire poplar genome multiple times. The pedigree consists of nearly 800 replicated lines maintained in an outdoor plantation at the US Forest Service Institute of Forest Genetics in Placerville, CA.

All lines within the subset were clonally propagated through stem cuttings from the field in multiple replicates (ramets) during the spring of 2018. Cuttings were planted with rooting hormone (Bontone) in individual 2.83-L pots filled with horticultural soil (Sungro Sunshine Mix #4) and fertilizer (Osmocote, approximately 14 g/kg soil) inside a greenhouse at the IFG. After a 2-month growth period, three healthy clonal replicates per line were randomly selected to include in a randomized complete block design. Plants were grown in a lathe house for 3 months, harvested, and moved inside a greenhouse to coppice and grown for a second 3-month period before harvesting a second time. Both crops were kept under well-watered conditions using a drip-irrigation system and monitored stem height and diameter growth until the end of the growing season in the fall of 2018. Greenhouse trees were kept at a near constant temperature of 23°C. All analyses and results involve the latter greenhouse-grown crop. A 6–8-cm woody stem segment was harvested from each tree at a fixed height of 10 cm from the point of emergence from the original cutting. Stems were immediately stored in 60% ethyl alcohol solution in 50 ml Falcon tubes.

Histology

Stem internodes were cut in 40 μm thick cross-sections with a sliding microtome (Spencer Lens) or a vibratome (Vibratome Series 1000). Sections were stained with and mounted in a mixture of phloroglucinol and Astra Blue, which stain lignin and cellulose, respectively. Sections were then photographed at ×5 or ×10 magnification under a microscope with a digital camera with standardized settings (Leica Microsystems). A 100-μm scale bar was included in each image, adjusted for specific magnification. Lastly, a high-quality micrograph of each replicate within a line was selected for image analysis.

Image Analysis

Stem cross-section micrographs were processed using Fiji ImageJ software (v2) to obtain wood anatomical trait data. Images were spatially calibrated using the known scale bar length to determine the number of pixels per micrometer. Bark thickness was calculated as the average distance between the cambial zone and the outer cork in unprocessed images. All non-xylem areas (bark and pith) were then manually cut out of the image before converting to grayscale. Images were divided into a "foreground" consisting of vessel lumens and a "background" made up of non-vessel lumen area by setting a standardized pixel thresholding value. Vessel lumen area and circularity values were obtained directly through the Analyze Particles tool with equivalent circle vessel diameters calculated from vessel lumen areas (Scholz et al., 2013). A MVD and MVC value was calculated for each image. A vessel frequency value was calculated for each image by dividing the number of vessels (obtained through the Analyze Particles tool) by the total xylem area (mm^2). NF was calculated by multiplying the mean vessel area by vessel frequency (Scholz et al., 2013). A VGI value was obtained for each image by dividing the number of vessels by the number of vessel groups. A vessel group consists of anything from a solitary vessel to any number of clustered vessels with secondary walls that are in contact (Carlquist, 2001). Vessel groups were counted manually using the Multi-point tool.

Height Corrected Traits

Because tree height is correlated with vessel diameter (Olson and Rosell, 2013), cMVD, and cVF values were calculated for each tree to assess the portion of trait variation that cannot be explained by height. The log10 of the final tree height at harvest was plotted against the log10 of each trait. The equation describing the linear regression of each plot was used to obtain expected trait values predicted from tree height. Expected values were subtracted from observed trait values to obtain residual values that were used as height-corrected trait data. Lines with residual values near 0 were considered to have vessel trait values expected for their height. Lines with significantly higher

residual values for MVD, for example, were considered to have unusually wide vessels for their height.

Estimating Broad-Sense Heritability

The broad-sense heritability (H^2) of each trait was estimated using the repeatability function in the CRAN heritability R package (version 1.3) developed by Kruijer et al. (2015). Repeatability, or intraclass correlation, is considered as the broad-sense heritability and was calculated by dividing the total genetic variance by the total phenotypic variance of a trait. The total genetic variance was estimated by subtracting the mean sums of squares for genotype and residual error obtained from an analysis of variance and dividing the results by the number of clonal replicates in each line. The total phenotypic variance was calculated by adding the total genetic variance to the mean sums of squares of the residual error (Kruijer et al., 2015).

Statistical Analysis

Trait data were transformed, when appropriate, through Box-Cox power transformations. Pearson's correlation tests were run to determine the relationship between all trait combinations. An ANOVA-based analysis was performed on each trait in base R, with genotype and final tree height at harvest as independent factors in each model, with the exception of height-corrected traits, which involved only a genotype factor. Tree height was also treated as a dependent variable in a separate model with genotype as the sole independent factor. Each analysis was followed by a Tukey's honest significance *post hoc* test.

Dosage-dependent quantitative trait locus analyses (dQTL) were performed on all traits. The start and end sites of all the indels of the genotypes included in the analysis were used to create the boundaries of genomic bins as previously described (Bastiaanse et al., 2019, 2021). A relative gene dosage score was calculated for each genotype at each genomic bin by dividing the gene dosage at the bin by the background ploidy of the particular line. A Kendall's tau coefficient was calculated at each bin to test for statistical dependence between the relative dosage score (RDS) and the phenotypic trait data (Schaeffer and Levitt, 1956). Most indels encompassed more than one chromosomal bin, and contiguous bins were thus correlated, as previously described for this population (Bastiaanse et al., 2021). Consequently, the resulting values of p were adjusted through a modified Bonferroni correction for multiple testing, in which the values of p were multiplied by the number of independent chromosomal bins (Bastiaanse et al., 2021). The number of independent bins was obtained through a dissimilarity matrix by calculating pairwise correlation coefficients between the relative dosage ratios of bins across all genotypes. These correlation coefficients were grouped using a hierarchical clustering method and individual branches were combined using a cutoff value of 0.7 (Bastiaanse et al., 2021). The original 469 genomic bins were merged into 40 independent bins through this method. The adjusted values of p below a threshold of 0.05 were considered as significant and signaled putative dQTL associated with a trait. The adjusted R-squared of the linear regression model fitting genomic bins was used to estimate the percentage of trait variance explained by dQTL.

RESULTS

Here, we used a subset of a previously described population of *P. deltoides* x *nigra* carrying genomically mapped indels (Henry et al., 2015) to investigate the effects of gene dosage variation on stem anatomical and vessel traits. Of the 201 genotypes included in the analysis, 173 carried insertions and/or deletions, with the remaining lines included as non-indel controls. Genomic bins were defined by the breakpoints of indels across all lines included in this experiment (see section "Materials and Methods"), which represented 469 genomic bins covering 91.5% of the genome, as shown in **Figure 1**. Genomic bin size ranged from 0.01 to 5.2 Mb with an average bin size of 0.78 Mb. Lesion coverage varied substantially between chromosomes, ranging from 1 to 16 indels per genomic bin, with a genome-wide average of six indels per bin.

Clonal replicates of all genotypes were grown and measured under permissive greenhouse conditions, prior to destructive sampling and measuring wood anatomical and vessel traits (see section "Materials and Methods"). For each tree, a basal stem cross section was stained, digitally imaged, and analyzed to extract anatomical trait data as illustrated in **Figure 2**. Traits directly measured or calculated are summarized in **Table 1** and include tree height (TH), MVD, vessel frequency (VF), VGI, MVC, non-lumen fraction (NF), and bark thickness (BT). Some hydraulic optimality models suggest that vessel width and quantity are a consequence of organ size (Olson and Rosell, 2013). Both MVD and VF are known to be highly correlated to tree height, where larger trees have wider and less numerous vessels compared to smaller trees at the same sampling height (Olson et al., 2014). To assess the portion of trait variation not explained by height, we evaluated correlations among raw anatomical and vessel trait data and tree height and included height-corrected adjuncts for traits with significant correlations (see section "Materials and Methods"). Two traits were corrected this way: cMVD and cVF (**Table 1**).

Pedigree Trait Distributions

Distributions of raw trait data are shown in **Figure 3**; trait distribution means, standard deviations, and ranges are summarized in **Table 1**. All traits showed continuous variation, consistent with multigenic variation expected for classical quantitative traits. The final tree height at harvest varied substantially within the population, ranging from 5 to 168 cm, with a mean height of 64 and a standard deviation of 32 cm (**Table 1**; **Figure 3A**). MVD within the 201 genotype pedigree subset ranged from 14 to 36 μm (**Figure 3B**), with an average of 26 and a standard deviation of 4 μm. VF distribution was strongly skewed right (**Figure 3D**) and ranged from 165 to 1,000 vessels/mm^2 of xylem, with an average of 365 and a

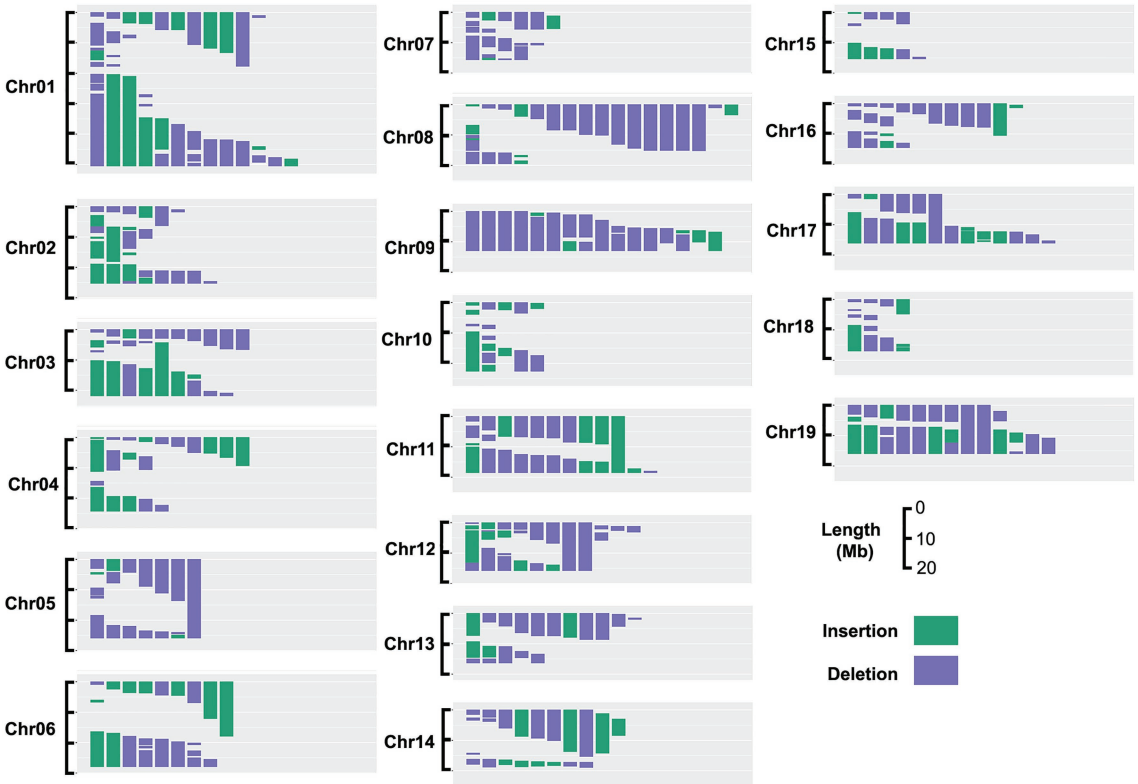

FIGURE 1 | Insertion and deletion (indel) coverage across the poplar genome for genotypes included in this study. Based on the indel size and location in the 201 genotypes chosen for this study, 95% of the genome is covered by at least one indel.

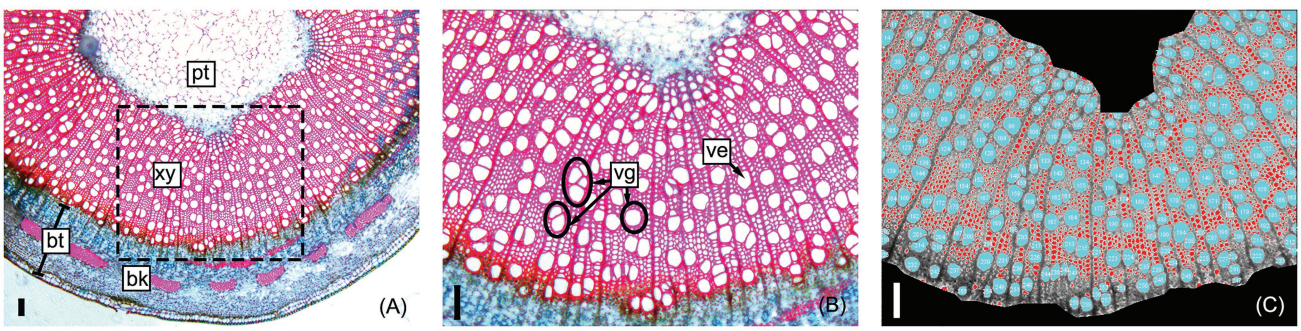

FIGURE 2 | Representative sample of a poplar stem cross-section used to obtain stem and vessel anatomical trait data. Section micrographs include the pith (pt), secondary xylem (xy), and bark (bk); bark thickness (bt) is measured before image processing **(A)**. Vessel elements (ve) and vessel group (vg) examples are shown within a close-up of the sampled section **(B)**; vessel groups are single vessels or any number of clustered vessels with secondary cell walls that are in contact. Image J software (v2) was used to measure xylem area, automatically count vessels, and measure vessel areas and circularities (see section "Materials and Methods") within the secondary xylem **(C)**. All scale bars are 100 μm.

standard deviation of 166 vessels/mm^2. VGI had a narrow distribution (**Figure 3F**) that ranged from 1.17 to 1.79 vessels/vessel group with a mean of 1.47 and a standard deviation of 0.1 vessels/vessel group. MVC had a narrow distribution (**Figure 3G**) that ranged from 0.68 to 0.87, with an average of 0.78 and a standard deviation of 0.03. NF distribution was narrow (**Figure 3H**) and ranged from 0.66 to 0.91 with a mean of 0.80 and a standard deviation of 0.04.

In comparison with non-indel control genotypes, indel genotypes extended the observed variation and defined the extremes of each phenotype as shown in **Figure 3** and **Table 2**. Thus, indels generated phenotypic variation beyond the variation caused by allelic segregation. Consistent with previous findings (Bastiaanse et al., 2019), as a group lines with lesions had an overall negative effect on growth, as illustrated here by significantly lower tree heights for the lesion group (**Table 2**).

TABLE 1 | The means, standard deviations (SD), and ranges of phenotypic traits measured in a 201 genotype poplar pedigree.

Trait	Abbr.	Units	Mean	SD	Range
Tree height	TH	cm	64	32	5–168
Mean vessel diameter	MVD	µm	26	4.0	14.0–34.9
Height-corrected MVD	cMVD	Unitless	0.0001	0.043	−0.136–0.123
Vessel frequency	VF	vessels/mm^2	365	166	165–1,000
Height-corrected VF	cVF	Unitless	−0.0004	0.084	0.341–0.282
Vessel grouping index	VGI	vessel/vessel group	1.47	0.1	1.17–1.79
Mean vessel circularity	MVC	Unitless	0.78	0.03	0.68–0.87
Non-lumen fraction	NF	Unitless	0.8	0.04	0.66–0.91
Bark thickness	BT	µm	608	349	169–779

Additional traits with significantly smaller means in the lesion line group included MVD and BT, while lesion lines had a larger mean for VF (**Table 2**). Thus, MVD, BT, and VF behave as growth-related traits with regards to response to lesion-induced dosage variation.

Genotype Effect and Broad-Sense Heritability

ANOVA tests showed that genotype had a significant effect on all measured traits (**Table 3**). Both genotype ($p < 0.0001$) and tree height ($p < 0.0001$) had a statistically significant effect on MVD. There was a significant interaction between genotype and tree height ($p < 0.0001$), indicating a departure from what would be expected if MVD was directly attributed simply to tree height. Genotype ($p < 0.0001$) and tree height ($p < 0.0001$) had significant effects on VF, but there was no significant interaction between genotype and tree height ($p = 0.0597$). Genotype also had a significant effect on cMVD ($p < 0.0001$) and cVF ($p < 0.0001$), indicating significant genetic variance for these traits not directly attributable to tree size. An example of

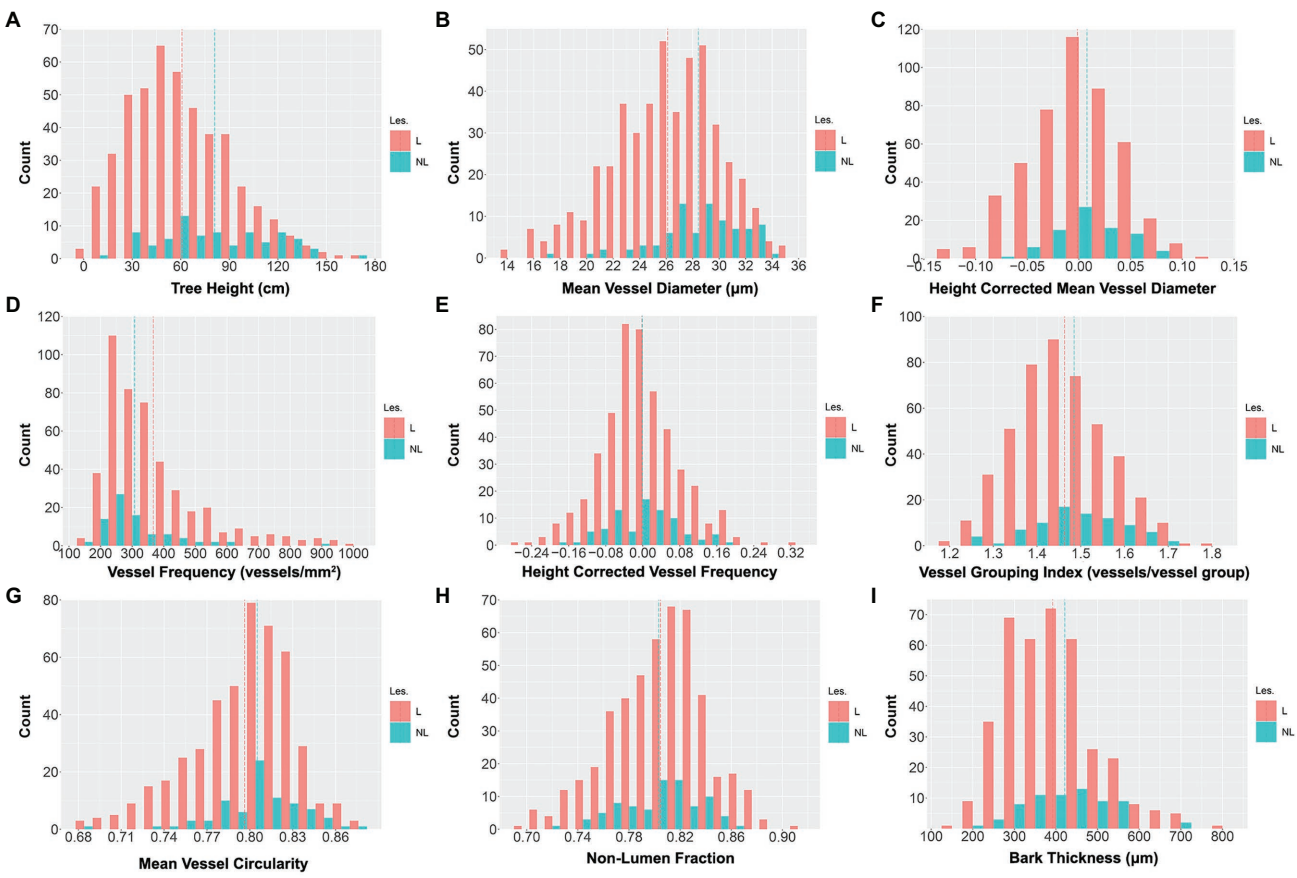

FIGURE 3 | Untransformed wood anatomical trait and stem trait data distributions across the 201 genotypes included in the study. Values are for three clonal replicates per genotype. The red bars represent indel genotypes (173), and the blue bars represent non-lesion genotypes (28). Traits include tree height (TH; **A**), mean vessel diameter (MVD; **B**), height-corrected mean vessel diameter (cMVD; **C**), vessel frequency (VF; **D**), height-corrected vessel frequency (cVF; **E**), vessel grouping index (VGI; **F**), mean vessel circularity (MVC; **G**), non-lumen fraction (NF; **H**), and bark thickness (BT; **I**). The red dotted lines represent the trait means of indel lines, and the blue dotted lines represent the trait means of non-indel lines.

FIGURE 4 | Representative stem cross-sections of three hybrid poplar genotypes that did not differ significantly in tree height (~30 cm), but show significant differences in vessel diameters. Genotype XXX_100_71 **(A)** had a MVD of 20 μm, XXX_100_70 **(B)** had a MVD of 25 μm, and XXX_100_93 **(C)** had a MVD of 29 μm. All scale bars are 100 μm.

TABLE 2 | The means, standard deviations (SD), and ranges of phenotypic traits measured in 201 genotype poplar pedigree across non-lesion (NL Lines) and lesion genotypes (L Lines).

Trait	NL Lines			L Lines		
	Mean	SD	Range	Mean	SD	Range
TH	80.9	34.6	9–166	60.8**	30.8	5–168
MVD	28.4	3.3	16.6–34.3	26.1**	4.0	14.0–34.9
cMVD	0.008	0.032	−0.064–0.082	−0.004	0.044	−0.136–0.123
VF	307	119	165–902	375*	171	168–1,000
cVF	0	0.074	−0.179–0.185	0	0.086	−0.282–0.341
VGI	1.48	0.1	1.25–1.69	1.46	0.1	1.18–1.79
MVC	0.81	0.030	0.69–0.87	0.80	0.035	0.68–0.87
NF	0.80	0.031	0.73–0.87	0.80	0.037	0.66–0.91
BT	421	99	221–690	392	105	169–779

*Means different at ≤ 0.05.
**Means different at ≤ 0.01.

TABLE 3 | ANOVA test results and broad-sense heritabilities (H^2) of phenotypic traits in a 201 genotype pedigree.

Trait	Line (*p*)	TH (*p*)	Line*TH (*p*)	H^2	95% CI
TH	<2e-16	–	–	0.45	±0.09
MVD	<2e-16	<2e-16	1.16E-06	0.49	±0.09
cMVD	<2e-16	–	–	0.44	±0.09
VF	<2e-16	<2e-16	0.0597	0.45	±0.09
cVF	9.93E-12	–	–	0.32	±0.09
VGI	1.38E-15	0.193	0.235	0.47	±0.09
MVC	<2e-16	0.186	0.393	0.51	±0.09
NF	<2e-16	4.70E-07	0.0799	0.5	±0.08
BT	5.45E-11	<2e-16	0.531	0.37	±0.09

The values of p were obtained from two-way ANOVA tests for each trait, with genotype (Line) and tree height (TH) as independent factors. TH, cMVD, and cVF were tested as dependent variables with line as the sole independent factor. H^2 was estimated through intraclass correlation, with 95% confidence intervals for each heritability estimate shown.

genotypes that significantly deviate from expected MVD based on tree height are shown in **Figure 4**. Genotype ($p < 0.0001$), but not tree height ($p = 0.193$), explained significant portions of VGI phenotypic variation. Genotype ($p < 0.0001$), but not tree height ($p = 0.186$), had a significant effect on MVC. Both genotype ($p < 0.0001$) and tree height ($p < 0.0001$) had a significant effect on NF.

Broad-sense heritabilities (repeatabilities) were calculated for all traits and are shown in **Table 3**. All wood and stem traits were moderately heritable. cVF had the lowest broad-sense heritability estimate among all traits ($H^2 = 0.32$) with confidence intervals ranging from 0.22 to 0.41. MVC had the highest broad-sense heritability estimate ($H^2 = 0.51$), with confidence intervals ranging from 0.42 to 0.59. As a reference to the estimation of vessel and stem anatomical trait heritabilities, tree height had a heritability of 0.45 in this study. All anatomical traits showed significant heritabilities suggest that the observed phenotypic variation for each trait has a substantial genetic basis. Together with the continuous phenotypic trait distributions, these results are consistent with the traits under study being quantitative traits influenced by multiple genes.

Pearson's Correlation Tests Between Traits

Correlations among all traits were calculated (see section "Materials and Methods") and are summarized in **Figure 5**. The final tree height at harvest was strongly positively correlated with MVD ($R = 0.76$, $p < 0.01$) and strongly negatively correlated with VF ($R = -0.78$, $p < 0.001$), similar to previous findings (Olson et al., 2014). Even after correcting for tree height, there was a negative correlation between cMVD and cVF ($R = -0.61$, $p < 0.05$), indicating potential interdependence of the size and frequency of vessel elements in wood that is independent of organ size. There was a weaker, but significant positive correlation between tree height and BT ($R = 0.52$, $p < 0.01$). VGI, MVC, and NF, however, were not significantly correlated to tree height or to any other trait, suggesting that these traits might be independently regulated from each other.

MVD and VF were strongly negatively correlated ($R = -0.79$, $p < 0.001$), as previously reported (Olson et al., 2014), and suggest either common regulation or direct influence of one trait on the other. BT was moderately but significantly positively correlated to MVD ($R = 0.48$, $p < 0.05$) and negatively correlated to VF ($R = -0.46$, $p < 0.01$). BT could be considered as a proxy for radial growth, and thus correlated with greater MVD and lower VF as expected for faster growing and larger trees.

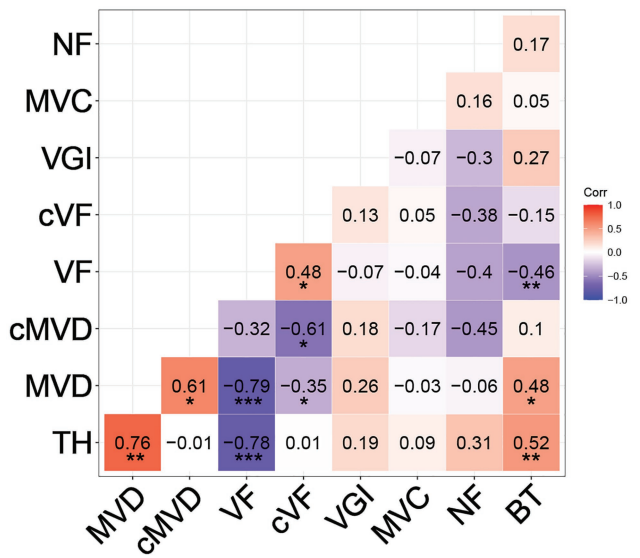

FIGURE 5 | Pearson correlation coefficients between different wood and stem traits. Traits include tree height at harvest (TH), MVD, cMVD, VF, cVF, VGI, MVC, non-lumen fraction (NF), and bark thickness (BT). Asterisks indicate significant correlations between traits (*$p \leq 0.05$; **$p \leq 0.01$; ***$p \leq 0.001$).

Dosage-Dependent QTL Analyses

We used our previously described approach (Bastiaanse et al., 2019, 2021) for correlating gene dosage at genomic bins with phenotypes, and mapping dosage QTL for all stem and anatomical traits (see section "Materials and Methods"). Briefly, genomic bins were established based on indel breakpoints across all lines (genotypes). For each bin within each line, RDS was defined as 0.5 for deletions, 1.5 for insertions, and 1 for normal diploid dosage. Correlations among relative dosage at each bin and each phenotype was then assessed across all lines genome-wide to identify dQTL. Adjacent bins were not independent and were frequently spanned by indels (**Figure 1**); thus values of p were adjusted for multiple testing based on the effective number of uncorrelated bins (see section "Materials and Methods").

Correlations of dosage at genomic bins and each trait are shown in **Figure 6** for TH, MVD, cMVD, cVF, VGI, and BT, and statistics for each dQTL bin including the percentage of phenotypic variance explained are summarized in **Table 4**. There were no significant correlations between the remaining traits (VF, MVC, and NF) and specific areas of the genome (not shown). Boxplots showing the relationship among dosage and trait values for each dQTL are shown in **Figure 7**. MVD and tree height were both significantly correlated with three contiguous genomic bins on chromosome 11, spanning 0.9 Mb (**Figures 6A,B**; **Table 4**). Lines with insertions in these regions

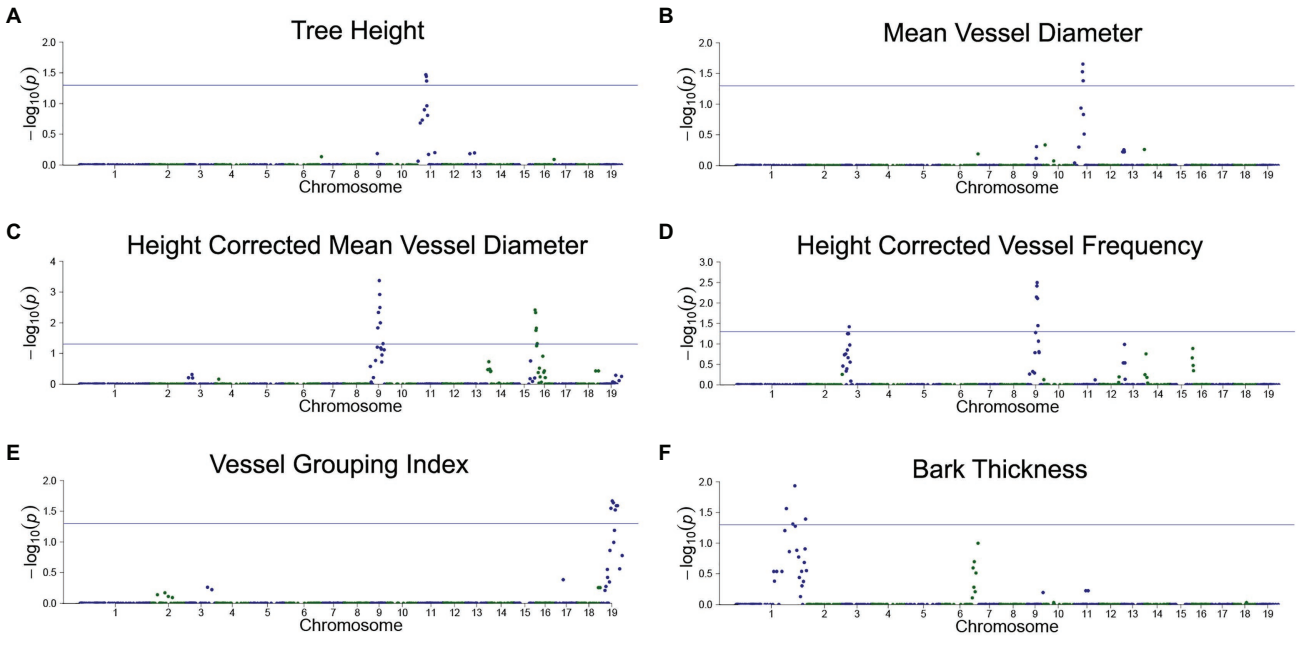

FIGURE 6 | Dosage-dependent quantitative trait loci (dQTL) of traits. Traits with significant dQTL included tree height **(A)**, MVD **(B)**, cMVD **(C)**, cVF **(D)**, VGI **(E)**, and bark thickness **(F)**. Genomic bin position is plotted against the –log10 of the value of p for each correlation test. A significance threshold corresponding to a value of p of 0.05 is depicted as a blue horizontal line. The values of p were adjusted using a relaxed Bonferroni correction (see section "Materials and Methods").

TABLE 4 | Locations of all genomic bins with significant correlations ($p < 0.05$) with stem or wood anatomical traits (dQTL).

Trait	Chr	Location (MBP)	*p*	Variance explained (%)
TH	11	6.10–6.65	0.0338	3.4
TH	11	6.60–6.75	0.0361	
TH	11	6.75–7.00	0.0429	
MVD	11	6.10–6.65	0.0297	4.1
MVD	11	6.60–6.75	0.0222	
MVD	11	6.75–7.00	0.0416	
cMVD	09	5.40–5.60	0.0147	14.9
cMVD	09	5.60–6.30	0.0046	
cMVD	09	6.30–6.80	0.0004	
cMVD	09	6.80–6.90	0.0012	
cMVD	09	6.90–7.10	0.0032	
cMVD	09	7.10–7.50	0.0100	
cMVD	09	8.50–9.90	0.0481	
cMVD	16	0–0.50	0.0038	
cMVD	16	0.50–0.80	0.0047	
cMVD	16	0.80–1.00	0.0178	
cMVD	16	1.00–1.30	0.0150	
cMVD	16	1.40–2.20	0.0478	
cVF	03	4.60–5.30	0.0383	11.2
cVF	09	6.30–6.80	0.0072	
cVF	09	6.80–6.90	0.0039	
cVF	09	6.90–7.10	0.0032	
cVF	09	7.10–7.50	0.0078	
cVF	09	7.50–7.70	0.0358	
VGI	19	7.20–8.10	0.0283	4.2
VGI	19	8.10–9.10	0.0215	
VGI	19	9.10–9.60	0.0230	
VGI	19	10.6–10.8	0.0301	
VGI	19	10.8–12.2	0.0257	
VGI	19	12.2–12.4	0.0256	
BT	01	34.9–36.8	0.0273	7.2
BT	01	39.1–41.8	0.0488	
BT	01	41.8–41.9	0.0116	
BT	01	49.3–49.6	0.0405	

The adjusted R-squared of the linear regression model fitting the genomic bins was used to estimate the percentage of trait variance explained by dQTL.

did not significantly differ in MVDs or tree heights from lines lacking indels, while lines with deletions had significantly lower values for these traits (**Figures 7A,B**), potentially uncovering a maternal allele with unique function or lack of function. These dQTL explained 4.1% of MVD variance and 3.4% of tree height variance (**Table 4**) and contained 63 annotated genes. cMVD was significantly correlated to seven genomic bins in chromosome 9, and five genomic bins on chromosome 16 (**Figure 6**). Together, these bins covered a length of 5.6 Mb and accounted for 14.9% of the total phenotypic variance of the trait (**Table 4**). The dQTL within chromosome nine included 380 annotated genes, while the dQTL within chromosome 16 included 370 annotated genes. Lines with deletions spanning either the chromosome 9 (**Figure 7C**) or the chromosome 16 dQTL (**Figure 7D**) showed increased cMVDs, while lines with insertions showed the opposite phenotype, as might be expected for a dosage-sensitive negative regulator of growth. cVF was significantly correlated to five genomic bins in chromosome 9 and one genomic bin in chromosome 3 (**Figure 6**). These dQTL jointly covered 2.1 Mb that contained 246 annotated genes and explained 11.2% of the total phenotypic variance of the trait. cVF was not statistically significantly different in lines carrying deletions in the chromosome 3 cVF dQTL region compared to lines lacking indels (**Figure 7E**), while lines with deletions of the chromosome 9 cVF region did significantly differ from lines lacking indels (**Figure 7F**). Lines carrying insertions covering either the chromosome 3 or 9 cVF dQTL regions exhibited significantly higher cVF values (**Figures 7E,F**). The five dQTL bins on chromosome 9 associated with cVF overlapped with five most significant bins correlated to cMVD, consistent with the idea of a common regulator affecting both traits. VGI was significantly correlated to six genomic bins spanning 4.2 Mb within chromosome 19 (**Figure 6**) that was not implicated in dQTL for any other trait. Along with the observation that VGI did not show significant correlations with other traits (**Figure 5**), these results suggest that this dQTL may identify a genetic factor specific to this trait. VGI for lines with deletions in the chromosome 19 VGI dQTL region did not statistically differ from lines lacking indels in this region, while lines with insertions had statistically greater VGI (**Figure 7G**). This dQTL explained 4.2% of the trait variance and contained 379 annotated genes. Finally, BT showed significant dQTL bins spanning a large region of chromosome 1 (**Figure 7H**), which explained 7.2% of the trait variance. Gene dosage in this region was positively correlated with BT and was not implicated in dQTL for other traits, despite correlations of BT phenotype with tree height, MVD, and VF (**Figure 5**).

DISCUSSION

The regulation of vessel element morphological traits remains poorly understood, despite the key role of vessel traits in determining the hydraulic physiology of plants, and trees in particular. One fundamental feature of vessel elements that makes their study complex is their extreme developmental plasticity. Vessel elements show dramatic morphogenic variation, as seen by contrasting vessel elements with narrow lumens and spiral secondary cell wall thickenings produced during elongative primary growth, and vessels with wide lumens and extensive secondary cell walls produced during secondary growth. Vessel element diameter and frequency have also been shown to be positively correlated with tree size (Olson and Rosell, 2013; Olson et al., 2014). And vessel development and final morphology are highly responsive to environmental conditions and can be modified to produce morphologies better suited to fast growth under permissive conditions or mitigating the effects of unfavorable conditions such as drought (Rodriguez-Zaccaro and Groover, 2019). A fundamental question is then, to what extent are vessel traits, such as final diameter, under genetic control, vs. non-genetic responses to environmental or physiological conditions?

Here, we took advantage of a genomically characterized population of *P. deltoides* x *nigra* to provide new insights into the genetic control of vessel traits associated with water transport physiology. This study is unusual as it presents trait distributions, correlations, heritabilities, and dQTL for wood anatomical traits

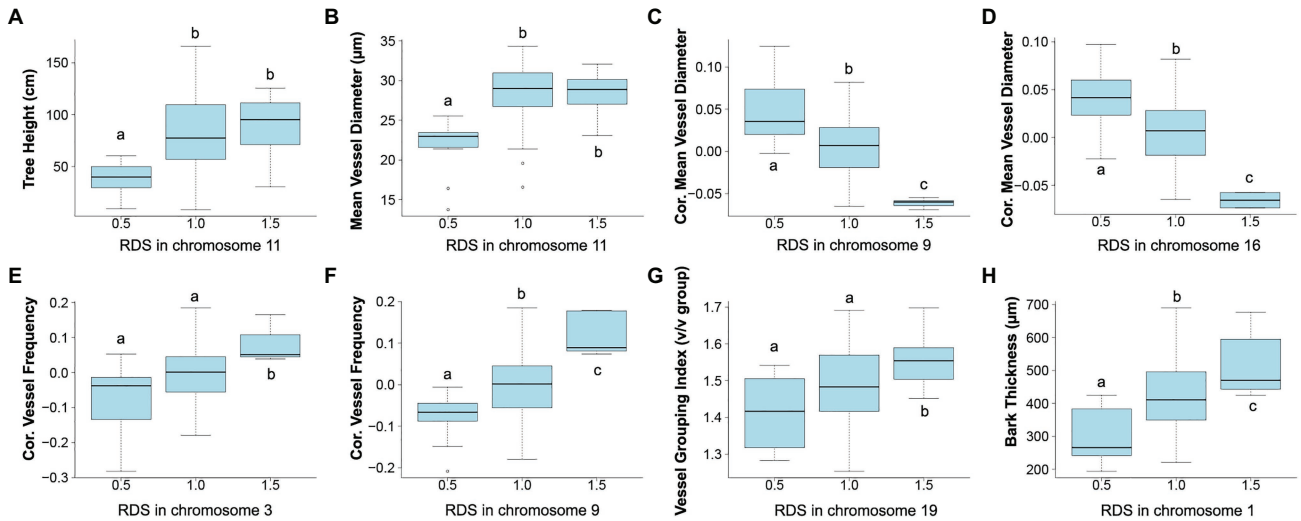

FIGURE 7 | Relationship between trait value and relative dosage scores (RDSs) at genomic bins detected by dQTL analyses. Each boxplot shows all genotypes grouped by RDS at the most significant dQTL detected for each trait. Selected dQTLs were located on chromosome 11 for tree height **(A)** and MVD **(B)**, chromosome 9 **(C)** and chromosome 16 **(D)** for cMVD, chromosome 3 **(E)** and chromosome 9 **(F)** for cVF, chromosome 19 for VGI **(G)**, and chromosome 1 for bark thickness **(H)**. Tukey pairwise comparisons were used to visualize significant differences in mean trait values between the groups; means that share a letter are not significantly different ($p > 0.05$).

directly in a forest tree species within a pedigree carrying indels that create additional, dosage-based variation. All the anatomical and vessel traits under study here showed significant heritabilities, indicating a significant degree of genetic control. As anticipated, some stem anatomical and vessel traits showed significant correlations with tree height. Specifically, significant positive correlations were found between tree height and MVD (0.76) and BT (0.52), while VF showed a significant negative correlation (−0.76) with height. One goal was thus to determine the amount of phenotypic variation in the MVD and VF is attributed to genetic variation not associated with height. We analyzed this by removing the effect of tree height in ANOVA to calculate cMVD and cVF that were "corrected" for the effect of tree height. This approach was effective and showed that genetic variation independent of tree height had significant heritabilities for cMVD (0.44) and cVF (0.32). Thus, in addition to scaling by tree height, we observed additional significant variation among genotypes for MVD and VF, suggesting that these are traits amenable to genetic manipulation and breeding independent of height or tree size.

Our irradiation hybrid germplasm also enabled analysis genome-wide scans for quantitative trait loci that are both responsive to gene dosage variation and that affect vessel traits. We found significant QTL for tree height, MVD, cMVD, cVF, VGI, and BT. Other traits, VF, MVC, and NF, did not reveal significant QTL, however. In each case, there are several types of genetic variation that would be transparent to our analysis here. These include genes that are involved in vessel trait regulation but that do not show dosage sensitivity, genes with segregating allelic variation, genes whose variation is masked by genetic redundancy or physiological compensation mechanisms, and genes with smaller effects. Regardless, some interesting conclusions can be reached about the genetic architecture and interplay of the traits under study here. For example, the correlation of tree height with MVD is reflected in a common dQTL on chromosome 11, perhaps representing a common regulator influencing each trait, or else a factor directly influencing one trait with indirect influence on the other. After correcting for tree height, significant genetic variation was still detected for cMVD, as reflected by a unique dQTL on chromosome 9. Interestingly, the cMVD trait was inversely proportional to dosage at this dQTL, predicting that a dosage-sensitive negative regulator of growth may be uncovered at this locus. Additionally, unique dQTL not shared by other traits were identified for cVF, VGI, and BT, suggesting potential trait-specific regulators at these loci. In addition to furthering our basic understanding of how these various wood anatomical traits are related to each other genetically, these results also provide insights into what traits may be independently targeted through breeding approaches. In this regard, an identification of dQTL for vessel traits that are not shared by tree height is encouraging for the ability to select or breed for trees through selection on both height growth and vessel traits.

Previous studies point to challenges in the genetic dissection of wood anatomy and vessel morphological traits. Quantitative genetic analyses of vessel traits in a *P. deltoides* mapping population identified a single QTL with the causative locus *ENLARGED VESSEL ELEMENT* (*EVE*) encoding a plasma membrane-localized protein affecting potassium uptake and presumably turgor in differentiating vessel elements (Ribeiro et al., 2020). Interestingly the EVE protein is not only specific to vessel elements but also found in fibers, but nonetheless is supportive of the notion that potassium plays a key role in vessel expansion. A large genome-wide association study in *Populus trichocarpa* identified a single QTL associated with intermediate wood vessel size,

encoding a putative double-stranded RNA binding protein (Chhetri et al., 2020). Multi trait associations with vessel area phenotypes were identified for an additional six genes, including genes encoding a leucine-rich repeat containing protein and a serine–threonine protein kinase that might play signaling roles during vessel element differentiation. Interestingly, some vessel traits were correlated with the latitude of accessions included in the study, emphasizing that these are adaptive traits are under genetic control and selection. Notably, there is no overlap among the QTL found in our study and any of these previous studies. Along with the modest number of QTL identified in these studies, it seems reasonable to speculate that the high responsiveness of vessel traits to environmental variation make it especially challenging to measure genetic signal against a background of uncontrolled environmental variation.

Our results clearly demonstrate that vessel traits are under genetic control and that dosage-responsive QTL can be identified. While this is encouraging, we also see the opportunity to increase the power of detection and characterization of the genetic regulation of vessel traits. Notably, future studies could exploit automated phenotyping systems to minimize uncontrolled environmental variation, impose water stress treatments to examine vessel trait responses, and capture physiological data using image-based phenotyping to correlate with those responses. Similarly, high throughput histological phenotyping combined with machine learning-based approaches could provide more insightful and uniform means for analyzing wood anatomy and vessel features. A systems genomics strategy integrating vessel phenotypes, genomic locations in indels, and gene expression data could now be used to both summarize mechanisms and identify candidate genes for functional characterization, as we recently used for dissecting poplar leaf morphology (Bastiaanse et al., 2021).

The magnitude of problems associated with climate change effects on forests is large with drought and increasing temperatures resulting in water stress that has already resulted in forest declines and associated wildfire in large areas of temperate and boreal forests. While vessel anatomy and hydraulics is only part of the picture, gaining new fundamental insights into how trees respond to environmental variation is a part of the needed information for producing solutions for managing and conserving forests in decades to come.

DATA AVAILABILITY STATEMENT

The datasets presented in this study can be found in online repositories. The names of the repository/repositories and accession number(s) can be found at: https://www.ncbi.nlm.nih.gov/genbank/. The genome sequencing datasets used for this study for detecting and defining indels can be found in NCBI SRA database under accession number SRP040492 and BioProject ID PRJNA241273.

AUTHOR CONTRIBUTIONS

AG, FDRZ, and IH designed the study. FDRZ led the data collection and the data analysis with direction from AG. FDRZ drafted the manuscript. AG and IH edited the manuscript. All authors contributed to the article and approved the submitted version.

FUNDING

FDRZ was supported by the NSF fellowship 1650042. Other funding for this study was provided by the US Forest Service Pacific Southwest Research Station.

ACKNOWLEDGMENTS

We thank Lucy Sullivan and Pakeeza Azizpor for assistance in performing histology and analysis of anatomical images. We also thank Courtney Canning for assistance in growing trees at the Institute of Forest Genetics. We also thank Heloise Bastiaanse for sharing code used in data analysis.

REFERENCES

Baas, P., Werker, E., and Fahn, A. (1983). Some ecological trends in vessel characters. *IAWA J.* 4, 141–159.

Barbour, M., and Whitehead, D. (2003). A demonstration of the theoretical prediction that sap velocity is related to wood density in the conifer *Dacrydium cupressinum*. *New Phytol.* 158, 477–488. doi: 10.1046/j.1469-8137.2003.00754.x

Bastiaanse, H., Henry, I., Tsai, H., Lieberman, M., Canning, C., Comai, L., et al. (2021). A systems genetics approach to deciphering the effect of dosage variation of leaf morphology in *Populus*. *Plant Cell* 33, 940–960. doi: 10.1093/plcell/koaa016

Bastiaanse, H., Zinkgraff, M., Canning, C., Tsai, H., Lieberman, M., Comai, L., et al. (2019). A comprehensive genomic scan reveals gene dosage balance impacts on quantitative traits in *Populus* trees. *Proc. Natl. Acad. Sci. U. S. A.* 27, 13690–13699. doi: 10.1073/pnas.1903229116

Brodribb, T., and Feild, T. (2000). Stem hydraulic supply is linked to leaf photosynthetic capacity: evidence from new Caledonian and Tasmanian rainforests. *Plant Cell Environ.* 23, 1381–1388. doi: 10.1046/j.1365-3040.2000.00647.x

Carlquist, S. (1984). Vessel grouping of Dicotyledon wood. *Aliso* 10, 505–525. doi: 10.5642/aliso.19841004.03

Carlquist, S. (2001). *Comparative Wood Anatomy – Systematic, Ecological, and Evolutionary Aspects of Dicotyledon Wood. 2nd Edn.* Berlin: Springer Verlag.

Chauhan, L., Raturi, R., and Gupta, S. (1999). Studies of anatomical variations in different clones of *Populus deltoides*. *Indian For.* 125, 526–532.

Chhetri, H., Furches, A., Macaya-Sanz, D., Walker, A., Kainer, D., Jones, P., et al. (2020). Genome-wide association study of wood anatomical and morphological traits in *Populus trichocarpa*. *Front. Plant Sci.* 11:545748. doi: 10.3389/fpls.2020.545748

Cochard, H., Froux, F., Mayr, S., and Coutand, C. (2004). Xylem wall collapse in water-stressed pine needles. *Plant Physiol.* 134, 401–408. doi: 10.1104/pp.103.028357

Cutter, B., and Morphey, W. (1978). Effects of potassium on growth and wood anatomy of a populus hybrid. *Wood Fiber Sci.* 9, 282–288.

Gleason, S. M., Westoby, M., Jansen, S., Choat, B., Hacke, U. G., Pratt, R. B., et al. (2016). Weak tradeoff between xylem safety and xylem-specific hydraulic efficiency across the world's woody plant species. *New Phytol.* 209, 123–136. doi: 10.1111/nph.13646

Groover, A., and Jones, A. (1999). Tracheary element differentiation uses a novel mechanisms coordinating programmed cell death and secondary cell wall synthesis. *Plant Physiol.* 119, 375–384. doi: 10.1104/pp.119.2.375

Hacke, U., Spicer, R., Schreiber, S., and Plavcova, L. (2016). An ecophysiological and developmental perspective on variation in vessel diameter. *Plant Cell Environ.* 40, 831–845. doi: 10.1111/pce.12777

Hajek, P., Leuschner, C., Hertel, D., Delzon, S., and Schuldt, B. (2014). Trade-offs between xylem hydraulic properties, wood anatomy and yield in *Populus*. *Tree Physiol.* 34, 744–756. doi: 10.1093/treephys/tpu048

Henry, I., Zinkgraf, M., Groover, A., and Comai, L. (2015). A system for dosage-based functional genomics in poplar. *Plant Cell* 27, 2370–2383. doi: 10.1105/tpc.15.00349

Kruijer, W., Boer, M., Malosetti, M., Flood, P., Engel, B., Kooke, R., et al. (2015). Marker-based estimation of heritability in immortal populations. *Genetics* 199, 379–398. doi: 10.1534/genetics.114.167916

Larson, P. (1994). *The Vascular Cambium: Development and Structure*. Berlin, Heidelberg: Springer-Verlag.

Lens, F., Sperry, J., Christman, M., Choat, B., Rabaey, D., and Jansen, S. (2011). Testing hypotheses that link wood anatomy to cavitation resistance and hydraulic conductivity in the genus *Acer*. *New Phytol.* 190, 709–723. doi: 10.1111/j.1469-8137.2010.03518.x

Loepfe, L., Martinez-Villalta, J., Pinol, J., and Mencuccini, M. (2007). The relevance of xylem network structure for plant hydraulic efficiency and safety. *J. Theor. Biol.* 247, 788–803. doi: 10.1016/j.jtbi.2007.03.036

Olson, M., and Rosell, J. (2013). Vessel diameter-stem diameter scaling across woody angiosperms and the ecological causes of xylem vessel diameter variation. *New Phytol.* 197, 1204–1213. doi: 10.1111/nph.12097

Olson, M., Tommaso, A., Rosell, J., Petit, G., Crivellaro, A., Isnard, S., et al. (2014). Universal hydraulics of the flowering plants: vessel diameter scales with stem length across angiosperm lineages, habits and climates. *Ecol. Lett.* 17, 988–997. doi: 10.1111/ele.12302

Pinosio, S., Giacommelo, S., Faivre-Rampant, P., Taylor, G., Jorge, V., Paslier, L., et al. (2016). Characterization of the poplar pen-genome by genome-wide identification of structural variation. *Mol. Biol. Evol.* 33, 2707–2719. doi: 10.1093/molbev/msw161

Ribeiro, C., Conde, D., Balmant, K., Dervinis, C., Johnson, M., McGrath, A., et al. (2020). The uncharacterized gene EVE contributes to vessel element dimensions in *Populus*. *Proc. Natl. Acad. Sci. U. S. A.* 117, 5059–5066. doi: 10.1073/pnas.1912434117

Rodriguez-Zaccaro, D., and Groover, A. (2019). Wood and water: how trees modify wood development to cope with drought. *Plants People Planet* 1, 346–355. doi: 10.1002/ppp3.29

Schaeffer, M., and Levitt, E. (1956). Concerning Kendall's tau, a nonparametric correlation coefficient. *Psychol. Bull.* 53, 338–346. doi: 10.1037/h0045013

Scholz, A., Klepsch, M., Karimi, Z., and Jansen, S. (2013). How to quantify conduits in wood? *Front. Plant Sci.* 4:56. doi: 10.3389/fpls.2013.00056

Searson, M., Thomas, D., Montagu, K., and Conroy, J. (2004). Wood density and anatomy of water limited eucalypyts. *Tree Physiol.* 24, 1295–1302. doi: 10.1093/treephys/24.11.1295

Sellin, A., Rohejärv, A., and Rahi, M. (2008). Distribution of vessel size, vessel density and xylem conducting efficiency within a crown of silver birch (*Betula pendula*). *Trees* 22, 205–216. doi: 10.1007/s00468-007-0177-4

Sperry, J., Hacke, U. G., and Pittermann, J. (2006). Size and function in conifer tracheids and angiosperm vessels. *Am. J. Bot.* 93, 1490–1500. doi: 10.3732/ajb.93.10.1490

Turner, S., Gallois, P., and Brown, D. (2007). Tracheary element differentiation. *Annu. Rev. Plant Biol.* 58, 407–433. doi: 10.1146/annurev.arplant.57.032905.105236

Turner, S., and Somerville, C. (1997). Collapsed xylem phenotype of *Arabidopsis* identifies mutants deficient in cellulose deposition in the secondary cell wall. *Plant Cell* 9, 689–701. doi: 10.1105/tpc.9.5.689

Tyree, M. (1989). Cavitation in trees and the hydraulic sufficiency of woody stems. *Ann. For. Sci.* 46, 330–337.

Tyree, M., and Sperry, J. S. (1989). Vulnerability of xylem to cavita-tion and embolism. *Annu. Rev. Plant Physiol.* 40, 19–36. doi: 10.1146/annurev.pp.40.060189.000315

Tyree, M., and Zimmermann, M. (2002). *Xylem Structure and the Ascent of Sap*. Heidelberg, Berlin: Springer-Verlag.

Venturas, M., Sperry, J., and Hacke, U. (2017). Plant xylem hydraulics: what we understand, current research and future challenges. *J. Integr. Plant Biol.* 59, 356–389. doi: 10.1111/jipb.12534

Villar-Salvador, P., Castro-Diez, P., Perez-Rontome, C., and Montserrat-Marti, G. (1997). Stem xylem features in three *Quercus* (Fagaceae) species along a climate gradient in NE Spain. *Trees* 12, 90–96.

von Arx, G., Kueffer, C., and Fonti, P. (2013). Quantifying plasticity in vessel grouping-added value from the image analysis tool RoXAS. *IAWA J.* 34, 433–445. doi: 10.1163/22941932-00000035

Wagner, K., Ewers, F., and Davis, S. (1998). Tradeoffs between hydraulic efficiency and mechanical strength in the stems of four co-occurring species of chaparral shrubs. *Oecologia* 117, 53–62. doi: 10.1007/s004420050631

White, F. (2011). *Fluid Mechanics*. New York: McGraw-Hill Higher Education.

Zanne, A., Westoby, M., Falster, D., Ackerly, D., Loarie, L., Arnold, S., et al. (2010). Angiosperm wood structure: global patterns in vessel anatomy and their relation to wood density and potential conductivity. *Am. J. Bot.* 97, 207–215. doi: 10.3732/ajb.0900178

Zhang, B., Zhu, W., Diao, S., Wu, X., Lu, K., Ding, C., et al. (2019). The poplar pangenome provides insights into the evolutionary history of the genus. *Commun. Biol.* 2:215. doi: 10.1038/s42003-019-0474-7

Conflict of Interest: The authors declare that the research was conducted in the absence of any commercial or financial relationships that could be construed as a potential conflict of interest.

Publisher's Note: All claims expressed in this article are solely those of the authors and do not necessarily represent those of their affiliated organizations, or those of the publisher, the editors and the reviewers. Any product that may be evaluated in this article, or claim that may be made by its manufacturer, is not guaranteed or endorsed by the publisher.

frontiers in Plant Science

ORIGINAL RESEARCH
published: 30 August 2021
doi: 10.3389/fpls.2021.704941

Association Study and Mendelian Randomization Analysis Reveal Effects of the Genetic Interaction Between *PtoMIR403b* and *PtoGT31B-1* on Wood Formation in *Populus tomentosa*

Liang Xiao[1,2†], Liting Man[1,2,3†], Lina Yang[1,2†], Jinmei Zhang[3], Baoyao Liu[3], Mingyang Quan[1,2], Wenjie Lu[1,2], Yuanyuan Fang[1,2], Dan Wang[1,2], Qingzhang Du[1,2] and Deqiang Zhang[1,2]*

[1] National Engineering Laboratory for Tree Breeding, College of Biological Sciences and Technology, Beijing Forestry University, Beijing, China, [2] Key Laboratory of Genetics and Breeding in Forest Trees and Ornamental Plants, Ministry of Education, College of Biological Sciences and Technology, Beijing Forestry University, Beijing, China, [3] Xining Forestry Science Research Institute, Xining, China

OPEN ACCESS

Edited by:
Meng-Zhu Lu,
Zhejiang Agriculture and Forestry University, China

Reviewed by:
Pankaj Bhardwaj,
Central University of Punjab, India
Jinhui Chen,
Hainan University, China

***Correspondence:**
Deqiang Zhang
DeqiangZhang@bjfu.edu.cn

[†] These authors have contributed equally to this work

Specialty section:
This article was submitted to Plant Biotechnology, a section of the journal Frontiers in Plant Science

Received: 04 May 2021
Accepted: 04 August 2021
Published: 30 August 2021

Citation:
Xiao L, Man L, Yang L, Zhang J, Liu B, Quan M, Lu W, Fang Y, Wang D, Du Q and Zhang D (2021) Association Study and Mendelian Randomization Analysis Reveal Effects of the Genetic Interaction Between PtoMIR403b and PtoGT31B-1 on Wood Formation in Populus tomentosa. Front. Plant Sci. 12:704941. doi: 10.3389/fpls.2021.704941

MicroRNAs (miRNAs), important posttranscriptional regulators of gene expression, play a crucial role in plant growth and development. A single miRNA can regulate numerous target genes, making the determination of its function and interaction with targets challenging. We identified PtomiR403b target to *PtoGT31B-1*, which encodes a galactosyltransferase responsible for the biosynthesis of cell wall polysaccharides. We performed an association study and epistasis and Mendelian randomization (MR) analyses to explore how the genetic interaction between *PtoMIR403b* and its target *PtoGT31B-1* underlies wood formation. Single nucleotide polymorphism (SNP)-based association studies identified 25 significant associations ($P < 0.01$, $Q < 0.05$), and *PtoMIR403b* and *PtoGT31B-1* were associated with five traits, suggesting a role for PtomiR403b and *PtoGT31B-1* in wood formation. Epistasis analysis identified 93 significant pairwise epistatic associations with 10 wood formation traits, and 37.89% of the SNP-SNP pairs indicated interactions between *PtoMIR403b* and *PtoGT31B-1*. We performed an MR analysis to demonstrate the causality of the relationships between SNPs in *PtoMIR403b* and wood property traits and that *PtoMIR403b* modulates wood formation by regulating expression of *PtoGT31B-1*. Therefore, our findings will facilitate dissection of the functions and interactions with miRNA-targets.

Keywords: PtomiR403b, *PtoGT31B-1*, association study, epistasis, Mendelian randomization, genetic interaction, *Populus*

INTRODUCTION

Trees are an abundant renewable source of pulp and are important in the emerging bioenergy industry (Jansson and Douglas, 2007). Secondary cell walls form the bulk of woody tissue and affect wood quality and quantity (Zhang et al., 2014). Genetic analyses of annual herbals and perennial trees have showed that the cell wall comprises mainly cellulose, hemicellulose, and pectin, along

with lignin and protein (Basu et al., 2016). The participation of genetic factors in the biosynthesis of cell wall components involves Galactosyltransferases and microRNAs (miRNAs) (Lu et al., 2013; Yu et al., 2014; Li et al., 2015; Fan et al., 2020).

Galactosyltransferases are encoded by a small gene family—glycosyltransferase 31 (GT31), include GALT and GALECTIN domains, and mediate the biosynthesis of cell wall polysaccharides, such as xyloglucan (XyG; the dominant component of hemicellulose) and rhamnogalacturonan I (RG-I; a pectin component) (Hennet, 2002; Jensen et al., 2012; Showalter and Basu, 2016; Matsumoto et al., 2019). The hemicellulose content of *Populus* wood is 16–23% on a dry weight (DW) basis, and the glucan content is 39–49% on a DW basis (Porth et al., 2013), suggesting an important role for galactosyltransferases in wood formation. But there are few functional analyses of galactosyltransferase genes in tree species, much of the research being conducted in *Arabidopsis thaliana* (Fagundes Lopes et al., 2010). For example, *GALT2* and *GALT5* function as AGP-Hyp-O-galactosyltransferases, and double mutants had altered phenotypes related to growth and development, including reduced silique length and plant height (Basu et al., 2015). *MURUS3* (*MUR3*) encodes a XyG-specific galactosyltransferase, which leads to dwarf mutants with short petioles and short inflorescence stems in *A. thaliana* (Kong et al., 2015). Overexpression of *EgMUR3* (the *MUR3* ortholog in *Eucalyptus grandis*) in *A. thaliana* resulted in similar phenotypes, implying a role for galactosyltransferase genes in wood formation (Fagundes Lopes et al., 2010).

MicroRNAs (miRNAs) are an endogenous class of *trans*-acting small non-coding RNAs (approximately 20–24 nucleotides) that are important posttranscriptional regulators of gene expression in eukaryotes (Ehrenreich and Purugganan, 2008). In plants, miRNAs play roles in numerous biological processes (Budak and Akpinar, 2015). For instance, miRNAs are implicated in wood formation in *Populus*—PtomiR397a downregulated the expression of *LACs* and reduced the Klason lignin content by as much as 22% in *Populus trichocarpa* (Lu et al., 2013). In addition, PtomiR6443 regulated *Ferulate 5-hydroxylase* (*F5H*) to alter lignin composition and enhance saccharification in *Populus tomentosa* (Fan et al., 2020). However, no systematic effort has been made to characterize the miRNAs that regulate the galactosyltransferase genes.

Association studies enable the identification of DNA variants associated with phenotypic variation, especially for the quantitative traits of perennial trees because of their abundant genetic variants and the large number of genomes sequenced (Cardon and Bell, 2001; Neale and Savolainen, 2004). This strategy has been used to identify single nucleotide polymorphisms (SNPs) associated with wood characteristics in several perennial tree species. For instance, Wegrzyn et al. (2010) explored the effects of SNPs in lignin and cellulose biosynthesis genes on wood chemistry traits and identified the polymorphisms responsible for phenotypic variation in *P. trichocarpa*. In Mendelian randomization (MR) analyses, a causal relationship between two heritable complex traits is inferred, with one reflecting exposure and the other taken as the outcome (Burgess et al., 2018). MR tests is a widely method to assess the causal relationship between complex traits and environmental factors or gene expression (Porcu et al., 2019). For example, MR studies have identified causal relationships between specific gene expression and clinical traits, with gene expression treated as an exposure risk factor for the manifestation of complex traits, indicating that MR analyses can bridge the causal relationship between genetic variation, gene expression, and complex traits (Li et al., 2016; van der Graaf et al., 2020). MiRNAs are *trans*-regulators of gene expression, implying that MR can be used to uncover causal relationships between miRNAs and desirable traits. Therefore, by combining an association study and a MR analysis, insight into how genetic interactions between miRNAs and their targets affect desirable traits can be obtained.

We report here that PtomiR403b, a conserved miRNA, was highly expressed in the developing xylem. An association study and epistasis analysis were conducted to explore the genetic effects of PtomiR403b and its target *PtoGT31B-1* on tree growth and wood formation in an association population of *P. tomentosa*, and an MR analysis was performed to assess the causative relationship between *PtoMIR403b* and *PtoGT31B-1* underlying the wood characteristic traits. Collectively, our aim was to identify significant SNPs in *PtoMIR403b* that are associated with wood characteristic traits, analyze the genetic interaction between *PtoMIR403b* and *PtoGT31B-1*. Ultimately, our findings provide a strategy to characterize the genetic interaction of miRNA and its targets, and also contribute to the improvement of *Populus* wood yield and quality via marker-assisted breeding.

MATERIALS AND METHODS

Association Population and Phenotypic Data

Association Population

The *P. tomentosa* association population used in this study consisted of 435 unrelated individuals representing almost the entire natural distribution (30–40°N, 105–125°E). The accessions were cloned via root segments in a randomized complete block design with three blocks in 2009 in Guan Xian County, Shandong Province, China (36°23′N, 115°47′E). The total genomic DNA from each accession was extracted from fresh leaves of each individual using a DNeasy Plant Mini kit (Qiagen, Shanghai, China) following the manufacturer's protocol.

Phenotypic Data

We measured 10 wood characteristic traits for the 435 individuals of *P. tomentosa*—diameter at breast height (DBH), tree height (H), stem volume (V), α-cellulose content (AC), holocellulose content (HC), hemicellulose content (HEC), lignin content (LC), fiber length (FL), fiber width (FW), and microfiber angle (MFA). Measurements were conducted following the method described in Du et al. (2014).

Identification and Isolation of *PtoMIR403b* and Its Target Genes

To clone the full-length sequence of *PtoMIR403b* in *P. tomentosa*, we used gene-specific primers based on the primary sequence

of PtomiR403b, which contains the pre-miRNA region of the *PtoMIR403b* sequence and 600 bp of flanking region on each side. Next, psRNATarget[1] was used to predict putative target genes of PtomiR403b in the genome-wide transcript of *P. tomentosa*, with the expectation cutoff set to 2.0. In addition, degradome sequencing of pooled samples of six tissues (leaf, shoot apex, phloem, cambium, developing xylem, and mature xylem) was performed to identify potential cleavage sites and verify the psRNATarget results, in which *PtoGT31B-1* was identified as a putative target of PtomiR403b. Finally, we cloned the full-length sequence of *PtoGT31B-1* from the genome of *P. tomentosa*.

Degradome sequencing enables the identification of miRNA cleavage sites in target genes via the sequencing of RNA ends. We performed degradome sequencing using equal pooled RNA samples of six tissues (leaf, shoot apex, phloem, cambium, developing xylem, and mature xylem) from *P. tomentosa*. The pooled RNA samples were used with biotinylated random primers to build a degradome-sequencing library as described previously (German et al., 2008). MiRNA cleavage sites were identified using the CleaveLand pipeline based on *P. tomentosa* genome transcripts (Addo-Quaye et al., 2009). The detailed methods have described in **Supplementary Methods 1**.

RNA Ligase-Mediated 5′ Rapid Amplification of cDNA Ends

To identify cleavage sites in target genes, RNA ligase-mediated 5′ rapid amplification of cDNA ends (RLM-5′ RACE) was conducted using the SMARTer RACE Kit (TaKaRa, Shiga, Japan) in accordance with the manufacturer's instructions with modifications. Briefly, extracted total RNA was ligated to a 5′ RACE adapter using T4 RNA ligase, followed by cDNA template synthesis via reverse transcription with 5′-RACE CDS Primer A [5′-(T)25 V N-3′; N = A, C, G, or T; V = A, G, or C]. Next, 5′ RACE PCR was performed using a universal primer (forward) and a gene-specific primer (reverse, **Supplementary Table 1**), with cDNA as the template. The products were gel purified, cloned, and sequenced.

Real-Time Quantitative PCR

To evaluate the expression of PtomiR403b and its targets, we used the phloem, cambium, developing xylem, mature xylem, leaf, and shoot apex tissues of a 1-year-old *P. tomentosa* clone. Total RNA was extracted using the Plant Qiagen RNeasy Kit (Qiagen China, Shanghai) following the manufacturer's instructions and purified using the RNase-Free DNase Set (Qiagen). mRNAs were reverse transcribed into cDNA using the Reverse Transcription System (Promega Corporation, Madison, WI) according to the manufacturer's instructions. MiRNAs were reverse transcribed into cDNA using the miRcute Plus miRNA First-Strand cDNA Synthesis Kit (Tiangen, Beijing, China). Gene-specific primers were used for real-time quantitative PCR (RT-qPCR) on the 7500 Fast Real-Time PCR System with SYBR Premix Ex Taq (TaKaRa) and the miRcute Plus miRNA qPCR Kit (SYBR Green; Tiangen) (**Supplementary Table 1**). All reactions were performed with three technical and biological replicates with poplar *actin* (accession number: EF145577) used as the internal control. The PCR amplification program (Xiao et al., 2017) was as follows: initial denaturation at 94°C for 5 min; 40 cycles of 94°C for 30 s, 58°C for 30 s, and 72°C for 30 s; and a final melting curve from 70 to 95°C.

Phylogenetic Analysis of miR403

For the phylogenetic analysis of miR403, we downloaded all precursor sequences of miR403 from miRbase,[2] thus obtaining 40 members from 22 species (including four members of PtomiR403). We used Muscle in MEGA ver. 7.0 software with the default settings to perform multiple sequence alignments (Kumar et al., 2016). Phylogenetic trees were constructed using the maximum-likelihood method in MEGA ver. 7.0 software; branch support was estimated with 1,000 bootstrap replicates. Figtree software[3] was used to visualize the phylogenetic tree.

Identification of SNPs in *PtoMIR403b* and *PtoGT31B-1*

The association population of 435 accessions was resequenced on the Illumina GA2 sequencing platform at an average depth of 15 × genome coverage (raw data). To obtain the clean data, the Raw reads were trimmed through a series of quality control (QC) procedures. QC standards as the following: (1) Removing reads with ≥ 10% unidentified nucleotides (N); (2) Removing reads with > 50% bases having phred quality < 5; (3) Removing reads with > 10 nt aligned to the adapter, allowing ≤ 10% mismatches; (4) Removing putative PCR duplicates generated by PCR amplification in the library construction process (read 1 and read 2 of two paired-end reads that were completely identical). Then, the clean reads were mapped to the *P. tomentosa* reference genome and used for SNP calling. VCFtools software was used to extract gene-derived biallelic SNPs from the full-length sequences of *PtoMIR403b* (including the pre-miRNA and 600-bp flanking sequences on each side) and *PtoGT31B-1* (including the 2-kb upstream promoter sequence and 500-bp downstream flanking sequence). We identified 54 and 165 high-quality SNPs in *PtoMIR403b* and *PtoGT31B-1*, respectively, with a minor allele frequency of > 5% and a miss rate of < 20% across 435 accessions. The detailed methods described in the **Supplementary Method 2**.

Nucleotide Diversity Analysis and Linkage Disequilibrium Test

To evaluate nucleotide diversity, we estimated π (the average number of pair-wise differences per site between sequences) and θw (the average number of segregating sites per site) using Tassel ver. 2.0 software. For linkage disequilibrium (LD) analysis, we calculated the squared correlation of allele frequencies (r^2) between pairs of SNPs in *PtoMIR403b* and *PtoGT31B-1*. To assess the pattern of LD in *PtoMIR403b* and its target, the decay of LD with physical distance (base pairs) within each SNP was estimated

[1]http://plantgrn.noble.org/psRNATarget/

[2]http://www.mirbase.org/

[3]http://tree.bio.ed.ac.uk/software/figtree/

in 10^5 permutations of the genotype data using non-linear regression. Singletons were excluded from the LD analysis.

Single SNP-Based Association Analysis

A single SNP-based association analysis was performed for all SNP-trait associations between 219 common SNPs and 10 traits using Tassel ver. 5.0 software with a mixed linear model (MLM) that controls for kinship coefficients (K) and population structure (Q) (Bradbury et al., 2007). The K and Q matrices were obtained as described by Du et al. (2019). The QVALUE package in R was used to correct for multiple testing based on the positive false discovery rate method. The significance threshold for a single SNP-based association was defined as $P < 0.01$ and $Q < 0.05$.

Multi-SNP Epistasis Association Analysis

Multifactor Dimensionality Reduction (MDR) ver. 3.0.2 software was used to detect epistatic effects among the SNPs (Hahn et al., 2003). The ReliefF algorithm in MDR 3.0.2 was used to improve the reliability of probability approximation by filtering all unlinked SNPs ($r^2 < 0.1$ or different genes) and identify the best five loci for each trait. An entropy-based measure was used to detect significant interactions between SNP-SNP pairs and calculate information gains (IGs) to evaluate epistatic effects.

Expression Level of *PtoGT31B-1* in a Natural Population of *P. tomentosa*

Developing xylem tissues from the 435 accessions in a natural population of *P. tomentosa* were collected. Total RNA was extracted, reverse transcribed into cDNAs, and subjected to RT-qPCR to assess the expression level of *PtoGT31B-1* in 435 accessions of *P. tomentosa*. All reactions were performed with three technical replicates with poplar *actin* as the internal control. Relative mRNA levels were calculated using the comparative threshold cycle method.

Mendelian Randomization (MR) Analysis

MR analysis was performed to evaluate the causality of the relationships between genetic variants and traits. To estimate the genetic effects of SNPs on the expression of *PtoGT31B-1*, we conducted an association analysis of the SNPs and *PtoGT31B-1* expression in the 435 accessions using Tassel 5.0 software with an MLM. The SNPs significantly associated with wood characteristic traits were subjected to MR analysis. The MendelianRandomization package in R was used for MR analysis with the inverse-variance weighting (IVW) method to summarize the effects of multiple SNPs (Yavorska and Burgess, 2017).

RESULTS

Identification of PtomiR403b and Its Potential Targets in *P. tomentosa*

The miRNA transcription profiles in the leaf, mature xylem, cambium, developing xylem, shoot apex, and phloem tissues of *P. tomentosa*, indicated that miR403b was highly expressed in the shoot apex and phloem, suggesting a putative role for miR403b in *Populus* growth and development. Thus, we selected PtomiR403b for further analysis. We isolated the 1,300-bp primary sequence of *PtoMIR403b* from *P. tomentosa* containing a 21-bp mature region, 100-bp pre-miRNA region, and 600-bp flanking sequences around the pre-miRNA region. Prediction of the secondary structure of the precursor of PtomiR403b using RNAfold[4] revealed a typical stem-loop structure, verifying that PtomiR403b is a miRNA (**Supplementary Figure 1**).

To identify the target genes of PtomiR403b, we used the psRNATarget to predict the putative targets in the genome-wide transcripts of *P. tomentosa* identified Ptom.002G.02518 (encoding β-1,3-galactosyltransferase 2 isoform X1, *PtoGT31B-1*), which is cleaved by PtomiR403 with an expectation value of ≤ 2. *PtoGT31B-1* is a member of CAZy GT-family-31 and mediates the synthesis of β-(1,3)-Gal. Degradome sequencing verified *PtoGT31B-1* as a target of PtomiR403b. 5′-RACE confirmed that PtomiR403b cut *PtoGT31B-1* at 1,449 nt in the 3′-untranslated region (UTR) (**Figure 1A**). The *PtoGT31B-1* cDNA is 2,540 bp long, with a coding region of 969 bp (322 amino acids) flanked by a 440-bp 5′-UTR and an 1131-bp 3′-UTR (**Figure 1B**).

miR403 has diverse functions in different species. Therefore, we aligned all precursor sequences of miR403 from miRbase, which included 40 members from 22 species. Mature sequences were conserved across 18 species, whereas the number of miR403 members varied among species, with some absent from eudicots, suggesting that the functional role of miR403 has changed over the course of plant evolution (**Supplementary Figure 2**). Phylogenetic analysis showed that PtomiR403 exhibits high homology with miR403 from *P. trichocarpa*, indicating that the miR403 family is conserved in *Populus*.

Tissue Specific Expression Pattern Reveal the Negative Correlation Between PtomiR403b and *PtoGT31B-1*

RT-qPCR showed that PtomiR403b and *PtoGT31B-1* expression varied among the eight different tissues of *P. tomentosa*. PtomiR403b expression was highest in the shoot apex, followed by the phloem, and lowest in mature xylem (**Figure 1C**). By contrast, *PtoGT31B-1* expression was highest in developing xylem, followed by leaves, and lowest in the shoot apex, implicating that *PtoGT31B-1* involving in wood formation. The correlation between the expression of PtomiR403b and its target was significantly negative (Pearson $r = -0.713$, $P = 0.056$), suggesting that PtomiR403b might negatively regulated the expression of *PtoGT31B-1* (**Figure 1D**).

PtoMIR403 and *PtoGT31B-1* Exhibited High Nucleotide Diversity and Rapidly Declining LD

Genomic resequencing of 435 *P. tomentosa* accessions identified 54 and 165 common SNPs in *PtoMIR403b* and *PtoGT31B-1*, respectively (**Supplementary Table 2**). For *PtoMIR403b*, no SNP

[4]http://rna.tbi.univie.ac.at/cgi-bin/RNAWebSuite/RNAfold.cgi

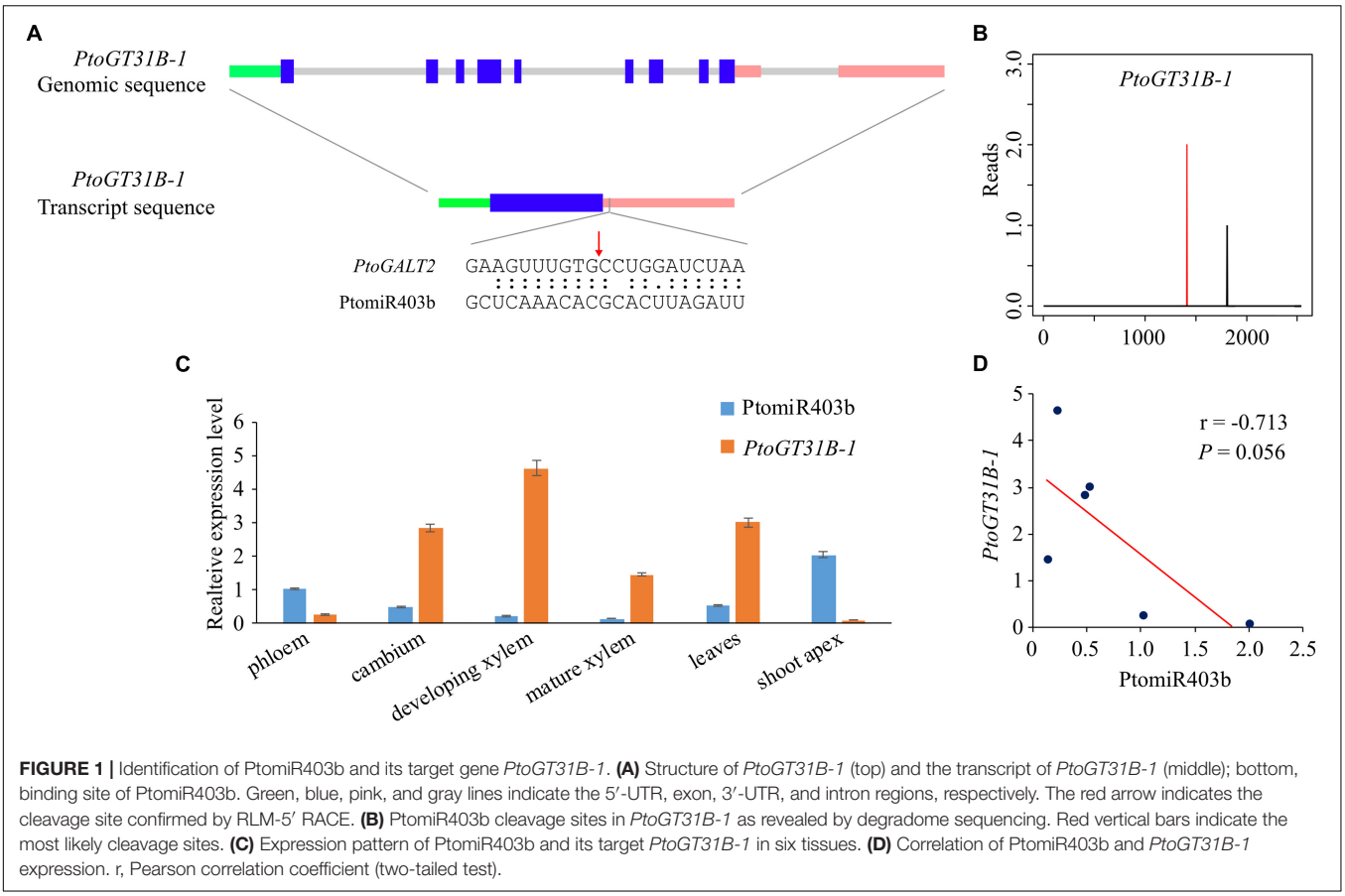

FIGURE 1 | Identification of PtomiR403b and its target gene *PtoGT31B-1*. **(A)** Structure of *PtoGT31B-1* (top) and the transcript of *PtoGT31B-1* (middle); bottom, binding site of PtomiR403b. Green, blue, pink, and gray lines indicate the 5′-UTR, exon, 3′-UTR, and intron regions, respectively. The red arrow indicates the cleavage site confirmed by RLM-5′ RACE. **(B)** PtomiR403b cleavage sites in *PtoGT31B-1* as revealed by degradome sequencing. Red vertical bars indicate the most likely cleavage sites. **(C)** Expression pattern of PtomiR403b and its target *PtoGT31B-1* in six tissues. **(D)** Correlation of PtomiR403b and *PtoGT31B-1* expression. r, Pearson correlation coefficient (two-tailed test).

was identified in the mature miRNA region, whereas three were detected in the precursor regions. We predicted the effect on the stem-loop structure and minimum free energy (MFE) of the SNPs in the precursor regions. PtoMIR403b_SNP31 and PtoMIR403b_SNP33 significantly altered the stability of secondary structure, whereas PtoMIR403b_SNP32 did not affect the stem-loop structure and MFE (**Supplementary Figure 1**). Moreover, these two deleterious variants had high LD ($r^2 = 0.948$) and affected the stem-loop structure more significantly. In addition, the primary sequence nucleotide diversity was higher than that of the precursor sequence, indicating different selective pressures in these regions. For *PtoGT31B-1*, the average synonymous diversity (d_S) of the coding region was higher than the non-synonymous diversity (d_N), with a d_N/d_S ratio of < 1 (0.83), indicating that the non-synonymous sites had experienced purifying selection. In addition, we also found that the nucleotide diversity of *PtoGT31B-1* ($\pi = 0.057$) was higher than that of *PtoMIR403b* ($\pi = 0.014$), implying that *PtoMIR403b* and *PtoGT31B-1* experienced different selection pressures.

The squared allelic correlation coefficient (r^2) between common SNP pairs was calculated to evaluate the overall patterns of LD for *Pto-MIR403b* and *PtoGT31B-1*. Non-linear regression showed that the LD decayed rapidly, decreasing to 0.1 within about 500 bp for *Pto-MIR403b* and about 2,500 bp for *PtoGT31B-1*. Therefore, the LD of *Pto-MIR403b* and *PtoGT31B-1* does not extend to the over entire gene sequences (**Supplementary Figure 3**).

Allelic Variation of *PtoMIR403b* and *PtoGT31B-1* Allelic Variation Affects Tree Growth and Wood Formation

To explore the effects of *PtoMIR403b* and its target *PtoGT31B-1* on tree growth and wood formation, we measured 10 wood characteristic traits of 435 individuals in a natural population of *P. tomentosa* that exhibited high phenotypic diversity. An association analysis to test the additive/dominant effects between SNPs in *PtoMIR403b* and its target gene and 10 traits using a MLM in Tassel 5.0 software. At the threshold of $P < 0.01$ and $q < 0.05$, we identified 25 significant associations, corresponding to 15 SNPs and 8 traits (**Supplementary Table 3**). Each SNP explained 0.61–16.35% of the phenotypic variance (R^2), with an average R^2 of 7.30%. Among the 25 significant associations, 10 out of 25 associations showed additive effects, 19 exhibited dominant effects, and four presented both additive and dominant effects.

For *PtoMIR403b*, we detected the deleterious variants PtoMIR403b_SNP31 and PtoMIR403b_SNP33 in the precursor region of *PtoMIR403b*; each had a high LD that altered the stem-loop structure of PtomiR403b. As expected, these two SNPs were significantly associated with HEC and AC,

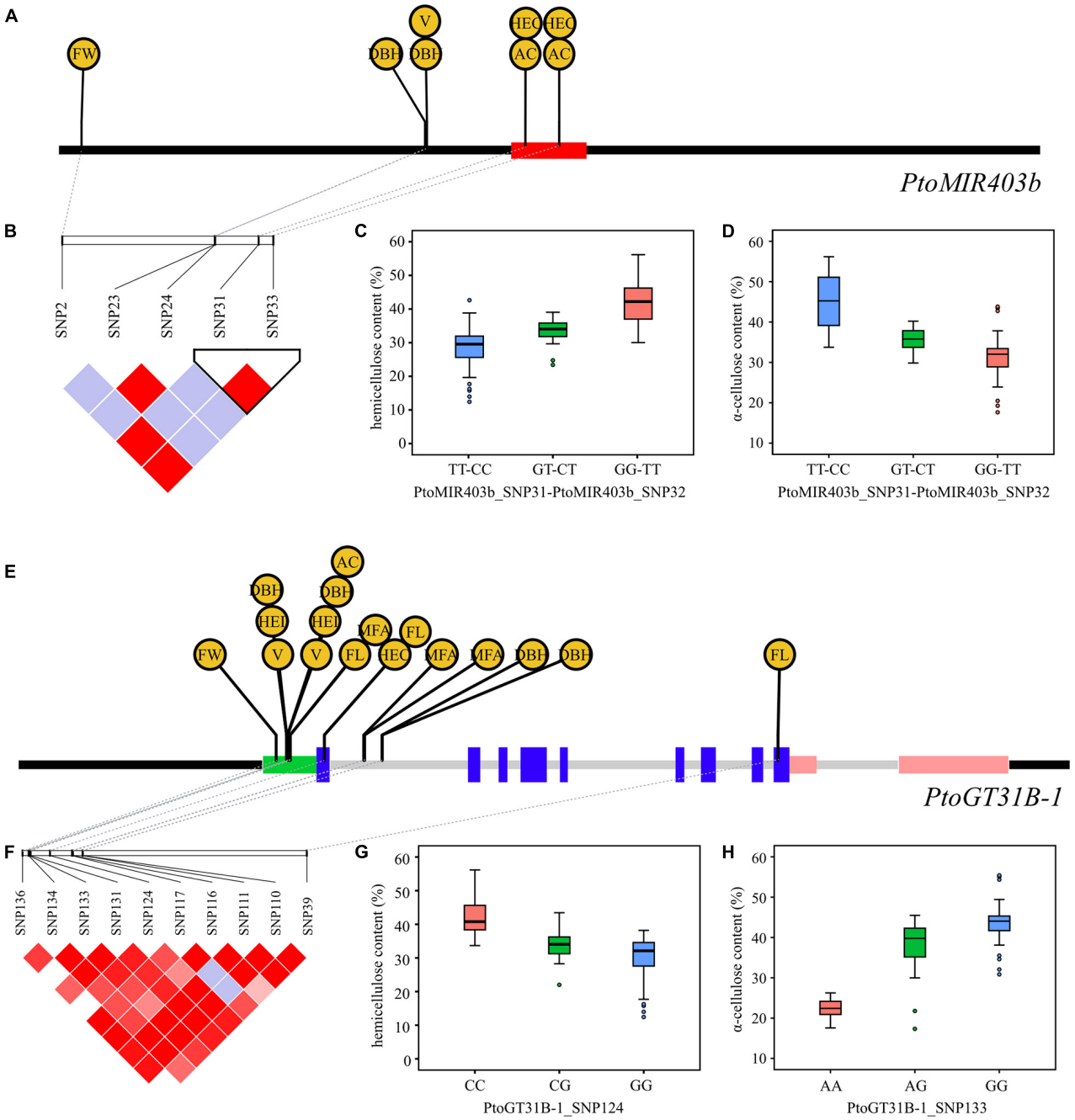

FIGURE 2 | Allelic loci in *PtoMIR403b* and *PtoGT31B-1* significantly affecting wood formation. **(A)** SNPs in *PtoMIR403b* significantly associated with wood characteristic traits. **(B)** Haploview plot of the LD coefficient r^2 for pairs of significantly associated SNPs in *PtoMIR403b*. PtoMIR403b_SNP31 and PtoMIR403b_SNP32 had a high LD coefficient r^2. **(C,D)** Combined genotypic effect of PtoMIR403b_SNP31 and PtoMIR403b_SNP32 on hemicellulose content **(C)** and α-cellulose content **(D)**. **(E)** SNPs in *PtoGT31B-1* significantly associated with wood characteristic traits. **(F)** Haploview plot of the LD coefficient r^2 for pairs of significantly associated SNPs in *PtoGT31B-1*. **(G)** Genotypic effect of PtoGT31B-1_SNP124 on hemicellulose content. **(H)** Genotypic effect of PtoGT31B-1_SNP133 on α-cellulose content.

indicating that allelic variation in *PtoMIR403b* affects wood formation (**Figures 2A–D**). *PtoMIR403b* and *PtoGT31B-1* were both associated with five traits, supporting a shared role of *PtoMIR403b* and *PtoGT31B-1* involving in the same regulatory pathway. For instance, PtoGT31B-1_SNP124 located in the exon region of *PtoGT31B-1* significantly associated with the HEC and PtoGT31B-1_SNP133 situated in the 5′-UTR that associated with the AC, and PtoMIR403b_SNP31 and PtoMIR403b_SNP33 significantly associated with both HEC and AC, indicating that PtomiR403b and its target gene co-regulate wood formation

(**Figures 2E–H**). We also detected SNPs in *PtoGT31B-1* associated with the other seven traits of wood formation, implying the important role of *PtoGT31B-1* in wood formation.

Pairwise Epistasis Revealed the Allelic Interaction Between *PtoMIR403b* and *PtoGT31B-1*

To assess the epistasis interactions between *PtoMIR403b* and its target gene *PtoGT31B-1*, we conducted epistatic analysis between each SNP pairs for 10 growth and wood formation traits via MDR software. Collectively, 95 significant pairwise epistatic associations were identified for 10 wood formation traits, including 14 unique SNPs in *PtoMIR403b* and 18 unique SNPs from *PtoGT31B-1* (**Supplementary Table 4**). The pairwise epistatic effects ranged from 0 to 10.34% (**Figure 3A**). Eight SNP-SNP pairs were associated with more than one trait. Moreover, the information gains (IGs) were used to estimate the mode of action of the epistatic interactions of the SNP-SNP pairs. We found that the IGs ranged from − 0.767 to 0.0437%, and most (86.32%) had negative IGs, indicating that the SNPs involved in the same process with functional overlap, and showed redundancy of genetic effects. For example, the PtoGT31B-1_SNP133-PtoGT31B-1_SNP114 exhibited epistasis effects on HC and V with different IGs of − 0.0273 for HC and 0.0437 for V (**Figures 3B,C**). The contrasting IGs for this SNP-SNP pair indicate the differential effects of epistatic interactions on growth and wood formation. Among all epistatic interactions, 37.89% showed the interaction between the *PtoMIR403b* and *PtoGT31B-1*; the remainder were intragenic SNP-SNP interactions. PtoGT31B-1_SNP19 interacted with four SNPs in PtomiR403b that showed epistatic effects on FW, implying the genetic interactions between PtomiR403b and *PtoGT31B-1*. The SNP-SNP pairs also exhibited pleiotropy, with eight SNP-SNP pairs contributing to at least one trait. For example, PtoMIR403b_SNP52 interacted with PtoGT31B-1_SNP133, which is responsible for phenotypic variation in HC and V. Only three SNPs of epistasis were detectable with additive or dominant effects, indicating that these SNP–SNP pairs exhibited more substantial epistatic effects than single SNPs.

To investigate the effects of single SNPs and SNP-SNP pairs underlying tree growth and wood properties, we focused and constructed the interaction graphs for HEC. We detected six SNP-SNP pairs showed epistatic effects on HEC, including four unique SNPs. PtoGT31B-1_SNP116 had a dominant effect on MFA and epistatic interactions with three SNPs associated with HEC, including two SNPs from PtoMIR403b. For example, we observed the different phenotypic values between genotypic combinations of PtoGT31B-1_SNP116 and PtoMIR403b_SNP18 led to different outcomes, with the AA-CC genotypic combination showed the highest phenotypic values of HEC (**Figure 3D**), indicating the epistasis effects of SNP pairs significantly contribute to the variation in HEC.

Mendelian Randomization Test Revealed That the *PtoMIR403b* Associated With Wood Formation by Regulating the Expression of *PtoGT31B-1*

Based on the association results of *PtoMIR403b* and the gene expression of *PtoGT31B-1* of these accessions, we performed MR

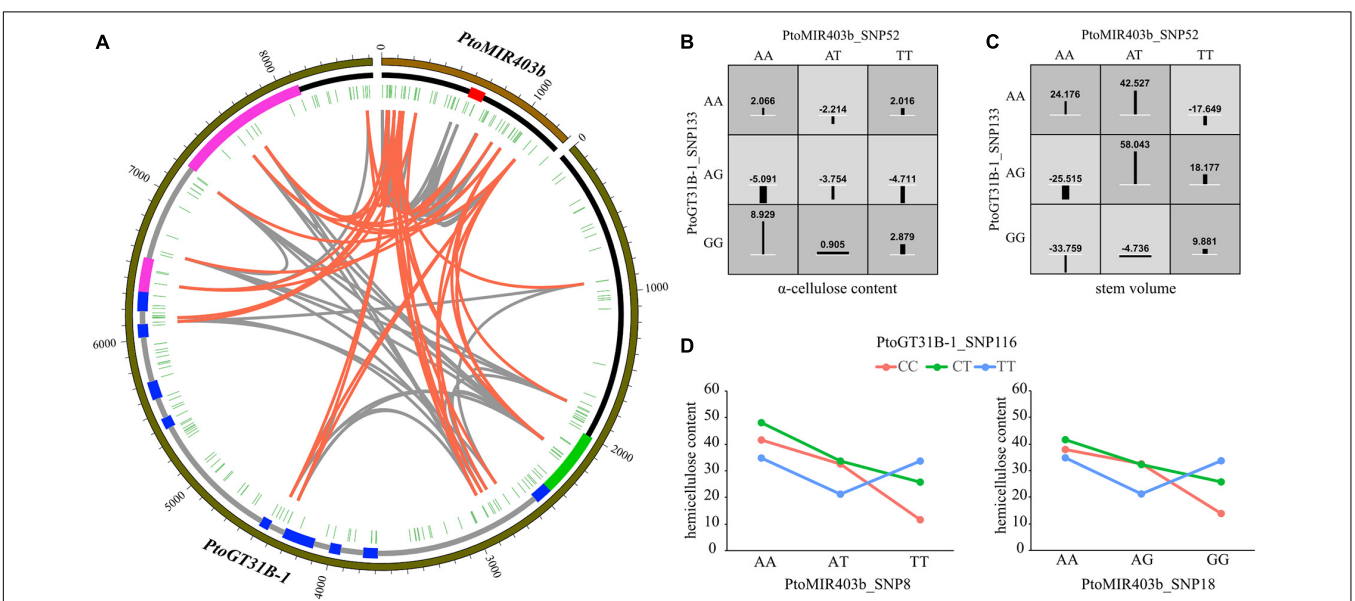

FIGURE 3 | Epistatic interaction between *PtoMIR403b* and *PtoGT31B-1* underlying wood formation. **(A)** Circos plot representing SNP pairwise interactions affect wood characteristic traits. The outer, middle, and inner circles show the length, structure, and location of each SNP, respectively, in *PtoMIR403b* and *PtoGT31B-1*. Interior lines represent the pairwise interactions underlying 10 wood characteristic traits. Gray and orange lines indicate intra-gene interactions and inter-gene interactions between SNP pairs, respectively. **(B,C)** Epistatic effects of the interaction between PtoMIR403b_SNP52 and PtoGT31B-1_SNP133 on a-cellulose content **(B)** and stem volume **(C)**. **(D)** Epistatic effects on hemicellulose content of PtoGT31B-1_SNP116 and two loci from *PtoMIR403b*.

test to identify traits whose variation is relevant to *PtoMIR403b* via affect the expression of target. First, we investigated the effects of causal SNPs within the *PtoMIR403b* for expression of *PtoGT31B-1*. Next, the genetic effects of significant SNPs in *PtoMIR403b* for expression of *PtoGT31B-1* and wood characteristics trait were integrated to perform MR test. The results of single-SNP based association have identified five SNPs which significantly associated with five traits, so we performed MR analysis using the IVW method of MR analysis to estimate the genetic effects arising from the expression of *PtoGT31B-1* on its corresponding trait. We identified that four of five traits were affected by the expression of *PtoGT31B-1*, which included expression of *PtoGT31B-1* positively contribute to FW, HEC, AC, and DBH trait, and expression of *PtoGT31B-1* negatively contribute to AC trait (**Supplementary Table 5** and **Figure 4**). Also, 80% of the associations have proved the causal relationships between SNPs and traits, indicating that the genetic variation in *PtoMIR403b* contributes to wood formation by modulating expression of *PtoGT31B-1*. Interestingly, we found that SNPs in the precursor region (which altered the stem-loop structure) for expression of *PtoGT31B-1* had a positive effect on HEC content, and had a negative effect on AC content. These results support our analytic strategy and the statistical power of the MR analysis to dissect the function of miRNAs and indicate that PtomiR403b post-transcriptionally regulates *PtoGT31B-1* to modulate wood formation.

Transcript Analysis of a Significant Haplotype Allele of *PtoMIR403b*

The results of association studies and MR test showed that a haplotype (PtoMIR403b_SNP31 and PtoMIR403b_SNP33) of *PtoMIR403b* significantly altered the expression of *PtoGT31B-1* and affected the HEC content. To further explore the effects of haplotype in the precursor region on the expression level of PtomiR403b and *PtoGT31B-1*, we next assayed the relative expression levels of PtomiR403b and *PtoGT31B-1* in developing xylem from 10 randomly selected individuals for each allele of the causal SNPs in the association population of *P. tomentosa*. The transcript abundances of PtomiR403b and *PtoGT31B-1* differed significantly among the alleles and exhibited opposite expression patterns (**Supplementary Figure 4**). PtomiR403b expression was high for the GG-TT allele but low for the TT-CC allele. By contrast, *PtoGT31B-1* expression was higher for the TT-CC allele than for the GG-TT allele, indicating that PtomiR403b downregulates *PtoGT31B-1* expression.

DISCUSSION

Wood formation is a complex trait of perennial tree species. Cellulose, hemicellulose, and lignin, the major components of wood tissue, have favorable relative proportions and structures in *Populus* wood (Porth et al., 2013). Genetic modification of genes involved in the biosynthesis of woody components can alter the woody growth and biomass of plants. In this study, we identified a conserved miRNA, PtomiR403b, which modulates wood formation by regulating its target *PtoGT31B-1*, a member of the galactosyltransferase family. Integration of association studies and Mendelian randomization test, we investigated the allelic interactions between *PtoMIR403b* and *PtoGT31B-1* underlying wood formation. Notably, we identified two SNPs in the precursor region of PtomiR403b that contributed

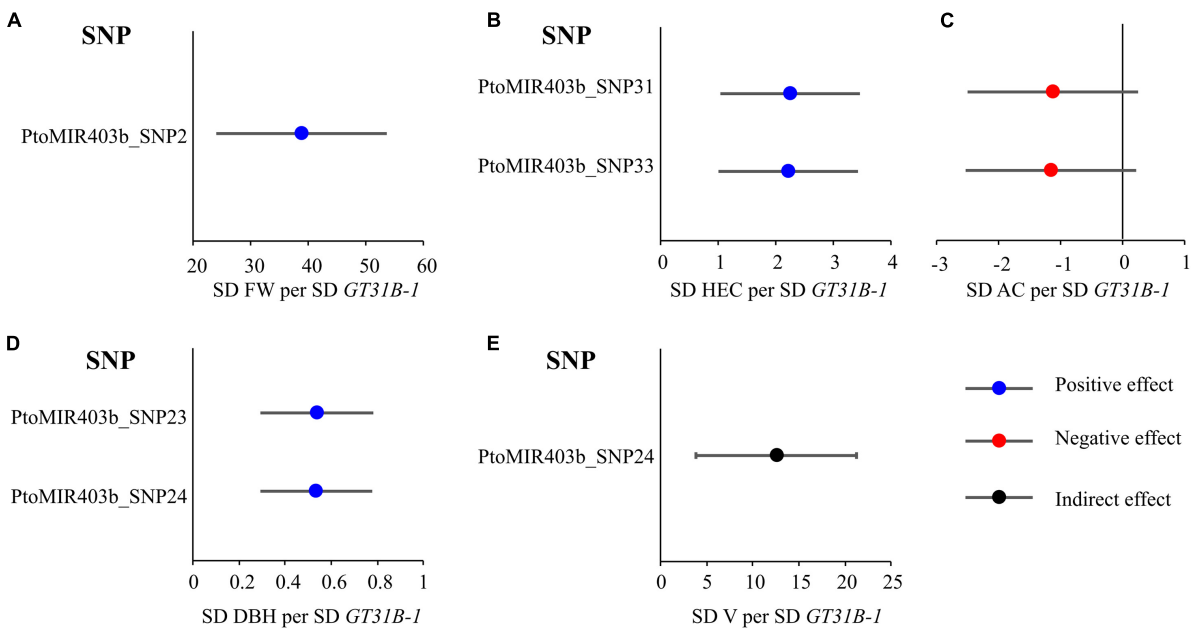

FIGURE 4 | Estimates of the genetic effects of SNPs in *PtoMIR403b* on the expression of *PtoGT31B-1* and wood characteristic traits. Estimates were derived via MR using the IVW method. Estimates of effects on FW **(A)**, HEC **(B)**, AC **(C)**, DBH **(D)**, and V **(E)** relative to *PtoGT31B-1* (*GT31B-1*) expression.

to HC variation by regulating the expression of *PtoGT31B-1*. We systematically explored the genetic interaction between PtomiR403b and its target *PtoGT31B-1* and identified the causal alleles responsible for wood formation, providing a theoretical basis for molecular-assisted breeding of *Populus*.

Characterization of PtomiR403b and Its Target PtoGT31B-1 in *Populus*

Wood formation in tree is highly plastic and requires the integration of complex developmental pathways. Molecular genetics studies in *Populus* have shown that woody growth is driven primarily by secondary cell wall formation. The secondary cell wall is predominantly composed of cellulose, hemicelluloses, and lignin. The biosynthesis genes for cellulose, hemicelluloses, and lignin have been characterized, as have those responsible for the supply of sugars and other secondary wall biosynthetic pathway precursors such as cellulose synthases (*CESAs*), cinnamoyl coenzyme A reductase (*CCR*), and trichome birefringence-likes (*TBLs*) (Zhong and Ye, 2014). In the recent years, the exhaustive data of RNA-seq from woody tissues have improved our understanding of transcriptional regulation during wood formation. Especially, miRNA as a short endogenous non-coding RNAs that posttranscriptionally regulate gene expression and are involved in various physiological processes. *In silico* analyses have identified numerous miRNAs involved in wood formation. Genetics studies in *Populus* have also characterized several miRNAs modulate the biosynthesis of woody components through its target genes. For example, Ptr-miR397a specifically down-regulated the expression of *laccases* (*LACs*), thus reducing lignin content (Lu et al., 2013), and PtomiR6443 alters lignin composition during stem development by modulating the expression of its target gene, *F5H*, which encodes the limiting enzyme in the biosynthesis pathway of sinapyl (S) monolignol (Fan et al., 2020). We found that miR403b regulates *PtoGT31B-1* in *Populus*, possibly modulating wood formation.

We found that miR403 is a conserved miRNA family in eudicots whose member number varies among species and is absent from 22 species in miRBase (**Supplementary Figure 2**). We identified four miR403 copies in *Populus* but only one in *Arabidopsis* with the same mature sequence. Surprisingly, miR403 targets AGO2 in *Arabidopsis* and is restricted to few plant species, whereas the target gene encoding AGO2 was lost in *Populus*, suggesting that the function of miR403 has been adapted during the course of plant evolution. Previous studies have predicted that miR403b target six genes in *Populus* (Xie et al., 2017), we focused on the interaction of miR403b-GT31B-1 to assess the role of miR403b in wood formation. The results of degradome sequencing, 5′-RACE, and expression patterns provided the evidence that miR403b cleave the *PtoGT31B-1*, suggesting *PtoGT31B-1* was the target of PtomiR403b (**Figure 1**). *PtoGT31B-1* is a member of the galactosyltransferase family glycosyltransferase 31 and harbors GALT and GALECTIN domains. This family is responsible for the biosynthesis of cell wall components, such as hemicelluloses and pectin. For instance, *AtGALT9* modulates cell wall pectin content, thereby controlling organ size (Zhang et al., 2021). An association study and MR testing indicated a causal relationship between PtomiR403b-*GT31B-1* and wood characteristic traits. Therefore, PtomiR403b targets *PtoGT31B-1* to modulate wood formation in *Populus*.

Moreover, we also found that the mature region of *PtoMIR403b* lacked SNPs and was conserved in the natural population of *P. tomentosa*. A haplotype block (including two SNPs) in the precursor region significantly altered the stem-loop structure and increased the MFE of pre-miR403b (**Supplementary Figure 1**). The transcript abundance of PtomiR403b differed significantly across the three genotypes (**Supplementary Figure 4**). The two SNPs in the precursor region were deleterious variants that alter the secondary structure and depress the generation of mature PtomiR403b, indicating that SNPs in the pre-miRNA region can have regulatory functions. SNPs in the precursor region can affect miRNA biogenesis, and most studies support the notion that causal SNPs in miRNAs can contribute to phenotypic variation (Xie et al., 2017). In this study, PtoMIR403b_SNP31 and PtoMIR403b_SNP33 had the top two association signals for HC and altered the expression of *PtoGT31B-1* to modulate HC variation. In addition, SNPs in *PtoMIR403b* were associated with DBH, V, and FW, implying a role for PtomiR403b in wood formation.

Allelic Variations in *PtoMIR403b* and *PtoGT31B-1* Affect Wood Formation in *Populus*

Ample study has revealed that SNPs in miRNA genes can alter miRNA biogenesis and function miRNA (Cai et al., 2009). Due to the SNPs may recruit or affect the combination of the miRNA to its target genes, thereby influence the regulation effects, and associate with the phenotypic variation (Mishra et al., 2008; Cai et al., 2009). For instance, Ehrenreich and Purugganan (2008) characterized the SNPs and nucleotide divergence in miRNAs and their binding sites in *Arabidopsis*. Several SNPs were predicted to affect the secondary structure of pre-miRNA. An SNP in the mature region of *PtoMIR6466* that alters the stem-loop structure and was associated with photosynthetic traits (Xiao et al., 2020). Herein, we identified five SNPs in PtoMIR403b significantly associated with wood characteristic traits, suggesting a role for PtomiR403b in wood formation (**Figure 2**). A haplotype (including two SNPs) in the precursor region was significantly associated with HC. Secondary structure prediction showed that the haplotype alters the stem-loop structure and increases the MFE of pre-miR403b. We also detected a different transcript abundance of PtomiR403b and its target *PtoGT31B-1* differed among the three genotypes. Therefore, this haplotype alters the secondary structure and depresses the generation of mature PtomiR403b, thus contributing to HC variation in *Populus*. MR test also revealed that this haplotype regulates the expression of its target *PtoGT31B-1* to modulate variation in HC. The PtoMIR403b_SNP31 and PtoMIR403b_SNP33 haplotype was a favorite allele combination for the marker-assisted breeding of high quality of *Populus*.

The *GT31B-1* is the target of miR403b in *Populus* but is absent in *Arabidopsis*, suggesting that miR403b has different functions in these species. Hence, to improve the understanding

of Pto-miR403b, we dissected the effects of allelic variation in *PtoGT31B-1*. Due to the putative function of *PtoGT31B-1* is implicated in the biosynthesis of cell wall components, we focused on the genetic effects in wood formation. We found 10 SNPs in *PtoGT31B-1* associated with nine wood characteristic traits, including the five associated with *PtoMIR403b*, implying that the function of PtomiR403b depends on the target and that PtomiR403b-GT31B-1 shares a wood-formation regulatory network. Interestingly, PtoGT31B-1_SNP133 was significantly associated with different genetic effects on four traits, indicating the pleiotropy of *PtoGT31B-1* in wood formation.

The epistatic effect is an important genetic component contributing to the genetic architecture of quantitative traits (Phillips, 2008; Mackay, 2014). Previous studies have shown that the most traits are a function of the actions of more than one gene or locus, particularly continuous variation traits, which are consequences of the actions of multiple loci (Roff and Emerson, 2006). Only three SNPs were identified in both single SNP-association and epistasis analyses, implying that epistatic interactions of multiple SNPs have complementary effects on a given trait. For example, PtoMIR403b_SNP38 interacted with 13 SNPs contributing to four wood characteristic traits and did not exhibit significantly additive or dominant effects. Regardless of the epistasis is the important effects underlying the desirable trait, it is still considered as a nuisance and ignored in plant breeding (Roff and Emerson, 2006; Sackman and Rokyta, 2018). Therefore, the incorporation of epistasis in breeding programs is challenging. VanRaden (2008) have first attempts to consider the epistasis in genomic selection, and several models have been developed to improve the prediction accuracy (Jiang and Reif, 2015). Additionally, the epistatic effect shapes phenotypic variation during domestication selection, suggesting an important role for gene-gene interactions in complex plant traits (Doust et al., 2014). We integrated additive, dominant, and epistatic effects to assess the genetic effects of *PtoMIR403b* and *PtoGT31B-1* on wood characteristic traits. The results provide insight into the role of PtomiR403b in wood formation and highlight several candidate SNPs for marker-assisted breeding of *Populus*.

Genetic Interactions Between *PtoMIR403b* and *PtoGT31B-1* Underlying Wood Properties

It is by now well established that miRNAs are dependent on their target genes (Chen, 2005; Chekulaeva and Filipowicz, 2009). Currently, a large number of evidence supports that the idea that miRNAs are involved in a broad spectrum of biological progresses through negative post-transcriptional gene regulation (Cai et al., 2009). Thus, only as target gene is confirmed will it be potential to establish commonalities that will enable more precisely predict miRNA-gene (Kuhn et al., 2008). A single miRNA may regulate hundreds target genes, thus it is a challenging to prove its function and interaction of miRNA-targets based on reverse genetics; however, association studies may provide a more relevant evaluation of the relationship between miRNA-targets.

Our results provide a robust evidence that the genetic interaction between *PtoMIR403b* and *PtoGT31B-1* underlies wood characteristic traits. The single SNP associations have revealed that *PtoMIR403b* and *PtoGT31B-1* were both associated with the wood characteristic traits and might be share the common functions in wood formation, and *PtoGT31B-1* was identified as a target of PtomiR403b. Epistasis is an interaction effect among multiple variants or genes that contribute to the same traits, and its analysis can reveal genetic interactions between two SNPs or genes underlying complex traits. We previously used the epistasis association study to construct a genetic interaction network for photosynthetic traits and revealed the allelic combinations among non-coding RNAs and protein-coding gene, suggesting the power of epistatic effects to illustrate the genetic interaction between miRNA and its target genes (Xiao et al., 2020). We identified 36 SNP-SNP pairs representing the interactions between *PtoMIR403b* and *PtoGT31B-1* and clarified how these interactions contribute to wood characteristic traits (**Figure 3**), revealing that *PtoMIR403b* and *PtoGT31B-1* interact and are involved the same regulatory pathway.

In addition, we also introduced the MR test to prove the causal relationship between *PtoMIR403b*, *PtoGT31B-1* and wood property traits, which uncovered the *PtoMIR403b* modulated the wood formation through regulate the expression of *PtoGT31B-1*. Conventionally, the MR test that uses genetic variants associated with a modifiable exposure level or intermediates to assess the causal relationship between variables and final outcomes (phenotypes) (Smith and Ebrahim, 2004; Evans and Davey, 2015). For instance, Su et al. (2021) investigated the genetic effects of SNP loci on rice yield using its component traits, suggesting the MR will be helpful for understanding the genetic basis of complex traits. Recently, the gene expression is regarded as an intermediate molecular phenotype that links genetic variants to plant traits. For example, MR test have prioritized 97 genes associated with drought tolerance and revealed that local variants regulate *abh2* expression and are negatively associated with drought tolerance in maize, indicating that gene expression bridges the genetic variation to phenotype (Liu et al., 2020). Moreover, miRNA as a *trans*-regulator modulate the expression of its target genes. Herein, we found that SNPs in precursors altered the stem-loop structure of PtomiR403b and were associated with target expression. Therefore, MR testing can demonstrate how genetic variants in miRNAs affect phenotype via *trans*-regulating target gene expression. Therefore, combining association analysis and MR test is a feasible approach for dissection of the function and interaction of miRNA-targets from massive bioinformatics prediction results.

DATA AVAILABILITY STATEMENT

The datasets presented in this study can be found in online repositories. The names of the repository/repositories and accession number(s) can be found in the article/**Supplementary Material**.

AUTHOR CONTRIBUTIONS

DZ designed the conception and experiment, obtained funding and was responsible for this article. LX, LM, LY, JZ, BL, and MQ collected the data and conducted statistical analysis. LX wrote the manuscript. LM, WL, YF, and DW provided valuable suggestion for the manuscript. LM, LY, and QD revised the manuscript. All authors read and approved the manuscript.

FUNDING

This work was supported by the Project of the National Natural Science Foundation of China (Nos. 31872671 and 31901336) and the 111 Project (No. B20050).

SUPPLEMENTARY MATERIAL

The Supplementary Material for this article can be found online at: https://www.frontiersin.org/articles/10.3389/fpls.2021.704941/full#supplementary-material

Supplementary Figure 1 | Stem-loop structure of PtomiR403b with SNPs. Three SNPs in the precursor region of PtomiR403b affect the secondary structure and MFE.

Supplementary Figure 2 | Phylogenetic tree of miR403 precursors. Left, unrooted maximum-likelihood tree. Bootstrap values are from 1,000 replicates. Right, alignment of mature miR403 sequences. Red, missing nucleotides. Precursor and mature sequences of miR403 were downloaded from miRbase.

Supplementary Figure 3 | Decay of LD in *PtoMIR403b* and *PtoGT31B-1*. Pairwise correlations between SNPs (r^2) plotted against the physical distance between SNP pairs. Red curves are non-linear regressions of r^2 based on physical distance.

Supplementary Figure 4 | Expression levels of PtomiR403b and *PtoGT31B-1* according to the genotype of the PtoMIR403b_SNP31 and PtoMIR403b_SNP33 haplotype.

Supplementary Table 1 | Oligonucleotide sequences of the primers used in this study.

Supplementary Table 2 | Common SNPs (minor allele frequency ≥ 5%) in *PtoMIR403b* and *PtoGT31B-1*.

Supplementary Table 3 | Significant SNPs in candidate genes associated with growth and wood characteristics in the association population of *P. tomentosa*.

Supplementary Table 4 | SNP pairs and their main effects among the two candidate genes in the association population of *P. tomentosa*.

Supplementary Table 5 | Results of MR analysis for SNP, *PtoGT31B-1* expression, and wood characteristic traits.

Supplementary Method 1 | Degradome sequencing.

Supplementary Method 2 | SNP calling following resequencing of the association population.

REFERENCES

Addo-Quaye, C., Miller, W., and Axtell, M. J. (2009). Cleaveland: a pipeline for using degradome data to find cleaved small RNA targets. *Bioinformatics* 25, 130–131. doi: 10.1093/bioinformatics/btn604

Basu, D., Tian, L., Debrosse, T., Poirier, E., Emch, K., Herock, H., et al. (2016). Glycosylation of a fasciclin-like arabinogalactan-protein (sos5) mediates root growth and seed mucilage adherence via a cell wall receptor-like kinase (fei1/fei2) pathway in *Arabidopsis*. *PLoS One* 11:e145092. doi: 10.1371/journal.pone.0145092

Basu, D., Wang, W., Ma, S., DeBrosse, T., Poirier, E., Emch, K., et al. (2015). Two hydroxyproline galactosyltransferases, galt5 and galt2, function in arabinogalactan-protein glycosylation, growth and development in *Arabidopsis*. *PLoS One* 10:e125624. doi: 10.1371/journal.pone.0125624

Bradbury, P. J., Zhang, Z., Kroon, D. E., Casstevens, T. M., Ramdoss, Y., and Buckler, E. S. (2007). Tassel: software for association mapping of complex traits in diverse samples. *Bioinformatics* 23, 2633–2635. doi: 10.1093/bioinformatics/btm308

Budak, H., and Akpinar, B. A. (2015). Plant mirnas: biogenesis, organization and origins. *Funct. Integr. Genomics* 15, 523–531. doi: 10.1007/s10142-015-0451-2

Burgess, S., Foley, C. N., and Zuber, V. (2018). Inferring causal relationships between risk factors and outcomes from genome-wide association study data. *Annu. Rev. Genomics Hum. Genet.* 19, 303–327. doi: 10.1146/annurev-genom-083117-021731

Cai, Y., Yu, X., Hu, S., and Yu, J. (2009). A brief review on the mechanisms of mirna regulation. *Genom Proteom Bioinf.* 7, 147–154. doi: 10.1016/S1672-0229(08)60044-3

Cardon, L. R., and Bell, J. I. (2001). Association study designs for complex diseases. *Nat. Rev. Genet.* 2, 91–99. doi: 10.1038/35052543

Chekulaeva, M., and Filipowicz, W. (2009). Mechanisms of mirna-mediated post-transcriptional regulation in animal cells. *Curr. Opin. Cell Biol.* 21, 452–460. doi: 10.1016/j.ceb.2009.04.009

Chen, X. (2005). Microrna biogenesis and function in plants. *FEBS Lett.* 579, 5923–5931. doi: 10.1016/j.febslet.2005.07.071

Doust, A. N., Lukens, L., Olsen, K. M., Mauro-Herrera, M., Meyer, A., and Rogers, K. (2014). Beyond the single gene: how epistasis and gene-by-environment effects influence crop domestication. *Proc. Natl. Acad. Sci. U S A.* 111, 6178–6183. doi: 10.1073/pnas.1308940110

Du, Q., Xu, B., Gong, C., Yang, X., Pan, W., Tian, J., et al. (2014). Variation in growth, leaf, and wood property traits of chinese white poplar (populus tomentosa), a major industrial tree species in northern china. *Can. J. Forest Res.* 44, 326–339. doi: 10.1139/cjfr-2013-0416

Du, Q., Yang, X., Xie, J., Quan, M., Xiao, L., Lu, W., et al. (2019). Time-specific and pleiotropic quantitative trait loci coordinately modulate stem growth in Populus. *Plant Biotechnol. J.* 17, 608–624. doi: 10.1111/pbi.13002

Ehrenreich, I. M., and Purugganan, M. D. (2008). Sequence variation of micrornas and their binding sites in *Arabidopsis*. *Plant Physiol.* 146, 1974–1982. doi: 10.1104/pp.108.116582

Evans, D. M., and Davey, S. G. (2015). Mendelian randomization: new applications in the coming age of hypothesis-free causality. *Annu. Rev. Genomics Hum. Genet.* 16, 327–350. doi: 10.1146/annurev-genom-090314-050016

Fagundes Lopes, F. J., Pauly, M., Brommonshenkel, S. H., Lau, E. Y., Diola, V., Passos, J. L., et al. (2010). The egmur3 xyloglucan galactosyltransferase from eucalyptus grandis complements the mur3 cell wall phenotype in *Arabidopsis thaliana*. *Tree Genet Genomes* 6, 745–756. doi: 10.1007/s11295-010-0288-8

Fan, D., Li, C., Fan, C., Hu, J., and Li, J. (2020). Microrna6443-mediated regulation of ferulate 5-hydroxylase gene alters lignin composition and enhances saccharification in Populus tomentosa. *New Phytol.* 226, 410–425. doi: 10.1111/nph.16379

German, M. A., Pillay, M., Jeong, D. H., Hetawal, A., Luo, S., Janardhanan, P., et al. (2008). Global identification of microrna-target rna pairs by parallel analysis of RNA ends. *Nat. Biotechnol.* 26, 941–946. doi: 10.1038/nbt1417

Hahn, L. W., Ritchie, M. D., and Moore, J. H. (2003). Multifactor dimensionality reduction software for detecting gene-gene and gene-environment interactions. *Bioinformatics* 19, 376–382. doi: 10.1093/bioinformatics/btf869

Hennet, T. (2002). The galactosyltransferase family. *Cell Mol. Life. Sci.* 59, 1081–1095. doi: 10.1007/s00018-002-8489-4

Jansson, S., and Douglas, C. J. (2007). Populus: a model system for plant biology. *Annu. Rev. Plant Biol.* 58, 435–458. doi: 10.1146/annurev.arplant.58.032806.103956

Jensen, J. K., Schultink, A., Keegstra, K., Wilkerson, C. G., and Pauly, M. (2012). Rna-seq analysis of developing nasturtium seeds (*Tropaeolum majus*): identification and characterization of an additional galactosyltransferase involved in xyloglucan biosynthesis. *Mol. Plant* 5, 984–992. doi: 10.1093/mp/sss032

Jiang, Y., and Reif, J. C. (2015). Modeling epistasis in genomic selection. *Genetics* 201, 759–768. doi: 10.1534/genetics.115.177907

Kong, Y., Pena, M. J., Renna, L., Avci, U., Pattathil, S., Tuomivaara, S. T., et al. (2015). Galactose-depleted xyloglucan is dysfunctional and leads to dwarfism in *Arabidopsis*. *Plant Physiol.* 167, 1294–1296. doi: 10.1104/pp.114.255943

Kuhn, D. E., Martin, M. M., Feldman, D. S., Terry, A. J., Nuovo, G. J., and Elton, T. S. (2008). Experimental validation of mirna targets. *Methods* 44, 47–54. doi: 10.1016/j.ymeth.2007.09.005

Kumar, S., Stecher, G., and Tamura, K. (2016). Mega7: molecular evolutionary genetics analysis version 7.0 for bigger datasets. *Mol. Biol. Evol.* 33, 1870–1874. doi: 10.1093/molbev/msw054

Li, C., Wang, X., Ran, L., Tian, Q., Fan, D., and Luo, K. (2015). PtoMYB92 is a transcriptional activator of the lignin biosynthetic pathway during secondary cell wall formation in *Populus tomentosa*. *Plant Cell Physiol.* 56, 2436–2446. doi: 10.1093/pcp/pcv157

Li, Y. I., van de Geijn, B., Raj, A., Knowles, D. A., Petti, A. A., Golan, D., et al. (2016). RNA splicing is a primary link between genetic variation and disease. *Science* 352, 600–604. doi: 10.1126/science.aad9417

Liu, S., Li, C., Wang, H., Wang, S., Yang, S., Liu, X., et al. (2020). Mapping regulatory variants controlling gene expression in drought response and tolerance in maize. *Genome Biol.* 21:163. doi: 10.1186/s13059-020-02069-1

Lu, S., Li, Q., Wei, H., Chang, M. J., Tunlaya-Anukit, S., Kim, H., et al. (2013). Ptr-miR397a is a negative regulator of laccase genes affecting lignin content in *Populus trichocarpa*. *Proc. Natl. Acad. Sci. U S A.* 110, 10848–10853. doi: 10.1073/pnas.1308936110

Mackay, T. F. (2014). Epistasis and quantitative traits: using model organisms to study gene-gene interactions. *Nat. Rev. Genet.* 15, 22–33. doi: 10.1038/nrg3627

Matsumoto, N., Takenaka, Y., Wachananawat, B., Kajiura, H., Imai, T., Ishimizu, T., et al. (2019). Rhamnogalacturonan i galactosyltransferase: detection of enzyme activity and its hyperactivation. *Plant Physiol. Biochem.* 142, 173–178. doi: 10.1016/j.plaphy.2019.07.008

Mishra, P. J., Mishra, P. J., Banerjee, D., and Bertino, J. R. (2008). MiRsnps or miR-polymorphisms, new players in microrna mediated regulation of the cell: introducing microRNA pharmacogenomics. *Cell Cycle* 7, 853–858. doi: 10.4161/cc.7.7.5666

Neale, D. B., and Savolainen, O. (2004). Association genetics of complex traits in conifers. *Trends Plant Sci.* 9, 325–330. doi: 10.1016/j.tplants.2004.05.006

Phillips, P. C. (2008). Epistasis–the essential role of gene interactions in the structure and evolution of genetic systems. *Nat. Rev. Genet.* 9, 855–867. doi: 10.1038/nrg2452

Porcu, E., Rueger, S., Lepik, K., Santoni, F. A., Reymond, A., Kutalik, Z., et al. (2019). Mendelian randomization integrating gwas and eQTL data reveals genetic determinants of complex and clinical traits. *Nat. Commun.* 10:3300. doi: 10.1038/s41467-019-10936-0

Porth, I., Klapste, J., Skyba, O., Hannemann, J., McKown, A. D., Guy, R. D., et al. (2013). Genome-wide association mapping for wood characteristics in Populus identifies an array of candidate single nucleotide polymorphisms. *New Phytol.* 200, 710–726. doi: 10.1111/nph.12422

Roff, D. A., and Emerson, K. (2006). Epistasis and dominance: evidence for differential effects in life-history versus morphological traits. *Evolution* 60, 1981–1990. doi: 10.1111/j.0014-3820.2006.tb01836.x

Sackman, A. M., and Rokyta, D. R. (2018). Additive phenotypes underlie epistasis of fitness effects. *Genetics* 208, 339–348. doi: 10.1534/genetics.117.300451

Showalter, A. M., and Basu, D. (2016). Extensin and arabinogalactan-protein biosynthesis: glycosyltransferases, research challenges, and biosensors. *Front. Plant Sci.* 7:814. doi: 10.3389/fpls.2016.00814

Smith, G. D., and Ebrahim, S. (2004). Mendelian randomization: prospects, potentials, and limitations. *Int. J. Epidemiol.* 33, 30–42. doi: 10.1093/ije/dyh132

Su, J., Xu, K., Li, Z., Hu, Y., and Hu, Z. (2021). Genome-wide association study and mendelian randomization analysis provide insights for improving rice yield potential. *Sci. Rep.* 11:6894. doi: 10.1038/s41598-021-86389-7

van der Graaf, A., Claringbould, A., Rimbert, A., Westra, H. J., Li, Y., Wijmenga, C., et al. (2020). Mendelian randomization while jointly modeling cis genetics identifies causal relationships between gene expression and lipids. *Nat. Commun.* 11:4930. doi: 10.1038/s41467-020-18716-x

VanRaden, P. M. (2008). Efficient methods to compute genomic predictions. *J. Dairy Sci.* 91, 4414–4423. doi: 10.3168/jds.2007-0980

Wegrzyn, J. L., Eckert, A. J., Choi, M., Lee, J. M., and Stanton, B. J. (2010). Association genetics of traits controlling lignin and cellulose biosynthesis in black cottonwood (*Populus trichocarpa*. Salicaceae) secondary xylem. *New Phytol.* 188, 515–532. doi: 10.1111/j.1469-8137.2010.03415.x

Xiao, L., Quan, M., Du, Q., Chen, J., Xie, J., and Zhang, D. (2017). Allelic interactions among *Pto-MIR475b* and its four target genes potentially affect growth and wood properties in *Populus*. *Front. Plant Sci*. 8:1055. doi: 10.3389/fpls.2017.01055

Xiao, L., Liu, X., Lu, W., Chen, P., Quan, M., Si, J., et al. (2020). Genetic dissection of the gene coexpression network underlying photosynthesis in Populus. *Plant Biotechnol. J.* 18, 1015–1026. doi: 10.1111/pbi.13270

Xie, J., Yang, X., Song, Y., Du, Q., Li, Y., Chen, J., et al. (2017). Adaptive evolution and functional innovation of populus-specific recently evolved microRNAs. *New Phytol.* 213, 206–219. doi: 10.1111/nph.14046

Yavorska, O. O., and Burgess, S. (2017). Mendelianrandomization: an r package for performing mendelian randomization analyses using summarized data. *Int. J. Epidemiol.* 46, 1734–1739. doi: 10.1093/ije/dyx034

Yu, L., Chen, H., Sun, J., and Li, L. (2014). PtrKOR1 is required for secondary cell wall cellulose biosynthesis in Populus. *Tree Physiol.* 34, 1289–1300. doi: 10.1093/treephys/tpu020

Zhang, J., Nieminen, K., Serra, J. A., and Helariutta, Y. (2014). The formation of wood and its control. *Curr. Opin. Plant Biol.* 17, 56–63. doi: 10.1016/j.pbi.2013.11.003

Zhang, H., Guo, Z., Zhuang, Y., Suo, Y., Du, J., Gao, Z., et al. (2021). MicroRNA775 regulates intrinsic leaf size and reduces cell wall pectin levels by targeting a Galactosyltransferase gene in *Arabidopsis*. *Plant Cell.* 33, 581–602. doi: 10.1093/plcell/koaa049

Zhong, R., and Ye, Z. H. (2014). Complexity of the transcriptional network controlling secondary wall biosynthesis. *Plant Sci.* 229, 193–207. doi: 10.1016/j.plantsci.2014.09.009

Conflict of Interest: The authors declare that the research was conducted in the absence of any commercial or financial relationships that could be construed as a potential conflict of interest.

Publisher's Note: All claims expressed in this article are solely those of the authors and do not necessarily represent those of their affiliated organizations, or those of the publisher, the editors and the reviewers. Any product that may be evaluated in this article, or claim that may be made by its manufacturer, is not guaranteed or endorsed by the publisher.

frontiers in Plant Science

ORIGINAL RESEARCH
published: 15 November 2021
doi: 10.3389/fpls.2021.704262

Transcriptomic, Proteomic, and Metabolic Profiles of *Catalpa bungei* Tension Wood Reveal New Insight Into Lignin Biosynthesis Involving Transcription Factor Regulation

Yao Xiao[1], Juanjuan Ling[1], Fei Yi[1], Wenjun Ma[1], Nan Lu[1], Tianqing Zhu[1], Junhui Wang[1], Kun Zhao[2] and Huiling Yun[3]*

[1] State Key Laboratory of Tree Genetics and Breeding, Key Laboratory of Tree Breeding and Cultivation of National Forestry and Grassland Administration, National Innovation Alliance of Catalpa bungei, Research Institute of Forestry, Chinese Academy of Forestry, Beijing, China, [2] Luoyang Academy of Agriculture and Forestry Sciences, Luoyang, China, [3] Xiaolongshan Research Institute of Forest Science and Technology, Tianshui, China

OPEN ACCESS

Edited by:
Meng-Zhu Lu, Zhejiang Agriculture & Forestry University, China

Reviewed by:
Bo Zhang, Zhejiang University, China
Sombir Rao, Robert W. Holley Center for Agriculture & Health, United States Department of Agriculture-Agricultural Research Service (USDA-ARS), United States

***Correspondence:**
Junhui Wang
wangjh@caf.ac.cn

Specialty section:
This article was submitted to Plant Metabolism and Chemodiversity, a section of the journal Frontiers in Plant Science

Received: *02 May 2021*
Accepted: *12 October 2021*
Published: *15 November 2021*

Citation:
Xiao Y, Ling J, Yi F, Ma W, Lu N, Zhu T, Wang J, Zhao K and Yun H (2021) Transcriptomic, Proteomic, and Metabolic Profiles of Catalpa bungei Tension Wood Reveal New Insight Into Lignin Biosynthesis Involving Transcription Factor Regulation. Front. Plant Sci. 12:704262. doi: 10.3389/fpls.2021.704262

Lignin is a complex polymer in plant cell walls whose proportion is second only to that of cellulose and plays an important role in the mechanical properties of wood and stress resistance of plants. Here, we induced tension wood (TW) formation in *Catalpa bungei* by artificial bending and analyzed the lignin metabolism of the TW. LC-MS analysis showed that a significantly higher content of coniferyl aldehyde was observed in the TW cell wall than in the opposite wood (OW) and normal wood (NW) cell walls. TW had significantly lower contents of coniferyl alcohol than OW and NW. Raman spectroscopy results indicated that TW had lower total lignin than OW and NW. The transcription and translation levels of most of the differentially expressed genes (DEGs) involved in lignin monomer biosynthesis indicated upregulation in TW/OW and TW/NW. We found no significant difference in the transcription levels of three collision gases (CADs) between TW and OW or between NW, but their translation levels were significantly downregulated in TW, suggesting post-transcriptional control for *CAD*. We predicted and analyzed transcription factors that could target DEGs involved in lignin monomer biosynthesis in TW. Based on the analysis of the relationships of targeting and coexpression, we found that NAC (evm.model.group1.695) could potentially target *4CLs* and *CCoAOMT*, that HD-Zip (evm.model.group7.1157) had potential targeting relationships with *CCoAOMT*, *F5H*, and *CCR*, and that their expression levels were significantly positive. It is speculated that the upregulation of NAC and HD-ZIP transcription factors activates the expression of downstream target genes, which leads to a significant increase in coniferyl aldehyde in TW. However, the decrease in total lignin in TW may be caused by the significant downregulation of CAD translation and the significant decrease in precursors (coniferyl alcohol). Whether the expression of CAD genes is regulated by post-transcriptional control and affects TW lignin metabolism needs further study.

Keywords: tension wood, *Catalpa bungei*, lignin metabolism, transcription factor, regulatory network

INTRODUCTION

Wood, the secondary xylem of trees, is a multipurpose renewable material and is commonly used in papermaking, architecture, furniture manufacturing, and energy production due to its varied properties (Nakahama et al., 2018; Papadopoulos et al., 2019). Wood formation is considered secondary growth and involves the formation of vascular tissue, secondary cell wall (SCW), lignification, programmed cell death, and heartwood formation (Tian et al., 2007). Wood quality is mainly determined by cellulose, hemicellulose, and lignin contents (Nakahama et al., 2018). Lignification can increase the hardness and mechanical supporting force of the secondary xylem cell wall and enhance the ability of plants to transport water over long distances and resist biological and abiotic stresses (Vance et al., 1980; Zhao, 2016; Hu et al., 2019). Lignin is related to the properties of pulp and paper (Liang et al., 2020). Therefore, it is of great significance to study the distribution, synthesis and regulation of lignin in xylem for the genetic improvement of wood properties.

The lignin synthesis pathway has been clearly elucidated (Zhao, 2016). Generally, lignin in higher plants is formed by the oxidative polymerization of three kinds of lignin monomers (p-hydroxyphenyl lignin, guaiacyl lignin, and syringyl lignin). Studies have found that lignin monomer synthesis pathways in different plants are significantly different (Li et al., 2014). For example, *caffeoyl shikimate esterase* (*CSE*) is a key gene for lignin monomer synthesis in *Arabidopsis thaliana*, and mutation of this gene will greatly reduce the lignin content in *A. thaliana* (Shen et al., 2013; Vanholme et al., 2013). Overexpression of the *F5H* gene in *A. thaliana* with a defective *COMT* gene leads to enrichment in unusual lignin (5H lignin) (Weng et al., 2010). These results indicate the flexibility of the lignification process. This flexibility is the starting point for the artificial regulation of lignin biosynthesis and will increase the possible applications of many economically important plants. Research has found that reducing the expression of the *4CL* gene during lignin synthesis in poplar will reduce Klason lignin by 30%, which reduces the elasticity modulus by 40% (Horvath et al., 2010). However, increasing *4CL* gene expression in poplar will increase lignin content by approximately 40%, reduce other carbohydrate contents and significantly increase wood strength (Hu et al., 2019). Altering the expression of genes in the lignin synthesis pathway has been shown to significantly influence the chemical composition of cell walls. Wu et al. (2019) confirmed that lignin monomer biosynthesis was strictly regulated by genes in synergy. They found that downregulation of *F5H* in COMT-RNAi transgenic switchgrass inhibits S lignin biosynthesis and increases guaiacyl lignin units. In contrast, overexpression of *F5H* in COMT-RNAi transgenic plants will reduce the number of G units. Deficient lignin biosynthesis could be partially compensated for or completely recovered with different degrees of *COMT* downregulation. These factors make it possible to artificially and precisely regulate the synthesis of lignin monomers.

Wood formation is a complicated process under the control of a large set of transcription factors (Sun et al., 2021). Lignin biosynthesis and lignification are two of the steps in wood formation. Transcriptional regulation is important for lignin synthesis. Studies have indicated that the lignin metabolic pathway usually has the same transcriptional regulation mode as cellulose and hemicellulose biosynthesis (Zhao and Dixon, 2011; Nakano et al., 2015). NAC transcription factors are usually the first-layer managers in the regulation network of wood chemical composition biosynthesis. NACs can target a number of *MYB* genes (second-layer managers) and promote their direct or indirect regulation of the formation of secondary walls for plants, including lignin biosynthesis. In *A. thaliana*, *MYB46*, *MYB58*, and *MYB63* are targeted by SND1, NST1, and NST2 (Zhou et al., 2009; Zhong et al., 2010). In *atnst1-1* and *atnst3-1-1* double mutants, secondary wall thickening was completely inhibited, and some lignin synthesis pathway genes were also inhibited (Mitsuda et al., 2005). Moreover, lignin biosynthesis and cellulose deposition genes were highly expressed in the *myb75-1* mutant with thickening of the fiber cell wall, increasing the lignin content and changing the S/G ratio in the stem (Bhargava et al., 2010). The *PtrWND* genes could induce the expression of wood biosynthetic genes, including related transcription factors and structural genes, leading to ectopic deposition of lignin in poplars (Zhong et al., 2010). Furthermore, several studies have shown that PtrMYB3 and PtrMYB20 can activate the lignin biosynthesis pathway (McCarthy et al., 2010). In addition to the NAC and MYB transcription factors, an increasing number of transcription factors have been found to be involved in wood formation. For example, homeobox genes are associated with lignification in bamboo (Xu et al., 2019), and *PtrHB7* expression enhances the differentiation of cambial cells toward xylem cells in Populus (Zhu et al., 2013). HD-ZIP also regulates lignin biosynthesis in plants (Sun et al., 2020). These studies suggest a new level of complexity in lignin biosynthesis regulation.

Catalpa bungei is native to China and is an economically important ring-porous tree species with high-quality wood (Li et al., 2019). Traditional breeding for rapid growth of *C. bungei* has been carried out for years (Xiao et al., 2019). However, currently, the forest industry demands not only high yields but also high quality. Thus, it is necessary to study the mechanism of wood formation in *C. bungei*. Recently, with the development of high-throughput sequencing techniques, multiomics analysis has played an important role in the selection of functional genes and the construction of gene expression regulatory networks for wood formation (Shinya et al., 2016; Bygdell et al., 2017; Wang et al., 2018). We combined transcriptome, proteome, and confocal Raman imaging techniques to analyze the xylem of tension wood (TW), opposite wood (OW), and normal wood (NW) in *C. bungei* and identified the key genes that regulate lignin biosynthesis, providing new insight for wood property improvement by genetic engineering in *C. bungei*.

MATERIALS AND METHODS

Plant Material

One-year-old *C. bungei* clone 8,402 was planted at the experimental base in Luoyang city, Henan Province. We used artificial bending to induce TW formation in July. The method

was as follows: one end of twine was tied to the top of the plant, and the other end was tied to a heavy object. The object was then dragged to bend the plant. The plants were kept in a bent state with a consistent angle of 45° in the same direction. Refer to the literature for a diagram of the bending treatment mode (Xiao et al., 2020). After 3 months of treatment, wood samples were collected at a height of 60 cm, and xylem was obtained to make tissue sections. The sections were double stained with saffron-fast green, and the detailed staining steps are described in the literature (Xiao et al., 2020). The staining results were used to identify the TW and OW.

Ultrastructure Observation

Sample preparation was carried out essentially as previously described by Xiao et al. (2020). The xylem samples were cut using a razor blade and immediately fixed in 3% (w/v) glutaraldehyde. Samples were dehydrated in an ethanol series (30, 50, 70, and 100%) and embedded in Spurr resin at 60°C. Transverse resin sections of xylem were cut using a diamond knife for ultrastructural observation under a transmission electron microscope (HITACHI HT-7700, Tokyo, Japan).

Confocal Raman Mapping

A LabRam Xplora confocal Raman microscope (Horiba Jobin–Yvon, Paris, France) with an Olympus confocal microscope (Olympus, Tokyo, Japan) and a linearly polarized 532 nm laser (Ventus VIS 532, Laser Quantum, Chester, United Kingdom) was used to measure the sample size. The power was set to 8 mW. Point-by-point scanning microprobe imaging was employed to acquire spectral data. The parameter settings were as follows: 1,200 mm^{-1} grating, 100 μm slit width, 300 μm numerical aperture, 0.7 μm scanning step, 1 s single-point spectral acquisition time, and 2 cm^{-1} spectral resolution. Every 15 spectra were acquired and averaged. Data were acquired and analyzed by LabSpec6 software. The entire experiment was carried out at a constant 25°C.

Liquid Chromatography-Mass Spectrometry (LC-MS) Determination of Metabolites in the Lignin Monomer Biosynthetic Pathway

A total of 100 mg of sample powder was weighed and extracted overnight at 4°C with 1.0 mL 70% aqueous methanol. Following centrifugation at 10,000 × *g* for 10 min, the extracts were subjected to SPE (CNWBOND Carbon-GCB solid phase extract (SPE) cartridge, 250 mg, 3 mL; ANPEL, Shanghai, China), and the eluates were filtered (SCAA-104, 0.22 μm pore size; ANPEL) before LC-MS analysis.

The sample extracts were analyzed using an LC-electrospray ionization (ESI)-MS/MS system [high performance liquid chromatography (HPLC), Shim-pack UFLC Shimadzu CBM30A system, Kyoto, Japan; MS, Applied Biosystems, Carlsbad, CA, United States]. The analytical conditions for HPLC were as follows: column, Waters ACQUITY UPLC HSS T3 C18 column (1.8 μm, 2.1 mm × 100 mm); solvent system, water (0.04% acetic acid): acetonitrile (0.04% acetic acid); gradient program, 100:0 V/V at 0 min, 5:95 V/V at 11.0 min, 5:95 V/V at 12.0 min, 95:5 V/V at 12.1 min, and 95:5 V/V at 15.0 min; flow rate, 0.40 mL/min; temperature, 40°C; and injection volume, 2 μL. The effluent was alternatively connected to an electrospray ionization (ESI)-triple quadrupole-linear ion trap (Q TRAP)-MS.

Linear ion trap (LIT) and triple quadrupole (QQQ) scans were acquired on a QQQ-LIT mass spectrometer (Q TRAP), API 6500 Q TRAP LC-MS/MS system, equipped with an ESI Turbo Ion-Spray interface, operating in positive ion mode and controlled by Analyst 1.6 software (AB Sciex). The ESI source operation parameters were as follows: ion source, turbo spray; source temperature, 500°C; ion-spray voltage (IS), 5,500 V; ion source gas I (GSI), 55 psi; gas II (GSII), 60 psi; curtain gas (CUR), 25.0 psi; and collision gas (CAD), high. Instrument tuning and mass calibration were performed with 10 and 100 μmol/l polypropylene glycol solutions in the 6500 Q TRAP and LIT modes, respectively. Q TRAP scans were acquired as multiple reaction monitoring (MRM) experiments with the CAD (nitrogen) set to 5 psi. The declustering potential (DP) and collision energy (CE) for individual MRM transitions were determined with further DP and CE optimization. A specific set of MRM transitions was monitored for each period according to the metabolites eluted within this period.

Transcriptome Sequencing and Transcript Quantification

Three biological replicates of TW (pool of five trees), OW (pool of five trees), and NW (pool of five trees) were used to carry out multiomic sequencing. Total RNA from the TW, OW, and NW of each sample was isolated using an RNA reagent kit (DP441; Tiangen Biotech, Beijing, China) following the manufacturer's protocol. RNA quality was assessed on an Agilent 2100 bioanalyzer (Agilent Technologies, Palo Alto, CA, United States) and checked using RNase-free agarose gel electrophoresis. In total, nine cDNA libraries (three libraries each for TW, OW, and NW) were constructed for mRNA and small RNA high-throughput sequencing using an Illumina HiSeq^{TM} 4000 platform (Illumina, United States) by Gene *Denovo* Biotechnology Co. (Guangzhou, China). Each base in the reads was assigned a quality score (Q) with a Phred-like algorithm using SOAPnuke software to assess the quality of the RNA-sequencing (RNA-seq) data (Li et al., 2012).

High-quality clean reads were obtained by removing adaptor sequences. RSEM software was used to quantify transcripts (Li and Dewey, 2011). Fragments per kilobase of transcripts per million mapped reads (FPKM) were used to normalize transcript expression. The transcripts with a fold change ≥ 1.5, a p-value < 0.05, and an FPKM > 1 in a comparison were significant differentially expressed genes (DEGs).

Protein Extraction and Labeling

Xylem samples of TW, OW, and NW were ground in liquid nitrogen into powder and transferred to 2 mL of lysis buffer [8 M urea, 2% SDS, 1 × Protease Inhibitor Cocktail (Roche Ltd., Basel, Switzerland)] and sonicated on ice for 30 min, and the homogenate was centrifuged for 30 min at 13,000 rpm and 4°C.

The supernatant was transferred to a fresh tube. For each sample, proteins were precipitated with ice-cold acetone at −20°C overnight. The precipitates were washed with acetone three times and redissolved in 8 M urea by sonication on ice. Protein quality was examined by SDS-PAGE (**Supplementary Figure 1**).

Then, 100 mL of 100 mM triethylammonium bicarbonate (TEAB) and 5 μL of 200 mM Tris(2-carboxyethyl)phosphine (TCEP) were added per 100 μg of protein. The mixture was incubated at 55°C for 1 h. Then, 5 μL of 375 mM iodoacetamide was added and incubated for another 30 min. Ice-cold acetone was added to precipitate proteins, which were then redissolved in 100 μL TEAB. Proteins were digested with trypsin (Promega, Madison, WI, United States), and the peptide mixture was labeled with tandem mass tags (TMT). The peptide mixture was redissolved in 20 mM ammonium formate solution, pH 10.0, and then an Ultimate 3000 system (Thermo Fisher Scientific, Waltham, MA, United States) was used to fractionate the mixture by high-pH separation *via* a linear gradient. The column was re-equilibrated under initial conditions for 15 min. The column flow rate was maintained at 1 mL/min, and the column temperature was maintained at 30°C. See the literature (Xiao et al., 2020) for more details.

Protein Identification and Quantification

Tandem mass spectra were extracted, charge state deconvoluted and deisotoped by Mascot Distiller version 2.6. Then, the mass spectrometry data were transformed into mascot generic file (MGF) files with Proteome Discovery 1.2 (Thermo Fisher Scientific, Pittsburgh, PA, United States) and analyzed using the Mascot search engine (Matrix Science, London, United Kingdom; version 2.3.2). The Mascot database was set up for protein identification using the *C. bungei* reference transcriptome assuming the digestion enzyme trypsin with one missed cleavage allowed. Mascot was searched with a fragment ion mass tolerance of 0.050 Da and a parent ion tolerance of 20.0 ppm. Carbamidomethyl of cysteine and iTRAQ8plex of lysine and the n-terminus were specified in Mascot as fixed modifications. Deamidation of asparagine and glutamine and oxidation of methionine and acetyl groups at the n-terminus were specified in Mascot as variable modifications.

Protein identifications were accepted if they could achieve an false discovery rate (FDR) <1.0% by the scaffold local FDR algorithm. Proteins were classified to satisfy the principles of parsimony if they contained similar peptides and could not be differentiated based on MS/MS analysis alone. In total, 17,548 unique peptides corresponding to 5,366 proteins were quantified. Proteins identified with unique spectra ≥2 in all the samples were used for quantification. The ratios of reporter ions reflect the relative abundances of peptides to ensure relative protein quantification. Medians were used to average and quantify the Mascot search results. Proteins with a fold change >1.2 or <0.83 in a comparison and with an unadjusted significance level $P < 0.05$ were significant differentially expressed proteins (DEPs).

Prediction of Key Transcription Factors

The DEGs related to lignin monomer synthesis between TW and OW or between TW and NW were selected. TBtools (Chen et al., 2020) was used to extract 2,000-bp sequences before the CDSs of key genes as potential promoter sequences based on the *C. bungei* genome data. The promoter sequences of functional genes were imported into the online database PlantTFDB,[1] and the potential transcription factors of target genes were predicted and regulated based on the Arabidopsis genome. The best match between Arabidopsis and *C. bungei* was found by basic local alignment search tool (BLAST). Then, we analyzed the differential expression of TFs between TW and OW and between TW and NW. The significantly differentially expressed TFs were candidate TFs.

Statistical Analysis

SPSS 22.0 was used for variance analysis to test the significant differences in metabolite content and gene expression among different wood types. The Duncan method was used for multiple comparisons after variance analysis. GraphPad Prism 6.0 was used to draw scatter plots of gene expression and linear regression analysis. Pearson correlation analysis of the gene transcription and translation levels was carried out by SPSS 22.0, and $P < 0.05$ was the threshold for significance.

RESULTS

The Anatomy of Tension Wood, Opposite Wood, and Normal Wood

Observation of the transverse section morphology of the *C. bungei* xylem showed that the differentiation of TW vessels was greatly affected. The number of vessels was significantly reduced, and their size was smaller than those in OW and NW (**Figure 1**). TW had a thinner cell wall than OW and NW according to the ultrastructure of the cell wall and the statistical results for cell wall thickness in our previous study (Xiao et al., 2020). Slice staining showed that TW could be dyed with fast green (**Figures 1B,C**), indicating lower lignification of TW. These results also suggested that the formation of the TW cell wall was inhibited and that its chemical composition might be greatly changed.

Raman Spectroscopic Imaging and Microspectroscopy of Tension Wood, Opposite Wood, and Normal Wood

Confocal Raman microscopy was used to obtain more information about lignin in different cell wall regions of TW, OW, and NW. Confocal imaging showed that the total lignin signal intensity from OW and NW fibers was greater than that from TW. This indicated decreased lignin deposition in TW (**Figure 2**). **Figure 3** shows that the Raman spectral intensities of the secondary layer (SL), middle layer (ML), and cell corner (CC) of TW were lower than those of OW and NW. According to previous literature (**Table 1**), characteristic Raman peaks at 1,210, 1,275, and 1,337 cm^{-1} reflect H, G, and S lignin, respectively. There was no obvious peak at 1,210 cm^{-1} from the fiber cell wall in this study. However, there was a weak peak at 1,275 cm^{-1}

[1] http://planttfdb.gao-lab.org/

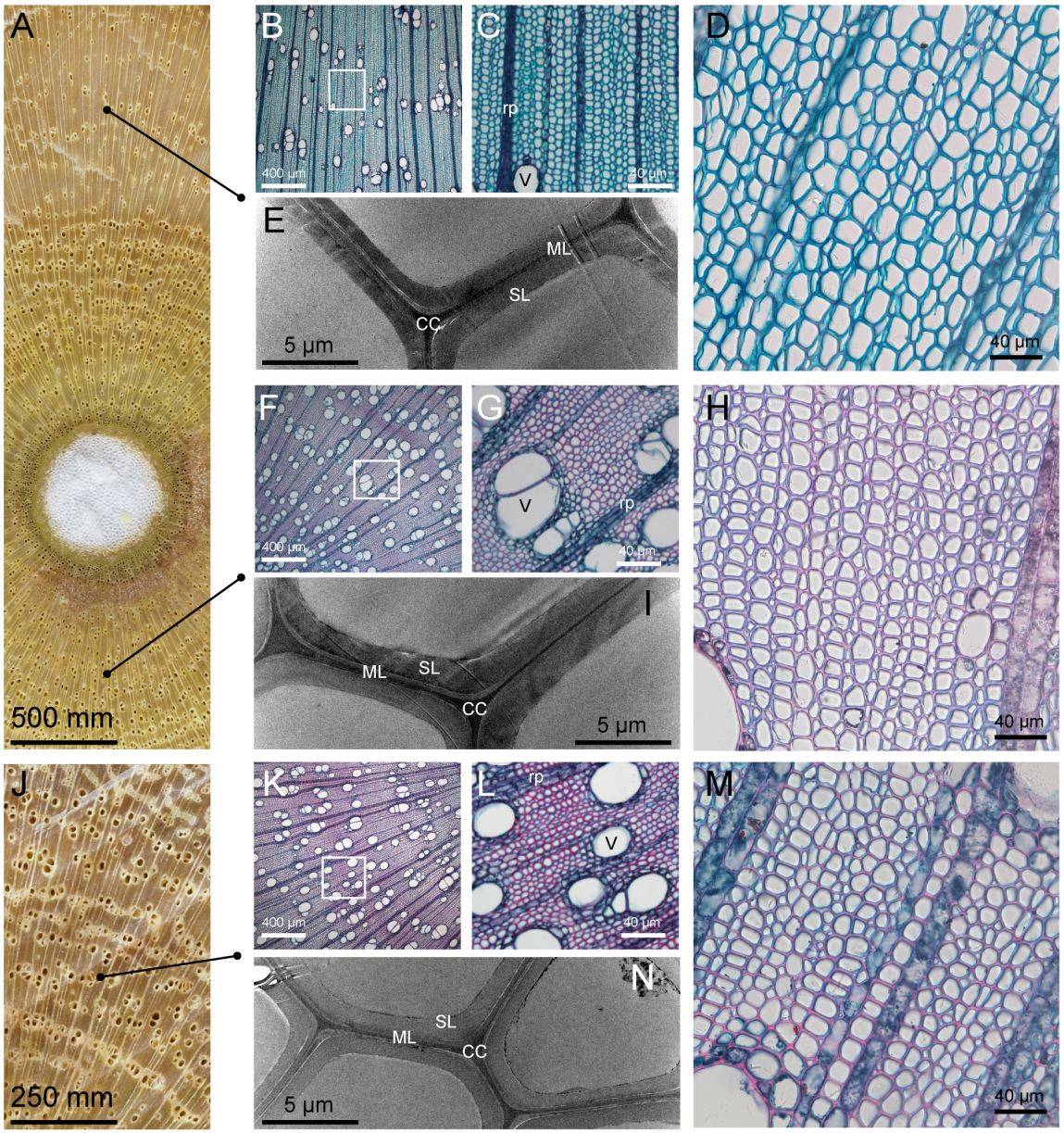

FIGURE 1 | Microstructure and ultrastructure of tension wood (TW), opposite wood (OW), and normal wood (NW). The tissue sections were stained with safranine and fast green. **(A)** Transverse TW and OW. **(B–D)** Light microscopy cross sections of TW. **(E)** Transmission electron microscopy illustrating TW; **(F–H)** light microscopy cross sections of OW. **(I)** Transmission electron microscopy illustrating OW; **(J)** transverse NW. **(K–M)** Light microscopy cross sections of NW. **(N)** Transmission electron microscopy illustrating of NW. rp, ray parenchyma; SL, secondary wall layer; ML, middle lamella; CC, cell corner; V, Vessel.

and a strong peak at 1,337 cm^{-1}, which indicated a high relative content of S lignin but no H lignin in *C. bungei* wood.

The peak at 1,607 cm^{-1} reflects the presence of aromatic lignin skeletal vibrations. In the SL, ML, and CC, the Raman intensity of this peak from OW was approximately 37.27, 14.42, and 15.64%, respectively, higher than that from TW. The Raman intensity of this peak from NW was also higher than that from TW, but the standard deviation in these intensities was large. This result suggests that the difference in lignin deposition between TW and OW or NW is mainly reflected in the S layer. Similarly, the characteristic peak at 1,275 cm^{-1}, which reflects G lignin in the ML layer, was not different between TW and OW, while in the S layer, there was a 28.31% higher value for OW than for TW. Although the intensity of the peak at 1,275 cm^{-1} in the ML was different between TW and NW, there was a slightly large error for NW; thus, we could not accurately assess the differences. The results above further confirmed that the lignin metabolism difference in TW fibers mainly occurred in the SL. The Raman intensities of each functional group

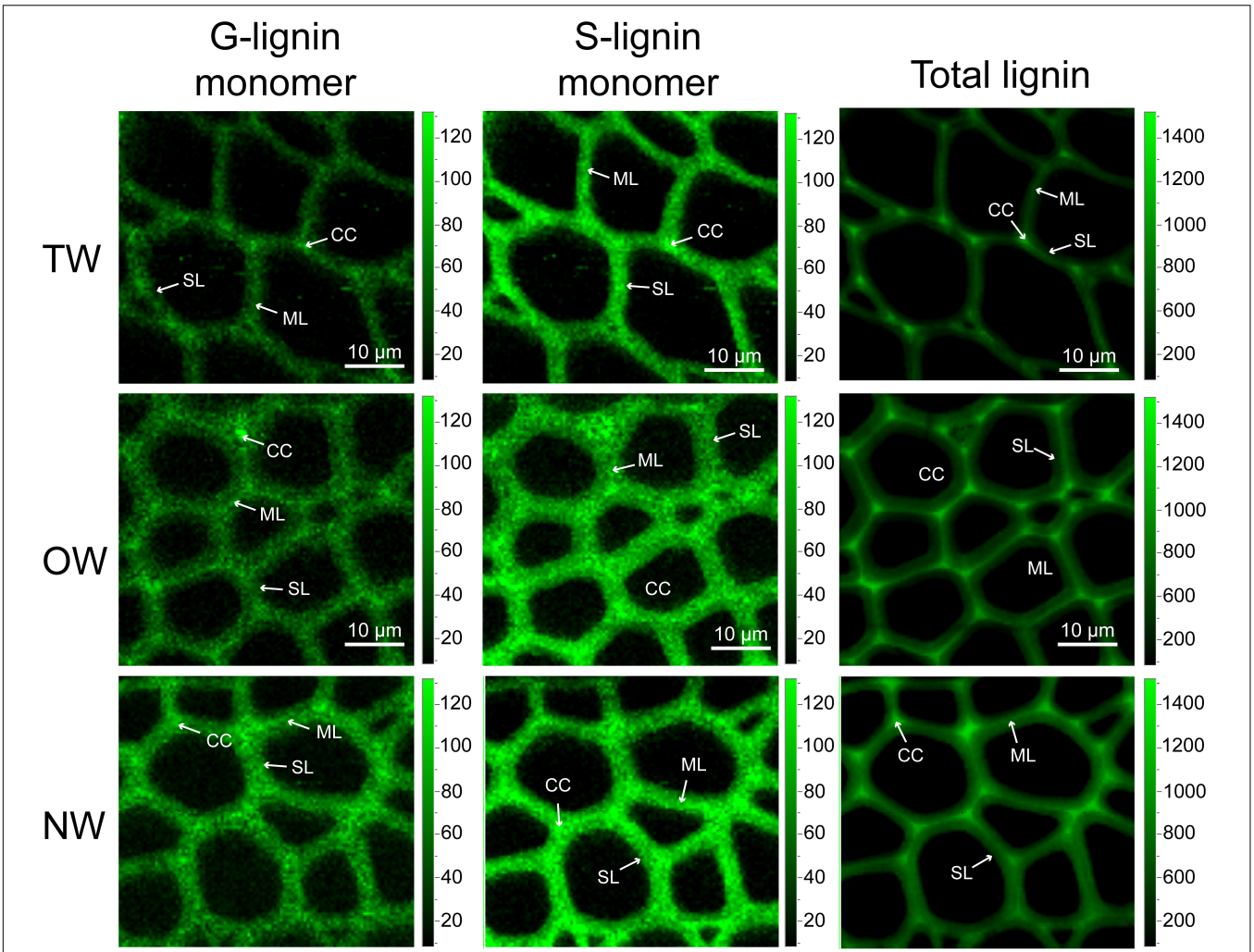

FIGURE 2 | Confocal Raman spectral imaging of tension wood (TW), opposite wood (OW), and normal wood (NW). Confocal Raman images of G-lignin monomer at 1,275 wavenumber/cm^{-1}, S-lignin monomer at 1,337 wavenumber/cm^{-1}, and total lignin at 1,607 wavenumber/cm^{-1}. SL, secondary wall layer; ML, middle lamella; CC, cell corner.

in lignin molecules in the CC layer were generally higher than those in the other layers, indicating that the lignin deposition in TW, OW, and NW began in the CC layer, and these peaks for OW were all greater than those for TW. Raman confocal imaging also clearly showed the strongest Raman spectral signals at 1,250–1,290 cm^{-1}, 1,320–1,338 cm^{-1}, and 1,590–1,620 cm^{-1} in CC. This implied that lignin synthesis and deposition in TW were inhibited from the beginning (**Figure 3C**).

LC-MS of Metabolites in the Lignin Monomer Biosynthesis Pathway in Tension Wood, Opposite Wood, and Normal Wood

To reveal the change in lignin metabolism during TW formation in *C. bungei*, we used LC-MS to determine the contents of metabolites in the monolignol synthesis pathways in TW, OW, and NW (**Figure 4**). The results showed that the content of *p*-coumaryl alcohol was very low in these three types of wood tissues, but coniferyl alcohol and sinapyl aldehyde in TW, OW, and NW were more abundant than *p*-coumaryl alcohol. This suggested that H lignin was almost absent from the fiber cell wall of *C. bungei*, and S lignin was dominant, which was consistent with the Raman spectroscopy results. Cinnamic acid and *p*-coumaric acid in TW were significantly more abundant than those in OW and NW. Interestingly, we found that both *p*-coumaryl alcohol and coniferyl alcohol were less abundant in TW than in OW, and the content of coniferyl alcohol in TW was significantly lower (41% of that in OW) than that in OW. Unfortunately, this study did not determine the amount of sinapyl alcohol, but we inferred that its content in TW would be lower than that in OW. The main reason why the total lignin content of TW was significantly lower than that of OW was the reduced biosynthesis of cinnamyl alcohol in TW.

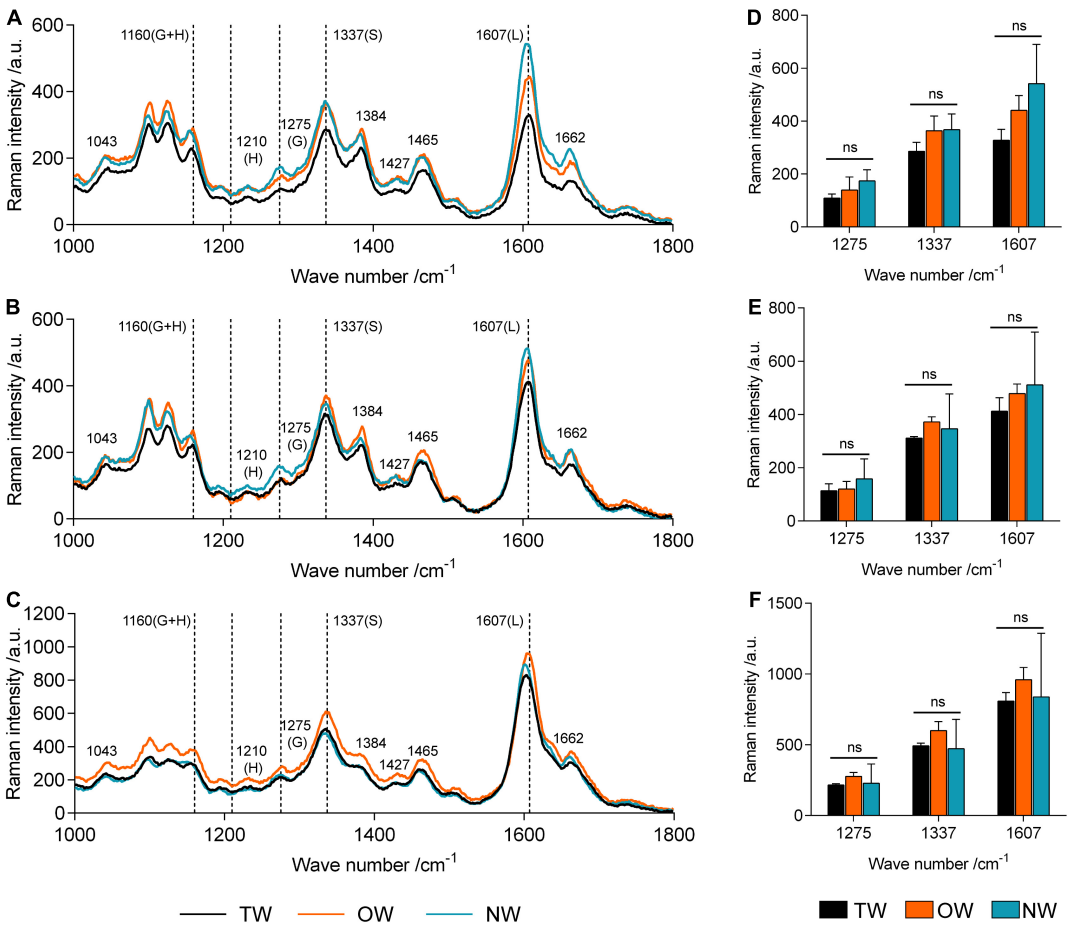

FIGURE 3 | Averaged Raman spectra in the range of 1,000–1,800 cm^{-1} in different cell wall layers of tension wood (TW), opposite wood (OW), and normal wood (NW). **(A)** Averaged Raman spectra of the secondary wall layer, **(B)** averaged Raman spectra of the middle lamella, and **(C)** averaged Raman spectra of the cell corner. **(D–F)** Raman intensities at 1,275, 1,337, and 1,607 of TW, OW, and NW in the secondary wall layer, middle lamella, and cell corner, respectively. G, G lignin; H, H lignin; S, S lignin; L, total lignin; ns, not significant. Duncan's method was used for multiple comparisons.

TABLE 1 | The Raman bands used for analysis and their assignment to lignins.

Wavenumber/cm^{-1}	Band assignment	References
1,043	OC stretch, ring deformation, CH3 wagging	Gierlinger and Schwanninger, 2006
1,143–1,209	Lignin hydroxyl COH bend, lignin methoxy vibrations	Agarwal et al., 1997
1,272	Ring deformation, CO stretch	Wiley and Atalla, 1987; Saariaho et al., 2005
1,331	Aliphatic OH stretch	Wiley and Atalla, 1987; Agarwal et al., 1997; Edwards et al., 1997
1,378–1,390	Phenolic OH stretch, CH bend	Edwards et al., 1997
1,427	Lignin methoxy deformation, methyl bending, aromatic skeletal vibration	Saariaho et al., 2005
1,465	CH3 out-of-phase bend, CH2 scissoring	Edwards et al., 1997
1,600	Lignin aromatic skeletal vibrations	Edwards et al., 1997; Gierlinger and Schwanninger, 2006
1,656	Lignin CC stretch of coniferyl alcohol and sinapyl alcohol	Agarwal et al., 1997; Saariaho et al., 2005

KEGG Pathway Enrichment of Differentially Expressed Genes and Differentially Expressed Proteins

Kyoto encyclopedia of genes and genomes (KEGG) pathway enrichment results showed that DEGs were significantly enriched into the phenylpropanoid biosynthesis pathway. The enrichment *Q*-value of this pathway was 0.01 and <0.001 in TW vs. NW and TW vs. OW, respectively (**Supplementary Figure 2A**). On the other hand, DEPs in TW vs. OW were also significantly enriched to phenylpropanoid biosynthesis (*Q*-value = 0.014) (**Supplementary Figure 2C**). The rich factor represents the proportion of DEGs in a metabolic pathway to the total number of genes, and the larger the value is, the higher the enrichment

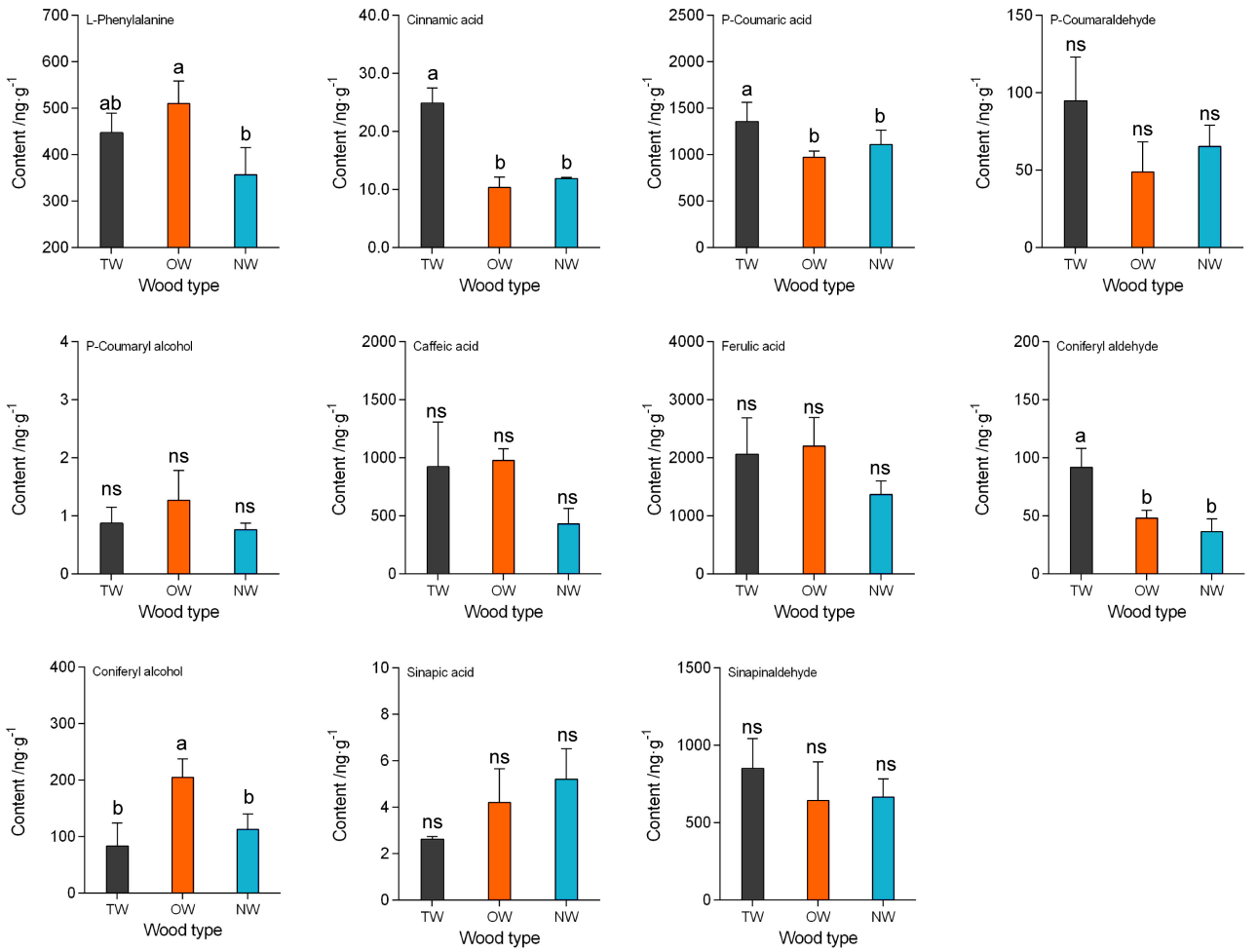

FIGURE 4 | The contents of metabolites in lignin monomer biosynthesis in tension wood (TW), opposite wood (OW), and normal wood (NW). Duncan's method was used for multiple comparisons. Different lowercase letters indicate a 5% significant difference. ns, not significant.

degree is. The rich factor of phenylpropanoid biosynthesis of DEGs was relatively high in TW vs. NW (0.06) and TW vs. OW (0.07) (**Supplementary Figure 2B**). And the rich factor of phenylpropanoid biosynthesis of DEPs in TW vs. OW was 0.13, it was higher than that in TW vs. NW (0.06) (**Supplementary Figure 2D**). This indicated the phenylpropanoid biosynthesis was more important for the difference between TW and OW. All of the above results showed the change of phenylpropanoid biosynthesis would influence the TW information.

Transcription and Translation Levels of Genes Involved in Lignin Monomer Biosynthesis in Tension Wood, Opposite Wood, and Normal Wood

The expression of genes and proteins involved in lignin biosynthesis was detected by transcriptome and proteome analyses. Detailed functional annotations of these genes can be found in **Supplementary Table 1**. Comparison of the expression levels of these genes or proteins between TW and OW and between TW and NW revealed that most of these genes had high levels of both transcription and translation in TW (**Figure 5**). The expression of *4CL* (evm.model.group13.1024), *PAL* (evm.model.group 7.3506), *CCoAOMT* (evm.model.group4.1455), *CCR* (evm.model.group6.1507), and *F5H* (evm.model.group3.991) significantly differed between TW and OW according to the transcriptome results (**Figure 5A**). Among them, 4CL and PAL had high levels of translation in TW according to the proteome (**Figure 5B**). Notably, most *CADs* in TW had higher transcription than those in OW and NW, but the translation of CADs in TW was lower than that in OW and NW. Correlation analysis of the gene expression levels showed that the transcription and translation levels of the two 4CLs and CCoAoMT genes were both significantly positively correlated (0.816–0.977). The transcription levels of *4CL* (evm.model.group6.1597) and *CCoAOMT* (evm.model.group4.1455) showed an obvious linear correlation with their translation levels (**Figure 5C**). In contrast, there was no obvious linear relationship between the transcription and translation levels of the three *CADs*, and

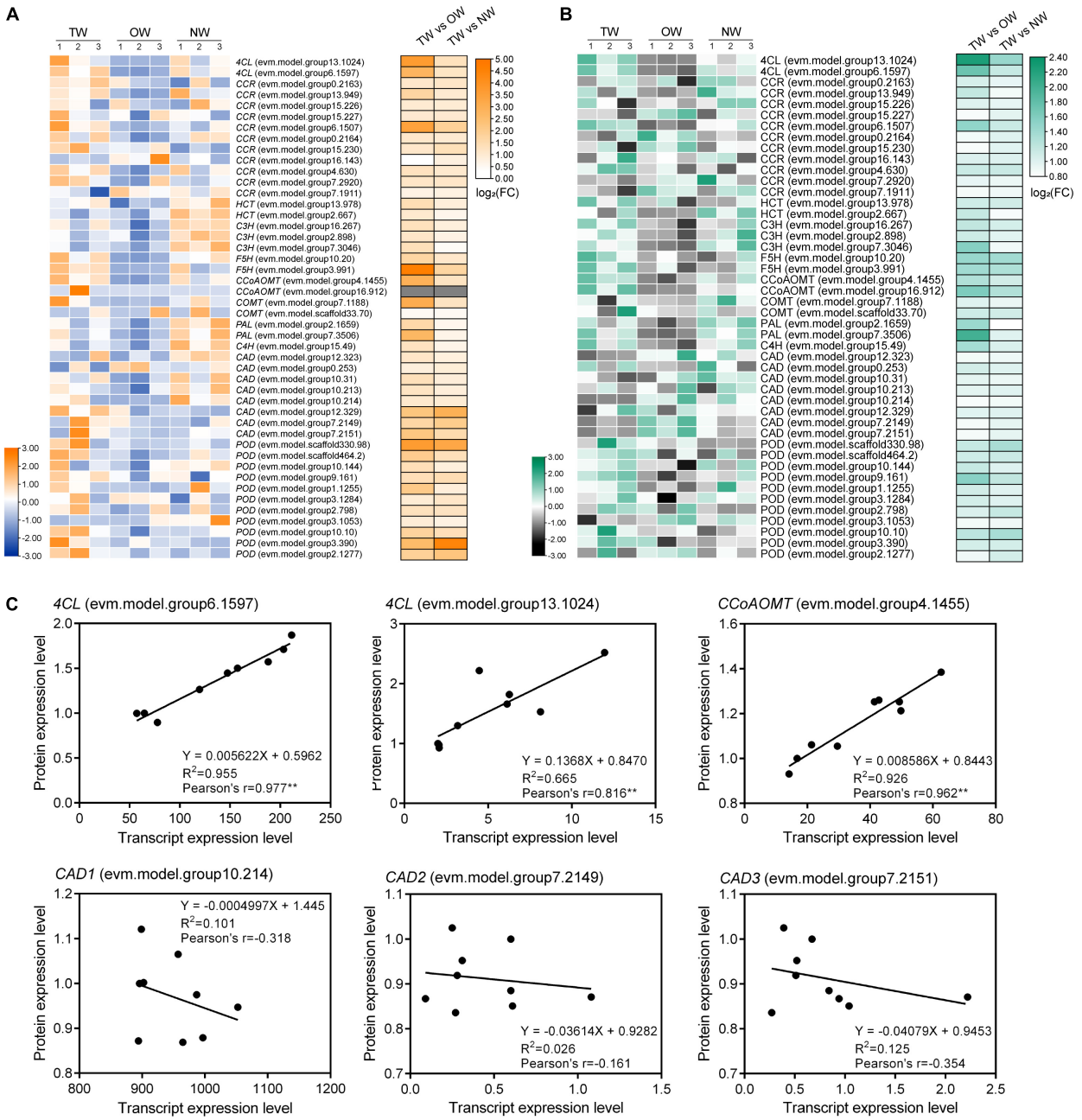

FIGURE 5 | Transcription and translation levels of genes involved in lignin monomer biosynthesis in tension wood (TW), opposite wood (OW), and normal wood (NW). The numbers in panels **(A,B)** represent the biological replicates. **(A)** Transcription levels in TW, OW, and NW and differential expression of genes involved in the lignin metabolism pathway between groups, **(B)** translation levels in TW, OW, and NW and differential expression of genes involved in the lignin metabolism pathway between groups, **(C)** correlation analysis of the transcription and translation levels of candidate genes. Pearson's r indicates the Pearson correlation coefficient. ** indicates 1% significance. Gene transcription levels and protein expression levels showed in heatmap were normalized.

the Pearson correlation of their transcription and translation levels was also weak.

Quantitative Real-time polymerase chain reaction (qRT-PCR) was used to validate the results of RNA-seq (**Figure 6A**). The transcription level of *4CL* (evm.model.group6.1597) in TW was significantly higher than that in OW and NW. This result was consistent with the transcription level of *CCoAOMT* (evm.model.group4.1455). Correlation analysis showed that the results of the qRT-PCR of *CCoAOMT* were positively correlated (0.810) with its FPKM value from the transcriptome. On the other hand, the transcription levels of the three *CAD* genes were not significantly different among TW, OW and NW. However, their qRT-PCR results were weakly correlated with the transcriptome sequencing results (**Figure 6B**), which may

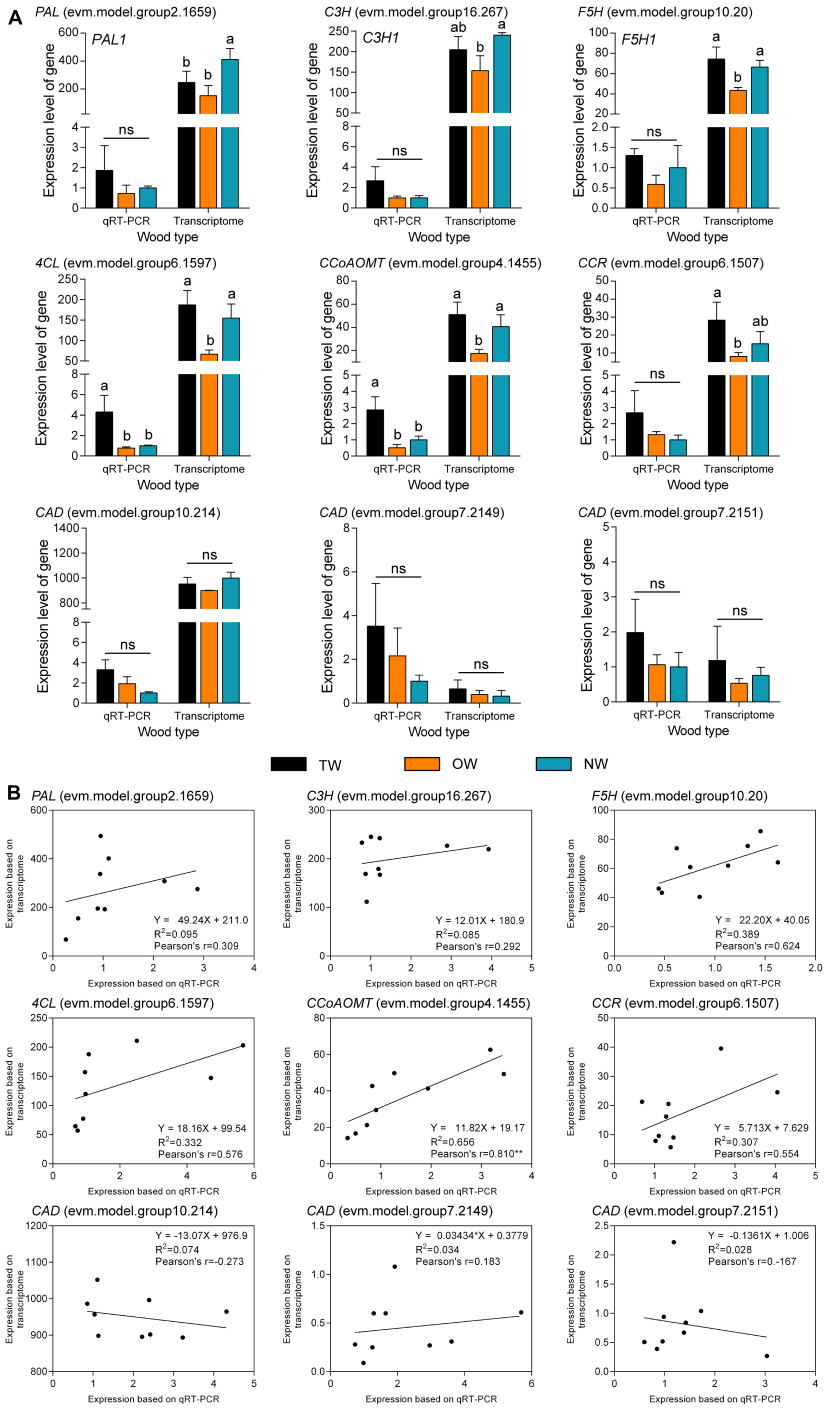

FIGURE 6 | qRT-PCR validation of transcripts involved in lignin monomer biosynthesis in tension wood (TW), opposite wood (OW), and normal wood (NW). **(A)** qRT-PCR of candidate genes. **(B)** Correlation analysis of qRT-PCR and transcriptome results for candidate genes. Duncan's method was used for multiple comparisons. Different lowercase letters indicate a 5% significant difference. ns, not significant. Pearson's r indicates the Pearson correlation coefficient. ** indicates 1% significance. The expression of NW was as the control in qRT-PCR experiment.

have been due to the specificity of primers or the difference in RNA samples used in this experiment. In contrast, two *4CLs* (evm.model.group13.1024, evm.model.group6.1597) and one *CCR* (evm.model.group6.1507) showed significantly higher transcription and translation levels in TW than in OW and NW. The translation level of 4CL (evm.model.group6.1597) in TW was 1.50 times that in OW and 1.14 times that in NW. However, the translation level of the three CADs

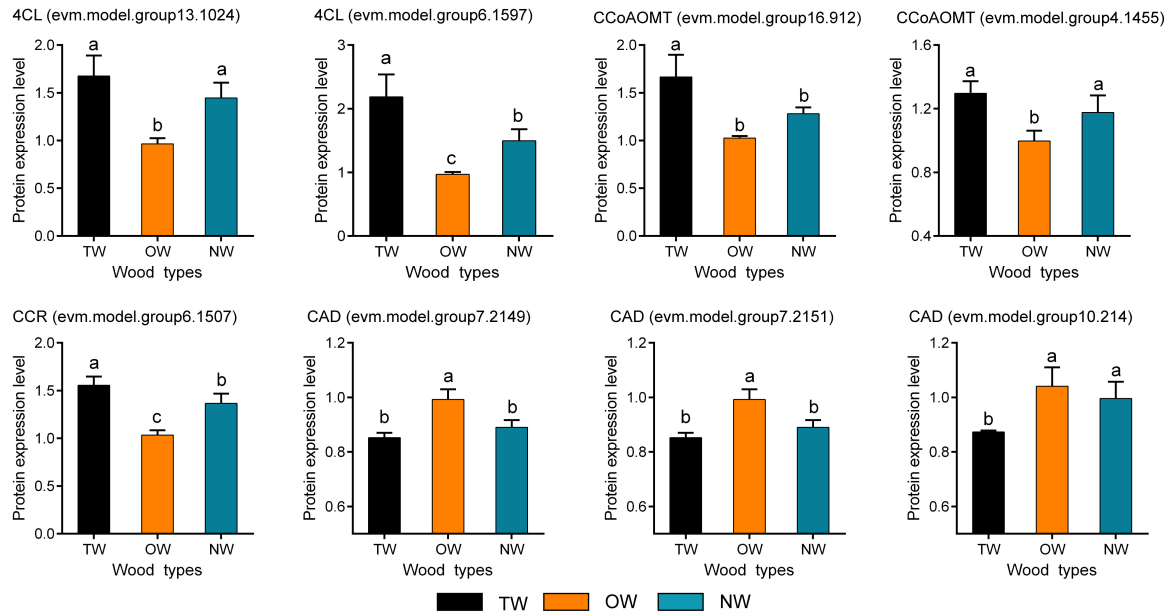

FIGURE 7 | The expression of candidate proteins involved in lignin monomer biosynthesis in tension wood (TW), opposite wood (OW), and normal wood (NW). Duncan's method was used for multiple comparisons. Different lowercase letters indicate a 5% significant difference. One of the biological repetitions of OW serves as a reference for calculating protein relative expression.

in TW was significantly lower than that in OW, and the expression level of CAD (evm.model.group10.214) in TW was significantly lower than those in OW and NW (**Figure 7**). The translation levels of the three CADs in OW were approximately 16.38–19.20% higher than those in TW (**Figure 7** and **Supplementary Table 2**).

Proteins are better for explaining biological problems as the basis for their function in live organisms. Therefore, the significantly low level of CAD enzymes in TW was probably the main factor limiting monolignol biosynthesis, which eventually led to a decrease in lignin deposition. We further mapped the 17 DEGs whose transcription and translation levels were both significantly different in the lignin monomer metabolic pathways (**Supplementary Figure 3**). This figure visually shows the transcription and translation levels of genes involved in each chemical reaction in the lignin monomer synthesis pathway during TW formation, increasing the understanding of the mechanism of lignin monomer biosynthesis in *C. bungei*.

Transcriptional Regulatory Network of Lignin Monomer Biosynthesis in Tension Wood

Transcription factors are some of the most important molecules that regulate gene expression. We used the PlantTFDB online database to predict the transcription factors that potentially regulate 17 candidate genes involved in lignin monomer synthesis. On the basis of the targeted relationship, we selected the differentially expressed transcription factors in TW and OW or in TW and NW as candidate regulatory genes (**Table 2**). In this study, 14 transcription factors were identified. Unfortunately, these 14 proteins were not identified in the proteome. Therefore, only their transcriptional levels are shown here. HD-ZIP (evm.model.group7.1157), LBD (evm.model.scaffold464.1), MYB (evm.model.group2.1745), MYB_related (evm.model.group2.388), and NAC (evm.model.group1.695) were significantly differentially expressed in TW and OW, and the remaining transcription factors were significantly differentially expressed in TW and NW.

Figure 8A shows the regulatory relationship between the candidate transcription factor and 17 target genes. Each transcription factor has multiple target genes with a node degree between 3 and 11 (**Table 2**). The node degree could represent the importance of transcription factors in the metabolic pathway. The node degrees of bHLH (evm.model.group1.1335) and HD-ZIP (evm.model.group7.1157) were 11 and 10, ranking first and second, respectively. Thus, they are considered important transcription factors. They all had targeting relationships with the *CCoAOMT*, *F5H*, *CCR*, and *CAD* genes (**Figures 8B,C**). Second, we found that several genes that had a potential targeting relationship with NAC (evm.model.group1.695), including *4CL*, *CCoAOMT*, and *CCR*, were more directly related to cinnamaldehyde biosynthesis. Therefore, we believe that NAC is also an important regulatory factor affecting lignin monomer synthesis (**Figure 8D**). The matching sequence information of the three key transcription factors and target genes is shown in **Supplementary Table 3**.

The correlation analysis of gene expression (**Figure 9**) showed that although bHLHs (evm.model.group1.1335) had a high node degree, the correlation between their expression level and target gene transcription and translation levels was weak. Therefore, bHLHs were not considered to have a critical

TABLE 2 | The expression and annotation of candidate transcription factor-regulated genes involved in lignin monomer biosynthesis.

Gene ID	Family	Transcriptional expression (mean ± SD)			Different expression (TW/OW)		Different expression (TW/NW)		Node degree	Best hit in *A. thaliana*	Description
		TW	OW	NW	log_2(FC)	*P*-value	log_2(FC)	*P*-value			
evm.model.group0.1192.1	ARR-B	3.08 ± 1.22	5.67 ± 1.5	6.79 ± 0.96	−0.88	/	−1.14	0.011	3	AT4G16110	Response regulator 2
evm.model.group1.1335	bHLH	3.91 ± 1.14	1.25 ± 0.8	0.22 ± 0.11	1.65	/	4.15	<0.001	11	AT3G59060	Phytochrome interacting factor 3-like 6
evm.model.group13.293	bHLH	7.04 ± 3.69	10.79 ± 2.96	15.41 ± 4.15	−0.62	/	−1.13	0.003	9	AT5G08130	bHLH family protein
evm.model.scaffold294.22	C2H2	17.27 ± 10.8	11.76 ± 9.87	5.91 ± 0.21	0.55	/	1.55	0.004	6	AT1G27730	Salt tolerance zinc finger
evm.model.group19.297	ERF	7.55 ± 6.76	9.21 ± 4.92	2.55 ± 0.52	−0.29	/	1.57	0.039	7	AT4G17490	Ethylene responsive element binding factor 6
evm.model.group7.1157	HD-ZIP	46.08 ± 7.01	21.36 ± 2.57	25.51 ± 3.61	1.11	<0.001	0.85	/	10	AT2G46680	Homeobox 7
evm.model.group3.142	HD-ZIP	26.04 ± 5.23	30.17 ± 7.81	53.29 ± 5.64	−0.21	/	−1.03	<0.001	6	AT4G40060	Homeobox protein 16
evm.model.scaffold464.1	LBD	12.41 ± 4.62	3.5 ± 1.76	10.82 ± 3.66	1.83	0.006	0.20	/	6	AT2G30340	LOB domain-containing protein 13
evm.model.group2.1745	MYB	1.92 ± 0.61	0.07 ± 0.07	0.85 ± 0.14	4.78	0.011	1.18	/	7	AT3G53200	MYB domain protein 27
evm.model.group2.388	MYB_related	2.92 ± 1.81	9.31 ± 5.16	0.77 ± 0.54	−1.67	0.042	1.92	/	5	AT5G56840	MYB_related family protein
evm.model.group1.695	NAC	16.75 ± 3.08	6.57 ± 0.9	13.27 ± 3.06	1.35	<0.001	0.34	/	7	AT4G28500	NAC domain containing protein 73
evm.model.group1.1356	NAC	4.55 ± 4.33	4.71 ± 2.08	13.53 ± 7	−0.05	/	−1.57	0.021	8	AT2G43000	NAC domain containing protein 42
evm.model.group1.1859	NAC	5.44 ± 1.55	5.61 ± 1.48	2.26 ± 0.59	−0.04	/	1.27	0.045	4	AT3G15510	NAC domain containing protein 2
evm.model.group0.1498	WRKY	21.34 ± 2.63	13.28 ± 1.89	6.71 ± 1.58	0.68	/	1.67	<0.001	4	AT1G69310	WRKY DNA-binding protein 57

FC, Fold change; TW, Tension wood; OW, Opposite wood; NW, Normal wood.

regulatory role in the synthesis of lignin monomers. In contrast, the transcription level of *HD-ZIP* (evm.model.group7.1157) was significantly positively correlated with the transcription and translation levels of *CCoAOMT* (evm.model.group4.1455), *CCR* (evm.model.group6.1507) and *F5H* (evm.model.group3.991), and the correlation coefficient for the former two groups was >0.8. Similarly, *NAC* (evm.model.group1.695) was significantly positively correlated with the transcription and translation levels of *CCoAOMT* (evm.model.group4.1455) and two *4CLs* (correlation coefficient > 0.7) (**Figure 9**). *HD-ZIP* (evm.model.group7.1157) had a higher transcription level in TW (FPKM was 46.08), which was approximately twice that of OW and NW. It is speculated that this transcription factor is the most important transcription factor regulating lignin metabolism in *C. bungei* TW.

Regulation Pattern Mediated by Transcription Factors in Lignin Biosynthesis in Tension Wood

We preliminarily proposed the transcriptional regulation mechanism of lignin monomer synthesis of *C. bungei* TW according to the contents of metabolites in the lignin synthesis pathway, the transcription and translation of key genes and the potential regulatory relationship between candidate transcription factors and genes (**Figure 10**). When the stems of trees grew under stress, the expression levels of the NAC (evm.model.group1.695) and HD-ZIP (evm.model.group7.1157) transcription factors were significantly increased in the stress area. They could bind *4CL*, *CCoAOMT* or *F5H* genes and activate their expression at the transcription level, which may promote the production of feruloyl-CoA and sinapoyl-CoA. Then, HD-ZIP further promoted the expression of the *CCR* gene and enhanced the conversion of coenzyme A to cinnamaldehyde, significantly increasing the content of coniferyl aldehyde in TW. However, we speculated that the significantly lower protein content of the CAD gene in TW may inhibit the conversion of coniferyl aldehyde and sinapaldehydes into coniferyl alcohol and sinapyl alcohol, resulting in a significant decrease in lignin monomer and total lignin in TW. The normal transcription level of CAD and the significantly lower translation level in TW suggested that CAD may be regulated at the post-transcriptional level and affect the translation of CAD. However, the specific regulatory mechanism remains to be further explored.

DISCUSSION

Differences in Lignin Metabolism Among Tension Wood, Opposite Wood, and Normal Wood of *Catalpa bungei*

Tension wood is wood with unique anatomical and physical characteristics. Its properties have created a starting point for the study of wood formation mechanisms. Lignin is one of the main chemical components in wood. Changes in its content and structure will affect the quality and utilization of wood. Methods of directionally changing lignin are always popular research

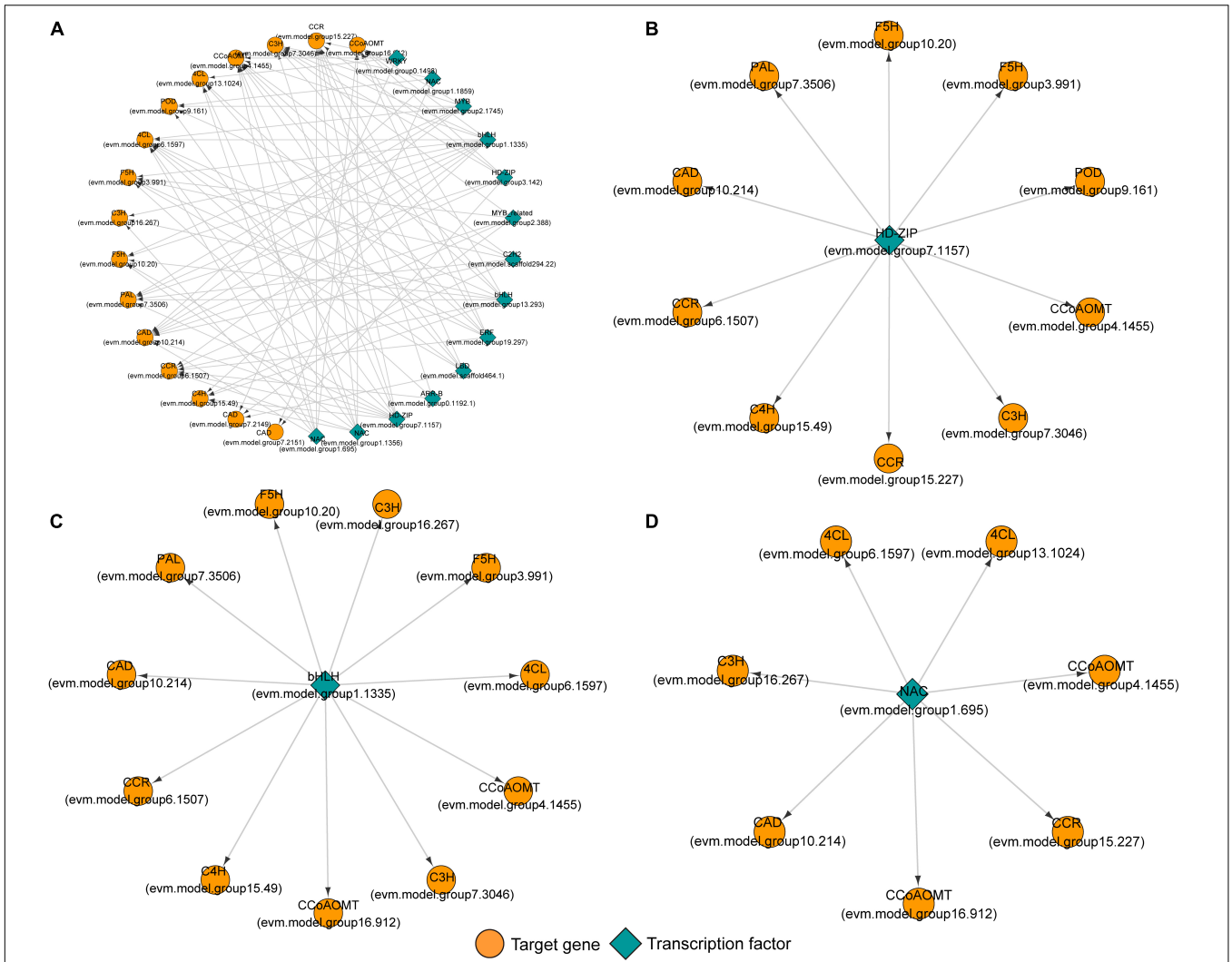

FIGURE 8 | The potential regulatory network between transcription factors and genes involved in lignin monomer biosynthesis in tension wood (TW) formation. **(A)** The regulatory network between candidate transcription factors and 17 key genes involved in lignin monomer biosynthesis. **(B)** The regulatory network of key HD-ZIP transcription factors and target genes. **(C)** The regulatory network of key bHLH transcription factors and target genes. **(D)** The regulatory network of key NAC transcription factors and target genes.

topics. In this study, the characteristics of lignin metabolism were evaluated by various methods. Histochemical staining showed that the lignin content of TW was significantly lower than that of OW, which agreed with previous studies (Jin and Kwon, 2009; Brereton et al., 2011; Mizrachi et al., 2015). The presence of a gelatinous layer (G layer) with no or an extremely low lignin content is considered the result of decreased lignification of TW (Pilate et al., 2004). Our previous work showed that the TW of *C. bungei* does not have a G-layer (Xiao et al., 2020); therefore, there may be a special regulation pattern for lignin metabolism during TW formation in *C. bungei*.

For a more comprehensive analysis of the changes in lignin metabolism during TW formation, LC-MS and confocal micro-Raman spectroscopy were used to further analyze the metabolic differences among TW, OW, and NW in the lignin monomer biosynthesis of *C. bungei*. Confocal micro-Raman spectrochemical imaging can reflect the differences in chemical components between samples more accurately without any chemical treatment and can also directly show the spatial distribution of lignin at the subcellular level (Gierlinger and Schwanninger, 2006). Analysis with this technique revealed an obvious difference in lignin metabolism between TW and OW or NW. In TW, not only was the total lignin content lower than that in OW and NW, but the contents of S lignin and G lignin were also lower than those in OW and NW. The Raman images of TW in poplar (Gierlinger and Schwanninger, 2006), maple, beech, and oak (Lehringer et al., 2008) were similar to our images. Notably, our results showed that TW had a significantly higher level of coniferyl aldehyde but a significantly lower level of coniferyl alcohol than OW and NW. Coniferyl alcohol, as one of the precursors of lignin monomers, had a great influence on the total lignin content. We speculate that the enzymes that catalyze

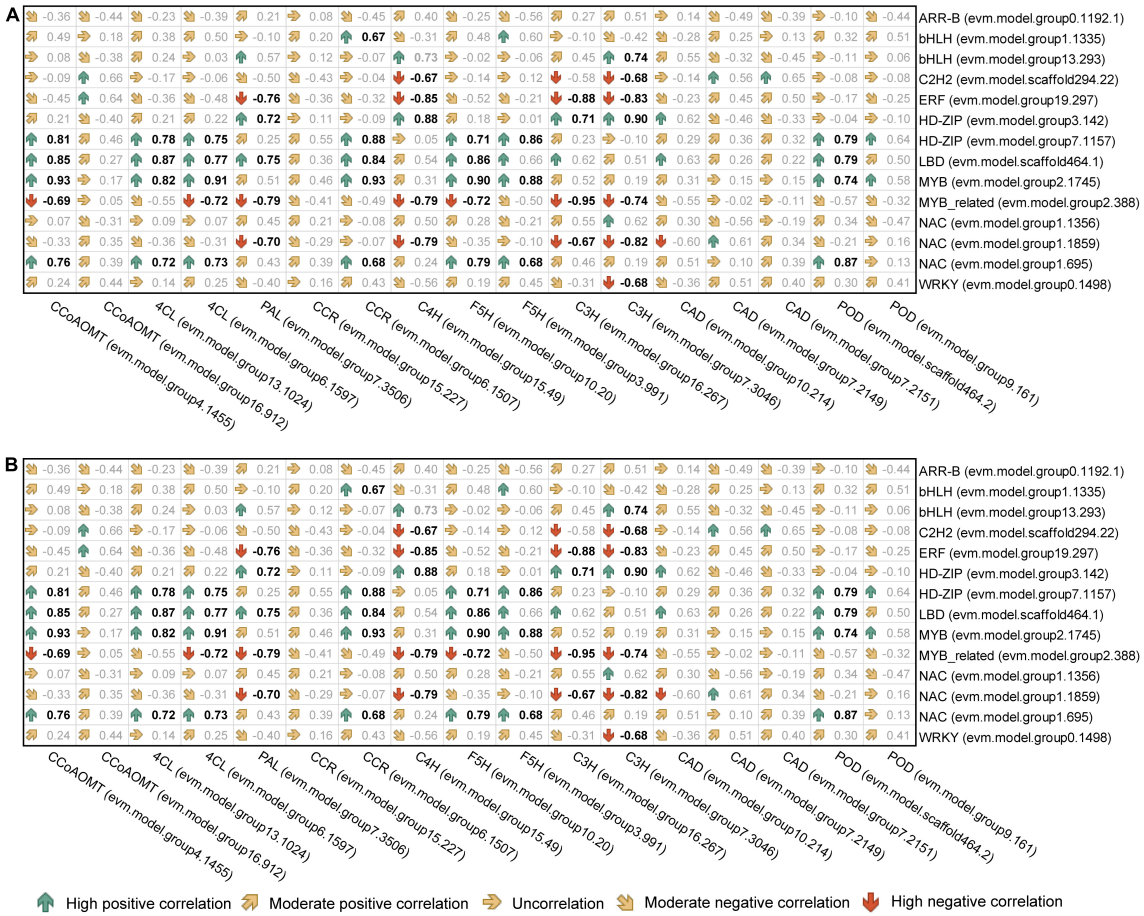

FIGURE 9 | Correlation analysis of the expression levels between candidate transcription factors and genes involved in lignin monomer biosynthesis. **(A)** The correlation coefficient between the transcription level of transcription factors and functional genes. **(B)** The correlation coefficient between the transcription level of transcription factors and the translation level of functional genes. Bold black indicates a $P < 0.05$ significance level.

this chemical process might have led to this result. In addition, higher contents of p-coumaraldehyde and sinapyl aldehyde and a lower content of *p*-coumaryl alcohol in TW than in OW and NW were also observed, although the difference did not reach the level of statistical significance. The conversion of cinnamaldehyde to cinnamyl alcohol is the main inhibitor of TW lignin biosynthesis. Unfortunately, sinapyl alcohol was not measured in this study, which is important evidence for our hypothesis.

Gene Expression Involved in Lignin Biosynthesis in the Tension Wood of *Catalpa bungei*

To test and verify our hypothesis, transcriptome and proteome sequencing of TW, OW, and NW were carried out. The results showed that most of the DEGs and proteins in the phenylpropanoid biosynthesis pathway between TW and OW were highly expressed in TW. The transcriptome of TW in *Betula luminifera* was similar to our transcriptome (Cai et al., 2018). However, the results were opposite for *Populus*, *Eucalyptus*, and *Betula platyphylla*, in which genes or proteins involved in lignin monomer synthesis were mostly downregulated during TW formation (Andersson-Gunneras et al., 2006; Chen et al., 2015; Mizrachi et al., 2015; Bygdell et al., 2017). This suggests that the expression of genes involved in lignin metabolism is highly dynamic during TW formation. In particular, we found that *4CL* (evm.model.group6.1597) and *CCoAOMT* (evm.model.group4.1455) had high transcription and translation levels in TW, and their transcription and translation levels were significantly positively correlated. Thus, we believe they might be the key to the change in TW lignin biosynthesis in *C. bungei*. Their high expression could lead to high contents of feruloyl-CoA and sinapoyl-CoA in TW. On the other hand, the high transcription and translation of *CCR* (evm.model.group6.1507) may be the reason for the high coniferyl aldehyde content in TW. However, in this study, we found that the content of lignin was lower in TW than in OW and NW, contrary to the increase in the expression of most genes involved in lignin monomer biosynthesis in TW. Interestingly, we found that the translation levels of the three CADs were significantly decreased in TW compared with OW, even though their transcription levels were not different between TW and OW.

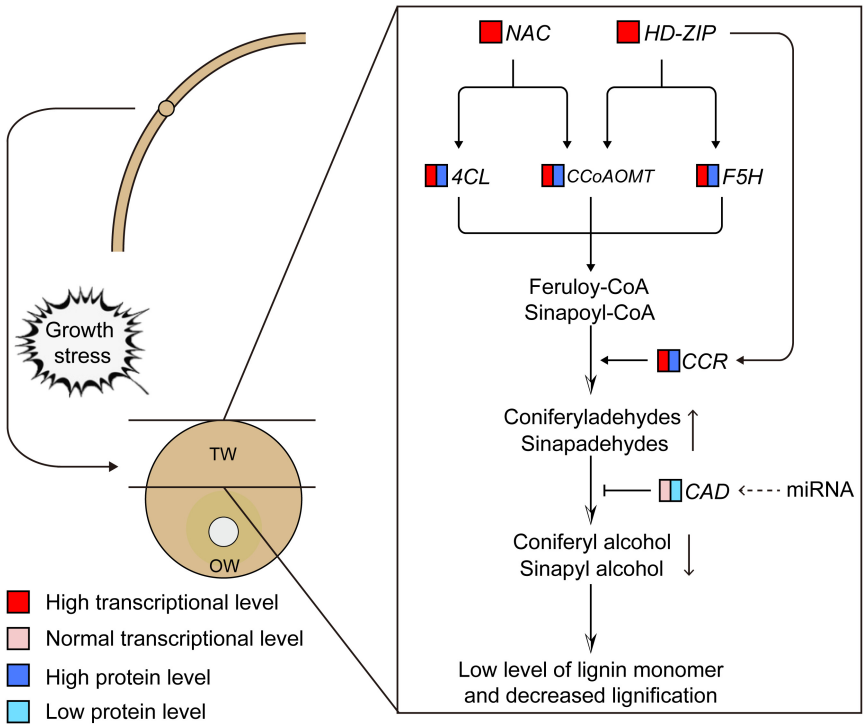

FIGURE 10 | Transcriptional regulation model of lignin monomer biosynthesis during tension wood (TW) formation in *C. bungei*. The dotted line represents the uncertainty.

Compared with mRNA, protein, as the final implementer of biological functions, plays a direct role in determining life processes. CAD is the key enzyme leading to the synthesis of coniferyl alcohol and sinapyl alcohol and catalyzes the final step of lignin monomer biosynthesis (Mansell et al., 1974). Therefore, the change in CAD translation levels may be a more important factor in the trait development of TW. Eudes et al. (2006) found that *AtCAD1* partially complemented the *A. thaliana CAD* mutant and resulted in the restoration of lignin units. Baucher et al. (1996) showed that the total lignin content was not changed in transgenic poplar trees with antisense inhibition of *CAD* gene expression compared with normal poplar, but the cinnamaldehyde level was significantly increased in the transgenic plants. Furthermore, an increase in cinnamaldehyde and an unchanging lignin content were observed in transgenic tobacco with inhibited expression of *CAD* (Halpin et al., 1994). Natural CAD mutants of pine showed not only high cinnamaldehyde levels but also a 9% decreased lignin content (Mackay et al., 1997). All these studies indicated that CAD plays an important role in lignin biosynthesis. According to our proteomic and LC-MS results, we believe that the low expression of CAD protein in TW resulted in inhibition of lignin monomer biosynthesis and a lower content of lignin in TW. Similarly, Mauriat et al. (2015) found that the CAD enzyme was less abundant in the TW than in OW of poplar. However, more information is needed to determine the difference between the transcription level and translation level of *CAD* genes in TW.

Molecular Regulation of Lignin Biosynthesis in the Tension Wood of *Catalpa bungei*

Many transcription factors, such as MYBs and NACs, have been proven to regulate lignin biosynthesis, and this regulatory hierarchy is similar to that of cellulose (Zhou et al., 2009; Zhao and Dixon, 2011). In our study, we also found that NAC (evm.model.group1.695) could regulate the expression of *4CLs* and *CCoAOMTs* to influence lignin monomer biosynthesis. Yang et al. (2019) found that overexpressed WOOD-ASSOCIATED NAC DOMAIN protein 3 (PdWND3A) in *Populus deltoides* can increase the lignin content and syringyl and guaiacyl lignin (S/G) ratio of transgenic plants, while the expression of *F5H* was increased. This result suggested that NAC may regulate the expression of the *F5H* gene to change lignin monomer synthesis in poplar. A recent study showed that the Eucalyptus NAC transcription factor can bind to the promoter of the *CCoAOMT* gene to activate its expression, and overexpression of this gene in *A. thaliana* will greatly promote xylem development and lignin synthesis (Sun et al., 2021). With the development of molecular biology techniques, more knowledge about the lignin synthesis mechanism, beyond the NAC-MYB transcriptional cascade, has been revealed (Zhao, 2016). In poplar, HD-ZIP transcription factors are highly expressed in the developing xylem (Schrader et al., 2004). Moreover, HD-ZIP transcription factors have been identified as important determinants of vascular bundle differentiation in *A. thaliana* (Zhong and Ye, 2004). With further

research, Roc8 (one HD-ZIP TF) was found to be able to target the expression of LAC, a lignin synthesis gene, in rice, while knocking out *OsRoc8* led to a significant decrease in the lignin content (Sun et al., 2020). These results supported our finding that there was a potential targeting relationship between HD-ZIP (evm.model.group7.1157) and several genes involved in lignin monomer synthesis, and the expression levels were significantly positively correlated with the target gene abundance. This implies that HD-ZIP plays a critical role in the wood formation of *C. bungei*. Interestingly, the high transcription level and low translation level of CAD in this study also suggest the existence of post-transcriptional regulation. And we guess maybe there were some miRNAs involved the regulation process, cause miRNAs were important to post-transcriptional regulation of genes. On the other hand, CAD is a key enzyme in the last step of the biosynthesis of lignin monomers, the low protein expression level of CAD is likely an important factor affecting the synthesis of lignin monomers when most lignin synthesis genes are highly expressed. Therefore, the hypothesis that miRNAs regulate CAD protein expression in translation inhibition and influence TW lignin metabolism is indeed worth exploring. Previous studies have shown that miRNAs are involved in the regulation of lignin metabolism; for instance, miR397 negatively regulates the LAC gene to change the lignin content of poplar (Lu et al., 2013). miR6433 influences the synthesis of S lignin by binding with the F5H gene (Fan et al., 2020). Overexpression of miR156 can reduce the S/G ratio in poplar (Rubinelli et al., 2013). All of the above results suggest a new level of complexity in lignin biosynthesis regulation.

CONCLUSION

In this study, we analyzed the differences in lignin biosynthesis in *C. bungei* at the transcription, translation, metabolism, and histochemistry levels between TW and OW or NW. We found that NAC and HD-ZIP transcription factors may be the key transcription factors regulating the biosynthesis of lignin monomers in *C. bungei* TW by analyzing the matching relationship between the transcription factors and the promoter sequences of key genes and the correlation of their transcription and translation levels. The significantly increased expression of NAC and HD-ZIP in TW may activate the expression of the *4CL*, *CCoAOMT*, *F5H*, and *CCR* genes and enhance the production of coniferyl aldehyde in TW. In contrast, the significantly decreased translation of CAD genes in TW may be the reason for the significantly decreased content of coniferyl alcohol, which ultimately limits lignin monomer biosynthesis in TW. However, the regulatory mode that changes the translation level of the CAD gene in TW needs further research.

DATA AVAILABILITY STATEMENT

The RNA-seq datasets are available in Sequence Read Archive (SRA) in NCBI with the accession number PRJNA559964.

AUTHOR CONTRIBUTIONS

YX performed the experiments, processed, analyzed, and interpreted the data, and wrote the manuscript with contributions from the other authors. JL, FY, and TZ assisted with the interpretation of the data and the writing of the manuscript. WM, KZ, and HY prepared the plant material and assisted in the data analysis. NL and TZ carried out the manuscript revision. JW conceived the original research plan and assisted with the design and interpretation of the data. All authors contributed to the article and approved the submitted version.

FUNDING

This work was supported by the Fundamental Research Funds of Chinese Academy of Forestry (CAFYBB2017ZY002) and the National Key Research and Development Program (Grant No. 2016YFD0600101).

ACKNOWLEDGMENTS

We would like to thank all colleagues and friends who have contributed to this study.

SUPPLEMENTARY MATERIAL

The Supplementary Material for this article can be found online at: https://www.frontiersin.org/articles/10.3389/fpls.2021.704262/full#supplementary-material

Supplementary Figure 1 | Protein SDS-PAGE.

Supplementary Figure 2 | The KEGG pathway enrichment of differentially expressed genes (DEGs) and differentially expressed proteins (DEPs). Gray indicates missing values.

Supplementary Figure 3 | Differentially expressed genes (DEGs) and Differentially expressed proteins (DEPs) involved in the lignin monomer synthesis pathways in tension wood (TW) vs. opposite wood (OW) and TW vs. normal wood (NW).

REFERENCES

Agarwal, U., and Ralph, S. (1997). Ft-raman spectroscopy of wood: identifying contributions of lignin and carbohydrate polymers in the spectrum of black spruce (Picea mariana). *Appl. Spectrosc.* 11, 1648–1655. doi: 10.1366/0003702971939316

Andersson-Gunneras, S., Mellerowicz, E. J., Love, J., Segerman, B., Ohmiya, Y., Coutinho, P. M., et al. (2006). Biosynthesis of cellulose-enriched tension wood in *Populus*: global analysis of transcripts and metabolites identifies biochemical and developmental regulators in secondary wall biosynthesis. *Plant J.* 45, 144–165. doi: 10.1111/j.1365-313X.2005.02584.x

Baucher, M. C., Pilate, B., Doorsselaere, C., Tollier, J. V., PetitConil, M. T., Cornu, M., et al. (1996). Red xylem and higher lignin extractability by down-regulating a cinnamyl alcohol dehydrogenase in poplar. *Plant Physiol.* 112, 1479–1490. doi: 10.1104/pp.112.4.1479

Bhargava, A., Mansfield, S. D., Hall, H. C., Douglas, C. J., and Ellis, B. E. (2010). MYB75 functions in regulation of secondary cell wall formation in the *Arabidopsis* inflorescence stem. *Plant Physiol.* 154, 1428–1438. doi: 10.1104/pp.110.162735

Brereton, N. P., Pitre, F. E., Ray, M. J., Karp, A., and Murphy, R. J. (2011). Investigation of tension wood formation and 2,6-dichlorbenzonitrile application in short rotation coppice willow composition and enzymatic saccharification. *Biotechnol. Biofuels* 4:13. doi: 10.1186/1754-6834-4-13

Bygdell, J., Srivastava, V., Obudulu, O., Srivastava, M. K., Nilsson, R., Sundberg, B., et al. (2017). Protein expression in tension wood formation monitored at high tissue resolution in *Populus*. *J. Exp. Bot.* 68, 3405–3417. doi: 10.1093/jxb/erx186

Cai, M., Huang, H., Ni, F., Tong, Z., Lin, E., and Zhu, M. (2018). RNA-Seq analysis of differential gene expression in *Betula luminifera* xylem during the early stages of tension wood formation. *PeerJ* 6:e5427. doi: 10.7717/peerj.5427

Chen, C. J., Chen, H., Zhang, Y., Thomas, H. R., Frank, M. H., He, Y. H., et al. (2020). TBtools: an integrative toolkit developed for interactive analyses of big biological data. *Mol. Plant* 13, 1194–1202. doi: 10.1016/j.molp.2020.06.009

Chen, J., Chen, B., and Zhang, D. (2015). Transcript profiling of *Populus tomentosa* genes in normal, tension, and opposite wood by RNA-seq. *BMC Genom.* 16:164. doi: 10.1186/s12864-015-1390-y

Edwards, H. G. M., Farwell, D. W., and Webster, D. (1997). FT Raman microscopy of untreated natural plant fibres. *Spectrochim. Acta A Mol. Biomol. Spectrosc.* 53, 2383–2392. doi: 10.1016/S1386-1425(97)00178-9

Eudes, A., Pollet, B., Sibout, R., Do, C. T., Seguin, A., Lapierre, C., et al. (2006). Evidence for a role of AtCAD 1 in lignification of elongating stems of *Arabidopsis thaliana*. *Planta* 225, 23–39. doi: 10.1007/s00425-006-0326-9

Fan, D., Li, C., Fan, C., Hu, J., Li, J., Yao, S., et al. (2020). MicroRNA6443-mediated regulation of FERULATE 5-HYDROXYLASE gene alters lignin composition and enhances saccharification in *Populus tomentosa*. *New Phytol.* 226, 410–425. doi: 10.1111/nph.16379

Gierlinger, N., and Schwanninger, M. (2006). Chemical imaging of poplar wood cell walls by confocal Raman microscopy. *Plant Physiol.* 140, 1246–1254. doi: 10.1104/pp.105.066993

Halpin, C., Knight, M. E., Foxon, G. A., Campbell, M. M., and Schuch, W. J. P. J. (1994). Manipulation of lignin quality by downregulation of cinnamyl alcohol dehydrogenase. *Plant J.* 6, 339–350. doi: 10.1046/j.1365-313X.1994.06030339.x

Horvath, L., Peszlen, I., Peralta, P., and Kelley, S. (2010). Use of transmittance near-infrared spectroscopy to predict the mechanical properties of 1- and 2-year-old transgenic aspen. *Wood Sci. Technol.* 45, 303–314. doi: 10.1007/s00226-010-0330-x

Hu, J. Q., Qi, Q., Zhao, Y. L., Tian, X. M., Lu, H., Gai, Y., et al. (2019). Unraveling the impact of Pto4CL1 regulation on the cell wall components and wood properties of perennial transgenic *Populus tomentosa*. *Plant Physiol Biochem.* 139, 672–680. doi: 10.1016/j.plaphy.2019.03.035

Jin, H., and Kwon, M. (2009). Mechanical bending-induced tension wood formation with reduced lignin biosynthesis in *Liriodendron tulipifera*. *J. Wood Sci.* 55, 401–408. doi: 10.1007/s10086-009-1053-1

Lehringer, C., Gierlinger, N., and Koch, G. (2008). Topochemical investigation on tension wood fibres of *Acer* spp., *Fagus sylvatica* L. and *Quercus robur* L. *Holzforschung* 62, 255–263. doi: 10.1515/HF.2008.036

Li, B., and Dewey, C. N. (2011). RSEM: accurate transcript quantification from RNA-Seq data with or without a reference genome. *BMC Bioinform.* 12:323. doi: 10.1186/1471-2105-12-323

Li, C. Y., Deng, G. M., Yang, J., Viljoen, A., Jin, Y., Kuang, R. B., et al. (2012). Transcriptome profiling of resistant and susceptible Cavendish banana roots following inoculation with *Fusarium oxysporum* f. sp. cubense tropical race 4. *BMC Genom.* 13:374. doi: 10.1186/1471-2164-13-374

Li, Q., Song, J., Peng, S., Wang, J. P., Qu, G. Z., Sederoff, R. R., et al. (2014). Plant biotechnology for lignocellulosic biofuel production. *Plant Biotechnol. J.* 12, 1174–1192. doi: 10.1111/pbi.12273

Li, S., Li, X., Link, R., Li, R., Deng, L. P., Schuldt, B., et al. (2019). Influence of cambial age and axial height on the spatial patterns of xylem traits in *Catalpa bungei*, a ring-porous tree species native to China. *Forests* 10:662. doi: 10.3390/f10080662

Liang, L., Wei, L., Fang, G., Xu, F., Deng, Y., Shen, K., et al. (2020). Prediction of holocellulose and lignin content of pulp wood feedstock using near infrared spectroscopy and variable selection. *Spectrochim. Acta A Mol. Biomol. Spectrosc.* 225:117515. doi: 10.1016/j.saa.2019.117515

Lu, S., Li, Q., Wei, H., Chang, M. J., Tunlaya-Anukit, S., Kim, H., et al. (2013). Ptr-miR397a is a negative regulator of laccase genes affecting lignin content in *Populus trichocarpa*. *Proc. Natl. Acad. Sci. U.S.A.* 110, 10848–10853. doi: 10.1073/pnas.1308936110

Mackay, J. J., O'Malley, D. M., Presnell, T., Booker, F. L., Campbell, M. M., Whetten, R. W., et al. (1997). Inheritance, gene expression, and lignin characterization in a mutant pine deficient in cinnamyl alcohol?dehydrogenase. *Proc. Natl. Acad. Sci. U.S.A.* 94, 8255–8260. doi: 10.1073/pnas.94.15.8255

Mansell, R. L., Gross, G. G., Stöckigt, J., Franke, H., and Zenk, M. H. J. P. (1974). Purification and properties of cinnamyl alcohol dehydrogenase from higher plants involved in lignin biosynthesis. *Phytochemistry* 13, 2427–2435. doi: 10.1016/S0031-9422(00)86917-4

Mauriat, M., Leplé, J.-C., Claverol, S., Bartholomé, J., Negroni, L., Richet, N., et al. (2015). Quantitative proteomic and phosphoproteomic approaches for deciphering the signaling pathway for tension wood formation in poplar. *J. Proteome Res.* 14, 3188–3203. doi: 10.1021/acs.jproteome.5b00140

McCarthy, R. L., Zhong, R., Fowler, S., Lyskowski, D., Piyasena, H., Carleton, K., et al. (2010). The poplar MYB transcription factors, PtrMYB3 and PtrMYB20, are involved in the regulation of secondary wall biosynthesis. *Plant Cell Physiol.* 51, 1084–1090. doi: 10.1093/pcp/pcq064

Mitsuda, N., Seki, M., Shinozaki, K., and Ohme-Takagi, M. (2005). The NAC transcription factors NST1 and NST2 of *Arabidopsis* regulate secondary wall thickenings and are required for anther dehiscence. *Plant Cell* 17, 2993–3006. doi: 10.1105/tpc.105.036004

Mizrachi, E., Maloney, V. J., Silberbauer, J., Hefer, C. A., Berger, D. K., Mansfield, S. D., et al. (2015). Investigating the molecular underpinnings underlying morphology and changes in carbon partitioning during tension wood formation inEucalyptus. *New Phytol.* 206, 1351–1363. doi: 10.1111/nph.13152

Nakahama, K., Urata, N., Shinya, T., Hayashi, K., Nanto, K., Rosa, A. C., et al. (2018). RNA-seq analysis of lignocellulose-related genes in hybrid Eucalyptus with contrasting wood basic density. *BMC Plant Biol.* 18:156. doi: 10.1186/s12870-018-1371-9

Nakano, Y., Yamaguchi, M., Endo, H., Rejab, N. A., and Ohtani, M. (2015). NAC-MYB-based transcriptional regulation of secondary cell wall biosynthesis in land plants. *Front. Plant Sci.* 6:288. doi: 10.3389/fpls.2015.00288

Papadopoulos, A. N., Bikiaris, D. N., Mitropoulos, A. C., and Kyzas, G. Z. (2019). Nanomaterials and chemical modifications for enhanced key wood properties: a review. *Nanomaterials* 9:607. doi: 10.3390/nano9040607

Pilate, G., Déjardin, A., Laurans, F., and Leplé, J. C. (2004). Tension wood as a model for functional genomics of wood formation. *New Phytol.* 164, 63–72. doi: 10.1111/j.1469-8137.2004.01176.x

Rubinelli, P. M., Chuck, G., Li, X., and Meilan, R. (2013). Constitutive expression of the Corngrass1 microRNA in poplar affects plant architecture and stem lignin content and composition. *Biomass Bioenergy* 54, 312–321. doi: 10.1016/j.biombioe.2012.03.001

Saariaho, A.-M., Argyropoulos, D. S., Jääskeläinen, A.-S., and Vuorinen, T. (2005). Development of the partial least squares models for the interpretation of the UV resonance Raman spectra of lignin model compounds. *Vib. Spectrosc.* 37, 111–121. doi: 10.1016/j.vibspec.2004.08.001

Schrader, J., Nilsson, J., Mellerowicz, E., Berglund, A., Nilsson, P., Hertzberg, M., et al. (2004). A high-resolution transcript profile across the wood-forming meristem of poplar identifies potential regulators of cambial stem cell identity. *Plant Cell* 16, 2278–2292. doi: 10.1105/tpc.104.024190

Shen, H., Mazarei, M., Hisano, H., Escamilla-Trevino, L., Fu, C., Pu, Y., et al. (2013). A genomics approach to deciphering lignin biosynthesis in switchgrass. *Plant Cell* 25, 4342–4361. doi: 10.1105/tpc.113.118828

Shinya, T., Iwata, E., Nakahama, K., Fukuda, Y., Hayashi, K., Nanto, K., et al. (2016). Transcriptional profiles of hybrid eucalyptus genotypes with contrasting lignin content reveal that monolignol biosynthesis-related genes regulate wood composition. *Front. Plant Sci.* 7:443. doi: 10.3389/fpls.2016.00443

Sun, J., Cui, X. A., Teng, S. Z., Zhao, K. N., Wang, Y. W., Chen, Z. H., et al. (2020). HD-ZIP IV gene *Roc8* regulates the size of bulliform cells and lignin content in rice. *Plant Biotechnol. J.* 18, 2559–2572. doi: 10.1111/pbi.13435

Sun, Y., Jiang, C., Jiang, R., Wang, F., Zhang, Z., and Zeng, J. (2021). A novel NAC transcription factor from eucalyptus, EgNAC141, positively regulates lignin

biosynthesis and increases lignin deposition. *Front. Plant Sci.* 12:642090. doi: 10.3389/fpls.2021.642090

Tian, M., Xia, Q. M., and Li, J. Y. (2007). The secondary growth in plant and its molecular regulation (in Chinese). *Heredita* 29, 1324–1330. doi: 10.1360/yc-007-1324

Vance, C. P., Kirk, T. K., and Sherwood, R. T. (1980). Lignification as a mechanism of disease resistance. *Ann. Rev. Phytopothol.* 18, 259–288. doi: 10.1146/annurev.py.18.090180.001355

Vanholme, R., Cesarino, I., Rataj, K., Xiao, Y., Sundin, L., Goeminne, G., et al. (2013). Caffeoyl shikimate esterase (CSE) is an enzyme in the lignin biosynthetic pathway in *Arabidopsis*. *Science* 341, 1103–1106. doi: 10.1126/science.1241602

Wang, J. P., Matthews, M. L., Williams, C. M., Shi, R., Yang, C., Tunlaya-Anukit, S., et al. (2018). Improving wood properties for wood utilization through multi-omics integration in lignin biosynthesis. *Nat. Commun.* 9:1579. doi: 10.1038/s41467-018-03863-z

Weng, J. K., Mo, H., and Chapple, C. (2010). Over-expression of F5H in COMT-deficient *Arabidopsis* leads to enrichment of an unusual lignin and disruption of pollen wall formation. *Plant J.* 64, 898–911. doi: 10.1111/j.1365-313X.2010.04391.x

Wiley, J. H., and Atalla, R. H. (1987). Band assignments in the Raman spectra of celluloses. *Carbohydr. Res.* 160, 113–129. doi: 10.1016/0008-6215(87)80306-3

Wu, Z., Wang, N., Hisano, H., Cao, Y., Wu, F., Liu, W., et al. (2019). Simultaneous regulation of F5H in COMT-RNAi transgenic switchgrass alters effects of COMT suppression on syringyl lignin biosynthesis. *Plant Biotechnol. J.* 17, 836–845. doi: 10.1111/pbi.13019

Xiao, Y., Ma, W., Lu, N., Wang, Z., Wang, N., Zhai, W., et al. (2019). Genetic variation of growth traits and genotype-by-environment interactions in clones of *Catalpa bungei* and *Catalpa fargesii* f. *duclouxii*. *Forests* 10:57. doi: 10.3390/f10010057

Xiao, Y., Yi, F., Ling, J., Wang, Z., Zhao, K., Lu, N., et al. (2020). Transcriptomics and proteomics reveal the cellulose and pectin metabolic processes in the tension wood (Non-G-Layer) of *Catalpa bungei*. *Int. J. Mol. Sci.* 21:1686. doi: 10.3390/ijms21051686

Xu, X., Lou, Y., Yang, K., Shan, X., Zhu, C., and Gao, Z. (2019). Identification of homeobox genes associated with lignification and their expression patterns in bamboo shoots. *Biomolecules* 9:862. doi: 10.3390/biom9120862

Yang, Y., Chang, G. Y., Rottmann, W., Winkeler, K. A., and Chen, J. G. (2019). Pdwnd3a, a wood-associated nac domain-containing protein, affects lignin biosynthesis and composition in *Populus*. *BMC Plant Biol.* 19:486. doi: 10.1186/s12870-019-2111-5

Zhao, Q. (2016). Lignification: flexibility, biosynthesis and regulation. *Trends Plant Sci.* 21, 713–721. doi: 10.1016/j.tplants.2016.04.006

Zhao, Q., and Dixon, R. A. (2011). Transcriptional networks for lignin biosynthesis: more complex than we thought? *Trends Plant Sci.* 16, 227–233. doi: 10.1016/j.tplants.2010.12.005

Zhong, R., Lee, C., and Ye, Z. H. (2010). Functional characterization of poplar wood-associated NAC domain transcription factors. *Plant Physiol.* 152, 1044–1055. doi: 10.1104/pp.109.148270

Zhong, R., and Ye, Z. H. (2004). Amphivasal vascular bundle 1, a gain-of-function mutation of the ifl1/rev gene, is associated with alterations in the polarity of leaves, stems and carpels. *Plant Cell Physiol.* 45, 369–385. doi: 10.1093/pcp/pch051

Zhou, J., Lee, C., Zhong, R., and Ye, Z. H. (2009). MYB58 and MYB63 are transcriptional activators of the lignin biosynthetic pathway during secondary cell wall formation in *Arabidopsis*. *Plant Cell* 21, 248–266. doi: 10.1105/tpc.108.063321

Zhu, Y., Song, D., Sun, J., Wang, X., and Li, L. (2013). *PtrHB7*, a class III HD-Zip gene, plays a critical role in regulation of vascular cambium differentiation in *Populus*. *Mol. Plant* 6, 1331–1343. doi: 10.1093/mp/sss164

Conflict of Interest: The authors declare that the research was conducted in the absence of any commercial or financial relationships that could be construed as a potential conflict of interest.

Publisher's Note: All claims expressed in this article are solely those of the authors and do not necessarily represent those of their affiliated organizations, or those of the publisher, the editors and the reviewers. Any product that may be evaluated in this article, or claim that may be made by its manufacturer, is not guaranteed or endorsed by the publisher.

frontiers in Plant Science

ORIGINAL RESEARCH
published: 14 January 2022
doi: 10.3389/fpls.2021.715809

A High-Throughput Screening System for *Populus* Wood-Associated Transcription Factors and Its Application to Lignin Regulation

Yamei Zhuang[1,2], Sihui Chen[2], Wenjun Lian[1], Li Xu[1], Dian Wang[2,3], Congpeng Wang[1,2], Jie Meng[1,2], Xianfeng Tang[2], Hua Xu[2], Shumin Wang[2], Lin Du[2], Yang Zhang[2], Gongke Zhou[1,2,4] and Guohua Chai[1,2,4]**

[1] College of Resources and Environment, Qingdao Agricultural University, Qingdao, China, [2] Qingdao Institute of BioEnergy and Bioprocess Technology, Chinese Academy of Sciences, Qingdao, China, [3] College of Agronomy, Qingdao Agricultural University, Qingdao, China, [4] Academy of Dongying Efficient Agricultural Technology and Industry on Saline and Alkaline Land in Collaboration With Qingdao Agricultural University, Dongying, China

OPEN ACCESS

Edited by:
Hong Luo,
Clemson University, United States

Reviewed by:
Concepcion Avila,
University of Malaga, Spain
Qingzhang Du,
Beijing Forestry University, China

***Correspondence:**
Gongke Zhou
zhougk@qau.edu.cn
Guohua Chai
chaigh@qau.edu.cn

Specialty section:
This article was submitted to Plant Biotechnology, a section of the journal Frontiers in Plant Science

Received: *27 May 2021*
Accepted: *09 December 2021*
Published: *14 January 2022*

Citation:
Zhuang Y, Chen S, Lian W, Xu L, Wang D, Wang C, Meng J, Tang X, Xu H, Wang S, Du L, Zhang Y, Zhou G and Chai G (2022) A High-Throughput Screening System for Populus Wood-Associated Transcription Factors and Its Application to Lignin Regulation. Front. Plant Sci. 12:715809. doi: 10.3389/fpls.2021.715809

Wood formation of trees is a complex and costly developmental process, whose regulatory network is involved in the protein-protein and protein-DNA interactions. To detect such interactions in wood development, we developed a high-throughput screening system with 517 Gal4-AD-wood-associated transcription factors (TFs) library from *Populus alba* × *P. glandulosa* cv "84K." This system can be used for screening the upstream regulators and interacting proteins of targets by mating-based yeast-one hybrid (Y1H) and yeast-two-hybrid (Y2H) method, respectively. Multiple regulatory modules of lignin biosynthesis were identified based on this *Populus* system. Five TFs interacted with the 500-bp promoter fragment of *PHENYLALANINE AMMONIA-LYASE 2* (*PAL2*), the first rate-limiting enzyme gene in the lignin biosynthesis pathway, and 10 TFs interacted with *Pa*MYB4/LTF1, a key regulator of lignin biosynthesis. Some of these interactions were further validated by EMSA and BiFC assays. The TF-*PaPAL2* promoter interaction and TF-*Pa*MYB4 interaction revealed a complex mechanism governing the regulation of lignin synthesis in wood cells. Our high-throughput Y1H/Y2H screening system may be an efficient tool for studying regulatory network of wood formation in tree species.

Keywords: wood, transcription factors, Y1H, Y2H, lignin, *Populus*

INTRODUCTION

The woody secondary cell walls of plants are the largest repository of renewable carbon biopolymers on the planet. They are widely used for timber, paper and pulp, and have potential as a source of bioenergy (Du and Groover, 2010). In tree species, wood (secondary xylem) is a complex biomass material constituted mainly of cellulose, hemicelluloses and lignin. Long cellulose microfibrils impart tensile strength, shorter hemicelluloses establish carbohydrate cross-linking, and lignin as a phenolic polymer fills in and cross-links the carbohydrate matrix (Albersheim et al., 2011).

Understanding the molecular regulation of wood formation is required for the improvement of biomass and wood characteristics.

Wood formation is finely controlled by a hierarchical transcription factor network (HTFN), which is relatively conserved between Arabidopsis and trees (Wang and Dixon, 2012; Lin et al., 2013; Nakano et al., 2015; Chen et al., 2019). Functional characterization of a serial of Arabidopsis mutants shows a three-layered regulatory network for secondary cell wall formation (Zhong et al., 2010; Wang and Dixon, 2012; Nakano et al., 2015). In Arabidopsis stems, SND1 is the highest level regulator of HTFN, and it directly activates the second-layered master switches MYB46 and its paralog MYB83, inducing the expression of multiple cell wall biosynthetic genes. A wood-associated HTFN involving TF-DNA and TF-TF regulations has been recently constructed using quantitative transcriptomics, yeast one/two hybrid (Y1H/Y2H) and chromatin binding assays (Chen et al., 2019). Similar to Arabidopsis SND1-mediated HTFN, in *Populus* stems *Ptr*SND1-B1 induces *Ptr*MYB21, a homolog of Arabidopsis MYB46/83, to regulate the expression of a number of genes associated with cell wall component and wood biosynthesis. However, *Populus* undergoes multiple gene duplication events during evolutionary process, resulting in the ratio of 1.4∼1.6 *Populus* homologs to each Arabidopsis gene (Tuskan et al., 2006). Duplicated genes may have divergent fates such as subfunctionalization, neofunctionalization, or non-functionalization, causing more complex regulation of wood formation in *Populus* compared with Arabidopsis. For instance, the TF protein-complex regulators (dimers and trimers) are shown to cooperatively or combinatorially mediate the biosynthesis of specific types of lignin in *Populus* stems (Chen et al., 2019).

Lignin is the generic term for a large group of aromatic polymers, and is one of the most important limiting factors in the conversion of plant biomass to pulp or biofuels (Vanholme et al., 2010; Liu et al., 2014; Zhao, 2016). These lignin polymers are resulted from the oxidative combinatorial coupling of 4-hydroxyphenylpropanoids. In plants, the main biosynthetic route of lignin is generally conserved and involved in a battery of enzymes (Vanholme et al., 2010). PHENYLALANINE AMMONIA-LYASE (PAL) is the first rate-limiting enzyme in the lignin biosynthesis pathway, and catalyzes the deamination of L-phenylalanine to cinnamic acid (Bate et al., 1994). Five *Populus* PAL isoforms (*Ptr*PAL1 to *Ptr*PAL5) exhibit essentially identical catalytic activities in secondary differentiating xylem (SDX) based on the Michaelis-Menten kinetic parameters, indicating functional redundancy in the synthesis of monolignol (Wang et al., 2014). 4-COUMARATE:CoA LIGASE (4CL) is the last enzyme in the phenylpropionic acid pathway, activating the hydroxycinnamic acids to their corresponding esters with coenzyme A, a rate-limiting enzyme connecting the phenylpropionic acid pathway and the lignin biosynthesis pathway (Lu et al., 2004). In *Populus*, there are two 4CL isoforms (*Ptr*4CL3 and *Ptr*4CL5) with distinct reaction kinetic parameters (Chen et al., 2013). *Ptr*4CL3 has the highest conversion rate for 4-coumaric acid, while *Ptr*4CL5 most effectively metabolizes caffeic acid (Wang et al., 2014). Transcriptional regulation of *PtrPAL2* and *Ptr4CL3* expression were experimentally proved during lignin biosynthesis (Chen et al., 2019; Gui et al., 2019). In the *Populus* SDX protoplasts, the expression of *PtrPAL2* is directly activated by *Ptr*MYB21 in *Ptr*SND1-B1-mediated network (Chen et al., 2019). LTF1/*Pd*MYB4 was identified as an upstream regulator of *Pd4CL3* by screening a *Populus* developing xylem library using Y1H (Gui et al., 2019). In response to environmental stimuli, phosphorylation of LTF1 by MPK3/6 functions as a sensory switch regulating lignin biosynthesis. Currently, it remains unclear how *Ptr*PAL2 and LTF1/*Pd*MYB4, two lignin-associated proteins, are precisely regulated in woody cells.

To understand the regulatory mechanism of wood formation at the transcriptional level, we here generated a wood-associated Gal4-AD–TF library that contains 517 TFs from poplar, a fast-growing tree species. High-throughput Y1H and Y2H screens were applied to verify the efficiency of this library using two lignin-associated genes (*PaPAL2* and *LTF1/PaMYB4*) as the baits. The interactions between 5 TFs and the promoter fragment of *PaPAL2* and between 10 TFs and LTF1/*Pa*MYB4 offer a clue as to how lignin biosynthesis is precisely controlled. Our high-throughput Y1H/Y2H screening system is a powerful tool to help dissect transcriptional regulatory networks of wood formation in trees.

MATERIALS AND METHODS

Construction of the Wood-Associated AD–TF Library

To generate the Gal4–AD-fused constructs, the coding regions of 517 TFs were amplified by PCR from the first-strand cDNA, that was prepared with the whole stem of 1.5-m-high *Populus alba* × *P. glandulosa* cv "84K" following the method described previously (Chai et al., 2014). After confirmation by sequencing, the PCR products were cloned into pGADT7 through the *Eco*RI site. The resulting constructs were transformed into the yeast strain Y187 using the PEG/LiAc method. The yeast cells containing the transformant was mixed with 30% sterilized glycerol in 2-ml 96-well plates and stored at −80°C for use.

Mating-Based Yeast-One Hybrid and Yeast-Two-Hybrid Screening

The 500-bp promoter fragment of *PaPAL2* was amplified from genomic DNA of "84K" and the coding region of *LTF1/PaMYB4* was amplified from the xylem cDNA using gene-specific primers (**Supplementary Table 1**). Following the methods described by Ou et al. (2011), this *PaPAL2* promoter fragment was inserted into the vector pHIS2.1 for mating-based Y1H screening, and the *LTF1* coding region was inserted into pGBKT7 for mating-based Y2H screening. Yeast strain AH109 carrying the two baits was grown in selective medium and the Gal4–AD–TF strains were grown on SD-Leu medium in 96-well plates overnight. 30 μL/well of donor and host strains were transferred to a new 96-well plate with 100 μL YPAD medium in each well. Mating was conducted for 20–24 h by shaking at 30°C and

200 rpm. After 10-fold dilution with water, the mating products (5 μL well^{-1}) were plated to different selective plates and incubated for 3 days at 30°C.

Yeast-One Hybrid Assay

The coding regions of *PaMYB21*, *PaMYBH*, *PaWRKY20* and *PaDF1*, four regulatory candidates of *PaPAL2* identified by mating-based Y1H, were amplified from the xylem cDNA of "84K" (primers in **Supplementary Table 1**) and cloned into the pGADT7 vector. Each of these pGADT7-TFs (pGADT7 as control) and pHIS-*proPaPAL2* were co-transformed into yeast stain Y187. The transformed cells were observed on the SD/-Leu-His plates and triple dropout plates (SD/-Trp-His-Leu) supplemented with 10 mM 3-amino-1,2,4-triazole (3-AT) for 3 days at 28°C, following the Y1H procedure described previously (Wang et al., 2020).

EMSA

EMSA was performed following the method described previously (Chai et al., 2014). The coding regions of *PaMYBH*, *PaWRKY20,* and *PaDF1* were fused in frame with MBP in pMAL-p4X and expressed in *Escherichia coli*. Recombinant protein was purified using amylose resin (New England Biolabs). The *PaPAL2* promoter fragments covering the corresponding binding sites of *PaMYBH*, *PaWRKY20,* and *PaDF1* were labeled with biotin at the 5' end and used as the probes (**Supplementary Figure 1**, BGI). The same unlabeled oligos were annealed for competition. Binding reactions were performed with a LightShift® Chemiluminescent EMSA Kit (Thermo Fisher Scientific) according to the manufacturer's instructions. The *Pa* MYBH-, *Pa*WRKY20- or *Pa*DF1-bound DNA fragments were separated from the unbound fragments by polyacrylamide gel electrophoresis. The DNA on a nitrocellulose membrane was detected by chemiluminescence. Three independent experiments were performed for each probe.

Yeast-Two-Hybrid Assay

The coding regions of *PaMYB21*, *PaGRAS2*, *PaWRKY20*, *PaANAC83,* and *PaDF1* identified by mating Y2H were amplified from the xylem cDNA of "84K" and cloned into the pGBKT7 vector (BD). Primers were shown in **Supplementary Table 1**. The pGADT7-LTF1/*Pa*MYB4 and pGBKT7-TF were co-transformed into yeast strain AH109. The transformed cells were cultured on SD/-Leu/-Trp plates for 2 days, and then dropped on the SD/-Leu/-Trp/-Ade/-His medium with or without 5 mM 3-AT for 3 days at 30°C following the Y2H procedure described previously (Tang et al., 2020). The empty vector pGADT7 was used as blank control.

BiFC

Bimolecular fluorescence complementation (BiFC) assays were conducted according to the method described previously (Tang et al., 2020). The coding region of *LTF1/PaMYB4* was cloned into the pSAT1-nVenus (pE3228) vector, and that of *PaMYB21*, *PaWRKY20* or *PaANAC83* was cloned into pSAT1-cCFP (pE3242) (Walter et al., 2004). Arabidopsis leaf protoplasts were isolated and transfected following the method established by Sheen (2001). Confocal microscopy was performed with an Olympus FluoView FV1000 confocal microscope using an excitation wavelength of 488 nm and detection at 499–535 nm. The experiments were repeated three times.

RESULTS

Construction of a Wood-Associated Transcription Factor Library

To obtain wood-associated transcription factors (WTFs), we extracted 4287 *Populus* TFs covering 58 gene families from both PlantTFDB[1] and Phytozome 12[2] (**Figure 1**). A total of 517 genes in 49 families were defined as WTFs based on the stringent filtering criteria as follows: genes show high (> 100) expression levels in xylem in Phytozome 12 and specific expression in wood tissues identified by the online software BAR[3]. Full-length ORFs of the 517 genes were amplified from the first-strand cDNA in the whole stems of *Populus alba* × *P. glandulosa* cv "84K." After validation by sequencing, All ORFs were independently inserted into the pGADT7 vector through the EcoRI site at multiple clone sites (MCS) and then transformed into the yeast strain Y187.

Identification of Transcription Factor That Binds to the *PaPAL2* Promoter

PaPAL2, the ortholog of Arabidopsis *PAL1* in *Populus*, is a rate-limiting enzyme that controls the deamination of phenylpropanoid to cinnamic acid during monolignol biosynthesis in woody cells (Wang et al., 2014). Further, *PaPAL2* is a direct target of *Pa*MYB21 that is the second-layered master regulator of wood formation (Chen et al., 2019). Thus, *PaPAL2* was selected to test the efficiency of this yeast library and to clarify the lignin biosynthesis pathway. Following the method described previously (Ou et al., 2011), we screened this library by mating the bait, a 500 bp promoter fragment upstream of ATG of *PaPAL2*, in Y1H assays. Yeast cells co-transformed with pHIS-*proPaPAL2* and each of five pGADT7-TFs that were identified were able to grow normally on medium SD-Trp-Leu-His with 10 mM 3-AT (**Figures 2A,B**). These five WTFs belong to the MYB (*Pa*MYB21), HD-ZIP (*Pa*HB5), MYB-related (*Pa*MYBH), Trihelix (*Pa*DF1), and WRKY (*Pa*WRKY20) family (**Table 1**). We further examined the cell-type expression patterns of *PaPAL2* and its five regulatory candidates in stems, based on high-spatial-resolution transcriptome data that were sampled across secondary stem tissues in *Populus* (Sundell et al., 2017). As revealed in **Supplementary Figure 2A**, *PaPAL2*, *PaMYB21*, *PaMYBH*, *PaHB5*, *PaDF1,* or *PaWRKY20* were expressed in wood-forming cells, including the cambial zone and secondary phloem/xylem cells.

*Pa*MYB21, *Pa*DF1, *Pa*MYBH, and *Pa*WRKY20, like *PaPAL2*, exhibited high expression in lignified xylem, and they were

[1]http://planttfdb.gao-lab.org/

[2]https://phytozome.jgi.doe.gov/pz/portal.html

[3]http://bar.utoronto.ca/efppop/cgi-bin/efpWeb.cgi

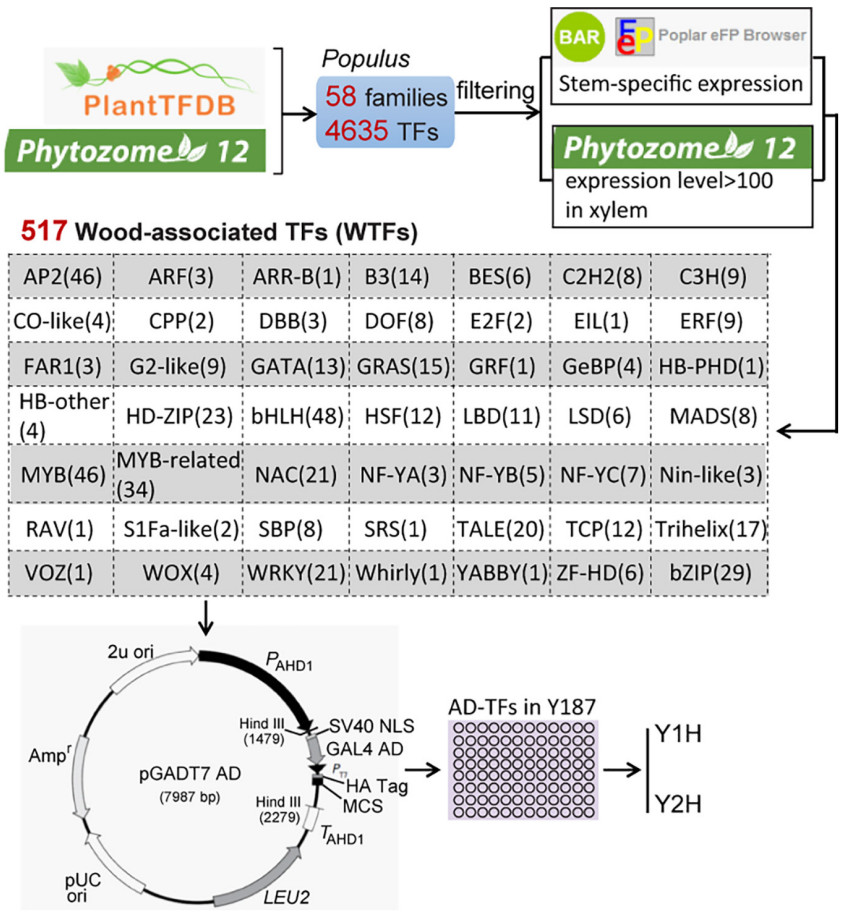

FIGURE 1 | The scheme of the construction of a wood-associated transcription factors (TFs) library. A total of 517 Wood-associated TFs (WTFs) were identified from 4287 *Populus* TFs of 58 gene families in two database (PlantTDB and Phytozome 12) using the stringent filtering criteria. All pGADT7-TFs were independently transformed into the yeast strain Y187 for throughout mating-based Y1H or Y2H screening.

selected for validation by Y1H method. Yeast cells co-transformed with pHIS-*proPaPAL2* and pGADT7-TF grew normally on the SD-Trp-Leu-His medium supplemented with 10 mM 3-AT (**Figure 2C**), indicating the binding of *Pa*MYB21, *Pa*DF1, *Pa*MYBH or *Pa*WRKY20 to the *PaPAL2* promoter in yeast. Analysis of the 500-bp *PaPAL2* promoter fragment showed the DNA-binding motifs of *Pa*DF1 (GT, Kaplan-Levy et al., 2012), *Pa*MYBH (MRE, Du et al., 2013) and *Pa*WRKY20 (W-box, Ulker and Somssich, 2004; **Supplementary Figure 2**). Not surprisingly, EMSA results revealed that *Pa*DF1, *Pa*MYBH, and *Pa*WRKY20 proteins were able to bind to these cis-elements of the *PaPAL2* promoter specifically *in vitro* (**Figures 2D–F**).

Identification of Transcription Factor That Interacts With *Pa*MYB4/LTF1

LTF1/*Pa*MYB4 is a key negative regulator of lignin biosynthesis in wood formation (Gui et al., 2019; Holwerda et al., 2019). To elucidate the regulatory mechanism of lignin biosynthesis, we screened the LTF1/*Pa*MYB4-interacting proteins in our TF library by mating the bait LTF1/*Pa*MYB4. Ten TF clones were obtained (**Figures 3A,B**). Three of them were in the Trihelix family, three were in the GRAS family, and one in the MYB, NAC, WRKY, or SBP family (**Table 2**). Interestingly, these TFs included *Pa*MYB21, *Pa*DF1, and *Pa*WRKY20, that were shown to directly regulate *PaPAL2* expression (**Figure 2**). Analysis of high-spatial-resolution wood transcriptome profiles revealed the high expression of LTF1/*Pa*MYB4 and its 10 interacting proteins in wood-forming tissues such as secondary phloem and lignified xylem (**Supplementary Figure 1B**).

Five TFs (*Pa*MYB21, *Pa*DF1, *Pa*GRAS2, *Pa*WRKY20, and *Pa*ANAC83) were selected to verify their interactions with *Pa*MYB4 using Y2H (**Figure 3C**). Yeast cells transformed with TF-BD and *Pa*MYB4-AD exhibited blue on SD/-Leu-Trp-His-Ade plate, confirming the interaction between the five TFs and LTF1/*Pa*MYB4. Of the five interacting TFs, only *Pa*MYB21 protein had self-activation in yeast, that can be effectively inhibited by addition of 5 mM 3-AT. BiFC assays were conducted in Arabidopsis leaf protoplasts to verify the *in vivo* interaction between *Pa*MYB4/TFL1 and *Pa*MYB21, *Pa*DF1, or *Pa*WRKY20 (**Figure 4**). Co-expression of *Pa*MYB4/LTF1 fused to the amino-terminal half of YFP (YFP^{NE}) and *Pa*MYB21, *Pa*DF1,

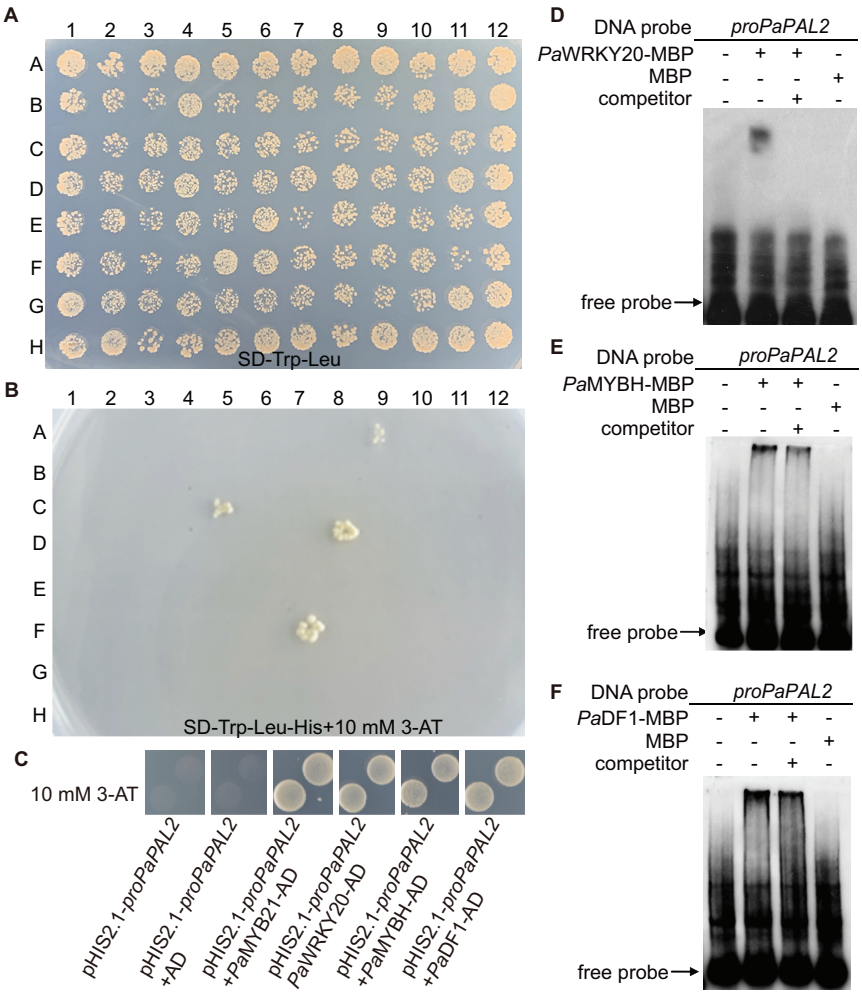

FIGURE 2 | Identification of TFs that bind to the *PaPAL2* promoter. **(A,B)** Y1H screening of the TFs library using 500-bp *PaPAL2* promoter fragment as a bait. Yeast growth on the non-selective medium SD-Trp-Leu showed the mating efficiency. The candidate TFs can be detected on medium with 10 mM 3-AT. **(C)** Y1H assays verifying that *Pa*MYB21, *Pa*WRKY20, *Pa*MYBH, or *Pa*DF1 was able to bind to the *PaPAL2* promoter fragment. Plasmids transformed into Y187 were screened on the SD/-Trp-Leu-His medium with 10 mM 3-AT. **(D–F)** EMSA results showing the specific bindings of *Pa*WRKY20, *Pa*MYBH, or *Pa*DF1 protein to the *PaPAL2* promoter *in vitro*. For competition assays, unlabeled probes (competitor) in 20-fold (+) molar excess relative to the labeled probe was include in the reaction.

or *Pa*WRKY20 fused to the carboxy-terminal half (YFP^{CE}) of yellow florescent protein led to visible fluorescence in the nucleus of co-transformed protoplasts. However, no YFP fluorescence was detected when *Pa*MYB4-YFP^{NE} was co-expressed with the carboxy-terminal half of YFP (cYFP) or *Pa*MYB21-, *Pa*DF1- or *Pa*WRKY20-YFP^{CE} was co-expressed with the amino-terminal half of YFP (nYFP).

DISCUSSION

Recent studies in the stem of *Populus* show that wood formation involves regulatory homeostasis determined by combinations of TF-DNA and TF-protein regulations (Petzold et al., 2017; Chen et al., 2019). Using Y1H and Y2H assays, 40 protein-DNA interactions involving 20 different TFs and 165 protein-protein interactions involving 162 different proteins are shown to be relevant to wood formation (Petzold et al., 2017). These interactions are incorporated into a network that includes 14 connected subnetworks, with the largest having 132 members. Integration of quantitative transcriptomics and chromatin binding data constructs a TRN, in which *Ptr*SND1-B1 directs

TABLE 1 | Transcription factors that bind to the *PaPAL2* promoter identified in the *Populus* wood-associated library using Y1H.

No.	Loci	Name	Arabidopsis homolog	Gene family
1	Potri.009G053900.1	*Pa*MYB21	MYB83	MYB family
2	Potri.002G068600.1	*Pa*DF1	DF1	Trihelix family
3	Potri.005G071900.1	*Pa*HB5	HB5	HD-ZIP family
4	Potri.001G189800.1	*Pa*MYBH	MYBH	MYB-related family
5	Potri.001G361600.1	*Pa*WRKY20	WRKY20	WRKY family

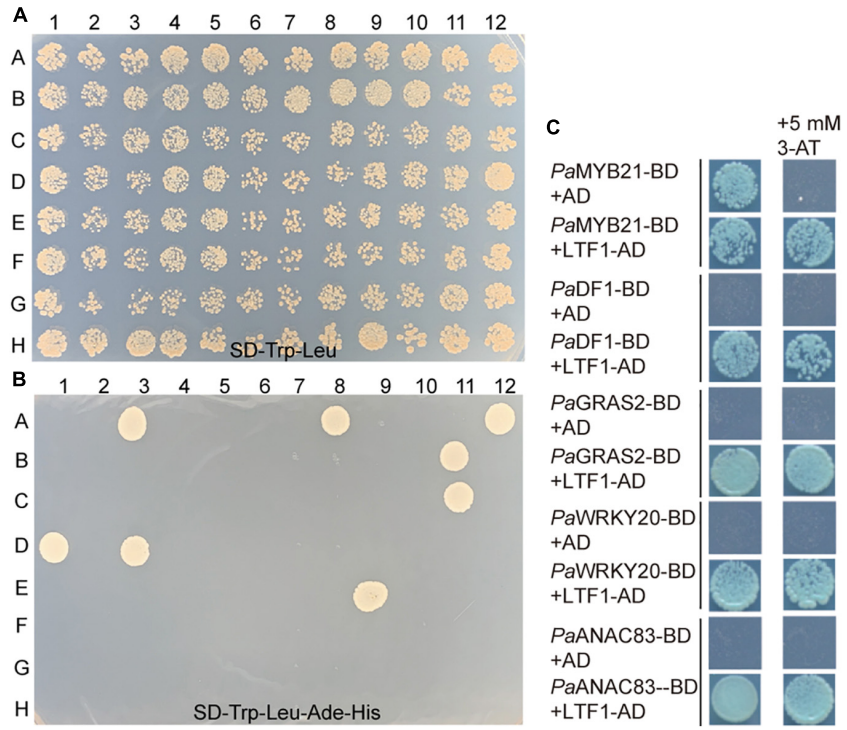

FIGURE 3 | Identification of TFs that interact with *Pa*MYB4/LTF1. **(A,B)** Y2H screening of this TFs library by mating the bait *Pa*MYB4/LTF1. Strong interaction can be detected on the stringent medium SD-Leu-Trp-His-Ade. **(C)** Y2H assays in yeast confirming the interaction between *Pa*MYB4/LTF1 and *Pa*MYB21, *Pa*DF1, *Pa*GRAS2, *Pa*WRKY20, or *Pa*ANAC83 *in vivo*. Plasmids transformed into AH109 were screened on the SD/-Trp-Leu-His-Ade medium with or without 5 mM 3-AT.

57 TF-DNA interactions through 17 TFs transregulating 27 cell wall genes (Chen et al., 2019). Of the multiple methods for determining TF-DNA and TF-protein interactions, Y1H and Y2H screenings are the most widely used in trees. However, a major limitation for the two methods is low expression levels of TFs in wood-forming tissues. To overcome this disadvantage, we set up a high throughout mating-based screening system that includes a Gal4-AD-TF library of 517 wood-associated TFs (WTFs). The 517 WTFs were filtered by the stringent criteria and accounted for 11% of all *Populus* TFs (4287). By mating yeast strains (bait) with a series of strains (prey) expressing WTF-AD protein, we were able to identify protein-DNA or protein-protein interactions and identify connected networks during wood formation. Importantly, our system is still effective for Y1H screening using a single fragment of up to 500 bp as a bait, which has an advantage of minimizing the effort to find out the exact cis-element and increasing the screening specificity. Thus, our library is a resource for Y1H and Y2H assay and functional analyses of genes associated with poplar wood formation.

TABLE 2 | Transcription factors that interact with *Pa*MYB4/LTF1 identified in the *Populus* wood-associated library using Y2H.

No.	Loci	Name	Arabidopsis homolog	Family
1	Potri.009G053900.1	*Pa*MYB21	MYB83	MYB family
2	Potri.002G068600.1	*Pa*DF1	DF1	Trihelix family
3	Potri.001G113600.1	Potri.001G113600	AT3G58630	Trihelix family
4	Potri.003G195300.1	Potri.003G195300	AT3G54390	Trihelix family
5	Potri.007G132000.1	*Pa*SHR	SHR	GRAS family
6	Potri.009G033300.1	*Pa*GRAS2	GRAS2	GRAS family
7	Potri.005G123800.1	Potri.005G123800	AT5G66770	GRAS family
8	Potri.001G361600.1	*Pa*WRKY20	WRKY20	WRKY family
9	Potri.001G061200.1	*Pa*ANAC83	ANAC083	NAC family
10	Potri.002G002400.1	Potri.002G002400	AT1G76580	SBP family

Lignin biosynthesis starts with the deamination of phenylalanine, followed by a series of hydroxylation, methylation and reduction resulting in the production of p-hydroxyphenyl (H), guaiacyl (G), and syringyl (S), three basic units of the lignin complex in trees (Zhao, 2016). In the *Populus* lignin biosynthesis pathway, *Ptr*MYB90, *Ptr*MYB161, *Ptr*NAC123, or *Ptr*WBLH1 targets G-specific *CCoAOMT* gene family members, and *Ptr*MYB90, *Ptr*MYB161, or *Ptr*WBLH1 targets *CAld5H* that is needed for the biosynthesis of the S subunits (Chen et al., 2019). In this study, we focus on *Pa*PAL2 that is rate-limiting enzyme in the lignin synthesis pathway, and LTF1/*Pa*MYB4 that targets *Pa*4CL3, a key enzyme of general phenylpropanoid metabolism that provides the precursors for both lignin biosynthesis (Lu et al., 2004; Chen et al., 2013, 2019; Wang et al., 2014; Gui et al., 2019).

With the help of a high-throughput Y1H/Y2H screening system, we identified five TFs that bound to the *PaPAL2* promoter fragment and 10 TFs interacting with *Pa*MYB4 in *Populus*,

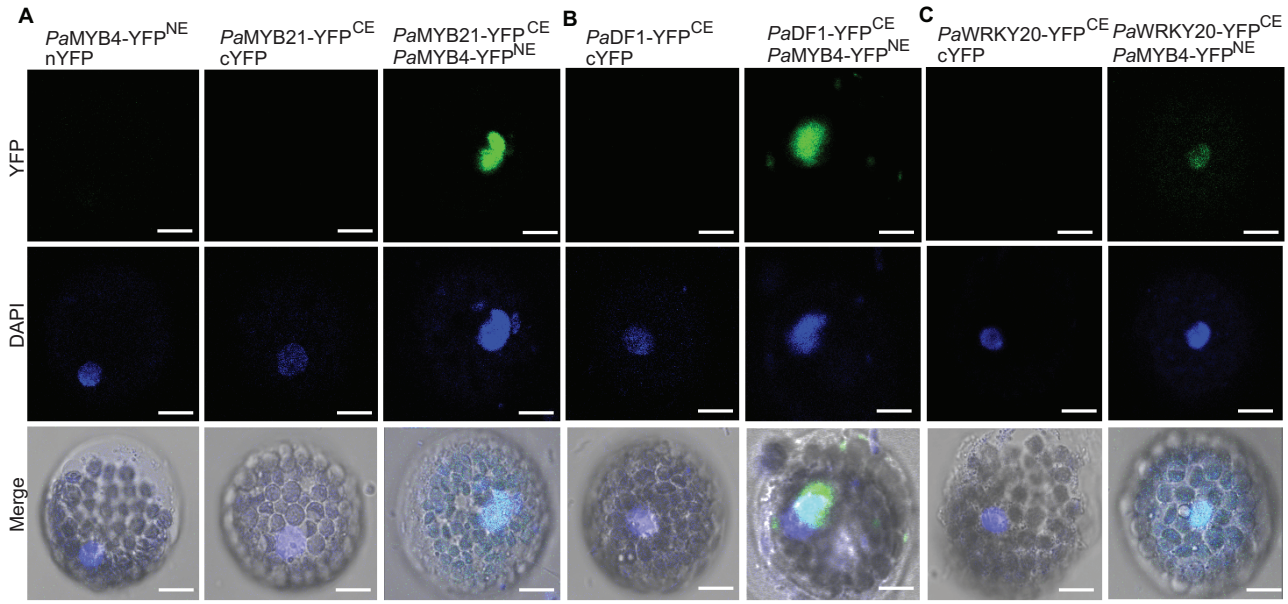

FIGURE 4 | BiFC validation of the *in vivo* interaction between *Pa*MYB21, *Pa*DF1, or *Pa*WRKY20 and *Pa*MYB4/LTF1. **(A–C)** *Pa* MYB21-, *Pa* DF1-, or *Pa*WRKY20-YFP^{CE} and *Pa*MYB4-YFP^{NE} interact to form a functional YFP in the nucleus of *Arabidopsis* leaf protoplasts. The DNA fluorochrome 4′, 6-diamidino-2-phenylindole (DAPI) was used to stain the cell nucleus (blue). Bar = 10 μm.

indicating a high efficiency of our library. Selected interactions were further verified by EMSA and BiFC independently. Of these TFs, *Pa*MYB21, *Pa*WRKY20, *Pa*DF1 were found to interact with the *PaPAL2* promoter or *Pa*MYB4 protein. Consistently, they exhibited overlapping expression with *PaPAL2* or *PaMYB4* in wood-forming tissues predicted by high-spatial-resolution wood transcriptome data (Sundell et al., 2017). Of these interactors, *Ptr*MYB21 is proven to directly activate *PtrPAL2* expression, promoting lignin biosynthesis during wood formation (Chen et al., 2019). Other TFs are not functionally characterized in trees, but the homologs of *Pa*DF1 and *Pa*WRKY20 in Arabidopsis were identified as the components of the gene regulatory network for secondary cell wall synthesis in stems (Taylor-Teeples et al., 2015). These preliminary results revealed a coordinated role of the TF-*proPaPAL2* and TF-*Pa*MYB4 interactions in lignin biosynthesis in *Populus* stems. The TF-DNA interactions for *Populus PAL4*, a paralog of *PaPAL2*, were also identified in xylem cells by Y1H assays (Petzold et al., 2017). Six TFs, including *Ptr*MYB2 that is a homolog of *Ptr*MYB21, are shown to bind to the *PtrPAL4* promoter. This suggests different TF-DNA interactions between homologs in woody cells. Our powerful system will facilitate to generate comprehensive interaction networks of TFs to understand the regulatory mechanism of wood formation in tree species.

DATA AVAILABILITY STATEMENT

The original contributions presented in the study are included in the article/**Supplementary Material**, further inquiries can be directed to the corresponding author/s.

AUTHOR CONTRIBUTIONS

GC designed the experiments, performed data processing, and drafted the manuscript. YZhu, SC, WL, LX, DW, CW, JM, XT, HX, SW, LD, and YZha prepared the materials and performed the experiments. GZ conceived the study and revised the manuscript. All authors read and approved the final version of the manuscript.

FUNDING

Financial support for this work was obtained from the National Key Scientific Research Project of China (2021YFD2200205), the National Natural Science Foundation of China (31670606, 31972955, 31770315, 32101549, and 31972860), the Taishan Scholar Program of Shandong (to GC), and the "First Class Grassland Science Discipline" Program of Shandong Province.

ACKNOWLEDGMENTS

We would like to thank Dr. Guoqing Dong (Wuhan Polytechnic University) for critical suggestions of this manuscript.

SUPPLEMENTARY MATERIAL

The Supplementary Material for this article can be found online at: https://www.frontiersin.org/articles/10.3389/fpls.2021.715809/full#supplementary-material

REFERENCES

Albersheim, P., Darvill, A., Roberts, K., Sederoff, R., and Staehelin, A. (2011). "Cell walls and plant anatomy," in *Plant Cell Walls: From Chemistry to Biology*, eds P. Albersheim, A. Darvill, K. Roberts, R. Sederoff, and A. Staehelin (New York: Garland Science), 1–42.

Bate, N. J., Orr, J., Ni, W., Meromi, A., Nadler-Hassar, T., Doerner, P. W., et al. (1994). Quantitative relationship between phenylalanine ammonia-lyase levels and phenylpropanoid accumulation in transgenic tobacco identifies a rate-determining step in natural product synthesis. *Proc. Natl. Acad. Sci. U. S. A.* 91, 7608–7612. doi: 10.1073/pnas.91.16.7608

Chai, G., Qi, G., Cao, Y., Wang, Z., Yu, L., Tang, X., et al. (2014). Poplar PdC3H17 and PdC3H18 are direct targets of PdMYB3 and PdMYB21, and positively regulate secondary wall formation in *Arabidopsis* and poplar. *New Phytol.* 203, 520–534. doi: 10.1111/nph.12825

Chen, H., Song, J., Williams, C. M., Shuford, C. M., Liu, J., Wang, J. P., et al. (2013). Monolignol pathway 4-coumaric acid:coenzyme A ligases in *Populus trichocarpa*: novel specificity, metabolic regulation, and simulation of coenzyme A ligation fluxes. *Plant Physiol.* 161, 1501–1516. doi: 10.1104/pp.112.210971

Chen, H., Wang, J. P., Liu, H., Li, H., Lin, Y. J., Shi, R., et al. (2019). Hierarchical transcription factor and chromatin binding network for wood formation in black cottonwood (*Populus trichocarpa*). *Plant Cell* 31, 602–626. doi: 10.1105/tpc.18.00620

Du, H., Wang, Y. B., Xie, Y., Liang, Z., Jiang, S. J., Zhang, S. S., et al. (2013). Genome-wide identification and evolutionary and expression analyses of MYB-related genes in land plants. *DNA Res.* 20, 437–448. doi: 10.1093/dnares/dst021

Du, J., and Groover, A. (2010). Transcriptional regulation of secondary growth and wood formation. *J. Integr. Plant Biol.* 52, 17–27. doi: 10.1111/j.1744-7909.2010.00901.x

Gui, J., Luo, L., Zhong, Y., Sun, J., Umezawa, T., and Li, L. (2019). Phosphorylation of LTF1, an MYB transcription factor in *Populus*, acts as a sensory switch regulating lignin biosynthesis in wood cells. *Mol. Plant* 12, 1325–1337. doi: 10.1016/j.molp.2019.05.008

Holwerda, E. K., Worthen, R. S., Kothari, N., Lasky, R. C., Davison, B. H., Fu, C., et al. (2019). Multiple levers for overcoming the recalcitrance of lignocellulosic biomass. *Biotechnol. Biofuels* 17:15. doi: 10.1186/s13068-019-1353-7

Kaplan-Levy, R. N., Brewer, P. B., Quon, T., and Smyth, D. R. (2012). The trihelix family of transcription factors-light, stress and development. *Trends Plant Sci.* 17, 163–171. doi: 10.1016/j.tplants.2011.12.002

Lin, Y. C., Li, W., Sun, Y. H., Kumari, S., Wei, H., Li, Q., et al. (2013). SND1 transcription factor-directed quantitative functional hierarchical genetic regulatory network in wood formation in *Populus trichocarpa*. *Plant Cell* 25, 4324–4341. doi: 10.1105/tpc.113.117697

Liu, C., Cai, Y., Zhang, X., Gou, M., and Yang, H. (2014). Tailoring lignin biosynthesis for efficient and sustainable biofuel production. *Plant Biotechnol. J.* 12, 1154–1162. doi: 10.1111/pbi.12250

Lu, H., Zhao, Y. L., and Jiang, X. N. (2004). Stable and specific expression of 4-coumarate: coenzyme A ligase gene (*4CL1*) driven by the xylem-specific *Pto4CL1* promoter in the transgenic tobacco. *Biotechnol. Lett.* 26, 1147–1152. doi: 10.1023/B:BILE.0000035487.91628.9e

Nakano, Y., Yamaguchi, M., Endo, H., Rejab, N. A., and Ohtani, M. (2015). NAC-MYB-based transcriptional regulation of secondary cell wall biosynthesis in land plants. *Front. Plant Sci.* 6:288. doi: 10.3389/fpls.2015.00288

Ou, B., Yin, K., Liu, S., Yang, Y., Gu, T., Hui, J. M. W., et al. (2011). A high-throughput screening system for Arabidopsis transcription factors and its application to Med25-dependent transcriptional regulation. *Mol. Plant* 4, 546–555. doi: 10.1093/mp/ssr002

Petzold, E., Rigoulot, S. B., Zhao, C., Chanda, B., Sheng, X., Zhao, M., et al. (2017). Identification of new protein-protein and protein-DNA interactions linked with wood formation in *Populus trichocarpa*. *Tree Physiol.* 38, 362–377. doi: 10.1093/treephys/tpx121

Sheen, J. (2001). Signal transduction in maize and Arabidopsis mesophyll protoplasts. *Plant Physiol.* 127, 1466–1475.

Sundell, D., Street, N. R., Kumar, M., Mellerowicz, E. J., Kucukoglu, M., Johnsson, C., et al. (2017). AspWood: high-spatial-resolution transcriptome profiles reveal uncharacterized modularity of wood formation in *Populus tremula*. *Plant Cell* 29, 1585–1604. doi: 10.1105/tpc.17.00153

Tang, X., Wang, D., Liu, Y., Lu, M., Zhuang, Y., Xie, Z., et al. (2020). Dual regulation of xylem formation by an auxin-mediated PaC3H17 and PaMYB199 module in *Populus*. *New Phytol.* 225, 1545–1561. doi: 10.1111/nph.16244

Taylor-Teeples, M., Lin, L., de Lucas, M., Turco, G., Toal, T. W., Gaudinier, A., et al. (2015). An Arabidopsis gene regulatory network for secondary cell wall synthesis. *Nature* 517, 571–575. doi: 10.1038/nature14099

Tuskan, G. A., Difazio, S., Jansson, J., Grigoriev, I., Hellsten, U., Putnam, N., et al. (2006). The genome of black cottonwood, Populus trichocarpa. *Science* 313, 1596–1604. doi: 10.1126/science.1128691

Ulker, B., and Somssich, I. (2004). WRKY transcription factors: from DNA binding towards biological function. *Curr. Opin. Plant Biol.* 7, 491–498. doi: 10.1016/j.pbi.2004.07.012

Vanholme, R., Demedts, B., Morreel, K., Palph, J., and Boerjan, W. (2010). Lignin biosynthesis and structure. *Plant Physiol.* 153, 895–905. doi: 10.1104/pp.110.155119

Walter, M., Chaban, C., Schutze, K., Batistic, O., Weckermann, K., Nake, C., et al. (2004). Visualization of protein interactions in living plant cells using bimolecular fluorescence complementation. *Plant J.* 40, 428–438. doi: 10.1111/j.1365-313X.2004.02219.x

Wang, D., Xu, H., Huang, J., Kong, Y., AbuQamar, S., Yu, D., et al. (2020). The Arabidopsis CCCH protein C3H14 contributes to basal defense against *Botrytis cinerea* mainly through the WRKY33-dependent pathway. *Plant Cell Environ.* 43, 1792–1806. doi: 10.1111/pce.13771

Wang, H. Z., and Dixon, R. A. (2012). On-off switches for secondary cell wall biosynthesis. *Mol. Plant* 5, 297–303. doi: 10.1093/mp/ssr098

Wang, J. P., Naik, P. P., Chen, H. C., Shi, R., Lin, C. Y., Liu, J., et al. (2014). Complete proteomic-based enzyme reaction and inhibition kinetics reveal how monolignol biosynthetic enzyme families affect metabolic flux and lignin in *Populus trichocarpa*. *Plant Cell* 26, 894–914. doi: 10.1105/tpc.113.120881

Zhao, Q. (2016). Lignification: flexibility, biosynthesis and regulation. *Trends Plant Sci.* 21, 713–721. doi: 10.1016/j.tplants.2016.04.006

Zhong, R., Lee, C., and Ye, Z. H. (2010). Functional characterization of poplar wood-associated NAC domain transcription factors. *Plant Physiol.* 152, 1044–1055. doi: 10.1104/pp.109.148270

Conflict of Interest: The authors declare that the research was conducted in the absence of any commercial or financial relationships that could be construed as a potential conflict of interest.

Publisher's Note: All claims expressed in this article are solely those of the authors and do not necessarily represent those of their affiliated organizations, or those of the publisher, the editors and the reviewers. Any product that may be evaluated in this article, or claim that may be made by its manufacturer, is not guaranteed or endorsed by the publisher.

frontiers in Plant Science

ORIGINAL RESEARCH
published: 25 January 2022
doi: 10.3389/fpls.2021.679230

Chemical and Structural Responses to Downregulated *p*-Hydroxycinnamoyl-Coenzyme A: Quinate/Shikimate *p*-Hydroxycinnamoyltransferase in Poplar Cell Walls

*Minglei Su[1,2], Yingli Liu[3], Jianxiong Lyu[1], Shutang Zhao[3] and Yurong Wang[1]**

[1] Research Institute of Wood Industry, Chinese Academy of Forestry, Beijing, China, [2] Key Laboratory of National Forestry and Grassland Administration/Beijing for Bamboo and Rattan Science and Technology, International Centre for Bamboo and Rattan, Beijing, China, [3] State Key Laboratory of Tree Genetics and Breeding, Research Institute of Forestry, Chinese Academy of Forestry, Beijing, China

OPEN ACCESS

Edited by:
Taku Demura, Nara Institute of Science and Technology (NAIST), Japan

Reviewed by:
Akiyoshi Kawaoka, Akita Jujo Chemicals Co. Ltd., Japan
Igor Cesarino, University of São Paulo, Brazil

***Correspondence:**
Yurong Wang
yurwang@caf.ac.cn

Specialty section:
This article was submitted to Plant Biotechnology, a section of the journal Frontiers in Plant Science

Received: *11 March 2021*
Accepted: *22 December 2021*
Published: *25 January 2022*

Citation:
Su M, Liu Y, Lyu J, Zhao S and Wang Y (2022) Chemical and Structural Responses to Downregulated p-Hydroxycinnamoyl-Coenzyme A: Quinate/Shikimate p-Hydroxycinnamoyltransferase in Poplar Cell Walls. Front. Plant Sci. 12:679230. doi: 10.3389/fpls.2021.679230

Unraveling the impact of lignin reduction on cell wall construction of poplar stems is important for accurate understanding the regulatory role of biosynthetic genes. However, few cell-level studies have been conducted on the changes in lignin, other important cell wall composition, and the structural properties of transgenic poplar stems at different developmental stages. In this work, the content and microdistributions of cell wall composition as well as the morphological characteristics of cells were studied for *p*-hydroxycinnamoyl-coenzyme A:quinate/shikimate *p*-hydroxycinnamoyltransferase (*HCT*) downregulated transgenic poplar 84K (*Populus alba* × *P. glandulosa cl. '84k'*) at different developmental stages. Results show that the lignin contents of the upper, middle, and basal parts of *HCT* transgenic poplar stems were significantly decreased by 10.84, 7.40, and 7.75%, respectively; and the cellulose contents increased by 8.20, 6.45, and 3.31%, respectively, compared with the control group. The cellulose/lignin ratio of *HCT* transgenic poplars was therefore increased, especially in the upper sections, where it was 23.2% higher. Raman results indicate the appearance of *p*-hydroxyphenyl units (H) and a decrease in the ratio of syringyl/guaiacyl (S/G) lignin monomers in fiber cell walls of *HCT* transgenic poplars. In addition, microstructure observations revealed that the fiber and vessel cells of the *HCT* transgenic poplars exhibited thin cell walls and large lumen diameters. Compared with the control group, the cell wall thickness of fiber and vessel cells decreased by 6.50 and 10.93% on average, respectively. There was a 13.6% decrease in the average ratio of the cell wall thickness to the lumen diameter and an increase in fiber length and width of 5.60 and 6.11%, respectively. In addition, downregulation of *HCT* did not change the orientation of cellulosic microfibrils, but it led to an 11.1% increase of the cellulose crystallinity in cell walls compared to the control poplars. The information obtained herein could lead to a better understanding of the effects of genetic modifications on wood cell walls.

Keywords: poplar, *HCT*, lignin, cell wall components, structural properties

INTRODUCTION

Lignocellulosic material is poised to be the primary source for biorefinery processes, and it can be used to produce liquid biofuels, chemicals, and materials (Vanholme et al., 2013). Wood is the main source of lignocellulosic biomass for the production of liquid biofuels, which consists of carbohydrates (including cellulose and hemicellulose) and lignin. However, the presence of lignin in plant cell walls is one of the most important reasons for biomass recalcitrance and the removal of lignin is costly and environmentally damaging because of the use of chemicals (Hu et al., 1999; Pauly and Keegstra, 2008). A high proportion of syringyl/guaiacyl (S/G) lignin monomers in wood can greatly improve biorefining efficiency (Reddy et al., 2005). Thus, lignin genetic engineering is considered to be a promising route to improve enzymatic digestion and delignification efficiency by reducing the lignin content or changing the lignin monomeric composition (Vanholme et al., 2010, 2012).

The *p*-hydroxycinnamoyl-coenzyme A:quinate/shikimate *p*-hydroxycinnamoyltransferase (*HCT*) is on the upstream and downstream in the phenylpropanoid pathway of *p*-coumarate 3′-hydroxylase (*C3′H*), and co-catalysis with *C3′H* of the conversion process from *p*-coumaroyl coenzyme A to caffeoyl coenzyme A (Hoffmann, 2002; Ralph et al., 2012). Previous studies have found that *HCT* gene silencing resulted in depression of lignin content and changes in lignin monomeric composition in *Arabidopsis* and *Pinus radiata* (Hoffmann et al., 2004; Wagner et al., 2007). It has also been found that downregulation of the *C3′H* and *HCT* in alfalfa had a significant effect on the structure of ball-milled lignin (Pu et al., 2009). Traditional studies of lignin content and monolignol composition have tended to use Klason lignin and nuclear magnetic resonance (NMR) spectroscopy analysis. However, the obtained native lignin samples for structural characterization are usually pretreated by physical and chemical methods, which may alter the natural molecular structure of lignin (Ralph et al., 2012; Peng et al., 2014). Therefore, further *in situ* studies on the lignin monomeric composition and its distribution in transgenic poplars are needed. With the development of Raman technology, the attribution peaks of G, S, and H monomers in Raman spectra are becoming clearer (Saariaho et al., 2003; Jin et al., 2018). This article uses Raman technology to observe the changes in lignin monomers in different regions of *HCT* transgenic poplar cell wall.

The downregulation of lignin biosynthetic genes not only causes changes in cell wall components, but also causes morphological changes in cells, which leads to plant growth phenotypic changes (Jung et al., 2012; Wang et al., 2014; Zhang et al., 2014). For example, when *C3′H* and *HCT* were simultaneously downregulated in alfalfa, the plants could not continue to grow upright beyond a certain height, and plant cell walls became thinner (Tong et al., 2015). When downregulating *HCT* in poplars, the thickness of their fiber and vessel cell walls have been shown to decrease (Zhou et al., 2018). However, studies are lacking regarding the effect of downregulation of *HCT* on the chemical composition and morphology of cell walls in *HCT* transgenic poplars and other transgenic plants at different developmental stages of stems.

The ultrastructure of wood fiber cell walls has an important influence on the physical and mechanical properties of wood. Indeed, the alteration of lignin content and composition in transgenic plants have been observed to affect the ultrastructure of fiber cell walls. In both *Arabidopsis* and tobacco limited in cinnamoyl-CoA reductase *(CCR)* activity, disordered cellulose microfibril organization was observed in fibers (Ruel et al., 2001, 2009). However, studies on the ultrastructure of *HCT* transgenic poplars have not been reported. Tracking the changes in cell wall structure, crystallinity, and microfibril angle (MFA) of transgenic poplar is essential to understand the responses of wood cell walls to downregulation of *HCT*.

In this study, we conducted a comprehensive study on *HCT* downregulated poplars using multiple techniques, combining chemical and structural analyses. The lignin and cellulose content and micro-region distribution of *HCT* transgenic poplars stems at different developmental stages, as well as the lignin monomers were observed to understand the responses of cell walls' chemical properties to downregulated *HCT*. Further, structural properties, such as fiber and vessel cell thickness and lumen diameter, fiber length and width, cell wall ultrastructure, cellulose crystallinity, and MFA of *HCT* transgenic poplars were obtained.

MATERIALS AND METHODS

Plant Materials

The tested specimens were prepared from control 84K (CK) poplars (*Populus alba* × *P. glandulosa cl.*) and downregulated *HCT* transgenic poplars. A RNAi construct for downregulating *HCT* gene (Orthologous of Potri.001G042900) expression in poplar was made in the pBIRNAi vector and transformed into poplars previously (Peng et al., 2014). Transgenic poplars with significantly reduced *HCT* gene expression were obtained, and the expression of the *HCT* was reduced by more than 65% compared with the control poplars. The CK and *HCT* transgenic poplars were planted in a greenhouse with 16 h natural light during the daytime (22°C) and 8 h of darkness at night (15°C). Poplar trees (98–124 cm height) were harvested after one growth season (6 months). The stem diameter of *HCT* transgenic poplars (4.72 mm) was thinner than that of CK poplars (5.25 mm). The sampling process for transgenic and CK poplars is shown in **Figure 1**. The leaves were manually removed from the poplars' stems and cut into three parts from the 11 internodes to the base. Next, some of the samples obtained from the upper, middle, and basal parts were preserved in FAA (70% alcohol: formalin: acetic acid = 90:5:5) fixative and 2.5% glutaraldehyde; some samples were packed in foil and placed in a refrigerator for subsequent structural and ultrastructural observation. The remaining stems were air-dried and prepared for analysis of cell wall composition. Sample preparation of the middle parts is illustrated in **Figure 1**.

Cell Wall Composition Analyses

The samples from upper, middle, and basal parts of the CK and *HCT* transgenic poplar stems were selected from the

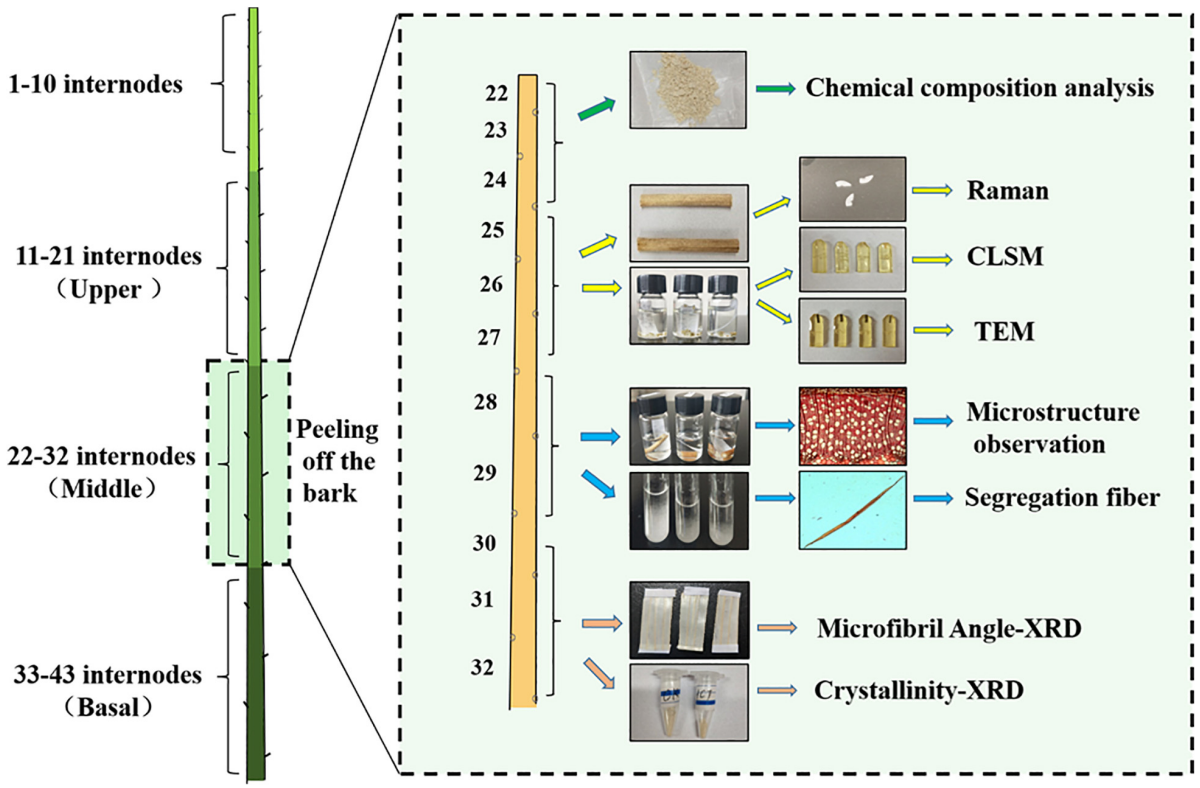

FIGURE 1 | Sampling and preservation from poplar stems; the preparation of wood samples from the middle parts for chemical and structural analyses is illustrated.

air-dried materials and treated with alcohol to obtain insoluble residues. The monosaccharide composition was determined using gas chromatograph mass spectrometry (Agilent) as described previously (Zhang and Zhou, 2017). For cellulose contents, the remains obtained above after trifluoroacetic acid treatment are hydrolyzed with sulfuric acid. After development of color with anthrone in concentrated sulfuric acid, the absorption at 625 nm is measured and the contents are determined based on standard curves (Zhang and Zhou, 2017). The lignin content of the wood was determined using the acetyl bromide method as previously reported (Foster et al., 2010). Five biological replicates were taken to ensure the accuracy of the results.

Confocal Laser Scanning Microscopy Analysis

The samples of the upper, middle, and basal parts of the CK and *HCT* transgenic poplars were taken from 2.5% glutaraldehyde and prepared at sizes of 1 mm × 1 mm × 3 mm. The samples were washed with 0.1 M phosphate-buffered saline (PBS) and deionized water three times (10 min each wash), then dehydrated by gradient alcohol. Next, the ethanol was replaced by propylene oxide gradually. The samples were then permeated in propylene oxide and Epon812 resin at ratios of 2:1, 1:1, and 1:2 three times, and placed in vacuum for 1.5–2 h. Finally, the embedded samples were put in vacuum and polymerized for 12 h at 37°C, 12 h at 45°C, and for 24 h at 60°C, respectively. Serial of 1.5-μm-thick cross-sections were cut from samples using an ultramicrotome (Leica EMUC6, Wetzlar, Germany), stained with acridine orange solution (0.001%) for 10 min, mounted with 70% glycerol, and then observed using a confocal laser scanning microscope (ZEISS LSM510META). A 488-nm argon laser was used for excitation.

Confocal Raman Microscopy Analysis

The samples for Raman analysis were taken from the air-dried stems. Serial of 16-μm-thick cross-sections were cut using a sliding microtome (Leica SM 2010R, Wetzlar, Germany) from the three parts of CK and transgenic poplars for Raman analysis. A LabRam Xplora exquisite full-automatic confocal Raman microscope (Horiba Jobin Yvon, Paris, France) equipped with an MPlan 100× oil immersion microscope objective (Olympus, NA = 1.40) was utilized. A linear polarized laser (diode-pumped green laser, λ = 532 nm), focused with a diffraction-limited spot size (0.61λ/NA), was used to conduct measurements. The laser power on the sample was approximately 8 mW. For mapping, an integration time of 2 s was chosen and every pixel corresponds to one scan with a spectrum acquired every 0.4 μm by averaging 2 s cycles. The Spectrum 6 software package was used for spectra analysis and image processing.

Observation of Anatomic Construction

The samples from three different parts of CK and transgenic poplars stems were taken from FAA fixative. Slices with a thickness of 20 μm were prepared using a sliding microtome.

The samples were stained with safranine (2%) for 12 h and washed with deionized water for three times (10 min for each), then a graded ethanol series was carried out. Finally, permanent sections were made with resin, which was used to observe the microstructure and measure the morphological parameters of fibrous cells. The ZEISS Imager A1 light microscope and Axiovision image processing software were used. Hundred fibers and 100 vessels were selected to measure cell wall thickness and lumen diameter.

Determination of Fiber Length and Width

The wood samples with a size of 1 mm × 1 mm × 10 mm (R × T × L) were cut from air-dried stems of three parts in the CK and transgenic poplars. Then, the samples were put into a centrifuge tube and 30 ml of dialysis solution was added (40% hydrogen peroxide: glacial acetic acid: water = 4:5:21) before heating in an oven (80°C) for 3 days. The isolated samples were cleaned three times with deionized water. After staining with safranine, the samples were observed under the ZEISS Imager A1 light microscope and images of the samples were taken. Hundred fibers were selected and their lengths and widths were measured using Axiovision image processing software.

Ultrastructure Observation

The samples of the middle part of poplar stems were obtained from 2.5% glutaraldehyde and cut into 1 mm^3 blocks for ultrastructure observation. The tissues were washed with 0.1 M PBS (1 h each wash) and deionized water three times (10 min each wash), then fixed in 1% osmium acid solution at 4°C. After 8 h, the samples were washed with PBS and water, then dehydrated and embedded in Epon812 resin. The embedding process is the same as that for confocal laser scanning microscopy analysis (CLSM) samples above. Transverse, ultrathin sections were cut with a 70 nm thickness using an ultramicrotome (Leica EMUC6, Wetzlar, Germany). Observations were carried out with a transmission electron microscope (TEM) (HT7700, Hitachi, Japan) at 100 kV accelerating voltage.

Measurements of Microfibril Angle

The slices with a 100 μm thickness were used for MFA analysis, which were cut from the middle and basal parts of the air-dried stems in *HCT* transgenic and control poplars. The MFAs were measured by an X'pert PRO polycrystalline X-ray diffractometer (PANalytical Company, Netherlands). The basic parameters of the diffractometer are as follows: diffraction angle = 22.4°, rotation range = 0–360°, rotation step = 0.5°, tube voltage = 40 kV, and tube current = 40 Ma. After rotating 360°, the 002 plane diffraction pattern was obtained. The average MFA was calculated by the 0.6T method (Wang et al., 2012). Three replicates of each sample were carried out.

Determination of Crystallinity

The wood powers from middle and basal parts of the air-dried stems in *HCT* transgenic and control poplars were used for determination of crystallinity. A D/max-rB type rotating anode X-ray diffractometer (Rigaku Company, Japan) was used for this purpose. The operating parameters for the measurements are as follows: radiation tube voltage = 40 kV, scanning range = 5°–40°, step length = 0.02°, and scanning speed = 4°/min. The crystallinity was calculated for the *HCT* transgenic and CK poplars by the Segal method, based on the diffraction patterns. The crystallinity equation is $C_rI = (I_u - I_a)/I_u \times 100\%$, where I_u is the maximum integral intensity of wood fiber diffraction intensity at $2\theta = 22°$ and I_a represents the minimum integral intensity at $2\theta = 18°$. Three replicates of each sample were carried out.

RESULTS

Chemical Changes of Cell Wall in Hydroxycinnamoyltransferase Transgenic Poplars

The contents and microdistributions of cell wall composition of the *HCT* transgenic poplars xylem at different developmental stages were studied to understand wood cell wall responses to downregulated *HCT*.

Chemical Composition Changes of Cell Wall

The lignin, cellulose, and hemicellulose content were determined from the stems of poplars at different developmental stages. Compared with the CK poplars, the lignin content of *HCT* transgenic poplars was significantly decreased by 10.84, 7.40, and 7.75% in the upper, middle, and basal parts, respectively (**Table 1**). And there was a significant increase in cellulose content in the upper and middle parts of transgenic poplars, by 8.20 and 6.45%, respectively. In comparison, the cellulose content of the basal part increased by only 3.31%. The cellulose/lignin ratio of *HCT* transgenic poplar increased (**Table 1**), and the increasing of upper parts was higher (23.2%) than those of the middle and basal sections (increased by 11.2 and 11.8%). The content of hemicelluloses (depicted by the cell wall-related monosaccharides rhamnose, fucose, arabinose, xylose, mannose, and galactose) does not change significantly in upper and basal part of *HCT* transgenic plants. But the hemicelluloses content in middle part significant decreased compared with the CK, and significant changes in the content of almost all cell wall-related monosaccharides. In which, the rhamnose, fucose, arabinose, and xylose content decreased and the mannose, galactose, and glucose content increased. In addition, the *HCT* transgenic poplars had higher mannose content in all three parts of stems.

The poplars at different stages of development showed some variation in their cell wall composition. Results revealed that more hemicellulose was deposited in younger internodes (upper part) and more cellulose was present in older internodes (middle and basal parts) for the transgenic and CK poplars. After the downregulation of *HCT*, poplars show more reduced lignin and increased cellulose in younger internodes.

Distribution of Lignin in the Xylem Cell

As can be seen from **Figure 2**, CLSM images were obtained in a large field of view for the lignin distribution in poplar cross sections. The cell wall corner (CC) and the compound middle

TABLE 1 | Chemical composition of *HCT* transgenic and CK poplar cell wall at different developmental stages.

Composition	CK (μg/mg)			*HCT* (μg/mg)		
	Upper	Middle	Basal	Upper	Middle	Basal
Lignin	161 (±3.3)^{B}	158 (±4.7)^{B}	159 (±2.5)^{B}	141 (±4.6)^{A}	151 (±6.4)^{AB}	146 (±3.3)^{A}
Cellulose	386 (±15.4)^{A}	423 (±13.0)^{BC}	430 (±5.1)^{BCD}	418 (±11.2)^{B}	450 (±19.8)^{D}	444 (±8.0)^{CD}
Hemicellulose	250 (±11.0)^{B}	249 (±11.7)^{B}	244 (±10.3)^{B}	247 (±2.69)^{B}	225 (± 10.4)^{A}	234 (±8.67)^{AB}
Cellulose/lignin	2.41	2.68	2.71	2.97	2.98	3.03
Rhamnose	5.39 (±0.25)^{B}	5.26 (±0.28)^{B}	4.73 (±0.34)^{A}	5.51 (±0.29)^{B}	4.60 (±0.24)^{A}	4.65 (±0.07)^{A}
Fucose	1.15 (±0.04)^{BC}	1.10 (±0.07)^{B}	1.03 (±0.07)^{A}	1.20 (±0.01)^{C}	1.02 (±0.04)^{A}	1.01 (±0.03)^{A}
Arabinose	4.45 (±0.14)^{D}	3.82 (±0.18)^{C}	3.44 (±0.23)^{B}	4.53 (±0.12)^{D}	3.30 (±0.13)^{AB}	3.15 (±0.09)^{A}
Xylose	220 (±10.8)^{C}	220 (±9.1)^{C}	215 (±9.7)^{BC}	214 (±9.3)^{BC}	194 (±9.3)^{A}	204 (±2.6)^{AB}
Mannose	10.3 (±0.54)^{A}	11.6 (±0.66)^{B}	12.7 (±0.34)^{C}	12.2 (±0.53)^{BC}	14.0 (±0.51)^{D}	13.8 (±0.64)^{D}
Galactose	8.50 (±0.45)^{B}	7.98 (±0.34)^{B}	7.22 (±0.62)^{A}	9.23 (±0.36)^{C}	8.01 (±0.25)^{B}	7.15 (±0.30)^{A}
Glucose	49.2 (±3.66)^{A}	56.6 (±2.97)^{B}	54.9 (±2.89)^{B}	54.0 (±2.38)^{B}	64.6 (±3.52)^{C}	55.8 (±2.42)^{B}

All values are expressed as means ± SD (n = 5, biological replicates). A, B, C, and D in the table indicated multiple analysis results, the same letter meant that there were no significant differences, and the different letters meant there were significant differences, $p < 0.05$ (Student Newman–Keuls test).

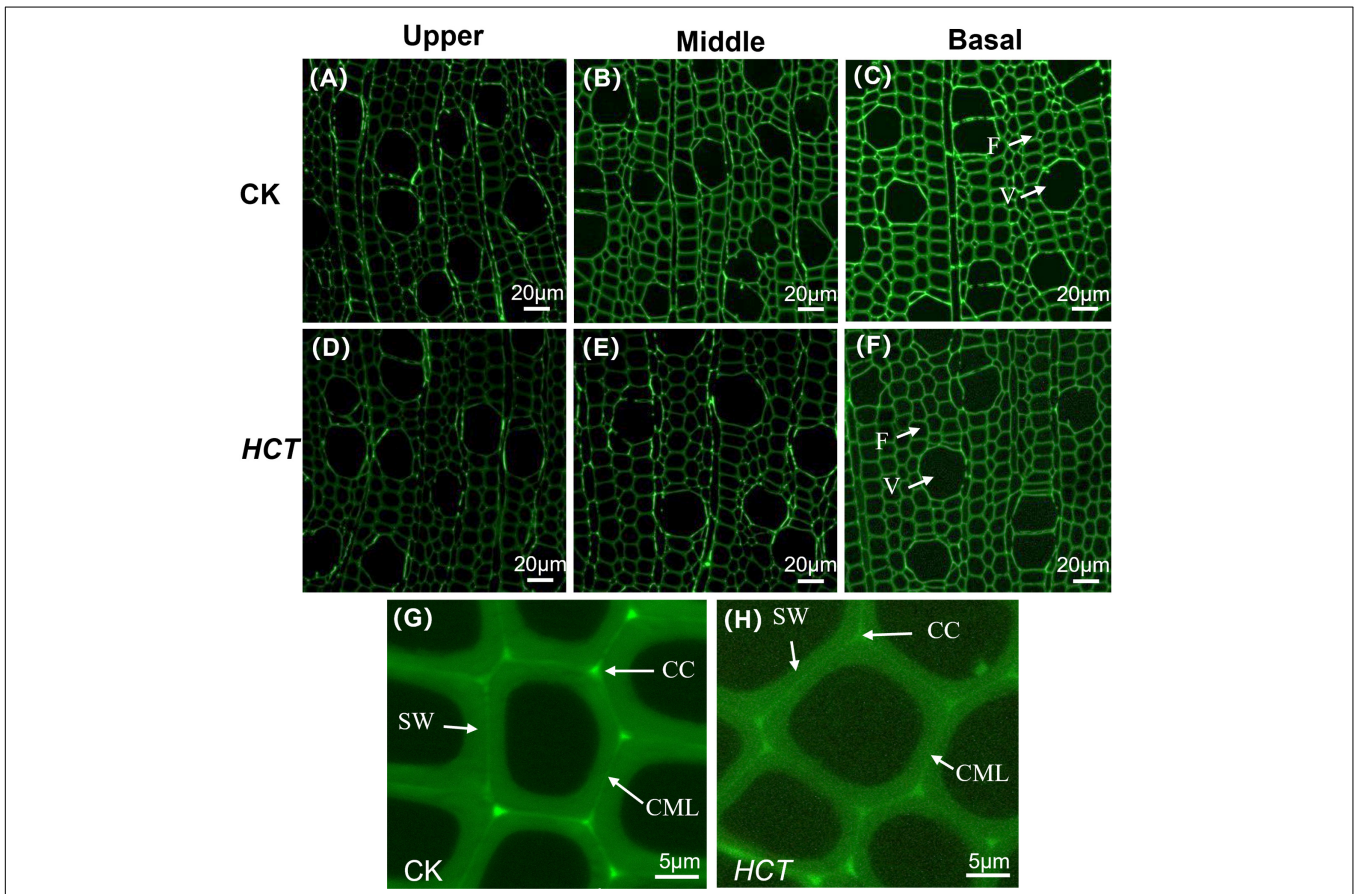

FIGURE 2 | Microscopic images of *HCT* transgenic and CK poplars stems by CLSM at different developmental stages. CK poplar, **(A)** the upper part; **(B)** the middle part; **(C)** the basal part; *HCT* transgenic poplar, **(D)** the upper part; **(E)** the middle part; **(F)** the basal part. Bar = 20μm. **(G)** The magnified image of CK poplar; **(H)** the magnified image of *HCT* transgenic poplar. Bar = 5 μm. F, fiber; V, vessel.

lamella (CML) regions have stronger fluorescence intensity, indicating that these regions had a higher degree of lignification. Compared with the CK poplars, a lower fluorescence intensity was observed clearly in the upper, middle, and basal parts of the *HCT* transgenic poplars (**Figures 2D–F**). Besides, the intensity in the CC, CML, and the secondary wall (SW) region of the *HCT* transgenic poplars were all decreased when compared with those of CK (**Figures 2G,H**). This indicated that the

TABLE 2 | Raman spectral characteristic peaks and their attribution of cell wall composition.

Composition	Wavenumber/ cm^{-1}	Band assignments
Lignin	1272	Aryl-O of aryl-OH and aryl-O-CH_3 of the G lignin
	1332	Aryl-O-CH_3 vibration of the S lignin
	1216	Aryl-O of aryl-OH and aryl-O-CH_3, ring deformation of the H lignin
	1600	Symmetric aryl ring stretching
	1654	Ring-conjugated C = C stretch of coniferyl alcohol; C = O stretch of conifer aldehyde
Cellulose	377	C-C-C ring deformation vibration, heavy atom stretching cellulose I
Cellulose and hemicellulose	1095 1122	Asymmetric stretch of C-O-C linkages Symmetric stretch of C-O-C linkages
Cellulose and lignin	1460	CH_3 bending in the O-CH_3 group, CH_2 scissoring

According to the literatures Wiley and Atalla (1987), Schenzel and Fischer (2001), Saariaho et al. (2003), Agarwal (2006), Agarwal and Ralph (2008), Kanbayashi and Miyafuji (2015), and Jin et al. (2018).

downregulation of *HCT* reduced the lignin concentration, which is coincident with the findings from cell wall composition analysis. The downregulation of *HCT* did not change the characteristics of lignin distribution, whose content remained CC > CML > SW. At different developmental stages of poplar stems, lignin concentrations increased gradually with the degree of lignification.

Distribution of Lignin and Cellulose in Wood Cell Wall

Raman spectroscopy technology can clearly visualize the distribution of lignin, lignin monomers, and carbohydrates in poplar cell wall *in situ*. Raman spectral characteristic peaks and their attribution of cell wall composition are listed in supporting **Table 2**. Typical Raman images of lignin are shown in **Figure 3** for the CK and *HCT* transgenic poplars at different developmental stages by calculating the Raman band ranges from 1550 to 1700 cm^{-1}. High lignin concentration was visualized in CC and then CML; SW was the lowest for both the *HCT* transgenic and CK poplars. The intensities in the upper, middle, and basal parts of the cell wall in the *HCT* transgenic poplars were all lower than those in CK poplars, due to the decline of lignin concentration. At different developmental stages of poplar stems, lignin concentrations increased gradually with the degree of lignification.

The middle part of poplars was used as tested specimen to study the distribution of lignin monomer and cellulose in wood cell walls. And average Raman spectra in the region of 300–1800 cm^{-1} of CC and SW were obtained (**Figure 4**). Stretching vibrations at 1600 and 1654 cm^{-1} were assigned to the lignin. Additionally, the results from previous studies reported that the peaks of G, S, and H lignin monomer in poplars were verified at 1272, 1333, and 1216 cm^{-1}, respectively (Saariaho et al., 2003; Agarwal et al., 2011; Jin et al., 2018). Although the spectra of *HCT* plants tended to be similar to those of the CK, the lignin spectrum intensities of CC and SW of the *HCT* transgenic poplars at 1600 cm^{-1} were lower than those of CK poplars. As shown in the Raman images, there were no obvious changes in the G lignin monomer of the transgenic and CK poplars. However, the S lignin monomer in CK poplars occurred at a higher intensity than *HCT* poplar at SW regions, suggesting a decrease of S lignin monomer in the secondary cell walls of the *HCT* transgenic poplar, which was also observed in Raman spectra (**Figure 4H**). But no obvious difference was found about microdistribution of cellulose, both at Raman images (**Figures 4C,F**) and spectra (**Figures 4G,H**). Notably, the CC of *HCT* transgenic poplars was recorded with higher intensities at 1216 cm^{-1}, which was assigned to the H lignin monomer (**Figure 4**).

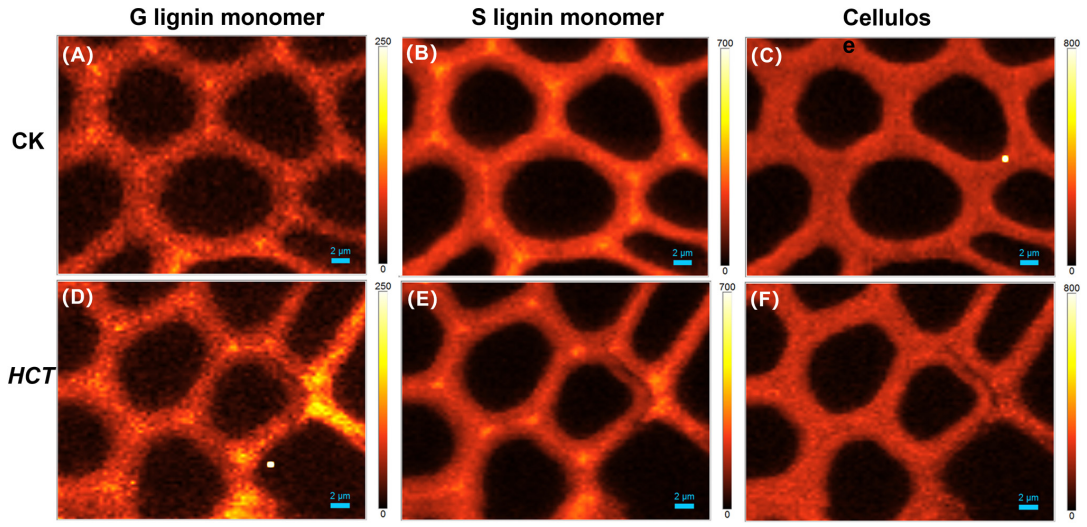

FIGURE 3 | Raman images of the lignin distributions for *HCT* transgenic and CK poplars at different developmental stages. CK poplar, **(A)** the upper part; **(B)** the middle part; **(C)** the basal part; *HCT* transgenic poplar, **(D)** the upper part; **(E)** the middle part; **(F)** the basal part. Bar = 2 μm. The lignin was integrated from 1550 to 1700 cm^{-1}.

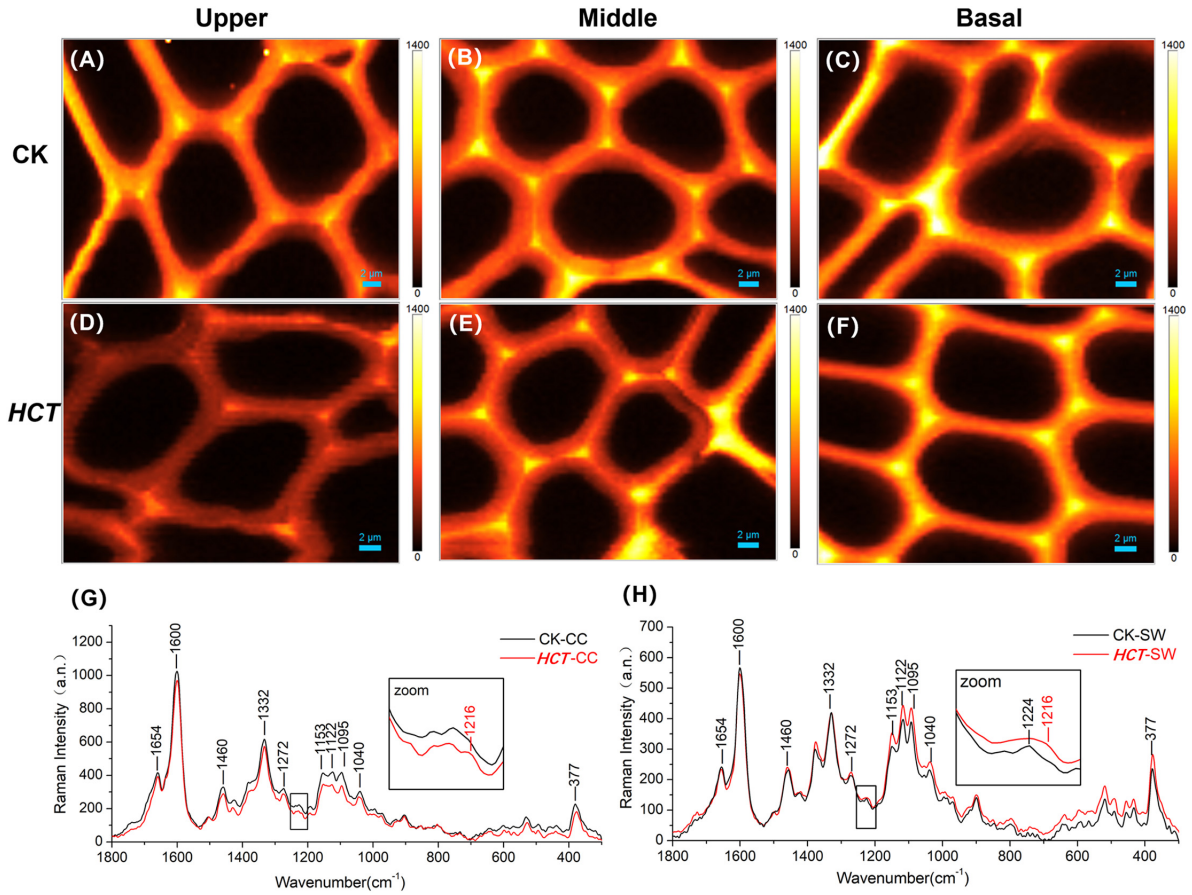

FIGURE 4 | Raman images of the lignin monomers and cellulose distributions, and extracted average spectra in the middle parts of *HCT* transgenic and CK poplars. CK poplar, **(A)** G lignin monomer; **(B)** S lignin monomer; **(C)** cellulose; *HCT* transgenic poplar, **(D)** G lignin monomer; **(E)** S lignin monomer; **(F)** cellulose. Bar = 2 μm. **(G)** Raman spectra obtained from the CC regions in cell wall; **(H)** Raman spectra obtained from the SW regions in cell wall. G lignin monomer integrating from 1247 to 1289 cm^{-1}; S lignin monomer from 1306 to 1359 cm^{-1}; cellulose from 344 to 400 cm^{-1}. The spectra of the transgenic lines exhibit a shoulder at around 1216 cm^{-1} (assigned to aryl-O of aryl-OH and aryl-O-CH_3 from H lignin).

Semiquantitative Analysis of Cellulose/Lignin and S/G Ratio

To extend the cell wall composition changes of cellulose/lignin and S/G ratio in *HCT* transgenic poplars at the cell level, a semiquantitative investigation was conducted. The ratio of I_{377}/I_{1600} and I_{1332}/I_{1272} represent the cellulose/lignin and S/G ratio, respectively. As illustrated in **Table 3**, the I_{377}/I_{1600} (cellulose/lignin) ratio is higher in the SW region of *HCT* transgenic fibers, which is consistent with the results of the traditional chemical method (**Table 1**). However, no significant difference was found in the CC region, where the lignin concentration was high. Notably, the I_{1332}/I_{1272} (S/G) ratio is lower both at the CC and SW regions in *HCT* transgenic fibers than those of the control, indicating that downregulation of *HCT* in poplars indeed decreased the S/G lignin monomer ratios at different regions of the cell wall.

TABLE 3 | Relative intensity ratios of the cellulose/lignin and S/G lignin monomer in CC and SW regions of cell walls in the middle part of *HCT* transgenic and CK poplars.

Poplar	I_{377}/I_{1600} (CC)	I_{377}/I_{1600} (SW)	S/G = I_{1332}/I_{1276} (CC)	S/G = I_{1332}/I_{1276} (SW)
CK	0.20 (±0.02)	0.43 (±0.04)	4.37 (±0.48)	3.90 (±0.70)
HCT	0.20 (±0.02)	0.47 (±0.03)*	3.98 (±0.58)*	3.37 (±0.49)*

All values are expressed as means ± SD (n = 7). Asterisk denotes significance at $p < 0.1$ (one-way ANOVA).

Structural Characteristics of Cell Wall in Hydroxycinnamoyltransferase Transgenic Poplars

The microstructure and ultrastructure characteristics of the *HCT* transgenic poplars were revealed to understand the response of structural properties of cell walls to downregulated *HCT*.

Morphology of Xylem Cell

From the images in **Figures 5A,B**, it can be discerned that the fibers of the two kinds of poplars are similar to each other. They are arranged regularly and distributed uniformly in the radial

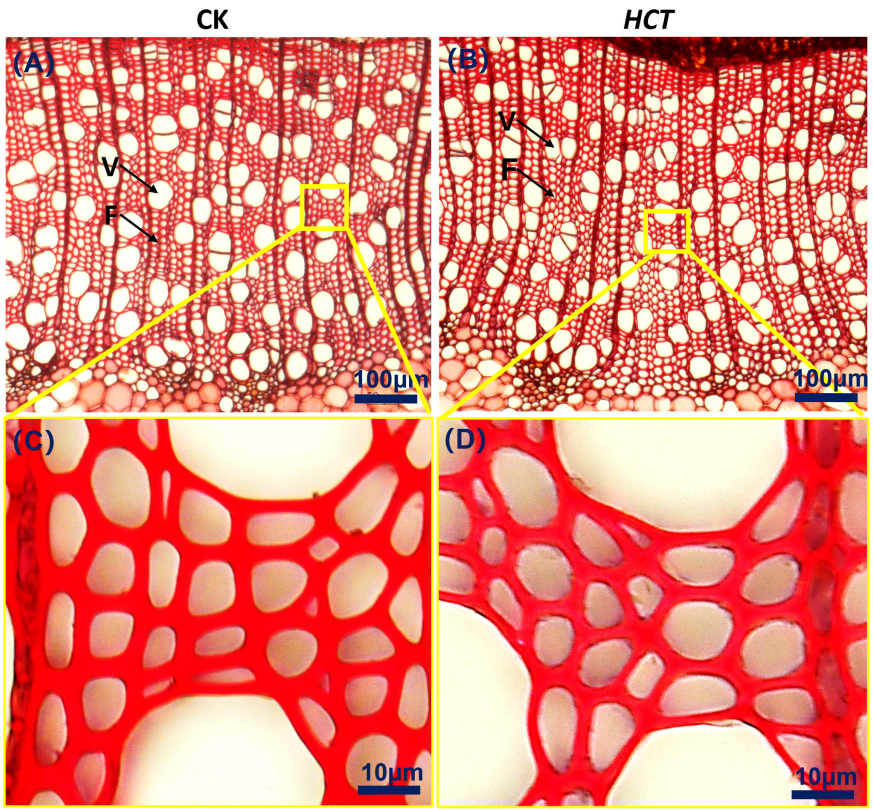

FIGURE 5 | Cross-sectional microstructure images of upper parts in poplars. **(A)** CK poplar; **(B)** *HCT* transgenic poplar, Bar = 100 μm. **(C)** Enlarged version of **(A)**; **(D)** enlarged version of **(B)**, Bar = 10 μm. F, fiber; V, vessel.

direction. The enlarged **Figures 5C,D** suggest that the fiber cell walls of *HCT* transgenic poplars are thinner. Fibers and vessels are the main cells of xylem in poplars, so the fiber and vessel cell thickness, lumen diameter and fiber length, and fiber width of the *HCT* transgenic poplars were measured.

Fiber Cell Thickness and Lumen Diameter

The fiber cell thickness and lumen diameter of the CK and *HCT* transgenic poplars are presented in **Table 4**. The average fiber cell wall thickness of the *HCT* transgenic poplars was 6.50% lower than that of the CK poplars. At different developmental stages of poplar stems, the cell wall thickness of the upper, middle, and basal parts of *HCT* transgenic poplars decreased by 6.47, 7.63, and 5.42%, respectively, and the fiber lumen diameter increased by 7.40, 11.88, and 5.45%, respectively, compared with the CK poplars. The ratio of the cell wall thickness to the lumen diameter of fiber cell walls is an important index for evaluating the quality of fiber cells. The results showed that the ratios in the upper, middle, and basal parts of transgenic poplars were all smaller than those of the control poplars in the corresponding parts and were reduced by 13.6% on average.

Fiber Length and Width

To further reveal the microscopic morphological characteristics of transgenic poplars, the wood was dissociated, and the length and width of individual fibers were measured (**Table 4**). The average fiber length of the *HCT* transgenic poplars (490 μm) was 5.60% higher than that of the CK poplars (464 μm), and the average fiber width of the *HCT* poplars (19.1 μm) was 6.11% higher than that of the control poplars (18.0 μm). At different developmental stages of poplar stems, the average fiber lengths of the three parts of the *HCT* transgenic poplars were 5.16, 4.07, and 7.50% greater than those of the CK poplars, respectively. The fiber width of the three parts of *HCT* poplars increased by 5.00, 9.09, and 3.80%, respectively. However, there was no significant difference in the ratio of fiber length to width between the two types of poplars.

Vessel Cell Thickness and Lumen Diameter

Table 5 shows the vessel cell wall thickness and its lumen diameter of poplars at different developmental stages of poplar stems. Thinner cell walls and larger lumen diameters of vessel cell in *HCT* transgenic poplars were observed. Vessel cell thickness in the three parts of the *HCT* transgenic poplars was reduced by 9.84, 13.97, and 8.37%, respectively, which significantly decreased compared with the CK poplars (an average decrease of 10.93%). The vessel lumen diameters of the upper, middle, and basal parts of the transgenic poplars were 10.12, 8.12, and 13.4% larger than those of the control poplars, respectively, and with an average increase of 9.83%. The vessel numbers and vessel area proportions obtained using Image J are listed in **Table 5**.

TABLE 4 | Fiber cell parameters of *HCT* transgenic and CK poplars at different developmental stages.

Line	Parts	Cell wall thickness/μm	Lumen dimeter/μm	Cell wall thickness/lumen dimeter	Length/μm	Width/μm	Length/width
CK	Upper	2.32 (±0.211)^{B}	9.59 (±2.01)^{A}	0.242 (±0.023)^{C}	446 (±72)^{A}	18.0 (±4.51)^{AB}	24.8 (±3.06)^{A}
	Middle	2.36 (±0.306)^{B}	10.1 (±1.46)^{A}	0.233 (±0.031)^{C}	467 (±69)^{B}	17.4 (±2.29)^{A}	26.5 (±4.00)^{AB}
	Basal	2.40 (±0.256)^{B}	11.0 (±2.15)^{B}	0.218 (±0.037)^{B}	480 (±79)^{B}	18.4 (±2.73)^{BC}	26.1 (±3.50)^{AB}
HCT	Upper	2.17 (±0.244)^{A}	10.3 (±1.10)^{A}	0.210 (±0.028)^{B}	469 (±72)^{B}	17.9 (±2.65)^{AB}	24.8 (±3.51)^{A}
	Middle	2.18 (±0.360)^{A}	11.3 (±3.24)^{B}	0.193 (±0.027)^{A}	486 (±101)^{B}	19.2 (±2.55)^{C}	25.3 (±4.47)^{AB}
	Basal	2.27 (±0.364)^{AB}	11.6 (±2.70)^{B}	0.196 (±0.032)^{A}	516 (±77)^{C}	19.1 (±2.68)^{C}	27.0 (±4.22)^{B}

All values are expressed as means ± SD (fiber cell wall thickness and cell lumen diameter, n = 100; fiber length and fiber width, n = 100). A, B, and C in the table indicated multiple analysis results, the same letter meant that there were no significant differences, and the different letters meant there were significant differences, $p < 0.05$ (Student Newman–Keuls test).

TABLE 5 | Vessel cell parameters of *HCT* transgenic and CK poplars at different developmental stages.

Line	Parts	Cell wall thickness/μm	Lumen dimeter/μm	Area proportions %	Number
CK	Upper	1.83 (±0.325)^{B}	30.8 (±4.59)^{A}	21.1 (±2.05)^{C}	39.5 (±3.25)^{C}
	Middle	1.86 (±0.255)^{B}	30.4 (±5.36)^{A}	17.7 (±1.98)^{B}	26.4 (±4.63)^{A}
	Basal	1.79 (±0.274)^{B}	32.1 (±5.16)^{AB}	18.0 (±2.02)^{B}	24.5 (±2.19)^{A}
HCT	Upper	1.65 (±0.242)^{A}	33.3 (±3.45)^{AB}	20.3 (±2.90)^{C}	42.2 (±5.69)^{C}
	Middle	1.60 (±0.152)^{A}	35.1 (±4.81)^{B}	16.1 (±2.60)^{A}	27.6 (±6.15)^{A}
	Basal	1.64 (±0.215)^{A}	35.6 (±3.29)^{B}	19.4 (±0.80)^{C}	30.8 (±0.96)^{B}

All values are expressed as means ± SD (vessel cell wall thickness and lumen diameter, n = 100; vessel area proportions and vessel numbers, n = 3). A, B, and C in the table indicated multiple analysis results, the same letter meant that there were no significant differences, and the different letters meant there were significant differences, $p < 0.05$ (Student Newman–Keuls test).

The vessel numbers of the *HCT* transgenic poplars were slightly higher than those of CK poplars, but the vessel area proportions were similar. At different developmental stages of poplar stems, the vessel numbers and the vessel area proportions of the upper part were higher than those of the middle and basal parts for both *HCT* transgenic and CK poplars.

Ultrastructure of Wood Cell Wall

In terms of cell wall layer structure, typical TEM images are shown in **Figure 6** for the *HCT* transgenic and CK poplars. It can be seen that the morphology of the fiber cell walls was similar between the *HCT* transgenic and CK poplars. The intercellular layer and the secondary cell wall (contain S_1, S_2, and S_3 layers) of the CK poplars could be observed clearly under TEM (**Figures 6A,B**). However, the cell wall layer structure of the transgenic poplars was less distinct, as shown in **Figures 6C,D**. The *HCT* transgenic poplar with thinner cell wall than that of the CK poplars is shown in **Figures 6E,F**. In addition, as can be seen in **Figures 6D,F**, the cell wall boundary of the transgenic poplars was not as smooth as that of the CK poplars.

The orientation of cellulose microfibrils in the SW and crystallinity of cellulose are the most important ultrastructural characteristics that determine the properties of wood and its products (Cave and Walker, 1994). Hence, average values of the MFA were obtained by using XRD and the 0.6T method. The average MFA of the *HCT* transgenic and CK poplars was 20.13° and 19.21°, respectively (**Table 6**), which coincide with typical values measured for juvenile wood (Gorisek and Niko, 1999). Although slightly higher, the MFA of transgenic lines is not significantly different from that of the CK. The *HCT* transgenic poplar showed an average relative crystallinity of 39.1%, whereas that of the CK had averaged crystallinity of 35.2%, according to Segal's method (**Table 6**). The cellulose crystallinity of *HCT* transgenic poplars increased by 11.1% compared with that of the CK poplars, and this difference was statistically significant. This suggests that downregulation of *HCT* does not change the orientation of cellulosic microfibrils but increased the cellulose crystallinity of cell walls.

DISCUSSION

The reducing lignin content or changing lignin monomeric composition through breeding and genetic regulation has the potential to reduce costs in biomass processing such as pulp, paper, and lignocellulosic ethanol industries. Hitherto, the downregulation of *HCT* on the chemistry and structure at different developmental stages of poplar stems, as well as the ultrastructure of poplar trees had not been explored.

Cell Wall Composition

The poplar cell walls are primarily composed of lignin, cellulose, and hemicellulose. In this study, we found that the downregulation of *HCT* led to a reduction in the lignin content and an increase in cellulose, as well as changes in monosaccharide content. A previous study exploring changes in the cellulose and hemicellulose contents of *HCT-C3′H* co-downregulated alfalfa, yielded similar results (Tong et al., 2015). The phenomenon of reduced lignin content accompanied by increased cellulose content has also been reported for hybrid poplars (Coleman et al., 2008) and aspens (*Populus tremuloides* Michx.) (Hu et al., 1999). This balancing mechanism between lignin and cellulose

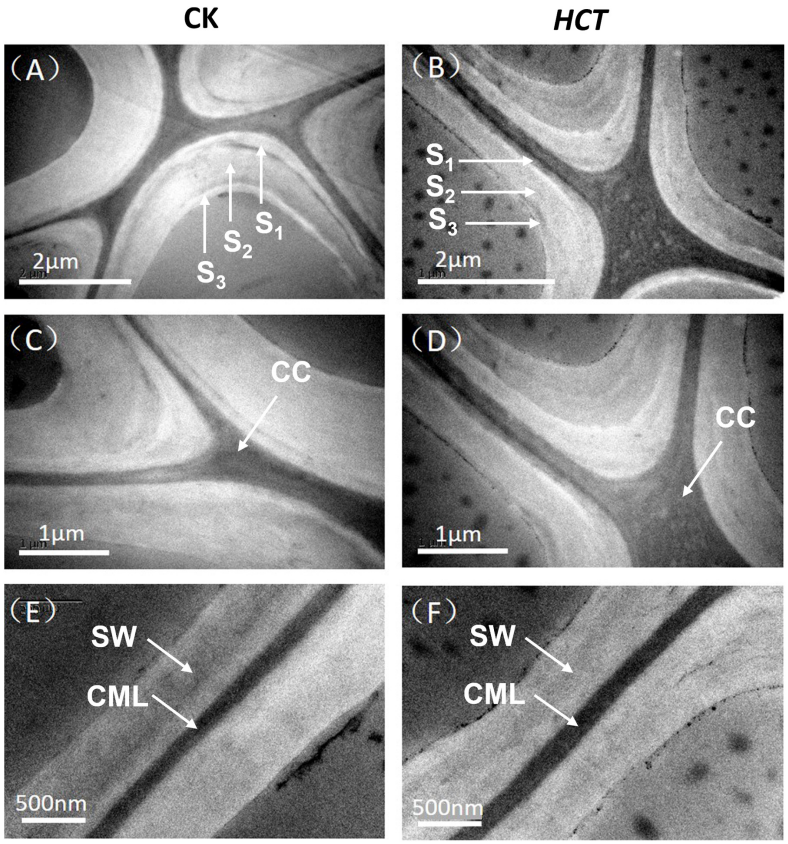

FIGURE 6 | Transmission electron microscope images of the *HCT* transgenic and CK poplars. **(A)** The cell corner of CK poplar; **(B)** the cell corner of *HCT* transgenic poplar; **(C)** enlarged version of **(A)**; **(D)** enlarged version of **(B)**; **(E)** the cell wall of CK poplar; **(F)** the cell wall of *HCT* transgenic poplar.

biosynthesis can be interpreted as the adaptability of trees to environmental change (Hu et al., 1999). To maintain the mechanical strength of lignin-deficient cell walls, plants may contribute to the conversion of glycosidic esters to cellulose and structural components (Tong et al., 2015). The production of fuel ethanol mainly uses cellulose and hemicellulose, so a higher cellulose/lignin ratio in *HCT* transgenic poplars facilitates the hydrolysis and fermentation process, increasing yields and ultimately reducing costs.

The composition of lignin, cellulose, and hemicellulose varied in poplars at different developmental stages. Lignin formation and deposition in cell walls is development tally controlled and reflects changes in gene expression. The results herein showed that lignin decreased more and cellulose increased in young internodes (upper) of poplar after downregulation of *HCT*. This is mainly because the basal part is the oldest internode, which is already highly lignified. Younger internodes, where lignification is still actively taking place, have high enzymatic activity and high levels of *HCT* gene repression expression (Chen et al., 2002).

TABLE 6 | Microfibril angle and cellulose crystallinity of *HCT* transgenic and CK poplars.

Sample	MFA[a]	CV[b]/%	Crystallinity/%	CV/%
CK	19.2 (±0.90)	4.70	35.2 (±1.17)	3.32
HCT	20.1 (±1.73)	8.61	39.1 (±0.20)*	5.21

[a]*Microfibril angle.* [b]*Coefficient of variation. All values are expressed as means ± SD, except CV values (MFA, n = 6; crystallinity, n = 3). Asterisk denotes significance at p < 0.05 (one-way ANOVA).*

Lignin Structure

The reduced lignin concentration and/or altered monolignol composition have been studied extensively to reduce the recalcitrance of cell walls in biomass crops to deconstruction for sugar release and conversion to biofuels. In this study, suppression of *HCT* in poplars resulted in an increase of H lignin monomer with a commensurate reduction in S lignin monomer. These results accord with those of similar studies, e.g., a large increase in H lignin monomer and strongly reduced S lignin monomer were found when *HCT* was downregulated in transgenic alfalfa plants (Shadle et al., 2007). Similarly, *C3′H* gene downregulation resulted in a significant increase of H lignin monomer at the expense of S lignin monomer in eucalyptus (*Eucalyptus urophylla* × *E. grandis*) (Sykes et al., 2015).

The *HCT* gene is only involved in the synthesis of S and G monomers and does not include H monomers. Thus, when downregulation of HCT, lignin tends to synthesize H lignin monomers via another pathway (Aymerick et al., 2016). And in this study, *HCT* downregulated poplar tend to produce H

lignin monomers at the expense of S lignin monomers. The multibranched structure of the G lignin monomers leads to tight cross-linking between carbohydrates, so that more retention facilitates normal plant growth and increases the strength of the cell wall support (Barsberg et al., 2013). However, lignin rich in S monomers is more likely to depolymerize than lignin rich in G monomers because there are fewer C–C bonds and a higher content of β-O-4 chains that are easier to remove (Ziebell et al., 2016). Therefore, the decrease in S/G ratio in *HCT* transgenic poplars may not benefit the hydrolysis process of lignocellulose. Reduced lignin content in eucalyptus was found to have a much greater effect on reducing recalcitrance than changing the lignin monomers ratio (Sykes et al., 2015). On the whole, the decrease in lignin content and the alteration of lignin structure in *HCT* transgenic poplars favors in reducing the recalcitrance cell walls, but enzyme hydrolysis efficiency and sugar release require further study.

Fiber Features

The poplars are an important raw material for pulp and paper making in China. Hence, the morphological characteristics of fiber are an important basis for evaluating fiber quality. Studies have shown that thicker and longer fibers are more likely to be resistant to abrasion and breakage. In addition, thin cell walls and large cavity fibers are easy to crush (Wei et al., 2008). Previous studies have reported that reduced lignin content affects fiber quality in transgenic poplars, e.g., Song et al. (2010) discovered that the ratio of fiber length to width in transgenic poplars was reduced following downregulation of the *CCR* gene. *HCT* transgenic poplar has thinner fiber cell walls and larger cell lumens, the characteristic that can make fibers easier to flatten down and become more adhesive (Wu et al., 2013). Fibers isolated from the *HCT* transgenic poplars were longer and wider than those from the CK poplars. These characteristics of the cell structures enable the fiberboards and paper made from *HCT* transgenic poplars to have a relatively high mechanical strength. In general, the fiber characteristics of *HCT* transgenic poplars are more favorable for paper applications.

Ultrastructure of Cell Wall

Both cellulose MFA and crystallinity are important indicators that affect wood quality. Results of this study have shown that downregulation of *HCT* does not change the orientation of cellulosic microfibrils but increased the cellulose crystallinity of cell walls. Previous studies have also shown that there was no significant difference in the MFA following downregulation of cinnamate 4-hydroxylase (*C4H*) in poplars (Ingela et al., 2010). However, decreases in lignin content and MFA were both revealed in the *Arabidopsis CCR1* mutant, suggesting that different gene regulatory pathways have different effects on MFA (Ruel et al., 2009). It should be noted that the cellulose crystallinity of cell wall in *HCT* poplar has increased (from 35.2 to 39.1%). And, cell wall composition results indicate that the decrease in lignin content lead to a compensatory increase in cellulose content, which is well-accompanied by an increase in crystalline area. Lignin has a mechanically supportive effect on cell walls, and previous studies have demonstrated that reduced lignin content may decrease mechanical stiffness and strength (Özparpucu et al., 2017, 2019). However, the increased cellulose crystallinity is beneficial to improve the physical mechanics of transgenic poplars, including mechanical support. Because, in most woods, the greater the crystallinity, the better the fracture strength and tensile strength of woods (Borrega et al., 2015; Shi et al., 2017).

CONCLUSION

The response mechanisms of chemical components and structural properties of wood cell walls to downregulated *HCT* in poplars were revealed. The lignin content of the *HCT* transgenic poplars was decreased with a compensatory increase in cellulose. The cell wall composition changes in the upper part were more obvious than those in the basal part for the *HCT* transgenic poplars. The results of *in situ* observation by Raman technology showed that *HCT* downregulation does not change the distribution of lignin monomers or cellulose in the cell walls. However, the lignin structure changed, and a small intensity of *p*-hydroxyphenyl (H) units was observed, as well as a decrease in the S/G ratio. Compared with the CK poplars, the fiber and vessel cells of the *HCT* transgenic poplars exhibited relatively thin cell walls and bigger lumen diameters. In addition, the fiber length becomes longer. Ultrastructure observations revealed that downregulation of *HCT* does not change the orientation of cellulosic microfibrils, but it led to an increase in the cellulose crystallinity of cell walls.

DATA AVAILABILITY STATEMENT

The raw data supporting the conclusions of this article will be made available by the authors, without undue reservation.

AUTHOR CONTRIBUTIONS

YW and JL designed the project. YW and MS designed the experiments and wrote the manuscript. MS performed the experiments. SZ performed the genomic analysis. YL and MS cultivated the transgenic poplars. All authors read and approved the submitted version of the manuscript.

FUNDING

This work was funded by the Central Public Interest Scientific Institution Basal Research Fund (CAFYBB2018GD001) and the National Natural Science Foundation of China (31370562).

ACKNOWLEDGMENTS

The authors are grateful to Jianfeng Ma and Kexia Jin (International Centre for Bamboo and Rattan, Beijing, China) for their assistance with the experiments.

REFERENCES

Agarwal, U. P. (2006). Raman imaging to investigate ultrastructure and composition of plant cell walls: distribution of lignin and cellulose in black spruce wood (*Picea mariana*). *Planta* 224, 1141–1153. doi: 10.1007/s00425-006-0295-z

Agarwal, U. P., and Ralph, S. A. (2008). Determination of ethylenic residues in wood and TMP of spruce by FT-Raman spectroscopy. *Holzforschung* 62, 667–675. doi: 10.1515/HF.2008.112

Agarwal, U. P., McSweeny, J. D., and Ralph, S. A. (2011). FT–Raman investigation of milled-wood lignins: softwood, hardwood, and chemically modified black spruce lignins. *J. Wood Chem. Technol.* 31, 324–344. doi: 10.1080/02773813.2011.562338

Aymerick, E., Pereira, J. H., Sasha, Y., Wang, G., Veronica, T. B., Baidoo, E. E. K., et al. (2016). Exploiting the substrate promiscuity of Hydroxycinnamoyl-CoA:shikimate Hydroxycinnamoyl Transferase to reduce lignin. *Plant Cell Physiol.* 57, 568–579. doi: 10.1093/pcp/pcw016

Barsberg, S., Selig, M. J., and Felby, C. (2013). Impact of lignins isolated from pretreated lignocelluloses on enzymatic cellulose saccharification. *Biotechnol. Lett.* 35, 189–195. doi: 10.1007/s10529-012-1061-x

Borrega, M., Ahvenainen, P., and Serimaa, R. (2015). Composition and structure of balsa (*Ochroma pyramidale*) wood. *Wood Sci. Technol.* 49, 403–420. doi: 10.1007/s00226-015-0700-5

Cave, I. D., and Walker, J. (1994). Stiffness of wood in fast-grown plantation softwoods: the influence of microfibril angle. *Forest Prod. J.* 44, 43–48. doi: 10.1007/BF02615226

Chen, L., Auh, C., Chen, F., Cheng, X., Aljoe, H., Dixon, R., et al. (2002). Lignin deposition and associated changes in anatomy, enzyme activity, gene expression, and ruminal degradability in stems of tall fescue at different developmental stages. *J. Agric. Food Chem.* 50, 5558–5565. doi: 10.1021/jf020516x

Coleman, H. D., Park, J., Nair, R., Chapple, C., and Mansfield, S. D. (2008). RNAi-mediated suppression of p-coumaroyl-CoA 3′-hydroxylase in hybrid poplar impacts lignin deposition and soluble secondary metabolism. *Proc. Natl Acad. Sci. U.S.A.* 105, 4501–4506. doi: 10.1073/pnas.0706537105

Foster, C. E., Martin, T. M., and Pauly, M. (2010). Comprehensive compositional analysis of plant cell walls (*lignocellulosic biomass*) Part II: carbohydrates. *Jove J Vis. Exp.* 37, 1837. doi: 10.3791/1837

Gorisek, Z., and Niko, T. (1999). Microfibril angle in juvenile, adult and compression wood of spruce and silver fir. *Phyton* 39, 129–132. doi: 10.1016/S0031-9422(98)00387-2

Hoffmann, L. (2002). Purification, cloning, and properties of an acyltransferase controlling shikimate and quinate ester intermediates in phenylpropanoid metabolism. *J. Biol. Chem.* 278, 95–103. doi: 10.1074/jbc.M209362200

Hoffmann, L. Besseau, S., Geoffroy. P., Ritzenthaler, C., and Legrand, M. (2004). Silencing of hydroxycinnamoyl-coenzyme a shikimate/quinate hydroxycinnamoyltransferase affects phenylpropanoid biosynthesis. *Plant Cell.* 16, 1446–1465. doi: 10.1105/tpc.020297

Hu, W. J., Harding, S. A., Lung, J., Popko, J. L., Ralph, J., Stokke, D. D., et al. (1999). Repression of lignin biosynthesis promotes cellulose accumulation and growth in transgenic trees. *Nat. Biotechnol.* 17, 808–812. doi: 10.1038/11758

Ingela, B., Anne-Mari, O., Bo, Z., Lorenz, G., Manoj, K., Lars, A. B., et al. (2010). Ultrastructure and mechanical properties of populus wood with reduced lignin content caused by transgenic down-regulation of cinnamate 4-hydroxylase. *Biomacromolecules* 11:2359. doi: 10.1021/bm100487e

Jin, K., Liu, X., Wang, K., Jiang, Z., Tian, G., Yang, S., et al. (2018). Imaging the dynamic deposition of cell wall polymer in xylem and phloem in *Populus* × *euramericana*. *Planta* 248, 849–858. doi: 10.1007/s00425-018-2931-9

Jung, Y. H., Cho, H. J., Lee, J. S., Noh, E. W., and Kim, K. H. (2012). Evaluation of a transgenic poplar as a potential biomass crop for biofuel production. *Bioresour. Technol.* 129, 639–641. doi: 10.1016/j.biortech.2012.12.074

Kanbayashi, T., and Miyafuji, H. (2015). Raman microscopic study of japanese beech (*Fagus crenata*) as treated with the ionic liquid, 1-ethyl-3-methylimidazolium chloride. *J. Wood Chem. Technol.* 36, 224–234. doi: 10.1080/02773813.2015.1112404

Özparpucu, M., Gierlinger, N., Cesarino, I., Burgert, I., Boerjan, W., and Rüggeberg, M. (2019). Significant influence of lignin on axial elastic modulus of poplar wood at low microfibril angles under wet conditions. *J. Exp. Bot.* 70, 4039–4047. doi: 10.1093/jxb/erz180

Özparpucu, M., Rüggeberg, M., Gierlinger, N., Cesarino, I., Vanholme, R., Boerjan, W., et al. (2017). Unravelling the impact of lignin on cell wall mechanics: a comprehensive study on young poplar trees downregulated for cinnamyl alcohol dehydrogenase (CAD). *Plant J.* 91, 480–490. doi: 10.1111/tpj.13584

Pauly, M., and Keegstra, K. (2008). Physiology and metabolism 'Tear down this wall'. *Curr. Opin. Plant Biol.* 11, 233–235. doi: 10.1016/j.pbi.2008.04.002

Peng, X. P., Sun, S. L., Wen, J. L., Yin, W. L., and Sun, R. C. (2014). Structural characterization of lignins from hydroxycinnamoyl transferase (HCT) down-regulated transgenic poplars. *Fuel* 134, 485–492. doi: 10.1016/j.fuel.2014.05.069

Pu, Y., Chen, F., Ziebell, A., Davison, B. H., and Ragauskas, A. J. (2009). NMR characterization of C3H and HCT down-regulated alfalfa lignin. *BioEnerg. Res.* 2, 198–208. doi: 10.1007/s12155-009-9056-8

Ralph, J., Akiyama, T., Coleman, H. D., and Mansfield, S. D. (2012). Effects on lignin structure of coumarate 3-hydroxylase downregulation in poplar. *Bioenerg. Res.* 5, 1009–1019. doi: 10.1007/s12155-012-9218-y

Reddy, M. S. S., Chen, F., Shadle, G., Jackson, L., Aljoe, H., and Dixon, R. A. (2005). Targeted down-regulation of cytochrome p450 enzymes for forage quality improvement in alfalfa (*Medicago sativa* l.). *Proc. Natl. Acad. Sci. U.S.A.* 102, 16573–16578. doi: 10.1073/pnas.0505749102

Ruel, K., Berrio-Sierra, J., Derikvand, M. M., Pollet, B., Thévenin, J., Lapierre, G., et al. (2009). Impact of CCR1 silencing on the assembly of lignified secondary walls in *Arabidopsis thaliana*. *New Phytol.* 184, 99–113. doi: 10.1111/j.1469-8137.2009.02951.x

Ruel, K., Chabannes, M., Boudet, A. M., Legrand, M., and Joseleau, J. P. (2001). Reassessment of qualitative changes in lignification of transgenic tobacco plants and their impact on cell wall assembly. *Phytochemistry* 57, 875–882. doi: 10.1016/S0031-9422(01)00118-2

Saariaho, A., Jääskeläinen, A., Nuopponen, M., and Vuorinen, T. (2003). Ultra violet resonance raman spectroscopy in lignin analysis: determination of characteristic vibrations of p-hydroxyphenyl, guaiacyl, and syringyl lignin structures. *App. Spectrosc.* 57, 58–66. doi: 10.1366/000370203321165214

Schenzel, K., and Fischer, S. (2001). NIR FT raman spectroscopy–a rapid analytical tool for detecting the transformation of cellulose polymorphs. *Cellulose* 8, 49–57. doi: 10.1023/A:1016616920539

Shadle, G., Chen, F., Reddy, M. S. S., Jackson, L., Nakashima, J., and Dixon, R. A. (2007). Down-regulation of hydroxycinnamoyl coa: shikimate hydroxycinnamoyl transferase in transgenic alfalfa affects lignification, development and forage quality. *Phytochemistry* 68, 1521–1529. doi: 10.1016/j.phytochem.2007.03.022

Shi, J. T., Ding, X. H., Zhang, X., and Chen, L. (2017). Comparison of characteristics of branch and truck of *Cunninghamia lanceolata* from natural secondary forest. *J. For. Eng.* 2, 20–24.

Song, E., Cai, C., Wei, G., Gao, H., and Xiang, Y. (2010). Cultivation of low lignin poplar by RNA interference. *Sci. Silvae Sin.* 46, 39–44.

Sykes, R. W., Gjersing, E. L., Foutz, K., Rottmann, W. H., Kuhn, S. A., Foster, C. E., et al. (2015). Down-regulation of p-coumaroyl quinate/shikimate 3′-hydroxylase (C3′H) and cinnamate 4-hydroxylase (C4H) genes in the lignin biosynthetic pathway of *Eucalyptus urophylla* × *E. grandis* leads to improved sugar release. *Biotechnol. Biofuels* 8:128. doi: 10.1186/s13068-015-0316-x

Tong, Z., Li, H., Zhang, R., Ma, L., Dong, J., and Wang, T. (2015). Co-downregulation of the hydroxycinnamoyl-CoA:shikimate hydroxycinnamoyl transferase and coumarate 3-hydroxylase significantly increases cellulose content in transgenic alfalfa (*Medicago sativa* L.). *Plant Sci.* 239, 230–237. doi: 10.1016/j.plantsci.2015.08.005

Vanholme, B., Cesarino, I., Goeminne, G., Kim, H., Marroni, F., Van Acker, R., et al. (2013). Breeding with rare defective alleles (BRDA): a natural *Populus nigra* HCT mutant with modified lignin as a case study. *New Phytol.* 198, 765–776. doi: 10.1111/nph.12179

Vanholme, R., Demedts, B., Morreel, K., Ralph, J., and Boerjan, W. (2010). Lignin biosynthesis and structure. *Plant Physiol.* 153, 895–905. doi: 10.1104/pp.110.155119

Vanholme, R., Morreel, K., Darrah, C., Oyarce, P., Grabber, J. H., Ralph, J., et al. (2012). Metabolic engineering of novel lignin in biomass crops. *New Phytol.* 196, 978–1000. doi: 10.1111/nph.12028

Wagner, A., Ralph, J., Akiyama, T., Flint, H., Phillips, L., Tor, K., et al. (2007). Exploring lignification in conifers by silencing hydroxycinnamoyl-CoA:shikimate hydroxycinnamoyl transferase in *Pinus radiata*. *Proc. Natl. Acad. Sci. U.S.A.* 104, 11856–11861. doi: 10.1073/pnas.0701428104

Wang, S., Li, E., Porth, I., Chen, J. G., Mansfield, S. D., and Douglas, C. J. (2014). Regulation of secondary cell wall biosynthesis by poplar R2R3 MYB transcription factor PtrMYB152 in Arabidopsis. *Sci. Rep.* 4:5054. doi: 10.1038/srep05054

Wang, Y., Leppänen, K., Andersson, S., Serimaa, R., Ren, H., and Fei, B. (2012). Studies on the nanostructure of the cell wall of bamboo using X-ray scattering. *Wood Sci. Technol.* 46, 317–332. doi: 10.1007/s00226-011-0405-3

Wei, J., Wang, Y., Wang, H., Li, R., Lin, N., Ma, R., et al. (2008). Pulping performance of transgenic poplar with depressed Caffeoyl-CoA O-methyltransferase. *Chinese Sci. Bull.* 53, 3553–3558. doi: 10.1007/s11434-008-0477-0

Wiley, J. H., and Atalla, R. H. (1987). Raman spectra of celluloses. *Struct. Cellulose* 340, 151–168. doi: 10.1021/bk-1987-0340.ch008

Wu, Q., Chen, H. L., Wang, B. B., and Cao, B. B. (2013). Analysis on fast-growing black poplar branch used as raw materials for APMP pulping and papermaking. *Appl. Mech. Mater.* 448-453, 972–977.

Zhang, B., and Zhou, Y. (2017). "Carbohydrate composition analysis in xylem," in *Xylem – Methods in Molecular Biology*, Vol. 1544, eds M. de Lucas and J. Etchhells (New York, NY: Humana Press), 213–222. doi: 10.1007/978-1-4939-6722-3_15

Zhang, G., Zhang, Y., Xu, J., Niu, X., Qi, J., Tao, A., et al. (2014). The CCoAOMT1 gene from jute (*Corchorus capsularis* L.) is involved in lignin biosynthesis in *Arabidopsis thaliana*. *Gene* 546, 398–402. doi: 10.1016/j.gene.2014.05.011

Zhou, X. W., Ren, S. H., Lu, M. Z., Zhao, S. T., Chen, Z., Zhao, R. J., et al. (2018). Preliminary study of cell wall structure and its mechanical properties of C3H and HCT RNAi transgenic poplar sapling. *Sci. Rep.* 8:10508. doi: 10.1038/s41598-018-28675-5

Ziebell, A., Gjersing, E., Hinchee, M., Katahira, R., Sykes, R. W., Johnson, D. K., et al. (2016). Downregulation of p-coumaroyl quinate/shikimate 3′-hydroxylase (C3H) or cinnamate-4-hydrolylase (C4H) in *Eucalyptus urophylla* × *Eucalyptus grandis* leads to increased extractability. *Bioenerg. Res.* 9, 1–9. doi: 10.1007/s12155-016-9713-7

Conflict of Interest: The authors declare that the research was conducted in the absence of any commercial or financial relationships that could be construed as a potential conflict of interest.

Publisher's Note: All claims expressed in this article are solely those of the authors and do not necessarily represent those of their affiliated organizations, or those of the publisher, the editors and the reviewers. Any product that may be evaluated in this article, or claim that may be made by its manufacturer, is not guaranteed or endorsed by the publisher.

Advantages of publishing in Frontiers

OPEN ACCESS
Articles are free to read for greatest visibility and readership

FAST PUBLICATION
Around 90 days from submission to decision

HIGH QUALITY PEER-REVIEW
Rigorous, collaborative, and constructive peer-review

TRANSPARENT PEER-REVIEW
Editors and reviewers acknowledged by name on published articles

Frontiers
Avenue du Tribunal-Fédéral 34
1005 Lausanne | Switzerland

Visit us: www.frontiersin.org
Contact us: frontiersin.org/about/contact

REPRODUCIBILITY OF RESEARCH
Support open data and methods to enhance research reproducibility

DIGITAL PUBLISHING
Articles designed for optimal readership across devices

FOLLOW US
@frontiersin

IMPACT METRICS
Advanced article metrics track visibility across digital media

EXTENSIVE PROMOTION
Marketing and promotion of impactful research

LOOP RESEARCH NETWORK
Our network increases your article's readership